GEOSYNTHETICS CONFERENCE 2001

Portland, Oregon USA

Economics, Performance & Constructibility • February 12-14, 2001

Main Menu

Conference Proceedings

Organized by:

IFAI
Industrial Fabrics Association International

NAGS
North American Geosynthetics Society

GMA
Geosynthetic Materials Association

Under the auspices of

IGS
International Geosynthetics Society

SITE EVALUATION/PERFORMANCE OF SEPARATION GEOTEXTILES

L. DAVID SUITS, NEW YORK STATE
DEPARTMENT OF TRANSPORTATION, UNITED STATES OF AMERICA
GEORGE KOERNER, PHD, GEOSYNTHETIC INSTITUTE
UNITED STATES OF AMERICA

ABSTRACT

In the transportation industry one of the major uses of geotextiles is a separator between fine grained subgrade soils, and the drainable base course materials in a pavement system. The purpose being to prevent the intrusion of the fine grain soils into the drainable base materials.

There is currently a study under the auspices of the Geosynthetic Institute located in Folsom, PA, USA, to evaluate the performance of geotextiles as separators under various foundations and environmental conditions. One of the sites under investigation is located in northern New York state, USA.

This paper will describe the site in New York, the geotextiles used, and the results of falling weight deflectometer testing which has been done in conjunction with the investigation.

INTRODUCTION

Since their inception as " filter fabrics," and continuing through to the present time as geotextiles, one of the major applications for these materials has been as a separator between fine grained subgrade soils, and the drainable base course materials in a pavement system. The geotextile serves to prevent intrusion of the fine grained soils into the drainable base materials.

Over the history of the use of geotextiles in this application, there have been small, isolated investigations as to their performance on specific projects. There has not been a coordinated study to evaluate performance under varying environmental and climatic conditions. Currently, a study under the auspices of the Geosynthetic Institute is evaluating several sites located in various regions of the United States to determine the effectiveness of various geotextiles in this application under differing climatic and environmental conditions. The sites under investigation are located in the states of Pennsylvania, New York, Minnesota, Washington, South Carolina, and Virginia.

On the site located in New York State, five different geotextiles were installed, plus a control section, for a total of six test sections. Investigation of the site has included both visual inspection and the performance of falling weight deflectometer tests during the different seasons of the year, on an annual basis.

This paper will describe the New York State site as to location, soil conditions, installation procedures, and the results of the falling weight deflectometer test which have been done to date. Conclusions will be drawn as to the performance of each geotextile to date at the site.

NEW YORK STATE SITE DESCRIPTION

Site Location

The site under investigation in New York is a rural, two lane road over which traffic is primarily agricultural equipment. It is located in northern New York, near Watertown. The project consisted of the replacement of the Vorce Road bridge over the Deer River just outside the village of Copenhagen in Lewis County. The original bridge was constructed in 1890, and the deteriorated condition would have prevented the implementation of a rural-road system plan for the area of Lewis County in which it is located. The length of the project was 482 meters (1583 feet).

The climatic region of the area falls into the FHWA Climatic Zone 1-A. As a result, the site is an area with a high potential for the presence of moisture in the pavement year round, severe winters, and frost penetration to appreciable depths. The monthly average precipitation is about 75 mm/month (3 inches/month), and an annual snowfall of 2,540 mm (8 feet +). During the winter months, the daytime temperature averages 0 ^{0} C, with nighttime lows below -15 ^{0} C. Freezing conditions run from early October through late April and early May.

The two-way average annual daily traffic for 1996 was 103, of which nine percent was truck traffic. The projected two-way average annual daily traffic for 2031 is 140, with the truck traffic remaining at nine percent.

Soil Conditions

There were three soils encountered on the project: two different subgrade soils, and the base soil. The subgrade soils are generically described as a Brown Till, and a Gray Sandy Silt. The base soil is generically described as a Well Graded Gravel. Table 1 summarizes the characteristics of each. The characteristics were determined by testing performed at the Geosynthetics Institute.

Table 1. Soil Characteristics

Property	Unit	Method*	Subgrade #1	Subgrade #2	Base
Soil Description	na	na	Brown Till "Hard Pan"	Wet, spongy, Gray Sandy Silt	Well graded Gravel
USCS Classification	na	D854	SC	SM	GW
AASHTO Classification	na	T100	A-2-6	A-2-4	A-1-a
d10	mm	D422	0.0065	0.04	0.3
Cu**	na	D422	31	21	27
Cc***	na	D422	1.2	2.7	1.4
Passing # 200	%	D422	43	15	4
Liquid Limit	na	D4318	25.5	14	na
Plastic Limit	na	D4318	4.9	2.5	na
Average CBR	na	D4429	9	<1	21
Avg. Cone Penetration	kPa	CN973	1427.2	379.2	>2068
Opt. Moist. Content	%	D698	14.3	9.2	na
Max. Dry Density	kg/m^3	D698	1866.2	2178.5	na
Avg. In-situ Density	kg/m^3	D1556	1681.9	1794.1	1906.2
Avg. Insitu Wc	%	D2216	9.2	16.5	6
Min. Dry Density	kg/m^3	D4253	na	na	1393.6
Max. Dry Density	kg/m^3	D4253	na	na	2066.4

* Methods denoted by a "D" are ASTM Standards, by a "T" are AASHTO Standards, and by "CN" are Us Army Corp of Engineers Standards,** Coefficient of Uniformity, *** Coefficient of Curvature

Figure 1 is a plan view of the Vorce Road site. The limits of the various geotextiles are shown on this view. Figures 2a and 2b show typical sections for the project. Figure 2a shows the typical built up section, while 2b shows a typical undercut section.

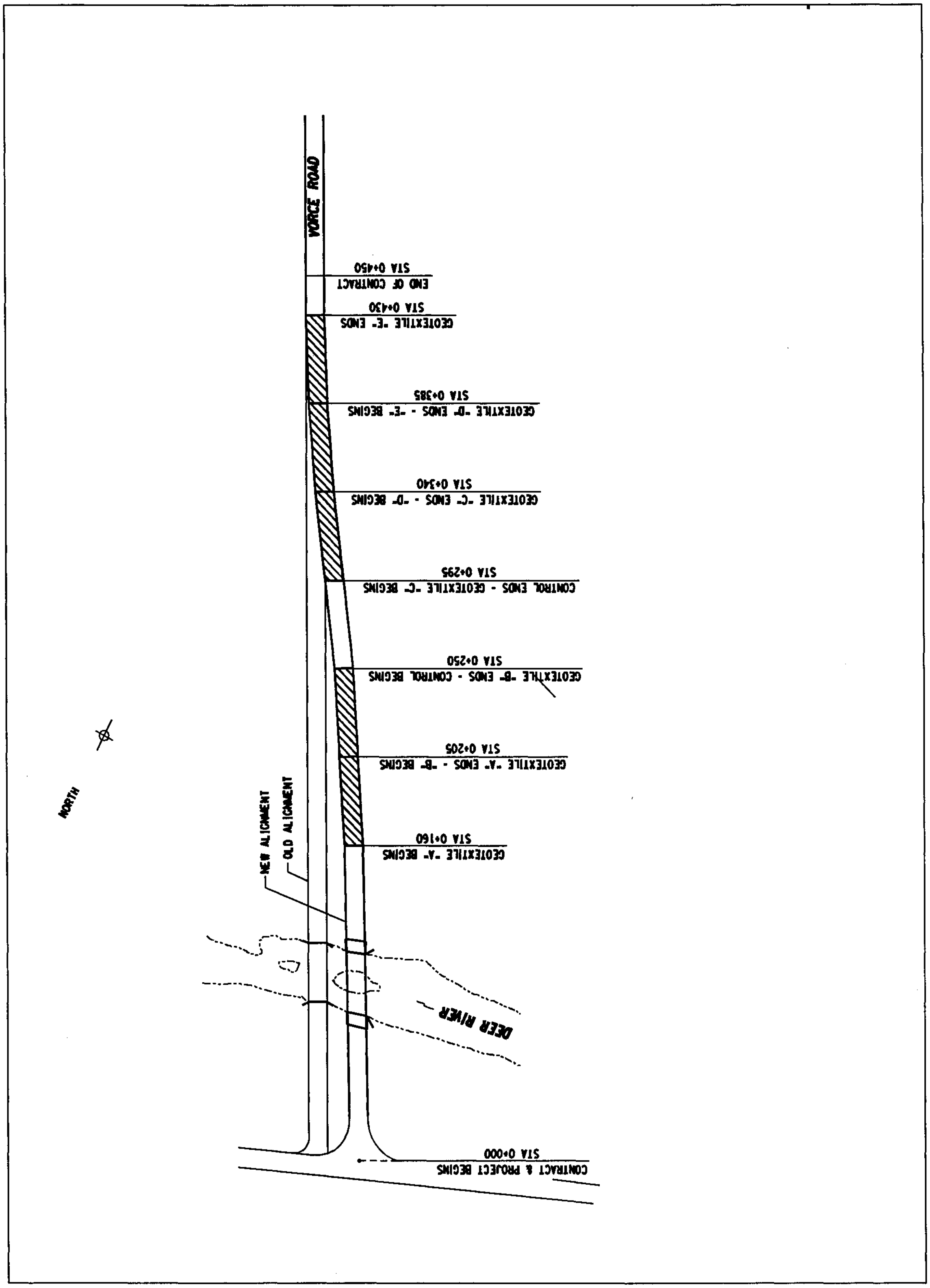

Figure 1- Plan View - Vorce Road over Deer River

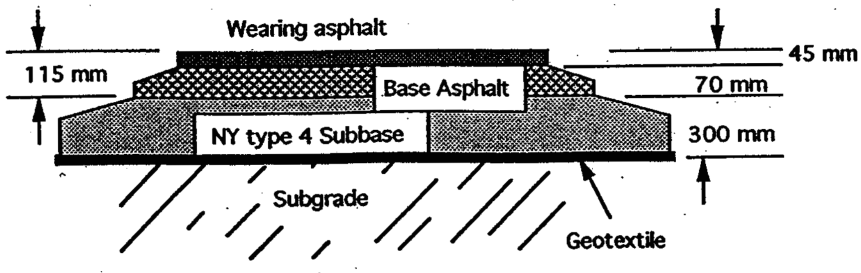

2a – Typical Section

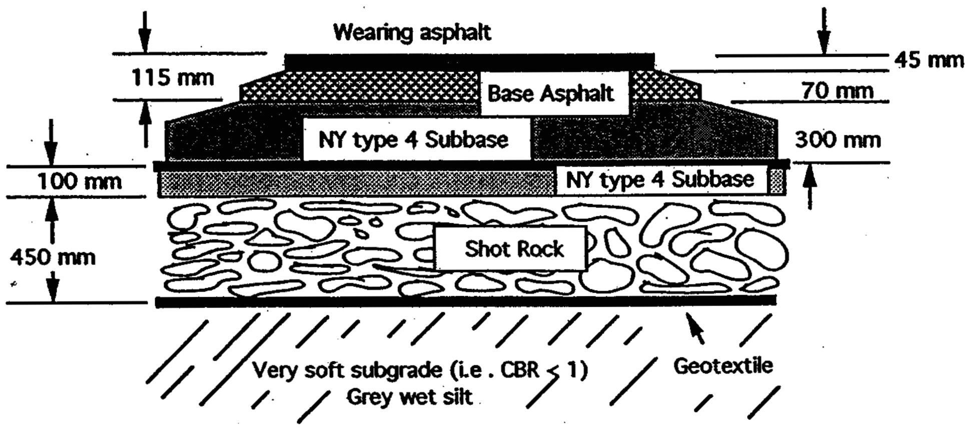

2b - Typical Undercut Section

Figure 2 - Typical Sections for Vorce Road

Geotextile Descriptions

Five different geotextiles were installed at the site. The range of mass per unit area for the geotextiles used was 169 g/ sq m to 264 g/ sq m. Table 2 lists the individual characteristics for each of the geotextiles used. Each was supplied by their respective manufacturer for inclusion in this study.

Table 2 - Geotextile Characteristics

Property	**Unit**	**ASTM**	**GT - A**	**GT - B**	**GT - C**	**GT - D**	**GT - E**
Structure*	-	-	CF/NW/NP/PE	S/NW/NP/PP	CF/NW/HB/PP	W/SF/PP	CF/NW/NP/PP
Thickness	mm	D5199	2.13	1.96	0.48	0.69	2.08
MD Grab Strength**	kN	D4632	0.89	0.80	0.78	1.80	0.98
MD Grab Elong.	%	D4632	79	56	98	30	103
MD Tear Strength	kN	D4533	0.35	0.36	0.34	0.66	0.49
Puncture Strength	kN	D4833	0.44	0.56	0.30	0.70	0.41
MD Wide Width Strength	kN/m	D4595	11.87	10.80	6.15	35.70	7.35
MD Wide Width Elong.	%	D4595	49	56	81	29	90
5 % Secant Modulus	kN/m	D4595	29.70	24.15	51.60	150.30	22.95
XD Wide Width Str.***	kN/m	D4595	8.25	17.85	8.40	37.35	9.15
XD Wide Width Elong.	%	D4595	54	62	67	18	24
5 % Secant Modulus	kN/m	D4595	17.10	26.70	62.70	307.95	82.95
Permittivity	1/sec	D4491	1085	1.20	0.70	0.28	1.30
AOS****	Sieve #	D4751	70	70	100	50	60

* CF:Continuous Filament; S: Staple Filament; NW:Woven; W:Woven; SF:Slit Film; NP:Needle Punched; HB:Heat Bonded; PE:Polyester; PP:Polypropylene; ** MD = Machine Direction; *** XD = Cross Machine Direction; **** AOS = Apparent Opening Size

DESIGN CONSIDERATIONS

The site is a roadway cut. A sloped field borders the southwest side of the roadway that drains into the Deer River. Unfortunately, Vorce Road intersects the natural drainage flow path of this field. For precautionary measures, an underdrain was designed and installed to handle the seepage from this field. The underdrain extends from Station 0+310 to 0+210, with the drain crossing the roadway at Station 0+210 emptying into a northern drainage swale.

CONSTRUCTION SEQUENCE

The construction sequence started by removing the old existing pavement, and cutting the realigned roadway. Upon completion of the highway cut, rough grade of the subgrade was obtained by the use of a heavy dozer. The subgrade was then proof rolled with a vibratory, steel wheeled roller, and then tested for competency. Upon establishing competency, final grade was made with a light dozer. The subgrade was then rolled with a vibratory, steel wheeled roller. The geotextile was then placed on the subgrade. It was covered with the subbase materials immediately to avoid any deterioration due to exposure to ultraviolet radiation. The subbase was placed using the light dozer, and compacted using the vibratory, steel wheeled roller.

Details

While the majority of the project was underlain by firm glacial till, between Stations 0+350 and 0+375 a soft section of wet, gray silty sand existed. The area was undercut, a reinforcement geotextile placed over the area, approximately 450 mm of shot rock was placed over the reinforcement geotextile. In order to facilitate grading, and to fill the voids in the shot rock, 100 mm of NYSDOT Type 4 Subbase was used. The section was then completed as typical over the repaired undercut section. See Figure 2b.

In typical sections, 300 mm of NYSDOT Type 4 Subbase material was placed over the separation geotextile. The cross section was finished by the application of an asphaltic roadway consisting of approximately 70 mm of asphaltic base, and 45 mm of asphaltic wearing coarse. A roadway edge drain was installed along the southern edge of the roadway between Stations 0+210 and 0+310. The drain consists of a 100 mm perforated pipe imbedded in approximately 455 mm of pea gravel.

The geotextile sections were constructed beginning at the southern end of the project and progressing to the northern end. The geotextiles were unrolled in such a manner to assure that the overlap was shingled so that any water flowing down gradient would not undermine the adjoining geotextile panel. Steel targets were place at the transitions of the geotextile panels to aid in the position of the geotextile panels in the future. These targets act as a redundant means of locating the panels. A survey crew marked the location of the panels by painting surface striping at the location of the panel edges.

Figures 3-4 show the construction sequences, including the installation of the geotextile panels. The project was completed in November of 1997at a cost of $621,953 US.

FIELD MONITORING AND TESTING

It is planned to visit the site at least annually and perform visual checks, along with the performance of field tests to evaluate the performance of the five geotextiles. The first site visit following completion of construction occurred approximately one year following completion of the project.

In October of 1998, the authors, along with falling weight deflectometer (FWD) testing personnel of the NYSDOT - Geotechnical Engineering Bureau visited the site for the visual inspection as well as the field testing. Falling weight deflectometer tests were performed over the entire length of the project. These details will be presented in the following section. The site was again visited in August of 1999 by the FWD personnel to perform further FWD testing. No visual observations were recorded on this visit. The site was visited again in May of 2000 for a visual inspection along with the FWD testing. Figures 5-6 show photographs of the falling weight deflectometer testing. Figures 7-9 are photographs taken during the May 2000 site visit. As of May 2000 there was no noticeable visual change in the wearing surface of the project.

The long term evaluation of the performance of the geotextiles on this project will be done by utilizing the New York State Department of Transportation's Dynatest Falling Weight Deflectometer. This will be done on at least an annual basis, with every attempt being made to perform the testing more often, in order to develop a seasonal factor for performance.

As the FWD was not available immediately following completion of the construction sequence in 1997, the first testing was performed in October 1998. A second series of testing was performed in August 1999, and a third series in May 2000.

FWD testing is ideal for monitoring the performance of a roadway over time. The data can be used to investigate the in-situ structural properties of the roadway. Knowing the applied load, the deflection data can be entered into an algorithm to calculate modulus of various layers of the pavement system.

The testing for this project consisted of dropping the weight from a height such that a 4082 kgf was applied to the pavement. The weight was dropped 3 times from a 10 mm height at each drop location. The testing was performed every 3 m for the entire length of the project. Testing progressed from the north to the south end of the project. Results of the FWD testing performed to date appear in Figures 10 and 11.

Figure 3 - Preparation of Undercut Section

Figure 4 - Geotextile Being Placed

Figure 5 - Falling Weight Deflectometer and Tow Vehicle

Figure 6 - Falling Weight Deflectometer Test In Progress

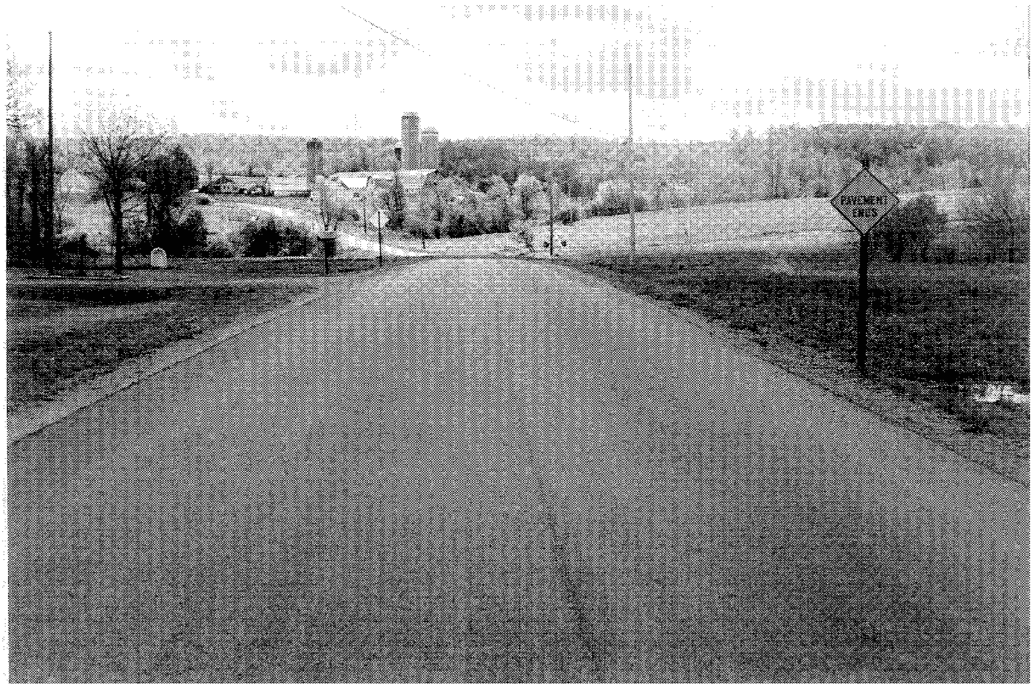

Figure 7 - May 2000 - Looking South Near Sta. 0+340

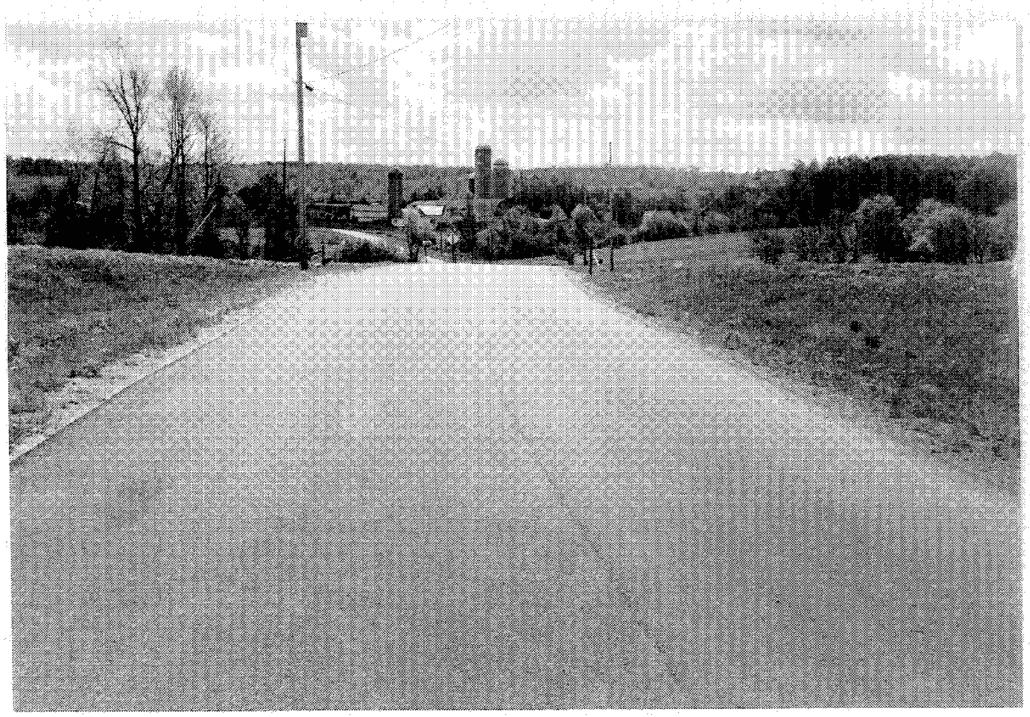

Figure 8 - May 2000 - Looking South Near Sta 0+250

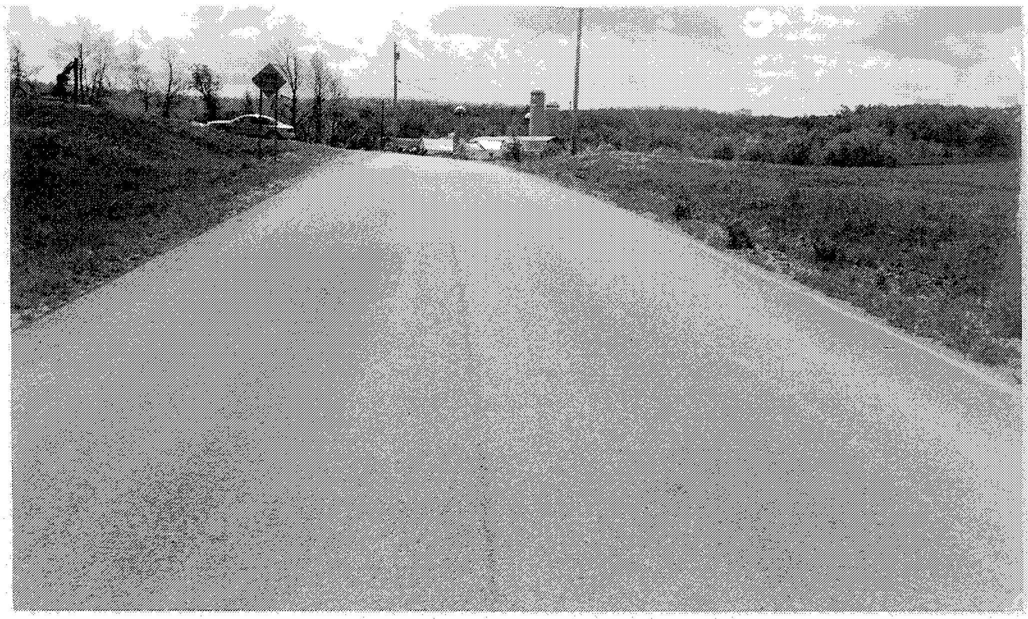

Figure 9 - May 2000 - Looking South Near Sta. 0+160

From a review of FWD literature the reader should be aware of the following:

1. Deflection monitored from geophones is inversely proportional to the subgrade modulus. Hence, the greater the measure of deflection, the lower the modulus. This applies to all geophones independent of their distance from the dropped weight. Subgrade modulus is calculated from the following formula:

$$E = \frac{(A)0.8775}{(\pi)(B)(C)} \qquad (1)$$

Where:

E = subgrade modulus (kPa)
A = Load (kN)
B = Deflection measured at geophone (m)
C = Distance from drop weight to geophone (m)

2. Factors affecting FWD results include temperature, moisture, and other environmental changes due to seasonal variations.

3. FWD experimental error with the same piece of calibrated equipment, and the same operator is of the order of 6,900 kPa (1000 psi). Variation of 34,500 kPa (5,000 psi)are deemed significant, particularly if they represent a doubling or greater of the original reading.

Discussion of FWD Test Results

There are four sets of data presented in Table 3 and shown graphically in Figure 10. Figure 11 is a plot of the average subgrade modulus versus time for each geotextile and the control section. The data spans three years since the test sections were constructed. When comparing the sections to one another, it appears that Geotextiles A, and C are showing relatively high subgrade modulus values, where Geotextiles B, D, and E, and the Control Section are showing relatively low subgrade modulus values. It would be convenient to say that these differences were due to modulus and strength differences in the geotextiles. However, it is more likely that these differences are due to variations in depth from grade to bedrock and initial in-situ subgrade conditions such as density and moisture content.

Table 3. Summary of Subgrade Resilient Modulus Values from Vorce Road

Section	10/1998 Mr Avg (kPa)	Cv*	8/1999 Mr Avg. (kPa)	Cv	5/2000 Mr Avg (kPa)	Cv	7/2000 Mr Avg (kPa)	Cv	% Drop 10/98 - 7/00
GT A	239006	79	192343	47	120713	49	124802	36	48
GT B	51669	33	71071	19	31867	29	38686	29	25
Control	70034	65	119072	55	46698	62	44409	55	37
GT C	93541	14	142390	11	56468	14	75580	10	19
GT D	64858	38	83936	43	38438	36	49593	39	24
GT E	26034	10	41134	9	19057	11	24821	10	5

*Cv = Coefficient of Variation

SUMMARY AND CONCLUSIONS

The paper has presented the to date results of an on-going case study of a geotextile separator full scale field test section. The site involved the re-construction of an actual rural roadway in the northern area of New York State. The test section has five different geotextile sections, plus a control section with no geotextile installed. The site has been in service since late 1997. Over the past four years we have had the opportunity to access the site for visual inspection as well as performing falling weight deflectometer testing. Visually the site shows no sign of distress since construction.

Upon comparing the results year after year of a given section itself, the following generalizations can be made about each section:

1 Geotextile A is showing the largest result scatter and as an overall we have seen a 48% decrease in subgrade resilient modulus values over the past three years.
2 Geotextile B is showing a 25% decrease in subgrade resilient modulus values over the past three years after an irregular set of initial readings in 1998
3. The Control Section is showing low subgrade resilient modulus values over the past three years and has exhibited a 37% decrease.
4. Geotextile C is showing a 19% decrease in subgrade resilient modulus values over the past three years.
5. Geotextile D has decreased 24% over the past three years.
6. Geotextile E has decreased 5% decrease over the past three years.

In all cases it appears that the subgrade resilient modulus of each of the respective sections is decreasing over time. This indicates that the subgrade is getting weaker over time as anticipated. In cases where there were upward trends in the data, it is felt that this could be explained by densification of the subgrade by trafficking, consolidation and/or moisture cycling.

It is the intention of the investigation plan to continue visual inspection and FWD testing o this site over the next 15 - 20 years to develop a true evaluation of geotextiles as separators. Results of this continuing investigation will be made available upon request.

ACKNOWLEDGMENTS

This project was jointly funded by a 1995 North American Geosynthetic Society Environmental Award of Excellence and the Geosynthetic Institute. The financial assistance of these two groups is sincerely appreciated. In addition the authors would like to thank Mr Ronald Duma of the NYSDOT for performing falling weight deflectometer testing and the geotextile manufacturers for donating the geotextiles used for this project.

Figure 10 - FWD Results - Vorce Rd.

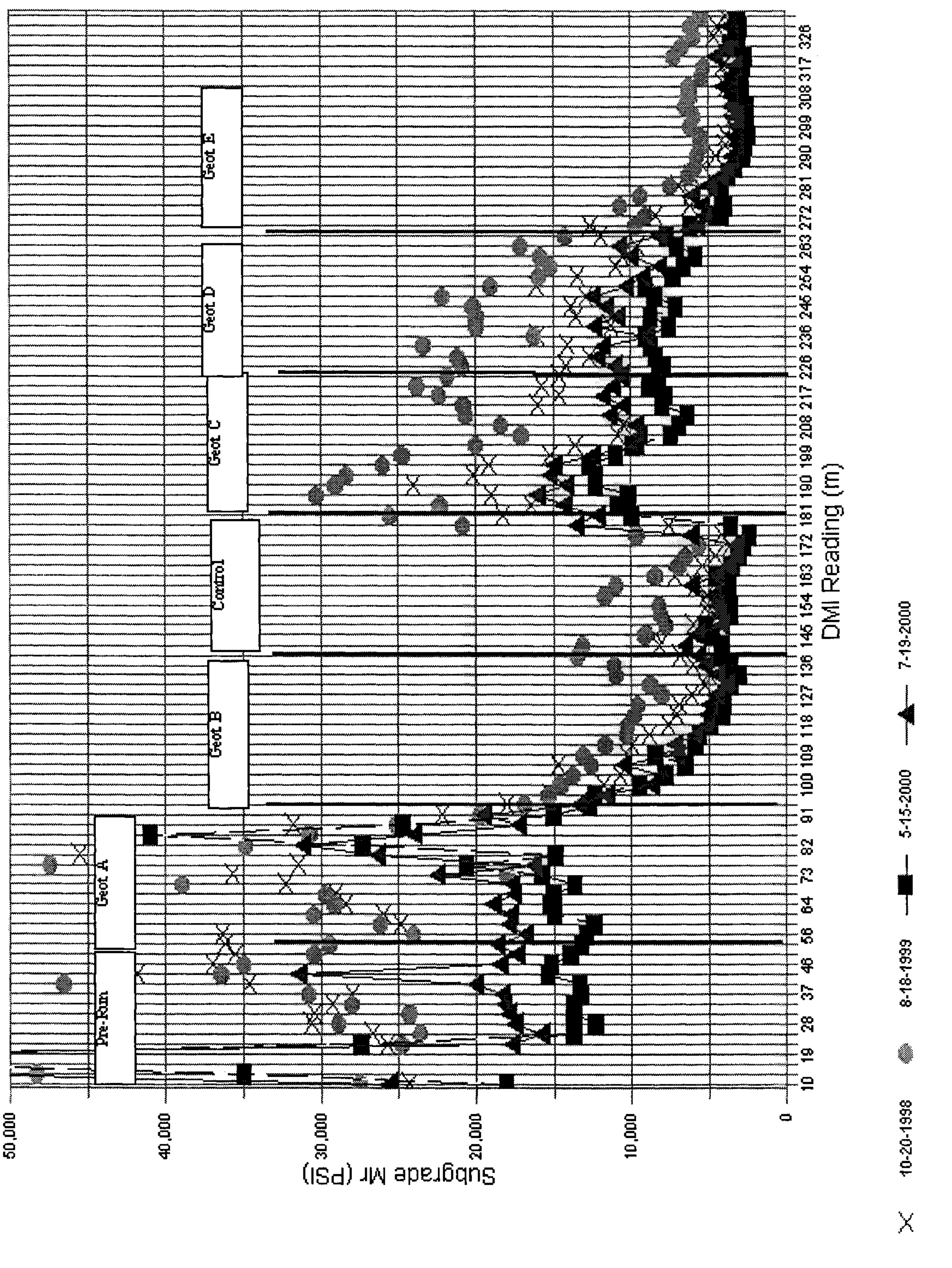

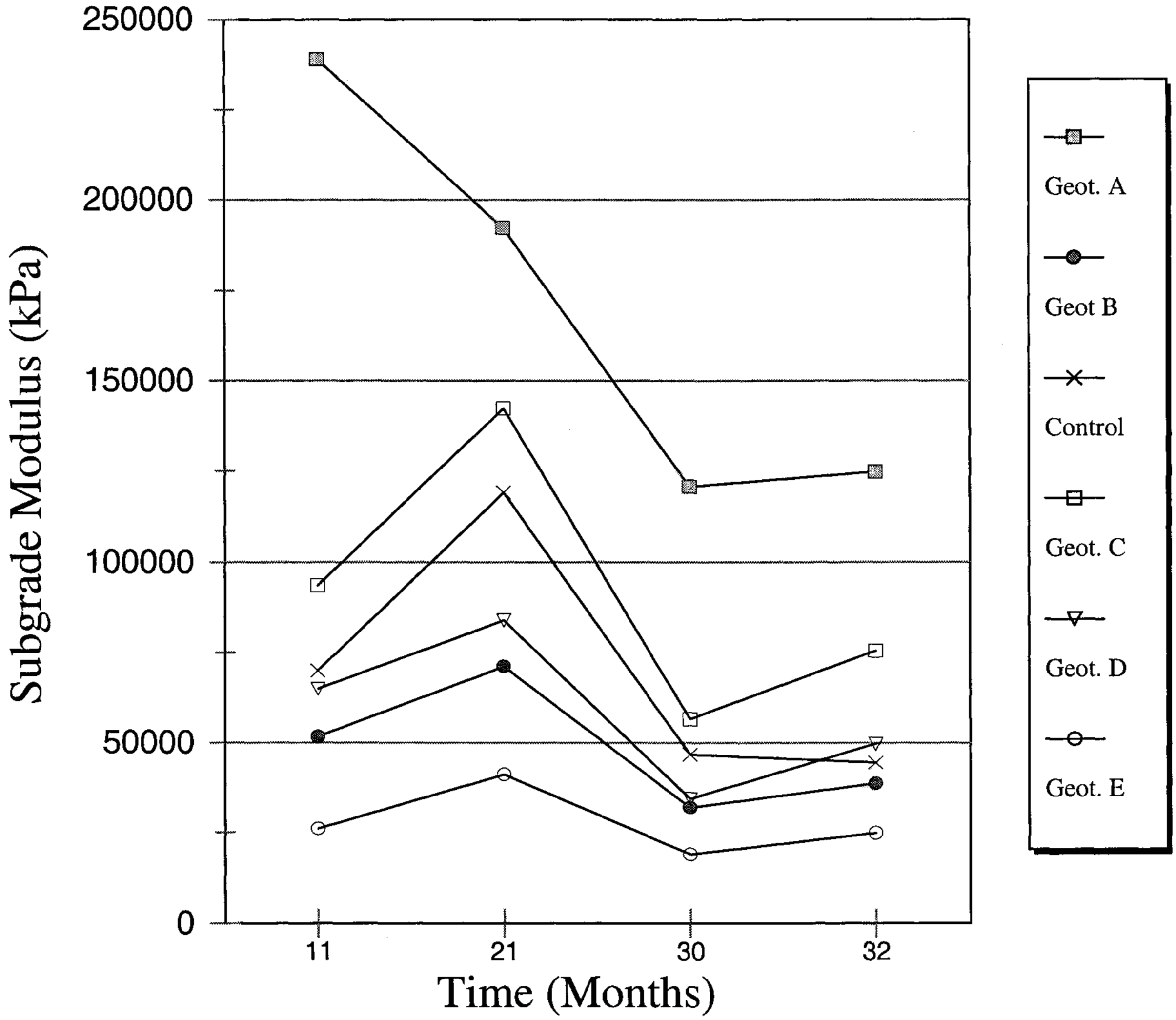

Figure11 - Average Subgrade Modulus from Table 3 - Vorce Rd.

REFERENCES

Barksdale, R. D., 1989, " Benefits of Geosynthetics in Flexible Pavement Systems," *NCHRP 315,* Transportation Research Board, Washington, DC, 55 pages

Cedegren, H.R., 1989, " *Seepage, Drainage and Flow Nets,* " Wiley and Sons, New York, New York

Koerner, R. M., Koerner, G. R, " Separation: Perhaps the Most Underestimated Geotextile Function," *Geotechnical Fabrics Report,* Vol. 12, No. 1, IFAI, St. Paul, MN, pp 4-10

Smith, T.E., Brandon, T.L., Al-Quadi, I.L., Lacina, B.A., Bhutta, S.A., and Hoffman, S.E., 1995, " Laboratory Behavior of Geogrid and Geotextile Reinforced Flexible Pavements," *Final Report to ACF Inc.,* Blacksburg, VA, 94 pages

Sprague, C.J., Cicoff, G.A., 1993, " A Study of the Cost Effectiveness of Using Separation Geotextiles as Separators in a Full Scale Road Test," *Proceedings of the Geosynthetics 1993 Conference,* Vancouver, BC, Canada, pp 49-63

MEASURING CONFINEMENT – THE PRINCIPLE COMPONENT OF BASE REINFORCEMENT

C. Joel Sprague, TRI/Environmental, Inc., USA
Claudia Kern, Texas Department of Transportation, USA

ABSTRACT

Traditional index properties for geogrids, such as aperture size or junction strength, have not been shown to relate to performance, so there is little argument to include them in specifications. Performance-based properties have been the subject of much research, but this large-scale testing is normally impractical for specific projects. One property - confinement of the base aggregate - is generally recognized to be of primary importance in achieving base reinforcement. Yet, no standard test has been available to measure this property.

This paper presents an overview of subgrade stabilization and base reinforcement issues and design approaches along with the details and results of a test program designed to quantify the ability of various geosynthetics to confine aggregate under load. The test is a modification of an existing ASTM standard test for out-of-plane loading. The test program used a typical base course material and a range of geosynthetics. The measured level of confinement was then correlated to more easily measured and specified index properties. Junction stiffness and pullout force were shown to correlate well. While, admittedly, the confinement test is NOT a performance test, as a measurement of the primary component of base reinforcement, it is likely to be a reasonable indicator of performance and may provide a bridge of understanding between pure index properties and the geosynthetic-aggregate system being modeled in large-scale tests.

INTRODUCTION

Efforts to develop specifications for the application of geosynthetics in various road applications have long relied on index properties which, to-date, have not been shown to consistently relate to performance. Yet, design approaches for subgrade separation, stabilization, and base reinforcement using geosynthetics generally rely on theoretical performance properties to account for the necessary interaction between the soil/aggregate and the geosynthetic. In base reinforcement, there is a special emphasis on the importance of aggregate confinement, yet the measurement of this unique property has proven elusive.

This paper provides background information on the current approach to integrating geosynthetics into road applications and then details a new effort, based on existing ASTM standard tests, to quantify relevant properties that may be more useful in the design and specification of geosynthetics in base reinforcement applications.

SUBGRADE SEPARATION, STABILIZATION, AND BASE REINFORCEMENT

Introduction to the Problem and Typical Solutions

Subgrade stabilization and/or base reinforcement geosynthetics and corresponding design theories apply when live loads (i.e. wheel loads) govern the design. This is commonly the case on unpaved low volume roads and paved roads and parking lots.

Temporary roads used for hauling and low volume access roads are often constructed without a paved surface. A layer of aggregate is placed on a graded subgrade to create a "gravel" or "dirt" road that is initially sufficient for temporary or low-volume traffic. Permanent roads carry larger traffic volumes and typically have a paved surface over a base layer of aggregate. The combined surface and base layers act together to support and distribute traffic loading to the subgrade. Problems are usually encountered when the subgrade consists of soft clays, silts and organic soils because these soils soften when they become wet. When wet, these subgrades become unable to adequately support traffic loads causing the gravel surface to deform and be pushed into the soft subgrade. If unimproved, the condition of the subgrade will worsen over time as a result of aggregate and subgrade mixing and increasing subgrade moisture content.

Commonly, excavation and replacement of unsuitable materials is used in road building, but it is a costly and time consuming subgrade stabilization process. Other less common, but still costly, methods of subgrade improvement include adding lime, cement, or stone.

The Geosynthetic Solution for Unpaved Roads – Separation and Stabilization

Geosynthetics are proving to be a cost effective alternative to traditional road construction methods when dealing with soft soil subgrades. As a result, the application of geosynthetics to the construction of roads over soft subsoils has become quite popular.

Design of unpaved roads has focused on the reinforcement of the aggregate and has led to the identification of two important functions: lateral restraint and membrane action. Lateral restraint is the lateral interaction between the aggregate and the geosynthetic. The presence of the geosynthetic creates pressure in the aggregate that improves the strength and stiffness of the road structure. Membrane action is the ability of a geosynthetic material to reduce and spread stress arising from the weak subgrade. Additionally, when a geogrid is involved, a third function has been proposed: enhanced load distribution within the aggregate.

Separation

At small rut depths, the strain in the geosynthetic is also small. At these low strain levels, the membrane action benefit of the geosynthetic will not be achieved. Consequently, the strength and stiffness properties of the geosynthetic are not important. Without the membrane action, the aggregate savings or benefit of the geosynthetic is essentially independent of the geosynthetic's modulus. In this case, the geosynthetic only acts as a separation between the soft subgrade and the aggregate. Any geosynthetic that survives construction will work as a separator.

Stabilization

For larger rut depths, more strain is induced in the geosynthetic. Thus the stiffness properties of the geosynthetic are essential. A considerable reduction in aggregate thickness is possible by the use of a geosynthetic that has a high modulus in the direction perpendicular to the road centerline; however, the benefits of the geosynthetic are not wholly dependent on the membrane action achieved with a stiff geosynthetic. Lateral restraint produced by the interaction between the geosynthetic and the aggregate is also important.

Practical Stabilization Design Methods

There are several available methods for designing geosynthetic-reinforced unpaved roadways. One commonly used approach was developed for geotextiles by Giroud and Noiray (1981) and expanded by Giroud, Ah-Line, and Bonaparte (1984) to include geogrids. These methods combine theoretical analysis with an empirical formula deduced from full-scale tests on aggregate roads as a function of soil properties and traffic. The methods consider subgrade strength and geogrid modulus and, for geogrids, load distribution capability in determining the required thickness of an aggregate layer. Both on- and off-highway vehicles can be considered. The assumptions in the model are the same as those used for stress distribution and bearing capacity calculations in foundation engineering. These methods provide a simple way of calculating aggregate savings when using a geosynthetic in unpaved road structures.

The Giroud, et al (1994) design model shows that the base layer thickness is not proportional to the tensile stiffness of the geosynthetic because, for an unpaved structure, base layer material / geosynthetic interaction is at least as important as geosynthetic tensile stiffness. In general, the following improvements can be expected by including an appropriate geosynthetic within the road structure.

- Separation only - load distribution improvement ratio in the range of 1.1 to 1.4.
- Reinforcement only - load distribution improvement ratio in the range of 1.7 to 2.2.
- Separation + Reinforcement - load distribution improvement ratio in the range of 2.0 to 2.5.

The Geosynthetic Solution for Paved Roads – Base Reinforcement

As was noted earlier, geosynthetics are proving to be a cost effective alternative to traditional road construction methods. In paved roads, lateral restraint also called confinement is considered to be the primary function of the geosynthetic. With the addition of an appropriate geosynthetic, the Soil-Geosynthetic-Aggregate (SGA) system gains stiffness. The stiffened SGA system is better able to provide the following structural benefits:

- Preventing lateral spreading of the base
- Increasing confinement and thus elastic modulus of the base
- Improving vertical stress distribution on the subgrade
- Reducing shear stress in the subgrade

Base Reinforcement Design

The Geosynthetics Materials Association (GMA) has commissioned an in-depth review of base reinforcement performance testing and associated design methodologies. A number of large-scale performance tests have determined the Traffic Benefit Ratio (TBR) associated with using geosynthetic base reinforcement. The TBR is a "measure" of base course reinforcement performance. The TBR relates the ratio of reinforced load cycles to failure (excessive rutting) to the number of cycles that cause failure of an unreinforced road section. In general, geogrids were found to provide a TBR in the range of 1.5 to 70 while geotextiles were in the range of 1.5 to 10. Still, large-scale performance testing to-date reflects a wide range of testing protocols and has produced no concurrence on a generally accepted associated design methodology.

Therefore, base reinforcement design is currently based on theory. For the purposes of theoretical design, if lateral restraint is taken into account as the primary function of the geosynthetic occurring simultaneously with membrane action, a much stiffer behavior of the Soil-Geosynthetic-Aggregate (SGA) system can be expected, allowing design of geosynthetics in paved roads. Incorporating this lateral restraint, or confinement, Sellmeijer (1990) provides a rational model for the SGA system, taking account of equilibrium and constitutive properties of the components. The aggregate behavior is modeled by elasto-plastic shear theory, the geosynthetic by membrane action and lateral restraint, and the subsoil by its bearing capacity. Due to the elasto-plastic behavior of the aggregate associated with higher traffic volumes, the concept of mobilized friction plays an important role. The model can be anything from a low volume road to a wide parking area.

Separation And Survivability

Both subgrade stabilization and base reinforcement using geosynthetics is affected over time by any changes taking place in the aggregate. The aggregate will lose strength if it is contaminated with fine soil particles from the subgrade. This being the case, the properties of the aggregate used in design should reflect the long-term condition – which may be a substantially reduced shear modulus, interaction coefficient and/or load distribution angle if a separation geotextile is not used.

Geosynthetics can be damaged if not properly handled and installed. Typically, specifications include empirically derived properties, such as a minimum unit weight, to insure that the geosynthetic is substantial enough to resist installation damage. Alternatively, when the tensile strength is critical, a reduction factor can be determined from installation damage testing.

THE SEARCH FOR A PERFORMANCE BASIS FOR SPECIFICATIONS: TxDOT PROJECT – BASE REINFORCEMENT GEOGRIDS

In January of 1999, TRI/Environmental (TRI) was retained by TxDOT to provide consulting and testing associated with establishing performance-based criteria and recommendations for road base reinforcement specifications using geogrids. TRI undertook the following 3-phase process:

Phase 1: Research and select a "reasonable" performance-based design approach upon which to base the selection of specification properties.
Phase 2: Develop "straw" specifications which present the selected performance-based properties and associated test methods. Additionally, develop new testing methodologies where existing tests are insufficient.
Phase 3: Test a selection of geogrid products to determine the applicability of the proposed specifications to currently available materials and propose final specifications based on the results of testing.

The resulting recommended specifications are to facilitate the selection of any appropriate geogrid product for base reinforcement based on a performance criteria established by the design engineer.

The work for TxDOT was performed simultaneously with, but not as a part of, an industry effort funded by the Geosynthetic Materials Association to develop a guide specification. The resulting "White Paper II" (WPII) was submitted to AASHTO on January 9, 2000, <u>without</u> proposed specifications. The review of large-scale performance tests to-date identified the determination of a Traffic Benefit Ratio (TBR), a Base Course Reduction percentage (BCR) or a Layer Coefficient Ratio (LCR) as the "measure" of base course reinforcement performance. Yet, only general conclusions could be drawn from the testing to-date because there was little uniformity between tests. In general, geogrids were found to provide a TBR in the range of 1.5 to 70 while geotextiles provided TBRs in the range of 1.5 to 10.

Industry efforts to present guideline base reinforcement specifications have stumbled when confronted with the need to include geosynthetic "index" properties that are acceptable to all parties. Traditional index properties for geogrids, such as aperture size or junction strength, have not been shown to relate to performance, so there is little argument to include them. Performance-based properties have been the subject of much research, but this large-scale testing is normally impractical for specific projects. Therefore, no generally accepted properties, let alone property values – index or performance – are available to the specifying community.

Still, WPII does give important guidance as to what components *are likely* to be important in base reinforcement, including the preventing lateral spreading of the base; increasing confinement and thus elastic modulus of the base; improving vertical stress distribution on the subgrade; and reducing shear stress in the subgrade

Further, WPII describes the importance of the "shear interaction" between the "relatively stiff" geosynthetic and the aggregate in achieving the necessary components of reinforcement.

Recognizing the difficulties inherent in standardizing and specifying purely performance tests, TRI's effort on behalf of TxDOT has focused on trying to quantify these "shear interaction" and "relatively stiff" characteristics of base reinforcement geosynthetics through the measurement of the confinement using a geosynthetic-aggregate system test. The test is a modification of an existing ASTM standard test for out-of-plane loading. The test program used a typical base course material and a range of geosynthetics. The measured level of confinement was then correlated to more easily measured and specified index properties. While, admittedly, the confinement test is NOT a performance test, as a measurement of the primary component of base reinforcement, it is likely to be a reasonable indicator of performance and may provide a bridge of understanding between pure index properties and the geosynthetic-aggregate system being modeled in large-scale tests.

PHASE 1 RESULTS – IDENTIFICATION OF PERFORMANCE-BASED PROPERTIES

An in-depth review of available base reinforcement design methodologies was performed. Most methodologies were found to be product-specific or based on large-scale testing of a very limited number of geogrids. These methodologies were dismissed, because they did not provide a basis for identifying specific properties of the geogrid which relate to measured performance. One generic methodology, known as the Sellmeijer (1990) method, was identified which presented the reinforced base system in terms of a series of free-body diagrams and associated equations relating the various components of the system under load. Though not independently validated by large-scale testing, the methodology proved to provide reasonable results when subjected to a sensitivity analysis and compared to the Giroud-Noiray design methodology for unpaved roads and the Asphalt Institute design technique for unreinforced paved roads.

Sellmeijer's method for geosynthetic-reinforced road base design clearly identifies the following properties as directly related to the performance of a reinforced road base:

- Geosynthetic Strength/Stiffness
- Geosynthetic/Aggregate Interaction

Along with these properties, certain typical relationships were identified, as follows:

- Paved road base reinforcement is primarily based on lateral confinement of the aggregate base by frictional interaction with the geosynthetic.
- Vertical displacement must be minimized, and is controlled by the aggregate.

PHASE 2 RESULTS – "STRAW" SPECIFICATIONS

The properties and relationships identified in Phase 1 formed the basis for "straw" specifications. So-called "straw" specifications provide a general specification outline, including appropriate properties and typical values. It is expected that actual spec values should be project-specific. The body of the proposed specifications was patterned after similar draft specifications which had been developed by the Geosynthetic Materials Association (GMA) and submitted to AASHTO for consideration. This assured consistency with geosynthetic industry manufacturing and certification standards. Material property requirements were not adopted from the GMA draft specifications because there was no evidence that they were performance based, as required by TxDOT. The "straw" specifications with performance-based properties, but no specific values, were submitted to TxDOT for concurrence prior to beginning product testing. Product testing would be used to establish "reasonable", generic property values.

Phase 1 had identified the importance of geosynthetic tensile strength, stiffness and interaction to the enhancement of road base performance. While these properties have been measured for years in situations where the load is applied in the plane of the reinforcement, no test methods have been developed to measure these properties when the load is applied perpendicular to the plane of the reinforcement as is the case in base reinforcement. Resistance to this out-of-plane loading has been referred to as "confinement", but has to-date not been quantified through laboratory testing. As part of Phase 2, TRI developed a "multiaxial" confinement test based on an existing ASTM standard to provide results for a reinforced aggregate system. While the modeled system does not include a paved surface or cyclic loading

– and therefore does not replicate base reinforcement – it does provide a way to accurately and reproducibly measure "confinement" associated with a specific reinforced aggregate system subject to out-of-plane loading. Additionally, the ability to run numerous confinement tests along with extensive strength and interaction tests on a range of products can facilitate the correlation of geogrid index properties to a geogrid's ability to confine aggregate.

PHASE 3 RESULTS – PRODUCT TESTING AND CORRELATIONS

Materials and Tests

The final, and key, phase of the project involved the testing of a wide range of geosynthetic products. The testing included standard tests commonly included in base reinforcement specifications as well as the newly developed "confinement" test, in order to identify those properties which correlate well with a geosynthetic's ability to provide confinement of an aggregate. Testing was done with a single base aggregate type, thickness, compaction effort, and confinement stress. Multiple replicates were performed of each test to identify and account for variability in the testing. Results from the various tests were related to each other on the basis of the out-of-plane displacement (in.) / in-plane elongation (in.) / in-plane strain (%) relationship identified in test method ASTM D 5617 as shown in Table 1.

Table 1. Equivalence of Deflections, Elongations and Strains (for 24-in. diameter specimen)

Δ = centerpoint deflection, in.	ε = elongation, in	ξ = strain, %
0.25	0.007	0.03
0.5	0.028	0.12
1.0	0.111	0.46
1.5	0.249	1.03
2.0	0.442	1.84

The following materials and tests were used:

Aggregate – Coarse Base Aggregate (referred to as TxDOT #1 and having a $D50 \approx 15$mm)

Geogrids - 5 geogrid types, including: Punched, drawn PP; Knitted, coated PET; Knitted, coated PP; Woven, coated PET; Extruded, drawn PP (Note: products are given a random letter designation in Figure 1 to avoid premature product comparisons.)

Index / Performance Tests - Interface friction tests (ASTM D 5321)
Multiaxial confinement tests (ASTM D 5617- modified)

Index Tests - Rib spacing, width, and thickness
Junction strength – strain characteristics (GRI GG2-modified)
Wide width tensile strength – strain characteristics (ASTM D 4595)
Initial wide width tensile strength – strain characteristics (No Preload)
Flexural Rigidity; Aperture Size; Percent Open Area

Calculations - Junction secant and offset stiffnesses
Wide width tensile secant and offset stiffnesses
Initial wide width tensile secant and offset stiffnesses
Pullout resistance (based on Demo 82 methodology)

Additional Material – TRI also included a woven PP geotextile in the above testing in order to provide some, though admittedly limited, reference to the larger field of "geosynthetic" reinforcements.

Test Method Details

Confinement - The confinement test is a modification of ASTM D 5617 which incorporates a four (±) inch layer of aggregate overlain by the candidate geosynthetic, both sandwiched between flexible membranes and subject to a vacuum to simulate confining pressure. Neither the aggregate nor the geosynthetic is anchored around the edges, though the flexible membranes are. The layered system is then subjected to an out-of-plane loading via a smooth pressure ramp (not cyclic impact like traffic). The centerpoint deflection of the sandwich is monitored during pressurization, producing a multiaxial pressure – vertical deflection record. Confinement occurs when the multiaxial pressure is greater at a given vertical deflection than for an unreinforced (control) layered system at the same deflection.

Reinforcement Strength/Stiffness – The tensile strength that appears to relate to confinement occurs at a very small amount of movement – generally less than 6.35 mm (0.25 in). This movement can be masked by the application of a preload or, in the case of grids, be accounted for in the deflection of transverse members as they transfer load to the junctions. Therefor, junction strength at the specific level of expected movement is relevant to confinement. This requires determination of the strength-elongation behavior associated with the junction, not just the highest, or ultimate, strength.

Reinforcement stiffness also relates to the interaction between the aggregate and the geosynthetic as measured by interface testing. A reinforcement material will distribute a shear load more or less uniformly over its surface depending on its stiffness. Elias and Christopher (1996) reported that the structural factor, α, that describes this load distribution varies from 1.0 for very stiff (i.e. steel) reinforcements to 0.6 for those that are significantly less stiff (i.e. nonwoven geotextiles). "Full" wide width strength-elongation curves (no preload applied) provide guidance in assigning an appropriate α for the reinforcement in question when interpreting the interaction performance. A visual examination of the curves below the 1% strain level was used to estimate α for each product based on the lag of each curve.

Aggregate/Geosynthetic Interaction – The interaction occurring as a result of out of plane loading is not strictly interface friction, or sliding over the geosynthetic, but its not strictly pullout, or extracting the geosynthetic, either. It appears to be more like a series of micro-pullouts happening simultaneously along the geosynthetic/aggregate plane. In order to address this unique behavior, an attempt was made to "derive" pullout behavior from direct shear results in accordance with the FHWA's Demo 82 guidance document. The calculation uses rib geometries and the structural factor, α, described above to account for the additional interaction resulting from aggregate bearing on transverse ribs. The measurements of longitudinal and transverse rib spacing, rib width, and rib thickness is necessary for calculating pullout.

$$\text{Confinement Factor} = \text{Pressure}_{\text{Reinforced @ }\Delta} \,/\, \text{Pressure}_{\text{Unreinforced @ }\Delta} \qquad \text{Eq. 1}$$

$$\frac{\text{Avg Junction Strength}_{@\,\varepsilon}}{\text{Area per Junction}}\,(\text{psf}) = \frac{(\text{MD J-Strength}_{@\,\varepsilon} + \text{XD J-Strength}_{@\,\varepsilon})}{2\,(s_t \times s_l)} \qquad \text{Eq. 2}$$

$$\text{Pullout Force per Area}_{@\,\varepsilon}\,(\text{psf}) = \frac{(\text{MD Pullout}_{@\,\varepsilon} + \text{XD Pullout}_{@\,\varepsilon})}{L_e} \qquad \text{Eq. 3}$$

$$\text{Pullout, } P = C\,\sigma'_v\,L_e\,\alpha\,(\tan\delta + (\sigma'_b/\sigma'_v)((1 - r/s_l)t/2s_t)) \qquad \text{Eq. 4}$$

Where:

MD = machine direction	r = rib width
XD = cross-machine direction	t = rib thickness
Δ = centerpoint deflection, in.	s_l = longitudinal rib spacing
ε = strain, in	s_t = transverse rib spacing
ξ = strain, %	L_e = embedment length

C = effective unit perimeter - 2 for geogrids and geotextiles;
σ'_v = effective vertical stress
α = scale effect correction factor (0.6 for very extensible to 1.0 for inextensible)
$\tan\delta$ = tangent of the interface friction angle
σ'_b/σ'_v = ratio of bearing to vertical stress (from Ref. 1)

Preliminary Recommendations / Suggestions

All index results were compared to the multiaxial confinement results using least squares regression. Those comparisons producing promising correlations (generally $R^2 > 0.80$) are included herein. The following points summarize the findings of the comparative testing:

1. There is no meaningful correlation between geogrid confinement as measured via multiaxial testing and aperture size, flexural rigidity, percent open area, ultimate junction strength, ultimate wide width tensile strength/stiffness, and interface friction.

2. Conversely, there appears to be significant and meaningful correlation between geosynthetic confinement as measured via multiaxial testing and junction stiffness and pullout force.

3. All geogrids enhanced the stiffness of the aggregate, though to different degrees, as measured via the multiaxial test. The geotextile did not. (Reference Figure 1, Product F)

4. Initial junction stiffness appears to be relevant to confinement at very low strain levels as shown in Figure 2.

5. Aggregate confinement involves a pullout interaction with the geogrid which can be calculated from direct shear, initial stiffness, and aperture and rib data as shown in Figure 3.

6. The inability to accurately measure interaction properties at very low levels of strain/displacement makes the identification of meaningful property correlations at these levels impossible.

7. The results of this program reflect testing using only one aggregate type (called TxDOT #1), one thickness (4 in.), one level of compaction (hand packing), and one confining pressure (1600 psf). The conclusions presented herein, therefore, should be considered as indicative of the geosynthetic/aggregate combinations tested herein, but not necessarily characteristic of all aggregates/confinement conditions.

Table 2 summarizes the preliminary recommendations resulting from this program.

Table 2. Preliminary Recommendations for Property Specifications

Reinforcement Characteristic	Property Measurement	Test Method	Value
Confinement	Confinement Factor @ 12.7 mm (0.5 in.) Centerpoint Deflection	ASTM D 5617 - modified	1.25
Reinforcement Stiffness	Avg Junction Strength @ 0.76 mm (0.03 in.) Elong. / Area per Junction	GRI GG2 - modified	14.4 kPa (300 psf)
Aggregate/Geosyn-thetic Interaction	Pullout Force per Area @ 2.54 mm (0.1 in.) Elongation	ASTM D 5321 + Calcs	1.4 kPa (30 psf) @ σ = 4.8 kPa (100 psf)

The preliminary recommendations include only "suggested" specification values because of the limited range of aggregate materials and conditions tested. A follow-up testing program that examines a range of aggregate conditions along with a survey and correlation with full-scale performance results would facilitate the recommendation of specification values.

As noted in the report, the Phase 3 testing provided a substantial amount of insight into the question of confinement – the primary component of base reinforcement. Much was learned about those material properties which are and aren't relevant to confinement. The results provide strong evidence that, through confinement testing and associated junction and pullout characterization, it is possible to specify generic material properties that relate directly to performance. Still, the assignment of specific values to a material specification is a sensitive issue that must be supported by thorough documentation. The results to-date, though substantial, still leave unanswered questions, such as:

- Does the level of compaction effect the level of confinement or interface friction?
- Would greater compaction reduce the importance of junction strength?
- Does the aggregate thickness or confining pressure have any affect on the results?
- Does a thin 100 mm (4 in) layer overestimate the likely benefits of a reinforcement?
- Much has been suggested about torsional rigidity. Is this an indicator of performance?
- Are sandy materials easier or harder to confine than aggregates?
- Do some geogrids confine sand better than aggregate and vice-versa?
- How reproducible are confinement results?

TRI has begun additional testing on a broader range of aggregates, confining pressures, and aggregate thicknesses in an effort to begin answering these questions. Also, TRI is performing torsional rigidity testing on the geosynthetics to investigate any possible correlation to this proposed index property. Firm recommendations will not be made until the results of this additional testing verify the preliminary recommendations.

CONCLUSIONS

This paper provides an introduction to subgrade separation, stabilization, and base reinforcement and the associated relevancy of confinement provided by geosynthetics. A testing program is described which attempts to quantify confinement and correlate confinement to index properties of geosynthetics. Graphs are presented which demonstrate the most relevant relationships between confinement and other geosynthetic index properties. There appears to be significant and meaningful correlation between geosynthetic confinement as measured via multiaxial testing and junction stiffness and pullout force.

The results of this effort to quantify and correlate relevant base reinforcement material properties are very encouraging, and, we think, an important contribution to road construction technology. Further testing is underway in an effort to refine the understanding of the benefits of using geosynthetic reinforcement in road base construction.

REFERENCES

Elias, V. and Christopher, B.R. (1996), "Mechanically Stabilized Earth Walls and Reinforced Slopes, Design & Construction Guidelines," FHWA-SA-96-071, p. 320.

Giroud, J.P., Ah-Line, C., and Bonaparte, R. (1984), "Design of Unpaved Roads and Trafficked Areas with Geogrids", Proceedings of the Symposium on Polymer Grid Reinforcement in Civil Engineering, London: ICE, pp. 116-127.

Giroud, J.P. and Noiray, L. (1981), "Design of Geotextile Reinforced Unpaved Roads," Journal of Geotechnical Engineering Division, ASCE, Vol. 107, No. GT9, pp. 1233-1254.

Sellmeijer, J.B. (1990), "Design of Geotextile Reinforced Paved Roads and Parking Areas", Proceedings of the 4th International Conference of Geotextiles, Geomembranes, and Related Products, The Hague, Balkema, pp. 177-182.

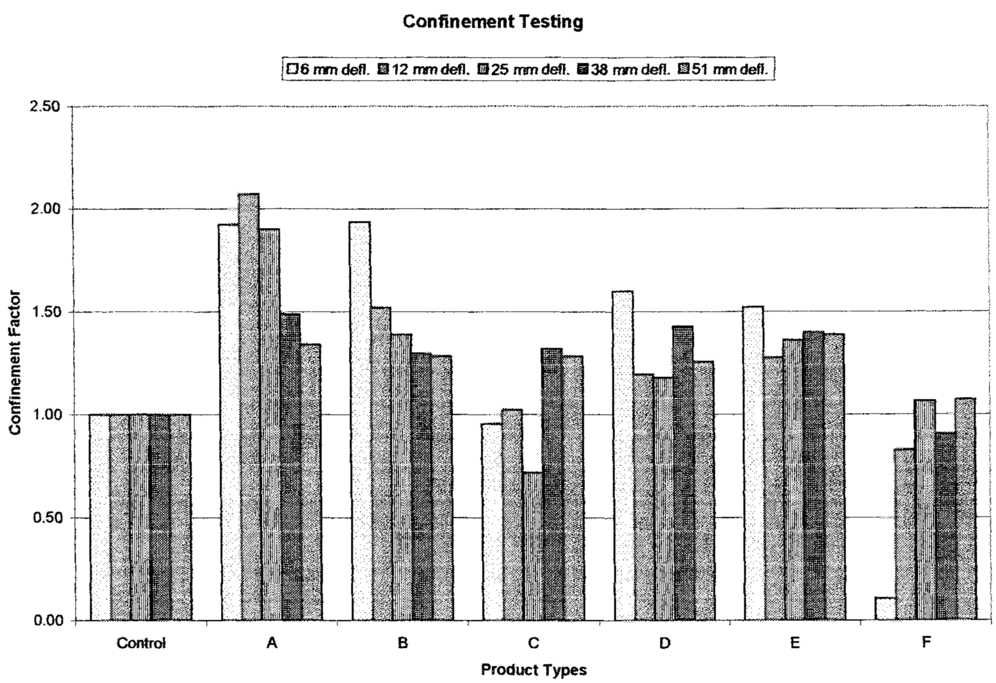

Figure 1. Confinement Testing Results vs. Product Type

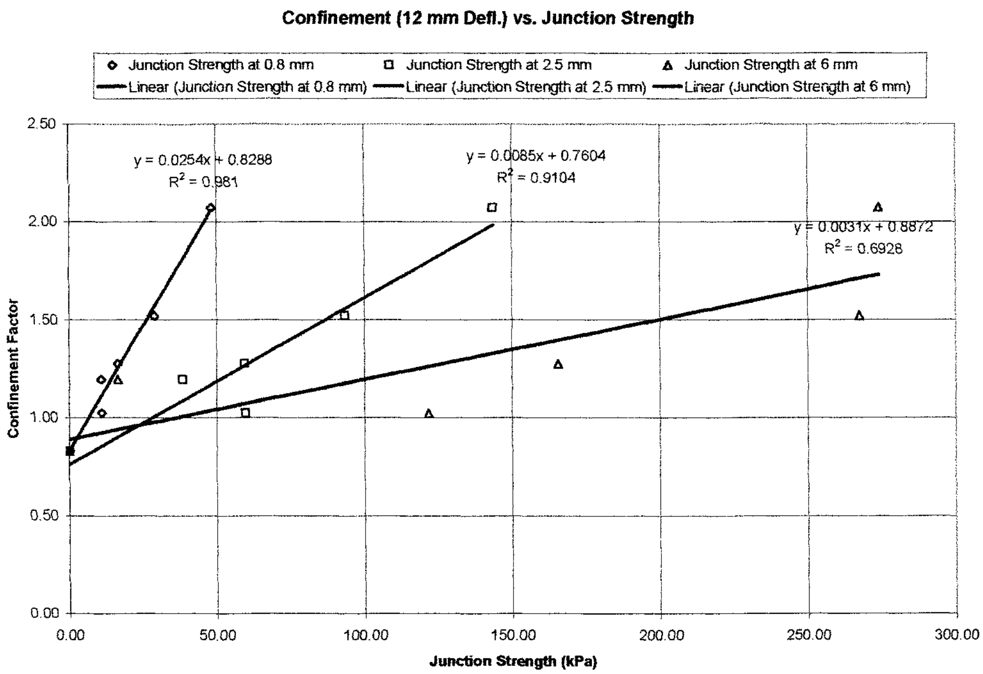

Figure 2. Correlation Between Confinement and Junction Strength at Various Strain Levels

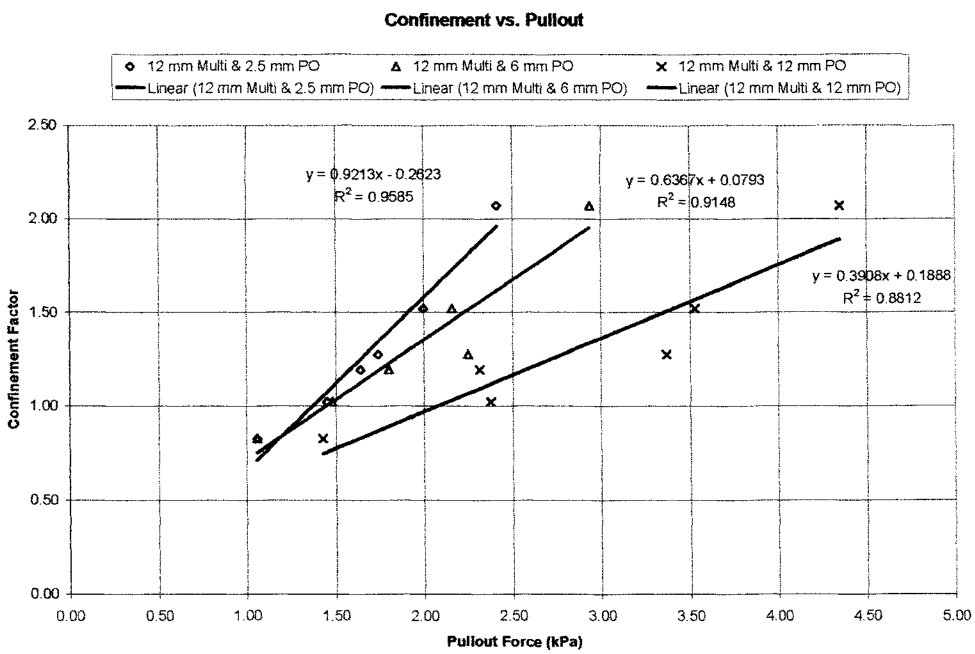

Figure 3. Correlation Between Confinement and Pullout Resistance at Various Strain Levels

WALLS, SLOPES & EMBANKMENTS I

EARTH RETAINING WALL COSTS IN THE USA

ROBERT M. KOERNER, GEOSYNTHETIC RESEARCH INSTITUTE, DREXEL UNIVERSITY
JAMIE KOERNER, GEOSYNTHETIC INSTITUTE
TE-YANG SOONG, EARTH TECH CONSULTANTS, INC.
UNITED STATES OF AMERICA

ABSTRACT

This paper presents the results of a survey of state transportation engineers in the USA as to the installed (bid) costs of different types of earth retaining walls in different height categories. As such, the reported costs (in units of dollars per square meter of wall face) include footings, facing, backfill, drainage, reinforcement (if any), finishing details and contractors/manufacturers mark-up. Furthermore, these 1998 costs are counterpointed to three earlier retaining wall cost studies conducted by others in 1973, 1981 and 1988.

The resulting mean values of wall costs show a significant increase in all types of earth retaining walls over a 10-year period (from 33% to 71%) and over a 25-year period (from 21% to 387%). The relative positioning of the different types of walls have, however, remained the same over the 25-year period. In order of decreasing cost per unit of wall face area they are as follows:

- R/C Gravity walls (the highest cost)
- Crib/Bin walls (somewhat lower cost)
- MSE (metal) walls (still lower cost)
- MSE (geosynthetic) walls (the lowest cost)

For all four wall categories, the higher the wall, the higher the cost on the basis of wall face area in an approximately linear manner.

Of importance in using the generated cost data generated herein is the scatter in the resulting costs. Scatter in wall cost data varied from four-times (for gravity walls), to two-times (for MSE geosynthetic walls). Other wall categories were intermediate in their respective costs. Earlier retaining wall cost studies only presented mean values. Thus, the mean values were the main comparative terms in this study.

The data was further analyzed in the basis of FHwA Region where each region was compared to the national mean value of all DOTs. Significant geographic differences were apparent. Finally, a comparison was made to wall costs of privately owned facilities (versus the majority of the report which is based on publicly owned facilities). It is seen that privately financed walls are significantly less expensive than publicly financed walls.

INTRODUCTION

This paper presents the results of a survey sent to the 50-state Departments of Transportation (DOT) in the United States as to the installed costs of earth retaining walls. It is also available in report form; Koerner, et al. (1998). The walls are in four classification categories:

- Gravity walls, e.g., reinforced concrete (R/C) cantilever types
- Crib/Bin walls, both metal and concrete types
- Mechanically Stabilized Earth (MSE) - metal reinforcement using steel strips and mesh
- Mechanically Stabilized Earth (MSE) - geosynthetic reinforcement using polymeric geogrids and geotextiles

Each wall category (with appropriate subdivisions) is arbitrarily placed in three height categories:

- High walls; greater than 9.0 m
- Medium walls; from 4.5 to 9.0 m
- Low walls; less than 4.5 m

The data resulting from the survey and subsequently analyzed is presented on the basis of dollars per square meter (dollars/m^2) of wall face. The value includes footings, facing, reinforcement (if applicable), drainage soil and/or pipe, backfilling, ancillary details and contractor/ manufacturers mark-up. Thus, the costs reported and analyzed are complete wall costs for all aspects of the respective wall types based on state DOT bid-prices.

A relatively small subsidiary survey was conducted as to private sector bid costs of MSE walls using geosynthetic reinforcement. It included both commercial and residential walls. This data will be counterpointed against the comparable data for publicly financed walls.

BACKGROUND OF PAST SURVEYS

Retaining wall cost surveys of the type to be described herein have undoubtedly been performed by many public agencies, private owners, design engineers, contractors and manufacturers in the past. The perspective for this survey, however, begins in the early 1970's. This coincides with the introduction and use in the United States of mechanically stabilized earth (MSE) retaining walls using steel straps. Data was reported in 1973 by Professor K. Lee of

UCLA and was predominately the result of a design-oriented project which included different corrosion rates of the steel reinforcement. Wall costs related to three corrosion rates (0, 0.025 and 0.050 mm/year) were presented and these results were compared to reinforced concrete cantilever walls and to metal bin walls, see Figure 1. The MSE walls were the least expensive, even at the maximum corrosion rates associated with the steel reinforcement. As seen in Figure 1 the economy of the MSE walls occurs at all wall heights, however, the data seems curious in a number of aspects:

- Reinforced concrete walls had been constructed to heights significantly greater than 11 m, yet such cost data is not reported in the figure.
- Metal bin walls were rarely constructed to 11 m heights, yet cost data are reported to such heights in the figure.
- MSE (metal) walls were generally not constructed to 18 m heights at that time, yet cost data are shown accordingly in the figure.
- There is no indication of the statistical scatter in the cost data, the presumption being that these are average (or mean) values.

While the data is somewhat suspect at this point in time, it is nevertheless instructive in providing a base line for this report and it certainly was the forerunner of many studies to follow.

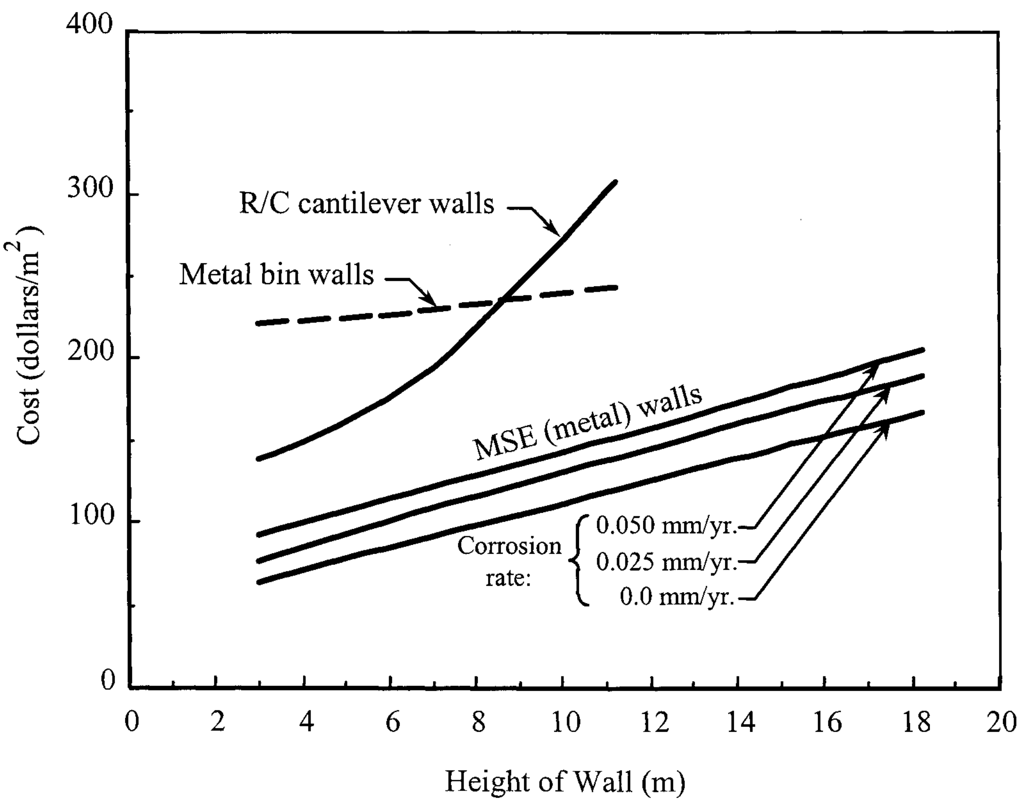

Figure 1 - Results of comparative retaining wall costs, Lee et al (1973)

In 1981, the VSL Corporation published their results on retaining wall costs. They included the same three wall types as discussed previously, but subdivided crib/bin walls into reinforced concrete and metal types, see Figure 2. Again the MSE walls were the most economic, however, this data is also curious insofar as the following considerations:

- The reinforced concrete retaining wall costs are limited to 9 m in the figure, while these walls have been constructed to considerably greater heights.
- The crib/bin wall costs are shown up to 9-11 m height in the figure which is somewhat large for this type of wall system.
- The MSE (metal) wall costs are shown for heights of 13 m in the figure, which was rather high for the time… some state DOTs limit MSE walls to either 7.6 m or 10.7 m.
- There was no distinction made of MSE (metal) wall costs on the basis of corrosion rates. Presumably, the steel reinforcement was galvanized at this time and corrosion was not considered to be a major issue.
- There is no indication of the statistical scatter in the cost data, the presumption being that these are average (or mean) values.

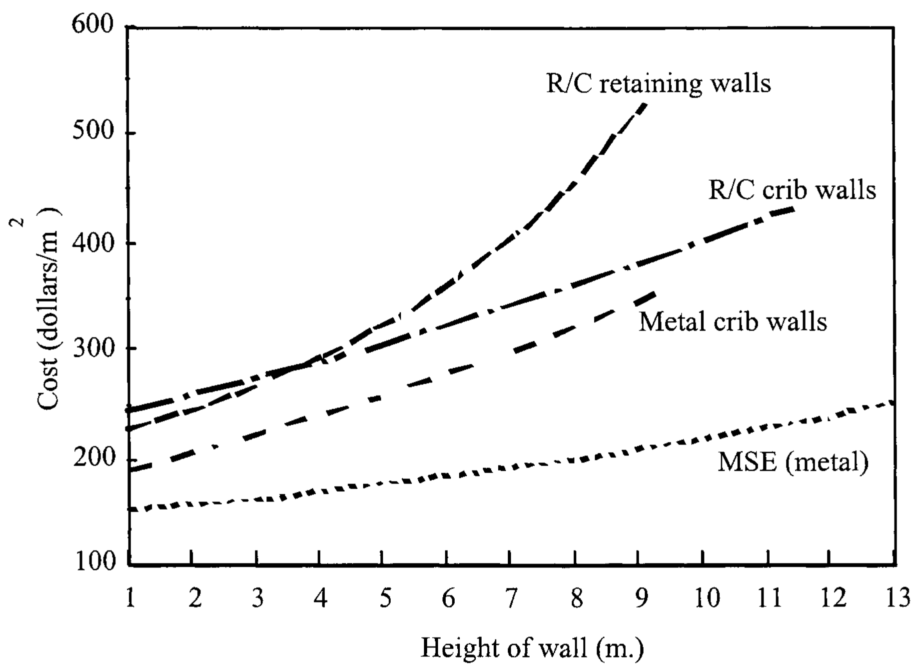

Figure 2 - Results of comparative retaining wall costs, VSL Corp. (1981)

The first MSE walls reinforced with geosynthetics were constructed by the U.S. Forest Service in the early 1970's; see Bell, et al. (1975), Bell, et al. (1977), Steward and Mohney (1982). These walls were of the wrap-around face type using nonwoven and woven geotextiles. Geogrid reinforced walls began with a wall used to stabilize a landslide in Oregon in 1983, see Yako and Christopher (1988). This same reference produced the cost analysis presented in Figure 3. The addition of the MSE (geosynthetic) walls was the first attempt at quantifying geogrid and geotextile reinforced retaining wall costs and was (and continues to be) of great interest. Figure 3 shows that MSE-geosynthetic walls are the least expensive of all wall types when less than 6.5 m, but were limited to wall heights of 8 m at the time. However, there are some curious aspects to the data of Figure 3:

- As with the other surveys, the reinforced concrete retaining wall costs cut off at 9 m height in the figure, yet such walls are known to have been constructed too much greater heights.
- The concrete and metal crib/bin wall costs are shown up to 9-11 m in height in the figure, yet these heights are rather large for these types of wall systems.
- The MSE-metal reinforced walls are shown to 13 m of height in the figure which is significantly greater than those used in practice, particularly by public agencies such as Departments of Transportation.
- The above three types of wall costs are the same (within scaling accuracy limits) as the VSL Corp. study conducted seven years earlier. The same VSL data may have been used in the figure except for the MSE-geosynthetic wall cost data which were the added feature to the study.
- There is an anomalous crossover in costs between MSE (metal) and MSE (geosynthetic) reinforced wall costs at approximately 7 m in height.
- These is no indication of the statistical scatter in the cost data, the presumption being that these are average (or mean) values.

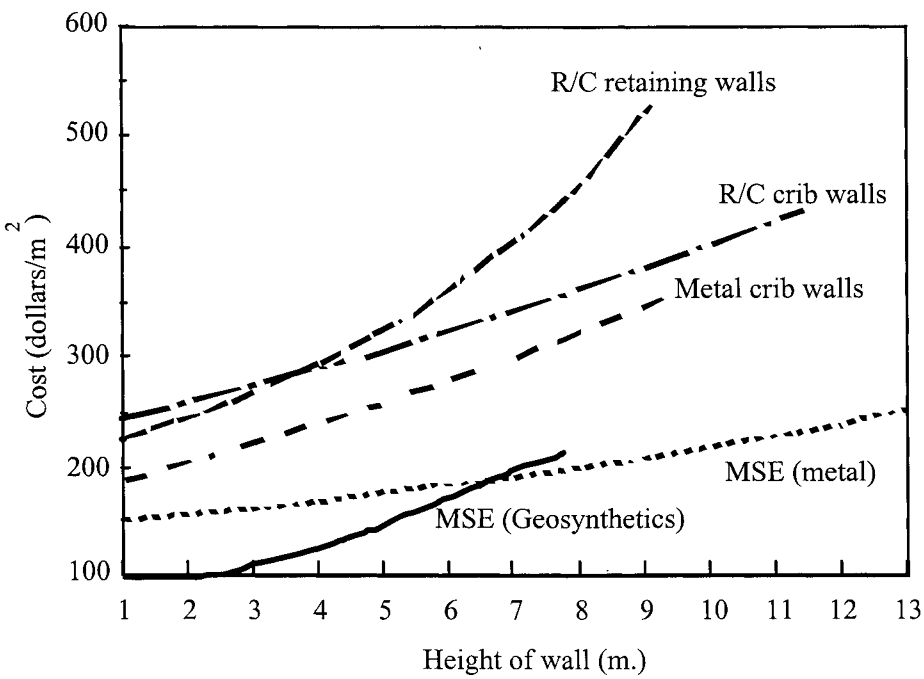

Figure 3 - Results of comparative wall costs, Yako and Christopher (1988)

These three economic studies, i.e., Lee, et al. in 1973, VSL Corp. in 1981 and Yako and Christopher in 1988, allow for a comparison of wall costs over the published time frames, see Table 1. Here the four types of walls are itemized according to three arbitrary wall heights:

- High walls; greater than 9.0 m
- Medium walls; 4.5 to 9.0 m
- Low walls; less than 4.5 m

Note that crib and bin walls made from different materials (concrete, metal, timber, etc.) are collectively listed as one wall category. Also note that the Yako and Christopher data appears to have been taken directly from the VSL Corp. study which was conducted 7-years previous.

Table 1 - Comparison of Retaining Wall Costs Based on Past Studies
(units are in U.S. dollars per square meter)

Wall Category	Wall Height		Lee, et al. (1973)	VSL Corp. (1981)	Yako & Christopher (1988)	GRI Study (1998)
	relative	meters				
Gravity Walls	high	>9.0	300	570	570	?
	med.	4.5-9.0	190	344	344	?
	low	<4.5	190	344	344	?
Crib/Bin Walls	high	>9.0	245	377	377	?
	med.	4.5-9.0	230	280	280	?
	low	<4.5	225	183	183	?
MSE (metal) Walls	high	79.0	140	300	300	?
	med.	4.5-9.0	100	280	280	?
	low	<4.0	70	172	172	?
MSE (geosynthetic) Walls	high	>9.0	N/A	N/A	250	?
	med.	4.5-9.0	N/A	N/A	180	?
	low	<4.5	N/A	N/A	130	?

note: N/A = not available at that time

Using Table 1 as a template or model, it now remains to counterpoint the existing data to current retaining wall cost data for the wall types and wall heights indicated. The remainder of the report is focused toward this task.

DETAILS OF 1998 GRI SURVEY

Recognizing that retaining wall costs built by the public versus private sections might be considerably different, it was decided to separate the two ownership groups. The main thrust of this paper is on publicly financed walls. This was done on the basis of convenience; since public agencies are approachable, known and interested in the information. An initial attempt, however, of obtaining data regarding privately financed walls will be included at the end of the paper.

Having decided to focus on public agencies, the obvious choice was the 50-state Departments of Transportation, i.e., the DOTs. There are of course other public agencies building retaining walls, but the majority of the walls considered herein are probably constructed as part of new construction or remediation of highways, structures, and related transportation systems. The list of contact persons was supplied by the Federal Highway Administration (FHwA). It should be noted, however, that this survey was not an official survey of the FHwA, nor was it funded as a special project by any agency, company or special interest group. The cover letter and survey template used to request the various retaining wall cost data is provided in the Appendix. Note that the data was requested in conventional units and was subsequently converted to S.I. units for this paper. Also note that the four wall categories noted previously are actually categories within themselves, each having at least three sub-types within each category.

As might be expected of an unofficial survey of this type, the diligence in providing the requested information varied from state-to-state and from individual-to-individual within the state organizations. In fact, many follow-up telephone calls were necessary to obtain a statistically meaningful population. The following responses were ultimately obtained and used in preparing this report (out of a possible 50):

- States responding = 34
- States willing but not able to respond (due to inadequate time or personnel) = 6
- States not responding = 10

Several state DOT engineers asked additional questions, or could not respond for various reasons. Some of these issues follow:

- Data was not available on the basis of cost per square unit of wall face
- Data was not available on the basis of wall height
- Some types of walls were not used by the responding DOT, e.g., ten (10) states do not use MSE-geosynthetic reinforced walls
- Some states had wall height limitations (or practices)
- Some states made a major effort in pulling data from recent past projects, whereas some made only a token effort
- A few individuals asked how far back in time should the data be reported

In response to these questions, we asked for whatever data was felt to be authoritative within the time frame of the past 2-3 years.

RESULTS OF 1998 GRI SURVEY

The raw data as obtained from the survey responses described in the previous section is plotted in Figure 4. Included therein are 167 individual data points where some points may have

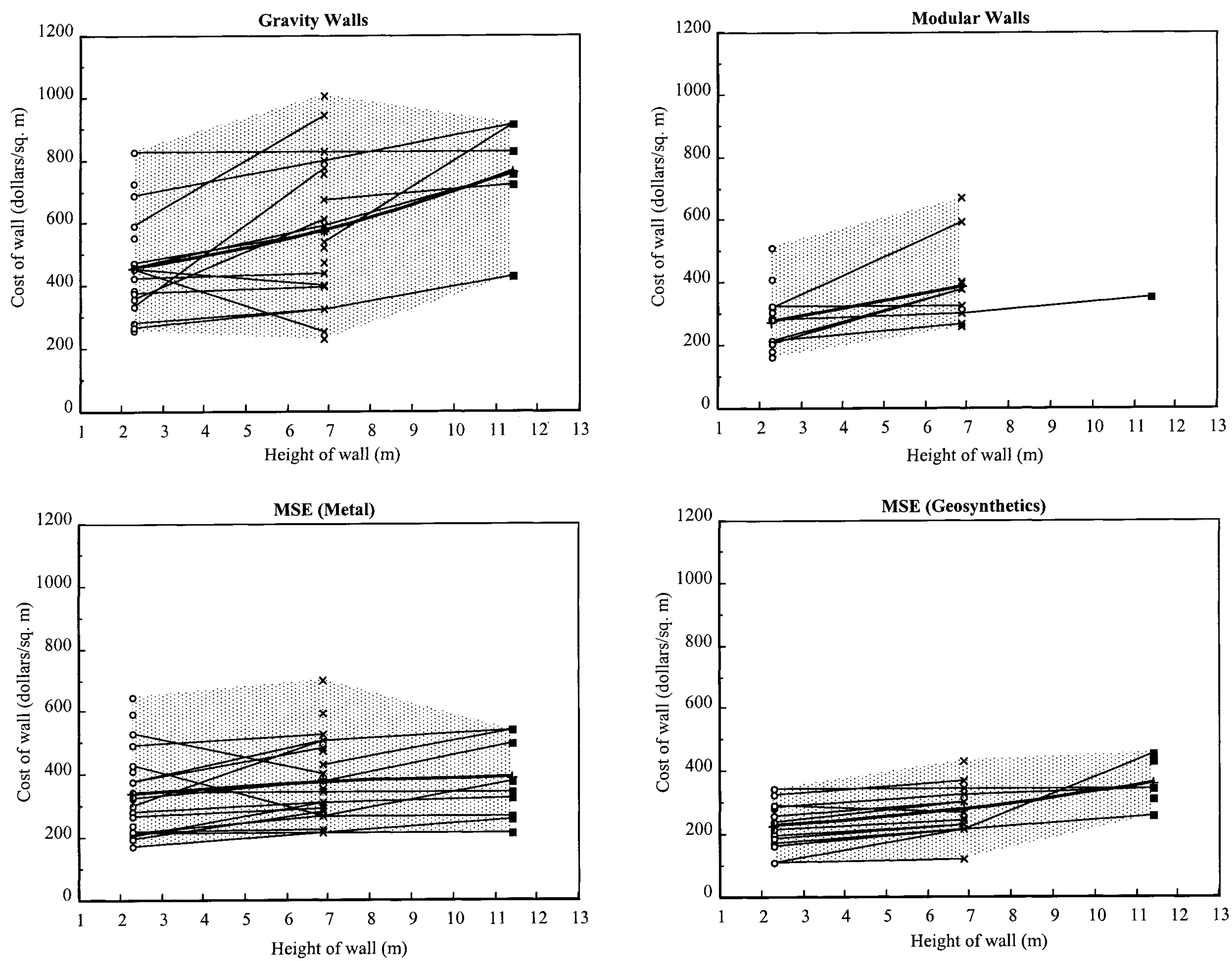

Figure 4 – Retaining wall (raw) cost data categorized by wall type

been for an individual wall, while others may have been averages for many walls. *Thus, the actual number of walls included in the study is unknown, but is probably in the thousands.* Each of the four respective wall categories is plotted separately. Where points are connected with fine lines across wall heights, that data was supplied by a single state agency. In general, the slope of these individual lines is positive, signifying an increasing unit cost with increasing wall height. Many points are not provided in this manner and appear as an isolated point signifying that certain wall categories are associated with specific wall heights.

Regarding the variation in the data of Figure 4, it is seen to be very large. This is somewhat understandable in that the data is national in its scope. Unfortunately, this variation cannot be compared to previous surveys since such data was not provided. The following can also be observed in the figure:

- Gravity walls have the greatest cost variation being separated by a factor of approximately four times from lower to higher costs.
- Crib/bin walls and MSE (metal) have intermediate cost variations being separated by a factor of approximately three times.
- MSE (geosynthetics) have the lowest cost variation being separated by a factor of approximately two times.

Also note in Figure 4 that crib/bin walls were only higher than 7.0 m in one case. In future analysis it will be omitted and these walls will be arbitrarily included as low and medium wall heights only.

The bold lines in Figure 4 within the individual wall types is the arithmetic average (mean) of the cost data provided. These mean values have been superimposed on one another in a single figure in Figure 5. It is arguably the most important curve in the paper. In all cases the mean values have a positive slope; the highest cost being gravity walls, and the least being MSE (geosynthetic) walls. The crib/bin walls and MSE (metallic) walls have intermediate costs.

The raw data of Figures 4 and 5 has been further analyzed to result in the mean, standard deviation and variance. Plotted on Figure 6 is the mean wall cost plus/minus one standard deviation for all four wall types at the three respective wall heights. As expected from the raw data provided earlier, the gravity walls have the greatest standard deviation, the MSE (geosynthetic) walls have the least standard deviation and the other two wall categories are intermediate between these extremes. Table 2 further quantifies the statistical data resulting from their survey. In this table, the gradually lower mean costs and standard deviations seen in the figures is readily apparent as one goes through the various wall categories. Not surprisingly, the variance (mean divided by standard deviation) is relatively constant.

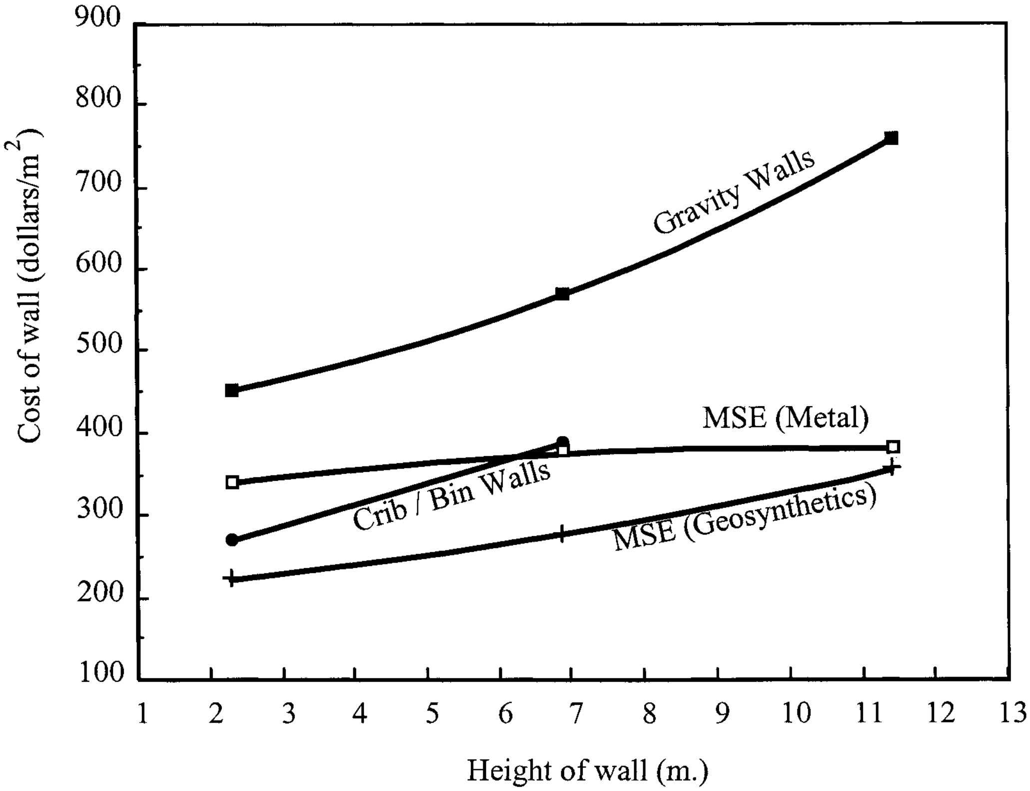

Figure 5 - Mean values of various categories of retaining wall costs

Table 2 - Statistical Data for Retaining Wall Costs from 1998 GSI Survey

Wall Category	Wall Height (m)	Cost in dollars/sq. m of wall force		
		mean	std. dev.	variance (%)
Gravity walls	>9.0	760	180	24
	4.5 to 9.0	573	224	39
	<4.5	455	166	37
Crib/bin walls	>9.0	I/D	I/D	I/D
	4.5 to 9.0	390	129	33
	<4.5	272	98	36
MSE (metal)	>9.0	385	122	32
	4.5 to 9.0	381	126	33
	<4.5	341	135	40
MSE (geosynthetic)	>9.0	357	73	20
	4.5 to 9.0	279	81	29
	<4.5	223	67	30

note: I/D = inadequate data

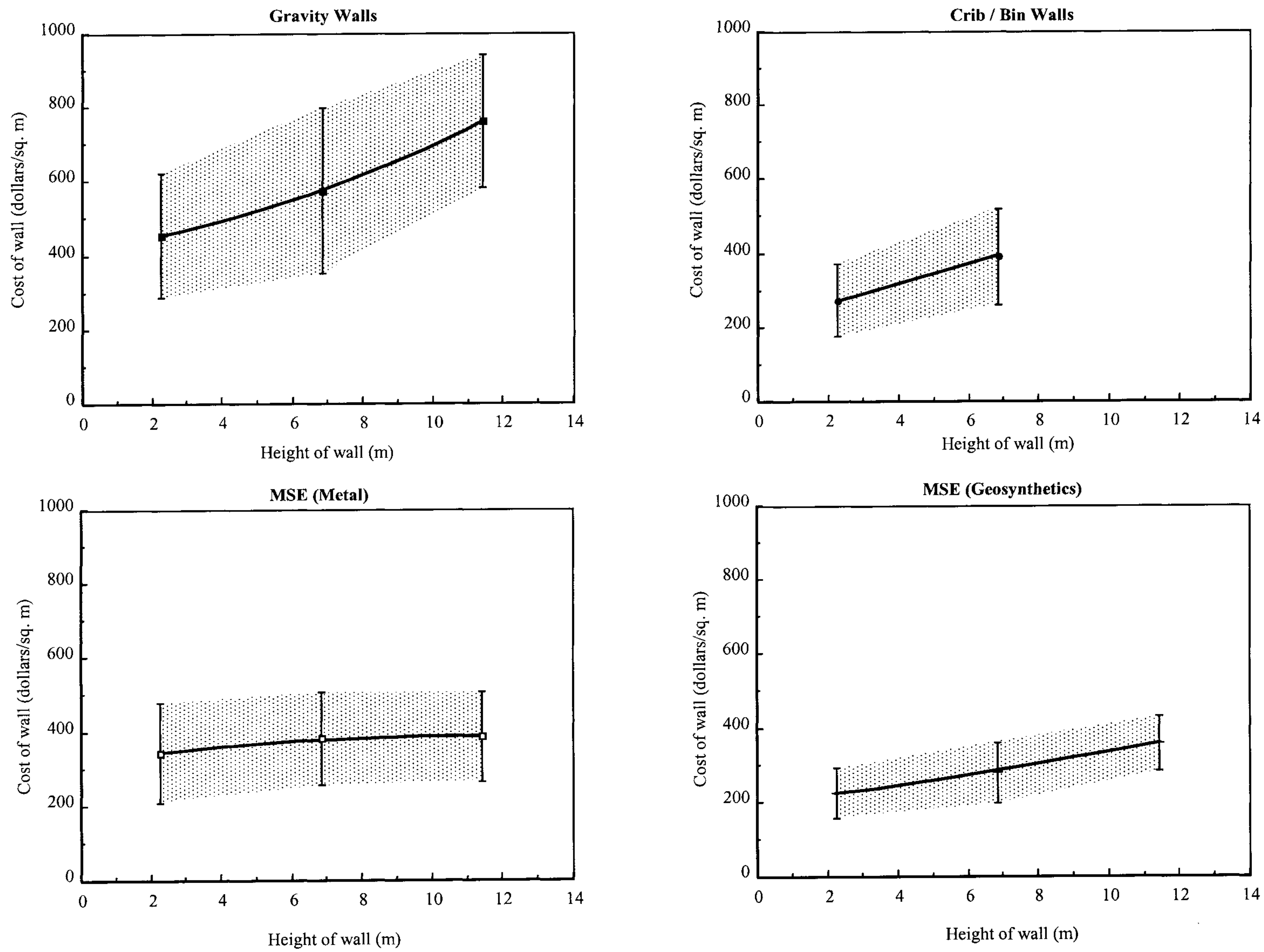

Figure 6 – Retaining wall cost data (mean value ± 1.0 standard deviation)

1998 GRI SURVEY COMPARED TO PAST SURVEYS

As described in the background section to this paper, surveys on retaining wall costs have been conducted in the past by numerous individuals and organizations. Most notable for the purpose of this report are the Lee, et al. (1973), VSL Corp. (1981) and Yako and Christopher (1988) surveys which were compared to one another in Table 1. We are now in a position to counterpoint this past data with results from the current study. Table 3 provides the comparative information.

Table 3 - Comparison of Past Retaining Wall Costs with Current (1998) GRI Survey Results

Wall Category	Wall Height (relative)	Lee, et al. (1973)	VSL Corp. (1981)	Yako & Christopher (1988)	GRI (1998)
Gravity Walls	high	300	570	570	760
	medium	190	344	344	573
	low	190	344	344	573
Crib/Bin Walls	high	245	377	377	I/D
	medium	230	280	280	390
	low	225	183	183	272
MSE (metal) Walls	high	140	300	300	358
	medium	100	280	280	381
	low	70	172	172	341
MSE (geosynthetic) Walls	high	N/A	N/A	250	357
	medium	N/A	N/A	180	279
	low	N/A	N/A	130	223

notes: I/D = inadequate data
N/A = not available at that time

Immediate apparent in Table 3 is the increased cost of all wall categories over the years. The 10-year interval from 1988 to 1998 has seen wall costs rise for all wall categories at all wall heights. Increases in this time period were from 33% to 71%. For the time interval from the original 1973 study, i.e., 25-years, the increases were from 21% to 387%. Note that MSE-geosynthetic reinforced walls were not available for the 1973 and 1981 surveys.

Clearly, retaining wall costs have risen considerably over the years for all categories and for all wall heights. The essential ordering of wall costs, however, has not changed. In the order of decreasing cost per unit wall face area are the following:

- Gravity walls (the highest cost)
- Crib/Bin walls (somewhat lower cost)
- MSE (metal) walls (still lower cost)

- MSE (geosynthetic) walls (the lowest cost)

For all four wall categories, the higher the wall, the higher the cost on the basis of wall face area. Thus the trends in comparative wall categories hold for all wall heights.

Graphically the trends in wall costs between wall categories and wall heights can be seen in Figure 7 in a bar chart format.

ANALYSIS OF RESULTS BY STATE, FHWA REGION AND FEDERAL LANDS

This section provides some additional insight into the data that was generated by the results of the survey.

State Acceptance of MSE-Geosynthetic Walls

Considering that MSE-geosynthetic reinforced walls (generally reinforced by geogrids, but also by geotextiles) are the newest of the wall types considered, the acceptance (or otherwise) by state DOT's is of interest. Figure 8 presents this state-by-state comparison data on the basis of the three wall heights under consideration. The data (which speaks for itself) indicates the following:

- States using MSE-geosynthetic walls = 24
  - high walls only = 2
  - medium walls only = 4
  - low walls only = 5
  - low and medium walls = 9
  - low, medium and high walls = 4
- States that responded but do not use MSE-geosynthetic walls at this time = 10
- States that did not respond to survey = 16

Total = 50 states

It is of great interest to note that eight of the ten states that do not use MSE-geosynthetic walls are all in the mid-Atlantic/mid-West area and these states actually adjoin one another. As will be seen in the next section, these are FHwA Regions 3 and 5.

Wall Costs by FHwA Region

Figure 9 graphically identifies the Federal Highway Administration Regions. There is no FHwA Region 2. These Regions will be used in this analysis to illustrate that national means, standard deviations and variances cannot be applied unilaterally across the country.

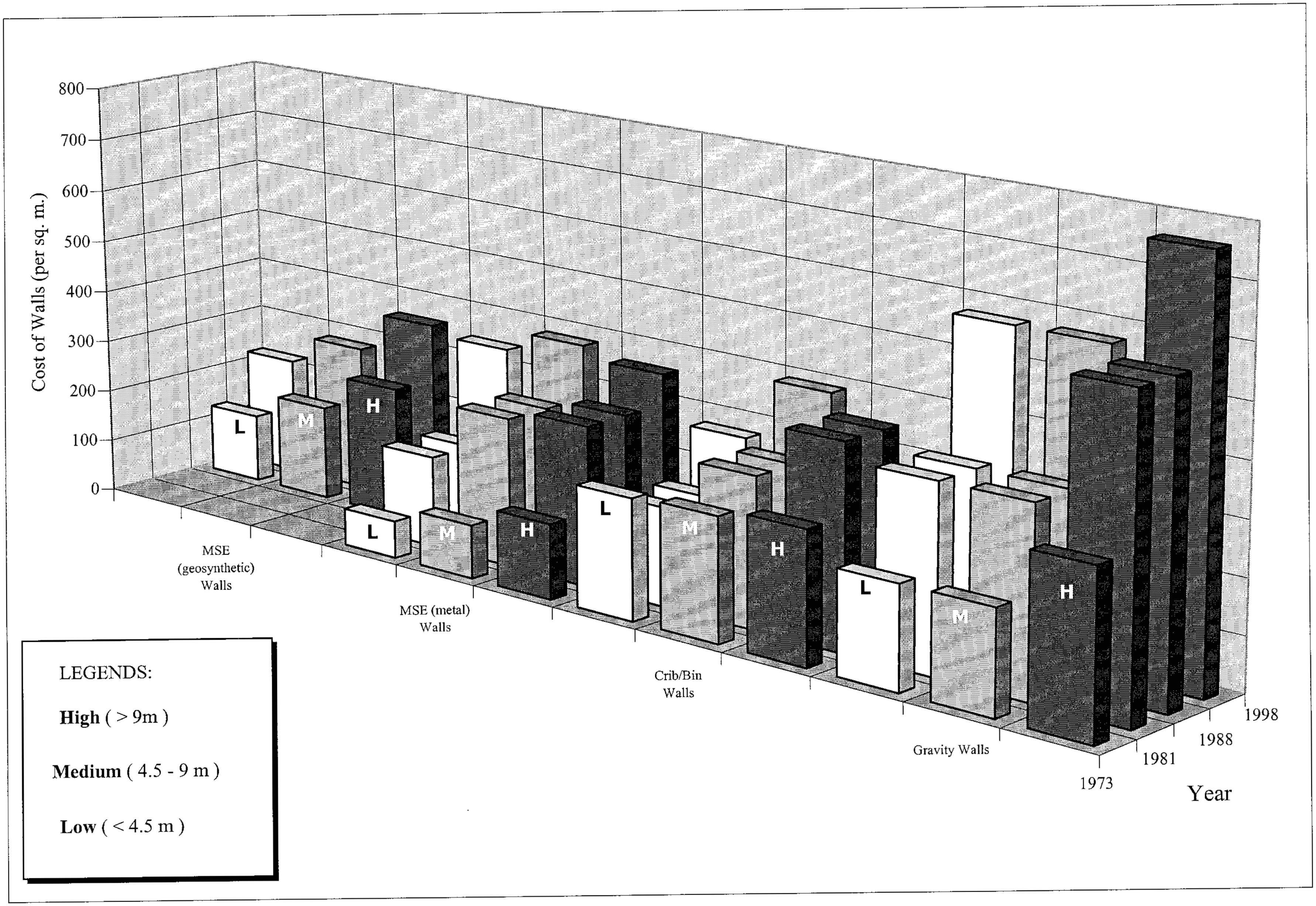

Figure 7 - Trends in retaining wall costs from 1973 to 1998 on the basis of wall categories and wall heights

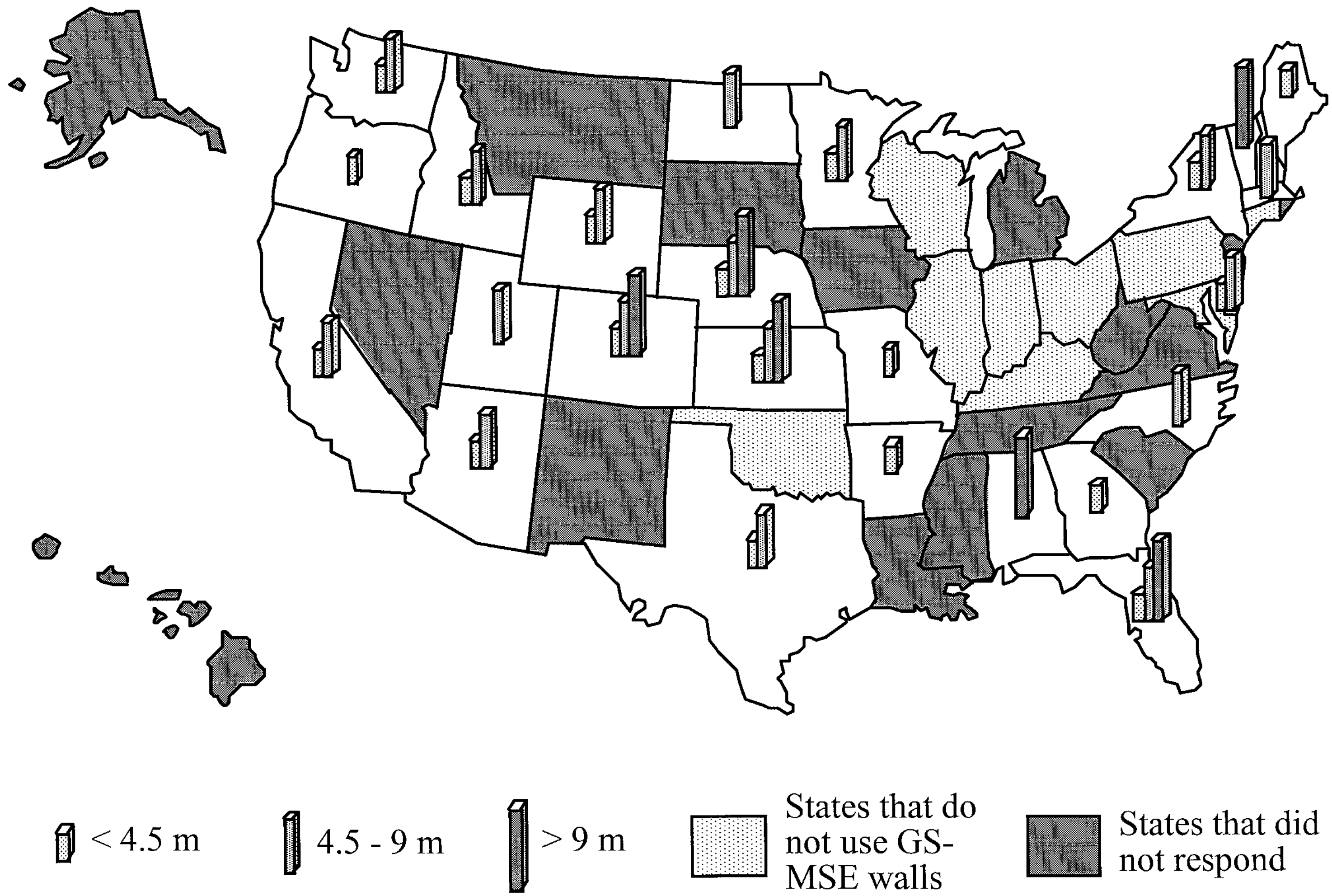

Figure 8 – Acceptance (by State DOT) of MSE geosynthetic reinforced retaining wall

The results of the survey have been individually analyzed for the various FHwA Regions, for each wall category and wall height and are plotted in Figure 10. The following observations are offered.

- Regions 1 and 3 always have higher wall costs (all categories and heights) than the national averages.
- Regions 5, 6, 8 and 10 always have lower wall costs (all categories and heights) than the national averages.
- Regions 4, 7 and 9 are intermediate in wall cost trends with respect to the above two comments, i.e., they are neither always higher nor always lower than the national averages.
- Gravity wall costs are very much higher than the national averages in Regions 1, 3 and 7, and lower than the natural averages in Regions 5 and 8.
- Crib/Bin wall costs are very much higher than the national averages in Regions 3 and 4, and lower than the national averages in Regions 6 and 10.
- MSE (metal) wall costs are very much higher than the national averages in Regions 1, 3 and 9, and lower than the national averages in Regions 6 and 8.
- MSE (geosynthetic) wall costs are very much higher than the national averages in Region 1, and lower than the national averages in Regions 5, 6 and 8.

Wall Costs on Federal Lands

The U. S. Bureau of Federal Lands contains a Highways Division which was kind enough to query its engineers on retaining wall costs. They responded in-toto as a national agency. The data that was supplied has been superimposed onto the mean values of all state DOTs (recall Figure 5) for the various wall types and wall heights. Figure 11 illustrates the mean values for the four wall categories from the two different agencies. The Bureau of Federal Lands retaining wall costs are either the same or higher than those of the DOTs. When the costs are higher, they are sometimes significantly higher which is the case as the wall heights increase. Perhaps the small size of projects and the sometimes remoteness of projects contribute to the cost differences, but these ideas are only conjecture on the part of the authors.

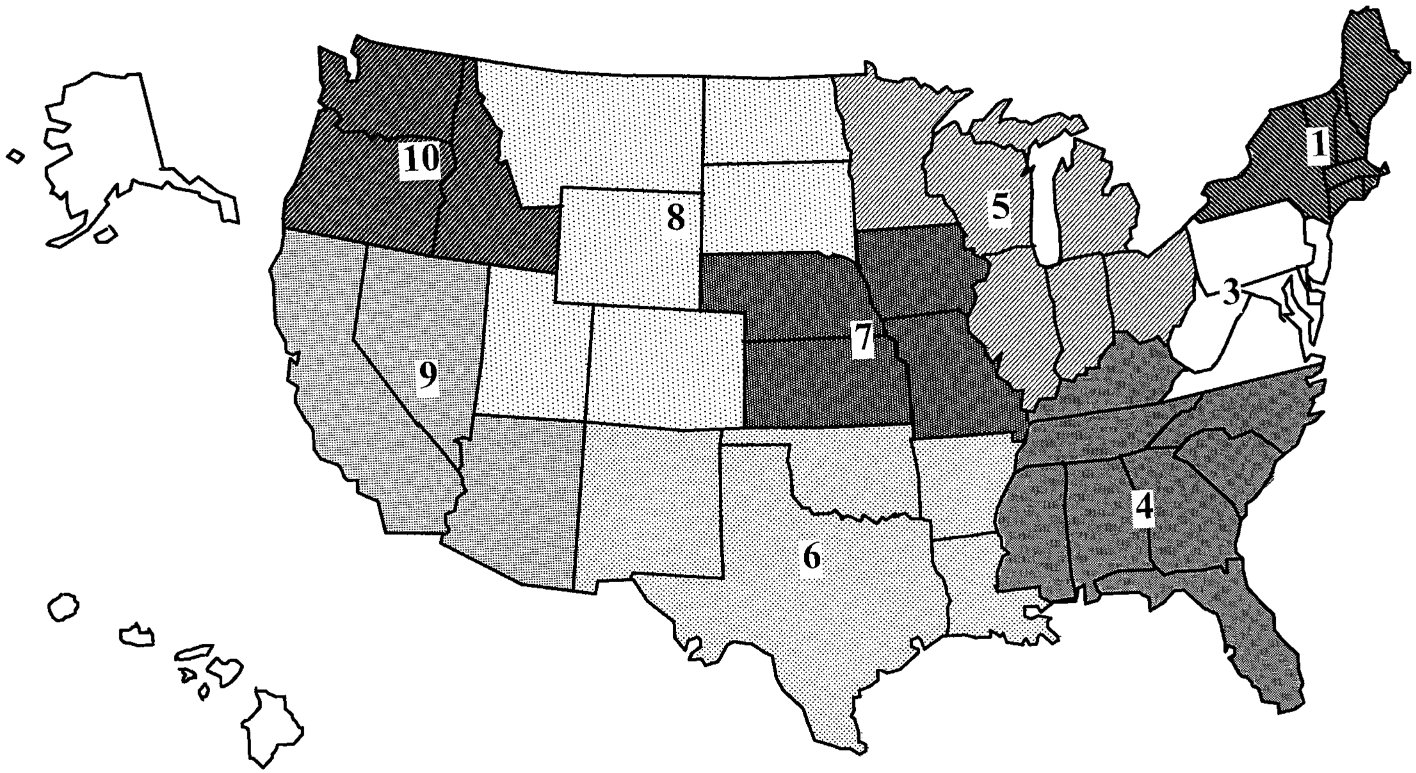

Figure 9 – FHwA regions

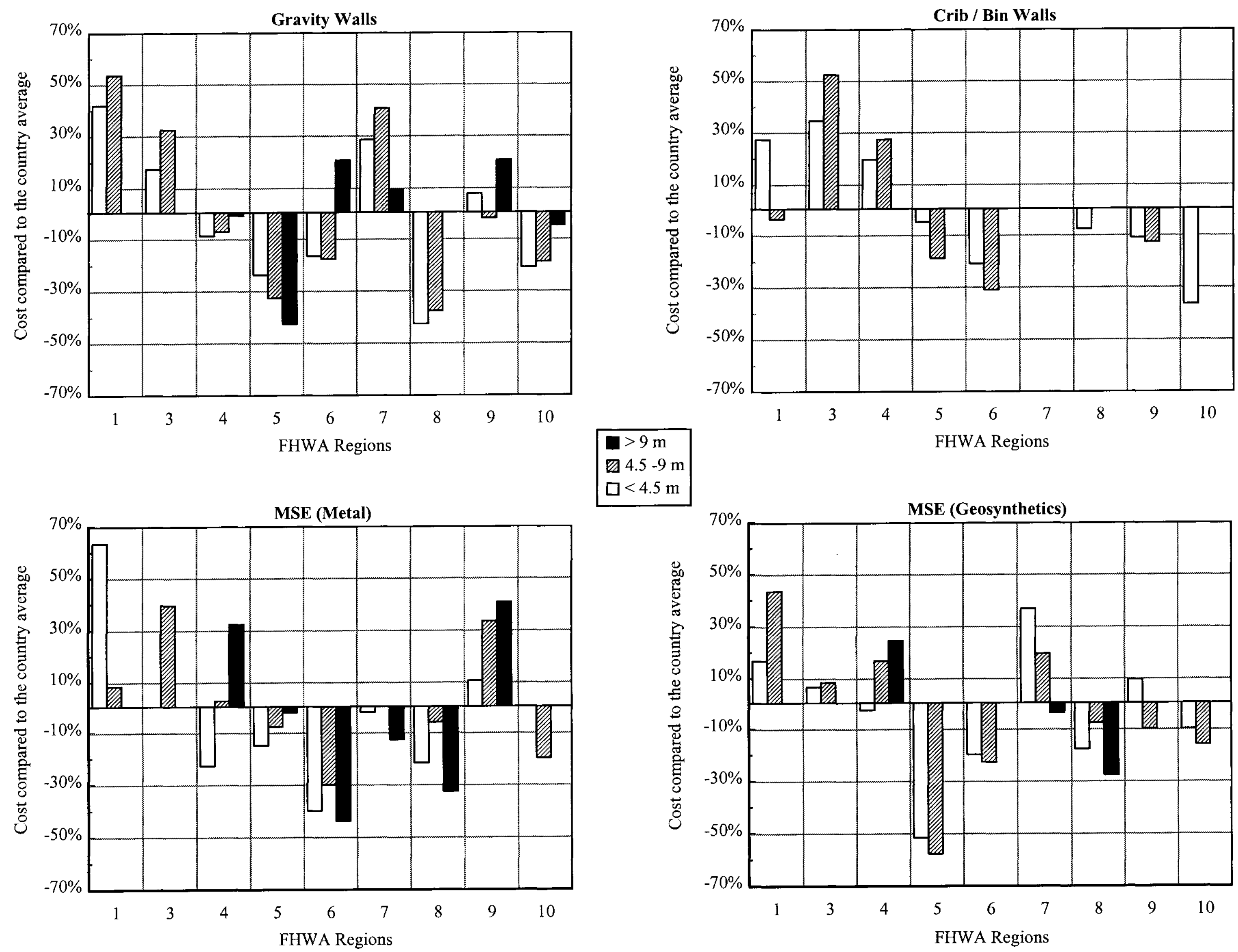

Figure 10 - Retaining wall costs by FHwA region

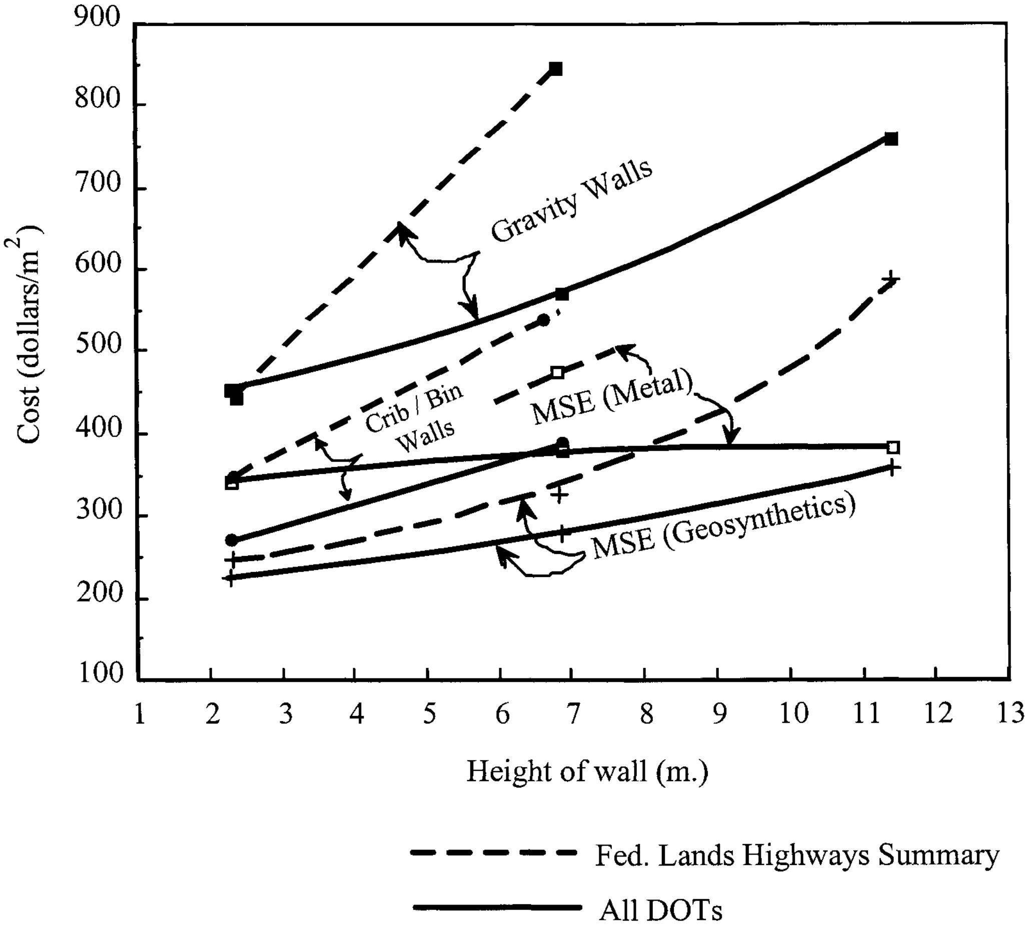

Figure 11 - U. S. Federal Lands (Highways Division) retaining wall costs compared to national mean values

Private Wall Costs

It was originally perceived that private wall costs of all wall types would be difficult to obtain. Yet having the data as exemplified in Figure 5, simply begs as to the question of privately financed wall costs. This includes both commercial and residential walls. Thus, it was decided to cut the scope of a second survey down to only MSE-geosynthetic reinforced walls. The same three wall height categories (low, medium, and high) were maintained. Even within this single wall category, data has not been easy to obtain. Approximately, 200 large owners/designers/architects/contractors of both commercial and residual walls have been contacted with relatively sparse results. The information we have gained to date is presented in Table 4.

Table 4 - MSE-Geosynthetic Reinforced Cost Data (in dollars per square meter of wall facing) of Privately Financed Walls

State	Type	Wall Height at maximum		
		< 4.5 m	4.5 – 9.0 m	> 9.0 m
Maryland	commercial	185	210	225
	residential	170	220	250
Virginia	commercial	n/a	150	150
	residential	180	n/a	n/a
North Carolina	commercial	n/a	150	150
	residential	180	n/a	n/a
Georgia	commercial	145	160	170
	residential	145	160	170
Ohio	commercial	160	195	260
	residential	160	195	260

A comparison of this admittedly sparse data to the large data base of publicly financed walls is quite tempting. We succumbed. In viewing the private wall cost data of Table 4 with the mean value curves of public wall costs in Figure 5, it is seen that all data is lower than the MSE (Geosynthetics) curve. This can be readily seen in Figure 12. Thus, privately financed walls are less expensive than publicly financed walls over all wall heights. The amount, is considerable, and is approximately as follows:

- for low wall heights; private walls are 17 to 35% less expensive than the public walls
- for medium wall heights; private walls are 21 to 46% less expensive than public walls
- for high wall heights; private walls are 27 to 58% less expensive than public walls

The paper does not delve into the reasons for such cost differences and the issue is left to the reader.

SUMMARY AND CONCLUSIONS

This survey of U. S. State Department of Transportation retaining wall costs was conducted during the winter of 1997-1998. The categories of walls surveyed were gravity, crib/bin, MSE-metal reinforced and MSE-geosynthetic reinforced. They were subdivided into three heights: high (>9.0 m), medium (4.5 to 9.0 m) and low (<4.5 m) walls. The costs were analyzed within themselves and also compared to three earlier surveys conducted by others in 1973, 1981 and 1988.

Insofar as general findings are concerned with respect to publicly financed walls, the following applies:

- Wall costs in all categories have risen from 33% to 71% over the past 10-years, and from

21% to 387% over the past 25-years.

- For all wall heights; gravity walls are the most expensive, followed by crib/bin walls, MSE metal walls and MSE geosynthetic walls, in that order.
- At all wall heights, gravity walls have the greatest variation in cost, followed by crib/bin walls, MSE metal and MSE geosynthetic wall costs, in that order.
- For high walls, i.e., walls 11.5 m and higher, the difference in mean value costs between MSE-metal and MSE-geosynthetic is quite small and considering the variation in the data may be statistically insignificant.
- The standard deviation in wall costs of the four categories of walls surveyed is high, as was expected for a national survey of this type.

Insofar as specific findings are concerned with respect to publicly financed walls, the following applies:

- Crib/bin walls are rarely used in heights over 7 m (only one state reported a single data point in this category).
- As of 1998, the following states do not use MSE-geosynthetic walls: PA, MD, OH, CT, NH, IN, WI, IL, KY, OK. With the exception of NH and OK, these states are all adjacent to one another and are in FHwA Regions 3 and 5.
- The states of FL, NE, KS and CO use MSE-geosynthetic walls in all height categories; i.e., high, medium and low as designated in this survey.
- The other states use MSE-geosynthetic walls in the low and medium height categories.
- Wall costs conducted in past surveys have presumably been on the basis of average values and this report has made a likewise comparison, but as discussed herein the statistical variation is quite high in this survey.
- Using plus/minus one standard deviation it was found that gravity walls vary by 4-times; bin/crib and MSE (metal) walls by 3-times; and MSE (geosynthetic) walls by 2-times.
- The data was subdivided according to FHwA Region which gave interesting insight; e.g., Regions 1, 3, 4 and 7 have wall costs higher than the national average, whereas Regions 5, 6, 8 and 10 have costs lower than the natural average.
- Retaining wall costs on highways of the Bureau of Federal Lands are generally higher than the natural average and for high walls significantly so.

Insofar as limited data for privately-financed walls are concerned, the following applies:

- Privately financed MSE-geosynthetic walls are considerably less expensive than comparable publicly financed walls.
- This applies to both commercial and residential MSE-geosynthetic walls.
- While the privately funded wall data is sparse, it appears that low walls are 17 to 35% less expensive, medium walls are 21 to 46% less expensive, and high walls are 27 to 58% less expensive than publicly financed MSE-geosynthetic reinforced walls.

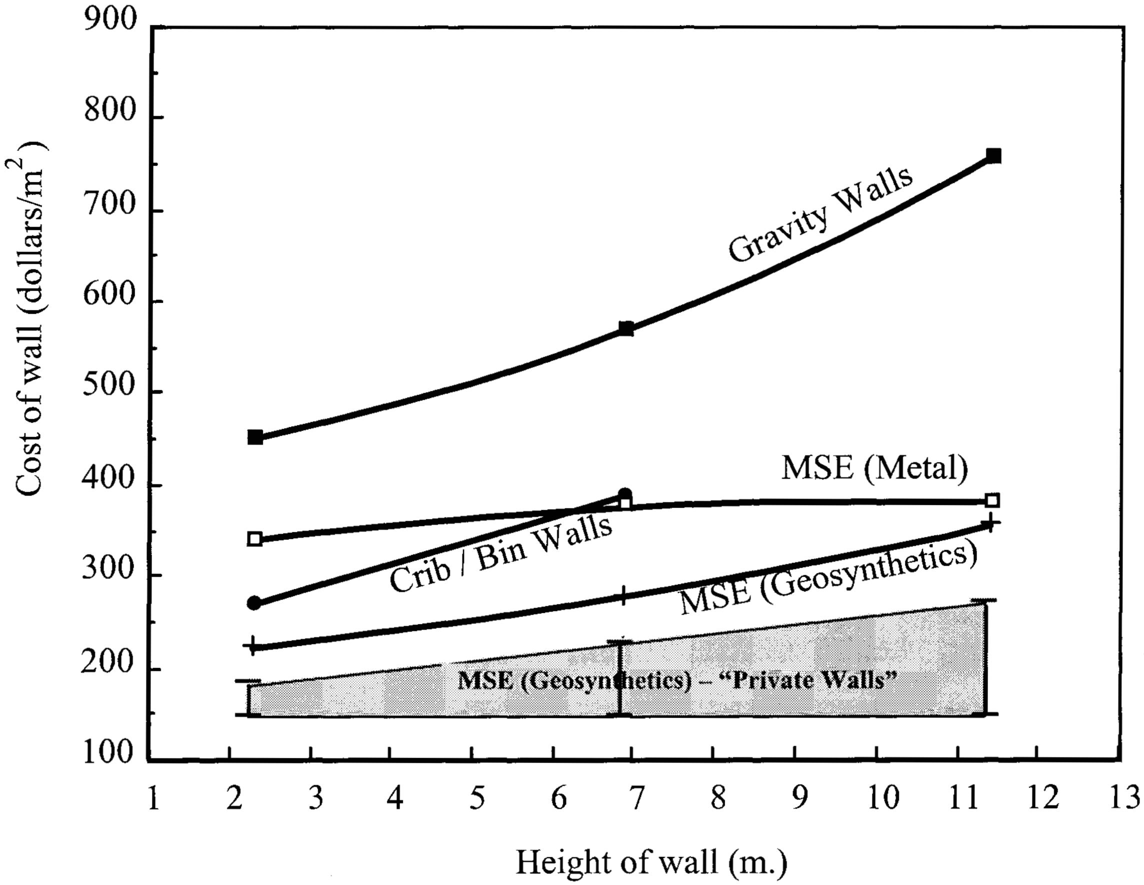

Figure 12 – Mean values of various categories of retaining wall costs from Figure 5, now showing a comparison of public-to-private wall costs for MSE-geosynthetics walls

ACKNOWLEDGEMENTS

The contributions of the wall cost data from which the paper was formed are acknowledged in total. Space precludes listing them all by name. The base report lists each by name and address. Sharing of this cost information is sincerely appreciated.

This study was funded through general membership fees of the organizations in the Geosynthetic Institute consortium. We are grateful for their generosity and support. The current organizations are as follows:

GSE Lining Technology, Inc.
Earth Tech Consultants, Inc.
U.S. Environmental Protection Agency
Polyfelt, GmbH
E. I. DuPont de Nemours & Co., Inc.
Federal Highway Administration
Golder Associates Inc.
Tensar Earth Technology, Inc.
Poly-Flex, Inc.
Colbond Geosynthetics
NOVA Chemicals Ltd.
Tenax, S.p.A.
Amoco Fabrics & Fibers Co.
U.S. Bureau of Reclamation
IT Corp.
Montell USA, Inc.
TC Mirafi, Inc.
CETCO - No. America
Huesker, Inc.
Solvay Polymers
Naue Fasertechnik GmbH
Synthetic Industries, Inc.
ExxonMobil Chemical Co.
BBA Nonwovens
NTH Consultants, Ltd.
TRI/Environmental Inc.
U. S. Army Corps of Engineers
Chevron Phillips Chemical Co.
Serrot International
Haley & Aldrich Consultants
URS/Greiner/WCC
S. D. Enterprise Co., Ltd.
Solmax Géosynthétiques
EnviroSource, Inc.
Strata Systems, Inc.
CARPI, Inc.
Rumpke Waste Service, Inc.
Civil & Environmental Consultants, Inc.
Agru America, Inc.
FITI (GSI-Korea)
Waste Management Inc.
CETCO Europe, Ltd.
NPU (GSI-Taiwan)

REFERENCES

Bell, J. R. and Steward, J. E., (1977), "Construction and Observations of Fabric Retained Soil Walls," *Proceedings, International Conference on the Use of Fabrics in Geotechnics*, Paris, France, Vol. 1, April, pp. 123-128.

Bell, J. R., Stilley, A. N. and Vandre, B. (1975), "Fabric Retained Earth Walls," *Proceedings, 13th Annual Geology and Soils Engineering Symposium*, Moscow, Idaho, pp. 271-287.

Koerner, J., Soong, T.-Y. and Koerner, R. M. (1998), "Earth Retaining Wall Costs in the USA", *GRI Report #20*, Geosynthetic Institute, Folsom, PA, 38 pgs.

Lee, K. L., Adams, B. D. and Vagneron, J. M. J. (1973), "Reinforced Earth Retaining Walls," *Journal of the Soil Mechanics and Foundation Division*, ASCE, Vol. 99, No. SM10, pp. 745-764.

Steward, J. E. and Mohney, J. (1982), "Trial Use, Results and Experience Using Geotextiles for Low-Volume Forest Roads," *Proceedings, 2nd International Conference on Geotextiles*, Las Vegas, Nevada, Vol. 1, August, pp. 335-340.

VSL Corporation (1981), "*VSL Retained Earth, Technical Data*," Rock and Soil Stabilization Systems, Los Gatos, California.

Yako, M. A. and Christopher, B. R. (1988), "*Polymerically Reinforced Retaining Walls and Slopes in North America*," P. M. Jarrett and A. McGown, Eds., The Application of Polymeric Reinforcement in Soil Retaining Structures, Kluver Academic Publishers, pp. 239-283.

APPENDIX

DREXEL
UNIVERSITY

Geosynthetic Research Institute
33rd & Lancaster Walk
Rush Building - West Wing
Philadelphia, PA 19104
TEL 215 895-2343
FAX 215 895-1437

Geotextiles
Geomembranes
Geogrids
Geocomposites
Geosynthetic Clay Liners
Geopipes
Geonets

July 30, 1997

re: Survey of Retaining Wall Costs

Dear _________________,

As you are well aware, there are numerous retaining wall systems available for use in DOT facilities. Safety is of course the highest priority, but cost also plays an important (albeit secondary) role. We are trying to assess these costs, via recent bid prices for walls built throughout the U. S. as a function of wall type and height. Our goal is to update and extend the following FHWA graph which is 10-15 years old. When time permits please fill out the following form and fax or mail it back to us. We realize that not all wall types are used in your state, so any information that you can supply is of value.
If you would like us to call yourself or a colleague (perhaps someone in your procurement department) please advise accordingly. Thank you in advance. You will be sent the results of the survey when it is tabulated and completed.

Very truly yours,

Robert M. Koerner, Ph.D., P.E.
Professor of Civil Engineering and Director - GRI

ma

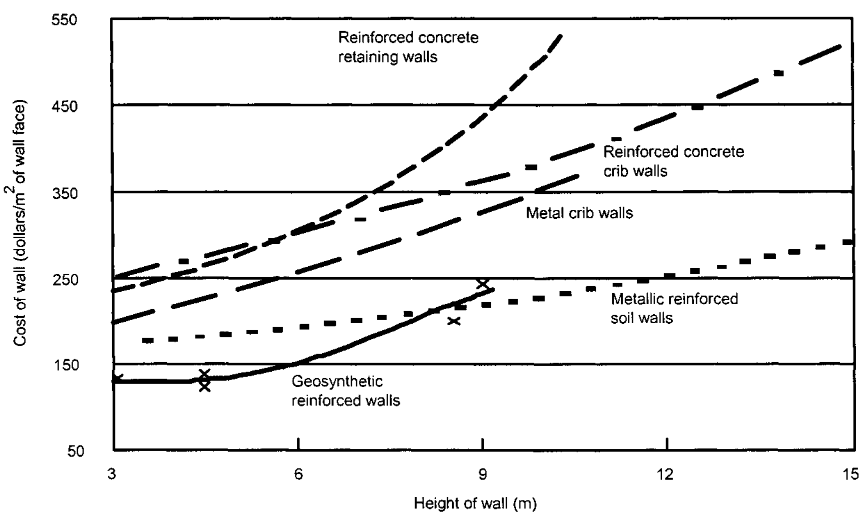

DREXEL UNIVERSITY

Geosynthetic Research Institute
33rd & Lancaster Walk
Rush Building - West Wing
Philadelphia, PA 19104
TEL 215 895-2343
FAX 215 895-1437

Recent Retaining Wall Costs* (via Bid Prices) In The

State of ________________________________

*Includes facing, reinforcement (if any), drainage, backfill and all construction costs.
(if not the case, please mark accordingly)

Category and Type of Wall	Height	Cost/ft^2	Height	Cost/ft^2	Height	Cost/ft^2
1. Rigid and/or Gravity Walls						
a. concrete cantilever	<15 ft		15-30 ft		>30 ft	
b. concrete cantilever with counterforts	<15 ft		15-30 ft		>30 ft	
c. rubble masonry	<15 ft		15-30 ft		>30 ft	
d. cylinder pile	<15 ft		15-30 ft		>30 ft	
e. soldier piles with tiebacks	<15 ft		15-30 ft		>30 ft	

2. Prefabricated Modular Gravity Walls						
a. metal bins	<15 ft		15-30 ft		>30 ft	
b. precast concrete cribs	<15 ft		15-30 ft		>30 ft	
c. precast concrete bins	<15 ft		15-30 ft		>30 ft	
d. gabions	<15 ft		15-30 ft		>30 ft	

3. Mechanically Stabilized Earth - with Nonextensible Reinforcement (Metal)						
a. precast concrete facing panels	<15 ft		15-30 ft		>30 ft	
b. cast-in-place facing	<15 ft		15-30 ft		>30 ft	
c. modular concrete block facing	<15 ft		15-30 ft		>30 ft	

4. Mechanically Stabilized Earth - with Extensible Reinforcement (Geosynthetics)						
a. precast concrete facing panels	<15 ft		15-30 ft		>30 ft	
b. cast-in-place facing	<15 ft		15-30 ft		>30 ft	
c. modular concrete block facing	<15 ft		15-30 ft		>30 ft	

Compiled by ________________________________
Address and/or Phone ________________________________

____

____

Please mail completed form to above address by October, 1997 or fax to (215) 895-1437.

STRESS DISTRIBUTION AND DEFORMATIONS IN MODULAR BLOCK FACED GRS WALLS SUBJECTED TO INCREASING SURCHARGE

FADZILAH SAIDIN, UNIVERSITY OF WASHINGTON, USA
R. J. RACE, KEYSTONE RETAINING WALL SYSTEM, USA
R. D. HOLTZ, UNIVERSITY OF WASHINGTON, USA

ABSTRACT

A verified numerical model based on a finite difference program FLAC was used to study the response of a 7.1m high modular block faced GRS wall to increasing surcharge load. Analyses were carried out for two geosynthetic reinforcement tensile moduli at a uniform spacing of 0.6m. The friction angle of the backfill was kept constant at 28° to represent a lower quality material. However, the dilation angles were assumed to be 0°, 10° and 20°. Analyses were also performed to investigate the effect of two types of reinforcement-facing connections on the response of the wall to increasing surcharge. Results indicated that at failure, the maximum tension in the reinforcement was well below its capacity and that failures were due to localized instability of the facing. It was also found that the type of connection at the facing did not have a significant effect on the response of the wall.

INTRODUCTION

Current design procedures for internal stability of GRS retaining structures are based on limit equilibrium or ultimate limit state concepts. Measurements on test walls and the fact that very few failures of well-designed and well-constructed GRS walls have occurred indicate that this approach is overly conservative (Bell et al. 1983; Rowe and Ho, 1993). Furthermore, this design approach does not consider deformations or interactions between the individual components of the wall system, and as a result, it cannot adequately describe the real behavior of reinforced soil walls.

In order to improve internal stability design procedures, reliable information on the internal stress-strain response of GRS structures is necessary. However, predicting the behavior of GRS retaining structures is difficult. Apart from external loading, the behavior of GRS structures is significantly affected by the complex interactions of the individual components of the wall system, namely the facing, backfill, reinforcement and foundation. Stresses and deformations in GRS walls prior to failure are also of great interest because they can validate design assumptions. The reinforcement for GRS walls is normally designed as the maximum force that the reinforcement needs to resist at failure. Questions arise whether this force is fully mobilized prior to failure and whether the reinforcement tensile modulus affects its mobilization. One of the ways to answer these questions is to load the wall to failure. This is hardly feasible due to the high cost involved, which is the reason why so little information is available in the literature on the stresses induced in GRS walls with load, especially at failure.

Numerical methods can be used to economically simulate the behavior of GRS wall systems once models are calibrated to observations on instrumented walls of similar configurations. One of the primary advantages of numerical technique is that parametric studies can readily be performed to explore the relationship between the behavior of the wall and the design parameters that affect its behavior (load, reinforcement, etc).

For this study, the numerical method we used was the finite difference program FLAC, a program which is efficient in modeling large strains (Itasca, 1993). Large strain analyses were appropriate in this case since the deformations of the soil and reinforcement due to the loads were often significant and analyses were carried out to failure. The study was conducted in two phases:

(1) Numerical models of GRS retaining structures were developed that were capable of reproducing instrumentation measurements on full scale walls
(2) Parametric analyses were performed using the developed numerical models to examine the influence of important parameters on the wall behavior.

The first phase, which involved modeling and verification of full-scale test walls, was carried out with acceptable results (Holtz and Lee, 1997; Lee, 1999; Lee, Holtz and Allen, 1999, Lee, 2000). For example, Lee (2000) showed that FLAC models adopted in the present study were capable of modeling with reasonable accuracy deformations and reinforcement strains observed in three FHWA test walls built in Algonquin, Illinois. The models also performed well in three large-scale GRS wall tests carried out at the Royal Military College of Canada. The present study is part of the second phase in which numerical models developed in Phase 1 were used to further investigate the behavior of GRS walls.

Verified numerical models were used to investigate the stresses in the reinforcement and the deformations induced in modular block-faced GRS retaining walls subjected to increasing surcharge loads. The model was also used to investigate whether the response was affected by the strength of the reinforcement. For this study, the reinforcement strength was represented as the tensile modulus at 5% strain. The effect of the dilation angles of the backfill was also studied because Lee (2000) found that the deflection of the wall facing was significantly affected by the value of the dilation angles used. Another important issue for segmental retaining structures is the connection to the facing. Since the behavior of GRS walls is affected by the components of the wall system, it is also important to see whether the results would be different if a different type of facing-reinforcement connection is used. This paper presents and discusses these analyses and their implications on our understanding of internal reinforcement behavior and wall design.

NUMERICAL SIMULATION

The Model Wall

The mesh used to model a typical generic GRS wall, 7.1m high, is shown schematically in Fig.1. The wall facing consisted of modular concrete blocks, 300mm thick, stacked on top of each other with a 3° batter. The height of each modular block was 200mm. The reinforcement consisted of eleven horizontal layers of geogrids, each having a length of 4.45m. The vertical spacing was uniform at 0.6m, which is equivalent to a reinforcement layer at every three blocks. A drainage layer consisting of 300mm thick crushed stone was placed behind the facing.

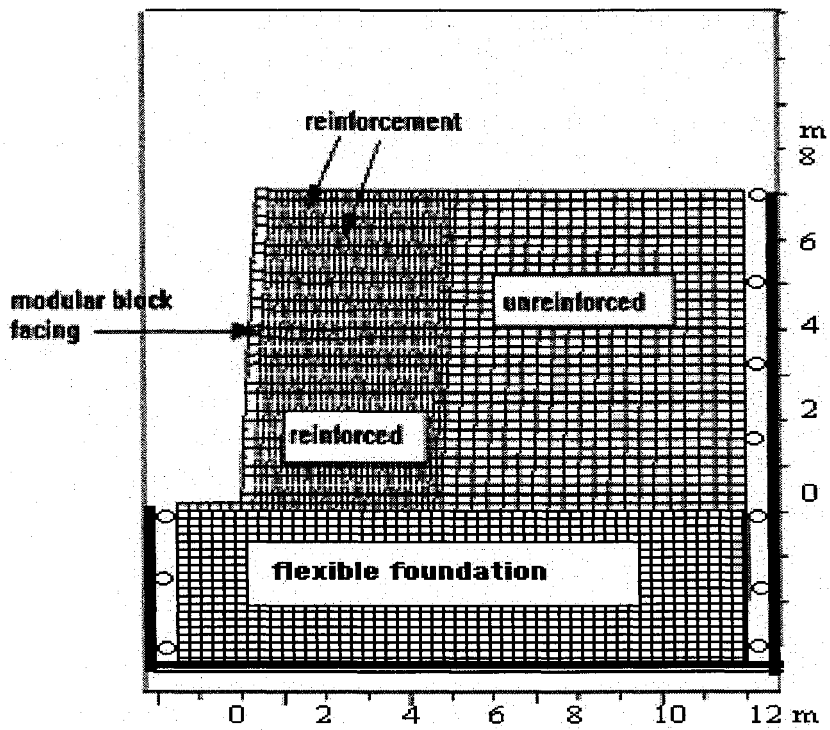

Fig.1: Generic wall (the foundation is not drawn to scale)

For the numerical model, the modular concrete block facing units were represented by linear elastic blocks separated by interfaces to allow movements to occur between the blocks at their common interfaces. The reinforcement was modeled as one-dimensional cable elements attached to the soil elements so that the cable elements developed forces along their lengths as the soil deformed. Elastic modulus properties of the reinforcement and the strength properties of the soil were assumed to describe the interaction between the cable elements and the soil elements. The reinforcements were divided into elements that coincided with the soil elements for convenience. The backfill was represented as plane strain quadrilateral soil elements with a nonlinear stress dependent stress-strain-strength behavior represented by the modified Duncan-Chang soil model (Duncan et al., 1980).

The model wall was constructed in lifts of 0.2m thickness. With each successive lift, an equilibrium condition was first established before new stresses were calculated. The vertical sides of the model wall were restrained horizontally (Fig. 1). A restraint in the vertical direction was imposed at a depth approximately equal to the height of the wall to simulate a flexible foundation.

Input Parameters

The backfill was assumed to be purely frictional with a constant internal friction angle of 28°. Lower strength backfill was selected to reflect the increasing trend to use locally available materials, but with a lower strength than ideal granular backfill. Because the backfill is hypothetical and actual test data was not available, three dilation angles of 0°, 10° and 20° were assumed. Analyses were performed using two reinforcement tensile modulus values of 320 kN/m and 640 kN/m, values that are typical of PVC coated flexible polyester geogrids. Two types of connections between the reinforcement and the facing blocks were assumed. One was a frictional connection that was modeled as cable elements with elastic properties of the reinforcement interacting with a frictional material having a friction angle of 55° and zero cohesion. The second type of connection was a fixed connection; it was modeled also as cable elements with elastic properties of the reinforcement interacting with the host medium consisting of grout having a friction angle of 10° and a cohesion of 5.5×10^3 kPa. For both types, the connection was assumed to be in effect through the full thickness of the facing blocks. The variables adopted in the study are summarized in Table 1.

Analysis

For analysis of effect of reinforcement tensile modulus, the dilation angle was assumed zero with frictional connection at the reinforcement-facing connection. For effect of the connection type, the reinforcement tensile modulus was kept constant at an arbitrarily chosen value of 640 kN/m. For the study on the effect of dilation angle, the reinforcement tensile modulus was also maintained at 640 kN/m and a frictional type of connection assumed. For the first study on the effect of reinforcement tensile modulus, the wall was subjected to increasing surcharge loads in increments of 10 kPa from an initial value of 0 kPa until “failure” occurred. Surcharge consisted of uniformly distributed horizontal loads that extended the full width of the wall to the edge of the backfill. Failure was assumed to have occurred when the relative displacement of the grid elements became so large that it caused mathematical instability and computation could not proceed. For the other two studies on the effect of connection type and dilation angle, the analyses were not carried to failure. Instead, the maximum surcharge found in the first analysis was applied. Response parameters investigated in this study were the average reinforcement tension at the reinforcement-facing connection, the maximum tension in the reinforcement and the maximum lateral displacements of the wall facing. The average reinforcement tension at the connection was calculated by averaging the tension values at four nodes in the vicinity of the connection. The maximum tension is the largest force along the length of the reinforcement.

Design variables	Values
Wall height	7.1m (constant)
Facing	
Density	2.0 Mg/m^3 (constant)
Bulk modulus	1.1x10^7 kPa (constant)
Shear modulus	1.0x10^7 kPa (constant)
Reinforcement	
Tensile modulus	320 , 640 kN/m
Vertical spacing	0.6m (constant)
Backfill	
Density	1.93 Mg/m^3 (constant)
Bulk modulus	6.7e^3 kPa (constant)
Shear modulus	3.3e^3 kPa (constant)
Duncan-Chang's parameters	k=450,r_f=0.7,n_d=0.5 (constant)
Poisson's ratio	0.25 (constant)
Friction angle	28^o (constant)
Cohesion	0 (constant)
Dilation angles	0^o, 10^o, 20^o
Drainage layer	
Duncan-Chang's parameters	k=1300,r_f=0.7,n_d=0.5 (const.)
Friction angle	50^o (constant)
Soil-reinforcement friction angles	28^o (constant)
Foundation	flexible
Reinforcement-facing connection	frictional, fixed
Surcharge	Increased in increments of 10 kPa

Table 1: Typical values of variables used in the study

RESULTS AND DISCUSSION

Effect of Reinforcement Tensile Modulus

For reinforcement tensile modulus of 320kN/m and dilation angle of 0°, the model failed at a uniform surcharge of 55kPa, suggesting that the maximum surcharge load before failure is between 50-54 kPa. A check on the deformed wall grids (Fig.2) showed that at a surcharge of 50 kPa, the blocks have separated and there is already a local instability at a height of about 3m. Recall that reinforcement was placed at every three blocks of facing which were arranged in a tier (Fig.1), at this level failure occurred at the blocks where there was no reinforcement attached.

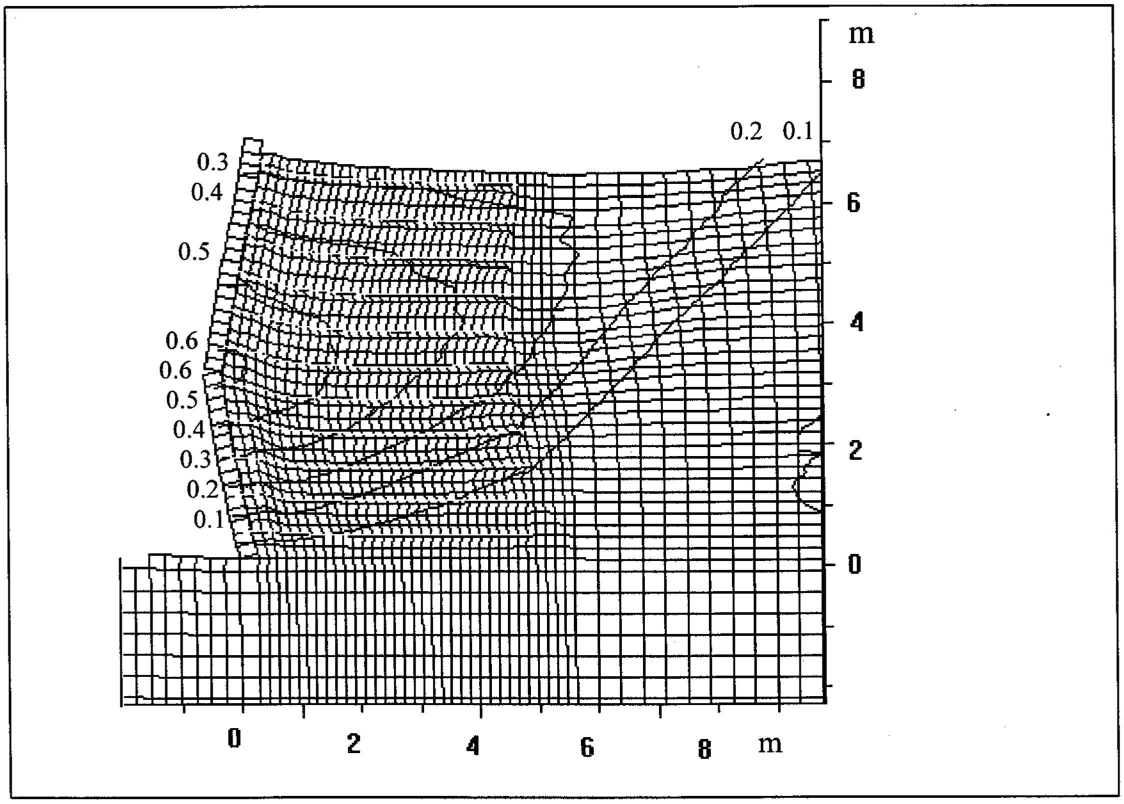

Fig.2: Deformed shape at surcharge of 50kPa with contours of horizontal displacement in m

A plot of the tension values with surcharge (Fig.3) yielded an approximately linear variation of the tension at the facing-reinforcement connection with load. Similar results were obtained for the maximum tension in the reinforcement. The average tension at the facing connection is lower than the maximum tension in the reinforcement. The plots also showed that even at the point of failure, the full capacity of the reinforcement has not been fully mobilized. In fact, it is still below the yield value of the reinforcement divided by a factor of 1.5. Failure occurred due to high shear stress in the blocks causing the blocks to separate.

The relationship between the reinforcement tension and surcharge for reinforcement tensile modulus of 640 kN/m is shown in Fig.4. The plots showed that the relationship for tension at the reinforcement-facing connection followed an approximately bilinear relationship. The behavior is similar to that for reinforcement tensile modulus of 320 kN/m (Fig. 3) for surcharge up to about 40 kPa, above which, the slope of the line changed. This indicated a higher increase in tension with surcharge for surcharges in excess of 40 kPa.

The plot of the maximum tension showed that the relationship is approximately linear for surcharges up to 50 kPa, also similar to Fig. 3. The slope of the line is slightly less, indicating that the increase in tension with surcharge is less for the higher modulus reinforcement. However, the difference in maximum tension values at a surcharge of 50 kPa is less than 10%, which is rather insignificant compared to the 100% increase in modulus of the reinforcement. Beyond the surcharge of 50 kPa, the relationship became nonlinear in the case of the higher modulus reinforcement. The change in response above a surcharge of 40 kPa for tension at the reinforcement-facing connection, and 50 kPa for maximum tension suggests a strain hardening of the reinforcing system.

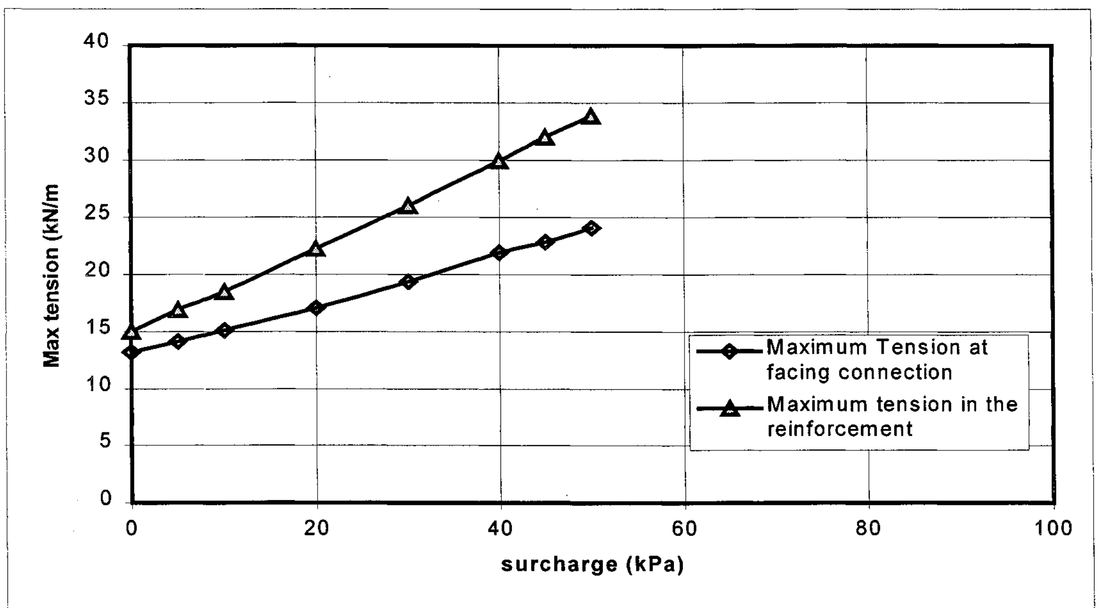

Fig. 3: Maximum tension in the reinforcement with surcharge
for reinforcement tensile modulus of 320 kN/m

The results of the analyses for effect of reinforcement tensile modulus are summarized in Table 2. It was found that the maximum tension at failure is approximately 34kN/m and 45kN/m for reinforcement tensile modulus of 320kN/m and 640kN/m, respectively. These forces are well below the ultimate tensile capacity of the reinforcement, which have the yield values of 64kN/m and 145kN/m respectively. Increasing the tensile modulus from 320kN/m to 640kN/m almost doubled the surcharge load that can be carried by the wall with everything else remaining constant. However, the maximum tension increased by only about 10 kN/m suggesting that there is some form of load transfer to the reinforcing system, which is stronger in the second case.

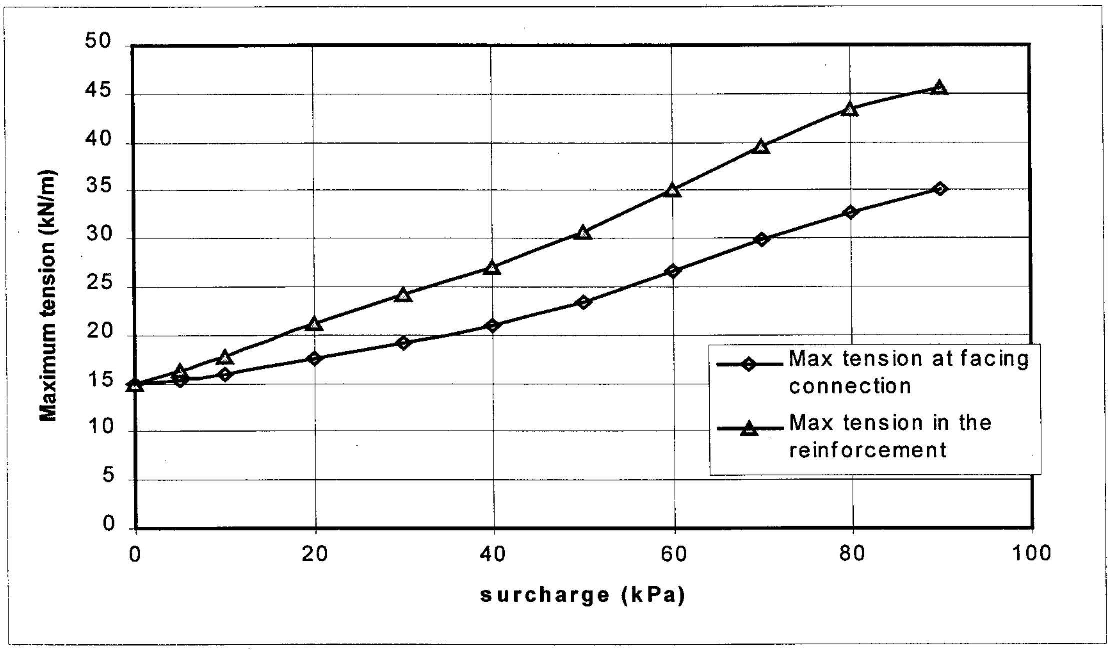

Fig. 4: Maximum tension in the reinforcement with surcharge for reinforcement tensile modulus of 640 kN/m

Reinforcement tensile modulus	320 kN/m	640 kN/m
Maximum surcharge load	50 kPa	90 kPa
Tension at connection at maximum surcharge load	24 kN/m	35 kN/m
Maximum tension at maximum surcharge load	34 kN/m	45 kN/m
Yield value of reinforcement	64 kN/m	145 kN/m

Table 2: Comparison for effect of reinforcement tensile modulus

The effect of reinforcement tensile modulus on wall displacement was also investigated. Fig. 5 shows the maximum displacement normalized by the height of wall versus surcharge for the reinforcement tensile modulus of 320 kN/m and 640 kN/m. The plot shows, as expected that the displacement is significantly lower in the case of the stronger reinforcement.

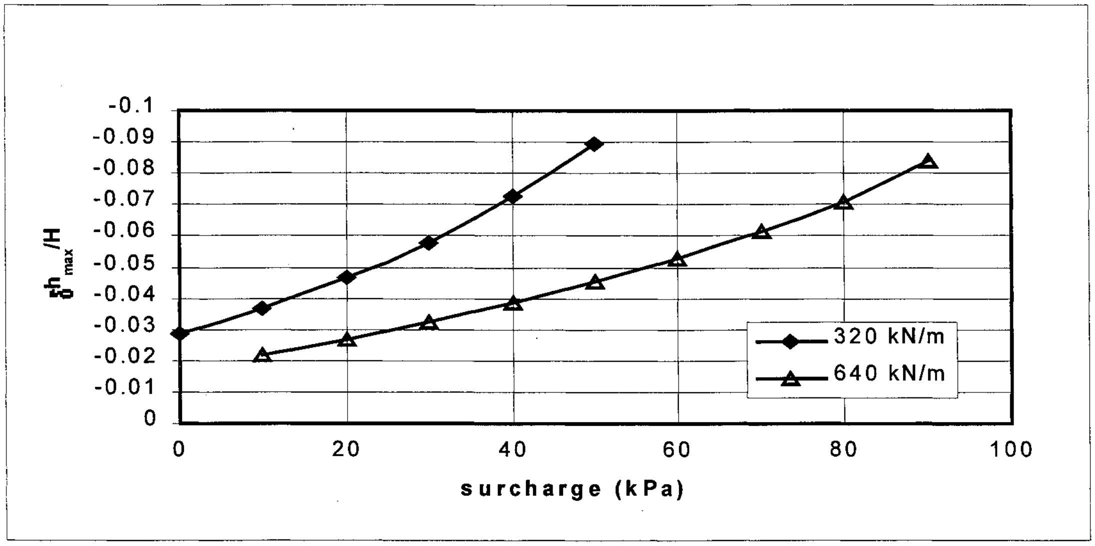

Fig. 5: Normalized maximum displacement at the facing with surcharge at different reinforcement tensile modulus

Effect of Connection Type

The results for tension in the reinforcement with surcharge are shown in Fig. 6. For tension at the reinforcement-facing connection, the plots showed that even though the fixed connection showed lower tension values, the decrease is not appreciable. For the maximum tension in the reinforcement, there is hardly any difference in the results. As shown in Fig. 7, the fixed connection also did not have a significant effect on displacement although it tends to predict slightly less deflection at higher surcharges.

Effect of Dilation Angle

Fig. 8 showed the effect of dilation angle on the maximum tension in the reinforcement at the facing connection. The dilation angle resulted in higher values of maximum tension at reinforcement-facing connection for lower surcharges but made no significant contribution at higher surcharges. There is only a slight increase in tension values between the dilation angles of 10^o and 20^o.

For maximum tension in the reinforcement (Fig. 9), the effect of dilation angle is not apparent. There is no obvious trend in the relationship though for lower surcharges (0 to 40kPa), it seems to indicate that increasing dilation angle increases the maximum tension in the reinforcement while at higher surcharges (70 to 90kPa), it has the opposite effect.

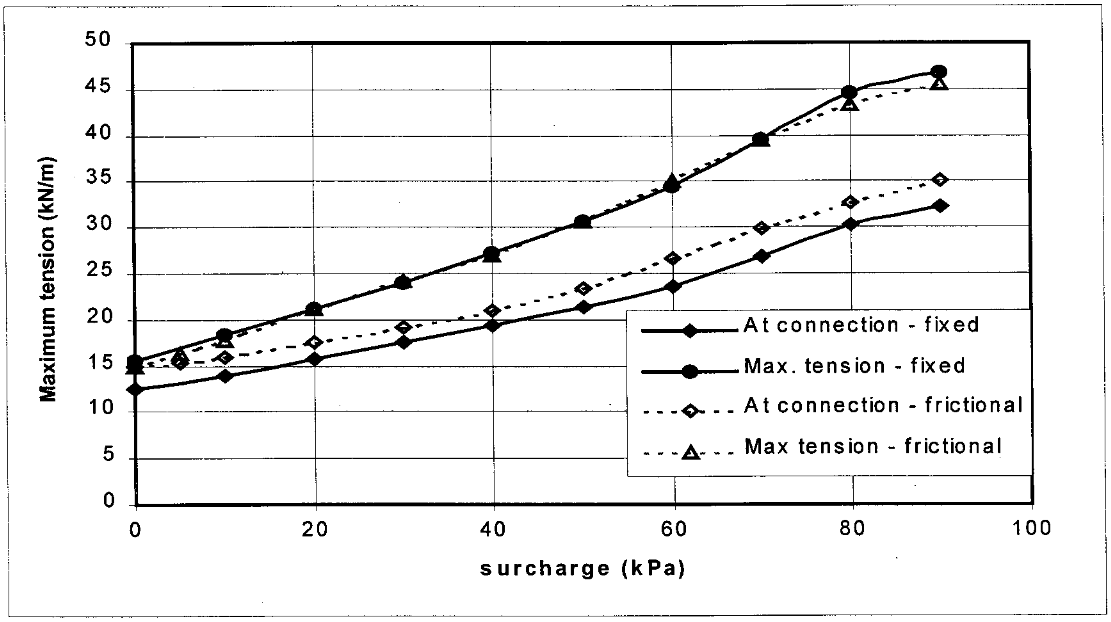

Fig. 6: Maximum tension and surcharge with types of connection

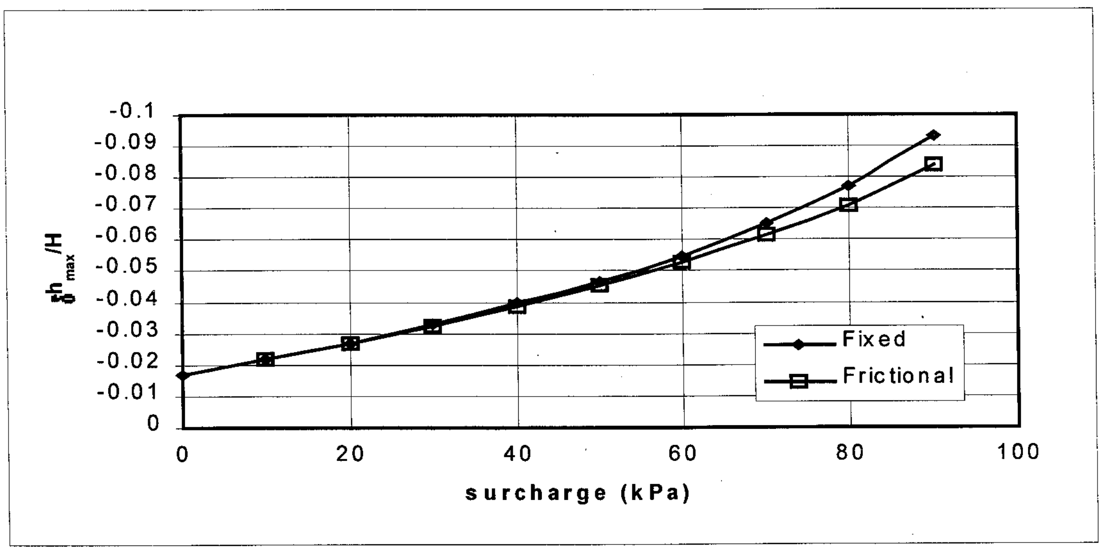

Fig.7: Normalized maximum displacement at the facing and surcharge with types of connection

For maximum displacement at the facing (Fig. 10), the effect of dilation angle is very significant at higher surcharges beyond 30 kPa. The dilation angle reduces the maximum deflection appreciably, the reduction increases as the surcharge increases. At surcharge in excess of 70 kPa, the effect of the dilation angle is more when the dilation angle is increased from 0° to 10° than from 10° to 20°. From these results it can be seen that the effect of dilation angle should be taken into account in predicting deflections of the facing.

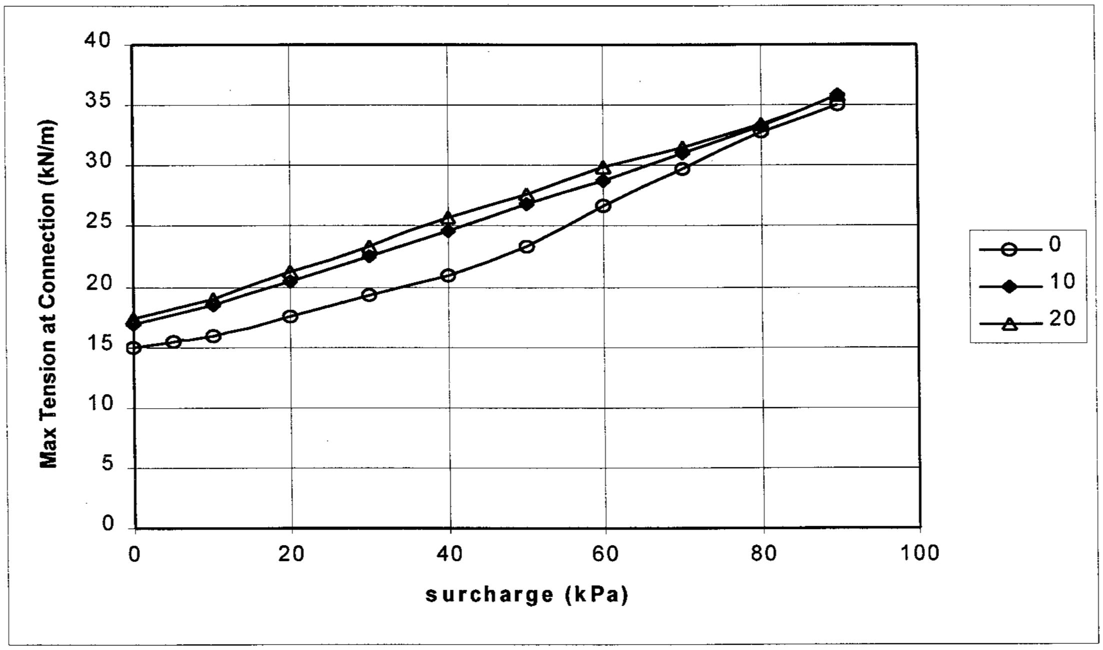

Fig. 8: Maximum tension at reinforcement-facing connection
with surcharge for various dilation angles

Implication for Design

The above findings suggest that in designing segmental GRS walls, apart from designing for the strength of the reinforcement, it is also important to check for the strength of the modular facing itself. The strength of the modular block facing is more critical unless reinforcement is attached to all the block facings as for example in the case of the concrete panel facing. The findings also point to the greater potentials of segmental GRS walls constructed using lower strength backfill to sustain greater loading or having greater heights, by having stronger reinforcing systems. For a lower strength backfill, this can be in the form of greater reinforcement density or strength, or a combination of the two. The greater displacement experienced by segmental walls can also be reduced by having a stronger reinforcing system.

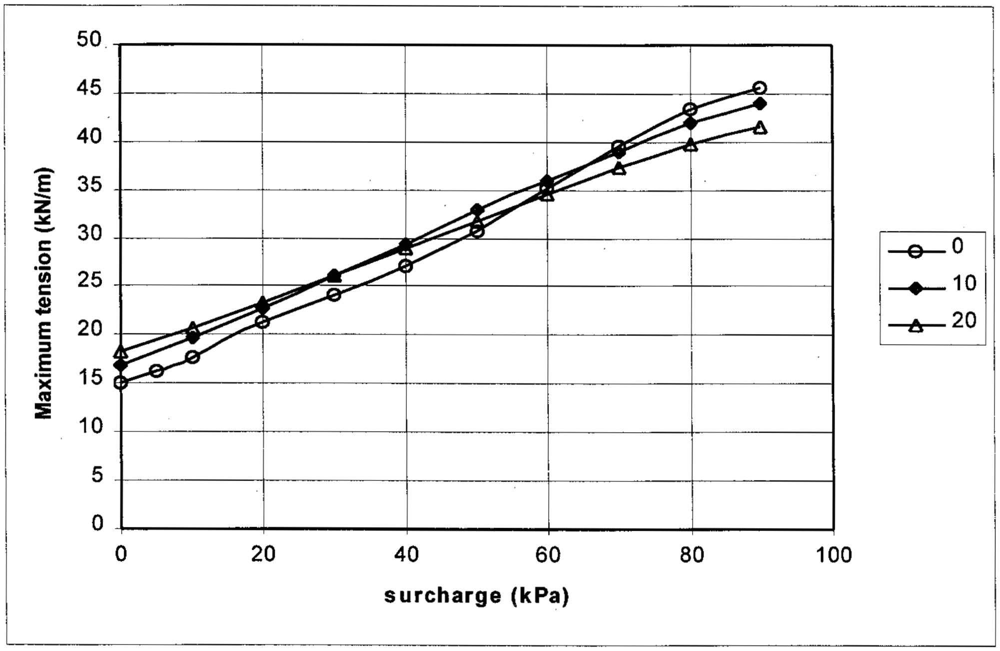

Fig. 9: Maximum tension in the reinforcement
with surcharge for various dilation angles

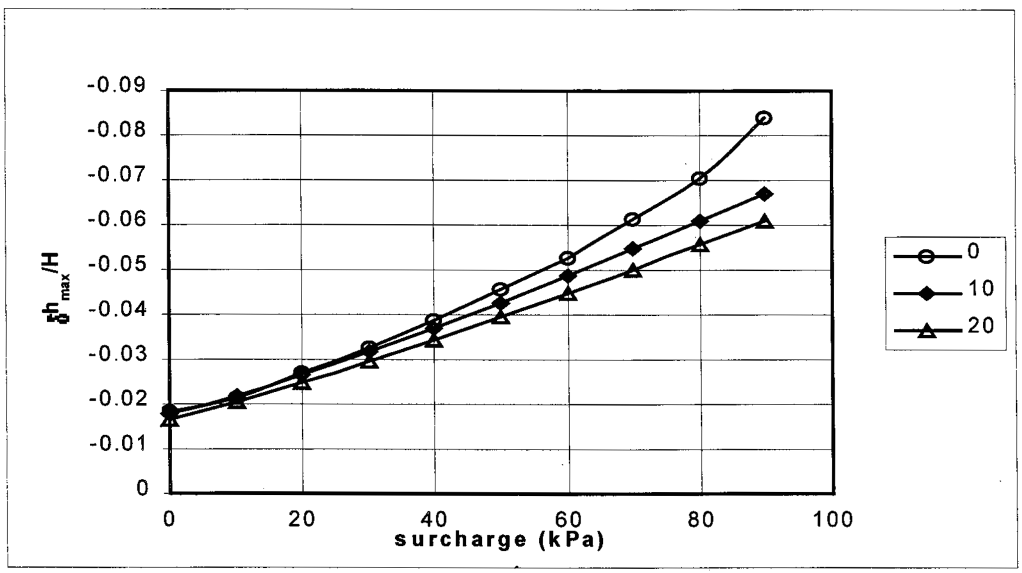

Fig. 10: Normalized maximum deflection with surcharge
for various dilation angles

CONCLUSIONS

Based on the results obtained, the following conclusions can be drawn:

1. The design capacity of the reinforcement is not fully mobilized even though the wall sustains high surcharges. For the wall configuration studied, failure of the wall was due to local excessive deflection of the modular block facing rather than pullout or rupture of the reinforcement be at the connection or in the reinforced soil mass. The wall failed at reinforcement tension values well below the yield values.
2. The connection capacity is not a critical issue for the wall configuration studied. The wall failed due to local failures that occurred at the blocks where reinforcement was not attached. The wall failed well before the maximum capacity of the connection can be mobilized.
3. Reinforcement tensile modulus has a significant effect on the amount of load that the wall can carry. It also has a significant effect on the maximum displacement induced at the wall facing.
4. The types of facing connection as considered in this study do not have a significant influence on the behavior of GRS walls.
5. The effect of dilation angle is significant in predicting the maximum deflection at the facing and should be taken into account to ensure its accurate prediction.

REFERENCE

Bell, J. R., Barrett, R. K., and Ruckman, A. C., 1983, "Geotextile Earth-Reinforced Retaining Wall tests: Glenwood Canyon, Colorado," *Transportation Research Record 916*, Washington, DC, pp. 59-69.

Duncan, J. M., Byrne, P., Wong, K. S. and Mabry, P., (1980), "Strength, Stress-Strain and Bulk Modulus Parameters for Finite Element Analyses of Stresses and Movement in Soil Masses", *Geotechnical Engineering Report* No. UCB/GT/80-01, University of California, Berkeley, 70p.

Holtz, R. D. and Lee, W.F. (1997), "Summary Report on Geosynthetic Reinforced Wall Analysis Phase II" Washington State Department of Transportation WSDOT, Olympia, WA.

Itasca Consulting Group, (1993), *Fast Lagrangian Analysis of Continua Version 3.2,* Itasca Consulting Group Inc., Minneapolis, MN, Vol. I, II, III.

Lee, W. F., (1999), "Distribution of Lateral Earth Pressure and Reinforcement Tension Inside the Geosynthetic Reinforced Retaining Walls", *Proceedings Geosynthetics '99*, Boston, MA, Vol. 2, pp.651-660.

Lee, W. F., (2000), *Internal Stability Analyses of Geosynthetic Reinforced Retaining Wall*, Ph.D. Dissertation, University of Washington, , Seattle, WA 98195, USA. pp.355
Lee, W.F., Holtz, R. D. and Allen, T. M. (1999), "Full Scale Geosynthetic Reinforced Retaining Walls: A Numerical Parametric Study " *Proceedings Geosynthetics '99*, Boston, MA, Vol. 2.

Rowe, R.K and Ho, S.K. (1993), "Keynote Lecture: A Review of the Behavior Reinforced Soil Walls, *Earth Reinforcement Practice*,. Ochiai, Hayashi, and Otani, eds. Balkema, Rotterdam, pp. 801-830.

CORPS OF ENGINEERS CRITERIA FOR MSE WALLS AND REINFORCED SOIL SLOPES

NEIL T. SCHWANZ, PE, US ARMY CORPS OF ENGINEERS, ST. PAUL DISTRICT, USA
MARK S. MEYERS, PhD, PE, UNIVERSITY OF WISCONSIN-PLATTEVILLE, USA
RYAN R. BERG, PE, RYAN R. BERG & ASSOCIATES, USA
JAMES G. COLLIN, PhD, PE, THE COLLIN GROUP, USA

ABSTRACT

The US Army Corps of Engineers (USACE) is typically cautious of accepting new technologies for use on USACE projects. A long project design life and applications that often involve special considerations, such as waterfront usage and potential for loss of life, combine to create a desire to design using methods that are time proven. USACE is recognizing that the continuing use of mechanically stabilized earth (MSE) wall and reinforced soil slope (RSS) structures is providing a history of performance that demonstrates these structures can achieve a long, safe design life. Design guidance and guide specifications for MSE and RSS structures have been prepared by USACE in response to the expanding library of performance data, the potential for significant retaining wall cost savings, and the potential use of steeper slopes to reduce real estate costs. The design guidance summarizes the design procedures and criteria for different applications and modes of failure; the guide specifications provide guidance for use by designers and specification engineers during the development of plans and specifications for USACE projects. Industry experience was used in the development of this guidance through the use of two peer reviewers funded by the Geosynthetic Materials Association (GMA) and the National Concrete Masonry Association (NCMA). This paper discusses the USACE design guidance and the special considerations that need to be addressed when using MSE walls and RSS structures on USACE projects. This paper is directed towards both government and private designers and specifiers of materials and methods for these structures.

INTRODUCTION

Mechanically stabilized earth (MSE) walls and reinforced soil slope (RSS) structures have readily become accepted construction for use on private and many public funded projects. The use of these structures on publicly funded projects appears to vary between agencies. The Federal Highway Administration (FHWA) and many State Departments of Transportation (DOTs) have widely used MSE structures on a variety of projects. The use of MSE structures by the US Army Corps of Engineers (USACE) to date has been minimal, but appears to be increasing with an expanding experience base. The continuing use of these structures is providing a history of performance, helping to assure the designers that these structures can achieve a long design life.

The use of segmental retaining wall (SRW) systems has proven to be very cost effective when compared to traditional cast-in-place gravity walls or cantilever or anchored sheetpile structures (Koerner (1999)). It is this economical aspect that has led to the rapidly expanding use of these wall systems. The combined efforts of private industry and the transportation departments of federal and state governments has resulted in sufficient past and ongoing research and testing such that these walls can be designed and constructed with confidence. The FHWA has a significant amount of experience in MSE wall construction and has completed much research in support of these walls on federally funded projects. Much of this experience has led to the use of MSE walls in nearly every type of application where conventional earth retaining structures have been used in the past. Experience in waterfront projects will continue to expand the potential use of these walls to many USACE civil works projects.

USACE Missions/Projects

USACE supports a number of different missions for the military and for civil works. USACE is the executive agent for contract and construction management of Army and Air Force facilities and infrastructure construction throughout the world. Traditional USACE projects for civil works applications include navigation, flood control, water supply and emergency response for disaster declarations. These missions often involve construction associated with: locks and dams; dredging of harbors and channels; dams (earth, rockfill, concrete); levees; floodwalls; channels; etc.

Retaining structures are required for a number of differing applications. Besides retaining earthen materials for grade separation, structures often retain floodwaters caused by rain, snowmelt or wind generated waves. In a channel environment, retaining walls may be exposed to turbulent as well as non-turbulent flow conditions. These flows can carry various types of debris or ice. Approach walls on hydraulic structures “train” inflow so that passage of water will be as efficient and economical as possible. Guidewalls on lock facilities aid in aligning incoming or outgoing navigation vessels. These few examples of different applications for walls used on USACE projects identify the varying uses that are typical of USACE projects, but atypical of most other public agencies.

Design Issues

The differing functions of USACE project walls, as noted above, often require designing for a number of different load and impact conditions. Since many walls are used in wet environments, differing water conditions require designs that accommodate flow into or out of the bank. Walls may be exposed to normal, or usual, water levels, but must also be designed for unusual load conditions that may be applied by very high or very low water levels. Recognizing that some load conditions are rare, USACE criteria is set accordingly by accepting more risk for those design cases through the use of lower minimum acceptable factors of safety.

In addition to different load cases and water-related concerns, USACE projects are typically designed for a long project life. A 100-year design life is often sought for flood control projects and a 50-year life can be expected for many navigation structures. MSE structures, used for these applications would also be expected to perform for those lengths of time. If walls have to be replaced prior to reaching the project design life, replacement costs need to be considered in the economic analyses. This could affect the decision as to the type of wall used.

Another consideration for use of MSE structures on USACE projects is the risk associated with failure of a critical project component. Failure of an approach wall on a navigation structure could close a river to traffic, resulting in significant economic loss. Failure of a floodwall could induce significant flood damages with the potential for loss of life. Failure of a wall used for an embankment dam raise could result in overtopping, and potential dam break, putting many lives at risk.

The number of design issues that must be considered for USACE projects has likely contributed to a slower acceptance of MSE applications than has been experienced by other public agencies. The need to address these design issues led to the development of USACE Engineering Circular (EC) EC 1110-2-311, *Design of Mechanically Stabilized Earth Walls and Reinforced Soil Slopes* (USACE, 2000). USACE (2000) is a design guidance document addressing MSE walls (specifically for SRW facing units and geosynthetic soil reinforcement) and geosynthetic reinforced soil slopes for USACE applications. Design considerations for MSE structures have been combined with USACE design criteria. In addition to the design document, guide specifications have been prepared for construction of segmental retaining walls and reinforced steepened slopes.

DESIGN CRITERIA FOR MSE WALLS

Design Methods

The current state-of-the-practice for designing MSE SRWs for private industry applications is presented in NCMA (1997), and for transportation structures in FHWA (1997) and AASHTO (1996). These design procedures may be performed using the NCMA's SRWall software (Earth Improvement Technologies and Bathurst (1997 and 2000)) and the FHWA's MSEWall design software (ADAMA, 1998), respectively. Koerner and Soong (1999) have compared FHWA and NCMA design methods, concluding that: the FHWA approach is the more conservative of the two procedures; both design procedures are considered adequate for current MSE SRW projects; and the selection of which method to use is site-specific or owner/specifier specific. Either method is considered acceptable for use on USACE projects. The limitations of the NCMA and FHWA design procedures, with respect to USACE projects, include: the documents do not address the varying load cases, including water effects, that are typical of USACE projects; and, slope stability requirements vary depending on the design conditions required to be analyzed. Most standard USACE design requirements are applicable to the design of SRWs. The USACE EC 1110-2-311 (USACE, 2000) design guidance is intended to supplement NCMA (1997) and FHWA (1997) for use on USACE applications.

Internal and Local Stability of SRW Units

NCMA (1997) identifies internal stability analyses as that necessary to *"... examine the effectiveness of the geosynthetic reinforcement in holding the reinforced soil mass together so the geosynthetic layers and soil function as a monolithic block."* The internal analyses address: tensile overstress in the geosynthetic reinforcement; pullout of the reinforcement through the reinforced soil mass; and internal sliding along reinforcement layers.

Local stability evaluates the column of SRW units. These analyses consider: facing connection between the SRW units and the reinforcement; bulging of the SRW units between reinforcement layers; and the maximum unreinforced height of the SRW units at the top of the wall. The procedures for these analyses are discussed in detail in NCMA (1997). These analyses are based on conditions that do not involve partial submergence or forces due to seepage. An assumption that is often made during design of SRWs that are fully or partially inundated is that the most critical load condition for these analyses will occur after the submerged period when moist soil unit weights may be higher than normal and are not offset by uplift conditions. In waterfront applications, care should be taken to assure drainage aspects have been fully addressed and that assumed pore water pressures reflect the field conditions to be encountered.

External Stability

External stability evaluates the minimum length of geosynthetic reinforcement necessary to satisfy base sliding, overturning and bearing capacity factors of safety. The SRW units and the reinforced soil zone are treated as a rigid body and are analyzed following the same procedures as for rigid gravity walls except for the bearing capacity analyses. FHWA (1997) states *"Due to the flexibility and satisfactory field performance of MSE walls, the adopted values for the factors of safety for external failure are in some cases lower than those used for reinforced concrete cantilever or gravity walls. For example, the factor of safety for overall bearing capacity is 2.5 rather than a higher value, which is used for more rigid structures. Likewise, the flexibility of MSE walls should make the potential for overturning failure highly unlikely. However, overturning criteria (maximum permissible eccentricity) aid in controlling lateral deformation by limiting tilting and, as such, should always be satisfied."* This empirical evaluation appears appropriate for USACE applications.

The external stability analyses utilize active lateral earth loads on the driving side. Passive resistance is neglected in the NCMA and FHWA procedures due to the potential for removal of these soils resulting from erosion or unforeseen excavation. Due to the relatively shallow depth of embedment used for many MSE walls, the passive resistance is generally small and neglecting this resistance is not overly-conservative. The selection of using the Coulomb earth pressure theory for determining the lateral earth pressure is partially consistent with the USACE approach for evaluating the sliding stability of concrete structures. USACE procedures utilize the Coulomb earth pressure theory and the General Wedge method to estimate the at-rest earth pressures, used for design of cast-in-place structures, by applying a strength mobilization factor to the shear strength of the backfill soil. These loads are then applied to the retaining wall, generally neglecting wall friction. The Coulomb earth pressure theory, as applied in NCMA (1997), is considered acceptable by USACE for the design of both reinforced and unreinforced SRWs.

Sliding, overturning and bearing capacity of retaining structures is discussed in USACE (1989). This manual provides detailed guidance for designing concrete gravity and T-type cantilever reinforced concrete retaining walls subject to hydraulic loading. The factors of safety recommended in USACE (1989) expand beyond those recommended in NCMA (1997) or FHWA (1997) to account for differing loading and foundation conditions. The stability criteria for sliding, overturning, and bearing capacity analyses for MSE wall design utilizing SRWs, as recommended in USACE EC 1110-2-311(2000) are summarized in Table 1. Values for the usual load condition are described in USACE (1989) as "*The backfill is in place to the final elevation; surcharge loading, if present, is applied (stability should be checked with and without the surcharge); the backfill is dry, moist, or partially saturated as the case may be; any existing lateral and uplift pressures due to water are applied. This case also includes the usual loads possible during construction which are not considered short-duration loads.*" Unusual loading is considered to be the same as the usual "*except the water table level in the backfill rises, for a short duration, or another type of loading of short duration is applied; e.g., high wind loads, equipment surcharges during construction, etc.* Earthquake loading is also the same as the usual load condition "*with the addition of earthquake-induced lateral and vertical loads, if applicable; the uplift is the same as for (the usual load case).*" Use of these values for flexible SRW structures have not been fully researched, but appear reasonable until further investigations or field experience is available.

Due to the flexible nature of MSE walls, computations for bearing capacity differ from those recommended for rigid structures. Instrumented MSE walls indicate that the stress distribution along the base of the walls can be reasonably modeled using a Meyerhof-type stress distribution. A Meyerhof-type stress distribution assumes that loading is applied uniformly over the effective base width. Bearing capacity factors for embedment and ground slope are applied to the general bearing capacity equation, but factors for base tilt (MSE walls are generally constructed with no base tilt) and load inclination are not included. Lack of inclusion of the load inclination factor provides a reasonable basis for USACE adopting the FHWA (1997) bearing capacity design factor of safety of 2.5, for the usual loading condition, rather than the bearing capacity factor of safety of 2.0 recommended for MSE structures in USACE (1989).

Table 1. Sliding, Overturning and Bearing Capacity Stability Criteria (USACE, 2000).

Loading Condition	Sliding Factor of Safety	Overturning Criteria Minimum Base Area in Compression		Minimum Bearing Capacity Safety Factor
		Soil Foundation	Rock Foundation	
Usual	1.5	100%; $e \leq B/6$	75%; $e \leq B/4$	2.5
Unusual	1.33	75%; $e \leq B/4$	50%; $e \leq B/3$	2.0
Earthquake	1.1	Resultant within base	Resultant within base	≥ 1.0

Global and Compound Stability

Global stability refers to the overall slope stability analysis involving the wall or wall system. Compound stability is a slope stability analysis where the failure surface passes through both the reinforced and unreinforced fill (Berg et al. 1989). The extensible nature of the reinforcement and the integral manner in which it is placed in the backfill creates a reinforced soil mass that can sustain minor deformations. A practice that has been used in the past to model the reinforced soils, for the purposes of analyzing slope stability, and perhaps may be used [incorrectly] by some designers today, was to assign an artificially high shear strength to the entire reinforced soil mass. The philosophy behind this methodology was that search routines used in locating the critical failure surface would not find critical surfaces that may have passed through or within what was perhaps perceived as a zone of high shear strength soil due to the inclusion of the reinforcement. This procedure, however, does not evaluate those potential failure surfaces passing between or through the reinforcement layers, which may have lower factors of safety against slope stability failure. Instead, both global and compound slope stability should be modeled using slope stability software that has the capability to include reinforcement in the model as discrete reinforcing elements.

The wall designer needs to understand the characteristics of the slope stability software and how it computes the factor of safety. Some slope stability programs compute the factor of safety by applying the resisting forces from the reinforcement as a resisting moment; other programs will treat the resisting force as a reduction to the driving moment. If the program does not apply the iterated factor of safety to the reinforcement strength, the allowable tensile strength (i.e., long-term strength reduced by a factor of safety) of the reinforcement should be used in the model. If the program does apply the computed factor of safety to the reinforcement, the long-term strength may be used.

The influence of water on global and compound stability can be significant and must be considered to the same extent that is routinely given to USACE projects (USACE, 1970; USACE, 1978). Table 2 presents and summarizes the minimum required factors of safety, as presented in EC 1110-2-311 (USACE, 2000), for various design conditions. These factors of safety are considered applicable for walls designed in conjunction with embankment dams or along rivers or streams. Walls designed in conjunction with other uses (i.e. grade control structures; wingwalls; landscaping applications; etc.) should also follow this criteria. Levee stability criteria would govern for most design projects and dam stability criteria should be followed for walls that may be considered critical. Such projects would include instances where failure would involve loss of life or significant economic loss. Discussions on appropriate shear strength parameters to use for the differing design conditions are discussed in USACE (1970 and 1978).

Table 2. Slope Stability Minimum Factors of Safety (USACE, 2000).

Design Condition	Dam Stability Factor of Safety (min)	Levee Stability Factor of Safety (min)
End of Construction (EOC)	1.3	1.3
Sudden drawdown from max. pool for dams or from significant saturation elevation on levees	1.0	1.0
Sudden drawdown from spillway crest or top of gates	1.2	N/A
Intermediate river stage	N/A	1.4
Steady seepage (SS) with max. storage pool	1.5	N/A
Steady seepage with surcharge pool for dams or from full flood stage for levees	1.4	1.4
Earthquake (EOC; SS)	1.0	1.0

The NCMA and FHWA design procedures both include a seismic coefficient method for a pseudo static analysis. NCMA (1998) provides a detailed discussion of the revised equations in the design procedure. Both design procedures base the seismic coefficient on an "A value", which is the pseudo acceleration with a 10% probability of exceedance in 50 years. The NCMA manual stipulates that the seismic coefficient method is only applicable for a value of A less than or equal to 0.4. If the A value is beyond this stated limit, a response spectrum (dynamic) analysis is recommended. With the FHWA procedure, it is recommended that if the seismic coefficient is 0.29, a seismic design specialist should review the stability and potential deformation for the structure. If the structure could cause hazardous conditions related to loss of human life, appreciable property damage, disruption of lifeline services, or unacceptable environmental consequences, then the design requirements in USACE (1995), which includes more stringent requirements for response spectrum or time-history analyses, should be followed.

Drainage

Surface water and pore water pressures can be detrimental to the internal stability when destabilizing seepage forces are present. The current design procedures for SRWs assume completely drained conditions; this assumption affects all modes of failure. Seepage forces, in the case of a sloping phreatic surface, will increase the lateral loading on the blocks, while at the same time reducing the pullout resistance of the geosynthetic reinforcement. The resulting seepage conditions will have an effect on the wall stability, thereby illustrating that drainage of the reinforced backfill is very important to properly constructed SRWs. All walls should include a minimum 12 inches of gravel drainage aggregate behind the facing elements.

For typical applications in upland areas, the drainage requirements are easily met. Open graded gravel is often placed for drainage in all soil types without consideration for filter criteria. Without any significant flow across the soil/drain interface, there is no mechanism for deterioration of the structure.

For waterfront applications, there is commonly a strong gradient near the water body. Along rivers and reservoirs, the case of rapid drawdown imposes the most critical loading for drains. For waterfront applications, design considerations for drainage and filters become much more important than for typical commercial applications.

Redundancy in drainage is necessary for critical applications. A perforated pipe at the toe of the wall (interface between retained backfill and reinforced backfill) may be used to reduce water levels in the infill soil. Additionally, the reinforced fill should not create resistance to drainage of the retained fill; therefore, it is recommended that the reinforced fill have a higher permeability than the retained fill. Another design consideration is the permeability of the geosynthetic reinforcement when used in projects that may be adversely impacted by infiltration and groundwater seepage. Geotextiles, if used for reinforcement, should be designed with a permeability greater than that of the reinforced soil so water flow within the reinforced fill is not impeded.

Saturation levels in the reinforced fill for external, global, and compound stability analyses should be determined following the procedures for dams (USACE, 1986) and levees (USACE, 1978). The derivation of the equations for internal stability tacitly assumes that a phreatic surface does not exist within the reinforced fill. It is recommended that drainage be designed to minimize horizontal seepage forces within the reinforced fill and facing materials.

To avoid loss of backfill through the blocks, the backfill material immediately behind the blocks usually consists of clean gravel. The gravel is predominantly in the ½ to ¾ inch size range to provide satisfactory retention when considering movement through block gaps that may form from settlement or from poor construction practice. The gravel, however, does not retain most soils and requires a filter at the interface between the drainage and reinforced fills. Due to the difficulty in maintaining a uniform thickness of near vertical layers of filters, geotextile filters become an attractive option for SRWs.

Walls constructed in areas where drains will frequently be active should be designed with consideration of clogging potential of geotextile filters. The appropriate geotextile should be used for the project soil conditions; the apparent opening size and percent open area should be important design considerations (Holtz, et al. 1997).

Ice and Impact Conditions

Ice expansion on lakes has been reported to move blocks laterally by impinging on the wall face. Ice loads can be estimated in accordance with USACE (1999). In addition to expansion, ice may adhere to the blocks and pull them out of alignment with changing reservoir levels. The following should be considered: water/ice levels near the top of the wall (little confining stress on the blocks) and reservoirs that are regulated in the winter so that water levels fluctuate when the ice sheet is bonded. Also, ice sheets driven by wind effects might impact walls causing movement of blocks.

Little information is available regarding the effects of impact loads on the face of SRWs. It can be envisioned that blocks can be displaced or broken by impacts from vehicles, ice or debris and that solid blocks would be more resistant to damage from impacts than hollow blocks. The wall designer should consider the potential for impact damage when specifying SRW units.

Cold Regions

Walls designed for use in cold regions need to address block durability and foundation treatment in frost zones. Freeze-thaw damage is being studied by the Minnesota DOT, FHWA and NCMA. Freeze-thaw damage in concrete is aggravated by saline water, such as in coastal applications or due to road deicing chemicals. Wall designers should consult FHWA/AASHTO or NCMA criteria for the most recent required material specifications for blocks. The current block durability requirements in American Society for Testing and Materials (ASTM) Designation C 1372 are default for warm weather climates; some state DOTs may have standard specifications for block durability requirements that are more appropriate to their climate. In the absence of specific information, Table 3 provides criteria for inclusion in project specifications. The above studies have determined that increasing the concrete compressive strength of the blocks, decreasing the allowable absorption of the block materials, and spraying the surface of the blocks with a sealer to reduce absorption, may reduce the rate of degradation.

DESIGN CRITERIA FOR REINFORCED SOIL SLOPES

Incorporating reinforcement in a soil slope is not a new procedure and has been used on many projects applying current design methods (Holtz, et al. 1997). Use of reinforcement can greatly

Table 3. Suggested SRW Unit Material Requirements for Cold Climates (USACE, 2000).

Testing Procedure	No Freezing	Freezing – No Deicing Salts	Freezing – Use of Deicing Salts
Minimum 28-day Compressive Strength (ASTM C 140)	28 MPa (4000psi)	28Mpa (4000 psi)	40 Mpa (5800 psi)
Maximum Moisture Absorption Rate (ASTM C 140)	7%	5%	5%
Freeze-Thaw Durability (ASTM C 1262)	None	Less than 1% weight loss after 150 cycles for 5 of 5 specimens OR less than 1.5% weight loss after 200 cycles for 4 of 5 specimens (tested in water)	Less than 1% weight loss after 40 cycles for 5 of 5 specimens OR less than 1.5% weight loss after 50 cycles for 4 of 5 specimens (tested in 3% saline)

increase a slope angle resulting in cost savings associated with increased land utilization, reduced fill quantities or eliminating the need for a more costly retaining wall. Schedule benefits may also be realized from decreased construction time by allowing "less desirable onsite material" to be used within the reinforced zone than would typically be allowed with other retaining structures. As in SRWs, geogrids and geotextiles have both been used successfully in RSS construction.

Reinforced Soil

FHWA (1997) states, "*Because a flexible facing (e.g. wrapped facing) is normally used, minor distortion at the face that may occur due to backfill settlement, freezing and thawing, or wetting and drying can be tolerated. Thus, lower quality backfill than recommended for MSE walls can be used. The recommended backfill is limited to low-plasticity, granular material [i.e., a plasticity index (PI) less than or equal to 20 and less than or equal to 50 percent of the infill soil should be finer than a particle diameter of 0.075 mm]. However, with good drainage, careful evaluation of soil and soil-reinforcement interaction characteristics, field construction control, and performance monitoring ... most indigenous soil can be considered.*" These recommended backfill requirements should be followed for USACE projects.

Internal Stability

The recommended method for determining the amount of primary reinforcement required for the RSS is a trial and error method incorporating reinforcement directly into a slope stability program (e.g., UTEXAS) capable of handling individual reinforcement layers. Reinforcement lengths, strengths and locations can be changed in the computer model until stability requirements are met. Anchorage lengths must be determined and incorporated in the model.

Since some slope stability codes can readily apply internal reinforcement, it is relatively easy to design the internal reinforcement in the following manner. This is a simplified description and the designer is referred to the FHWA (1997) or to Holtz et al. (1997) for further clarification and details.

a. Assume a primary reinforcement layout (layers spaced not greater than 24 inches vertically if intermediate reinforcement is not proposed).

b. Set the reinforcement lengths longer than is necessary in order for program search routines to locate the critical failure surface within the reinforced soil.

c. Vary the reinforcement spacing and strength for an optimal design. The reader is referred to FHWA (1997) for design suggestions.

Global/Compound Stability

These stability concerns are discussed in detail in the design for MSE walls and are applicable to RSS structures. Once the internal stability has been designed following the above procedure, the reinforcement lengths can be shortened until the sliding and global and compound stability requirements are just met. Minimum factors of safety for varying design conditions are presented in Table 2.

Sliding Stability

Sliding along reinforcement layers is checked using a wedge failure surface. Multiplying by the coefficient of direct sliding reduces the infill shear strength to model the interface conditions. Stability results are found by fixing the failure surface along the reinforcement location and then increasing the reinforcement lengths if required.

Seismic Conditions

Seismic conditions can be modeled following current USACE procedures.

Drainage

Since many USACE civil works projects are water related, it is reasonable to assume that most applicable RSS structures need to address seepage and drainage aspects. Less restrictive requirements on infill soil translates into use of lower permeability materials and an increased concern for raising the phreatic surface within the RSS mass. The steep slope face will inherently be unstable when subjected to emerging seepage. Drains should typically be installed on projects with seepage concerns, but also on many projects without visible seepage problems. The cost of installing a drain can be a relatively inexpensive component in the RSS system.

Facing

Slope face treatment may consist of vegetation (sod; seed) or hard facing (gabions; shotcrete; stone). The face may be wrapped with reinforcement or left unwrapped. Temporary or permanent erosion control mats (ECM) may be incorporated. Whatever method is used, some type of slope face treatment is required to inhibit erosion. Table 4 provides recommendations for facing treatments for differing project conditions (Collin, 1996 and FHWA, 1997).

SUMMARY

Engineering design criteria has been established for MSE wall and RSS structures used on USACE projects. This criteria and discussion of design procedures and recommendations is included in an Engineer Circular, EC 1110-2-311, Design of Mechanically Stabilized Earth Walls and Reinforced Soil Slopes (publication pending). This criteria is an extension of, and builds upon, existing FHWA and industry guidelines. In addition to the design guidance document, two guide specifications have been prepared for the construction of segmental concrete block faced, geosynthetic reinforced MSE retaining walls (USACE, 1999a) and geosynthetic reinforced soil slopes (USACE, 1999b). These documents are currently available on the USACE TechInfo website: www.hnd.usace.army.mil/techinfo/cegs/cegstoc.htm.

ACKNOWLEDGEMENTS

The authors would like to thank the USACE Headquarters and the Mississippi Valley Division for their support and recommendations throughout the development of the MSE wall and RSS design guidance documents. Additionally, the authors thank GMA and NCMA for funding the involvement of peer reviewers on the project.

Table 4. RSS Slope Facing Options and Guidelines for Selection (modified from Collin, 1996).

Slope Face *Angle and soil type*	**Type of Facing**			
	When geosynthetic is not wrapped at face		When geosynthetic is wrapped at face	
	Vegetated Face	*Hard Facing*	*Vegetated Face*	*Hard Facing*
> 50° All soil types	Not recommended	Gabions	Sod; Permanent erosion blanket w/ Seed	Wire baskets Stone; Shotcrete
35° to 50° Clean sands; Rounded gravel	Not recommended	Gabions; Soil-Cement	Sod; Permanent erosion blanket w/ seed	Wire baskets; Stone; Shotcrete
35° to 50° Silts; Sandy silts	Bioreinforcement; Drainage Composites[1]	Gabions; Soil-Cement; Stone Veneer	Sod; Permanent erosion blanket w/ seed	Wire baskets; Stone; Shotcrete
35° to 50° Silty sands; Clayey sands; Well graded sands and gravels	Temporary Erosion blanket W/ seed or sod; Permanent erosion mat w/ seed or sod	Hard facing not needed	Geosynthetic wrap not needed	Geosynthetic wrap not needed
25° to 35° All soil types	Temporary Erosion blanket W/ seed or sod; Permanent erosion mat w/ seed or sod	Hard facing not needed	Geosynthetic wrap not needed	Geosynthetic wrap not needed

Notes: [1]Geosynthetic or natural horizontal drainage layers to intercept and drain the saturated soil at the face of the slope

REFERENCES

ADAMA Engineering, Inc. (1998) *Mechanically Stabilized Earth Walls Software (MSEW 1.0),* Federal Highway Administration, Washington, DC 20590.

ASTM C 1372-99a, "Standard Specification for Segmental Retaining Wall Units", Annual Book of ASTM Standards.

Berg, R.R., Chouery-Curtis, V.E., and Watson, C.H., "Critical Failure Planes in Analysis of Reinforced Slopes," Proceedings of Geosynthetics '89
Conference, San Diego, California, February 21-23, 1989, pp. 269-278.

Collin, J.G. (1996) "Controlling Surficial Stability Problems on Reinforced Steepened Slopes," *Geotechnical Fabrics Report* IFAI.

Earth Improvement Technologies and Bathurst, Richard J. (1997) *Program Manual and Users Guide: Design Software for Segmental Retaining Walls (SRWall ver. 2.1)*, National Concrete Masonry Association, Herndon, VA.

Federal Highway Administration (1997) *Mechanically Stabilized Earth Walls and Reinforced Soil Slopes Design and Construction Guidelines*, *FHWA-SA-96-071,* Washington, DC.

Holtz, R. D., Christopher, B. R., and Berg, R. R. (1997), *Geosynthetic Engineering*, BiTech Publishers Ltd., Richmond, British Columbia, Canada, 452 p. [Also available as: Holtz, R.D., Christopher, B.R. and Berg, R.R.,[Technical Consultant - DiMaggio, J.A.], *Geosynthetic Design and Construction Guidelines*, U.S. Department of Transportation, Federal Highway Administration, Washington, D.C., FHWA-HI-98-038, 1998, 460 p.]

Koerner, R. M. and Soong, T.Y. (1999) "Geosynthetic Reinforced Segmental Retaining Walls," American Society of Civil Engineers Journal of Geotechnical and Geoenvironmental Engineering (pending).

Meyers, M. S., Schwanz, N. T. and Berg, R. R. (1997) "Specifying and Bidding Segmental Concrete Faced MSE Walls on U. S. Army Corps of Engineers, St. Paul District Projects", *Geosynthetics '97, IFAI*, Long Beach, CA, USA, pp. 789-801.

National Concrete Masonry Association (1997) *Design Manual for Segmental Retaining Walls (Modular Block Retaining Wall Systems), second Edition*, J. G. Collin, Ed., Herndon, Virginia, USA.

National Concrete Masonry Association (NCMA), 1998, *Segmental Retaining Walls – Seismic Design Manual*, Bathurst, R. J., Author, Herndon, Virginia, 118 pp.

US Army Corps of Engineers (2000) *EC 1110-2-311, Design of Mechanically Stabilized Earth Walls and Reinforced Soil Slopes,* US Army Corps of Engineers, Washington, DC, USA.

US Army Corps of Engineers (1999a) *CEGS 03832, Segmental Concrete Block Retaining Wall,* US Army Corps of Engineers, Washington, DC, USA.

US Army Corps of Engineers (1999b) *CEGS 02332, Reinforced Soil Slope,* US Army Corps of Engineers, Washington, DC, USA.

US Army Corps of Engineers (1999) *EM 1110-2-1612, Engineering and Design, Ice Engineering*, US Army Corps of Engineers, Washington, DC, USA.

US Army Corps of Engineers (1995) *ER 1110-2-1806, Earthquake Design & Evaluation of Civil Works Projects,* US Army Corps of Engineers, Washington, DC, USA.

US Army Corps of Engineers (1986) *EM 1110-2-1901, Engineering and Design, Seepage Analysis and Control for Dams*, US Army Corps of Engineers, Washington, DC, USA.

US Army Corps of Engineers (1978) *EM 1110-2-1913, Engineering and Design, Design and Construction of Levees*, US Army Corps of Engineers, Washington, DC, USA.

US Army Corps of Engineers (1970) *EM 1110-2-1902, Stability of Earth and Rock-Fill Dams,* US Army Corps of Engineers, Washington, DC, USA.

US Army Corps of Engineers (1989) *EM 1110-2-2502, Engineering and Design, Retaining and Flood Walls*, US Army Corps of Engineers, Washington, DC, USA.

GEOSYNTHETIC REINFORCED HIGHWAY EMBANKMENT OVER PEAT

J.R. KERR
TENSAR EARTH TECHNOLOGIES, INC., CANADA
B. BENNETT
MINISTRY OF TRANSPORTATION OF ONTARIO, CANADA
O.N. PERZIA
VEDO CONSTRUCTION LIMITED., CANADA
P.A. PERZIA
TENSAR EARTH TECHNOLOGIES, INC., CANADA

ABSTRACT

A highway embankment was constructed over peat on Highway 69 north of Port Severn in Ontario, Canada. The purpose of the embankment was to support two additional lanes in the twinning of the highway. Due to the proximity of the existing highway embankment and the limited right of way, it was not feasible to remove the soft underlying soils without undermining the existing structure. After considering a number of alternatives, an embankment reinforced with geogrid was selected as the most feasible solution.

This case study will review the design, cost, construction and performance of the embankment. Site investigation and design were completed during the later part of 1991 and into 1992 with construction starting on November 18, 1992. Construction and post construction settlements were monitored including the effect of a surcharge lift placed during 1993. Ongoing settlement observations are still being recorded.

A total fill thickness in the order of five meters (including surcharge) has resulted in settlement ranging from 0.4 to 1.02 meters. The stratigraphy of the foundation soils consisted of 2.5 m. saturated peat overlying 2.5 to 5.5 m of weak clay overlying bedrock.

INTRODUCTION

In late 1991, Ministry of Transportation Ontario (MTO) began evaluating alternatives for the construction of a new highway embankment to run parallel to an existing two lane embankment in central Ontario. The highway section was part of an overall twinning required to meet increasing traffic loads occurring on Highway 69 north of Port Severn. Problems were encountered along one section where the proposed alignment for the new embankment was constrained by a deep swamp on the west side and the proximity of the existing embankment on the east side. Further complications were associated with potentially undermining the existing embankment which was also founded upon soft soils.

There are a number of alternatives that can be typically considered for a project such as this. These include techniques such as dredging, piling, staged construction, and a variety of both unreinforced and reinforced embankment configurations. The solution that was finally selected consisted of a geosynthetic reinforced embankment (Figure 1).

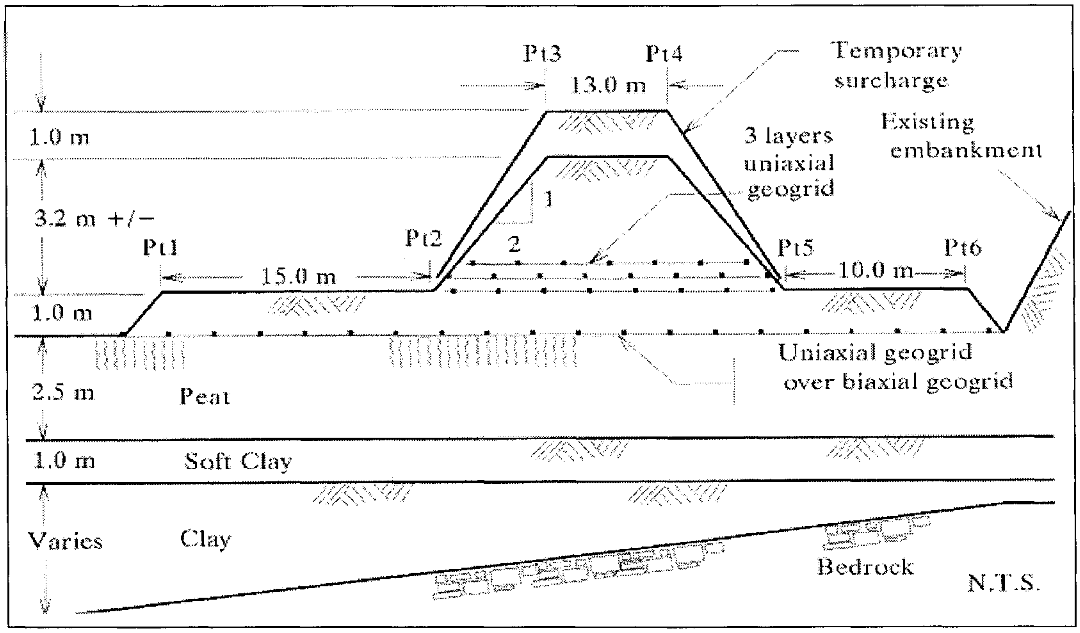

Figure 1. Typical Cross Section

SITE DESCRIPTION

The project is located on the southern edge of the physiographic area known as the Canadian Shield which comprises nearly half of the area of Canada. It is composed mainly of granitic and metamorphic Precambrian rock. The region is characterized by its innumerable lakes, rivers and wet lands. The preponderance of rock and wet land make this a challenging area for highway design and construction.

Site Soil Conditions. The soil conditions at the site consisted of saturated peat overlying soft clay overlying firm clay over bedrock. The water table was at the existing surface elevation.

Peat Saturated, organic peat was encountered to a depth of 3.0 m below existing grade. This fine fibrous to fibrous peat was dark brown to black with moisture contents varying from 92 to 581 percent with an average of 320 percent. For design purposes, the undrained shear strength of the unconsolidated peat was estimated as 5 kPa with a unit weight of 16 kN/m^3.

Clay. Underlying the peat, a layer of soft to firm clay was encountered to a depth of 4.9 m on the east side of the embankment and 8.5 m below surface on the west side. The moisture content of the medium plastic clay varied from 10 to 60 percent (decreasing with depth). The clay was subdivided into two layers for design purposes. The upper meter of the deposit was characterized by an undrained shear strength of 5 kPa and a unit weight of 18 kN/m^3 and the lower zone was 10 kPa and 18 kN/m^3 respectively.

Bedrock. Bedrock was encountered beneath the clay.

PROJECT DESCRIPTION AND CONSTRAINTS

The centerline of the new Highway 69 alignment alternately traversed rock outcropping and wet lands (Figure 2). The construction technique over most of the alignment consisted of full depth dredging of the bogs and replacement with blast rock obtained from adjacent cut sections. In most cases the new embankment could be constructed far enough away from the existing embankment so that the dredging operation would not undermine the existing embankment (sometimes also founded upon soft soils). Where this separation could not be achieved, due to site constraints, alternate design and construction methods had to be selected. Alternate methods, however, would also have to meet the timely construction schedule required by the project.

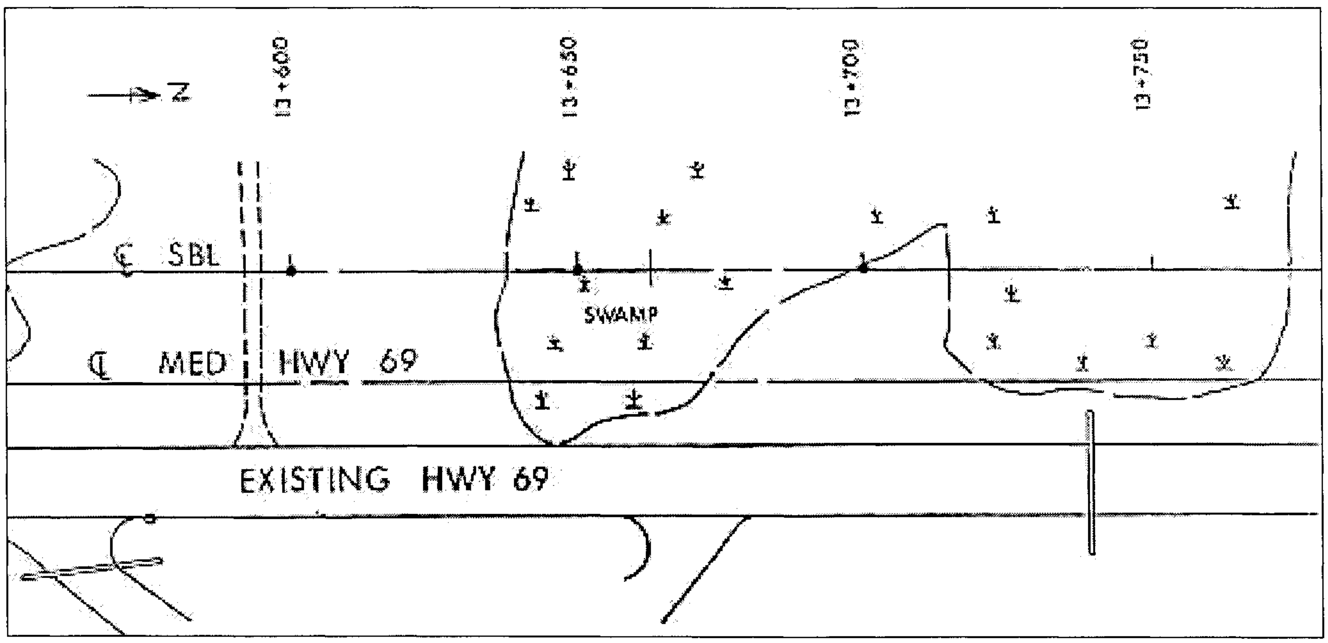

Figure 2. Highway 69 Alignment

DESIGN ALTERNATIVES

A number of factors influenced the selection of alternatives on the project. The main concern of MTO was the safety of the existing highway embankment on the immediate east side of the new embankment. Any movement of the existing embankment either during or after construction had to be avoided. Another consideration was maximizing the use of the coarse, angular blast rock from the cut sections of the new highway right of way. The proximity of the wetlands to the western edge of the project also presented the need to minimize the extent of intrusion for both technical and environmental reasons.

Constraints associated with project schedules, costs and technical complications ruled out closer evaluation of a number of alternatives. These included pile foundation support and longer term, unreinforced, staged construction. The two main alternatives that were considered were the dredging technique already being used on other sections of the highway and a geosynthetic reinforced embankment founded upon the soft foundation soils.

Dredging and Replacement. Dredging and replacement with blast rock had already been used along most of the right-of-way to the north and south of the site. Along the section in question, however, the proper alignment could not be achieved without positioning the new embankment as close as possible to the existing embankment. Dredging was discounted due to the potential for undermining the adjacent embankment. Economic considerations were considered secondary to technical complications. For purposes of comparison, however, it was of interest to evaluate the cost and time required to construct this alternative. An in depth evaluation of project cost was completed by Perzia (1993). Using the standard cross section being constructed elsewhere on the project, a total cost of \$226,500 and a construction time of 21 days was calculated.

Reinforced Construction. Mainly from a technical standpoint, this option was considered by MTO to be the best alternative; although, it was subsequently estimated to be cost efficient as well. The main advantages offered by this solution consisted of minimizing the negative influence on the adjacent embankment, eliminating the need to dispose of dredged material and meeting the construction schedule required by the project. The use of geosynthetic reinforcement enabled the width of the embankment to be reduced from that of an unreinforced embankment. This had the advantage of providing an embankment that was lighter and required less fill. This reduced width also minimized the intrusion into the wet lands on the west side of the embankment. At a total cost of, \$237,300, the reinforced embankment was comparable to the dredging alternative; but, with a total construction time of 11 days, it was completed in close to half the time that would have been required by the dredging alternative.

COST ANALYSIS

A thorough cost analysis of the project was carried out by Perzia (1993). The component and total cost of the two main alternatives are shown in Table 1.

Table 1. Cost Comparison

Alternative	Fill Vol. m^3	Fill Cost @ $10/$m^3$	Other	Total Cost
Dredging	21,251	$212,506	$14,000 Fill disposal	$226,500
Reinforced Embankment	6,733	$67,326	$170,000 Geosynthetics	$237,300

Although the selection of the final alternative was not primarily cost, the two alternatives were still reasonably similar. If total cost were the only consideration then the decision to use either one of the alternatives would be primarily influenced by the unit cost of the fill. Perzia (1993) went on to evaluate the relationship between total cost and unit fill cost for the two alternatives. The analysis yielded a unit fill cost of $10.75 per m^3 as the break even cost between the two construction alternatives for this specific site (Figure 3). Depending upon factors such as dredging depth, and haul distance, the reinforced alternative can be shown to have economic advantages as well as technical preference.

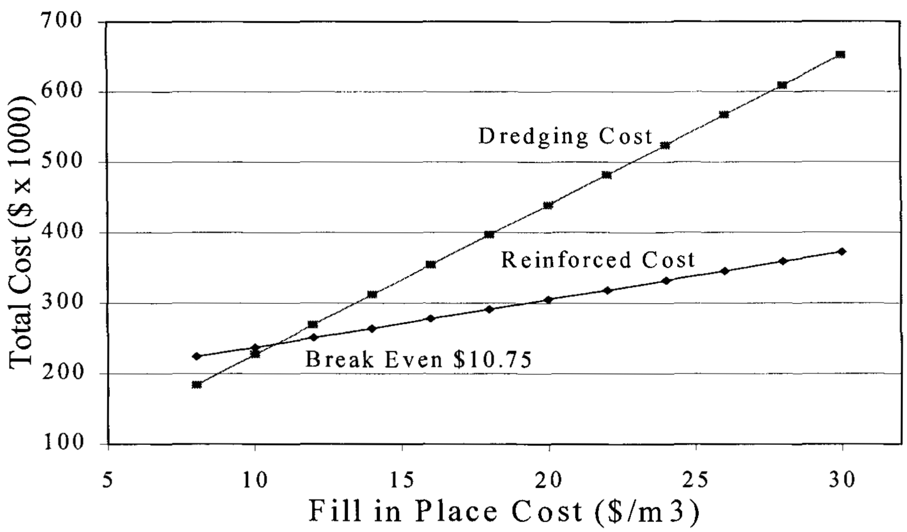

Figure 3. Reinforced Costs vs Dredging Costs

RATIONALE FOR GEOSYNTHETIC USE AND SELECTION

The need for geosynthetic reinforcement was identified when the width of an unreinforced embankment became too wide for the space available. The west side of the unreinforced structure intruded too far into the deepening marsh. If the foundation was not dredged and the embankment was founded on the peat deposit, a narrower, lighter reinforced structure would be required.

The readily available blast rock had three main advantages; low cost, high permeability and low unit weight. Because of the economic and technical advantages of utilizing the rock, the reinforcement would have to be resistant to a relatively high level of construction damage. For this reason, MTO selected the heaviest geogrid that was available at that time. The main reinforcement used in the embankment consisted of uniaxial, HDPE geogrid that had a prior record of success in blast rock structures of this type. The geogrid had a creep limited strength of 61.3 kN/m and a 2% secant modulus of 21.9 kN/m.

To facilitate placement of the first stage of construction, a stiff biaxial geogrid was unrolled parallel to the centerline immediately on the surface of the peat. The biaxial geogrid provided a stable platform for workers as they placed the first layer of uniaxial geogrid at right angles to the centerline. The uniaxial geogrid was placed immediately on top of the biaxial layer. The presence of biaxial reinforcement prevented the separation of the uniaxial geogrid sheets as the first layer of rock (one meter thick) was placed.

ANALYSIS AND DESIGN

Stability of the reinforced embankment was evaluated using Bishop's Method applied to the Swedish Method of Slices A minimum factor of safety of 1.4 was used for both internal and external stability.

The undrained strength of the foundation was found to govern stability for both unconsolidated and consolidated states. For design purposes an unconsolidated, undrained strength of 5 kPa was used for the peat and the upper zone of the underlying clay. The lower clay zone was characterized by an undrained, unconsolidated strength of 10 kPa.

At 19 kN/m^3 the blast rock used had the advantage of having a light unit weight which added to the stability of the embankment. A drained friction value of 35 degrees was used in the design.

The stability was checked for the addition of a 1.0 to 1.5 m surcharge five months later. The consolidated, undrained strength of the peat layer was estimated to be 8 kPa. The underlying clay was conservatively assumed to have the same strength characteristics used for the start of construction.

A variety of cross sectional shapes and reinforcement quantities were investigated to find the optimum configuration. The parametric study involved a 5.5 m high trapezoidal embankment with a variety of side slopes, with and without lower height berms on either side. Parametric analyses were also carried out varying the height and width of the side berms. The optimum configuration was found to be a central embankment with one meter high berms on either side. On the east side the berm extended 10 m to abut the existing embankment. On the west side, the berm extended 15 m beyond the toe of the central embankment. Both the central embankment and the side berms were built with side slopes of two horizontal to one vertical.

CONSTRUCTION

The swamp area to be traversed was 70 m long and was covered with water to a maximum depth of approximately one meter. Trees and shrubs were cleared leaving the root mat and vegetative surface undisturbed. Once the bog was cleared, construction of the reinforced embankment commenced on November 18,1992.

Biaxial Reinforcement. The first step required was to place 4 m by 50 m geogrid rolls on the surface of the swamp (Figure 4). These rolls were placed with the long axis parallel to the centerline of the new embankment. The rolls were placed with a one meter overlap and were tied every 2 to 3 meters with plastic ties. With the initial construction platform in place the first layer of the main embankment reinforcement could be placed.

Figure 4. Biaxial Geogrid Layer

Uniaxial Reinforcement. Immediately over the biaxial geogrid, 1.3 by 55.5 m rolls of uniaxial geogrid were placed at right angles to the highway centerline. The geogrid was abutted along the edges with no overlap and spanned toe to toe with no splices. Roll lengths for the project were custom cut at the manufacturing plant. Instead of having to unroll the geogrid across the ground in the conventional way, the contractor was able to position a truck mounted spindle on the adjacent, existing embankment and the geogrid was simply unwound and pulled across the site (Figure 5). This enabled the four man crew to increase the laydown rate from 220 m^2 to 470 m^2 per hour.

Figure 5. Placing Uniaxial Geogrid

Placement of Fill. On top of the uniaxial geogrid, a one meter thick layer of rock fill with a maximum particle size of 500 mm was placed in one lift (Figure 6). This fill was obtained from a blast site situated at the north end of the swamp. A single 980C Caterpillar front end loader was used to place the fill over the bog. The rock was first placed in the center of the structure to create a central construction platform. Once this was completed, fill was then spread laterally toward each side to the edge of the embankment. This leading edge was completed by the caterpillar hauling fill from a dump area on the north side of the swamp. Once the fill extended far enough into the swamp, two haul trucks were used to deliver rock fill to the front end loader operating at the edge of the fill. These delivered loads and the trucks were restricted from being closer than two meters from the leading edge of the fill. The front end loader then moved and spread the rock the rest of the way. The construction rate was governed by the two trucks as there was not enough room to operate a third truck.

Figure 6. Placing Rock Fill

As the rock fill layer reached about half way across the swamp, a small mud wave started to form where the loader was pushing out in the center. The wave was contained by subsequently pushing fill from the shallow side (east) of the swamp.

Central Embankment. Once the wider foundation fill was completed, the 26 m wide central embankment was started. At the base of the embankment, three layers of uniaxial geogrid were placed and abutted the same way as for the first layer of uniaxial geogrid (Figure 7). Each of the geogrid layers were separated by a 300 mm thick layer of rock fill with a maximum particle size of 150 mm and layer at right angles to the centerline of the highway. These three layers were constructed much more efficiently due to the fact that a solid one meter thick working platform already existed and that the crew was already experienced and had an effective method of placing the geogrid. For the three layers of geogrid, the four man crew achieved a laydown rate of 650 m^3 per hour.

Figure 7. Central Embankment Fill

A one meter thick zone of rock fill was then placed above the reinforced zone. This rock fill had a maximum particle size of 500 mm. Standard, coarser rock fill was then used to bring the total structure up to a final grade of approximately four meters. This work was completed on December 20, 1992 followed by a surcharge of 1.0 to 1.5 m on April 18, 1993. The final embankment is shown in Figure 8.

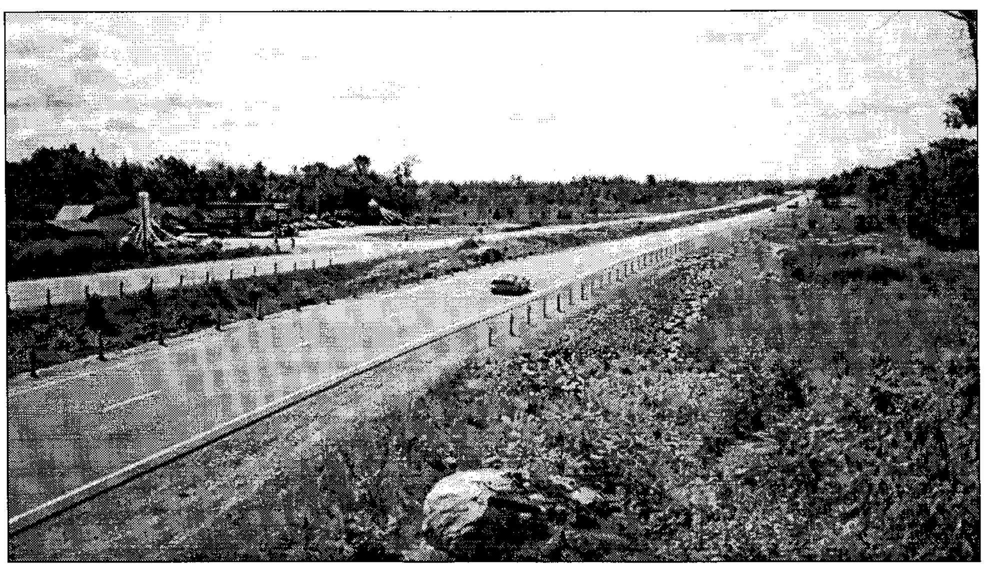

Figure 8. Completed Embankment

PERFORMANCE

Existing Embankment. Protection of the existing embankment from structural distress and settlement was the main objective of this project. To date, no structural distress or settlement has been observed in this embankment. This represents an elapsed period of over seven years since initial construction of the additional embankment.

New Embankment. The main objectives for the new embankment consisted of achieving stability and reducing the settlement to tolerable limits. Although competitive construction costs were also achieved, economics were secondary to the objectives stated above.

Settlement of the new embankment was monitored by observing a series of benchmarks installed on the surface of the structure at Stations 13+720,+735,+750 and +765. A typical cross section showing benchmark locations and observed settlements is shown on Figure 9. Typical observations of settlement vs. time are shown on Figure 10. Settlement observations obtained on June 15,1994 (19 months elapsed time) showed a maximum settlement of 1.02 m on the centerline of Station 13+750. The settlement observations obtained from the project are comparable to 1.0 to 1.5 m total settlement estimated at the time of design.

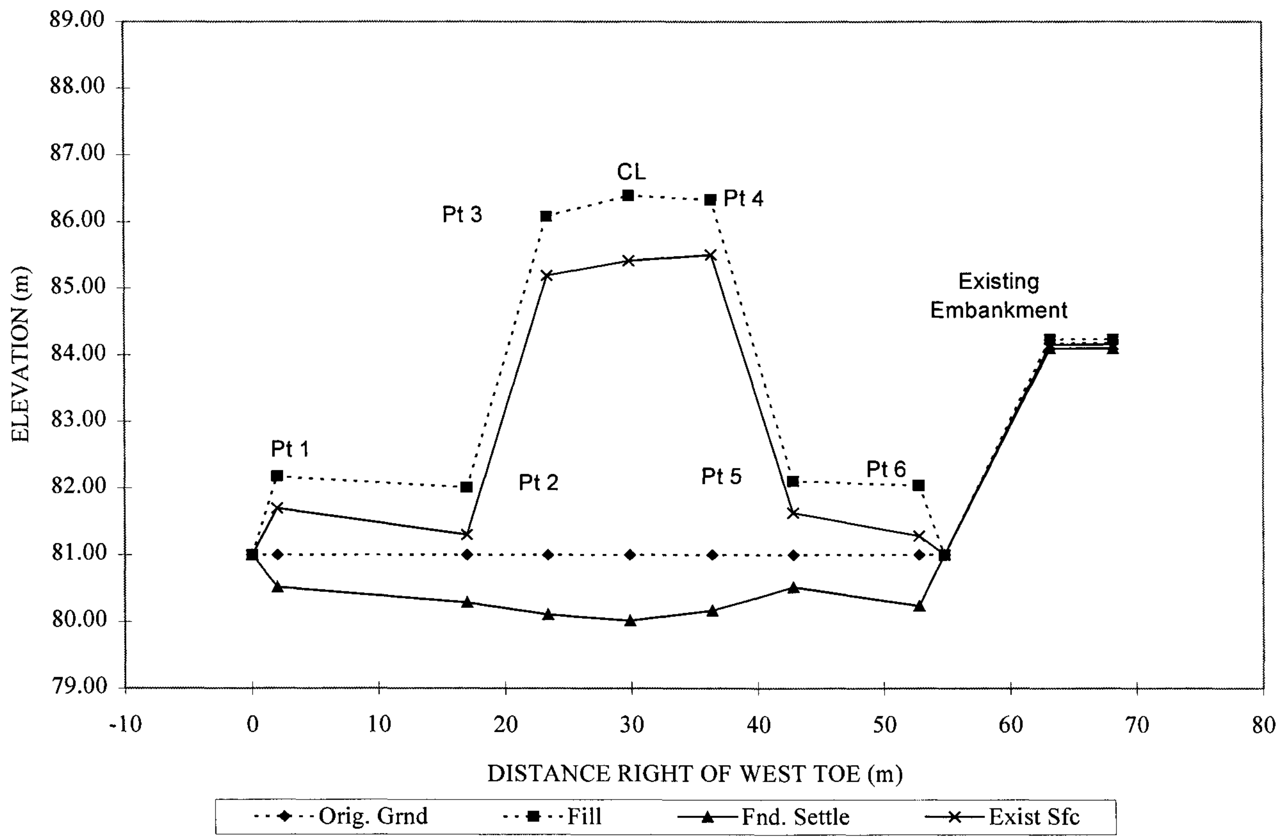

Figure 9. Typical Cross Section

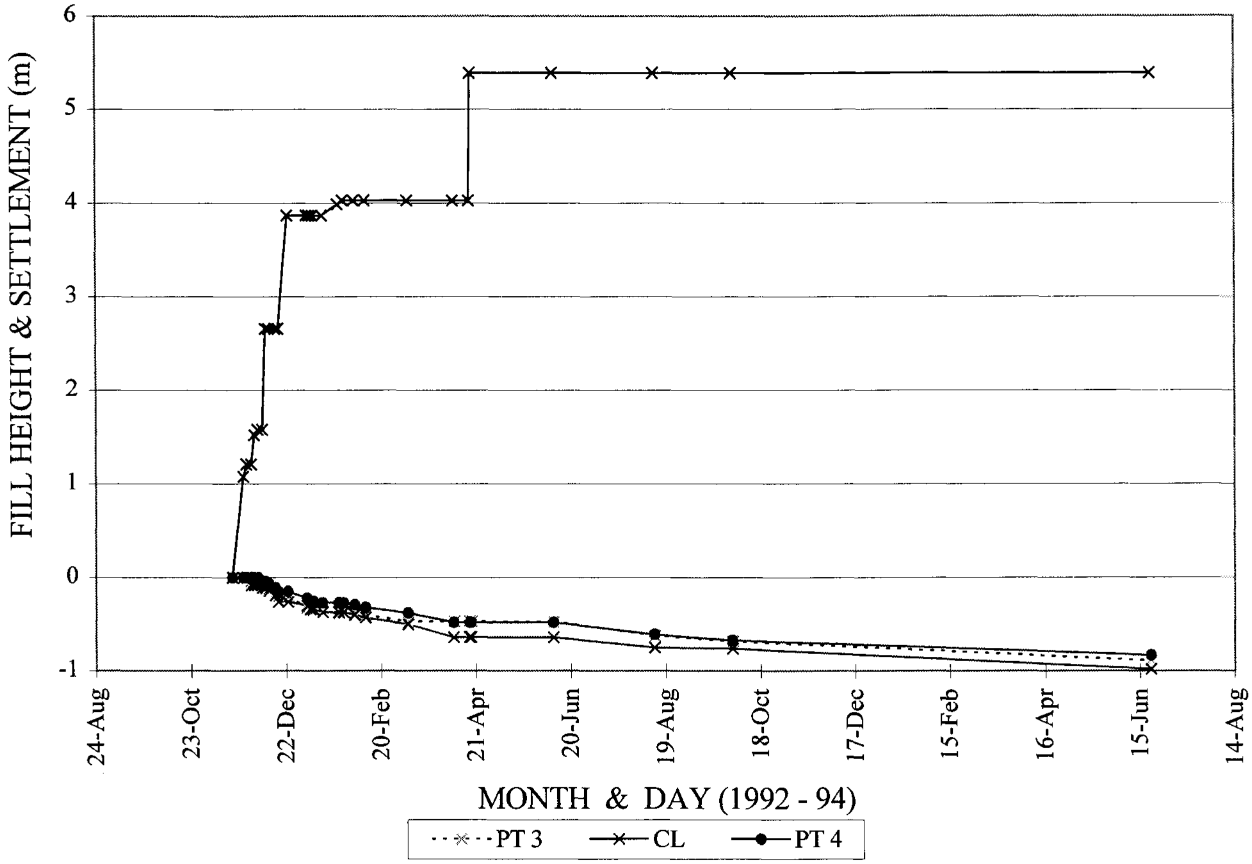

Figure 10. Settlement vs. Time

During construction, no structural distress was observed in the embankment and the work proceeded as expected. However, on October 21, 1993, approximately 10 months after completion of construction, a tension crack was observed on the southern edge of the embankment at Station 13 + 720. The crack, with a width of approximately 50 mm, was observed on the surface of the main embankment at a right angle to the highway centerline. It was found that the embankment at this location saddled a finger like rock outcropping extending from the east side to approximately two thirds across the embankment. The orientation of this outcrop was approximately at a right angle to the highway cross section. The crack was judged to be the result of differential settlement resulting from settlement of the embankment on either side of the outcrop. As the bulk of settlement had occurred at this time, repair simply consisted of patching the crack. This was achieved by excavating a 300 mm deep strip on either side of the crack, placing a biaxial geogrid in the base and refilling the area with compacted gravel. No further structural distress has been observed to date.

CONCLUSIONS

A geosynthetic reinforced embankment was successfully designed and constructed over a swamp in northern Ontario. The objective of preventing damage to existing, adjacent embankment was achieved and its safety was not compromised. This embankment was situated in close proximity to the new embankment for reasons of horizontal alignment constraints. Soft foundation conditions existed beneath both of the embankments necessitating the need to minimize settlement in the new embankment so as not to negatively impact the existing embankment. This was achieved. The maximum observed settlement as of June 15 was 1.02 m. This was comparable to 1.0 to 1.5 m total settlement estimated at the time of design. Overall settlement has been on the low side of prediction. The tension catinery formed in the geogrid layer on the bottom of the structure may be contributing to the settlement behavior of the embankment. This should be confirmed in future structures with appropriate instrumentation and site investigation.

Cost consideration was not a specific factor in this project other than to ensure the selected alternative was economic from a project management standpoint. It was determined, however, that the cost of a geosynthetic reinforced embankment was comparable with the usual method of dredging and replacement.

Although the reinforced method may be more labor intensive, it is cost comparable with dredging and, depending on the cost of fill, can be a more favorable alternative to dredging. From a construction aspect, the amount of fill material required for the reinforced method is approximately half of that required by dredging. In addition, the time of construction of the reinforced method is twice as fast as the tedious dredging method.

The geosynthetic reinforced embankment alternative achieved a number of environmental objectives:

- encroachment of the adjacent wet land was minimized;
- dredging and disposal of foundation soils was avoided; and,
- by leaving the existing foundation soils undisturbed, groundwater was not contaminated.

Time constraints did not permit the installation of more sophisticated instrumentation on this project. However, the settlement information obtained indicated that this investment is warranted in future work. This project has shown that a reinforced embankment with side berms can have technical, economic, and environmental superiority over other alternatives.

ACKNOWLEDGMENTS

Permission from the Ministry of Transportation Ontario to publish this paper is gratefully acknowledged. This project would not have happened without the Foundation Design Section's ongoing interest in geosynthetic technology and the cooperation of the Northern Regional

Construction Office both during construction and in providing ongoing monitoring of the structure. The authors also wish to acknowledge the construction contractor, E. E. Seegmiller, for their care and attention in completing this project.

REFERENCES

MacFarlane, Ivan C., Editor, 1969,"*Muskeg Engineering Handbook*", University of Toronto Press, Ontario, Canada, 248 p.

Perzia, O. S., 1993,"Geogrid Reinforced Highway Embankment Constructed Over Soft Soils On Highway 69 In Baxter Township", Department of Civil Engineering, University of Toronto, 56p.

MATERIAL SCIENCE & DURABILITY II

GEOSYNTHETICS CONFERENCE 2001
Portland, Oregon USA
Economics, Performance & Constructibility • February 12-14, 2001

THE INSTALLATION DAMAGE OF WOVEN RIB GEOGRIDS UNDER VARIOUS BACKFILLS

CHIWAN HSIEH, JENG HAN WU & CHAIN KWUE LIN
DEPARTMENT OF CIVIL ENGINEERING,
NATIONAL PINGTUNG UNIVERSITY OF SCIENCE AND TECHNOLOGY, TAIWAN

ABSTRACT

Four different strengths of PVC-coated PET flexible geogrids from a single manufacture were placed in five different typical soils for the purpose of evaluating the amount and degree of installation damage. A series of single rib strength tests (GRI-GG1) and in-isolation junction strength tests (GRI-GG2) were performed. Based upon the test results, the tensile strength retained for flexible geogrid placed within fine grained soil, sandy soil, gravel with some fine soil, and crushed stone gravel are 83% to 99%, 85% to 96%, 66% to 95%, and 57% to 88%, respectively. The reduction factor for tensile strength due to installation damage is significantly related to soil type and varies from 1.05 to 1.70. The retained strength of junction for flexible geogrid is ranging from 71% to 100% for various type soils. The reduction factor for junction strength due to installation damage varies from 1.00 to 1.40 for different type of soils.

INTRODUCTION

The family of Geosynthetics includes geotextile, geogrid, geomembrane, geonet, geocomposite, geopipe, geosynthetic clay liner, and geo-others. These products are generally produced using polymer materials in manufacture and usually consist of a very good quality control process. Since these materials are relatively easier to handle in comparison with conventional construction materials, they have been widely used in the construction site to replace some virgin materials in the areas of transportation, environmental, geotechnical, and hydraulics engineering.

Geogrid is a member of geosynthetic family. The primary function of geogrid is reinforcement and separation. In order to satisfy these functions, geogrids typically are placed within soils with equal spacing and forming a soil/geogrid composite material. The tensile strength of geogrid in combine with the interlocking phenomena within the soil/geogrid system provides the function of reinforcement. As the results, this improves the bearing capacity and the compressive strength of soil-geogrid system.

Geogrids are currently being used in a number of different soil reinforcement applications, such as retaining walls, steep soil slope stabilization, and improve bearing capacity of foundation soils. All of these applications require design procedures that are based on the tensile strength of geogrid. Generally, the wide width tensile strength according to ASTM standard D-4595 or the single rib tensile strength according to GRI-GG1 specification would be measured in the laboratory. Such laboratory-measured strength is not the allowable value to be used in the final design. The as-received materials test specimens usually do not include such items as installation damage, long term creep, chemical degradation, etc. Thus the design value must be suitably reduced so as to reflect the anticipated in-situ behavior. The allowable strength can be related to one another on a site-specific basis as follows (Koerner 1998):

$$T_{allow} = T_{ult} \left(\frac{1}{RF_{ID} \times RF_{CR} \times RF_{CD} \times RF_{BD}} \right) \quad (1)$$

Where T_{allow} = allowable wide width tensile strength for use in design; T_{ult} = ultimate wide width tensile strength on the as-received material; RF_{ID} = reduction factor for installation damage; RF_{CR} = reduction factor for creep deformation; RF_{CD} = reduction factor against chemical degradation; RF_{BD} = reduction factor against biological degradation.

At present, the standard method for evaluating the installation damage of Geosynthetics is not available. This paper focuses on providing a database for the installation damage of flexible geogrids for retaining wall and steep soil slope applications and similar reinforcement situations. Since flexible geogrid is getting popular for construction industry, the PVC-coated PET geogrids produced from a local manufacture are used in the study. The manufacture design strength of the test are 60 kN/m, 100 kN/m, 150 kN/m, and 200 kN/m. Five different soils were used in the study, which include a low plasticity silty clay (CL), a poorly graded fine sand (SP), a poor graded silty gravel (GP-GM), a clayey gravel (GC), and a well graded gravel (GW, crushed stone). The test geogrids were placed parallel and perpendicular to the compaction roller traveling direction with 15 cm and 30 cm lift thickness. The compaction effort of the test soils was evaluated by the sand cone method or the nuclear density gage method after each layer of compaction. The strength behavior of the geogrids before installation and after exhuming was evaluated according to the Geosynthetic Research Institute test standards GG1 and GG2. The comparison of the single rib ultimate tensile strength, 5% tensile strength, elongation at failure, and junction strength before and after installation was also performed. The reduction factor for installation damage for the flexible geogrid was also evaluated.

Note that the term has been called "survivability" by Christopher and Holtz (1984) and is defined as the "resistance to damage during construction and initial operation". Up to now, a number of studies related to the survivability of geotextiles and geogrids had been performed; for example see Bonaparte, et al. (1998), Koerner and Koerner (1990), Koerner et al. (1993), Rainey and Barksdale (1993), Richardson (1998), and Troost and Ploeg (1990). However, geotextiles and rigid geogrids are the primary materials used in those studies. Thus, the objective of the study is to fill the gap of the current database and to provide the test data of the installation damage of flexible geogrids. The concern of this paper is not focused on "durability" which can be defined as "resistance to damage by long-term degradation of biological, chemical or aging mechanisms".

FHWA/AASHTO SURVIVABILITY CRITERIA

Recent work by FHWA has led to development of reduction factor for installation damage to reduce the allowable tensile strength of geosynthetic reinforcement used in retaining wall and slope-stabilization applications. Table 1 gives current FHWA presumptive installation-damage reduction factors for a variety of geosynthetics. Recommended values from IFAI's Geotextile Division (now the Geosynthetic Materials Association, GMA) also are shown. These installation-damage reduction factors reflect potential stone/stone applications.

Table 1. FHWA Reduction factors for Degradation of Geosynthetics. (Suits 1996)

Geosynthetic	Reduction Factors for Degradation		
	FHWA Recommendation		IFAI Recommendation
	Type 1. Backfill Max. Size 100mm D50 about 30mm	Type 2. Backfill Max. Size 20mm D50 about 0.7mm	Type 3. Backfill Max. Size 20mm 0.1mm□D50□ 0.5mm
HDPE Uniaxial geogrid	1.20-1.45	1.10-1.20	1.05-1.15
PP Biaxial geogrid	1.20-1.45	1.10-1.20	1.05-1.15
PVC-coated PET geogrid	1.30-1.85	1.10-1.30	1.05-1.20
Acrylic-coated	1.30-2.05	1.20-1.40	1.15-1.30
Woven geotextiles (PP and PET)	1.40-2.20	1.10-1.40	1.05-1.20
Nonwoven geotextiles (PP and PET)	1.40-2.50	1.10-1.40	1.05-1.20
Slit-film woven PP geotextile	1.60-3.00	1.10-2.00	1.10-1.75

PP = polypropylene, PVC = polyvinyl chloride,
PET = polyester, HDPE = high density polyethylene

FIELD SURVIVABILITY TEST PROGRAM

The field survivability study was performed during the development of an industry park near Shin-Chun, Taiwan in the middle of September 1999. Five different test pits were prepared for each test soil. The test soils included a low plasticity silty clay (CL), a poor graded fine sand (SP), a poor graded silty gravel (GP-GM), a clayey gravel (GC), and a well-graded gravel (GW). The gradation curves of the test soils are shown in Figure 1.

Four different tensile strength uniaxial geogrids from a single manufacture were used in the study. The tensile strengths of the test geogrids are 60 kN/m, 100 kN/m, 150 kN/m, and 200 kN/m. The flexural rigidity values are less than 1000 g-cm measured using ASTM D1388 test method. The manufacture roll width is 3.8 meters. The size of test sample is 1.9 m wide and 2.9 m long. In order to evaluate the effect of compaction roller traveling direction on the strength of geogrid, the warp ribs of test sample were placed parallel (MDC test) and perpendicular (XMC test) to the roller traveling direction for these four types of geogrids. The schematic view of the placement of geogrid for MDC and XMC tests is shown in Figure 2. Totally 8 pieces of test samples were placed within each test pit. Thus, the minimum size of test pit is 8 meters by 11 meters.

First of all, the entire test site was compacted to reach a minimum 95% of the standard compaction density (ASTM D698). A lift of 15 to 20 cm test soils was then placed and compacted to the desired density. The eight pieces of test samples were placed in the desired arrangement as shown in Figure 3. Thereafter, the test soils were carefully placed over the test geogrid samples with the lift thickness of 15 cm or 30 cm by using a backhoe and a dozer. During the placement, the dozer was not allowed to make any significant turns on the geogrids. Then the test soils were compacted using a vibratory steel wheel compactor. The density of the cover soils was then evaluated by the sand cone method and the unclear density gage method. The compaction density of the test soils was found in the range from 91% to 97 % of the standard compaction density. Exhuming of the geogrids at each test pit and under different lift thickness consisted of dozing off the upper materials and then carefully hand shoveling the remaining thickness, about 10 cm covers. Due to short time interval between placement and exhuming of the geogrids, which varied from 1 to 4 hours, there was no bonding of geogrids to the soil beneath or above them. Thus, it was assumed that whatever damage may have occurred to the geosynthetics was done during the backfilling and compaction process, i.e., it is "installation damage" and not due to any other possible types of long-term degradation.

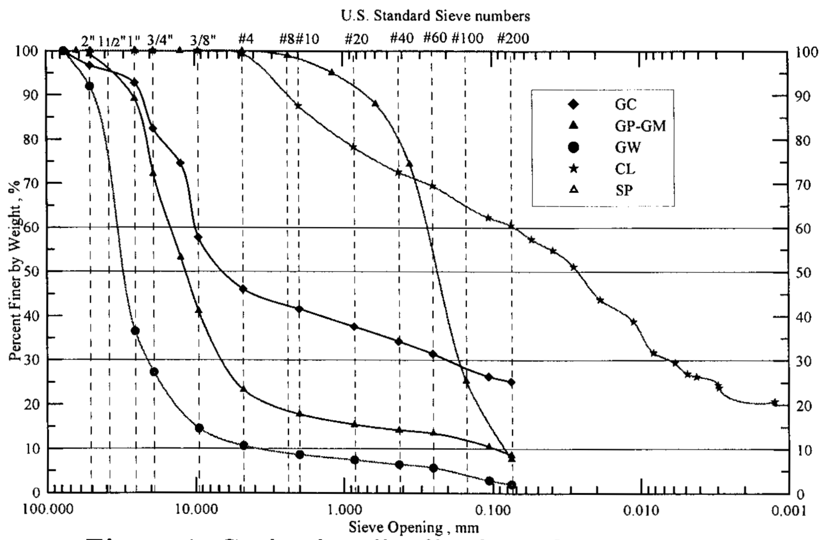

Figure 1. Grain size distribution of the test soils.

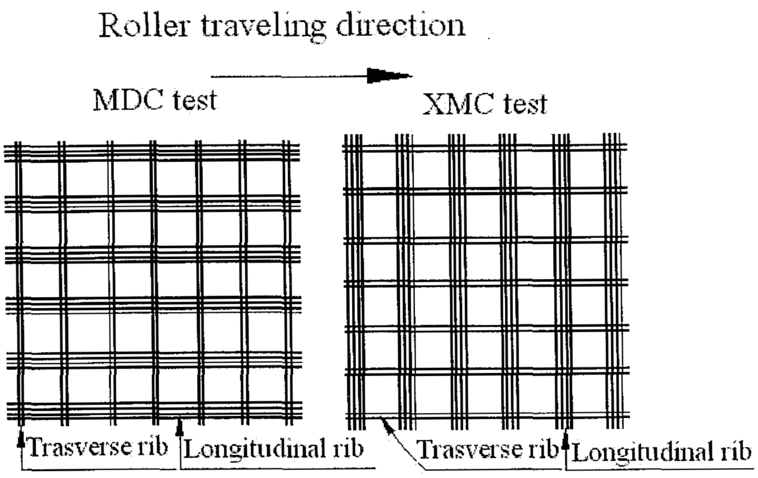

Figure 2. Schematic view of geogrid layout for the installation test.

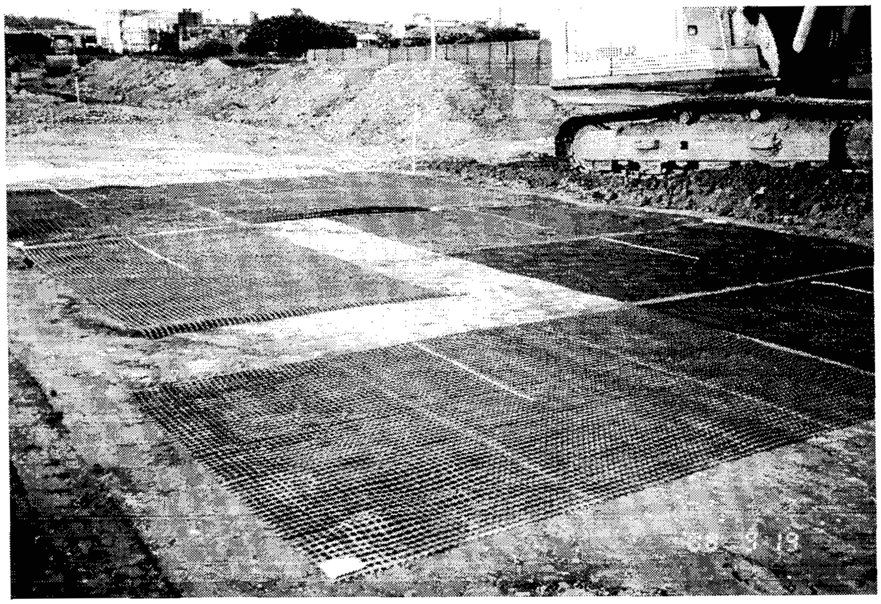

Figure 3. Typical geogrid samples layout.

TEST DATA AND RESULTS

Upon exhuming the installed geogrids, a visual damage survey was made. The number of ribs broken per square meter was reported. The exhumed geogrid samples were then labeled and shipped back to laboratory for testing. The single rib tensile strength test and junction strength test according to GRI-GG1 and GRI-GG2 test standards were performed. For each geogrid sample, 20 specimens were tested for both test methods.

Single Rib Tensile Test

Generally tensile strength is the most important design parameter for geogrid reinforcement applications, and ASTM D-4595 and GRI-GG1 are the most common test methods in the design. For simplicity, the GRI-GG1 standard test method was used in the analysis. In addition, 5% strain tensile strength and elongation at failure were also examined. The results of these tests were then compared to the average test values obtained from the pre-construction geogrid samples. The result of such a comparison is the retained percentage for each different conditions of evaluated. Finally, the inverse of this value will be the reduction factor for installation damage.

Test Data for Pre-construction Samples

As mentioned earlier, only four types of geogrids were analyzed in the study. The manufactured tensile strength of the analyzed geogrids was 60 kN/m, 100 kN/m, 150 kN/m, and 200 kN/m. The manufacture roll width of the test samples is 3.8 meters. A number of 124 warp ribs are counted for the raw samples (equivalent 32 warp ribs per meter). The rib opening is about 2 cm by 2 cm, and the opening area is about 47%. In order to understand the effect of preload on tensile strength of geogrid, a series of single rib tensile tests with various preloads was performed for these four types of geogrids. Typical test results for various preload conditions are shown in Figure 4. As shown on the figure, the tensile strength versus elongation curves for 1% and 2% preload conditions are quite similar. In addition, the results of statistical analysis for the single rib tensile tests of 60-kN/m geogrid under various preload conditions are shown in Table 2. It is very clear to us, the test results obtained from 2% preload condition consist the lowest measurement uncertainty and 95% confidence interval. Thus, 2% preload was used for the rest of the single rib tensile tests. The junction strengths of the pre-construction geogrid samples are shown in the Table 3. The average junction strength efficiencies vary from 9.5% to 14.6% for the test samples.

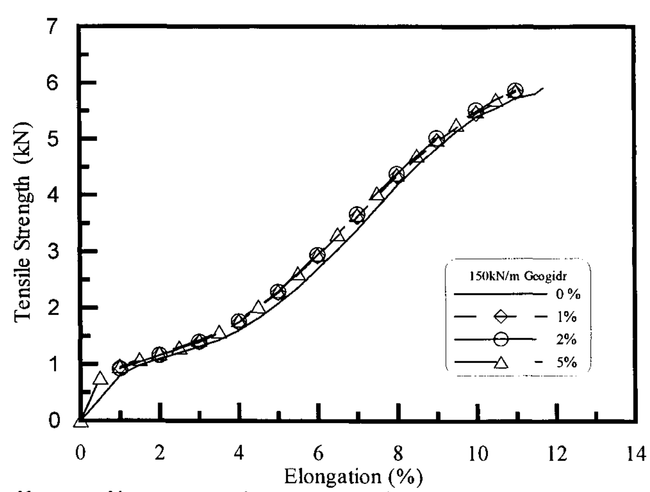

Figure 4. Typical single rib tensile strength test results for 150-kN/m geogrid under various preload conditions.

Table 2. The results of statistical analysis of typical single rib tensile tests for 60-kN/m geogrid under various preload conditions.

Preload	0%	1%	2%	5%
Tensile Strength (kN)	1.488	1.457	1.525	1.497
Standard Deviation (kN)	0.031198	0.062548	0.028191	0.041110
Measurement Uncertainty (kN)	0.009865	0.019779	0.006304	0.013000
Confidence Level (kN)	0.022318	0.044744	0.013194	0.029408
Elongation (%)	10.677	14.798	12.0375	11.421
5%Strain Strength (kN)	0.570	0.357	0.5005	0.511

Table 3. Typical junction strength test results for the pre-construction geogrid samples.

Geogrid Type	Single Junction Strength (N)	No. of Junction (No./m)	Junction Strength (kN/m)	Junction Strength Efficiency (%)
60kN/m	145.58	40	5.823	9.546
100kN/m	633.54	32	20.273	14.631
150kN/m	693.79	32	22.201	11.582
200kN/m	749.80	32	23.994	9.155

Tensile Strength of the Geogrid Placed in the Poor Graded Silty Gravel

As mentioned earlier, 20 test specimens were used for the tensile tests of each test condition. The single rib tensile strength of the 150 kN/m geogrid samples placed in the poor graded silty gravel (GP-GM) with 30 cm cover thickness under XMC test condition in comparison with the average tensile strength of the pre-construction samples is shown in Table 4. The average retained percentages for the ultimate and 5% strain tensile strength are 86.0% and 85.0%, respectively. The average of elongation at failure is about 90.0% of pre-construction sample. The results of 150 kN/m geogrid samples placed under the poor graded silty gravel for different cover thickness and compaction roller traveling direction are summarized in the Table 5. As shown in the table, the compaction direction has very low influence on rib tensile strength. However, the percentages strength retained associated with 15-cm lift thickness are slightly less than those associated with 30-cm lift thickness. The variance is not significant. The percentages strength retained are ranging from 81.4% to 86.0% for various conditions.

Table 4. The comparison of single rib tensile test results between pre-construction and installed samples (150 kN/m) placed 30 cm under the poor graded silty gravel with XMC condition.

	Tensile Strength		Elongation		5% Strain Strength	
Items	Test Values (kN)	Retain Percentage (%)	Test Values (%)	Retain Percentage (%)	Test Values (kN)	Retain Percentage (%)
Average Values	5.149	85.95993	10.2275	90.03081	1.954	84.95652
Standard Deviation	0.348544	5.81877	1.091454	9.607872	0.181177	7.87728
Interval	1.36	22.70451	3.61	31.77817	0.72	31.30435
Min. Value	4.33	72.28715	8.53	75.08803	1.59	69.13043
Max. Value	5.69	94.99165	12.14	106.8662	2.31	100.4348
Total	102.98	1719.199	204.55	1800.616	39.08	1699.13
Confidence Level	0.163124	2.723269	0.510816	4.496624	0.084794	3.686682

Table 5. Summary of the test results between the pre-construction and installed samples (150 kN/m) placed under the poor graded silty gravel for various test methods and test conditions.

Compactor type	Cover Thickness	Tensile Strength Retain Percentage	Elongation Retain Percentage	5% Strain Strength Retain Percent-age	Junction Strength Retain Percent-age
MDC	15cm	81.386	88.050	80.304	91.926
	30cm	84.958	89.969	83.587	75.116
XMC	15cm	83.402	89.979	79.840	76.086
	30cm	85.960	90.031	84.957	87.355

Comparison of Tensile Strength for The Five Backfill Materials

In order to provide complete data base for the installation damage of flexible geogrids, the average test values and percentages strength retained for the 60 kN/m woven geogrids placed within the test soils for XMC and MDC test conditions are summarized in the Table 6. Since the effect of soil cover thickness on rib tensile strength is not very significant for the condition tests, the data shown in the table are the average values for conditions associated with both 15-cm and 30-cm cover thickness. The data shown in the tables were obtained base upon the results analyzed from the single rib tensile tests and junction strength tests. In conclusion, the percentages strength retained for the 60-kN/m geogrid are about 95% for fine-grained soils, 94% for sands, and 69% to 88% for gravels. The test values and percentages strength retained for 100-kN/m, 150-kN/m, and 200-kN/m geogrids installed within the test soils are summarized in Tables 7, 8, and 9, respectively. It was found that those test geogrids consisted similar installation damage behavior as the 60-kN/m geogrid.

Table 6. The test result and retained percentages of the 60-kN/m geogrid under five different soils for XMC and MDC test conditions.

Soil type	Test condition	Tensile Strength		Elongation		5% Strain Strength		Junction Strength	
		Test Value (kN)	Retained Percentage (%)	Test Value (%)	Retained Percentage (%)	Test Value (kN)	Retained Percentage (%)	Test Value (N)	Retained Percentage (%)
CL	XMC	1.453	95.30	11.479	95.34	0.483	96.60	139.48	95.81
	MDC	1.447	94.89	10.950	90.95	0.515	103.01	132.65	91.12
SP	XMC	1.430	93.74	11.900	98.84	0.444	88.85	139.70	95.96
	MDC	1.438	94.31	11.992	99.60	0.431	86.15	138.18	94.92
GW	XMC	1.060	69.51	9.105	75.63	0.472	94.35	114.19	78.44
	MDC	1.037	68.02	9.062	75.27	0.461	92.10	117.18	80.49
GC	XMC	1.330	87.24	10.938	90.84	0.459	91.78	125.61	86.28
	MDC	1.376	90.25	12.178	101.14	0.426	85.25	125.63	86.29
GP-GM	XMC	1.141	74.82	9.464	78.60	0.482	96.34	116.47	80.00
	MDC	1.025	67.20	9.207	76.47	0.460	91.95	110.02	73.70

Table 7. The test result and retained percentages of the 100-kN/m geogrid under five different soils for XMC and MDC test conditions

Soil type	Test condition	Tensile Strength		Elongation		5% Strain Strength		Junction Strength	
		Test Value (kN)	Retained Percentage (%)	Test Value (%)	Retained Percentage (%)	Test Value (kN)	Retained Percentage (%)	Test Value (N)	Retained Percentage (%)
CL	XMC	4.043	93.36	12.13	103.70	1.258	71.47	616.85	97.38
	MDC	4.009	92.59	11.98	102.45	1.253	71.20	591.50	93.38
SP	XMC	3.810	87.99	11.43	97.75	1.276	72.49	659.81	104.16
	MDC	3.889	89.81	11.90	101.82	1.231	69.94	596.14	94.11
GW	XMC	3.419	78.95	11.15	95.38	1.124	63.87	618.98	97.71
	MDC	3.507	81.00	11.83	101.22	1.034	58.77	599.60	94.66
GC	XMC	3.828	88.41	11.42	97.70	1.292	73.41	624.74	98.62
	MDC	3.955	91.32	13.31	113.88	1.014	57.62	552.39	87.20
GP-GM	XMC	3.420	78.97	10.30	88.11	1.250	71.03	553.40	87.36
	MDC	3.483	80.45	10.61	90.79	1.272	72.28	568.76	89.79

Table 8. The percentages and retained reduction factors of the 150-kN/m geogrid under five different soils for XMC and MDC test conditions

Soil type	Test condition	Tensile Strength		Elongation		5% Strain Strength		Junction Strength	
		Test Value (kN)	Retained Percentage (%)	Test Value (%)	Retained Percentage (%)	Test Value (kN)	Retained Percentage (%)	Test Value (N)	Retained Percentage (%)
CL	XMC	5.569	92.98	10.92	96.14	1.985	86.32	588.35	84.80
	MDC	5.859	97.81	11.71	103.06	2.055	89.36	599.55	86.42
SP	XMC	5.412	90.35	10.63	93.61	1.984	86.26	555.48	80.06
	MDC	5.516	92.09	11.04	97.18	1.928	83.81	586.06	84.47
GW	XMC	4.667	77.91	9.64	84.89	1.899	82.54	555.14	80.01
	MDC	4.910	81.97	9.99	87.94	1.923	83.60	566.76	81.69
GC	XMC	5.208	86.94	10.44	91.93	1.917	83.34	589.19	84.92
	MDC	5.290	88.32	10.92	96.10	1.791	77.89	592.08	85.34
GP-GM	XMC	5.073	84.68	10.22	90.00	1.895	82.40	566.97	81.72
	MDC	4.982	83.17	10.11	89.01	1.885	81.95	579.46	83.52

Table 9. The percentages and retained reduction factors of the 200-kN/m geogrid under five different soils for XMC and MDC test conditions

Soil type	Test condition	Tensile Strength		Elongation		5% Strain Strength		Junction Strength	
		Test Value (kN)	Retained Percentage (%)	Test Value (%)	Retained Percentage (%)	Test Value (kN)	Retained Percentage (%)	Test Value (N)	Retained Percentage (%)
CL	XMC	7.433	90.75	12.625	87.07	2.099	105.99	669.19	89.25
	MDC	7.587	92.63	12.634	87.13	2.206	111.41	743.46	99.15
SP	XMC	7.321	89.38	12.844	88.58	1.844	93.12	707.01	94.29
	MDC	7.275	88.83	13.358	92.12	1.855	93.66	725.08	96.70
GW	XMC	6.688	81.66	11.622	80.15	1.977	99.84	669.44	89.28
	MDC	6.571	80.23	10.254	70.71	2.387	120.53	688.14	91.78
GC	XMC	7.052	86.10	11.824	81.54	2.092	105.67	733.50	97.83
	MDC	7.386	90.19	13.046	89.97	1.896	95.73	695.89	92.81
GP-GM	XMC	6.866	83.83	45.486	90.26	1.735	87.61	663.75	88.52
	MDC	6.508	79.46	44.172	81.20	1.916	96.78	741.07	98.84

Tensile Strength at 5% Strain

Variation of the tensile strength at 5% strain for the 60-kN/m geogrid installed in the test soils for XMC and MDC test conditions are shown in Tables 6. As shown in the table, the effect of installation process on 5% strain tensile strength is relatively less that on rib ultimate tensile strength. Typically, the percent of strength retained varies from 94% to 99% for the conditions tested. By evaluating the data shown in tables 7 to 9, the effect of installation process on 5% strain tensile strength is relatively more significant for the geogrid with higher tensile strength.

Elongation at Failure

Compatibility is an important principle in the geogrid reinforcement application. Therefore, the rib elongation and tensile strength at desire strain are the important mechanical properties of geogrid. The elongations at failure of the 60-kN/m geogrid samples installed in the five different test soils are also shown in Table 6. Based upon the test results, the average elongation values at failure for the various type pre-construction samples range from about 11.4% to 14.5%. The elongations at failure for various types geogrids and different test conditions are also shown in tables 6 to 9. For the great majority conditions, the data shown in the tables indicate that the installation process would reduce the elongation of test sample at failure. The amount of reduction of strength could be related to the type of damage of geogrid rib due to installation damage. By further analyzed the data, it is found that the compaction roller traveling direction is also having no significant effect on the single rib elongation at failure.

Junction strength

Commonly, the opening area of geogrid is also an important physical property that controls the interlocking behavior of soil/geogrid system. In addition to provide surface friction, geogrid, junction strength is another mechanism that will transfer the pullout resistance of geogrid from soil to geogrid. Therefore, junction strength is another important mechanical property for geogrid. Tables 6 to 9 also consisted the junction strength for the tested geogrid samples installed in the five different test soils for XMC and MDC test conditions. As mentioned earlier, the average junction strength for the 150-kN/m pre-construction geogrid samples is about 693.8 Newtons. As shown in Table 8, the average junction strength for the150 kN/m geogrid samples installed was generally decreased in the range from 555 Newtons to 600 (80.0 to 84.8% of the pre-construction sample). In addition, the behavior of junction strength for XMC and MDC test conditions was found to be quite similar to each other. And the junction strength behavior for others type of geogrid samples is quite similar to that associated with the150 kN/m geogrid samples.

SUMMARY AND CONCLUSIONS

The installation survivability of four styles of flexible geogrids from one manufacture under various conditions was performed. The tensile strength of the tested geogrids were 60 kN/m, 100 kN/m, 150 kN/m, and 200 kN/m, and the test geogrid samples were placed and compacted in five different soils with 30 cm or 15 cm cover thickness. The samples then were carefully hand shoveling from the test field and sent to the laboratory for testing. The single rib tensile strength and junction strength tests according to the GRI-GG1 and GRI-GG2 specifications were performed. Base upon the test results, the reduction factor of the rib ultimate tensile strength, the tensile strength at 5% strain, elongation at failure, and junction strength were obtained.

The results of the study have indicated that installation damage to a flexible geogrid is a function of grain size distribution of backfill material, compactor traveling direction, and lift thickness. It is also clear that geogrid placed within the angular crushed stone gravel shown greater damage than other backfill materials, while the geogrid placed in a fine sand or fine grained soil shown little damage. Due to the time constrain, the degree of compaction, the type and weight of compaction equipments are not examined as the variables in the study.

In addition to provide the installation damage database for this type of flexible geogrid, the other goal of the study was to quantify a reduction factor for geogrid installation survivability. Based upon the results of the study, the recommended typical and average reduction factors for flexible geogrids placed within various types of soils are listed in Table 10. As shown in the table, geogrid installed in gravel backfill showed more severe damage than same material placed in fine grain soil or fine sand. The typical reduction factors of single rib tensile strength for fine grain soil, sandy soil, gravel with some fine soils, and the crushed stone gravel are about 1.01 to 1.20, 1.04 to 1.18, 1.05 to 1.52, and 1.14 to 1.74. In addition, the average reduction factors of junction strength for fine grained soil, sandy soil, gravel with some fine soils, and the crushed stone gravel are 1.09, 1.08, 1.12 to 1.18, and 1.16, respectively. The recommended values appear to agree with those values recommended by FHWA.

Table 10. Typical recommended reduction factor for installation damage of flexible geogrids

Soil Type	Tensile Strength		Junction Strength	
	Range of Reduction Factor	Average Reduction Factor	Range of Reduction Factor	Average Reduction Factor
CL	1.01□1.20	1.10	1.00□1.21	1.11
SP	1.04□1.18	1.11	1.00□1.31	1.16
GW	1.14□1.74	1.44	1.00□1.41	1.21
GC	1.05□1.19	1.12	1.00□1.25	1.12
GP-GM	1.13□1.52	1.33	1.00□1.40	1.20

ACKNOWLEDGEMENTS

The study is part of the generic research on geogrids by the Geosynthetic Laboratory of National Pingtung University of Science and Technology at Taiwan. The study was partially supported by Seven States Enterprise Co. Ltd. The field installation damage program was assisted and arranged by the President Tang-Hui Chang of All-Toffs Industrial Co., Ltd. The Graduate students Jen-Han Wu, Ming-Wen Hsieh, and Undergraduate students Ming-Cher Wong and Chain-Kwue Lin of the National Pingtung University of Science and Technology performed the field installation study and laboratory-testing program. The authors express sincere appreciation to all the members having great contribution to the study.

REFERENCES

Bonaparte, R., Ah-Line, C., Charron, R., & Tisinger, L. 1998. "Survivability and Durability of a Nonwoven Geotextile," *Proc. Geosynthetics for Soil Improvement, Geotech. Spec. Publ. 18, ASCE,* pp. 68-91.

Christopher, B. R. & Holtz, R. D. 1984. *Geotextile Engineering Manual*, FHWA DTFH 61-80-C-0094, Washington DC.

Halliburton, T. A., Lawmaster, J. D. & McGuffey, V. E. 1982. *Use of Engineering Fabrics in Transportation Application*, FHWA DTFH 0-C-0094, Washington DC.

Koerner, G. R. & Koerner, R. M. 1990. The Installation Survivability of Geotextiles and Geogrids, *Fourth International Conference on Geotextiles, Geomembranes, and Related Products.* The Hague, Balkema, Rotterdam. pp. 597-602.

Koerner, G. R., Koerner, R. M. & Elias, V. 1993. Geosynthetic Installation Damage Under Two Different Backfill Conditions, *Geosynthetic soil Reinforcement Testing Procedures, ASTM STP 1190,* West Conshohocken, PA, pp. 163-183.

Koerner, R. M. 1998. *Designing with Geosynthetics*, 4th. Edition, Prentice Hall.

Rainey, T. & Barksdale, R. 1993. Construction Induced Reduction in Tensile Strength of Polymer Geogrids, *Geosynthetics '93 Conference*, St. Paul, Minn.

Richardson, G. N. 1998. Field Evaluation of Geosynthetic Survivability in Aggregate Road Base, *Geotechnical Fabrics Report*. Vol. 16, No. 7, Sep. pp. 34-38.

Suits, L.D. and G.N. Richardson, 1996, "M288-96: The Updated AASHTO Geotextile Specifications", *Geotechnical Fabrics Report*, Vol. 16, No.2, March pp.39-41.

Troost, G. H. & Ploeg, N. A. 1990. Influence of Weaving Structure and Coating on the Degree of Mechanical Damage of Reinforcing Mats and Woven Geogrids, Caused by Different Fills, During Installation, *Proc. 4th IGS Conference,* The Hague, The Netherlands, pp. 609-614.

Troost, G. H. & Ploeg, N. A. 1990. Influence of Weaving Structure and Coating on the Degree of Mechanical Damage of Reinforcing Mats and Woven Geogrids, Caused by Different Fills, During Installation, *Proc. 4th IGS Conference,* The Hague, The Netherlands, pp. 1119-1124.

CREEP OF GEOGRID REINFORCEMENT FOR RETAINING WALL BACKFILLS

F. NAVARRETE
FLORIDA ATLANTIC UNIVERSITY
UNITED STATES OF AMERICA
CONSEJO NACIONAL DE CIENCIA Y TECNOLOGIA
MEXICO
D. V. REDDY
FLORIDA ATLANTIC UNIVERSITY
UNITED STATES OF AMERICA
P. LAI
FLORIDA DEPARTMENT OF TRANSPORTATION (FDOT)
UNITED STATES OF AMERICA

ABSTRACT

This paper describes the Creep and Creep-Rupture investigation carried out for two types of geogrids: High Density Polyethylene (HDPE) and Polyester Terephthalate (PET). The specimens were tested in different exposure environments, simulating Florida soil-water conditions, with super-ambient temperatures for accelerated testing. It was observed that HDPE geogrids undergo larger creep than PET geogrids, and the different exposures do not play an important role in the rate of creep. Exposure temperatures and load levels have a strong effect on the amount of creep strain and creep rupture, mainly for the HDPE geogrids. Creep rupture occurred in several of the HDPE specimens. The PET specimens did not experience creep rupture except for two specimens; for these two cases the rupture was attributed to either defects in the specimens or defective clamping.

INTRODUCTION

The ASTM D5262 (1992) defines a geogrid as "a geosynthetic formed by a rectangular network of integrally connected elements with apertures greater than 6.35mm (1/4 in.) to allow interlocking with the surrounding soil, rock, earth, and other surrounding materials to function primarily as a reinforcement". Geogrids are produced for biaxial and uniaxial load-carrying configurations.

Due to the relatively short experience with these polymeric materials, there are uncertainties regarding their durability, with respect to retainment of the design properties after being subjected to construction stresses and exposed to in-soil environments over the expected design life. Potential degradation of polymeric reinforcement, with time, will depend on the characteristics of a specific polymer, configuration, and the environment to which it is exposed. If geogrids have to be used as an alternative to steel reinforcement to overcome the corrosion problem, their performance has to be established based on laboratory and field testing for site specific conditions, e.g. high water tables and temperature ranges of 27° C to 38° C in Florida.

HDPE Geogrids

HDPE is the acronym for High Density Polyethylene, The uniaxial HDPE geogrids used in this research are manufactured by stretching punched sheets of extruded HDPE in one direction, under carefully controlled conditions, Table 1. This process aligns the polymer's long-chain molecules in the direction of drawing, and results in a product with high one-directional tensile strength and modulus.

Table 1 Properties of UX-1400 HDPE Geogrid

Properties	Test methods	Units	Value
Apertures: MD	Calipered	mm	137(nom.)
CDM	"	mm	137(nom.)
Open area	COE Method	%	60 (nom.)
Thickness: ribs	ASTM D1777-64	mm	1.8(nom.)
junctions	"	mm	5.8(nom.)
Creep Limited Strength	GRI GC3-87	kN/m	43.8(min.)
Flexural Regidity	ASTM D1388-64	mg-cm	6600000(min.)
Tensile Modulus MD	GRI GG1-87	kN/m	1896(min.)
Junctions: strength	GRI GG2-87	kN/m	102 (min.)
efficiency	"	%	90 (min.)

PET Geogrids

PET is the acronym for Polyester Terephthalate. PET geogrids are made of polyester multifilament yarns, which are interlocked by weaving to create a stable network, such that the yarns retain their relative positions, Table 2. Compared to HDPE, PET is more flexible in bending and exhibits a relatively lower junction strength.

Table 2 Properties of matrex-30 PET Geogrid

Properties	Test methods	Units	Value
Mass/Unit Area	ASTM D5261-92	g/m^2	332
Aperture size MD		mm	81.3
CDM		mm	12.7
Ultimate Tensile Strength	ASTM D-4595	kN/m	48
Creep Limited Strength			
-5 %	ASTM D-4595	kN/m	39
-5 %	GG3	kN/m	20
-10 %	GG3	kN/m	31

Creep and Creep Rupture

Creep is simply the viscoelastic response of the reinforcement due to a sustained load. It results in time-dependent deformation, which may continue to occur as long as the reinforcement is loaded. Creep is a material, load, temperature, and time-dependent phenomenon. It is associated with all the mechanical deformations: tensile, compression, torsion, and flexure (ASTM D 2990-93a, 1993). However, tensile creep is the only deformation that matters for geogrid, since it is a flexible material. It is of primary importance in the design of polymeric reinforced structures, (Allen 1991). The tensile creep test is carried out by applying in-plane stress and the compressive creep test by transverse loading. Creep and creep-rupture data must be taken into consideration for the determination of the creep modulus and strength of the material for long-term behavior (Cazzuffi et al, 1997). The creep test measures the dimensional changes of a specimen subjected to a constant load during a certain period of time, while the creep rupture test measures the time taken for rupture to occur under sustained constant loading (ASTM D 2990-93a, 1993).

Geosynthetic geometry tends to dominate primary creep, whereas the polymer material tends to dominate secondary and tertiary creep, (Allen et al. 1983). Soil confinement tends to restrict the movement of individual filaments, preventing their realignment in the direction of load, thereby substantially reducing the magnitude of the geosynthetic macrostructure creep i.e., primary creep, (McGrown et al. 1982). Chemical aging of geosynthetics is the result of both soil environmental factors and the polymer chemical structure. In general, chemical aging can affect creep at relatively high temperatures, as those encountered in Florida, with moderate high moisture conditions in soils which are chemically active.

Creep-rupture is expressed in terms of decreasing life with increasing stress and temperature, and the transition from ductile to brittle behavior. It is important to identify the "failure time transition" point in the creep-rupture plot for realistic estimation of life. Figure 1 shows the creep rupture behavior for a semi-crystalline polymer.

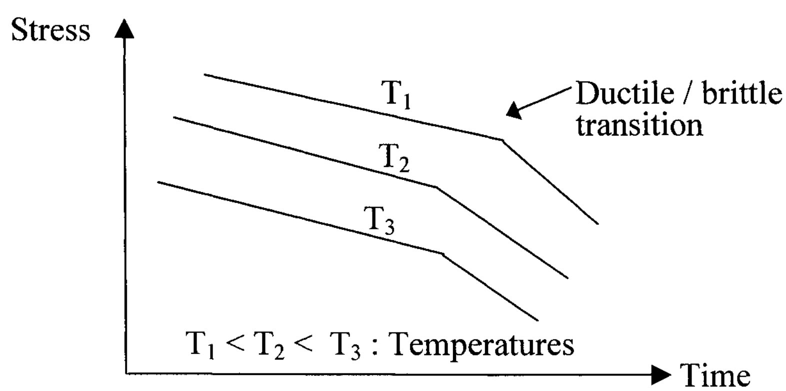

Figure 1 Creep-rupture Behavior for a Semi-crystalline Polymer. Ahn et al. (1998)

EXPERIMENTAL INVESTIGATION

To simulate different exposure conditions, 20 tanks were fabricated. The specimens were tested in different exposure environments simulating Florida soil-water conditions, with super ambient temperatures for accelerated testing. The specimens were exposed to the different environments during the entire test periods. The creep and creep rupture tanks were filled with different solutions and soils, with 6 single rib geogrid test specimens in each tank. The test setup comprised clamps for gripping each specimen, heaters and pumps to maintain the temperatures and compositions of the solutions, clocks for time measurement, dial gages with extensions to record the elongations, loading lever arms (1:5), and weights for the application of constant loads.

The temperatures were 30° C, 35° C, 45° C, 55° C and 65° C, with submergence in the following groundwater-simulating solutions:

HDPE specimens:
- Calcareous (pH 9.0)
- Phosphate (pH 4.5)
- Limerock
- Seawater

PET specimens:
- Calcareous (pH 9.0)
- Phosphate (pH 4.5)
- Limerock
- Seawater
- Freshwater

The load levels were 30 %, 40 % and 50 % of the ultimate load.

The results are presented for creep strain and creep rupture tests on both HDPE and PET test specimens. The values of creep strain were plotted for each of the two specimen types categorized as: "Specimen Set I" and "Specimen Set II". Each graph corresponds to a geogrid type, specimen set, temperature and load level, including all environmental exposures. Regression analysis was carried out for each specimen.

Creep

From the creep testing, it was observed that PET geogrids resist creep strain better than HDPE ones at similar temperatures and load levels, Figures 2 and 3. However, for both HDPE and PET specimens the increase in temperature and load level have a strong effect on the creep strain behavior, relatively larger for HDPE specimens.

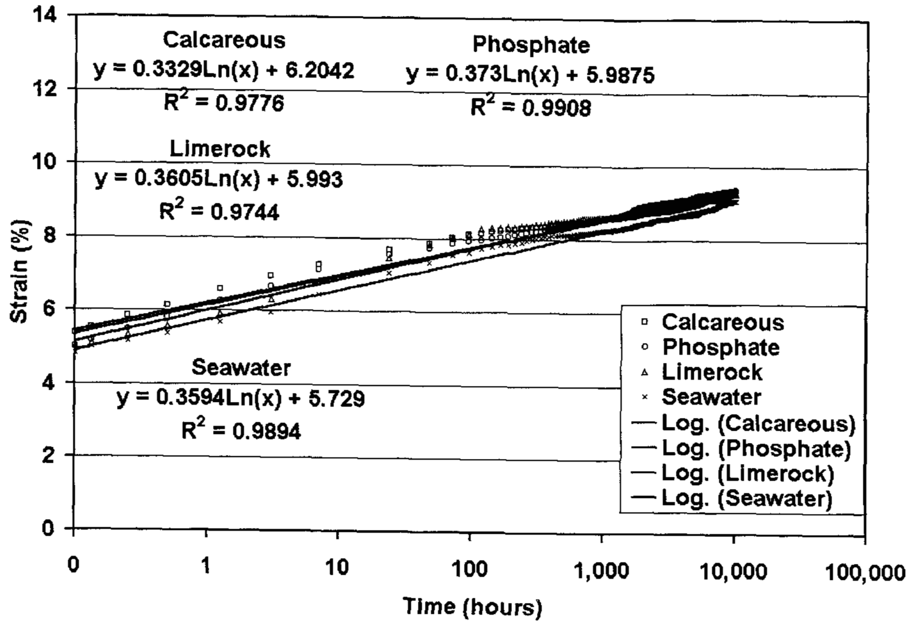

Figure 2 Creep Curves for HDPE Geogrids, T = 30°C, Load Level = 30% Ultimate Load - Specimen set I

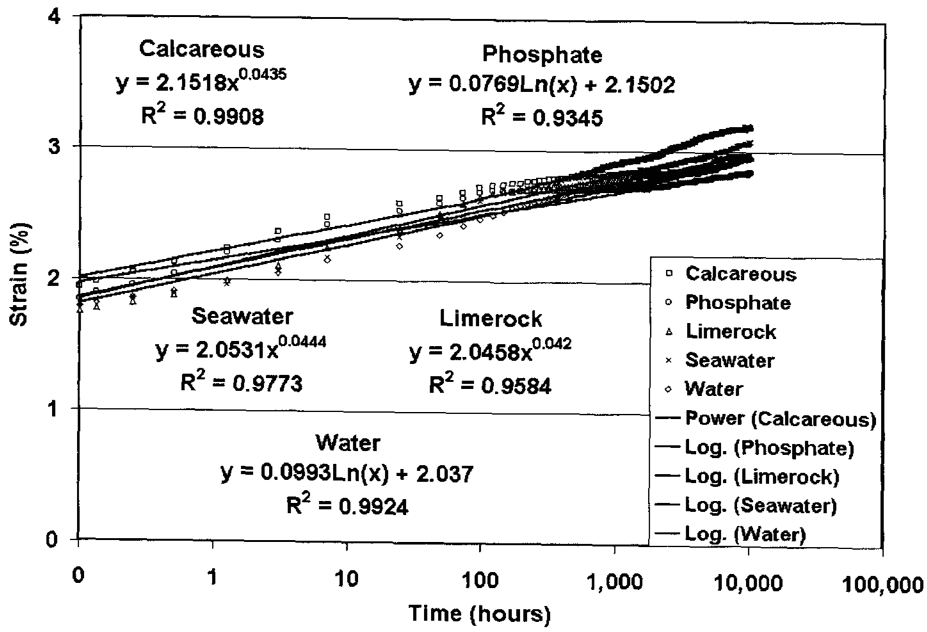

Figure 3 Creep Curves for PET Geogrids, T = 30°C, Load Level = 30% Ultimate Load - Specimen set I

It can be observed, that HDPE geogrids show large deformations, up to 55 % strain under the most extreme conditions (i.e. T= 65° C and Load level = 50% ultimate load, Figure 4), while for PET specimens the maximum creep strain was 14 % for the same conditions, Figure 5.

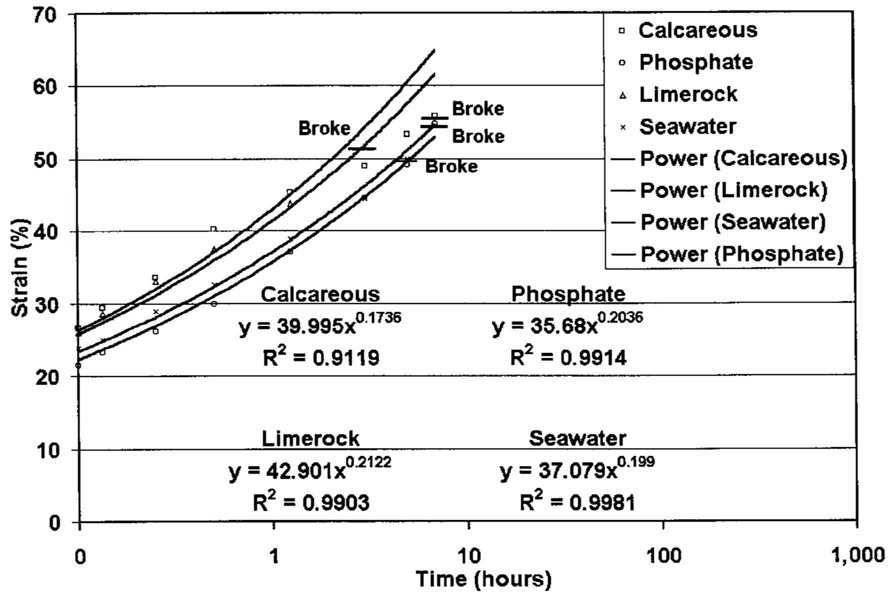

Figure 4 Creep Curves for HDPE Geogrids, T = 65°C, Load Level = 50% Ultimate Load - Specimen set II

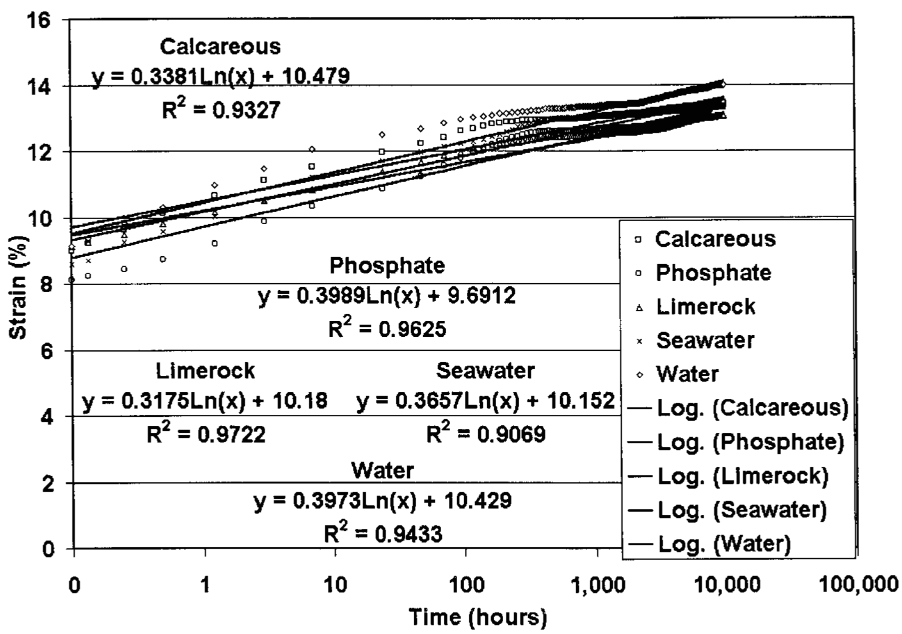

Figure 5 Creep Curves for PET Geogrids, T = 65°C, Load Level = 50% Ultimate Load - Specimen set II.

From the results shown in Tables 3 to 6, it can be seen that the increase in temperature has a large influence on the amount of creep strain, and that specimens exposed to higher temperatures will be subjected to larger amounts of creep strain before breaking than those exposed to lower temperatures. Also, the creep strain at breaking for the HDPE specimens was about 50% when exposed to 55° C or 65° C.

The increase in load level also increases the amount of creep strain in the specimens, but the influence is not as large as that due to the temperature. However, higher the temperature, the larger is the influence of the increase in load level. It should be noticed that the different solutions do not seem to influence the amount of creep strain.

Table 3 Creep Strain (%) for HDPE Specimens 30° C

Load level	30 %	40 %	50 %
Initial strain	4.5 - 5	4.5 - 6	7.5 - 8
Final strain	8.5 - 9	11 - 11.5	17.5 - 20.5

Table 4 Creep Strain (%) for HDPE Specimens 45° C

Load level	30 %	40 %	50 %
Initial strain	6 - 6.5	8.6 - 9.5	11 -13
Final strain	10 - 11	16 - 19	34 - 39

Table 5 Creep Strain (%) for HDPE Specimens 55° C

Load level	30 %	40 %	50 %
Initial strain	6.3 - 7	9.5 - 10.5	14 -16
Final strain	10.5 - 11.5	23 - 27	46 - 53

Table 6 Creep Strain (%) for HDPE Specimens 65° C

Load level	30 %	40 %	50 %
Initial strain	8 - 9	11 - 13	19 -26
Final strain	17 - 19	28 - 33	46 - 56

From the results shown in Tables 7 to 10, it can be seen that the increase in temperature has a large influence on the amount of creep strain , but not as much as that encountered in HDPE specimens; for PET specimens the effects of temperature and load level are similar. It should be noticed that the different solutions do not seem to influence the amount of creep strain.

Table 7 Creep Strain (%) for PET Specimens 30° C

Load level	30 %	40 %	50 %
Initial strain	1.8 - 2.1	2.6 - 2.9	4.9 -5.3
Final strain	2.7 - 3.2	3.4 - 4	6.3 - 6.9

Table 8 Creep Strain (%) for PET Specimens 45° C

Load level	30 %	40 %	50 %
Initial strain	3.8 - 4.2	4 - 5	6.3 - 7
Final strain	5.2 - 5.9	5.6 - 6.5	8.4 - 9.8

Table 9 Creep Strain (%) for PET Specimens 55° C

Load level	30 %	40 %	50 %
Initial strain	3.6 - 4	5.2 - 5.8	7.8 - 8.2
Final strain	5.3 - 5.9	7.9 - 8.8	10.2 - 11

Table 10 Creep Strain (%) for PET Specimens 65° C

Load level	30 %	40 %	50 %
Initial strain	3.4 - 4.3	6.7 - 7.2	8.4 - 9
Final strain	6 - 6.6	9.2 - 10.2	13 -14

Creep Rupture

The PET specimens did not experience creep rupture except for two specimens, and for those two cases the rupture can be attributed to either defects in the specimens or poor clamping. On the other hand, for the HDPE specimens, creep rupture was observed in all the specimens exposed to 50% of the ultimate load; and for the 55° C and 65° C temperatures, creep rupture occurred at 40% of the ultimate load. Tables 1 to 4 indicate that the specimens exposed to higher temperature undergo larger deformations before creep rupture occurs. Tables 9 to 11 show the time of rupture for the HDPE geogrids.

It can be observed in Table 11, that creep rupture occurred between 17.5 % and 20.2 % creep strain for the 30° C temperature and 50 % ultimate load, while for the 45° C temperature and 50% ultimate load the rupture occurred between 34.3 % and 39.1% creep strain . The rupture time for the 30° C temperature and 50 % ultimate load was between 6,768 and 8,520 hours, except for the limerock exposure, while for the 45° C temperature and 50% ultimate load, the time to rupture varied from 360 to 528 hours.

Table 11 Creep Rupture for HDPE Specimens, Load Level = 50% Ultimate Load, T= 30° C & 45° C

Time/Strain	30° C-set I Hours / %	30° C-set II Hours / %	45° C-set I Hours / %	45° C-set II Hours / %
Calcareous	8520 / 19.1	7752 / 18.9	528 / 39.1	408 / 35.4
Phosphate	6768 / 18.1	8040 / 19.7	408 /34.8	408 / 34.3
Limerock	3576 / 20.2	3696 / 17.5	408 / 38.7	480 / 37.4
Seawater	7584 / 19.5	6768 / 17.7	528 / 37	360 / 36.8

With these results it can be seen that the temperature has a strong effect on the percentage creep strain reached before creep rupture occurs and the time to creep rupture. The limerock exposure, at 30° C temperature and 50% ultimate load, reached creep rupture at only 3,576 to 3,696 hours. This can be attributed to non-uniform temperature exposure of the geogrid.

Table 12 Creep Rupture for HDPE Specimens, Load Level = 50% Ultimate Load, T= 55° C & 65° C

Time/Strain	55° C-set I Hours / %	55° C-set II Hours / %	65° C-set I Hours / %	65° C-set II Hours / %
Calcareous	120 / 46.2	48 / 52.5	5 / 46	7 / 55.9
Phosphate	120 / 51.2	120 / 50.3	5 /51.3	7 / 54.7
Limerock	96 / 51.5	96 / 52.2	7 / 48.4	3 / 51.7
Seawater	144 / 51.2	72 / 50.9	5 / 55.1	5 / 50

For the 55° C and 65° C temperatures shown in Table 12, the percentage of creep strain before creep rupture does not vary significantly suggesting that the creep strain limit for the material has been reached. The time to reach creep rupture was further reduced with the increment in temperature.

From Table 13, it can be seen that for the 55° C temperature and 40% ultimate load, the percentage of strain before creep rupture was between 23.3% and 27 %, while for the 65°C temperature and 40% ultimate load it was between 29.6% and 32.7%, showing again that temperature affects the amount of creep strain reached before creep rupture. Comparing Tables 12 and 13, it can be observed that the increase of load from 40% to 50% ultimate load also increases the creep strain before creep rupture.

It is clear from the results that the solution had no impact on the creep rupture, as the variabilities were principally from specimen to specimen. The only exception was limerock at 30° C temperature and 30% ultimate load. While this can be attributed to non-uniform distribution of temperature in the geogrid, which created regions, where the exposure temperature was higher than the 30° C required, not all findings permit this generalization.

Table 13 Creep Rupture for HDPE Specimens, Load Level = 40% Ultimate Load, T= 55° C & 65° C

Time/Strain	55° C-set I Hours / %	55° C-set II Hours / %	65° C-set I Hours / %	65° C-set II Hours / %
Calcareous	4392 / 23.3	2256 / 27	168 / 29.6	168 / 32.7
Phosphate	3576 / 23.5	3144 / 23.3	96 / 31	120 / 31.6
Limerock	3168 / 24.1	3432 / 24.2	168 / 31.7	168 /30.9
Seawater	2688 / 25.1	3192 / 23.6	240 / 29.9	240 / 30.2

CONCLUSIONS

In the creep plots, considerable variability of the data was encountered. This can be attributed to the testing of single rib specimens. The need to test more specimens for each condition has been identified. In the present research, it was not possible to test more than two specimens for each solution due to a large number of variables.

Regression analysis helped to address the variability and provide the equations to identify the creep strain at any given time. It can be observed that temperature and load have a strong effect on the creep behavior of HDPE geogrids. There is a large difference in creep strains between the HDPE geogrids exposed to 30° C and the ones exposed to 65° C, under the same load levels. Also, specimens exposed to higher temperatures showed a larger amount of creep strain before breaking, than those exposed to lower temperatures. Higher the temperature, the greater was the influence of increasing the load level. For PET specimens, the influence of temperature and the load level was similar.

It is clear that HDPE geogrids undergo larger creep strain than PET geogrids. The different exposures do not play an important role in the rate of creep strain. It can be observed that there are larger variabilities from specimen to specimen, than from different solutions.

Creep rupture occurred in all the HDPE specimens exposed to 50% of the ultimate load. For the specimens exposed to 40% of the ultimate load, creep rupture occurred for specimens exposed to 55° C and 65° C temperatures. From the results, it was found that specimens exposed to similar loading, but higher temperatures, underwent larger deformations before creep rupture occurred, and the time to failure is reduced. Also, an increase of the load level produced an increase in the amount of creep strain reached before creep rupture occurred.

For the 55° C and 65° C temperatures, the percentage of creep strain before creep rupture did not vary significantly, indicating that the creep strain limit for the material has been reached and was between 50% and 55% strain. The time to reach creep rupture was further reduced with the increment in temperature.

The PET specimens did not experience creep rupture except for two specimens; for these two cases, the rupture can be attributed to either defects in the specimens or defective clamping.

ACKNOWLEDGEMENTS

This paper is based on a Florida Department of Transportation (FDOT)-funded project entitled "Strength and Durability of Backfill Geogrid for Retaining Walls", Work Program # 0510738. The authors are grateful to FDOT for the funding. The support and encouragement of Dr. S.E. Dunn, Professor and Chairman of the Department of Ocean Engineering, and Dr. J.T. Jurewicz, Dean of Engineering, are gratefully acknowledged. Thanks are also due to Consejo Nacional de Ceiencia y Tecnologia (CONACYT) for its support to the second author (F. N.)

REFERENCES

Ahn, W. 1998. An Experimental and Analytical Investigation of Viscoelastic Pipe Soil Interaction, *Ph.D. Dissertation, Florida Atlantic University*, Boca Raton, Supervisor: Dr. D.V. Reddy, Florida DOT Research Contract Monitor: Powers, R. G

Allen, T. M. 1991. Determination of Long-Term Strength of Geosynthetics, *State-of-the-Art-Review, Proc., Geosynthetics 91 Conference*, Atlanta, USA. 351-379.

Allen, T. M., Bell, J. R., and Vinson T. S. 1983. Properties of Geotextiles in Cold Regions Applications, *Transportation Research Report No. 83-6*, Oregon State University, OR. USA.

ASTM D5265 1992 Standard Test Method for Evaluating the Unconfined Tension Creep Behavior of Geosynthetics, *Annual Book of ASTM Standards, Vol. 08 03.*

ASTM D 2990-93a: "Standard Test Methods for Tensile, Compressive, and Flexural Creep and Creep-Rupture of Plastics", 1993.

Cazzuffi D., Ghinelli A.: "European Experimental Approach to the Tensile Creep Behavior of High-Strength Geosynthetics", Geosynthetics '97 Conference Proceedings, Long Beach, 1997, pp.253-266.

McGrown, A., Andrews K. Z., and Kabir M. H. 1982 Load-Extension Testing of Geotextiles Confine In-Soil, *Second International Conference on Geotextiles Vol III*, Las Vegas, NV, USA. 793-798.

STUDENT PAPERS

THE PERFORMANCE OF A FULL-SCALE POLYESTER GEOGRID REINFORCED SEGMENTAL RETAINING WALL

Captain D.D. Saunders, P.Eng, Royal Military College of Canada

ABSTRACT

The Geotechnical Research Group at the Royal Military College of Canada (RMCC) is conducting a long-term research project that investigates the performance of a series of ten full-scale metallic and geosynthetic reinforced soil retaining walls. This paper describes the test program for the most recent wall (Wall 5), some instrumentation details, and presents some preliminary results that are compared with selected results from previous walls in the series. Wall 5 was loaded to stress levels well in excess of working load conditions and well beyond acceptable serviceability criteria using staged surcharge loading. Important performance features of reinforced soil structures have been identified from the data collected from this wall and earlier walls. In addition, the data has been instrumental in detecting sources of conservatism in current North American design methods. The project results will assist in the development of rational analysis and design methodologies for reinforced segmental soil retaining walls.

INTRODUCTION

Reinforced segmental soil retaining walls (Simac et al., 1993; Bathurst and Simac, 1994), as illustrated in **Figure 1**, consist of three main components: a facing which is comprised of dry-stacked modular concrete facing units, layers of metallic or geosynthetic reinforcement, and the backfill soil. Geosynthetic reinforced segmental soil retaining walls are a class of Mechanically Stabilized Earth (MSE) structures which, at heights greater than 6m, have been shown to cost approximately one-half that of conventional gravity walls based on the cost per square meter of exposed face (Koerner, 1998). However, the current North American design methodologies (AASHTO 1998; FHWA 1996; Simac et al., 1993) contain sources of conservatism which, once identified, may lead to further cost savings (Bathurst et al., 2000). In order to identify these sources of conservatism, the Geotechnical Research Group at the Royal Military College of Canada (RMCC) is conducting a long-term research project that investigates the design and per-

Figure 1. Construction of a geosynthetic reinforced segmental soil retaining wall.

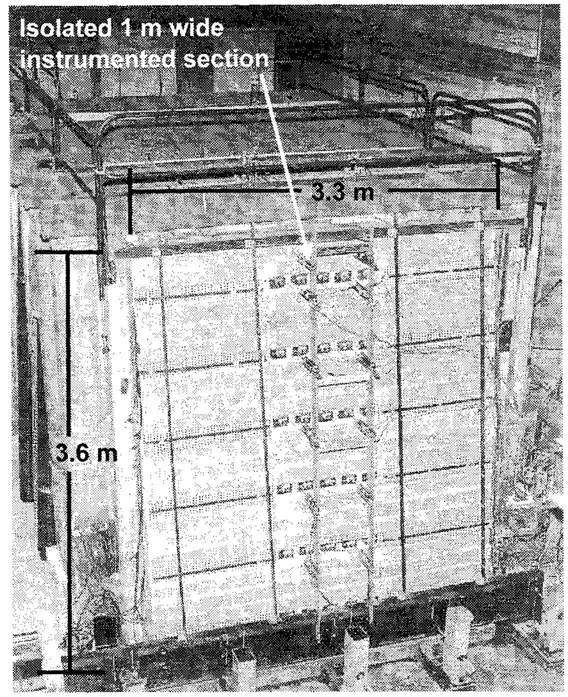

Figure 2. RMCC retaining wall test facility.

formance of geosynthetic and metallic reinforced segmental soil retaining walls. The experimental portion of this program involves the construction of ten full-scale, heavily instrumented reinforced soil retaining walls.

A total of five walls have been constructed and tested to date. Four of the walls were constructed using a column of dry-stacked modular concrete facing units (Walls 1, 2, 3, and 5) while another nominal identical wall was constructed with a wrapped-face (Wall 4). At the end of construction, each wall was stage surcharge loaded to stress levels in excess of working load conditions and well beyond acceptable serviceability criteria. This paper describes the test program for the most recent wall (Wall 5), some instrumentation details, and presents preliminary results that are compared with selected results from previous walls in the series.

RMCC RETAINING WALL TEST FACILITY

The RMCC retaining wall test facility (**Figure 2**) permits the construction and monitoring of soil retaining walls in a controlled indoor laboratory environment. The walls are 3.6 m high by 3.3 m wide with backfill soil extending 6 m from the front of the facility. The facility has a rigid concrete foundation while the soil is laterally restrained between two reinforced concrete counterfort walls that are bolted to the floor. The inside surfaces of these walls are lined with Plexiglass and multiple layers of polyethylene sheeting. Prior to constructing a wall, the inside surfaces of the side walls are lubricated to reduce the effects of side wall friction thereby ensuring that wall performance approaches a plane strain condition. A series of rigid reinforced concrete bulkheads is used to confine the rear of the soil mass. At the top of the facility six hollow steel sections are used as a restraining system for a timber joist and plywood ceiling. This ceiling confines a series of air bags that are used to apply uniform surcharge pressures up to 120 kPa (which equates to an additional 7 m of fill) to the entire backfill surface.

MATERIALS

Facing Units

The modular facing units used in this testing program were a solid masonry block with a continuous shear key. The location of the shear key combined with the block geometry provided a facing batter of 8 degrees from vertical. The blocks had an average mass of 20 kg and were 300 mm long (toe to heel), 200 mm wide, and 150 mm high. The wall face was constructed with a staggered block configuration (**Figure 2**) except for two vertical breaks to form three distinct columns: two 1.15 m outer columns and an isolated, instrumented 1 m wide central column.

Reinforcement

A knitted polyester geogrid reinforcement product was used in Wall 5. This reinforcement was selected because it had a similar strength to the biaxially extruded polypropylene reinforcement that was used in the four previous test walls. In-isolation constant load (creep) tests were conducted in order to develop isochronous load-strain data using the method described by McGown et al. (1984). Using the approach described by Bathurst and Benjamin (1990) and Bathurst (1990), the data may be used to infer the tensile loads in the reinforcement directly from the recorded strains and elapsed time measurements.

Soil

A locally procured clean, uniformly graded, rounded beach sand with a constant volume friction angle, $\phi_{cv} = 35^{\circ}$ and a plane strain friction angle, $\phi_{ps} = 44^{\circ}$ was used as backfill in these tests. The sand was placed in 150 mm lifts and was compacted to a dry unit weight of 16.8 kN/m^3 (relative density 50%) using a light-weight compactor. To avoid compaction induced stresses at the connections the area immediately behind the face was hand tamped to the same density using a 60 cm by 30 cm by 0.6 cm thick steel plate. Density and moisture content were measured using a nuclear densometer.

Instrumentation

Figure 3 shows the instrumentation plan for Wall 5, which used 242 instruments to record:

- Strain in the reinforcement layers;
- Connection loads between the facing column and reinforcement layers;
- Horizontal wall facing deflections;

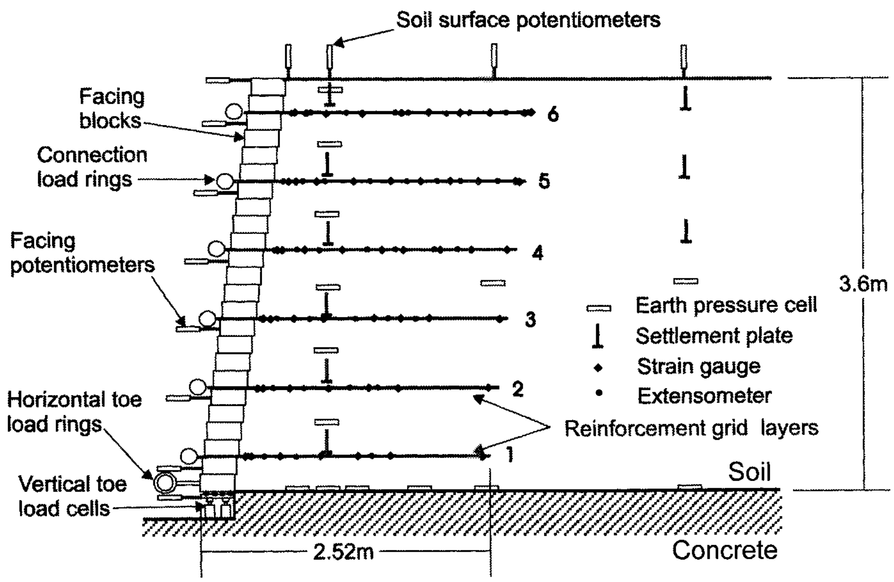

Figure 3. Wall 5 instrumentation plan.

- Horizontal and vertical toe loads;
- Vertical earth pressures both at the base and within the backfill soil mass; and
- Vertical deformations both within and at the surface of the backfill soil mass.

The polyester geogrid was instrumented using foil strain gauges (rated to 10%) bonded directly to the polyester fibres of selected longitudinal members. To ensure redundancy, the strain gauges were mounted in pairs at identical distances from the front of the reinforcement. It has been previously reported that the local strain measured by a strain gauge may differ from the average "global" strain recorded over a gauge length that incorporates several grid apertures (Bathurst, 1991). This is important since, for back-analysis purposes, the global strain readings are used to infer the reinforcement tensile forces. Therefore, in-isolation wide-width strip tensile tests (ASTM 4595) and single strand constant load (creep) tests (GRI GG3 Test Method) were used to determine the relationship between gauge strains and global strains of instrumented geogrid specimens.

Reinforcement displacements were measured using wire-line extensometers. These wire-line devices were sheathed in a stiff plastic tube in order to isolate the cable from the soil. One end of the cable was attached to a geogrid junction while the other end was attached to a displacement potentiometer located at the rear of the test facility. In addition to directly recording reinforcement displacements, displacement readings from pairs of extensometers were used to estimate the global strains in the reinforcement.

The facing units across the instrumented test section were modified with specially manufactured load rings to measure the reinforcement connection loads during construction, staged surcharging, and excavation. To simplify interpretation, the connections were designed to ensure that there was no slippage of the reinforcement layers at the interface between facing units.

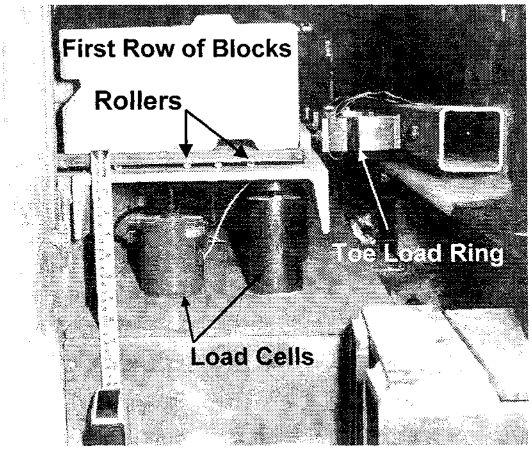

Figure 4. Profile view of instrumented footing.

The footing of the test facility was also instrumented, as illustrated in **Figure 4**. The facing column rested on a rigid steel plate that was in turn supported by a roller plate assembly. This assembly isolated the vertical and horizontal footing load components and allowed them to be measured independently for the duration of the test. Two rows of load cells were situated directly beneath the roller plate assembly to measure the facing column vertical load. The horizontal footing load was recorded using a row of specially manufactured toe load rings, which also restricted horizontal movement of the toe to less than 2 mm for the duration of the test. Therefore, the footing was essentially fully restrained with respect to vertical and horizontal degrees of freedom for the duration of the test.

An automated data acquisition system was used to record all instrumentation readings. The data was exported to spreadsheets so that a complete record of wall performance was available to the author within two hours of data downloading. Therefore, current data was available to make timely decisions regarding the experimental program, which was critical during the surcharge portion of the testing.

TEST PROGRAM

Bathurst et al. (2000) provide a detailed summary of the test program for the previous four walls tested to date in this long-term research project. Wall 1 was the control structure and was constructed with six layers of a polypropylene geogrid with low strength and stiffness properties in order to generate large strains and deformations under uniform surcharge loading. Wall 2 examined the influence of reinforcement strength and stiffness on wall performance by using a polypropylene geogrid having a strength and stiffness that was 50% that of the control structure. Wall 3 examined the influence of reinforcement spacing on wall performance and was constructed with only four layers of reinforcement. Wall 4 was constructed with a wrapped-face in order to examine the influence of the facing on wall performance.

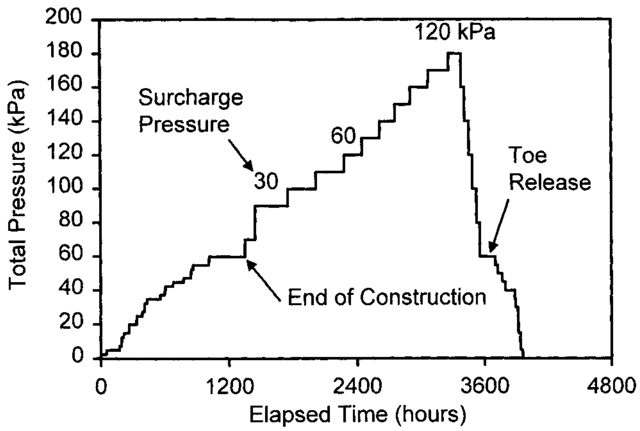

Figure 5. Wall 5 testing history.

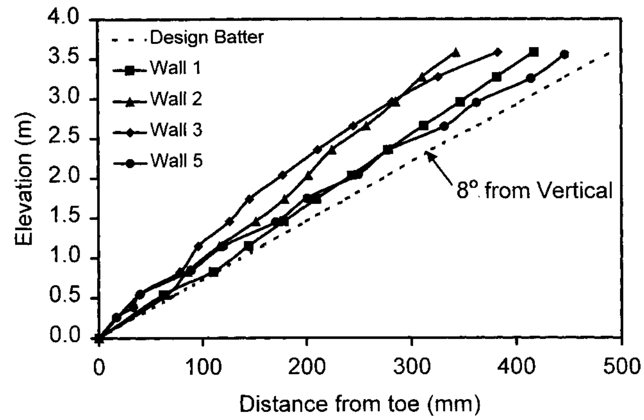

Figure 6. End-of-construction facing profiles.

Wall 5 incorporated a knitted polyester geogrid to examine the influence of reinforcement type on wall performance. At the end of construction Wall 5 was subjected to staged uniform loading (**Figure 5**) using the surcharge system described earlier in this paper. In the figure, the time datum is the beginning of construction, which commenced on 21 January 2000. Initially, a surcharge of 10 kPa was applied to confirm that all the instruments were functioning. The load was then increased to 30 kPa and each subsequent loading stage increased by 10 kPa until a surcharge of 120 kPa was reached, with each load increment being kept constant for a minimum of 100 hours. At the end of the surcharging program, the wall was unloaded in 20 kPa increments. After the wall was fully unloaded, the toe of the wall was released to examine the influence of the restrained toe on wall performance. Finally, while data acquisition continued, the wall was carefully excavated in 300 mm deep layers. This facilitated the visual confirmation of internal failure surfaces through the reinforced soil mass and the recording of any elastic rebound in the reinforcement layers due to the removal of the overburden soil.

RESULTS

Figure 6 compares the end-of-construction facing profiles for Walls 1, 2, 3 and Wall 5. The dashed line in the figure represents the target facing batter of 8 degrees from vertical. The figure shows that the actual facing alignment was steeper than the target batter. This change in alignment was a direct result of the incremental construction of the wall. In addition, the amount of construction-induced displacement ranges from 1 to 4% of the wall height. Furthermore, it may be seen that the Wall 5 displacement was similar to that of Wall 1, which was constructed with six layers of polypropylene reinforcement. However, the movement of Wall 5 was less than that of both Wall 2 (constructed with six layers of polypropylene reinforcement of reduced stiffness) and Wall 3 (constructed with four layers of polypropylene reinforcement).

Figure 7 compares the maximum observed outward movement for each of the walls constructed with a hard facing. Wall 2 facing displacements were significantly greater than those of the other walls since Wall 2 was constructed with a reinforcement stiffness that was one-half

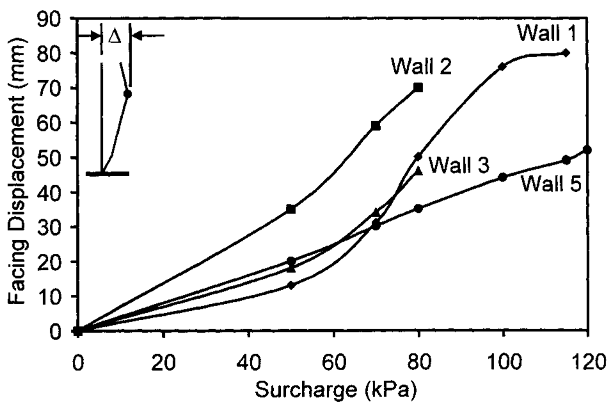

Figure 7. Maximum observed post-construction facing displacement.

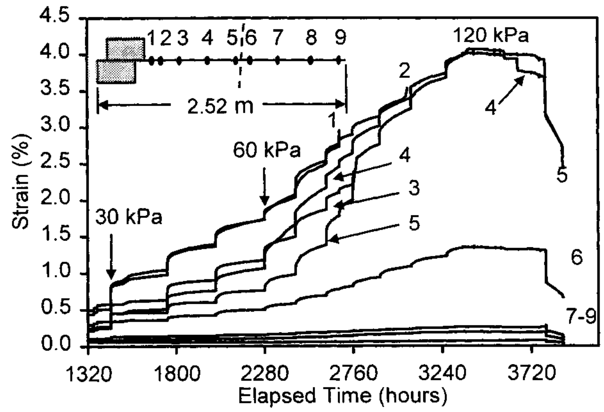

Figure 8. Strain gauge pair readings in Wall 5 reinforcement layer 4.

that of the control structure (Wall 1) and, therefore, greater displacements were anticipated. With the exception of Wall 2, at low surcharge levels the observed facing displacements were comparable. However, at surcharges greater than 70 kPa (i.e. at loads well in excess of predicted surcharge capacities) the measured facing displacements for Wall 5 were less than those recorded for the other walls. This effect may be attributed to differences in geogrid properties, stiffness, and geogrid-soil interaction.

Figure 8 illustrates the recorded strain in reinforcement layer 4 of Wall 5, which is located at an elevation of 2.1 m above the base. The data presented is the average of each strain gauge pair readings. It should be noted that the strain magnitude for Wall 5 was within the range recorded for the hard-faced walls incorporating polypropylene reinforcement (Walls 1, 2, and 3). Beyond the end of construction, each jump in the strain curve corresponds to the application of a new surcharge load. It may be seen that initially the largest measured strains were located at or near the facing connections. The generation of these strains may be attributed to the downward movement of the soil behind the relatively rigid facing. Finally, it may be seen that as the surcharge increased, the strain propagated further back into the soil as an internal failure plane developed. This is consistent with the active zone and the anchorage zone assumed in conventional tied-back wedge theories of design.

Figure 8 may also be used to illustrate creep of the reinforcement. During any given surcharge increment, it may be seen that the recorded strain increased with respect to time which is indicative of the time-dependent strain deformation characteristics of visco-elastic materials. In addition, during the subsequent unloading and excavation of the wall, the strain in the reinforcement decreased slightly, which is consistent with the notion of elastic rebound. Therefore, the instrumentation used in this experiment was sensitive enough to record not only the creep deformation but also the elastic rebound of the reinforcement layers.

Figure 9 shows the vertical loads recorded at the footing during the construction of Wall 5. The self-weight of the facing column (W) is plotted as the linear line. In addition, this figure

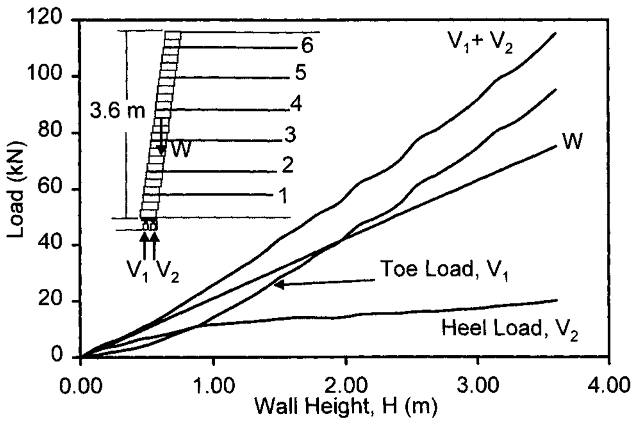

Figure 9. Vertical toe loads recorded for Wall 5 during construction.

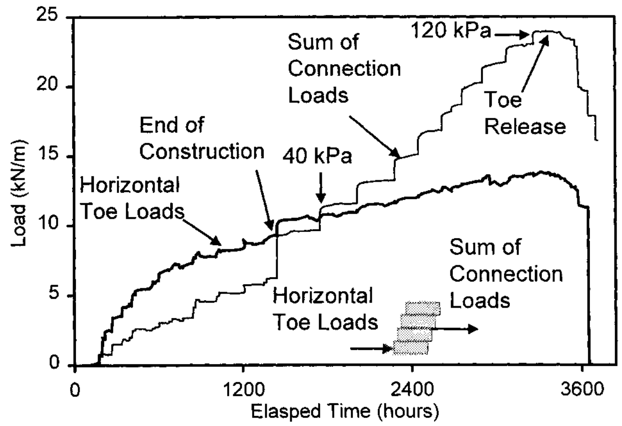

Figure 10. Comparison of Wall 5 horizontal toe loads and reinforcement connection loads.

plots the vertical footing load recorded by the load cells located at both the heel and the toe of the footing (**Figure 4**). It may be seen that the calculated sum of the vertical footing loads was greater than the facing column self-weight. This difference is attributed to the generation of soil down-drag forces behind the facing column. In addition, as construction progressed, the vertical load at the toe was significantly greater than at the heel, which indicates rotation about the toe. However, it is worthy to note that the heel of each block was not unloaded which implies that the wall batter was sufficient to maintain block-to-block interface contact. Similar results were observed with the other walls constructed with a hard facing (Bathurst et al., 2000). These measurements have two major implications on design. Firstly, the normal load on the reinforcement connections is higher than that presently assumed in design, and therefore the available frictional connection shear capacity is greater than that presently assumed in design. Secondly, the hinge height calculation for modular block walls (Simac et al., 1993; Bathurst and Simac, 1994) is conservative for design of walls with a similar geometry and steep facing batter.

Figure 10 depicts the history of horizontal toe load measurements recorded at the footing and the sum of the reinforcement connection loads recorded at each reinforcement layer for Wall 5. This figure illustrates that the essentially restrained toe initially attracted a significant portion of the total horizontal earth force acting on the facing column. However at 40 kPa, the tensile load was fully mobilized in the reinforcement. Similar qualitative results were observed with Walls 1, 2, and 3 (Bathurst et al., 2000). In all cases the toe carried approximately 40% of the total horizontal earth force. This load capacity is not accounted for in current design methods and is a source of conservatism.

The shortcoming of conventional earth pressure theories to predict the reinforcement loads and the load capacity of the restrained toe at the base of the facing column is magnified when one examines the influence of the soil friction angle, ϕ. Bathurst et al. (2000) noted that using the constant volume friction angle, ϕ_{cv} resulted in an excessively conservative (for design) prediction of the reinforcement loads whereas using the peak plane strain friction angle, ϕ_{ps} resulted in a less conservative estimate. Similar results were observed with Wall 5.

CONCLUSIONS

The data obtained from Wall 5 and the previous four walls continues to be analysed. However, some preliminary conclusions may be drawn:

- Detectable differences in wall performance were observed for walls constructed with similar strength polyester and polypropylene geogrid reinforcement.
- At the end of construction, connection loads at the facing units are the largest loads in the geogrid reinforcement layers.
- The measured vertical loads in the facing column indicate the presence of significant downdrag forces acting on the back of the facing column. These forces are not accounted for in present connection design methodologies and are a source of conservatism.
- The essentially rigid toe restraint carried a significant amount (40%) of the horizontal earth force acting on the back of the segmental wall facing column. This is not accounted for in current North American design methodologies and is a source of conservatism.
- Using excessively low estimates of soil friction angles exacerbates conservatism in current design methods. Peak plane strain friction angles should be used to reduce the conservatism in the analysis and design of geosynthetic reinforced retaining walls.

ACKNOWLEDGEMENTS

Funding for this research program has been provided by the Washington State Department of Transportation, the AASHTO MSE Pooled Fund, the National Concrete Masonry Association, Natural Sciences and Engineering Research Council of Canada, and grants from the Department of National Defence (Canada). The author recognizes the contributions of Dr R.J. Bathurst, G.P. Burgess (Walls 1 and 2), N. Vlachopoulos (Walls 3 and 4) and Research Assistants who helped construct the walls described in this paper. The support from Risi Stone Systems, who provided the facing units and permission to publish Figure 1 is greatly appreciated. Strata Systems Inc. donated the reinforcement materials and their support is also acknowledged.

REFERENCES

AASHTO, 1998, *Interims: Standard Specifications for Highway Bridges*, American Association of State Highway and Transportation Officials, Washington, D.C., USA.

ASTM 4595-86, 1995, "Standard Test Method for Tensile Properties of Geotextiles by the Wide-Width Strip Method", *ASTM Standards on Geosynthetics*, 4th Ed., American Society for Testing and Materials, West Conshohocken, Pennsylvania, USA.

Bathurst, R.J., 1990, "Instrumentation of Geogrid-Reinforced Soil Walls", *Transportation Research Board 1277*, pp. 102-111.

Bathurst, R.J., 1991, "Case study of a Monitored Propped Panel Wall", *Proceedings of the International Symposium on Geosynthetic-reinforced Soil Retaining Walls*, A.A. Balkema, Denver, Colorado, USA, August 1991, pp. 159-166.

Bathurst, R.J. and Benjamin, D.J., 1990, "Failure of a Geogrid-reinforced Soil Wall", *Transportation Research Board 1288*, pp. 109-116.

Bathurst, R.J. and Simac, M.R., 1994, "Geosynthetic Reinforced Segmental Retaining Wall Structures in North America", Invited keynote paper, *5th International Conference on Geotextiles, Geomembranes, and Related Products*, Vol. 4, Singapore, September 1994, pp. 1275-1298.

Bathurst, R.J., Walters, D.L., Vlachopoulos, N., Burgess, G.P., and Allen, T.M., 2000, "Full Scale Testing of Geosynthetic Reinforced Walls", *Advances in Transportation and Geoenvironmental Systems using Geosynthetics*, ASCE Geotechnical Special Publication No. 103, American Society of Civil Engineers, Reston, Virginia, USA, pp. 201-217.

FHWA, 1996, *Mechanically Stabilized Earth Walls and Reinforced Soil Slopes Design and Construction Guidelines*, Federal Highway Administration Demonstration Project 82, Washington, D.C., USA.

GRI GG3 Test Methd (b), 1992, "Tension Creep Testing of Flexible Geogrids", *GRI Test Methods & Standards*, Geosynthetic Research Institute, Philadelphia, Pennsylvania, USA.

Koerner, R.M., 1998, *Designing with Geosynthetics*, 4th Ed., Prentice-Hall Inc., Toronto, Ontario, Canada, 761 p.

McGown, A., Andrawes, K., Yeo, K., and Dubois, D., 1984, "The Load-Strain-Time Behaviour of Tensar Geogrids", *Symposium on Polymer Geogrid Reinforcement*, Thomas Telford, London, UK, March 1984, pp. 11-17.

Simac, M.R., Bathurst, R.J., Berg, R.R., and Lothspeich, S.E., 1993, *National Concrete Masonry Association Segmental Retaining Wall Design Manual*, National Concrete and Masonry Association (NCMA), Herndon, Virginia, USA, 250 p.

FIELD PERFORMANCE OF GEOTEXTILE REINFORCED SLUDGE CAPS

AHMET H. AYDILEK
UNIVERSITY OF WISCONSIN-MADISON
UNITED STATES OF AMERICA

ABSTRACT

Geosynthetic reinforced capping of highwater content waste materials is becoming an efficient and economic way of dealing with the confinement of the contaminants. To define the filtration performance of sludge-geotextile systems and investigate their durability, ten sludge lagoon test cells were constructed using of a lightweight fill, i.e. a wood chip/soil mixture over different geotextiles. Instrumentation of the cells included piezometers, settlement plates and surveying blocks. Various laboratory tests were performed on the field-exhumed geotextile samples to understand their filtration performance.

The laboratory and field investigations showed that woven geotextiles could be effectively used in filtering contaminated wastewater treatment sludges. Considering the constructability, woven geotextiles should also be preferred due to their higher strength. Laboratory observations performed on the exhumed samples can provide valuable information about the performance of the geotextile.

INTRODUCTION

Considerable evidence has been provided by the recent studies (Grefe 1989, Zeman 1994) that containment of contaminated soft sediments and sludges by capping may provide efficient solution for wastewater treatment sludges. An example of these sludges is currently available in Madison, WI. The Madison Metropolitan Sewerage District (MMSD) generates sludge as part of its water treatment process. This sludge has been disposed in lagoons and subsequently retrieved as fertilizer for application on farmlands. Some of the sludge contained polychlorinated biphenyls (PCBs), which are detrimental to human health, at concentrations above the allowable limit (50 mg/kg) and was banned from land applications. The MMSD evaluated different remediation alternatives to treat its sludge and the U. S. EPA agreed to permit capping as the method of remediation.

The design of such a cap would include a geosynthetic component, which would have three main functions: reinforcement, filtration and separation. While reinforcement is an important function of the geotextile for providing a good construction platform on soft sludge, filtration is another function that the geotextile should provide for long-term retention of the contaminated sludge solids during later movement. It becomes more important in case of sludge, since there is a common perception that sludge clogs geotextiles. In addition to an expected anti-clogging performance, openings of the geotextile should be small enough to prevent excessive piping and retain the contaminated sludge solids. Finally, the geotextile should separate sludge from the overlaying cap and should not allow intrusion of any sludge solids.

To define the filtration performance of sludge-geotextile systems and investigate their durability, ten sludge lagoon test cells were capped. A light-weight fill, i.e. a wood chip/soil mixture was used as a cap material along with ten different woven and nonwoven geotextiles (Figure 1). Piezometers installed at different depths in the sludge provided information about the pore pressure values therefore a measure of the clogging performance. Laboratory tests were performed on the field-exhumed geotextile samples to understand their field-clogging performance. Two of the cells used the same woven geotextile (Geotextile A), and were constructed in two different seasons, summer and winter to observe the seasonal effects on constructability. Detailed information about the construction, and field and laboratory investigations of the test cells can be found in Edil and Aydilek (1997) and Aydilek et al. (1999).

TEST CELLS

Properties of the Cap Material, Sludge and Geosynthetics

Field and laboratory tests were performed to assess the physical characteristics of the cap material. The field tests included determination of density of the cap material using sand cone tests (ASTM D1556), and measurement of the cap thickness. Samples of the field material were compacted in a compaction mold in the laboratory and constant head hydraulic conductivity tests were performed. The tests showed that hydraulic conductivity of the cap material ranges from 2.2×10^{-4} to 2.0×10^{-7} cm/sec depending on the compaction level. Sampling of the sludge, conducted by taking continuous core samples provided information about water content and solids content of the material before construction. Solids content of the sludge ranged from 17% to 26%. Solids content is defined as a ratio of the weight of sludge solids to the total specimen weight.

Six woven and four nonwoven geotextiles were used in the construction. The geotextiles were selected based on their polymer type, manufacture type, and mechanical and flow properties. The properties of the geotextiles are summarized in Table 1.

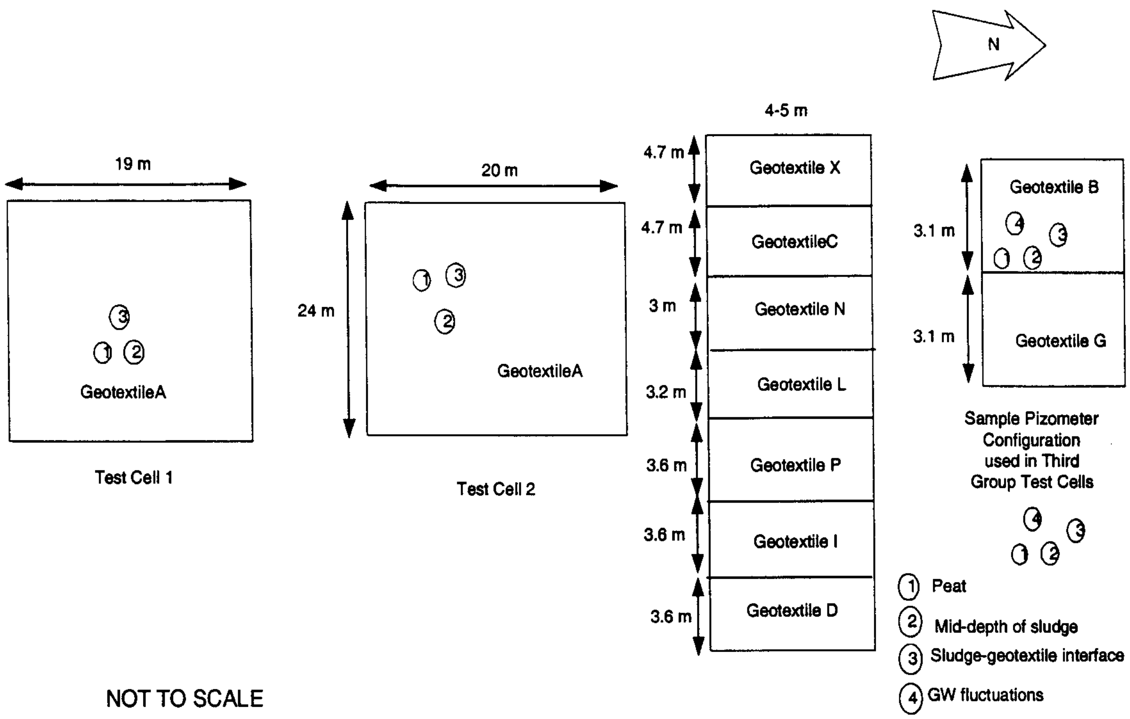

Figure 1. Layout of test cells.

Table 1. Physical and Hydraulic Properties of Geotextiles Used in the Study.

Geotextile name	Structure, polymer type[1]	Mass/unit area (gr/m^2)	Thickness (mm)	AOS[2] (mm)	POA[2] or porosity (%)	Permittivity (sec^{-1})
A	W-SF, PP	263	0.462	0.16	0.6	0.05
B	W-MU, PP	257	0.864	0.43	13.3	1.50
C	W-MF, PP	207	0.670	0.26	8.2	1.36
D	W-SF, PP	291	0.603	0.425	2.0	0.10
G	W-MF, PP	204	0.660	0.33	25	2.14
I	NW-STF, NP, PP	278	2.30	0.18	86.6	1.20
L	NW-STF, NP, PP	492	3.80	0.15	85.6	0.70
N	NW-CF, HB, PP	136	NA	0.212	NA	0.70
P	NW-STF, NP, PP	387	0.3	0.15	85.7	0.80
X	W-MU/SF, PP	225	NA	0.30	5.0	0.5

[1] W: woven, SF: slit-film, MF: monofilament, MU: multifilament, STF: Staple fiber, CF: Continuous filament, HB: Heat-bonded, NP: Needle-punched, PP: polypropylene.
[2] Apparent opening size (AOS) and percent open area (POA) values for wovens are determined using image analysis, except for Geotextile X reported value is used. Percent open area is applicable for wovens and porosity is for nonwovens. Porosity is determined using the method described by Wayne and Koerner (1994). NA = Not analyzed.

Construction and Instrumentation of the Test Cells

Construction of the first test cell was performed on an approximately 24 m long by 19 m wide section of the lagoons, on August 2, 1996 (Figure 2). Before construction, the sludge had an average solids content of 25% corresponding to a water content of 300%, and an average depth of 1.2 m. The pre-sawn geotextile (Geotextile A) was spread on the sludge in the east-west direction. The fill material, a mixture of 70% wood chip and 30% soil, was placed in three layers, resulting in an average total thickness of 0.6 m, by use of light construction equipment. The average wet unit weight of the material was 9 kN/m^3 and its initial water content 20%. The west section of the cap was generally compacted more than the east side due to higher number of equipment passes during construction. As a result, the cap thickness and the applied stress were not uniform over the sludge, being approximately 11 kPa on the west section and 7.6 kPa on the east section. Information about the settlement of the sludge was obtained from two settlement plates installed on the geotextile. Ten open tube piezometers placed at different locations and depths were used to observe groundwater levels and excess pore pressures during consolidation. Instrumentation of the cell also included nine surface survey blocks to monitor settlement of the cap.

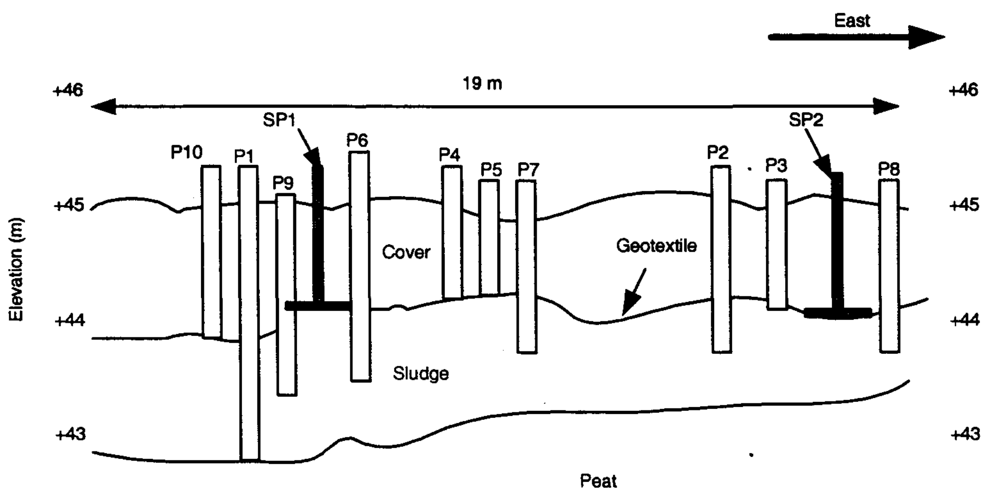

Figure 2. Cross sectional view of Test Cell 1

To investigate winter constructability of a cap on the sludge, a second test pad was constructed on an approximately 20 m long by 24 m wide section of the lagoons, on February 12, 1997. It is confined on three sides with dikes and open on the fourth side bordering some vegetative growth. Construction of the cap was facilitated by a 60 mm thick layer of ice over a 0.3 m thick layer of frozen sludge. The frozen sludge was underlain by a 1 m thick layer of soft sludge. Before construction, the sludge had an average solids content of 18%, corresponding to a water content of 470%. Test Cell 2 was constructed using the same reinforcement geotextile and the wood/chip soil mixture as in Test Cell 1. The wet unit weight of the cap material was

6.3 kN/m^3 on the northwest side and 10.5 kN/m^3 on the east side. The thickness of the cap ranged from 0.3 to 0.5 m, which corresponds to vertical stresses of 3 kPa to 9 kPa. These values are lower than those obtained for Test Cell 1. Instrumentation of the cell included four settlement plates, twelve piezometers and five surface survey blocks.

A third group of test cells using eight different woven and nonwoven geotextiles were built north of Test Cell 2, on April 5, 1999. The length of each cell is equal to the roll length of the geotextile, which ranged from 4 to 5 m as shown in Figure 1. The cap material was a 50% wood-chip and 50% soil mixture, being slightly less permeable than the material used in Test Cells 1 and 2 (ranges between 1 x 10^{-5} to 1 x 10^{-7} cm/sec depending on the compaction level). The wet unit weight of the cap material ranged from 10 kN/m^3 to 13 kN/m^3. The thickness of the cap ranged from 0.3 to 0.7 m, which corresponds to vertical stresses of 4 kPa to 8 kPa. Field instrumentation included two concrete survey blocks (surface markers) on each cell to determine the settlement of the sludge. Four piezometers were used in each cell, one in the sludge, one at the bottom of the sludge (sludge-peat interface), one at the sludge-geotextile interface, to understand the pore water pressure regime. The last set of piezometers was inserted above the geotextile (at the base of cap) to observe the ambient water level.

FIELD INVESTIGATIONS AND EXHUME OF GEOTEXTILES

The field investigations were conducted to exhume samples of geotextile, sludge and cap material. Samples were exhumed 6 months and 1 year after construction of Test Cells 1 and 2, and 1 year after construction of third group cells. An excavator was initially used, however, due to a light damage occurred in the geotextile, its use was discontinued. This method could also cause disturbance of the underlying sludge and piping of excessive material through the fabric. Instead a bucket auger and a hand shovel were used to dig the test holes. The excavations were approximately 1.2 m by 1.8 m in size, and when the excavation depth was within about 0.15 m of anticipated geotextile locations; cap materials were removed by hand to locate the geotextiles without much disturbance. Shelby tube sampling of sludge was conducted by inserting the tube with its sharpened end, into the sludge from the corner of the excavated hole. This method allowed collecting of the sludge samples from the geotextile-sludge interface and below the fabric. Two samples of the cap material were collected above (typically 20 mm) geotextile for future laboratory analysis. During the sampling, attempts were made to measure the thickness of zone of intermixing (sludge fines and cap material). This thickness was generally insignificant, being less than 0.05m in most cases. Therefore, it was concluded that no significant sludge intrusion into the overlying cap is occurring.

After the cap material is removed from the geotextile surface, a utility knife was used to cut the perimeter of the exposed geotextile. The geotextiles were carefully removed, sealed in zip lock bags and transported to the laboratory for further evaluation. Some leachate was added to the bags and the samples were kept in the humidity room until they are tested, along with the suggestions of Corcoran and Bhatia (1996). Sludge samples were also collected in zip lock bags for laboratory tests, i.e., water content, solids content, and PCB determinations. Geotextile patches were placed over the areas before the test pits were backfilled.

In addition to the geotextile exhume, pore water pressures are monitored during and after the construction. Excess pore pressures occurred due to loading of the sludge dissipated approximately 1.5 years after construction and followed the trend observed in the settlement data (Aydilek et al. 2000). No excess pore pressure build-up at the sludge-geotextile interface was observed.

LABORATORY INVESTIGATIONS

Clogging Behavior

After the samples were carried to the laboratory, a digital image camera was used to assess the damage on geotextiles. No apparent damage was observed on the exhumed geotextile samples. Some of the wood chips intruded into the cap-geotextile interface; however no puncture or tears were visible. The excess material on the surface of the geotextile samples was removed by a wet brush and the micrographs of the samples were taken. The removal of the excess material was necessary to expose the portion of the geotextile, if blinding or clogging has occurred.

Laboratory tests (i.e., permittivity tests, image analyses, filter press tests) performed on the field-exhumed geotextile samples provided valuable information about the clogging performance of the geotextiles. Image analyses were mainly performed to determine percent open area (POA)s of the woven geotextiles. Approximately 30-35 images of each woven geotextile specimen were taken and POAs were determined through a newly developed computer program named as PORE (Aydilek et al. 2000). POA_R is defined as ratio of the field-exhumed geotextile percent open area to the virgin geotextile percent open area, and any change in POA_R would indicate a reduction in open area and therefore, flow capacity. For instance, $POA_R = 0.75$ would indicate a 25% reduction in the open area of a woven geotextile.

Permittivity tests were performed on the samples, in conformance with the ASTM 4491, after determining their POAs. Permittivity ratio (Ψ_R), a ratio of the permitivity of the field-exhumed geotextile to virgin geotextile permittivity is determined for each sample. This ratio gives an idea about the percent clogging/blinding performance of the geotextile. Three tests were conducted on each sample and the mean value was used. Practically, for an unclogged/unblinded geotextile this ratio should be equal to 1.0. Table 2 summarizes the permittivity and percent open area ratios for each geotextile, exhumed 1 year after construction. As part of a laboratory research program at University of Wisconsin, the filtration performance of the same geotextiles was determined using gradient ratio testing procedure, and permittivity tests and image analyses were performed on the post-gradient ratio test specimens (Aydilek 2000). For comparison purposes, the permittivity and percent open area ratios determined from this testing program are also given in Table 2. Attempts were made to determine the porosity of exhumed and laboratory tested geotextiles using the procedure described by Wayne and Koerner (1994); however, due to a nonuniform clogging of the geotextile specimens, accurate thickness measurements were not possible.

Permittivity ratios are in an excellent agreement with the calculated percent open area ratios for most of the test cells, and both of the values are within the limits, 0.8 to 1.2, set based on the laboratory tests (Aydilek 2000). The values are also comparable with the ones determined from previous laboratory testing program, which might indicate that a successful laboratory testing can predict the field filtration performance of geotextiles. It could be observed from the table that woven geotextiles performed better than the nonwoven geotextiles. Two of the nonwoven geotextiles (L and N) clogged more due to their relatively low permitivity values. It should also be remembered that Geotextile N is a heat-bonded nonwoven geotextile, which is usually not preferred in filtration applications (Haliburton et al. 1982). Considering the constructability issues, it could be concluded that woven geotextiles should be preferred for capping of sludges.

Table 2. Clogging Performance of Geotextiles Used in the Study

Geotextile name	Percent open area, POA^2 or porosity (%)	Permittivity (sec^{-1})	Permittivity ratio (Ψ_R)		Percent open area ratio (POA_R)	
			Field exhumed geotextiles	After laboratory testing	Field exhumed geotextiles	After laboratory testing
A	0.6	0.05	0.91	1.0	0.92	1.0
B	13.3	1.50	0.97	1.0	0.92	0.97
C	8.2	1.36	0.83	0.80	0.85	0.90
D	2.0	0.10	0.95	0.53	0.87	0.53
G	25	2.14	1.0	0.93	0.81	0.88
I	86.6	1.20	0.86	0.82	NAP	NAP
L	85.6	0.70	0.70	0.73	NAP	NAP
N	NA	0.70	0.43	0.52	NAP	NAP
P	85.7	0.80	0.89	0.80	NAP	NAP
X	5.0	0.5	0.98	NA	0.90	NA

NA = Not analyzed, NAP: Not applicable.

An analysis is made to observe the effects of varying cap stresses on the sludge. Figure 3 shows the permittivity and percent open ratios obtained for samples of Geotextile A exhumed from Test Cells 1 and 2. The ratios obtained in the laboratory tests for this geotextile are also included in the same figure. The values obtained for Test Cell 1 is slightly lower than those obtained for Cell 2. This might be due to higher vertical stresses exerted on the sludge in Cell 1. The ratios calculated for samples exhumed after 6 months and 1 year of construction are nearly the same indicating that the geotextiles were successful in terms of their long-term anticlogging performance.

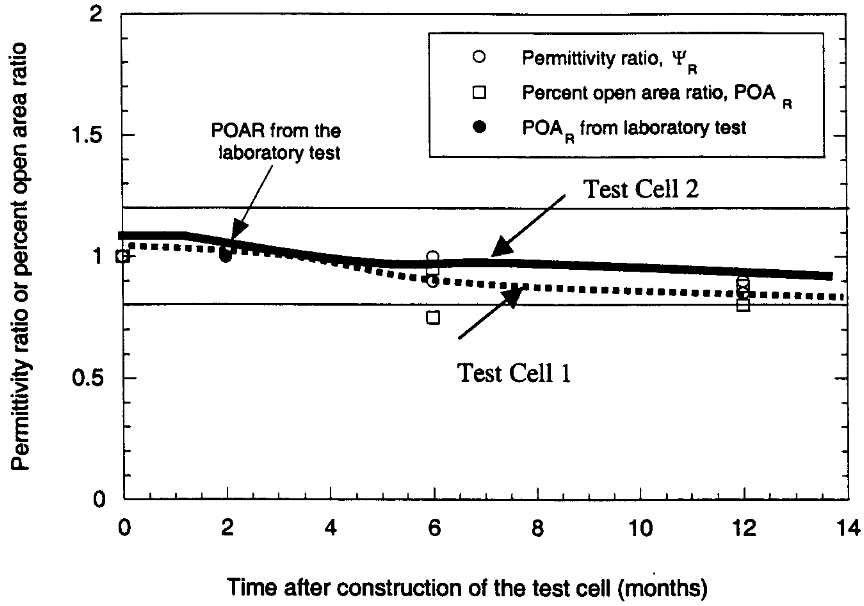

Figure 3. Change in the permittivity ratios and percent open area ratios of the geotextiles exhumed from Test Cells 1 and 2.

Retention and Separation Behavior

Observations during the exhuming showed no significant piping of the sludge through the geotextile. The supernatant collected at the top of the geotextile was sampled in zip lock bags and transferred to the laboratory. Samples of the cap material on the surface of the geotextile were also collected to investigate any intrusion of the sludge into the cap. The supernatant samples were sedimented in glass graduate cylinders for 48 hours, however no measurable amount of material (sludge solids) was visible. Samples of the cap material collected on the geotextile interface were dried and wood chip, soil and sludge particles were separated. Sludge solids were black in color and could be easily identified among the soil particles. The weight of the solids intruded was insignificant, in each case being less than 10 grams for 2,000 to 4,000 grams of collected cap material. This corresponded to a piping rate of less than 1,200 g/m^2, lower than a limit of 2,500 g/m^2 set by Lafleur et al. (1989) for laboratory tests. Field piping rates were higher than the ones observed in the laboratory tests (e.g., 1,200 g/m^2 versus100 g/m^2); however, this is most likely due to additional dynamic loads exerted on the sludge due to passages of trucks during the construction. Therefore, it is concluded that all of the geotextiles performed satisfactorily both in terms of separation of the sludge from the overlaying cap and retention of the sludge solids by means of preventing their excessive piping.

Filter press test, a widely used test by the petroleum industry to determine the flowability of the liquids, is slightly modified and was conducted on the samples of exhumed geotextiles. One test was conducted on each exhumed geotextile sample, and average value is reported. Control tests were also conducted on the virgin samples of the geotextile with the sludge procured from the lagoon and percent changes in the filtrate loss of the field-exhumed geotextiles were reported. Details of the testing program can be found in Aydilek (2000). The filtrate loss values for the samples exhumed after 1 year of construction shown in Figure 4 are consistent with the findings obtained from the permittivity tests (Table 2). For instance, a 52% decrease in the filtrate loss is obtained for Geotextile N, which is comparable to a 57% decrease in the flow capacity of the same geotextile (Ψ_R = 0.43 would indicate a 57% decrease in flow capacity).

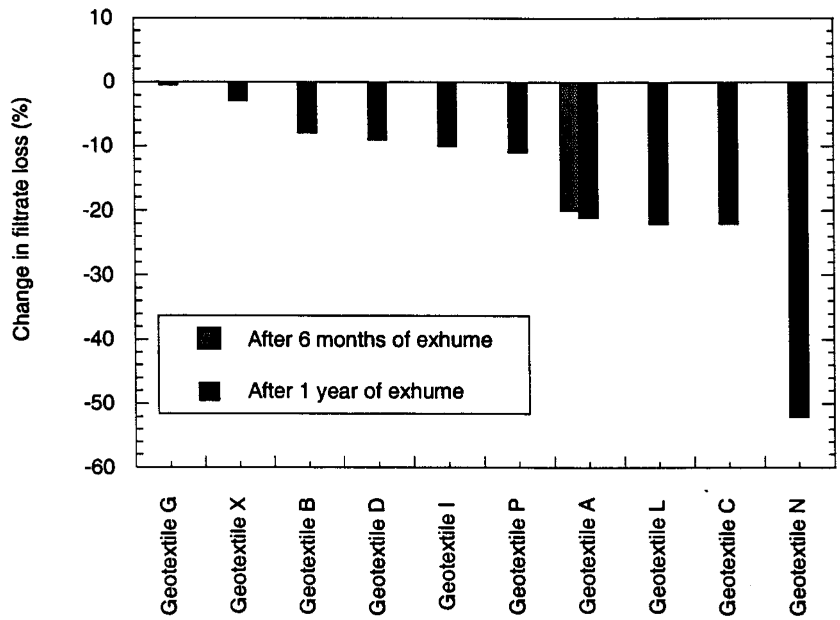

Figure 4. Change in the retention performance of field-exhumed geotextiles

CONCLUSIONS

The filtration performance of a wastewater treatment sludge was evaluated with ten different woven and nonwoven geotextiles in the field. Piezometers installed at different depths in the sludge provided information about the pore pressure regime in the cells. Permittivity tests, filter press tests and image analysis were conducted on the exhumed geotextile samples to understand the long-term filtration performance of these geotextiles. The results showed that woven geotextiles perform satisfactorily, and, considering the constructability of the cap, they should be preferred due their higher tensile strength. The following conclusions can be made based on the observations:

- Permittivity tests and image analyses performed on the field-exhumed geotextile samples showed that filtration capacity of a geotextile is related to its manufacturing type and percent open area/porosity.
- Piping rates were determined by measuring the sludge solids in the collected cap material samples. The rate was around 1,200 g/cm^2, being insignificant for field samples. The value was also less than the limit of 2,500 g/m^2 set by Lafleur et al. (1989) for the laboratory tests. Change in the retention performance and flow capacity of the exhumed fabrics was investigated by conducting filter press tests. The tests reflected the behavior observed in the permittivity tests.
- Field and laboratory observations showed no indication of sludge intrusion into the cap material and no apparent damage was visible. Therefore, the geotextile acted as an efficient separation layer between the sludge and the cap.

REFERENCES

Aydilek, A.H., Edil, T.B., and Fox, P.J., 2000, "Consolidation Characteristics of Wastewater Treatment Sludge", *Geotechnics of High-Water Content Materials*, ASTM STP 1374, T.B. Edil and P.J. Fox., Eds., Philadelphia, PA, pp.309-323.

Aydilek, A. H., 2000, "Filtration Performance of Geotextile-Wastewater Sludge Systems", Ph.D. Dissertation, University of Wisconsin-Madison.

Corcoran, B.W. and Bhatia, S. K, 1996, "Evaluation of Geotextile Filter in a Collection System at Fresh Kills Landfill", *Recent Developments in Geotextile Filters and Prefabricated Drainage Geocomposites*, ASTM STP 1281, S.K. Bhatia and L.D. Suits, Eds., Philadelphia, PA, pp.182-195.

Edil, T.B. and Aydilek, A.H., 1997, "Winter Construction and Performance Analysis of Sludge Lagoon Test Cell Cover", A Report Submitted to the Madison Metropolitan Sewerage District.

Grefe, R.P., 1989, "Closure of Papermill Sludge Lagoons Using Geosynthetics and Subsequent Performance", *Proceedings of the 12th Annual Madison Waste Conference*, University of Wisconsin-Madison, Madison, WI, pp.121-162.

Haliburton, T.A. and Wood, P.D., 1982, "Evaluation of the U.S. Army Corps of Engineers Gradient Ratio Test for Geotextile Performance", *Proceedings of the Second International Conference on Geotextiles*, Las Vegas, Vol.1, pp.97-101.

Wayne, M.H. and Koerner, R.M., 1994, "Correlation Between Long-Term Flow Testing and Current Geotextile Filtration Design Practice", *Proceedings of Geosynthetics '93*, Vol.1, pp. 501-517.

Zeman, A.J., 1994, "Subaqeous Capping of Very Soft Contaminated Sediments", *Canadian Geotechnical Journal*, Vol.31, pp.570-577.

PERFORMANCE TESTING OF GEOTEXTILE TUBES

VALERIE ZOFCHAK
DREXEL UNIVERSITY, USA

ABSTRACT

Geotextile tubes have become widely used in coastal and riverine environments to minimize erosion and scour, provide enclosure, containment, or buttress slopes and bulkheads. One of the most promising applications is the use of dredged materials in a continuous or semi continuous operation, where the excavated slurry fills the geotextile tube, drains, and is immediately deposited in its final location on site or nearby. This project described herein focuses on use of geotextile tubes in connection with dredging operations along the Delaware River, where a wide variety of soil types are encountered. The key operational parameters are those of filters in general, turbidity of the drained water, and rate of drainage. The problem addressed is developing a rapid performance-based test to support selection of the appropriate geotextile material for the soil being retained. This project has developed a hanging-bag test that simultaneously indicates dewatering rate and particle retention of a candidate geotextile in a scaled prototype of the actual final product, the filled geotextile tube.

The testing program included developing the test set-up, determining an appropriate mix design for the MH soil used, and performing full scale pilot testing. Two types of geotextile were tested. The soil mix design was based on a weight relationship of 10:1 between water and Delaware River soil. Full-scale pilot tests quantified flow rates and particle retention.

INTRODUCTION

Geotextile tubes are a popular and efficient method to stabilize banks and channels, and prevent coastal erosion by maintaining the integrity of soil as a flexible mass shielded from erosion. One of the most promising applications is the use of dredged materials in a continuous or semi continuous operation, where slurry fills the geotextile tube, drains, and is immediately deposited in its final location on site or nearby. The mechanical integrity of the fabric containment has been extensively studied, such that construction stresses appear to dominate. However, less well understood is the interplay between geotextile permeability, which controls the slurry dewatering rate, and filtration, which restricts particle loss through the pores. This might be especially critical in dredging industrial waterways. Potential contaminants are often sorbed (metals) or adhered (hydrocarbon globules) to the finer, more plastic particles. Lightly contaminated dredgings are a problem only if the cohesive particles are mobilized into open water. Hence, assuring that they stay within the geotextile tube can be critical. The indicator of fines release is turbidity of the effluent, however, the more rapidly the slurry drains through the geotextile, the more efficient the complete operation.

This paper describes development of a performance-based test that focuses on soil retention and the dewatering rate of the geotextile tubes. A test set-up and procedure have been developed to analyze the soil-geotextile tube system.

BACKGROUND

As defined by GRI Test Method GT10, a geotextile tube is a large tube made from a high strength woven geotextile, which can be filled either hydraulically or mechanically. The length is at least 6.1 meters (20 feet) and the circumference is a minimum of 2.3 meters (7.5 feet) (GRI 1999). These tubes have many uses in coastal and riverine environments.

Applications

Geotextile tubes have various uses as temporary or permanent structures including breakwaters, groins, and containment dikes (Cheng 1999). Geotextile tubes have also been used successfully as the core of restored sand dunes. One of the most visible sand dune reconstruction projects occurred in Atlantic City, New Jersey, where the natural dunes had eroded away over time due to storms. Exposure left the boardwalk, hotels, homes, and casinos at risk to damage from high tides. Geotextile tubes were placed at the center of the reconstructed dunes. The efficiency of this embedded core system was tested shortly after the completion of the project when Hurricane Luis produced waves 3 to 3.6 meters (10 to 12 feet) high. The beach in front of the tubes was scoured, but the land behind the tubes was barely touched. This installation saved many dollars in avoided damages (Torre 2000).

Another application of geotextile tubes is dewatering fine grained soils including dredge material and sewage sludge. These are materials that must be disposed of in designated sites. A problem is the high moisture contents of the soil as excavated, often as a suspension or slurry. For instance, a dredge material can have a moisture content of 800 percent. A simple, cost effective solution is to dewater the dredge material in geotextile tubes. This can help consolidate the material and reduce the water content significantly over a short period of time, leaving less material to haul and dispose, resulting in lower costs (Gaffney et al. 1999).

Typically, for these and other applications, geotextile tubes result in a lower cost, a lower volume of work, faster construction times, and the ability to use local materials. For low volume projects, locally available equipment can be used, such that a local contractor could perform the work under supervision of an expert (Pilarczyk 1995). Geotextile tubes can also reduce the amount of time it takes for dredge material to dewater when compared to a traditional disposal site due to the shorter path length and larger drain focus.

MATERIAL PROPERTIES

Soil

The soil used is a dredge material from the Delaware River, near Wilmington Harbor. The water content of the soil (when received) was 125%. It had been deposited in a flat, diked disposal area some years previously. The dark gray fine material had a strong odor of organics and was classified as MH. The soil has a liquid limit of 130 and the plastic limit is 90. The plasticity index for the soil is 40. A wet sieve performed on the soil showed 90% passing the #200 sieve. The fineness of most soil particles makes retention a critical factor as a substantial portion of the material could be readily mobilized as a highly turbid slurry.

Geotextiles

Two woven geotextiles were used as tube material in this project. One is a 175 x 175 kN/m (1000 x 1000 lb/in) woven polyester geotextile with an Apparent Opening Size (AOS) of 60. The second is a 70 x 105 kN/m (400 x 600 lb/in) woven polypropylene geotextile with an AOS of 40. Both fabrics are often used for geotextile tube construction. The textiles were obtained on rolls and were made into bags in the laboratory as discussed below.

TEST SET-UP

The test apparatus was designed with the goal of developing a standard test that can be performed quickly and easily in the field or in the laboratory. The set-up is based on the hanging bag test (Fowler 1996). The test set-up developed consists of an aluminum frame 0.76 meters (30 inches) high, with a 0.3 meter (12 inch) diameter opening for the hanging bag. The bag is fastened to the frame by placing the geotextile over six bolts around the opening, placing an aluminum collar over the geotextile and fastening the collar down with wing nuts. The set-up is pictured below in Figure 1.

The compactness and simplicity of the test has several advantages. Its small size makes it convenient for a lab technician to work with. The frame could also be readily transported to a job site if necessary. The smaller bag size requirement allows quicker drainage of fine grained soil mixtures allowing comparison of the relative performance of several candidate materials. This is important because it will lower lab expenses, which will make the test more attractive to designers. The test can also be performed off the side of a dredge vessel without the frame as long as there is a way to hang the bag. The small size of the bag makes it convenient to keep several types of textile bags on board an exploration vessel to test different fabrics before dredge operations begin. This can ensure the appropriate type of geotextile is used for the specific soil to be dredged.

Figure 1. Hanging Bag Test Set-up.

TESTING PROGRAM SUMMARY

The testing program consisted of three main phases: preparation of geotextile bags, soil/water mix design, and full scale pilot testing. The goal of the testing program is to develop the final procedure for the proposed test.

Preparation of Geotextile Bags

The bags were approximately 0.6 meters (24 inches) long and 0.3 meters (12 inches) in diameter. The bags were sewn together along one side and straight across the bottom since sewing a circular bottom onto a bag is virtually impossible for an unskilled lab technician using a hand held sewing machine. The size was roughly determined from the size of a 19 liter (5 gallon) bucket. This size is makes it easy to measure the amount of soil slurry when performing the test in the field. The hand held sewing machine that was used to sew the bags used a high strength Kevlar thread. The seam needed to be strong enough to not be an issue because ultimately it was the bag fabric that was to be tested.

A photograph of the bags used is shown in Figure 2.

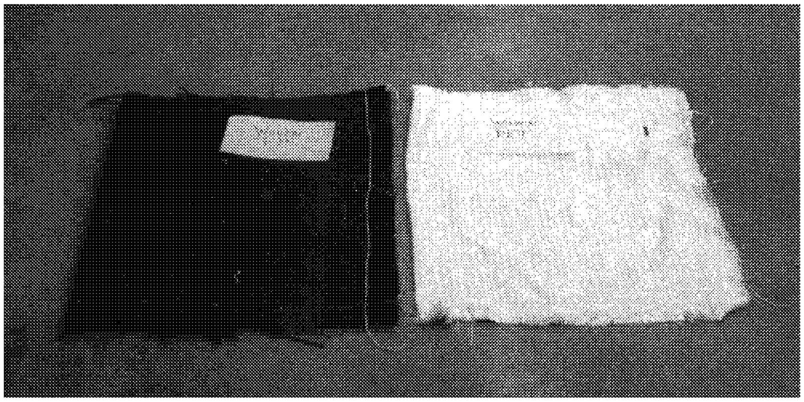

Figure 2. Photo of Geotextile Bags.

Mix Designs

Before the full scale testing began, it was necessary to develop a soil slurry that was similar to actual dredging operations and was easy to prepare in the laboratory. Four different mix designs were tested based on the weight relationship between the moist soil and water. The water used in the experiment was Philadelphia tap water, for which the Delaware River is the source, since in certain tests it has performed close to a mild leachate (Koerner 1998)

The slurries used were in the added water:moist soil ratios 7:1, 8:1, 10:1, and 12:1 to represent slurries from suction or cutterhead dredges. The first mix was based on the consistency of the mixture, while the following mix designs were based on the performance of the previous test. The mixes were tested for time to dewater, general mixability, quality of filter cake developed, time for the flow through the bag to change to a drip, and a qualitative comparison of the amount of soil lost through the bag.

To perform the mix testing, a small swatch of geotextile, about 0.35 meters (14 inches) in diameter was placed about 10 cm (4 inches) into a standard 6 inch Proctor mold. The geotextile was secured around the Proctor mold. Approximately 500 ml of the test mixture was prepared by mixing the soil and water with a standard laboratory mixer for several minutes until the mixture was uniform. The soil slurry was then placed in the geotextile and times were taken for the flow to turn to a drip and for the total drain time. The successful mix was the one that showed similar properties between the two different types of geotextile. The flow to drip times were consistently higher for the polyester geotextile, but the soil loss (drainage turbidity) was consistently higher for the polypropylene geotextile. There was a wide range of total drain times for both geotextiles, showing no discernable pattern. The mix selected was the 10:1 mixture since two geotextiles had similar total drain times. See Figure 3 for the total drain times for each mix. The polyester geotextile developed a very good (time to permeability) filter cake, while the polypropylene geotextile seemed to clog rather than develop a filter cake. This is probably due to the fact that the polypropylene is very smooth and the soil does not adhere to it as well as the polyester, which is more fibrous. The polyester fabric absorbs water readily, along with the soil particles, and creates a well bonded filter cake. The polypropylene fabric also released more soil particles until the pores became clogged. For each geotextile, once the filter cake developed or the pores clogged, the water seeping through the bag was clear, indicating that the geotextile was working properly in retaining the soil.

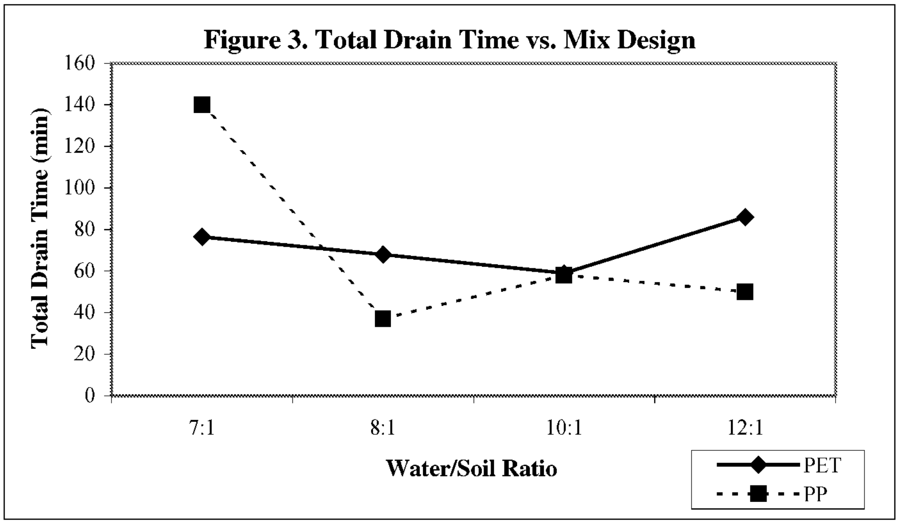

Full Scale Pilot Testing

Once the appropriate slurry proportion was determined, full scale pilot testing began. Each type of geotextile was tested. The goal of the pilot testing was to refine the test procedure to one that can be used in a normal testing situation. The full scale test used a 15 liter (4 gallon) mixture of the soil slurry. This slurry was based on the 10:1 weight relationship determined previously. The soil and water were mixed using a standard laboratory mixer until the slurry was uniform. This mixture was placed in the geotextile bag that was connected to the test set-up. The flow to drip time was recorded as well as flow measurements at designated time intervals. To determine the flow, each bag was marked at various lengths of time (30 s, 1 min., 2 min., 5 min., 15 min., etc.) and the volume of water that drained during that period was determined based on the measured dimensions of the bag. Other data collected was the amount of soil that passed through the bag and the quality of the filter cake.

The results of the pilot testing did provide some insight into changes that may be needed in the test. First, the test took almost 24 hours to complete. However, the flow rate decreased logarithmically for each type of geotextile. This information is useful because it may not be necessary to run such a large-scale test or run the test until completion depending on the variables that are sought. If soil retention is the property being analyzed, the test only needs to be run until the water seeping out of the bag is no longer turbid. This can easily be measured by taking samples at given intervals measuring turbidity with a meter or simply by placing a shiny object in the bottom of a pan (as in the Secchi dish test) and observing which sample allows more visibility. If dewatering rate is necessary, the test should be run to completion. To cut down on the testing time the amount of soil slurry could be decreased. It should not be decreased too much, however, because there needs to be enough to develop a good filter cake on the bag for it to function properly.

The filter cakes that developed on the test bags were similar to those found in the mix design testing. The polyester geotextile developed a very consistent filter cake over the area exposed to the soil slurry. The polypropylene geotextile again showed signs of pore clogging rather than filter cake development. When the mixture was added to the bags, the polypropylene bag released more soil particles than the polyester bag, but in a shorter amount of time. This shows that the pores clog quickly, but the filter function of the geotextile is not efficient until that occurs. The polyester geotextile released less soil, but it took a greater amount of time for the dripping to become clear. This could be because the soil particles were temporarily trapped in the polyester fibers, and were able to be washed away until the filter cake developed. The AOS of the polyester geotextile was 60, so it was expected that less soil would break through.

The flow rates for the first 3 hours of the test are shown in Figure 4. It can be seen that when plotted on a logarithmic scale, the data gives a straight line. This clearly indicates there is a fast initial release until the filter cake develops to the gradually slowing seepage as the test goes on a combination of lower permeability and falling head. The polyester geotextile shows a slightly lower seepage rate. The polypropylene shows a higher initial flow rate. This higher flow rate is most likely the reason more soil was lost through this geotextile. Overall, it can also be seen from this graph that the two types of geotextile behave very similar.

Figure 4. Flow Rate vs. Time

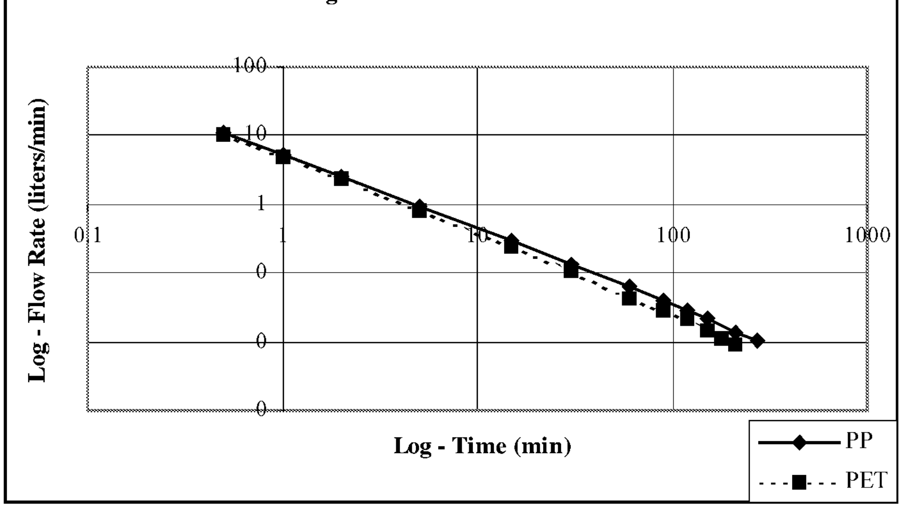

CONCLUSIONS

Based on the previous experiments, a performance based testing program for geotextile tubes is well underway. The test set-up developed has many advantages including a small size anyone can work with, it is easily transportable, it is easily adaptable to just about any situation, and it can provide important information relatively quickly. A mix proportioning was developed for this testing procedure. This mix may have to be changed depending on the type and gradation of specific site soils. The mix design is appropriate for fine grained soils. The pilot testing revealed many interesting points. First, the polypropylene geotextile does not develop a filter cake, but relies on pores clogging for fines retention. The polypropylene geotextile also showed a higher initial flow rate, which may have contributed to the higher volume of soil lost in the initial stages of testing. The polyester geotextile showed the ability to develop a good filter cake, but also showed that the dewatering rate was slightly lower. Overall, the two geotextiles performed similarly with regards to flow rates over time. Procedurally, this test will not change for full scale testing. Other aspects that need to be studied before the test can be complete include gradation of the soil that passed through the bag, formal turbidity measurements, and the behavior of the geotextiles under stress.

FUTURE WORK

This paper has been the first phase of a two-phase project for the author. Now that the initial testing has been completed and testing program has been refined, a full scale test of five different geotextiles and two different soils will be conducted. Based on the results of this study, items that were not previously studied, but need to be, are the turbidity of the of the water seeping form the bag, the gradation of the soil which passes through the bag compared to the gradation of the original soil, and the weave pattern of the geotextile. It is believed that under stress different weave patterns behave differently. An in depth look at the different weaves under stress will be conducted. It is the hope of the author that once these different parameters are studied it will be possible to develop a standard performance based test method for geotextile tubes.

ACKNOWLEDGEMENTS

I would like to thank Dr. Jonathan Cheng, Dr. Joseph Martin, Michael Carnivale, Dr. Robert Koerner, Doug Gaffney, Ed Trainer, Oscar Merida, Alyssa Koch, and Claire Zofchak for their help with this project.

REFERENCES

Cheng, S.C., 1999, "Application of Geotextile Containers: The Material Issue from Properties to Testing," *Workshop on New Topics of Geosynthetic Applications in Environmental Conservation and Earthquake Resistant Structures*, Vol.1, National Cheng Kung University, Tainan, Taiwan, August 1999, pp. 6-1-6-16.

Fowler, J., Bagby, R. and Trainer, E., 1996, "Dewatering Sewage Sludge with Geotextile Tubes," *Proceedings of the 49th Canadian Geotechnical Conference*, St. John's, New Foundland, Canada, September 1996.

Gaffney, D. A., Martin, S.M., Maher, M.H., and Bennert, T.A., 1999, "Dewatering Contaminated, Fine-grained Material Using Geotextiles," *Geosynthetics '99 Conference Proceedings*, IFIA, Boston, MA, USA, April 1999.

Koerner, R. M., 1998, *Designing with Geosynthetics*, 4th ed., Prentice Hall, Upper Saddle River, New Jersey, USA, p. 620.

Pilarczyk, K. W., 1995, "Geotextile Systems for Coastal Protection," *International Conference on Coastal and Port Engineering in Developing Countries*, Brazil, September 1995.

"Test Methods, Properties and Frequencies for High Strength Geotextile Tubes used as Coastal and Riverine Structures," GRI Test Method GT10, GRI, Folsom, PA, USA, 1999, pp.1-8.

Torre, M. A., 2000, "Geotextile Tubes Saving the Shore from Erosion," *CE News*, February 2000, 6 p.

EFFECTS OF SUSTAINED AND CYCLIC TENSILE LOADS ON GEOGRID EMBEDDED IN CLAY

AHMET PAMUK,
GRADUATE RESEARCH ASSISTANT,
DEPARTMENT OF CIVIL ENGINEERING,
RENSSELAER POLYTECHNIC INSTITUTE, TROY, NY,
USA

ABSTRACT

Most laboratory pullout tests have concentrated on static short-term loading for cohesionless soils. This experimental study attempted to improve the understanding of the long-term pullout behavior of a geogrid that was confined with cohesive soil and subjected to a combination of sustained and cyclic tensile loads. Strain gages utilized to measure the strain distribution along the length of embedded geogrid. The confining pressure had important effects on the creep strain rate and as well as on strain distribution along the reinforcement. Creep strain rate of the geogrid embedded was found to be a function of load amplitude. However, creep strain rate was not affected by the presence of the confining soil at the point of load application. Creep under repeated load was smaller than creep under sustained load

INTRODUCTION

Geosynthetic-reinforced soil systems in engineering practice are increasingly being used over conventional soil systems. Current design methods for reinforced soil structures require granular soils as backfill material (Elias et al, 1998). Limited number of earth structures constructed with cohesive soils has performed well (e.g., Hayden et al. 1991, Scott et al. 1987, Tatsuoka et al. 1986) showing that they can be used in place of granular soils and thus, reduce the cost of construction. However, the cost of backfill constitutes a major portion of the total cost of the structure. Therefore, it would be more economical to use poor quality soils.

The pullout resistance of geosynthetics is one of the key parameters in the design of reinforced soil structures. Laboratory pullout tests offer more realistic models of soil-geosynthetic interaction in design. To date, most of the research has been concentrated on the interaction between geosynthetics and granular soils and was limited to short-term static loading conditions. Previous research (e.g., Min et al., 1995) has shown that static and cyclic loading conditions may result in different approaches in design. Therefore, it is important to understand the behavior of geosynthetics embedded in clay under long-term repeated loading conditions.

The purpose of this study is to explore the long-term pullout behavior of geogrid embedded in clay subjected to a combination of sustained and cyclic loads. A series of sustained and cyclic loading tests were conducted using a pullout box. Some uniaxial tension tests were conducted to study the fundamental creep behavior under sustained and cyclic tensile loads, and were used as a baseline for all confined tests. Strain gages combined with a data acquisition system were utilized to measure the strain distribution along the length of embedded geogrid. The test results are presented, compared and discussed.

EXPERIMENTAL PROGRAM

A special apparatus used in this study was designed to carry out pullout tests. Figure 1 shows the schematics of the testing box. It provided the capability of both unconfined and confined tests. The test box was 60 cm long, 20 cm wide and 30 cm high. Pullout loads were applied using a load actuator controlled by a servo console system generating static and dynamic air pressures. The front end of the box had a slot at the mid-height. Through this slot the clamping plates were connected to a loading actuator. Applied load and front-end displacement were measured by a load cell and LVDT, respectively. Latex sheets were pasted onto the side walls, and a layer of lubricant grease was applied between the latex sheets and the walls, thus created ideally plane strain conditions. The confining pressure was applied through an air bag to assure uniform normal pressure distribution in the test box.

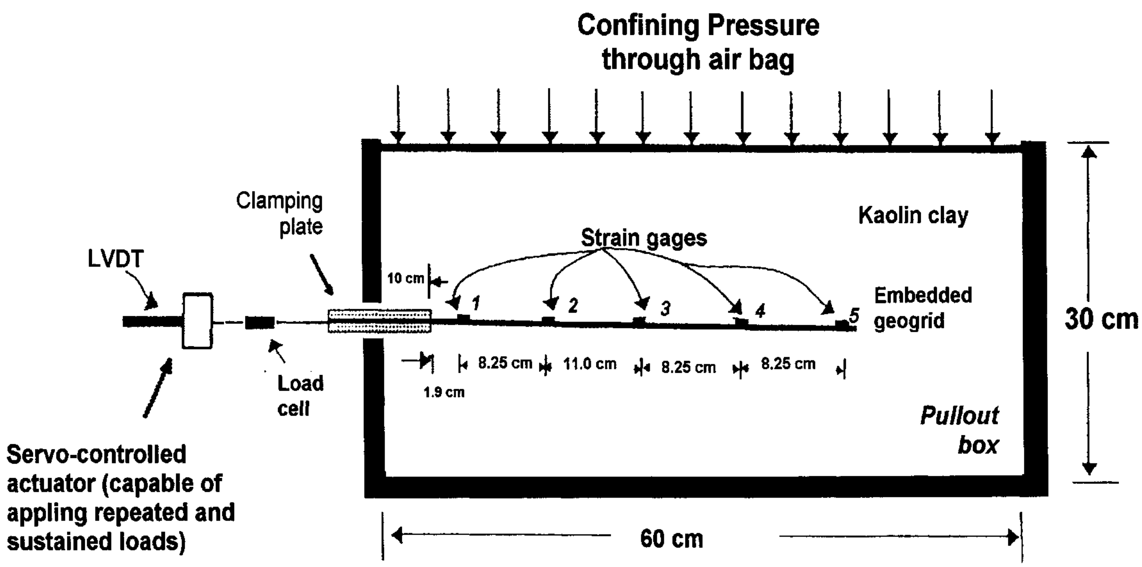

Figure 1. Schematics of test setup for confined tests

A biaxial polypropylene geogrid, 38 cm by 19 cm, was used for all tests. The tensile strength of the geogrid in the machine and transverse directions were 35 and 45 kN/m (Leshchinsky et al., 1994), respectively. The tensile loads were uniformly transferred to the geogrid using clamping plates in the transverse direction. Geogrid specimens were bonded, at one end for confined tests and at two ends for unconfined tests, with a pair of rigid metal plates by epoxy glue.

The soil used in all tests was kaolin clay with liquid and plastic limits of 59% and 25%. The maximum dry unit weight in standard proctor test was 14.7 kN/m3 and optimum moisture content was 26%. During the test, the soil was compacted at the optimum water content. A mechanical mixer was used to have a uniform distribution of water content of the soil specimen. Then the mixture was placed inside plastic bags to ensure the water content had been fully equalized before compaction. The soil was compacted in 3.75 cm-thick layers the day after mixing. After the box was filled with the soil, the required confining pressure was applied slowly through the airbag. The soil was kept under pressure for 24 hours to permit soil consolidating and equalization of moisture content, especially around the geogrid specimen. Direct shear tests were conducted on samples extracted from the soil mass in the testing box. Peak and residual internal friction angles were measured as 14° and 14.7° and apparent cohesion measured as 52 and 19 kPa, respectively.

Strains were measured using strain gages along the length of embedded geogrid. Strain distribution in the geogrid is not uniform because of its ununiform geometry. Therefore, strain gage outputs were calibrated so that the local strain gage output could give the average strain. A data acquisition system was used to record strain readings at five different locations (see Fig. 1) throughout the test. The strain gages output was important for studying the interaction mechanism between geogrid and confining clay under different types of loading conditions. Details of pullout box and testing procedures can be found in Pamuk et al. (1997).

Table 1. Testing program for confined tests

	Static Loading Tests		**Cyclic Loading Tests**		
Normal Pressure (kPa)	**Applied Initial Load (kN/m)**	**Load Increment Per Day (kN/m)**	**Applied Initial Load (kN/m)**	**Load Increment Per Day (kN/m)**	**Frequency (Hz)**
34.5	**1.75**	**1.75**	**0.25-1.75**	**1.75**	**0.1**
69.0	**1.75**	**1.75**	**0.25-1.75**	**1.75**	**0.1**
103.4	**1.75**	**1.75**	**0.25-1.75**	**1.75**	**0.1**

Three sets of confined tests with sustained loads were conducted. These tests were carried out under confining pressures of 34.5 kPa, 69 kPa and 103.4 kPa. Tests equivalent to the long-term sustained pullout tests were also conducted under cyclic loads. Testing program for confined soil tests are shown in Table 1. The cyclic loads were applied incrementally at a fixed frequency of 0.1 Hz (square wave). Unconfined tests were conducted to study the fundamental creep behavior under static and repeated tensile loads. First, unconfined and then confined tests were performed. For all tests the same loading pattern was followed; i.e., each load was kept constant for 24 hours and then increased by the prescribed increment. Information concerning the development of strain along the reinforcement and displacement at the front were recorded.

TESTING RESULTS

Typical results obtained from unconfined tests (i.e., creep tests) are shown in Figure 2. It compares strain-time relationship for different types and magnitudes of applied loads. Creep strain rate (i.e., strain/day) calculated for these tests are summarized in Figure 3. No rupture attained in these tests.

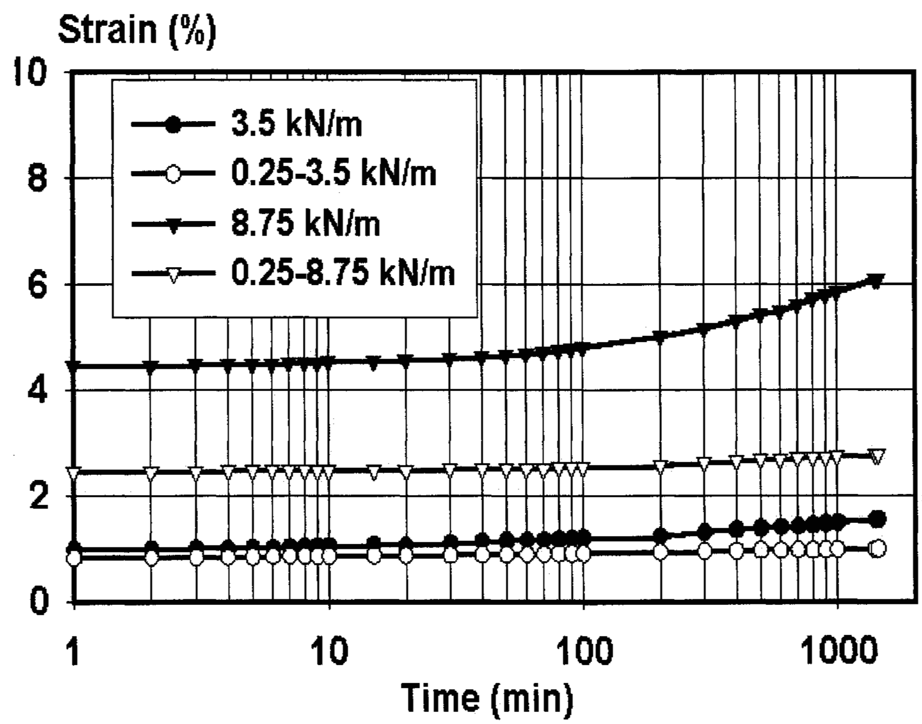

Figure 2. Strain vs. log-time curves (unconfined tests)

Three different long-term confined pullout tests were conducted under normal pressures of 34.5 through 103.4 kPa (see Table 1). Figure 4 and 5 show strain distributions measured (1 minute and 24 hours after load application) along the length of embedded geogrid under normal pressure of 34.5 kPa for sustained loads and cyclic loads, respectively. Total displacement measured using for sustained loading is shown in Figure 6. Both unconfined and confined tests were terminated when the load actuator reached its displacement or load capacity. During the tests the geogrid was not pulled out or ruptured.

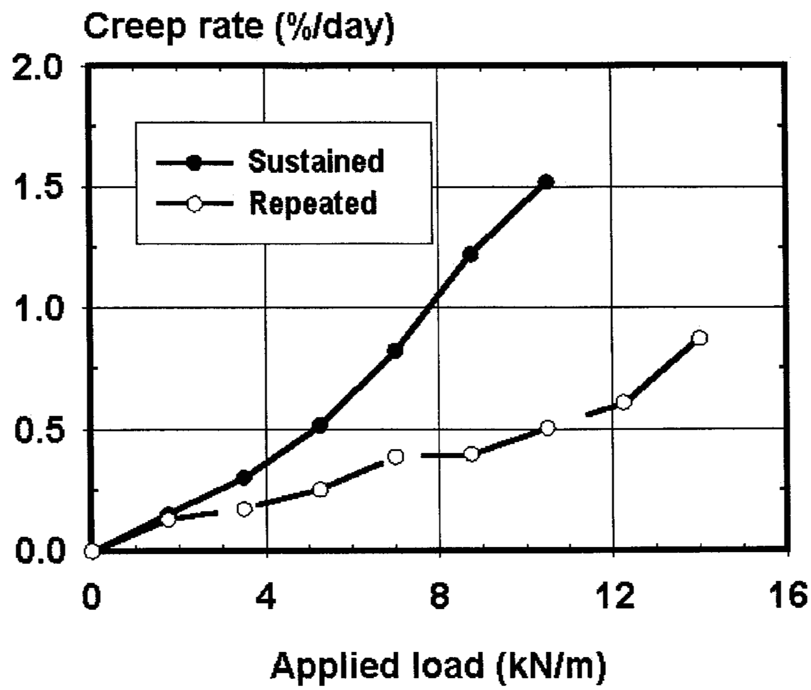

Figure 3. Creep strain rate vs. applied loads (unconfined tests)

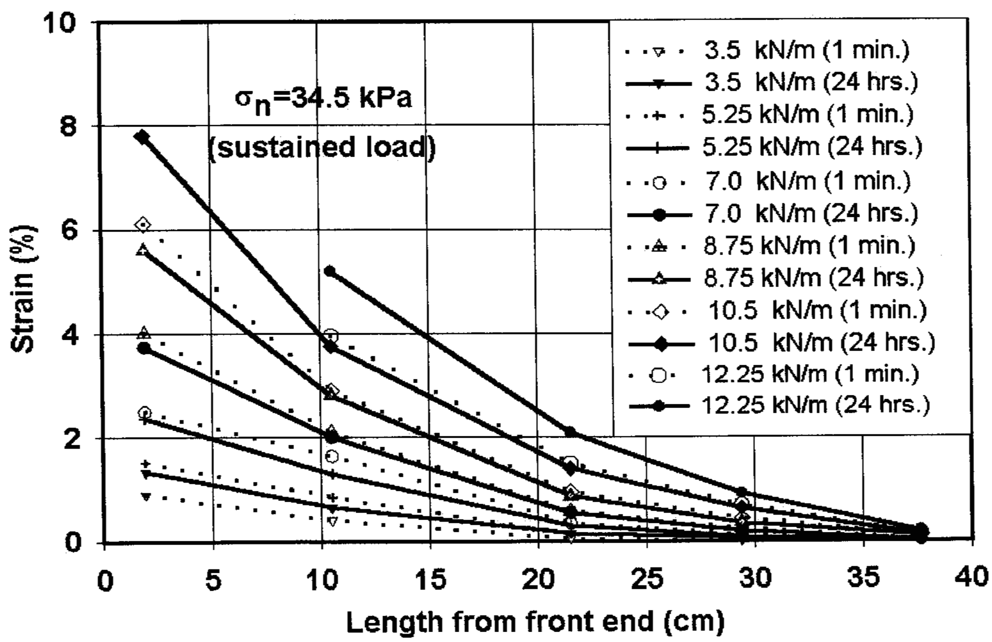

Figure 4. Strain distribution along the geogrid, σ_n=34.5 kPa, (sustained loading, strain measured 1 min. and 24 hrs. after load application)

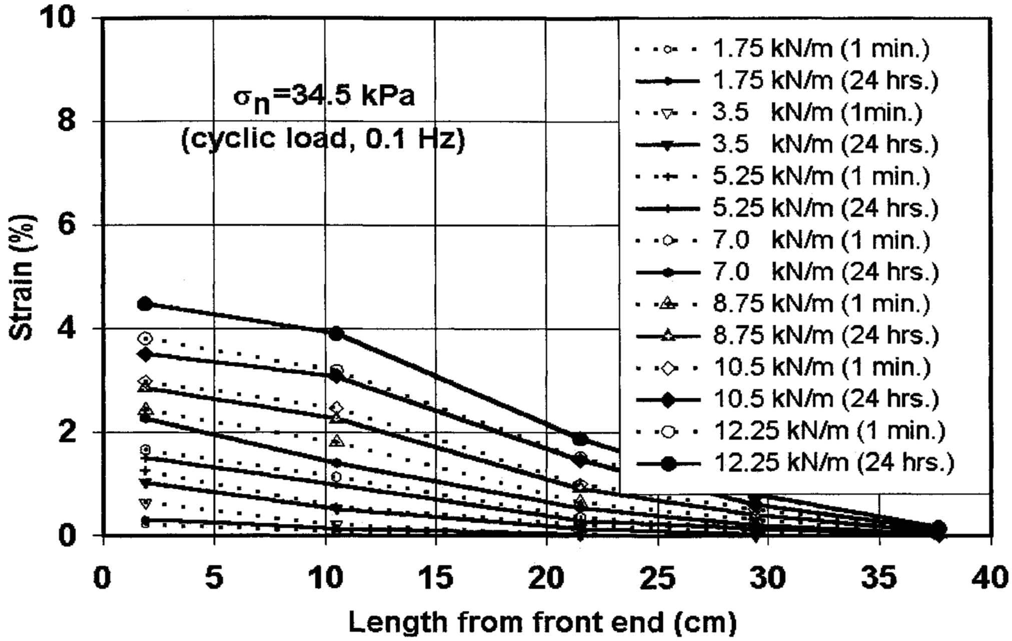

Figure 5. Strain distribution along the geogrid, σ_n=34.5 kPa, (cyclic loading strain measured 1 min. and 24 hrs. after load application)

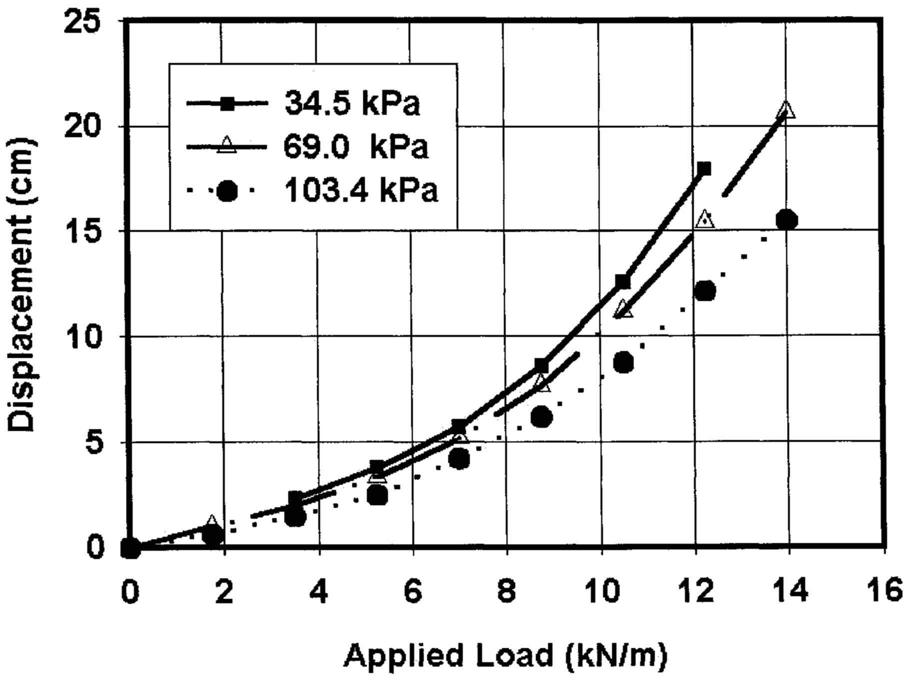

Figure 6. Load-displacement relationship measured at the front (sustained loading)

INTERPRETATION OF TEST RESULTS

Unconfined tension tests were conducted to provide baseline information to determine the influence of confining soil at different normal stress levels. The types of loading (i.e., sustained or repeated) and magnitudes of applied loads were compared (see Fig. 2). Significant creep developed, especially under sustained loads, and increased with applied load. Creep strain rates under sustained loads was almost twice that for cyclic loads.

Confined tests were performed to understand confined effects of the geogrid embedded in clay. For sustained loading tests, the creep strain was reduced by the presence of confining soil and confining pressure. Figure 7 demonstrates that significant creep developed only at the front end and then diminished quickly towards the rear end. This was especially true at lower magnitudes of sustained load. However, the creep strain increased with the tensile load. The interaction between soil and geogrid interface increased with confining pressure. That is, much load was transferred into the soil causing reductions in creep strain. However, the creep strain rate in the front end was not affected significantly by the presence of soil and confining pressure, as can be seen in Figure 8. The figure compares creep strain measured at the point of load application (see Fig.1, strain gage No. 1) with that measured from unconfined tests. Results similar to sustained load tests were obtained for cyclic load tests. Figure 9 shows the influence of the normal stress and magnitude of applied load on the stress distribution under cyclic loads.

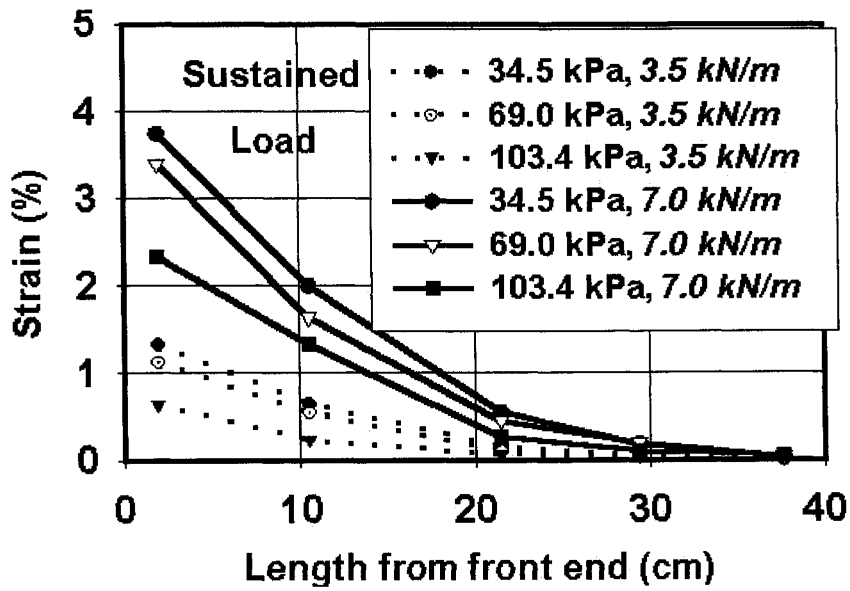

Figure 7. Strain distribution under various confining pressures and applied loads (sustained loading)

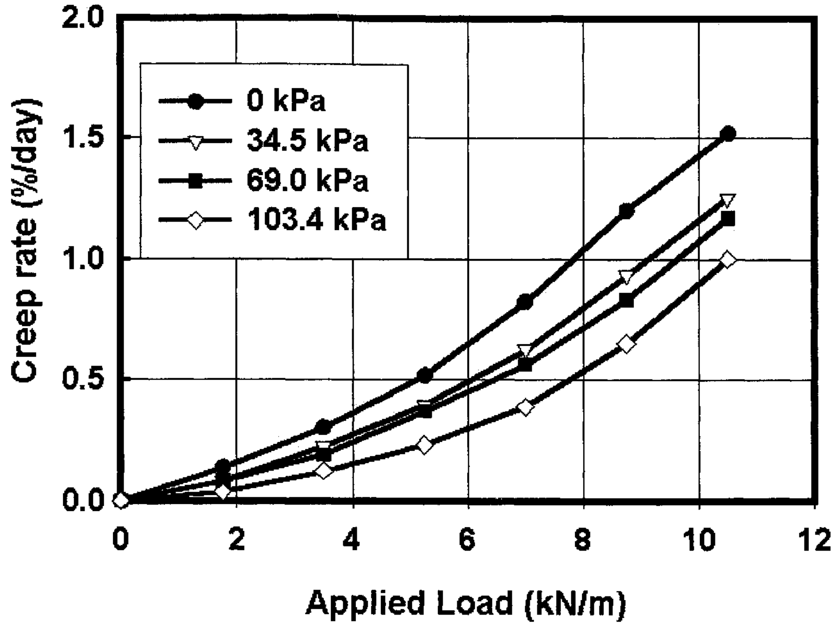

Figure 8. Creep strain at the point of load application
(sustained loading)

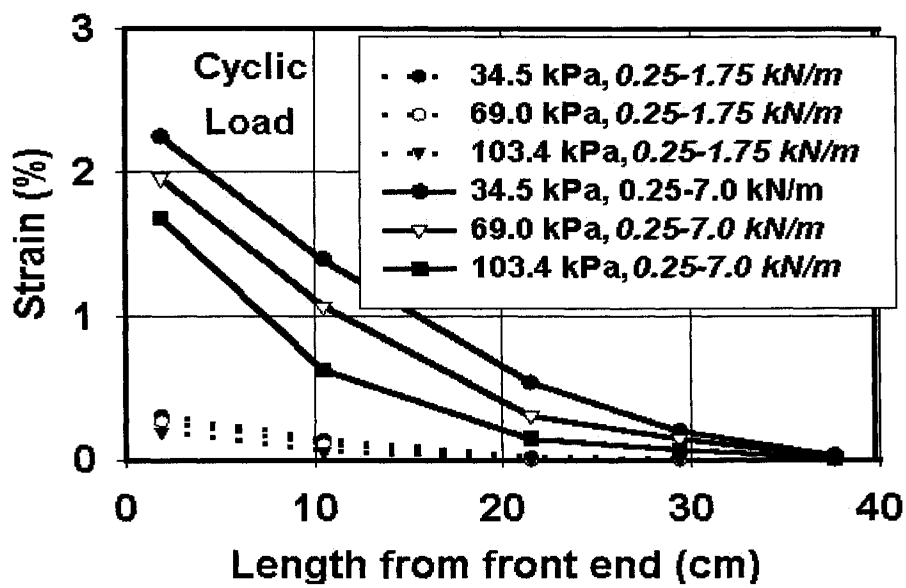

Figure 9. Strain distribution under various confining pressures and applied loads
(cyclic loading)

Figure 10 compares the effects of load type (i.e., sustained or cyclic load) and confining pressure on the strain distribution along the length of the geogrid under the same load magnitude. The only noticeable difference in creep strain took place at the front ribs of the geogrid. This difference eventually vanished along the length of the grid. Creep was higher for the case of sustained loading. That difference was higher in the front (i.e., at the point of load application) increased Creep was reduced with an increase in confining pressure. Therefore, creep strain was dependent on the magnitude of applied tensile load and normal stress.

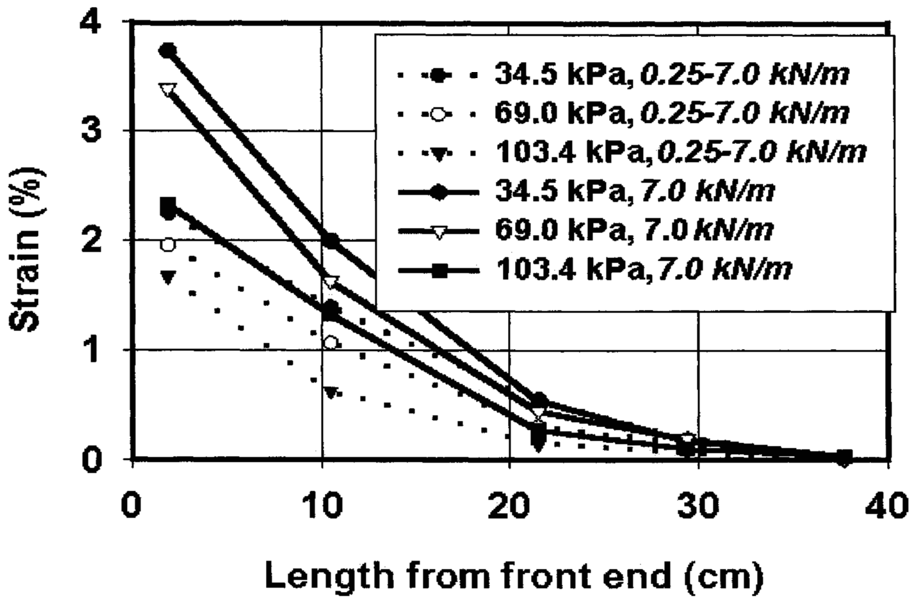

Figure 10. Strain distribution under various confining pressures for the same maximum load level (sustained and cyclic loading)

CONCLUSION

The long-term pullout behavior of a geogrid subjected to sustained and repeated loads was studied. Strain gages attached to the geogrid were utilized to investigate the influence of confining pressure and type of applied load on the interaction behavior of the embedded geogrid in clay. Unconfined creep tests were useful to interpret the confining effects. Creep developed along the geogrid under both sustained and cyclic loads, and increased with time. However, creep was larger under sustained load when compared to maximum cyclic load level and increased with tensile load. Confining pressure greatly influenced clay-to-geogrid interaction. However, creep rate at the point of load application was not greatly affected by the presence of confining pressure. That is, at a given tensile load in the geogrid, the strain rate remained constant regardless of the confining pressure. Therefore, creep strain appears to be largely dependent on the mechanical properties of the geogrid material.

ACKNOWLEDGEMENTS

This research was completed under supervision of Prof. Dov Leshchinsky, University of Delaware. The author is grateful for his valuable academic guidance and support. The author also thanks to Prof. Hoe I. Ling, Columbia University, and Prof. Victor Kaliakin, University of Delaware for their outstanding support during the study. This work was sponsored by Delaware Transportation Institute and was prepared in cooperation with Delaware Department of Transportation (DelDOT), and Federal Highway Administration (FHWA).

REFERENCES

Elias, V., Christopher, B.R., 1998, "Mechanically Stabilized Earth Walls and Reinforced Soil Slopes, Design and Construction Guidelines", US Department of Transportation, FHWA-SA-96-071.

Hayden R.F., Schmertmann, B.Q. and McGuire, M.S., 1991, "High Clay Embankment Over Cannon Creek Constructed with Geogrid Reinforcement", *Geosynhetics'91 Conference*, Atlanta, USA, Volume 2, pp. 799-821.

Leshchinsky, D., Kaliakin, V.N., Bose, P., and Collin J., 1994, "Failure Mechanism in Geogrid-Reinforced Segmental Walls: Experimental Implications", *Soils and Foundations*, Volume 34, N. 4, pp. 33-41.

Min, Y., 1994, "Pullout Behavior of Embedded Geogrid Subjected to Sustained and Repeated Loads", *Master's Thesis,* University of Delaware, Newark, Delaware.

Pamuk, A., Leshchinsky, D., Ling, H.I. and Kaliakin, V.N., 1997, "Interaction Behavior of Geogrids Embedded in Clay Subjected to Static and Repeated Loads", *Research Report,* Delaware Transportation Institute, DTI 105, University of Delaware.

Scott, J.D., Hofman, B.A., Richards, E.A. and Buch, E.R., 1987, "Design of the Devon Geogrid Testfill", *Geosynhetics'87 Conference*, New Orleans, USA, pp. 157-168.

Tatsuoka, F., Ando, H., Iwasaki, K. and Nakamura, K., 1986, "Performance of Clay Test Embankments Reinforced with a Non-Woven Geotextile", *Proceedings of 3rd International Conference on Geotextiles*, Vienna, Austria, Volume 2, pp. 355-360.

STRAIN DISTRIBUTION IN GEOSYNTHETIC-REINFORCED SLOPES USING DIGITAL IMAGE ANALYSIS

FABIANA ARRIAGA
UNIVERSITY OF COLORADO AT BOULDER

ABSTRACT

Geosynthetic-reinforced soil structures are conventionally designed using methods based on limit equilibrium, which require that assumptions be made regarding the distribution of tensile forces within the reinforcement layers. The uncertainties in reinforced soil behavior have been perceived to lead to conservative designs.

Digital image analysis was used in this investigation to analyze in-flight video images of geosynthetic-reinforced soil slopes models tested in a geotechnical centrifuge until failure. The use of digital image analysis techniques allowed the determination of the displacement distribution along the reinforcements for increasing g-levels. The raw displacement data was fitted to a sigmoid curve and the strain distribution in the reinforcement layers was calculated as the derivative of the smoothed displacement data function. The reinforcement layers were observed to strain proportionally to the overburden pressures defined by the vertical distance below the face of the slope. Consequently, the location of the maximum reinforcement strains was at approximately midheight of the slope. This location did not vary with increasing g-levels.

INTRODUCTION

Geosynthetic-reinforced soil structures are conventionally designed using methods based on limit equilibrium. In these methods, the distribution of tensile forces within the reinforcement layers must be assumed. Assumptions regarding the magnitude and distribution of the maximum reinforcement tensile forces with depth are of particular relevance for the design of geosynthetic-reinforced soil structures. The uncertainties in current understanding of the behavior of reinforced soil have been perceived to lead to conservative designs. Consequently, more realistic reinforcement strain distributions need to be incorporated in current design methods for geosynthetic-reinforced structures.

The purpose of this study is to investigate, using digital image analysis, the reinforcement strain distribution in a geosynthetic-reinforced slope tested in a geotechnical centrifuge. In particular, this study provides insight on: i) the distribution with depth of the maximum strain developed in the reinforcement layers for increasing g-levels, and ii) the magnitude and location of the maximum strain developed among all reinforcement layer for increasing g-levels.

A review on strain distribution obtained in full-scale geosynthetic-reinforced slopes reported in the literature is presented. Next, details of the digital image analysis of the in-flight images of the centrifuge geosynthetic-reinforced slope model are discussed. The procedures followed to obtain the reinforcements displacement and strain distributions are also included. Finally, evaluation of the reinforcement strain distribution data, its implications in current design methods and the conclusions of this investigation are presented.

STABILITY ANALYSIS OF REINFORCED SOIL SLOPES

Most reinforced soil stability analyses are modified versions of classical limit equilibrium slope stability methods in which reinforcement contributions are introduced as additional tensile forces in the computations. The modified stability analysis must include additional assumptions on top of those already introduced in the analysis of unreinforced slopes (i.e. shape of failure surface and the inclination and magnitude of inter-slice forces). These additional assumptions include the inclination (e.g. horizontal or tangential) and distribution (e.g. linear, constant with depth, etc.) of the reinforcement tensile force along the selected failure surface (Christopher and Leshchinsky, 1991; Zornberg et al., 1998).

A linear distribution of reinforcement tension with depth is usually assumed in design. Zero tension is assumed at the crest of the slope and a maximum tension value is commonly assumed at the toe. It is reasonable to assume that the maximum tension in the reinforcements resists the horizontal stresses that develop within the soil along the location of the potential failure surface (Zornberg et al., 1998). For reinforced vertical walls, the horizontal soil stresses along the potential failure surface are proportional to the overburden pressure, which increases linearly with depth below the top of the wall. Thus the triangular shape of the distribution of maximum reinforcement tension. Such assumption has not been validated for reinforced slopes, and it could lead to additional reinforcement of non-critical zones.

STRAIN DISTRIBUTION WITHIN FULL-SCALE GEOSYNTHETIC-REINFORCED SLOPES

A review of full-scale instrumented geosynthetic-reinforced soil slopes was undertaken as part of the present investigation in order to assess the distribution of strains within geosynthetic reinforced slopes. Although numerous projects were reviewed, only full-scale geosynthetic-reinforced slopes with granular backfill and flexible facing are evaluated herein (See Table 1). Measurement of the strain distribution in the reinforcement layers was a common characteristic of all the slopes reviewed. Analysis of the reported strain distribution data led to the following observations:

- As expected, the magnitude of the strain distribution along the reinforcement layers increases as the load increases (e.g. Fannin and Hermann, 1990).
- The strain distribution along the reinforcement layers usually exhibits a peak value (e.g. Fannin and Hermann, 1990; Ghinelli and Sacchetti, 1998). For geosynthetic-reinforced slopes with granular backfill and with extensible facing (i.e. wrapped-around), the maximum strain in each reinforcement layer is located away from the slope face.

Table 1. Full scale geosynthetic-reinforced slopes with granular backfill and reported strain distribution data

Slope Inclination	H (m)	Reinforcement Type	n	L (m)	S (m)	Reference
1H:1.2V	2.7	woven geotextile	6	3.5	n/a	Delmas et al., 1988
1H:2V	6.0	geogrid	4	<= 9.0	1.5, 1.0	Fannin & Hermann, 1988
0.7H:1V	3.0	geogrid	1 - 3	1.0 – 3.0	1.5 – 1.0	Miki et al., 1988
1H:2V	4.8	geogrid	8	2.2	0.6	Fannin & Hermann, 1990
1H:1.73V	5.3	geogrid	8	3.15, 4.5	0.65	Ghinelli & Sacchetti, 1998

H: slope height
S: spacing between reinforcement layers
n: number of reinforcement layers
L: length of reinforcement layer

Magnitude and Location of the Maximum Strain in the Reinforcements

The maximum reinforcement strain magnitudes typically ranged from 0.3% to 1.5%. Such strain levels corresponded to reinforcement loads much lower than the maximum tensile strength of the geosynthetic materials. The elevation of the reinforcement that showed the maximum strain ranged from approximately 0.25H to 0.65H, where H is the height of the slope. These results indicate that the common assumption that the maximum tensile force develops at the toe of the slope is not supported by field data obtained for slopes under working load conditions.

Zornberg et al. (1998) investigated the behavior of geosynthetic-reinforced soil structures at failure using models tested in a geotechnical centrifuge. Geotextile-reinforced slope models with granular backfill were tested under increasing centrifugal acceleration until failure. From the experimental results obtained, it was apparent that failure of the centrifuge models initiated at midheight of the slopes (i.e. 0.5H). The conventional triangular distribution of maximum tensile forces in the reinforcements with depth was also not supported by these results. Instead, the horizontal stresses resisted by the reinforcement layers were considered proportional to the overburden pressure defined by the vertical distance below the face of the slope (see Figure 1). It was also established that the location of the maximum tensile force in the reinforcements measured as the height h_p from the bottom of the slope would depend on the inclination of the slope face.

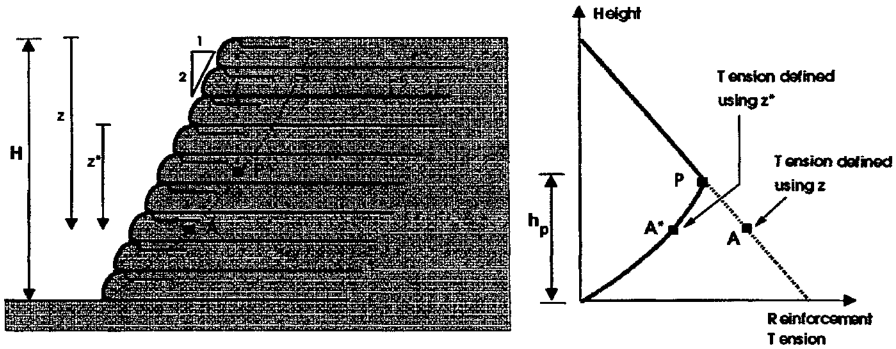

Figure 1. Distribution with depth of maximum reinforcement tension for reinforced soil slopes (after Zornberg et al., 1998)

DESCRIPTION OF THE CENTRIFUGE TESTING PROGRAM

Determination of the reinforcement strains in geotextile-reinforced slopes was undertaken as part of this investigation by applying digital image analysis techniques to in-flight video recordings of centrifuge tests on geotextile-reinforced slopes performed by Zornberg (1994). The strain distribution of the reinforcement layers was obtained for several of those slope models. However, the results for only one of those models, model B18, are presented herein. The characteristics of the centrifuge testing program relevant to this study are review in this section.

Model B18 was subjected to a gradually increasing centrifugal acceleration until failure occurred at 76.5 g. Details of the geometry, backfill material, geotextile reinforcement, and instrumentation are described below. Information on the geotechnical centrifuge, model construction and testing procedures is provided by Zornberg et al. (1997).

Characteristics of Centrifuge Slope Model B18

Model B18 was 254 mm high. It consisted of a 228 high geotextile-reinforced slope built on a 25 mm thick foundation layer. The slope inclination was 1H:2V. Air dried Monterey No. 30 sand was used both as backfill material and foundation soil. Model B18 was built with 18 reinforcement layers 203 mm long. The geotextile layers were wrapped at the face using a 50 mm long geotextile overlap. The geometry of models B18 is presented in Figure 2. The horizontal lines (green colored sand) in this figure correspond to the locations of the reinforcement layers.

The centrifuge model cross-section was visible through a Plexiglas wall and an image acquisition system consisting of a closed circuit television camera and video recording device was used. Green colored sand was placed against the Plexiglas wall along each reinforcement layer. In addition, black colored sand markers were placed at a regular horizontal spacing of 25 mm (1 in) (see Figure 2).

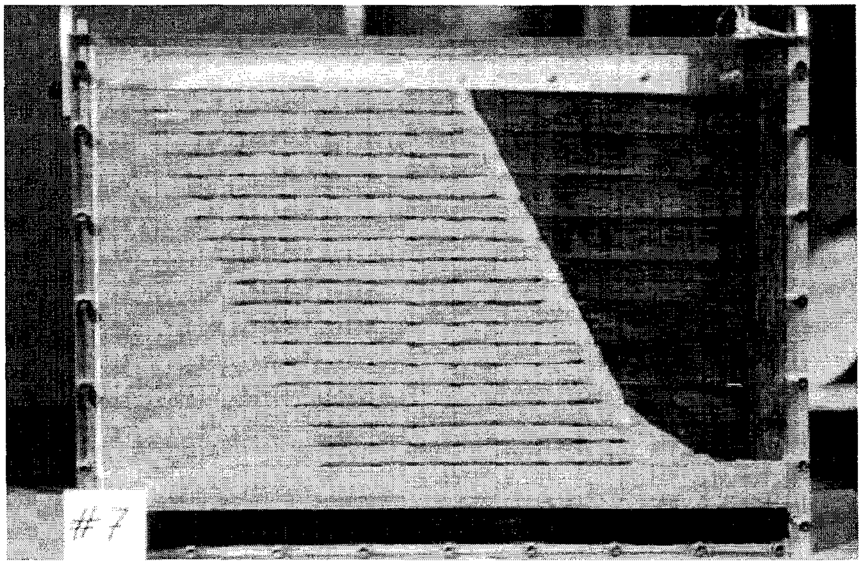

Figure 2. Model B18 after construction

Material Properties

The centrifuge models were built using Monterey No. 30 sand, which is a clean, uniformly graded sand classified as SP in the Unified System. the friction angle obtained from triaxial compression tests was ϕ=35° for a relative density of 55%. The corresponding unit weight for the Monterey No. 30 sand was 15.64 kN/m^3.

Model B18 was built using interfacing fabric as reinforcement material. The fabric used was a nonwoven with a unit weight of 24.5 g/m^2. An unconfined tensile strength value of 0.063 kN/m was obtained from a series of wide-width strip tensile tests ASTM D4595. However, the confined tensile strength was used in the analysis. A value of 0.123 kN/m was obtained from backcalculation of the centrifuge slope models.

DIGITAL IMAGE ANALYSIS OF GEOTEXTILE-REINFORCED CENTRIFUGE SLOPE MODELS

Instrumentation of geotextile reinforcements in centrifuge testing applications has proven to be difficult. Digital image analysis techniques can be used to retrieve displacement data from images of the centrifuge models in order to obtain the reinforcements strain distributions. This section contains the details of the digital image analysis performed using a videotape of a centrifuge test of a geotextile-reinforced slope model reported by Zornberg et al. (1998). A video capturing board was utilized in order to convert the videotape of the centrifuge test from analogue to digital signal.

The objective of the digital image analysis was to obtain the strain distribution in the geotextile reinforcements of the centrifuge slope models. The strain distribution along each reinforcement layer was obtained from the corresponding displacement distribution.

Reinforcement Displacement Distributions

Since the sand markers were placed at increasing distances from the slope face, relative displacements between markers could be obtained from the distances between them. The distance between markers was calculated by considering both vertical and horizontal changes in the coordinates of the markers' centers of mass. The edge of each sand marker was tracked on the centrifuge models images. The computer program automatically recognized the presence of an object (e. g. edge of marker) and calculated the coordinates of its center of mass. Calibration of the distance measurement was performed considering the known spacing of the square grid imprinted on the Mylar sheet lining the Plexiglas side wall.

Geotextile strain distributions were initially calculated by dividing the relative displacement between consecutive markers by the distance between them. However, minor scatter in the geotextile displacement distribution results in major oscillations in the calculated strain distribution. Consequently, the displacement distribution data was fitted to a monotonically increasing curve. The expression used to fit the displacement data is a sigmoid curve defined by:

$$d = \frac{1}{a + be^{-cx}}$$

where d is the marker displacement, x is the distance between the marker and the corresponding reference marker, e the natural logarithm base constant, and a, b, and c are parameters defined by fitting the displacement data to the sigmoid curve using least squares techniques. The displacement distribution for reinforcement layer 6 of model B18 at increasing g-levels is shown in Figure 3. The corresponding fitting curves are also shown in the figure.

Reinforcements Strain Distributions

The reinforcements strain distribution for the geotextile-reinforced slope model B18 was defined analytically as the derivative of the smoothed reinforcement displacement distribution. This strain distribution shows zero strain values closer to the face of the slope and at the embedded end of the reinforcement. This trend is consistent with the behavior of geosynthetic-reinforced slopes with extensible facing. Figure 4 shows the strain distribution for reinforcement layer 6 of model B18.

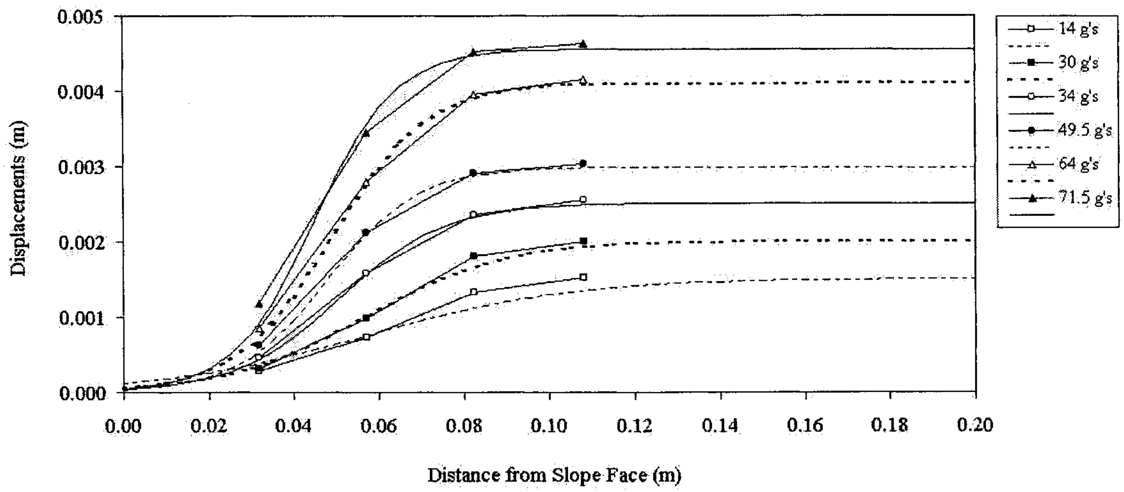

Figure 3. Displacement data and sigmoid fitted curves for reinforcement layer 6 of Model B18

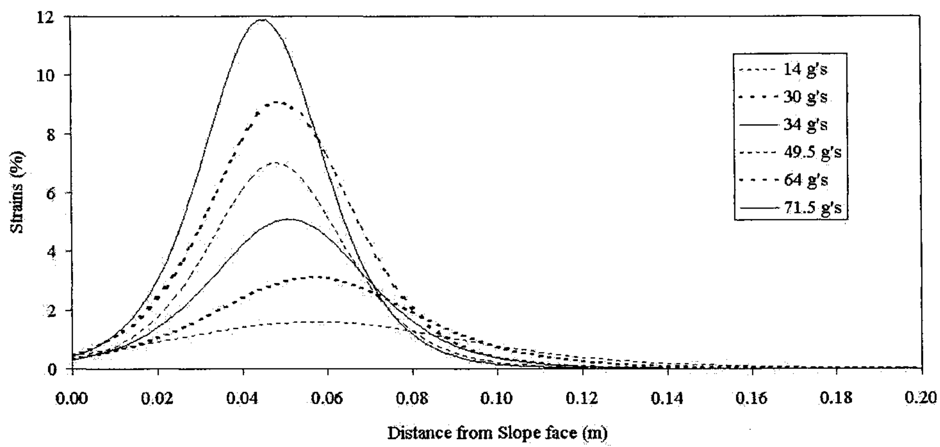

Figure 4. Strain distribution for reinforcement layer 6 of model B18

ANALYSIS OF RESULTS

Distribution of Maximum Reinforcement Strain with Depth

Identification of the maximum strain in each reinforcement layer has major implications in the design of geosynthetic-reinforced slopes. Current design procedures generally assume that the maximum strain among all the reinforcement layers occurs towards the base of the slope. This assumption is not supported by the results presented herein. The maximum strain for each reinforcement for increasing g-levels for model B18 is shown in Figure 5. The dashed lines in this figure represent the location of the geotextile layers.

As expected, Figure 5 shows that the maximum reinforcement strain increases for increasing g-levels. It can also be observed that the distribution of maximum reinforcement strain with depth for each g-level shows a maximum strain located at approximately midheight of the slope. The strain values decrease from this maximum towards the toe and the top of the slope.

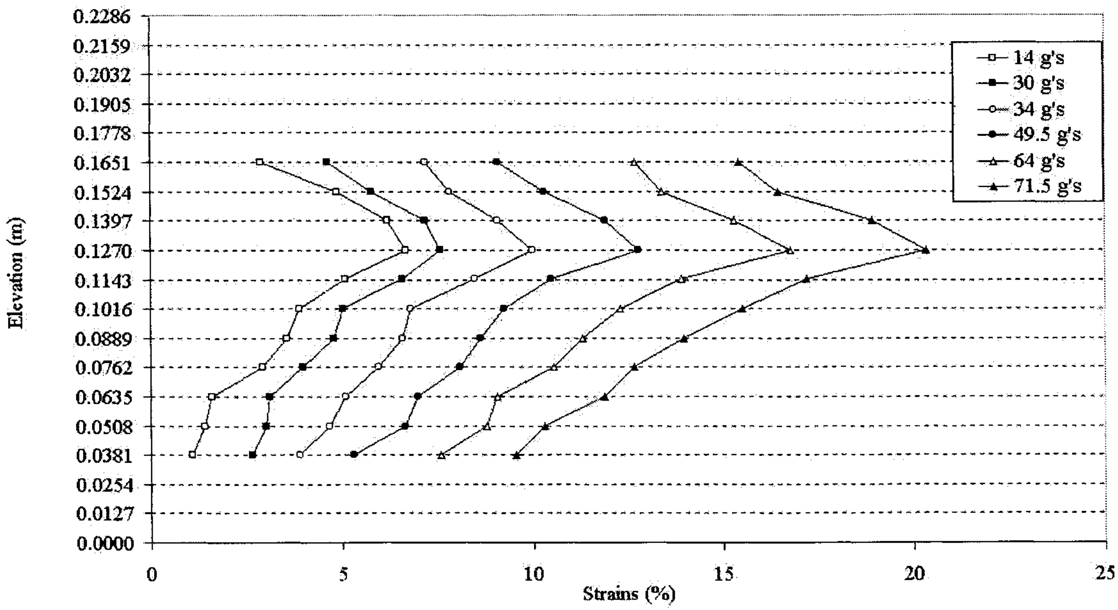

Figure 5. Maximum reinforcement strain vs elevation for model B18

Maximum Strains Developed among All Reinforcement Layers

Determination of the magnitude and location of the maximum strain developed among all reinforcement layers plays a major role in design of geosynthetic-reinforced slopes, as it defines the required reinforcement tensile strength and reinforcement layout. Figure 5 shows that the maximum reinforcement strains developed among all reinforcement layers for model B18 occurred in reinforcement layer 11 for all the g-levels considered in the analysis. This reinforcement layer was located at an elevation of 56% of the reinforced slope height.

The location with respect to the slope face of the maximum reinforcement strains for model B18 is plotted in Figure 6. A vertical dashed line through the crest of the slope is shown in Figure 6 to help identify the relative location of the maximum strains. It is apparent that the maximum strains are located directly below the crest of the slope. It is important to emphasize that this location was the same for different increasing g-levels and not only at failure. The results obtained in this investigation do not support the conventional triangular distribution of maximum tensile forces in the reinforcements with depth. Instead, the horizontal stresses resisted by the reinforcement layers were observed to be proportional to the overburden pressure defined approximately by the vertical distance below the face of the slope (see Figure 1), as proposed by Zornberg et al. (1998).

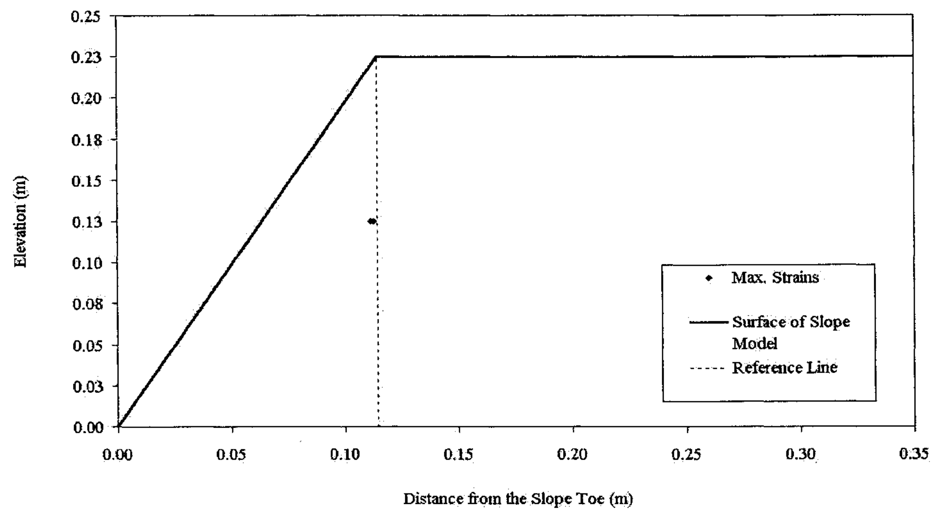

Figure 6. Location of the maximum reinforcement strain developed among all reinforcement layers for Model B18

The required reinforcement design tensile strength that would result from adopting the distribution of tensile stresses proposed herein is lower than the corresponding value obtained by assuming the conventional triangular distribution of maximum reinforcement tensile forces. Therefore, less conservative and more cost-effective designs of geosynthetic-reinforced slopes could be performed if a more representative tensile force distribution is adopted in design procedures.

CONCLUSIONS

The main objective of this investigation was to study the strain distribution in geosynthetic-reinforced slopes. For this purpose, centrifuge testing and digital image analysis techniques were combined to evaluate the reinforcement strain distribution in geotextile-reinforced centrifuge slope models. Performance data from projects involving full-scale instrumented geosynthetic-reinforced slopes with granular backfill and extensible facing was reviewed. The strain levels reported for geosynthetic-reinforced slopes under working stress conditions induce significantly lower reinforcement tensions than the ultimate tensile strength of the geosynthetic materials.

The reinforcement strain distribution in a geotextile-reinforced centrifuge slope models was evaluated. The following conclusions can be gathered:

- The distribution of maximum reinforcement strain with depth shows an increasing trend with increasing g-levels.

- The maximum reinforcement strains were located at an elevation of 56% of the reinforced slope height (model B18). Such location of the maximum strain remained the same for increasing g-levels.

- The results obtained in this investigation are in contradiction with the triangular distribution of maximum tensile forces with depth used conventionally for design. Instead, the horizontal stresses resisted by the reinforcement layers were observed to be proportional to the overburden pressure defined by the vertical distance below the face of the slope.

Overall, this investigation showed that the combination of digital image analysis and centrifuge modeling can provide significant insight regarding strain distribution in geosynthetic-reinforced structures.

ACKNOWLEDGMENT

This research was supported by a grant from the Colorado Advanced Software Institute (CASI). CASI is sponsored in part by the Colorado Commission on Higher Education (CCHE), an agency of the State of Colorado. This assistance is gratefully acknowledged.

REFERENCES

Chrsitopher, B. R., and Leshchinsky, D. (1991). "Design of geosynthetically reinforced slopes", Proceedings of the Geotechnical Engineering Congress 1991 sponsored by the Geotechnical Engineering Division of the ASCE, Boulder, CO, 988-1005.

Delmas, Ph., Gourc, J. P., Blivet, J. C., and Matichard, Y. (1988). "Geotextile-reinforced retaining structures: a few instrumented examples", Proceeding of the International Geotechnical Symposium on Theory and Practice of Earth Reinforcement, Japan, 511-516.

Fannin, R. J., and Hermann, S. (1988). "Field behavior of two instrumented, reinforced soil slopes", Proceedings of the International Geotechnical Symposium on Theory and Practice of Earth Reinforcement, Japan, 277-282.

Fannin, R. J., and Hermann, S. (1990). "Performance data for a sloped reinforced soil wall", Canadian Geotechnical Journal, (27), 676-686.

Ghinelli, A., and Sacchetti, M. (1998). "Finite Element Analysis of instrumented geogrid reinforced slope", Proceedings of the 6th International Conference on Geosynthetics, (2), 649-654.

Miki, H., Kutara, K., Minimi, T., Nishimura, J., Fukuda, N. (1988). "Experimental studies on the performance of polymer grid reinforced embankment", Proceedings of the International Symposium on Theory and Practice of Earth Reinforcement, Japan, 431-436.

Zornberg, J. G. (1994). "Performance of geotextile-reinforced soil structures", Thesis submitted in partial fulfillment of the requirements for the degree of Doctor of Philosophy, Department of Civil Engineering, University of California, Berkeley, California.

Zornberg, J. G., Mitchell, J. K., and Sitar, N. (1997). "Testing of reinforced slopes in a geotechnical centrifuge", Geotechnical Testing Journal, Vol. 20, No. 4, pp. 470-480.

Zornberg, J. G., Sitar, N., and Mitchell, J. K. (1998). "Performance of geosynthetic reinforced slopes at failure", Journal of Geotechnical Engineering, 124(8), 670-683.

MECHANISMS OF INTERFACE SYSTEMS IN FLEXIBLE PAVEMENT – A FINITE ELEMENT APPROACH

MOSTAFA A. ELSEIFI
UNITED STATES OF AMERICA
VIRGINIA POLYTECHNIC INSTITUTE AND STATE UNIVERSITY
THE CHARLES EDWARD VIA, JR., DEPARTMENT OF CIVIL AND ENVIRONMENTAL ENGINEERING

ABSTRACT

Although interface systems are recognized as feasible solutions to enhance the performance of flexible pavements, the contributing mechanisms are still unclear. To better understand the reinforcement and strain absorption mechanisms, an axisymmetric finite element model was developed based on the experimental results obtained from the Virginia Smart Road Project. In this full-scale instrumented facility, different interface systems were installed, including geocomposite membrane, steel reinforcing netting, and geotextile. The developed finite element model was used to investigate the effectiveness of the interface in the pavement system. Results of the developed finite element model indicated that a reinforced system significantly contributes to the pavement structure only if it is stiffer than the upper layer. In a cracked pavement structure, however, the performance of the interlayer as a strain energy absorber is controlled by its stiffness and surface interaction with the surrounding layers.

INTRODUCTION

Interface systems have received considerable attention in recent years as viable solutions to enhance flexible pavement performance. The introduction of these systems to the transportation field was mainly due to the unsatisfactory performance of traditional materials when exposed to a dramatic increase in loading and change in traffic patterns; a need that still exists. Among the new materials introduced to enhance flexible pavement performance are geosynthetics. In general, an interface system can provide five distinct functions to a pavement structure: reinforcement of a particular layer (by improving the tensile strength of a pavement layer and spreading the load over a larger area); separation (by maintaining the integrity of a particular layer by preventing intermixing); drainage or filtration (by allowing the water to flow, thereby dissipating pore water pressure while limiting soil movement); strain energy absorption (by allowing for larger deformations in the interlayer, which dissipates the excess amount of energy that otherwise may enhance the crack propagation); and moisture barrier (by preventing water movement between layers).

Although some of the benefits of interface systems can be easily identified, such as reinforcement (enhanced overall performance) and strain energy absorption (retardation or prevention of reflective cracking), the contribution mechanisms are poorly understood. The use of these materials based on field experiences and empirical rules resulted in contradicting experiences and opinions about their benefits. While some studies emphasized the surplus advantages, such as substantial savings in hot-mix asphalt (HMA) thickness (Kennepohl et al., 1985), others found that the use of interface systems is 'useless' (Donna, 1993). This contradiction is mainly due to the gap between in-situ performance and the understanding of the contributing mechanism.

To investigate the effectiveness of different interlayer systems, four of the twelve heavily instrumented flexible pavement sections at the Virginia Smart Road were built with different interface layers (geocomposite membrane as a moisture barrier and as a strain energy absorber, and steel nettings as reinforcement); five other sections include geotextile as a separator. More than 500 instruments were embedded in the road during construction to quantitatively measure the response of pavement systems to vehicular and environmental loading. For successful instrumentation strategy, at least two types of response (stress, strain or deflection) have to be compared simultaneously. Therefore, strain and stress are carefully monitored along the depth of the pavement system. Climatic parameters such as temperature, base and subbase moisture, and frost depth are monitored at different depths along the pavement. The calibration and installation of the instruments at the Virginia Smart Road has been presented elsewhere (Al-Qadi et al., 2000).

Parallel to the field-testing and evaluation of the interface systems, a theoretical approach was initiated to investigate and explain the contributing mechanisms. This paper presents the results of a finite element (FE) study evaluating the performance of interlayers with flexible pavement systems. A FE model was developed to simulate the vehicular loading. The results obtained from the FE model were compared with those obtained from the experimental measurements. The effects of different design parameters were also investigated.

BACKGROUND

The traditional approach to predict flexible pavement response to vehicular loading is by using the multilayer elastic theory. This approach assumes that pavement systems are loaded statically over a uniform area, and that the system responds linearly to the applied load. In addition, the subgrade is assumed to be a semi-infinite layer with a constant modulus. The compatibility of strains and stresses is also assumed to be satisfied at all the layer interfaces. Although this approach involves several assumptions that may be questionable, the simplicity of the multi-layer analysis is usually thought to overcome the uncertainty of the results (Zaghloul et al., 1993).

In contrast, the finite element method can be a complex and costly analysis tool; it is thus employed only when accurate results are needed. Although involving more complicate formulation, the application of FE techniques allows a "better" simulation of pavement problems. This method can include almost all controlling parameters (dynamic loading, discontinuities such as cracks and shoulder joints, viscoelastic and nonlinear elastic behavior, infinite and stiff foundations, system damping, quasi-static analysis, crack propagation, etc.). Although this technique still requires strong engineering knowledge, its flexibility and accuracy allows the understanding of more complicated systems such as reinforced flexible pavements.

During the last decade, FE techniques have been successfully used to simulate different pavement problems that could not be simulated using multi-layer elastic theory. In 1993, Zaghloul and White effectively employed three-dimensional (3D) dynamic finite elements to investigate the effect of load speed and asphalt mixture properties on the resulting rut depth (Zaghloul et al., 1993). In 1994, Uddin et al. investigated the effect of pavement discontinuities on pavement response using FE techniques (Uddin et al., 1994). In 1996, Cho et al. highlighted the advantages and disadvantages of three different finite element approaches: plane-strain (2D), axisymmetric, and 3D finite element models (Cho et al., 1996). According to this study, the two-dimensional plane-strain model is inaccurate in simulating actual traffic loading. On the other hand, the axisymmetric and 3D finite element approaches were found to yield accurate results in simulating actual traffic loading. Although 3D finite element models provide very accurate results, the dramatic increase in time and computer requirements may not justify the obtained level of accuracy. Vanelstraete et al. have employed a 3D FE model for the simulation of non-homogeneous interlayer systems (e.g. steel reinforcing nettings) (Vanelstraete et al., 2000).

In this study, an axisymmetric finite element approach is employed. The three-dimensional pavement structure is mathematically reduced to a two-dimensional one by assuming constant properties in all horizontal planes. Although the traffic load is assumed to be applied over a circular area, this model still provides a 3D solution based on a two-dimensional formulation using cylindrical coordinates (radius r and depth z). In this case, displacements are assumed to occur in the radial and axial directions only (no circumferential displacements are allowed); the formulation is presented in Figure 1.

MODEL FORMULATION

The commercial software ABAQUS version 5.8 was used for the finite element modeling of the pavement structure (Abaqus 1993). This finite element software allows for 2D and 3D analyses under static, dynamic or quasi-static conditions. Any type of material properties can be modeled (viscoelastic, linear and non-linear elastic, elastic-plastic, etc.). This program also allows for exact modeling of surface behaviors. Contacts between two deformable bodies or a rigid and a deformable body are allowed. This contact can be defined as a tied or a friction motion. Friction interaction can be defined as a regular Coulomb model or as a user-defined friction model.

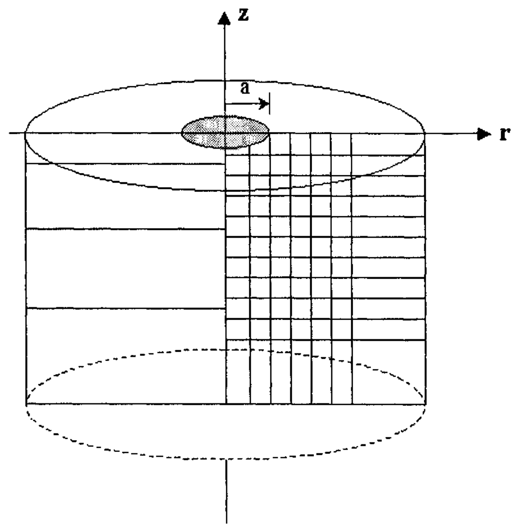

Figure 1. Axisymmetric finite element formulation.

Figure 2 illustrates the pavement structure under consideration. The cross-section shown in Figure 2 corresponds to the pavement structure constructed at the Virginia Smart Road (section K). Another finite element model that did not include an interface layer as a base for comparison was formulated for the same design. The assumed material properties were obtained using MICHBACK version 1.0 backcalculation software (Harichandran et al., 1994). All layers were assumed to behave linearly and elastically. Based on the vehicular loading measurements and the backcalculation results, the following section presents the general assumption made in the developed model.

Model Dimensions and Geometry

The dimensions of the modeled portion are 1016mm x 1511mm (40in x 59.5in). These dimensions were selected to reduce any edge effect errors while keeping the elements' sizes within acceptable limits (modeling constraints). The generated mesh distribution was designed to give an optimal accuracy (small elements around the load and large elements far from the load). While 6mm (0.25in) square elements were used in the region close to the load, 50mm (2in) square elements were used in the regions far from the load. All elements were 8-nodes biquadratic axisymmetric. Due to the large number of degrees of freedom (22430), reduced integration elements were selected to increase the rate of convergence. The original mesh was refined according to Bathe's criterion for mesh refinement: "A finite element mesh is sufficiently fine when jumps in stresses across inter-element boundaries become negligible"

(Bathe 1982). In this study, a jump in stresses across element boundaries of less than 0.7kPa (0.1psi) was assumed negligible. A convergence study was also established for the developed model, see Figure 3 for illustration. As the mesh is refined, the 'exact' solution becomes more stable.

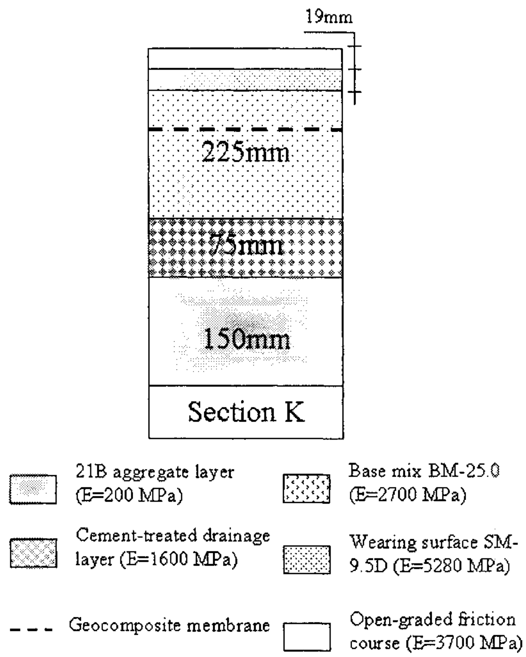

Figure 2. Pavement design for section K at the Virginia Smart Road.

Boundary Conditions

Infinite elements were assumed as the vertical support at the bottom of the model. Backcalculation evaluation indicated the presence of a stiff layer at a very high depth (3.30m). Therefore, the classical assumption of a fixed boundary at the bottom of the model was not considered as it may have resulted in a stiffer model than the actual pavement. Roller supports were assumed at the axis of symmetry allowing only for vertical displacement throughout this axis.

Surface Interaction

All hot-mix asphalt (HMA) layers were assumed fully bonded. This assumption was based on the expected good bonding between the different HMA layers due to the high temperature during placement, which leads to strong adhesion between the layers. On the other hand, the bonding between aggregate layers was assumed as friction-type (Mohr-Coulomb theory). This assumption is based on the fact that when granular surfaces are in contact, they usually transmit shear as well as normal forces across their boundary. Small sliding was also allowed between the aggregate layers. The values for the adhesion between the interlayer system and the surrounding HMA layers were based on the measured strains during vehicular loading. Three cases were investigated: full adhesion, unbonded to the upper layer, and friction.

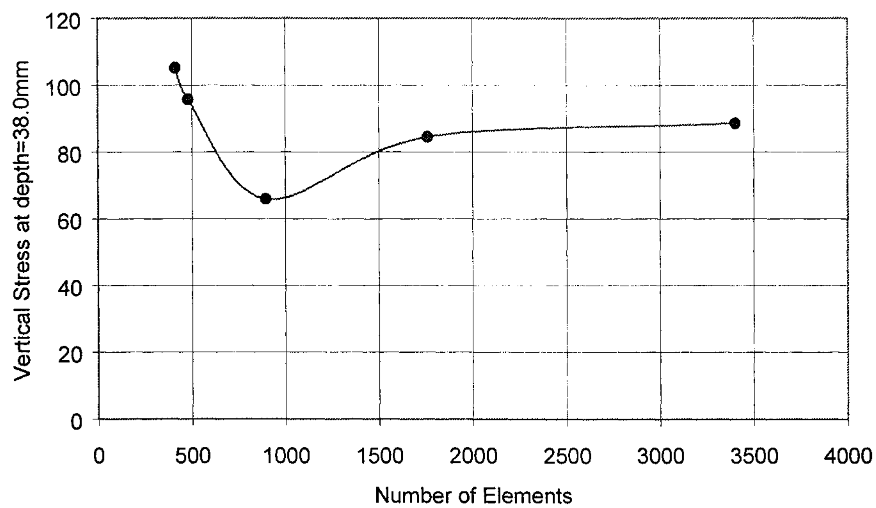

Figure 3. Mesh accuracy based on the number of elements used in the model.

Applied Load

A single tire load (26kN) was assumed with a uniform pressure of 724kPa applied over a circular area. A static analysis was considered and the obtained results were compared to those measured at very low speeds (8km/hr).

Model Validation

Before evaluating the interface system effectiveness, the results obtained using the developed model for the vertical stresses were compared to the measured values. Figure 4 illustrates the comparison between the measured and computed vertical stresses at different depths for a typical section without interlayer system at the Virginia Smart Road (Section B). As shown in this figure, there is a good agreement in stresses between field measurements and calculated ones.

INTERLAYER BENEFITS

Different cases were investigated to evaluate the potential benefits of the investigated interlayer system. As part of this parametric study, an uncracked cross-section (Figure 2) was investigated. The interface modulus was assumed to vary between 7 and 40000MPa (1 to 6000ksi). This range represents the expected modulus for the interlayer; 7MPa represents a typical geosynthetic material and 40000MPa is the average stiffness for steel reinforcing nettings. A geogrid material is expected to have a modulus around 1000MPa.

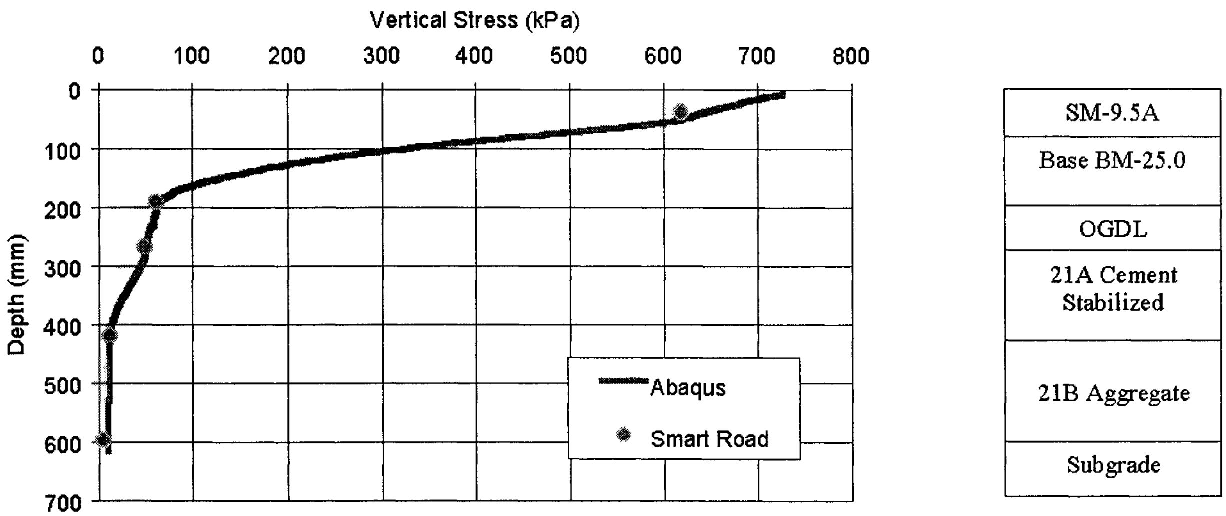

Figure 4. Computed and measured vertical stresses at different depths in section B at the Virginia Smart Road.

Figure 5 illustrates the variation of the tensile strain at different depths from the interface layer. It is clear from the figure that the interface layer causes a reduction in the tensile strain when its modulus is greater than the modulus of the surrounding HMA layer (E_{HMA} = 2700MPa). If the modulus of the interface layer is lower than the surrounding material, the interface may not be used to reinforce the pavement system. These results highly question the use of a geotextile with a modulus lower than HMA for reinforcement purposes. However, the use of such a geotextile may be justified for strain energy relief purpose only, not for reinforcement. As presented in the following section, such an application needs to be used carefully because its success highly depends on the bonding to the surrounding layers and the modulus of the material (the lower the modulus with high elongation, the better as a strain energy absorber). The decision of bonding strength is based on the crack location and propagation rate and direction.

The tensile strain at the bottom of the HMA surface layer can be related to the number of fatigue cycles to failure (N) through the following equation:

$$N = C_1 \varepsilon^{-C_2} \tag{1}$$

where N = the number of cycles to fatigue failure; ε is the tensile strain at the bottom of the asphalt layer; and C_1 and C_2 are mix constants. Typical reported values for the exponent constant (C_2) is between 3 to 5 (Bonaquist 1992). C_1 was assumed equal to 1.3 x 10^{-14} as found in the literature (Cebon 1986). Based on Equation (1), Figure 6 illustrates the expected fatigue life for the different interlayer systems shown in Figure 5.

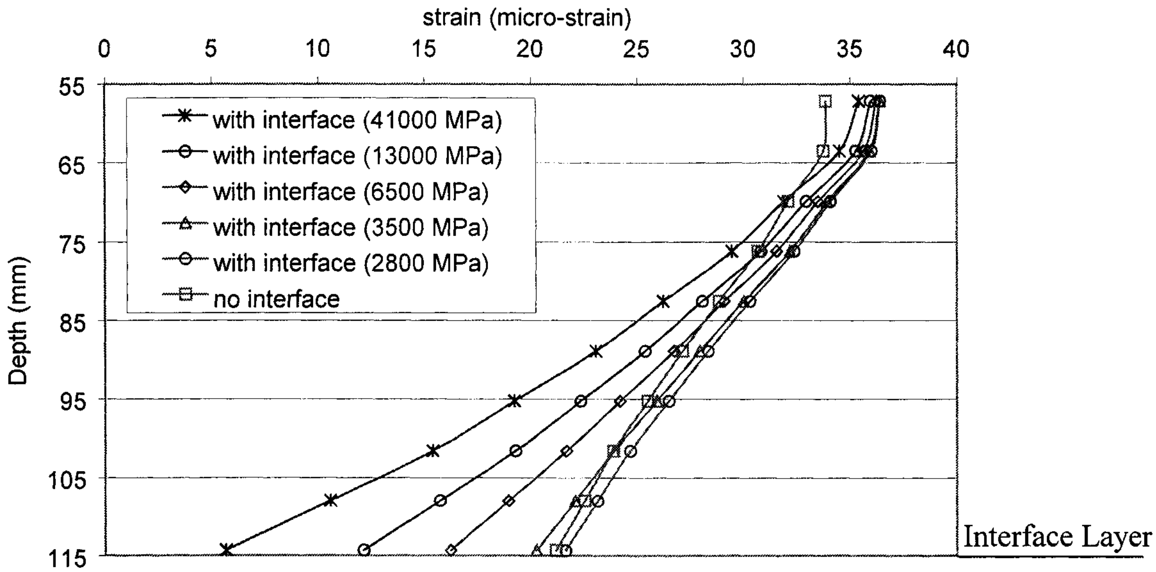

Figure 5. Variation of the tensile strain along the depth above interface.

As shown in Figure 6, an interlayer system with a modulus of 7MPa may reduce the fatigue life expectancy of the pavement structure if full bonding exists with both surrounding layers. Therefore, a low modulus material needs to have high elongation characteristics to provide strain energy absorption, which is important in many applications, especially the rehabilitation of cracked pavements. On the other hand, a strong interlayer system may effectively improve the overall performance of the pavement system if used as reinforcement.

The same analysis was performed by assuming the presence of a crack underneath the interface layer. In this case, the crack starts to propagate from its original position upward until it reaches the stress-relieving layer. If flexible enough, the interlayer will exhibit large deformations, which will be accompanied with a dissipation of energy, thus retarding the crack propagation process (Lytton 1989). Three different cases were considered for the bonding between the stress relieving layer and the upper layer: fully bonded, friction contact, and unbonded to the upper HMA layer. Figure 7 illustrates the three cases for an interface layer with a modulus of 2700MPa (400ksi). As shown in this figure, the behavior of the interlayer largely differs between the aforementioned cases:

- If the interface layer is fully bonded to the upper layer, the interface layer will cause an increase in the tensile strain at the crack tip (depth=120.65mm), which may result in debonding of the interface layer from the upper HMA layer.

- If the interface layer is unbonded to the upper layer, an increase in tension will occur at the bottom of the upper layer (depth=114.3mm). However, the crack tip region will be under compression, which will close the crack and may retard its propagation.

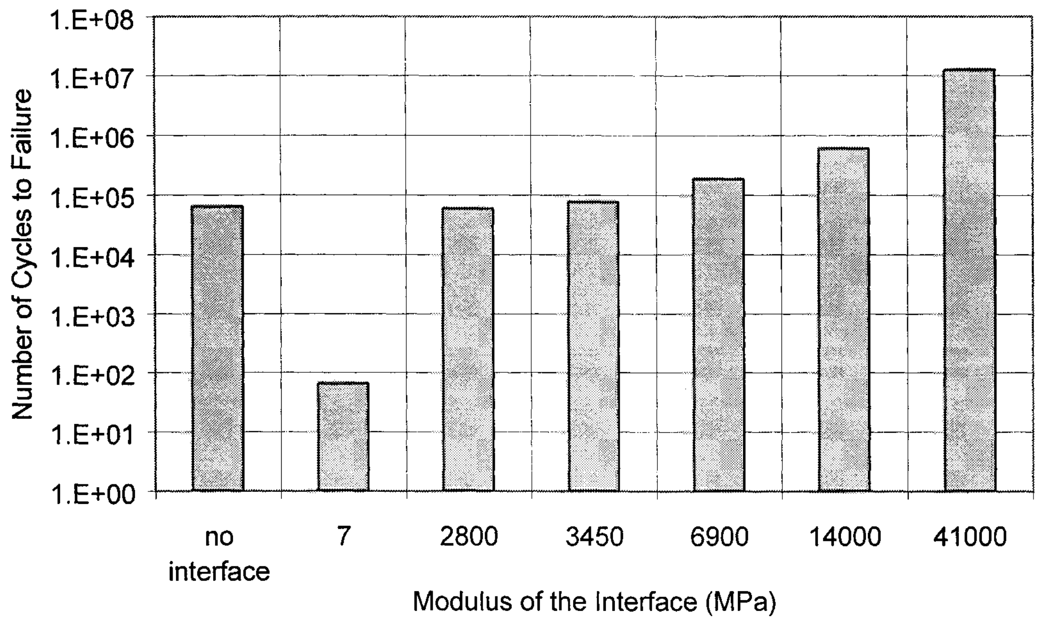

Figure 6. Fatigue life expectancy for the different reinforced sections.

- If friction is assumed at the interface, a similar situation to the unbonded case will occur with a smaller magnitude.

This analysis indicates that the bonding between the interface layer and the upper layer (probably an overlay) is extremely important and controls the overall performance of the strain absorption layer.

CONCLUSIONS

This paper presents a finite element investigation on the mechanistic behavior of interlayer systems used in flexible pavements. The following conclusions are drawn based on the results of this study:

- A good agreement was found between in-situ measured stresses in flexible pavements at the Virginia Smart Road and the developed axisymmetric FE model. The extent of this agreement depends mainly on the geometry of the model (model dimensions, boundary conditions, and surface interaction).

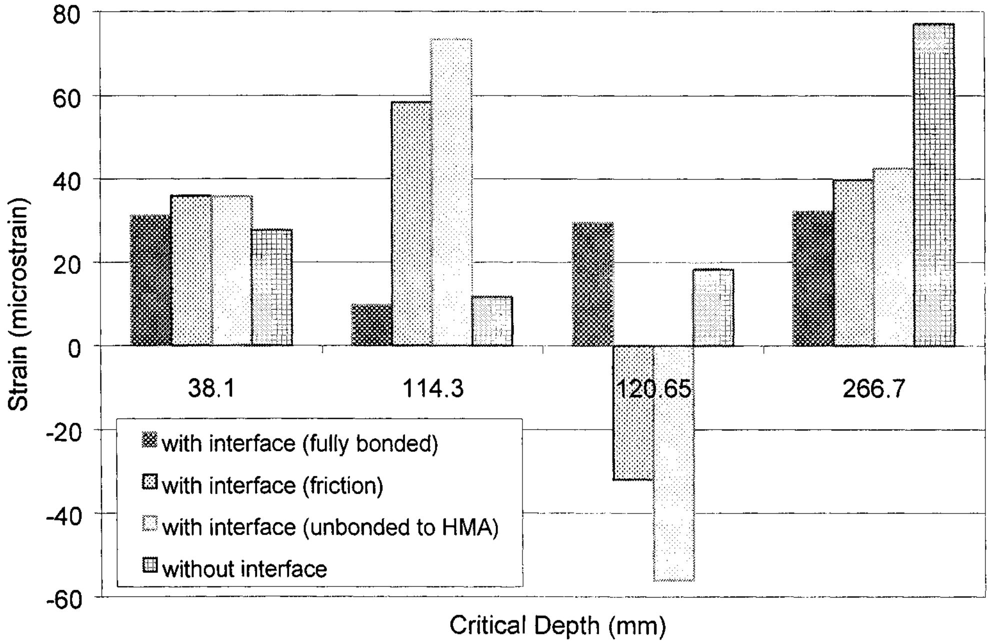

Figure 7. Contribution of the interface system (E= 2700MPa) to the pavement structure.

- The interface layer may positively contribute to the pavement structural capacity if its stiffness is higher or equal to the upper layer's stiffness. If the interface layer's stiffness is lower than the surrounding material, the system may not effectively contribute to the pavement structure capacity; however, it may provide strain energy absorption when it combines low modulus with high elongation.
- In a cracked pavement structure, the behavior of the strain absorption system is controlled by its bonding to surrounding layers. If full bonding exits between the interface layer and the upper layer, tensile strain will develop at the crack tip causing a faster propagation of the crack. However, if semi-bonding (friction) is induced during construction, the interface layer causes compression at the crack tip resulting in closing the crack and retarding its propagation. Therefore, the installation of such a system becomes very important.

ACKNOWLEDGEMENTS

This research, of which I.L. Al-Qadi is the Principal Investigator, has been sponsored by Carpi USA, Virginia Transportation Research Council, Virginia Department of Transportation, and Atlantic Construction Fabrics, Inc. The author would like to acknowledge the continuous help of his advisor, Professor I.L. Al-Qadi. Thanks are also given to R. Andruet and S. Holzer for their help in the finite element formulation. The assistance of the author's colleagues, especially A. Loulizi, W. Nassar, and S. Lahouar, is greatly appreciated.

REFERENCES

Kennepohl, G., et al., (1985). "Geogrid Reinforcement of Flexible Pavements Design Basis and Field Trials", Journal of the Association of Asphalt Paving Technologists, Vol. 54, pp. 45-75

Donna, H. S., (1993) "Crack-Reduction Pavement-Reinforcement Glassgrid", Colorado Department of Transportation, prepared in cooperation with the U.S. Department of Transportation, Federal Highway Administration

Al-Qadi, I. L., et al., (2000) "Flexible Pavement Instrumentation at the Virginia Smart Road", Paper No. 00-1275 presented at the Transportation Research Board 79th Annual Meeting

Zaghloul, S. and T. White, (1993) "Use of a Three-Dimensional, Dynamic Finite Element Program for Analysis of Flexible Pavement", Transportation Research Record 1388, pp. 60-69

Uddin, W., et al., (1994) "Finite Element Simulation of Pavement Discontinuities and Dynamic Load Response", Transportation Research Record 1448, pp. 100-106

Cho, Y-H., et al., (1996) "Considerations on Finite-Element Method Application in Pavement Structural Analysis", Transportation Research Record 1539, pp. 96-101

Vanelstraete, A., D., et al., (2000) "Structural Design of Roads with Steel Reinforcing Nettings", Proceedings of the 4th International RILEM Conference – Reflective Cracking in Pavements, Research in Practice, pp. 56-67

"ABAQUS, Finite Element Computer Program," (1993) "Theory Manual", Version 5.8, Hibbit, Karlsson and Sorensen, Inc, Pawtucket, USA

Harichandran, R. S., et al., (1994) "MICHBACK User's Manual", Michigan Department of Transportation, Lansing, MI.

Bathe, K. J., (1982) "Finite Element Procedures in Engineering Analysis", Prentice-Hall

Bonaquist, R., (1992) "An Assessment of the Increased Damage Potential of Wide Based Single Tires", Proceedings of 7th International Conference on Asphalt Pavements, pp. 1-16

Cebon, D., (1986) "Road Damaging Effects of Dynamic Axle Loads", Proceedings of the International Symposium on Heavy Vehicle Weights and Dimensions, pp. 37-53

Lytton, R. L., (1989) "Use of geotextiles for reinforcement and strain relief in asphalt concrete", Geotextiles and Geomembranes, Vol. 8, pp. 217-237

WASTE & LIQUID CONTAINMENT III—LININGS

FREEZE/THAW PROTECTION FOR A LINER SYSTEM UTILIZING GEOINSULATION BLANKETS

TIMOTHY J. SCHUMM, P.E.
MIDWEST ENVIRONMENTAL CONSULTANTS, INC.
UNITED STATES OF AMERICA
JAMES K. ADAMS, P.E.
MIDWEST ENVIRONMENTAL CONSULTANTS, INC.
UNITED STATES OF AMERICA
DONALD D. CASSEL, P.E.
ENVIROSOURCE
UNITED STATES OF AMERICA

ABSTRACT

To protect the underlying recompacted soil liner from potential freeze/thaw damage and to minimize the expansion and contraction of the geosynthetics, the side slopes of a landfill in northwest Ohio were covered with a geoinsulation blanket. The blankets were installed in December 1998 and are still in position at this time. The temperature of the recompacted soil liner and the atmospheric temperature were monitored through April 1999. Four thermocouples were placed near the surface of the recompacted soil liner to measure the temperature of the soil. The data for the first winter indicates that even though the air temperature fell to -22°C (-7°F), the temperature of the soil remained above 8°C (47°F). The results indicate that the blankets are an effective means to protect the liner system.

This paper details the use of the geoinsulation blanket and its benefits over other materials used to protect recompacted soil liners from potential freeze/thaw damage.

INTRODUCTION

There are times during the life of a landfill in certain areas of the country/world that the recompacted soil liner requires protection from potential freeze/thaw damage. For most scenarios, waste is utilized. However, there may be situations when waste is not an option. For such situations, materials such as soil, sand, shredded tires or other materials are utilized. While all of these materials meet the regulatory requirements for freeze/thaw protection, they each have their own disadvantages. This paper will describe the utilization of a geoinsulation blanket to protect a recompacted soil liner from potential freeze/thaw damage and the benefits of using a geoinsulation blanket as compared to other materials

Benson, et al (1995) conducted field tests to determine the effects of freezing and thawing on the hydraulic conductivity of compacted clay. In the study, a test pad was constructed and instrumented with thermocouples. A portion of the test pad was protected with a geoinsulation consisting of expanded polystyrene beads encased in a 0.8 mm PVC membrane. In the insulated portion of the test pad, no freezing occurred. The un-insulated portion of the test pad had temperature fluctuations throughout the winter and up to 10 freeze-thaw cycles. Comparing pre-winter hydraulic conductivity tests to post-winter hydraulic conductivity tests, the post-winter results indicated an increase in hydraulic conductivity of 50 to 300 percent in the un-insulated area within the zone of frost penetration. No increase in hydraulic conductivity was seen in the insulated area. The increase in hydraulic conductivity was also found by studies conducted by Zimmie and La Plante (1990).

Benson, et al (1996) analyzed five different methods for insulating the side slopes of landfills. Included in the study was sand, sand and tire chips, polyurea foam, polystyrene boards, and encapsulated fiberglass geoinsulation panels. The tests indicated that the encapsulated fiberglass geoinsulation was an effective insulator. Fluctuations in the geomembrane temperature were minimal. No below freezing measurements were experienced by the geomembrane beneath the black geoinsulation despite having air temperatures below 0°C for a majority of the test period. The tire chips and extruded polystyrene were also determined to be effective. However, the tire chips can be costly and the extruded polystyrene is difficult to place. The rigidity of the polystyrene prevented it from conforming to irregularities in the surface. Also, the seams between the panels separated and allowed air below the panels. This decreased the effectiveness of the polystyrene boards.

FREEZE/THAW PROTECTION ALTERNATIVES

To protect the recompacted soil liner from potential freeze/thaw damage, different materials can be used. When the landfill area is approved for waste placement prior to the on set of cold weather, waste can be used. This is usually the preferred method by operators. However, if the is not time to cover the area, then other materials are used. Depending on the site and the availability of the material, sand, soil or shredded tires are used. While these materials will protect the recompacted soil liner from potential freeze/thaw damage, there are some disadvantages.

The disadvantages of sand are the cost of installation and removal and the instability of placing a thin layer of material on a steep slope. The cost to purchase, install and eventually remove the sand could be approximately $20/cu m ($15/cu yd) or more. This would result in a cost of over $163,000 (based on an area of 9,100 sq m (98,000 sq ft)). The removal of the sand could also cause additional costs if damage was done to the liner system. This price could be lowered and the damage potential minimized if it was decided to not remove the sand. However, the sand would then take up valuable airspace and result in lost revenue.

The effectiveness of sand as an insulator was evaluated at a northwest Ohio landfill in 2000. The landfill completed construction in the fall of 1999 but was not able to begin filling waste in the cell until February 2000, due to required regulatory approval. Prior to waste placement, the facility installed four thermocouples below the leachate collection system and above the geomembrane liner to monitor temperature. Two thermocouples were installed on the north slope, one at the top and one at the toe, and two thermocouples were installed on the south slope, one at the top and one at the toe. The leachate collection system consisted of 30 cm (12 in) of sand. Temperatures were monitored from mid-January to mid-February. Figure 1 shows the recorded air temperature and readings from the four thermocouples. The data shows that there were two occasions when the temperature below the leachate collection system fell below 0°C (32°F).

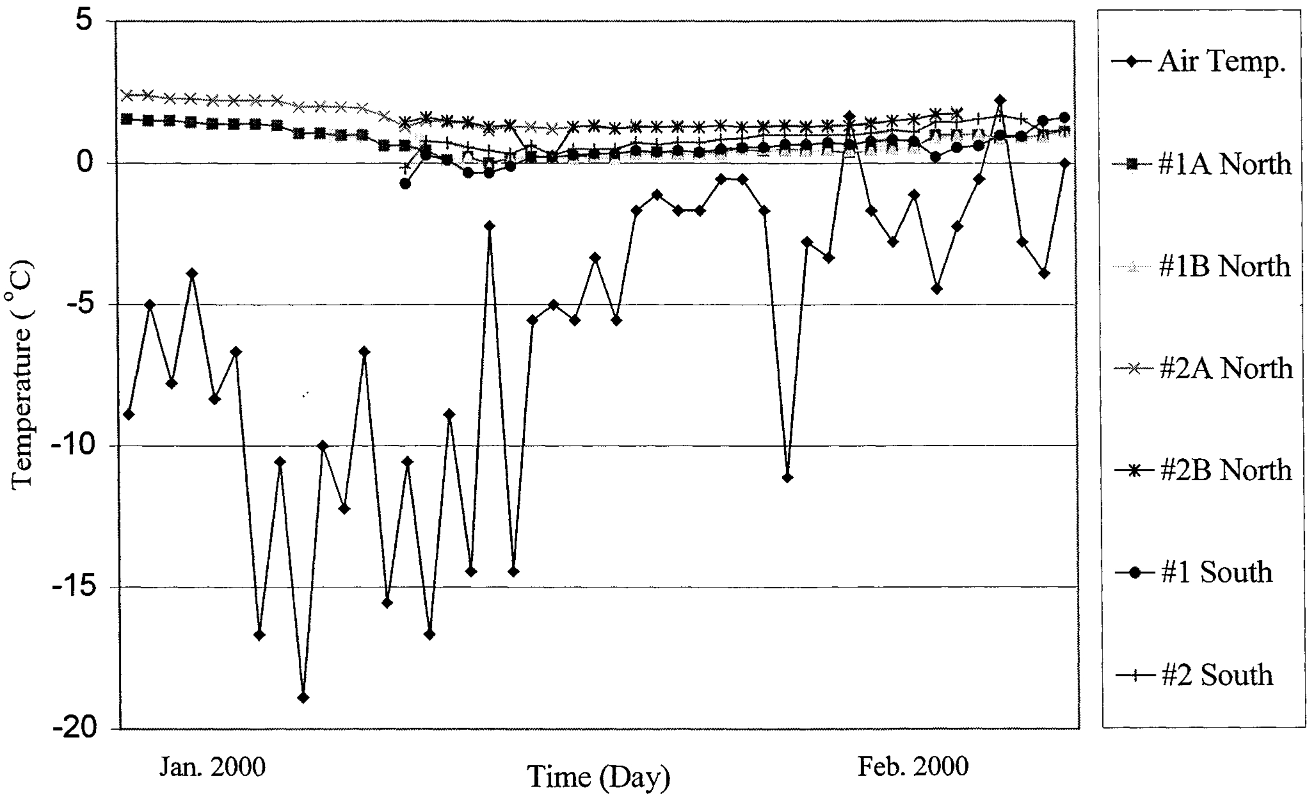

Figure 1. Liner and Air Temperature Measurements

The disadvantages of soil are similar to that of sand with the exception of the cost to purchase the material. Soil is available on-site and would not require purchasing. However the cost to install and remove would be approximately $11/cu m ($8.50/cu yd). The resulting cost would still be over $91,000 (based on an area of 9,100 sq m (98,000 sq ft)). As with sand, the removal of the soil could also damage the liner system and result in higher costs.

Similar to sand and soil, the use of shredded tires as a protective layer has its disadvantages. Depending on the availability and proximity of a shredded tire source, the cost to purchase install and remove shredded tires can vary. In Ohio, shredded tires can not be accepted for disposal and as such, disposal fees can not be charged. Another disadvantage of shredded tires is its workability. Shredded tires can not be placed or removed as easily as sand or soil. This results in additional costs. The cost to use shredded tires could be greater than or equal to that of soil.

The above mentioned costs are approximate. Actual costs will vary depending on the availability and proximity of the material source.

BENEFITS OF GEOINSULATION BLANKETS

One advantage of geoinsulation blankets is the ease of installation. The blankets arrive in rolls that can be easily handled by two people. The blanket is compressed in a roll to reduce the shipping size. Upon deployment of the roll, an air valve in the blanket is opened to allow the blankets to decompress to regain its original thickness. Air can be pumped into the vent to speed up the process. Each roll has a strip of hook and loop fasteners around the perimeter of the blanket to allow the blankets to be attached together (Abeltech). These blankets than can be easily removed prior to waste placement. In this case, the cost to install was $10.23 per square meter ($0.95 per square foot) for a total of approximately $93,000 (based on an area of 9,100 sq m (98,000 sq ft)).

Another advantage of geoinsulation blankets is the reuse potential. Depending on the stresses and UV damage encountered during the initial use, the blankets could be rolled up and stored for future use.

PROJECT DETAILS

The subject phase of the landfill was completed in June 1998. Due to the time needed for waste placement sequencing and regulatory review, the 3:1 (horizontal:vertical) sideslopes of the phase required protection from potential freeze/thaw damage. The floor of the phase has protective aggregate and clay layers that will protect the recompacted soil liner from potential freeze/thaw damage.

After discussions with the regulators, it was decided to utilize insulation blankets to protect the sideslopes. To monitor the effectiveness of the blankets, thermocouples were installed near the surface of the recompacted soil liner.

The geoinsulation blankets consisted of a 5 cm (2 in) thick fiberglass batting encapsulated within 0.2 mm (10 mil) thick black polyethylene film. Each blanket was equipped with strips of hook and loop fasteners around the perimeter and an air vent in one corner. The blankets were

2.4 m (8 ft) wide by lengths of 7.6 m (25 ft), 10.7 m (35 ft), 13.7 m (45 ft) and 15.2 m (50 ft) and 5 cm (2 in) thick.

Prior to installation of the secondary geomembrane liner (1998-1999 winter), four thermocouples were installed near the surface of the recompacted soil liner. The east sideslope had one thermocouple installed 2.5 cm (1 in) below the surface of the recompacted soil liner. On the west sideslope, three thermocouples were installed. Two thermocouples were installed 2.5 cm (1 in) below the surface of the recompacted soil liner and one thermocouple was installed 15 cm (6 in) below the surface of the recompacted soil liner. The thermocouples were installed about mid-slope on both the east and west sides. The thermocouple leads run to the top of each sideslope and have a jack attached to each end. These jacks are plugged into a handheld digital thermometer for temperature measurements.

GEOINSULATION BLANKET DEPLOYMENT

Prior to deployment of the geoinsulation blankets, anchor posts are installed at the top of the slope beyond the anchor trench. The geoinsulation blankets are then secured to these posts with polypropylene rope after they are deployed. As subsequent rolls are deployed, they are attached together using the hook and loop fasteners. The blankets are overlapped such that upper blanket shingles over the lower blanket. This allows water to freely flow down-slope without flowing directly into the seams. To minimize the potential for wind uplift, sandbags filled with gavel were placed approximately every 2.4 m (8 ft) along the perimeter of each blanket. These bags were tied together with polypropylene rope to form baglines and the baglines were tied to the anchor posts. Figure 2 shows the deployment of the blankets. Figure 3 shows the baglines and blankets tied to the anchor posts. Figure 4 shows the completed slope.

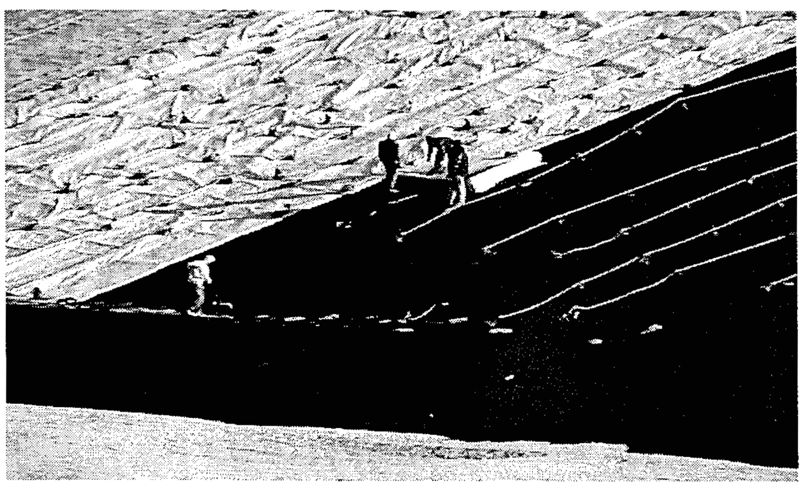

Figure 2. Deployment of Geoinsulation Blankets

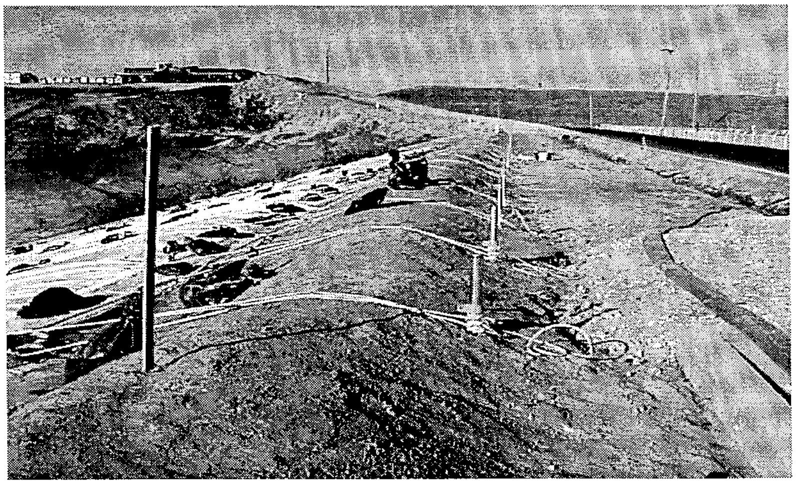

Figure 3. Anchoring of Blankets and Sandbags

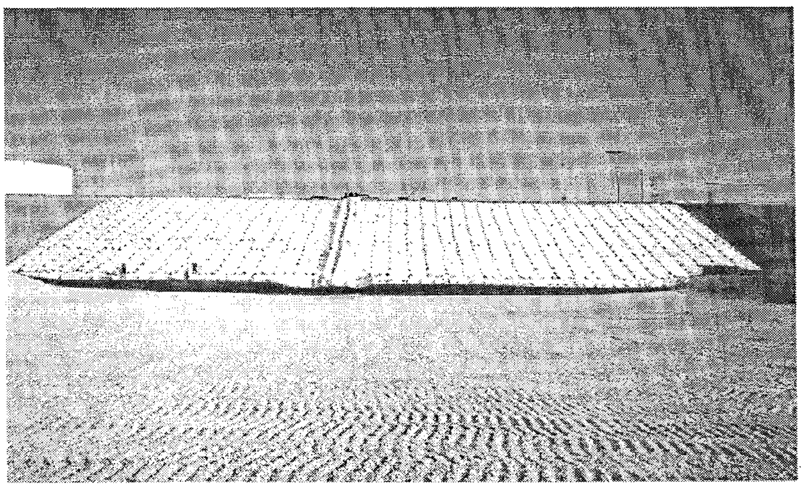

Figure 4. Completed Deployment on Slope

TEMPERATURE MEASUREMENTS

After the geoinsulation blankets were installed, the temperature of the monitoring probes was measured once per day from December 1998 through April 1999. The air temperature was also measured throughout the day and the minimum and maximum daily temperatures were logged. The measurements indicated that even though the air temperatures fell to -22°C (-7°F) the temperature of the recompacted clay remained above 8°C (47°F). Figure 5 shows the temperature measured by the four thermocouples and the associated minimum and maximum daily temperatures throughout the testing period.

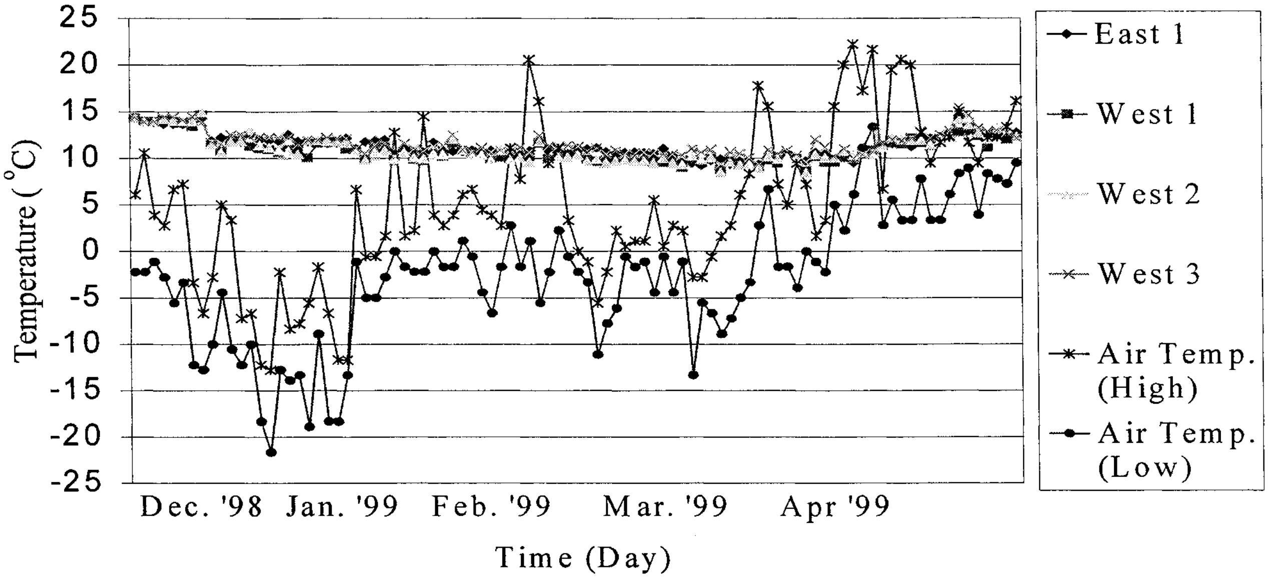

Figure 5. Clay Liner and Air Temperature Measurements

CONCLUSION

Based on the above information, the use of geoinsulation blankets were effective in preventing potential freeze/thaw damage in the recompacted soil liner. At no time during the monitoring period did the temperature of the liner go below 0°C (32°F). The geoinsulation blankets were more effective than sand since there were two occasions, in the cited example, in which the liner dropped below 0°C (32°F).

Not only were the blankets thermally effective, but they were also cost competitive. The cost to purchase and install the blankets was less than the cost to install and remove sand, soil or shredded tires. The ability to deploy the blankets by hand reduced the potential for damage to the liner system from equipment that would be needed when applying and removing material. The reuse potential is also a plus.

ACKNOWLEDGEMENTS

Michael A. Olson, P.E. of Abletech, Inc. was the supplier and project engineer for the installation of the blankets.

REFERENCES

Abletech, Inc., "Thermasure™ Insulating Blankets" brochure.

Benson, C.H., Abichou, T.H., Olson, M.A., and Bosscher, P.J., 1995, "Winter Effects on the Hydraulic Conductivity of a Compacted Clay", *Journal of Geotechnical Engineering"*, ASCE, Vol. 121, No.2, pp. 69-79.

Benson, C.H., Olson, M.A. and Bergstrom, W.R., 1996, "Temperatures of an Insulated Landfill Liner", *Transportation Research Record No. 1534*, Transportation Research Board, National Research Council, pp. 24-31.

Zimmie, T.F., and La Plante, C., 1990, "The Effect of Freeze/Thaw Cycles on the Permeability of a Fine-Grained Soil", *Proc. 22nd Mid-Atlantic Industrial Waste Conference*, Philadelphia, Pennsylvania, USA, July 1990, pp. 580-593.

COST-BENEFIT ANALYSIS OF ALTERNATIVE CANAL LININGS

Jay Swihart, P.E., US Bureau of Reclamation, USA
Jack Haynes, US Bureau of Reclamation, USA

ABSTRACT

Over the past 8 years, the US Bureau of Reclamation (Reclamation) has constructed 28 canal-lining test sections to assess durability and effectiveness (seepage reduction) over severe rocky subgrades. The lining materials include combinations of geosynthetics, shotcrete, roller compacted concrete, grout mattresses, soil cushions and covers, elastomeric coatings, and sprayed-in-place foam. Five of the 28 test sections have failed, while the remaining 23 test sections are in very good to excellent condition. Unit construction costs range from \$10 to \$40 per square meter. Full-scale pre- and post-construction ponding tests have shown effectiveness at reducing seepage between 70 and 95 percent, with the geomembrane alternatives having the highest effectiveness. Preliminary benefit/cost ratios have been calculated based on initial construction costs, maintenance costs, durability (service life) predictions, and seepage reduction. Alternatives utilizing a geomembrane with a concrete cover seem to offer the best long-term performance, as the geomembrane liner provides the water barrier, while the concrete cover provides protection from mechanical and environmental damage.

INTRODUCTION

Unlined canals typically lose 35 to 50 percent of their water to seepage. Canals in the Pacific Northwest have the highest losses as they are constructed through fractured volcanic basalt (Figure 1). Traditional canal-lining materials include compacted clay, reinforced or unreinforced concrete, and more recently buried geomembranes. However, these materials are not always viable because either 1) they are not locally available (such as compacted clay), 2) they are too expensive (such as reinforced concrete), 3) they require large right-of-way for heavy construction equipment, or 4) they require extensive over-excavation and subgrade preparation (such as buried geomembranes). In areas with rock subgrades, over-excavation requires blasting which is cost prohibitive. This study looks at alternative canal-lining materials and techniques that are less expensive, easier to construct with limited access, do not require over-excavation, and are compatible with severe rocky subgrades.

CONSTRUCTION

Over the past 8 years, Reclamation has constructed 28 canal-lining test sections to assess durability and effectiveness (seepage reduction) over severe rocky subgrades (Swihart, Haynes, and Comer, 1994) (Swihart, 1994). The lining materials include combinations of geosynthetics (geomembranes and geotextiles), shotcrete, roller compacted concrete, grout-filled mattresses, soil cushions and covers, elastomeric coatings, and sprayed-in-place foam. Typical construction is shown in Figures 2 through 5. The test sections are predominantly located in central Oregon, and each test section covers 1,500 to 3,000 square meters. The test sections now range in age from 1 to 8 years. Of the 28 test sections, five failed during their first year of service, and another five are not evaluated because they have been in service for less than 2 years. The remaining 18 test sections are all performing well and are in very-good to excellent condition. This paper presents preliminary Benefit-Cost analysis on those 18 test sections.

Figure 1 - Canals in the Pacific Northwest
are constructed through fractured volcanic basalt.

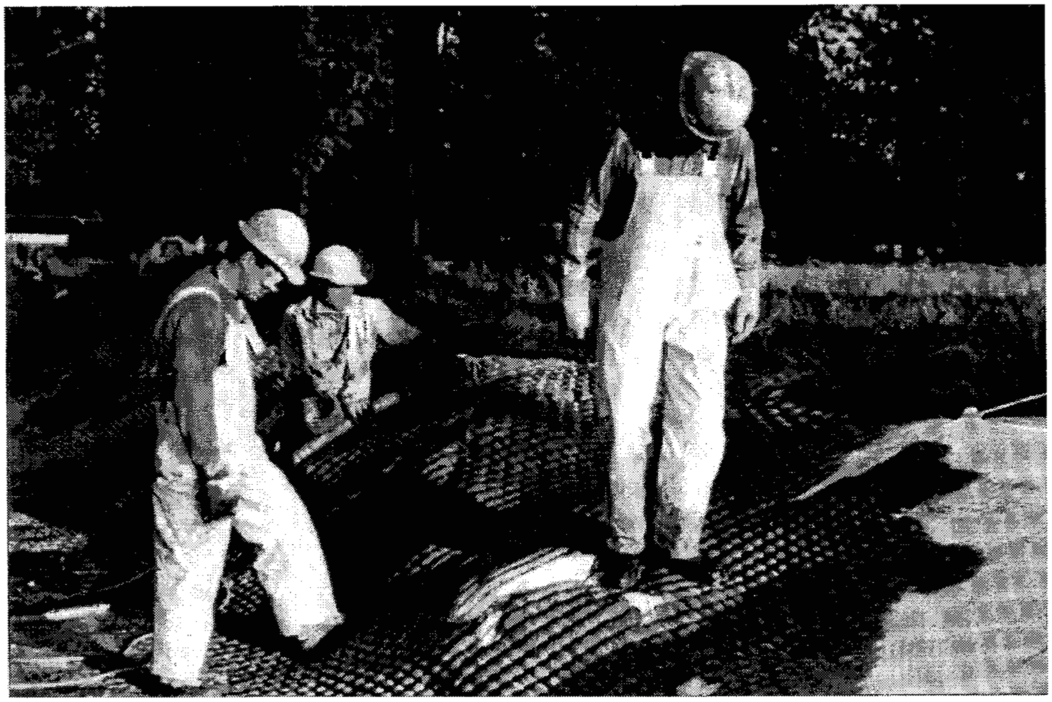

Figure 2 - Grout mattress is placed over PVC (polyvinyl chloride) geomembrane. Mattress consists of cement grout pumped into place between two layers of geotextile.

Figure 3 - Shotcrete is applied over geomembrane for mechanical protection. Geomembrane underliners include VLDPE (very low density polyethylene) and a thin PE (polyethylene) geotextile composite.

Figure 4 - Exposed geomembrane is pulled into place over geotextile cushion.
Exposed geomembranes included HDPE (high density polyethylene)
and CSPE-R (reinforced chlorosulfonated polyethylene).

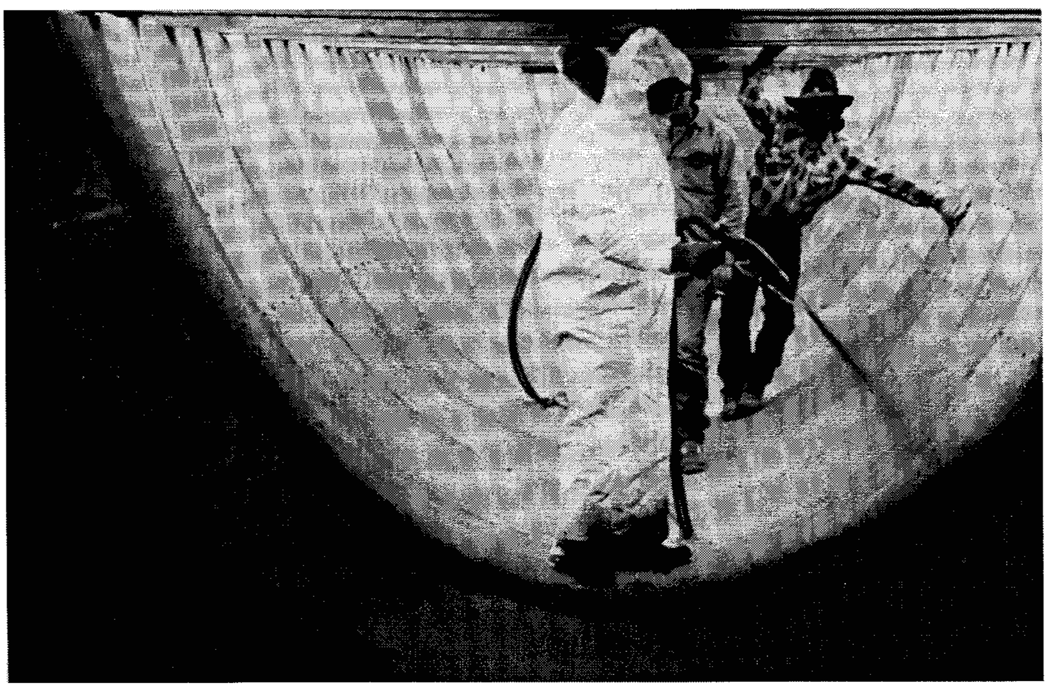

Figure 5 - Asphalt emulsion is spray-applied to steel flume.

BENEFIT-COST ANALYSIS

Preliminary benefit/cost ratios have been calculated for the canal-lining test sections (equation 1). Benefits are based on the market value of the conserved water. Costs are life-cycle costs, calculated from initial construction costs, maintenance costs, and service life predictions (equation 2). Based on the type of materials, the test sections are divided into 4 categories as shown in Table 1.

$$\text{Benefit-Cost Ratio} = \frac{\text{Benefit}}{\text{Cost}} = \frac{\text{Value of Conserved Water}}{\text{Life-Cycle Cost}} \qquad (1)$$

$$\text{Life-Cycle Cost} = \frac{\text{Construction Cost}}{\text{Service Life}} + \text{Annual Maintenance Cost} \qquad (2)$$

Seepage Studies - Full-scale ponding tests (Figure 6) were used to measure the amount of water conserved. Test sections were ponded both before and after lining of the canal. In addition, inflow-outflow measurements were taken over a 3-year period on a 40-km reach of canal. These seepage studies show that pre-construction seepage rates were highly site specific, and ranged from 0.2 up to 6.0 m/day depending on soil type, geology, and topography. Seepage was reduced by 70 to 95 percent, depending on the type of lining (Haynes and Swihart, 1999). The seepage studies are summarized in Table 2 including the value (Benefit) of the conserved water based on a market value of $0.04/m^3 ($50/acre-ft), a 180-day irrigation season, and an average pre-construction seepage rate of 0.3 m/day.

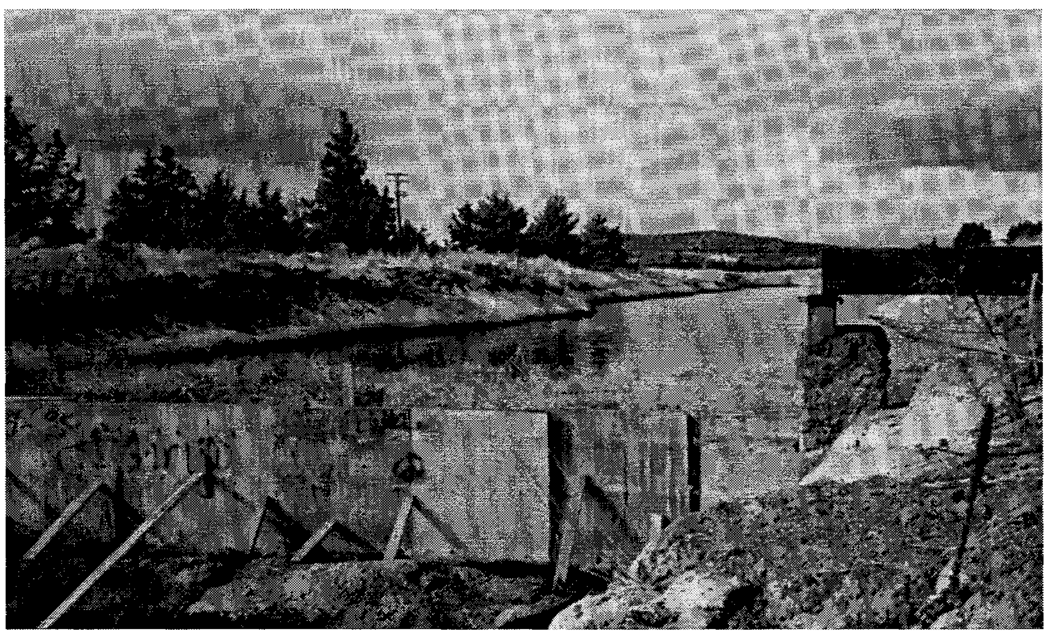

Figure 6 - Full-scale ponding test.
Water is ponded 1-m deep behind 100-mm-thick concrete dike.

Table 1 - Life-cycle Costs

Type of Lining	Construction Cost ($/m^2)	Maintenance Cost ($/m^2-yr)	Durability (years)	Life-Cycle Cost ($/m^2-yr)
Concrete				
RCC with Shotcrete Sideslope	$20.00	$0.05	40 - 60 yrs	0.45
75-mm Shotcrete with Steel Fibers	$22.00			0.49
75-mm Shotcrete with PolyFibers A	$21.40			0.48
75-mm Shotcrete with PolyFibers B	$21.40			0.48
75-mm Shotcrete - no fibers	$20.70			0.46
75-mm Grout-filled Mattress	$19.20			0.43
RCC - invert only	$17.40	$0.05	40 - 60 yrs	0.39
Exposed Geomembrane				
2-mm HDPE	$13.80	$0.10	20 - 40 yrs	0.56
0.75-mm PVC with Geotextile Cover	$10.50		10 - 20 yrs	0.80
1.1-mm CSPE-R	$11.10		20 - 40 yrs	0.47
0.9-mm CSPE-R	$10.30		15 - 35 yrs	0.51
4-mm Asphaltic Geomembrane A	$15.30		20 - 40 yrs	0.61
4-mm Asphaltic Geomembrane B	$15.30		20 - 40 yrs	
Geomembrane with Concrete Cover				
0.1-mm PE geocomposite with Shotcrete	$24.30	$0.05	40 - 60 yrs	0.54
0.75-mm VLDPE with Shotcrete	$25.20			0.55
1-mm PVC with 75-mm Grout Mattress	$25.40			0.56
Fluid-applied Membrane				
Spray Foam with Urethane Coating A	$43.30	$0.10	5 - 15 yrs	4.43
Spray Foam with Urethane Coating B	$39.20		5 - 15 yrs	4.02
Geotextile A with Urethane Coating	$26.40		1 - 5 yrs	8.90
Geotextile B with Urethane Coating	$26.40		1 - 5 yrs	8.90
Asphalt Emulsion over Existing Concrete	$17.00		5 - 15 yrs	1.55
Asphalt Emulsion over Sandblasted Steel	$21.60		10 - 20 yrs	1.54
Asphalt Emulsion over Broomed Steel	$14.00		10 - 20 yrs	1.03

Table 2 - Benefit-Cost Analysis

Type of Lining	Effectiveness (percent)	Value of Conserved Water ($\$/m^2$-yr)	Benefit-Cost
Concrete	70 %	$1.45	
RCC with Shotcrete Sideslope			3.2
75-mm Shotcrete with Steel Fibers			3.0
75-mm Shotcrete with Poly Fibers A			3.0
75-mm Shotcrete with Poly Fibers B			3.0
75-mm Shotcrete - no fibers			3.2
75-mm Grout-filled Mattress			3.4
RCC - invert only	40 %	$0.83	2.1
Exposed Geomembrane	90 %	$1.86	
2-mm HDPE			3.3
0.75-mm PVC with Geotextile Cover			2.3
1.1-mm CSPE-R			4.0
0.9-mm CSPE-R			3.6
4-mm Asphaltic Geomembrane A			3.0
4-mm Asphaltic Geomembrane B			3.0
Geomembrane with Concrete Cover	95 %	$1.96	
0.1-mm PE Geocomposite with Shotcrete			3.6
0.75-mm VLDPE with 75-mm Shotcrete			3.6
1-mm PVC with 75-mm Grout Mattress			3.5
Fluid-applied Membrane	90 %	$1.86	
Spray Foam with Urethane Coating A			0.4
Spray Foam with Urethane Coating B			0.5
Geotextile A with Urethane Coating			0.2
Geotextile B with Urethane Coating			0.2
Asphalt Emulsion over Existing Concrete			1.2
Asphalt Emulsion over Sandblasted Steel			1.2
Asphalt Emulsion over Broomed Steel			1.8

Maintenance - Through 8 years, maintenance costs have been relatively low for all the lining alternatives. As shown in Table 1, exposed geomembranes need about twice the maintenance of concrete linings. Maintenance activities include repairing thin spots in the concrete linings, and patching small tears and punctures in the exposed membrane linings (Figures 7 through 9). For all the lining alternatives, benefit/cost analysis shows that every $1 spent on maintenance returns $10 to $20 in conserved water by maintaining water tightness (effectiveness) and extending service life (Swihart and Haynes, 1999). Therefore more emphasis should be placed on maintenance. The irrigation districts are experienced with and quite capable of performing repairs to concrete linings. However for the exposed linings, the irrigation districts need to be supplied with patching materials and equipment, and periodically re-trained on proper repair methods.

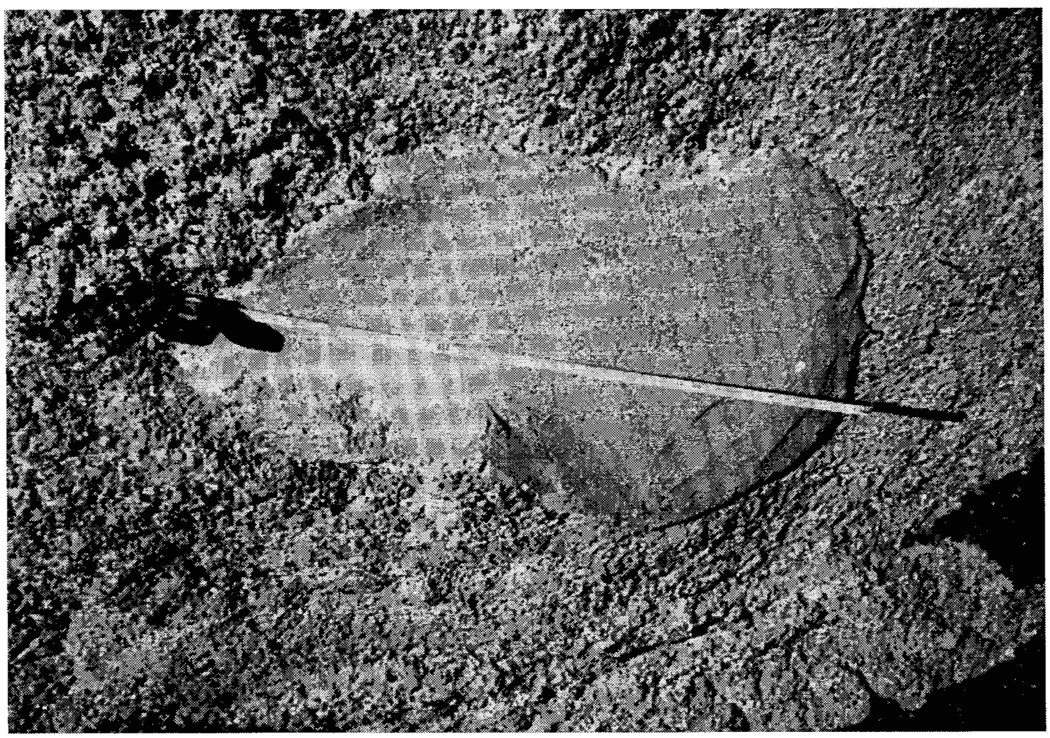

Figure 7 - Concrete patch where shotcrete was less than 25-mm thick and broke loose after 4 to 5 irrigation seasons.

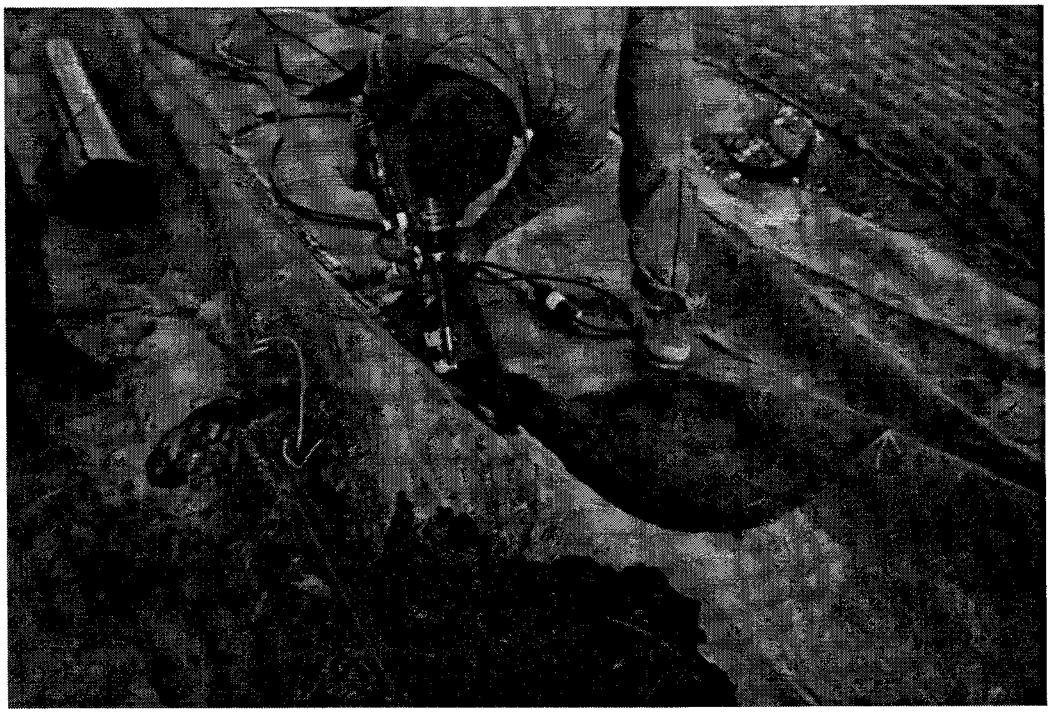

Figure 8 - Contractor uses extrusion welder to patch exposed geomembrane.

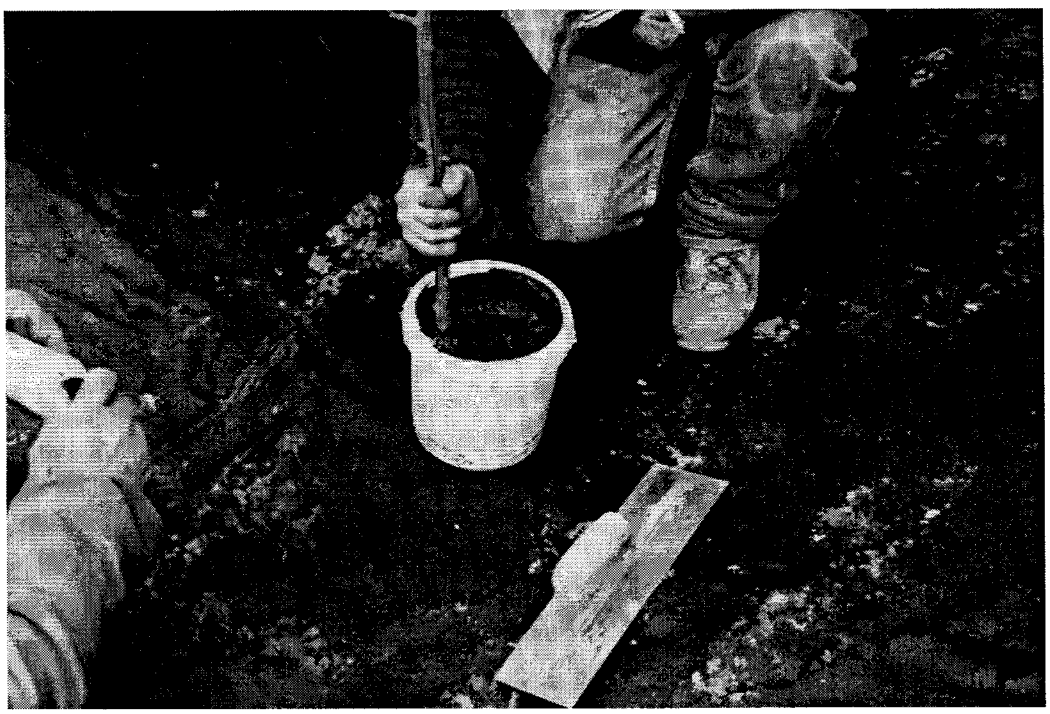

Figure 9 - Blisters in spray-applied asphalt emulsion are patched
with hand-mix repair material.

SUMMARY AND CONCLUSIONS

Preliminary benefit/cost (B/C) ratios have been calculated for the canal-lining test sections based on initial construction costs, maintenance costs, durability (service life), and effectiveness at reducing seepage. Based on the type of material, the lining test sections are divided into 4 categories as shown in Table 3.

Table 3 - Summary of Benefit-Cost Analysis

Type of Lining	Construction Cost ($/m^2)	Durability (years)	Maintenance Cost ($/m^2-yr)	Effectiveness at Seepage Reduction (percent)	B/C Ratio
Concrete alone	$19 - $24	40 - 60 yrs	$0.05	70 %	3.0 - 3.2
Exposed Geomembrane	$10 - $16	20 - 40 yrs	$0.10	90 %	3.0 - 3.9
Geomembrane with Concrete Cover	$24 - $26	40 - 60 yrs	$0.05	95 %	3.5 - 3.7
Fluid-applied Membrane	$14 - $44	1 - 20 yrs	$0.10	90 %	0.2 - 1.8

Each of the lining alternatives offer advantages and disadvantages. The geomembrane with concrete cover seems to offer the best long-term performance.

Concrete - Excellent durability, but only 70 percent long-term effectiveness. Irrigation districts are familiar with concrete and can easily perform required maintenance.

Exposed Geomembrane - Excellent effectiveness (90 percent), but is susceptible to mechanical damage from animal traffic, construction equipment and vandalism. Also often poorly maintained because irrigation districts unfamiliar with geomembrane materials, and need special equipment to perform repairs.

Concrete with Geomembrane Underliner - The geomembrane underliner provides the water barrier while the concrete cover protects the geomembrane from mechanical damage and weathering. System effectiveness estimated at 95 percent. Districts can readily maintain the concrete cover, but do not have to maintain the geomembrane underliner.

Fluid-applied Membrane - Many of these test sections have failed and have been removed from the study. Most of the problems related to poor quality control and poor bond because of adverse weather during construction. Unfortunately inclement weather is quite common as most canal work is in the irrigation off-season (early spring and late fall). These types of linings may have potential for special applications such as lining of existing steel flumes.

Maintenance - For all the lining alternatives, benefit/cost analysis shows that every $1 spent on maintenance returns $10 to $20 in conserved water. Therefore more emphasis should be placed on maintenance. For the exposed linings, the irrigation districts need to be supplied with repair materials and equipment, as well as kept fully trained on proper repair methods.

New Test Sections - The newest test sections have been in service for less than two years. These test sections include Exposed Polypropylene over an existing steel flume, Exposed GCL (geosynthetic clay liner), Buried GCL, Exposed LLDPE (linear low density polyethylene), and Exposed EPDM (ethylene-propylene diene monomer) Rubber. These test sections have some of the lowest construction costs; however, several irrigation seasons will be needed to evaluate.

Future Studies - The benefit-cost analysis presented in this paper is considered preliminary because of the uncertainties in the estimated service lives of the linings. Therefore, Reclamation will continue to monitor the test sections over the next several years to verify durability.

ACKNOWLEDGMENTS

The authors wish to thank the irrigation districts and geosynthetic manufacturers who participated in this study. Without their support and financial contributions, this study would not have been possible. In addition, the manufacturers also assumed risks by placing their products next to their competitors under adverse conditions and often in new applications.

REFERENCES

Haynes J.A., Swihart J.J. (April 1999) "Two Frequently Asked Questions about Canal Linings, "Do They Work?" and "How Much do They Cost?"", *Geosynthetics 99*, Boston MA, Vol. 1, pp137-150

Swihart J.J., Haynes J.A., Comer A.I. (May 1994) "Deschutes Canal-Lining Demonstration Project - Construction Report", Report No. R-94-06, US Bureau of Reclamation, Denver CO

Swihart J.J., (September 1994) "Deschutes Canal-Lining Demonstration - Construction Report", *Fifth International Conference on Geotextiles, Geomembranes and Related Products*, International Geotextile Society (IGS), Singapore, Volume 2, pp 553-556

Swihart J.J., Haynes J.A. (September 1999) "Canal-Lining Demonstration Project - Year 7 Durability Report", Report No. R-99-06, US Bureau of Reclamation, Denver CO

EFFECTS OF INORGANIC LEACHATE ON POLYMER TREATED GLC MATERIAL

DARWISH EL-HAJJI, P.E., D.E.E, CDM INC.
UNITED STATES OF AMERICA
ALAA K. ASHMAWY, P.E., UNIVERSITY OF SOUTH FLORIDA
UNITED STATES OF AMERICA
JERRY DARLINGTON
UNITED STATES OF AMERICA
NESTER SOTELO, UNIVERSITY OF SOUTH FLORIDA
UNITED STATES OF AMERICA

ABSTRACT

In regions where natural clay deposits are not available, the use of Geosynthetic Clay Liners (GCL) in landfill liner and cover systems may provide a cost benefit to landfill owners. The clay component of GCL materials may consist of either untreated or polymer-treated bentonite. Untreated GCL material is typically used in the lining system of municipal solid waste landfills. Polymer-treated GCL material is typically used where a high concentration of calcium is present in the leachate. Calcium is known to increase the permeability of clays by decreasing the double layer thickness and changing the clay structure through sodium-calcium cation exchange. Polymer treatment renders the clay non-reactive to many organic and inorganic chemicals.

This paper presents and discusses data from a laboratory research program on the long-term effect of high inorganic solution (high concentrations of calcium) on the hydraulic properties of untreated and polymer-treated GCLs. In addition, cost benefits to landfill owners and operators will be discussed.

INTRODUCTION

Municipal solid waste (MSW) landfills are required to be designed and constructed with a liner system to minimize the potential for groundwater contamination. The U.S. Environmental Protection Agency (EPA) established minimum design criteria that must be met when designing and constructing landfills. These criteria were established in the Code of Federal Regulations (40 CFR 258) under Subtitle D. The minimum design criteria require, among other things, the incorporation of low permeability soils, typically 1×10^{-7} cm/sec, in the liner design.

MSW and ash landfills are two of the most common landfill types in the United States. MSW landfills are used to dispose of unprocessed solid waste. Leachate generated from these landfills tends to have a high concentration of organic compounds. Ash landfills are those used to dispose of ash residue generated from the incineration of municipal solid waste. Leachate generated structureless, and slowly permeable clay barrier into an aggregated, structured, and more permeable barrier" (Anderson and Jones, 1983).

Testing Program

A laboratory-testing program (program) was developed to determine the long-term behavior of polymer treated GCL when exposed to solution containing elevated concentration of inorganic compounds (calcium and magnesium). Untreated GCL material was also tested for permeability with the inorganic solution for comparison purposes. The permeant used for the program consisted of a synthetic seawater solution containing inorganic chemical compounds that are similar to what is commonly found in ash leachate. The ions of concern are calcium and magnesium. These chemical components can negatively impact the permeability of GCL material. The synthetic solution had a calcium and magnesium concentration of 398 and 1,318 ppm, respectively.

Sample Preparation and Testing Method

The program tested multiple GCL samples with time duration varying between 19 and 175 days. The GCL samples used for the program were composed of Na-Bentonite and Ca-Bentonite bound between two layers of geotextile fabrics. Each sample had an approximate thickness of 1 cm and was cut from the parent material in a circular pattern having a 10-cm diameter. To prevent dry bentonite powder from falling out of the edges of the sample, the exposed sample edge was sealed with a bentonite paste made by mixing bentonite granular and tap water.

The testing program was conducted in general accordance with ASTM D5887, "Standard Test Method for Measurement of Index Flux through Saturated Geosynthetic Clay Liner Using a Flexible Wall Permeameter". For this testing program a flexible wall permeameter with a 10-cm diameter was used for the permeability measurement. Each sample was positioned between two porous filter stones and placed in the permeameter. The sample and the stones were encapsulated in a latex membrane and were allowed to hydrate with the synthetic seawater solution for a period of 48 hours using a back pressure of 3 psi prior to the start of the permeability measurements.

Confining Pressure

Generally speaking, when testing fine grained soil material, the higher the confining pressure the lower the hydraulic conductivity. When Daniel et al. (1997) conducted permeability testing on GCL material using a confining pressure between 5and10 kPa, the resulting hydraulic conductivity was 10^{-9} cm/sec. When the hydraulic gradient was increased to 300 kPa, the permeability decreased to 10^{-10} cm/sec.

The ASTM method D5887 specifies a maximum compressive stress value of 35 kPa; however, no minimum value is specified. For this testing program this compressive stress value was used for permeability measurement.

Hydraulic Gradient

Several studies have been conducted to determine the effect of the hydraulic gradient on the permeability of compacted clays, including those by Oakes (1960), Hansbo (1960), and Mitchell and Younger (1967). Due to the low permeability of fine-grained soils, it will take a considerable amount of time for the permeant to fully saturate and penetrate the soil layer under a low hydraulic gradient. Therefore, for laboratory measurement, it has been customary to test using high hydraulic gradients to determine the hydraulic conductivity of fine-grained soils. Zimmie (1981) recommended a hydraulic gradient between 5 and 20. Anderson and Brown (1981) conducted permeability measurements using hydraulic gradients as high as 362, and Lutz and Kemper (1959) used a hydraulic gradient of 900.

The ASTM D5084 standard recommends a maximum hydraulic gradient of 30 when testing low permeability soils. For this testing program a hydraulic gradient of 140 was used in an effort to provide an adequate quantity of flow during the testing period. The use of a high hydraulic gradient can shorten the testing duration and can simulate the exposure of GCL to the permeating liquid for extended duration.

Results

The permeability for each sample was calculated and recorded. Table 1 summarizes the test results for the Na-Bentonite GCL.

Table 1. Permeability of Na-Bentonite GCL
When Permeated with Synthetic Seawater Solution

Sample	GCL Type	Test Duration (days)	Initial Permeability (cm/sec) After 48 Hours of Saturation	Final Permeability (cm/sec)
A	Untreated	75	$1.7\text{x}10^{-9}$	$2.24 \text{ x } 10^{-6}$
B	Untreated	75	$1.50 \text{ x}10^{-9}$	$5.45 \text{ x } 10^{-7}$
C	Treated	75	$1.60 \text{ x } 10^{-9}$	$3.43 \text{ x } 10^{-8}$
D	Treated	75	$1.4 \text{ x } 10^{-9}$	$1.03 \text{ x } 10^{-7}$
E	Treated	175	$3.57\text{x } 10^{-9}$	$7.27 \text{ x}10^{-9}$

The following figures depict the variation of permeability with time for the above samples.

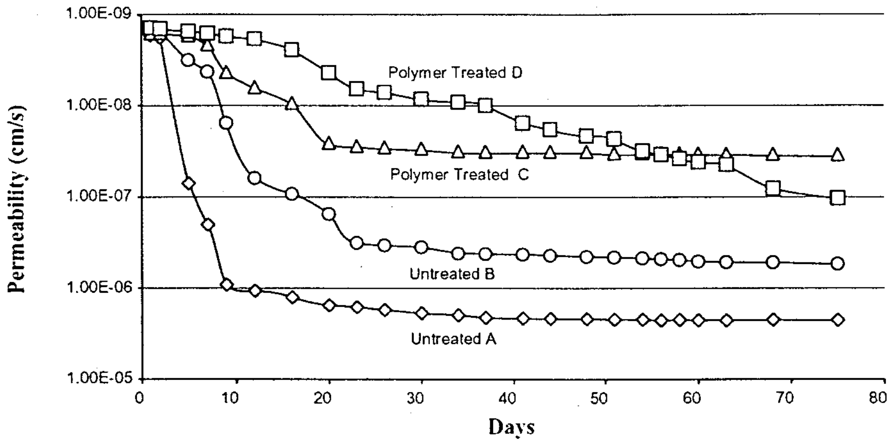

Figure 1
Performance with Time of GCL

The intent of the testing program was to evaluate the long-term performance of the Na-Bentonite GCL, when permeated with an inorganic solution, because it is the most commonly used GCL material in the United States. The Ca-Bentonite GCL is more commonly used in Europe. A short time duration test was conducted on the Ca-Bentonite using the same inorganic solution for informational purposes. Table 2 provides a summary of the test results.

Table 2. Permeability of Ca-Bentonite GCL
When Permeated with Synthetic Seawater Solution

Sample	GCL Type	Test Duration (days)	Initial Permeability (cm/sec) After 48 Hours of Saturation	Final Permeability (cm/sec)
F	Treated	19	5.73×10^{-9}	3.28×10^{-9}
G	Untreated	19	5.47×10^{-6}	2.98×10^{-6}

The results indicate that the permeability of the treated Ca-Bentonite GCL material remains low, at least for the short-time duration, when permeated with an inorganic solution containing a high concentration of electrolytes. However, the permeability of the standard Ca-Bentonite GCL material was three orders of magnitude higher than the treated sample. The following figures depict the permeability variation with time for the polymer treated and untreated Ca-Bentonite GCL material.

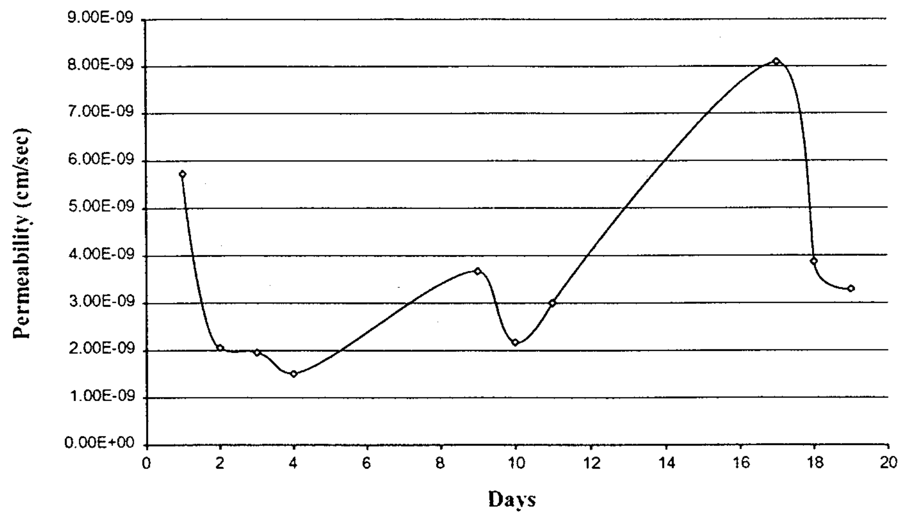

Figure 2
Performance with Time of Sample F

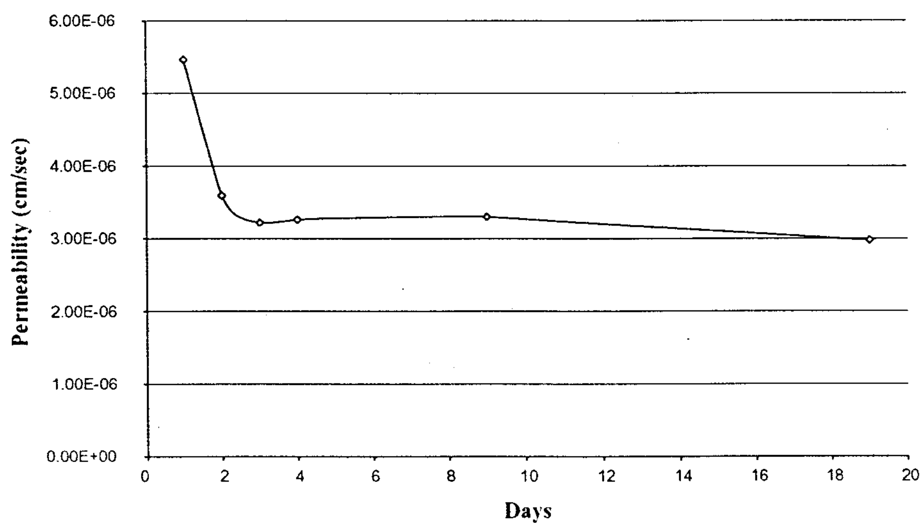

Figure 3
Performance with Time of Sample G

GCL Considerations

The use of polymer treated GCL material should be considered in lining applications when the permeating liquid being contained has elevated concentration of inorganic compounds such as calcium and magnesium. The permeability of the treated GCL remains somewhat unaffected by the inorganic compounds; however, the permeability of the untreated GCL material tends to increase when permeated with the same inorganic liquid. The increased GCL permeability may not provide adequate protection of the groundwater from the liquid being contained.

The use of GCL in liner applications will provide definite practical and economic advantages to design professionals, landfill owners and operators. Based on actual landfill, designed and advertised for bid by the authors, construction costs, the polymer treated GCL installed cost was \$4.50/m^2 versus \$7/m^2 for 60-cm thick compacted natural low permeability clay liner (10^{-7} cm/sec). The cost differential can be even more dramatic when standard GCL material is used in place of natural clay liners. For an actual landfill liner project, designed and advertised for bids by the authors, the material and installation cost for standard GCL was \$2.50/m^2.

The GCL material can be installed within short time duration. Typically one hectare of GCL can be installed on a daily basis. Additionally, the cost of implementing a field quality assurance/quality control program for natural clay installation is substantially higher than that for GCL material. The GCL offers other advantages including: consistent product quality, material manufacturing and shipping is not affected by wet weather periods, and it has less settlement when compared to thick natural clay liners.

CONCLUSION

This experimental testing program demonstrated that the polymer treated GCL using synthetic seawater as a Permeant performs better than untreated GCL. The results obtained under this program are assuring; however, they can not be generalized. When considering the use of GCL in lining applications, it is recommended that permeability compatibility testing be performed using the actual solution as the permeant. Additional studies are still needed to determine the long-term effect of actual inorganic solution on polymer treated GCL.

REFERENCES:

American Society for Testing and Materials (1994) D 5084-90 (1994), "ASTM Standards and Other Specifications and Test Methods on the Quality Assurance of Landfill Liner Systems" Publication Code Number 03-435193-38, Philadelphia

American Society for Testing and Materials (1990) Annual Book of ASTM Standard, "ASTM 5084-90 Standard Test Method for Measurement of Hydraulic Conductivity of Saturated Porous Materials Using a Flexible Wall Permeameter", Philadelphia

American Society for Testing and Materials (1999) D5887-99 Annual Book of ASTM Standard, "ASTM 5887-99 Standard Test Method for Measurement of Index Flux Through Saturated Geosynthetic Clay Liner Specimen Using a Flexible Wall Permeameter", Vol 4.09, West Conshohocken

American Society for Testing and Materials (1999) D4439-99 Annual Book of ASTM Standard, "ASTM D4439-99 Standard Terminology for Geosynthetics", Volume 4.09, West Conshohocken

Anderson and Jones (1983), "Clay Barrier-leachate Interaction", National Conference on Management of Uncontrolled Hazardous Waste Sites, Washington, D.C.

Anderson and Brown (1981), "Organic Leachate Effects on the Permeability of Clay Liners." National Conference on Management of Uncontrolled Hazardous Waste Sites, Washington, D.C.

Daniel et al. (1996) "Report of 1995 Workshop on Geosynthetic Clay Liners," EPA/600/R-96/149.

Daniel et al. (1997), "Laboratory Hydraulic Conductivity Testing on GCLs in Flexible-Wall Permeameters." ASTM STP 1308

Dunn (1983), "Hydraulic Conductivity of Soils in Relation To Subsurface Movement of Hazardous Wastes," Ph.D. Dissertation, Department of Civil Engineering, University of California, Berkley.

Egloffstein (1994), "Properties and Test Methods to Assess Bentonite Used in Geosynthetic Clay Liners," Proceedings of An International Symposium Nurberg/Germany/14-15 April 1994.

Goldman et al. (1990) " Clay Liners for Waste Management Facilities Design, Construction and Evaluation."

Hansbo, S. (1960), "Consolidation of Clay With Special Reference to the Influence of Vertical Sand Drains," Proceedings, 18th Swedish Geotechnical Institute, Stockholm.

Mitchell and Younger (1967), "Abnormalities in Hydraulic Flow Through Fine Grained Soil." ASTM STP 417 Disposal of Solid Wastes, Gerzensee, March 14-17, 1988.

Madsen (1994), "Characteristics and Sealing Effect of Bentonite," Proceedings of An International Symposium Nurberg/Germany/14-15 April 1994.

Lutz and Kemper (1959), "Intrinsic Permeability Of Clays as Affected by Clay-Water Interaction," Soil Science, Volume 88.

Madsen et al. (1988), "Chemical Effects on Clay Fabric and Hydraulic Conductivity," The Landfill Reactor and Final Storage Swiss Workshop on Land Disposal of Solid Wastes, Gerensee, March 14-17, 1988.

Mitchell, J. (Second Edition) 1993, "Fundamentals of Soil Behavior."

Oakes, D. (1960), "Solids Concentration Effects in Bentonite Draining Fluids, Clay and Clay Minerals," Volume 8.

Ruhl (1994), "Effects of Leachate on the Hydraulic Conductivity of Geosynthetic Clay Liners," M.S. Thesis, University of Texas, Austin.

U.S. Environmental Protection Agency (1991) 40 CFR Part 257 and 258 "Solid Waste Disposal Facility Criteria; Final Rule," Washington, D.C.

Zimmie et al. (1981), "Permeability Testing of Soils for Hazardous Waste Disposal Sites," Proceedings of the Tenth International Conference on Soil Mechanics and Foundation Testing, Stockholm, Sweden.

DESIGN AND INSTALLATION OF A GEOMEMBRANE CONTAINMENT SYSTEM TO LINE AN OFF-SHORE WASTE CONTAINMENT BUND

FELON R. WILSON, P.E, SEAMAN CORPORATION
UNITED STATES OF AMERICA

ABSTRACT

This paper details the design and installation of a geomembrane system to line an offshore containment bund for the government of Singapore. The Pulau Semakau project involved the construction of a 7½ Km rock bund and cost $1.6 billion (U.S. dollars). Geomembrane represented the most reliable and easily constructed barrier for the perimeter bund. About one half of the 400,000 square meters of geomembrane were installed under water prior to dewatering of the containment area. The selection of the geomembrane and subsequent packaging, transportation, and installation are detailed within this paper. The unique constructability issues centered around the geomembrane properties including density, flexibility, and pre-fabrication, particularly compared to conventional clay containment systems. Data is also presented from other independent studies comparing the relative containment features of alternative lining systems.

INTRODUCTION

The tiny tropical nation of Singapore covers only 90 hectares (225 square miles) and is located at the southern end of the Malay Peninsula (see Figure 1). This flourishing nation of three million inhabitants is the world's busiest port and a major center of trade, banking, tourism, and communications. All of this prosperity means increasing concerns for waste disposal. In the early 1990's, Singapore began planning for replacement of the long used state owned landfill which was to be at capacity by 1998. The unique solution, proposed by the Ministry of Environment of Singapore, called for an offshore waste disposal facility to contain inert incinerated residue for the next 30 years. Relying on land reclamation techniques long employed in Northern Europe, the facility called for the building of a 7½ km (4.2 mile) earth bund in water depths ranging from 10 m (33') to 20 m (66'), resulting in a 30 ha (75 acre) offshore waste pond. The bund served as a connecting wall between two offshore islands.

Therefore, installation techniques were required for both dry and wet scenarios. In conjunction with various other hydraulic considerations, the seawater was to be displaced as the solid waste filling progressed.

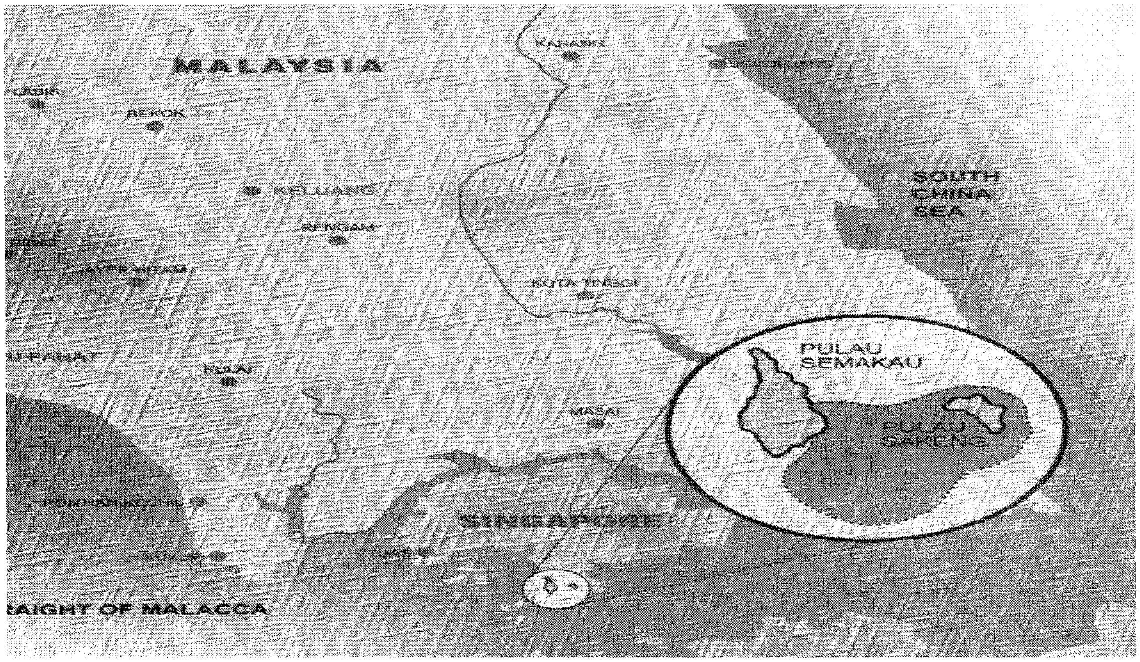

Figure 1. Location of Singapore

CONTAINMENT DESIGN

The offshore bund was constructed by transporting and dumping 4.5 million metric tons (5 million tons) of rock and 36 million metric tons (40 million tons) of sands. The construction materials were transported from Indonesia. Figure 2 is the General Layout Plan for the Bund Project. The earthen wall connected several islands offshore from Singapore. Figure 3 illustrates the typical bund cross section which varied depending on the ocean depth. The offshore bund was created using stone with geofabrics for separation and filtration and sand was hydraulically installed in the body of the bund. A geomembrane was used on the interior surface of the dike, which was keyed into the seabed. Offshore investigations had shown that the seabed soils consisted of silt and clay of depths up to 10m (33')' overlaying rock with permeabilities less than 10^{-8} cm/sec. The project designers considered vertical leachate migration not to be a problem. The facility was designed to be operated with no net head difference from internal to external water levels. Therefore, hydraulic head forces on the containment layer are minimized. Rather, the interior of the bund was lined with a geomembrane which was then covered with a clay layer under the water level and rock at shore level. Outer slopes utilized geofabrics on a 1:3 slope (for shore protection) and inner slopes employed a flatter slope at 1:5. The construction of the bund is shown in Figure 4.

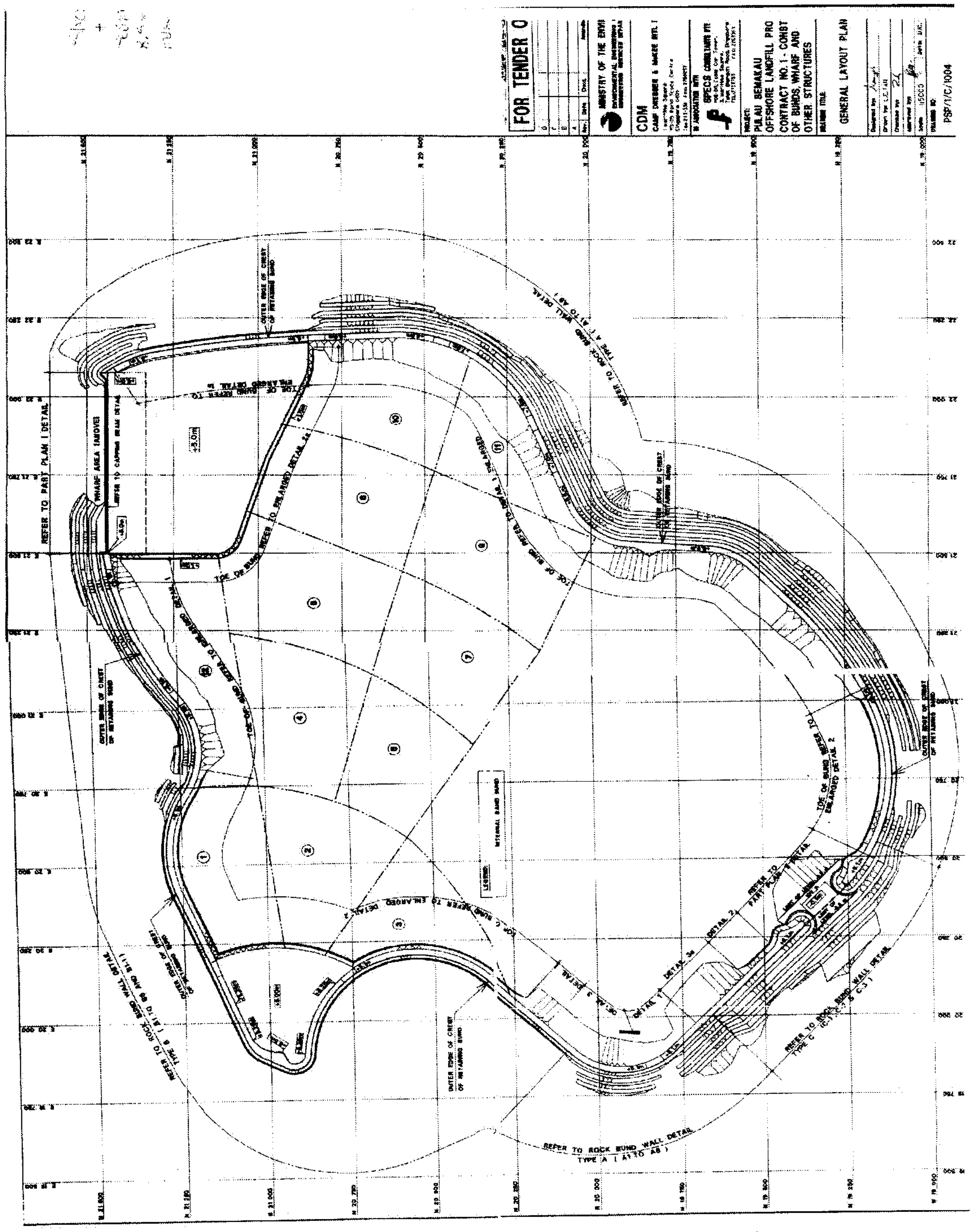

Figure 2. Bund Construction Layout

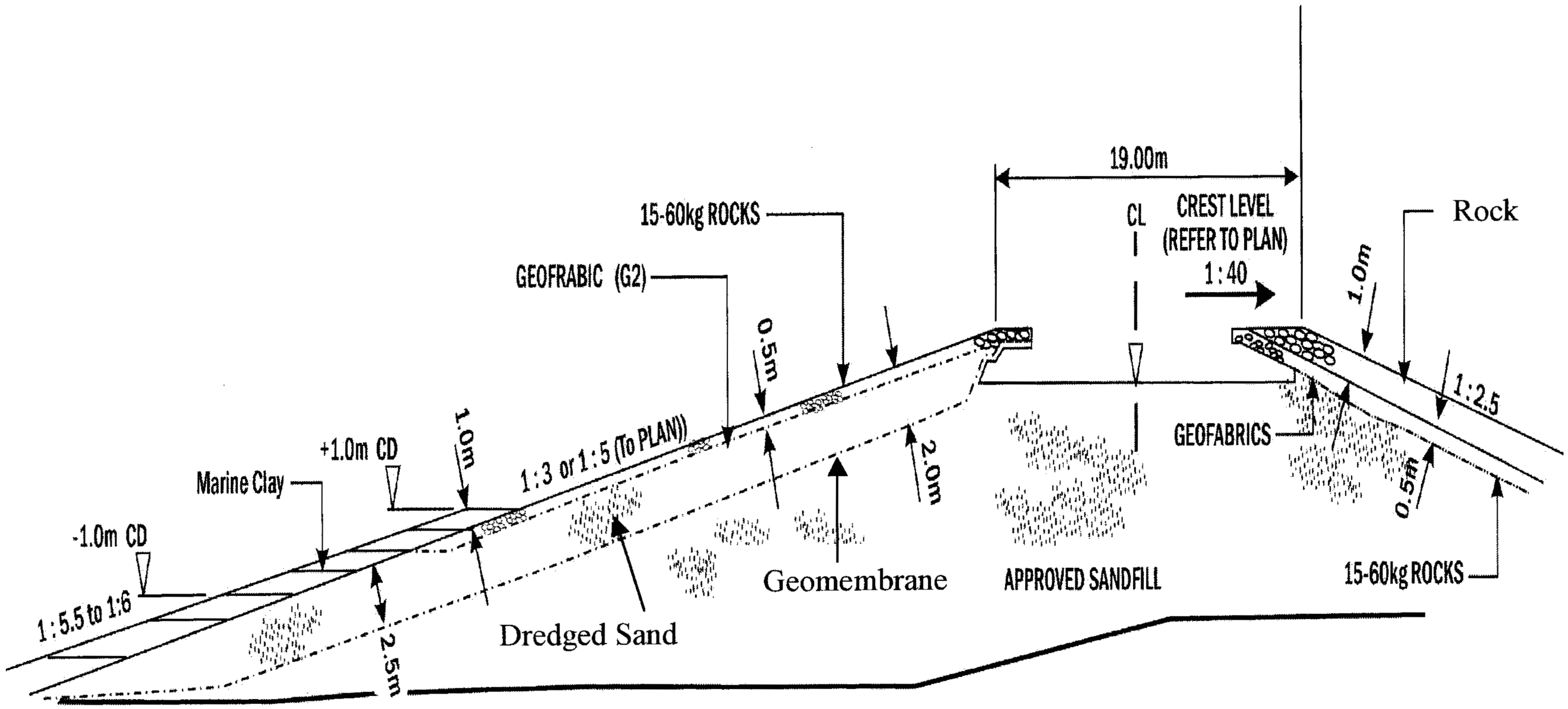

Figure 3. Typical Bund Cross Section

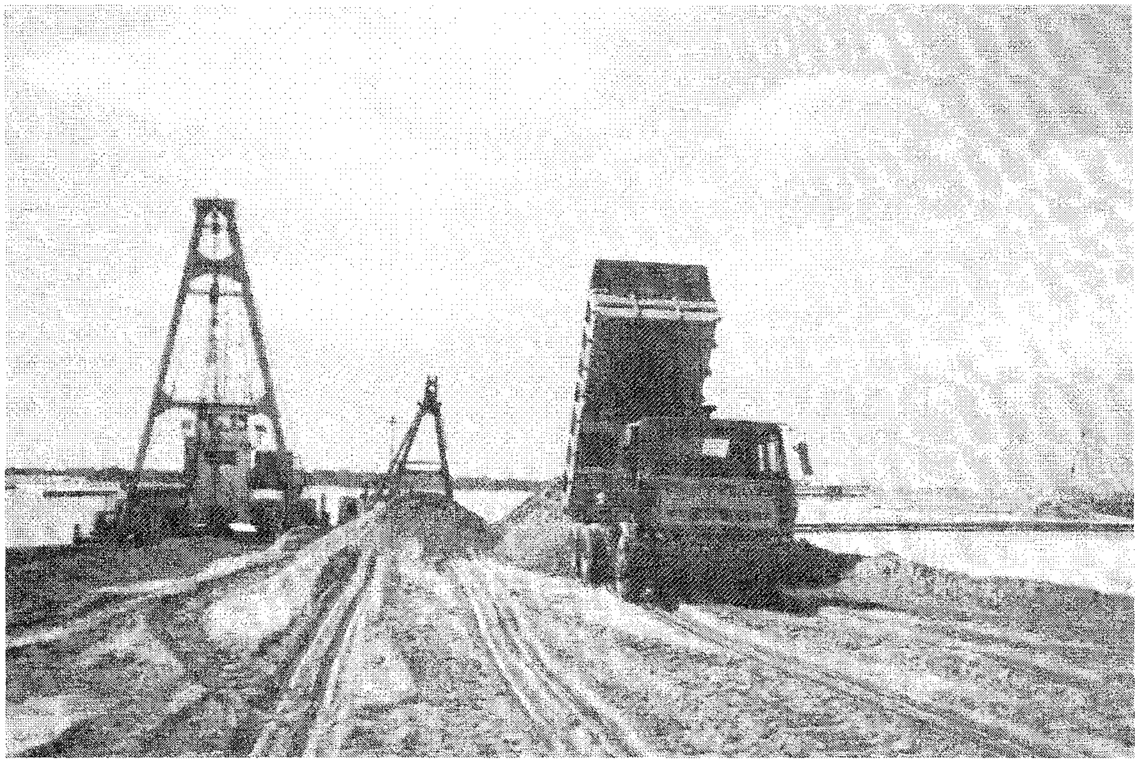

Figure 4. Bund Construction

SELECTION OF GEOSYNTHETICS

Several lining materials were considered for the containment portion of the project including clay layers, Geosynthetic Clay Liners (GCL's), and various geomembranes. Selection criteria included Leakage Rate (theoretical) and constructability. Because of the difficult construction techniques involved, cost considerations were a minor selection criteria.

Leakage Rate (theoretical)

Hydraulic modeling by Tan, et al, showed that significant leakage rate potential reductions could be achieved using a geomembrane as opposed to a single clay layer or a clay layer and a GCL. Figure 5 illustrates the conclusions drawn as a result of this modeling effort.

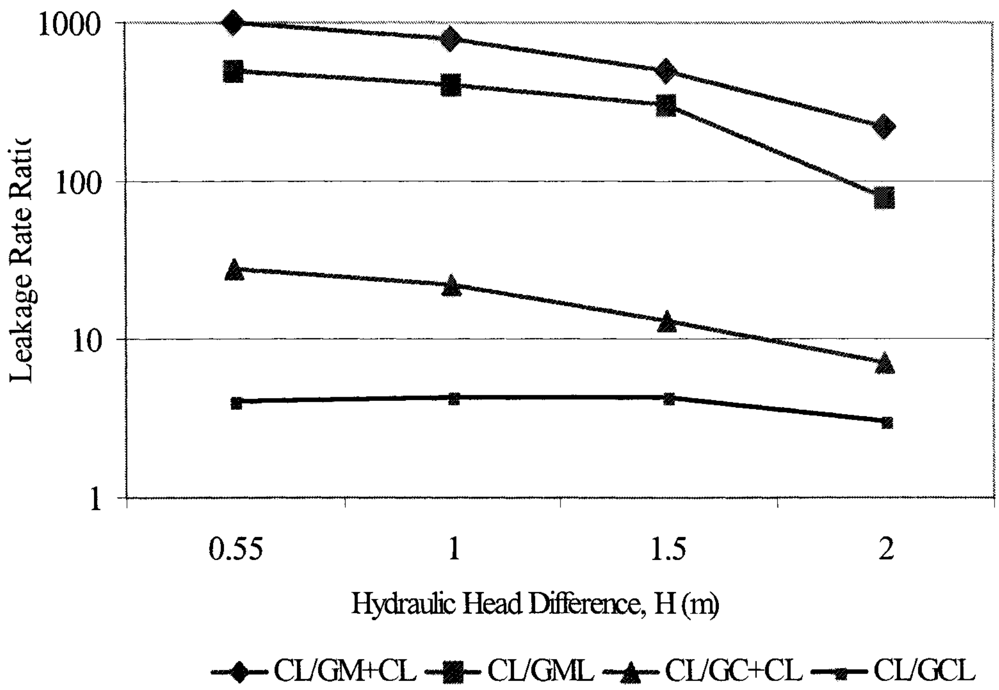

Figure 5. Results of Modeling with various Lining Systems (Tan,

This figure compares the lining alternatives on the basis of Leakage Rate Ratio, which is defined as:

$$\text{Leakage Rate Ratio} = \text{Leakage}_{\text{No Liner}} / \text{Leakage}_{\text{Liner}} \quad (1)$$

Note also the following designations:

CL/GCL – Clay Liner/Geosynthetic Clay Liner
CL/GCL + CL – Clay Liner/Geosynthetic Clay Liner + Clay Liner
CL/GM – Clay Liner/Geomembrane Liner
CL/GM + CL – Clay Liner/Geomembrane Liner + Clay Liner

Leakage for the liner various with the selected liner alternative. A GCL was shown to be 5-30 times better than the clay alone, a geomembrane liner 50-100 times better and a geomembrane with clay was 200-1000 times better. The ranges are dependent on head conditions.

Constructability

With the geomembrane/clay layer as the selected alternative, a material selection then concentrated on constructability. Field seaming the use of large mechanical equipment for panel placement had to be minimized due to site constraints. There were two site installation scenarios, one was a "dry" installation in the areas of existing land, and the other involved a "wet installation", where the geomembrane would be installed from a barge into the ocean leading to the land.

Three types of geomembranes were considered:

- Reinforced Coated Fabric: Ethylene Interpolymer Alloy (EIA-RCF)
- Reinforced Laminates: Polypropylene and Chlorosulfonated Polyethylene (PPE/CSPE)
- Unreinforced Films (HDPE).

In the evaluation of constructability, the weights of the panels, along with associated friction angles for the considered materials are contained in Table 1.

Material Type	Thickness	Panel weight	Friction Angle GM/Asphalt	Friction, Tan S GM/Asphalt
EIA-RCF	1 mm	30.2 KN	22^{0}	0.404
PPE/CSPE	0.9 mm	32.6 KN	25^{0}	0.466
HDPE	2 mm	45.5 KN	18^{0}	0.325

Table 1. Geomembranes Evaluated for Constructability Issues

CASE 1: DRY DEPLOYMENT

In the first (dry) construction scenario, published friction angles were used to determine a theoretical safety factor when dragging the geomembrane into place:

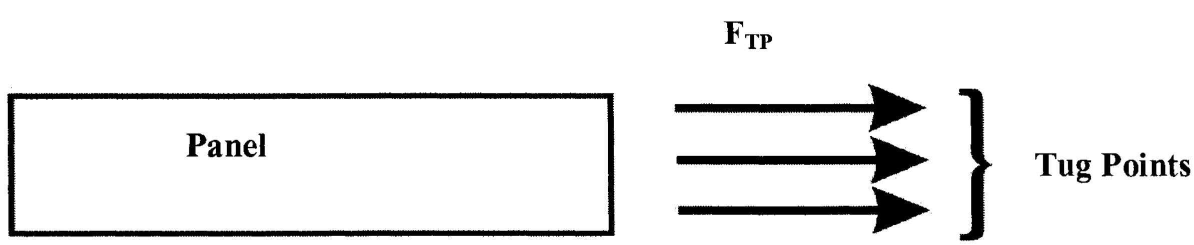

Assume: Impact Load Factor (Dynamic) = 1.1

1-meter clamp bar @ tug points (worst case)

F_{TP} = ForceTug Point = (Panel Weight x Tan S x Impact Load Factor)/No. Tug Points (2)

$F_{allowable}$ = Yield Tensile Strength (3)

Calculate Factor of Safety (F.S.) in onshore dragging operation:

F.S. = $F_{Allowable}$/FTP (4)

Table 2 summarizes the Force Tug Point, Allowable Force and Factor of Safety for each of the considered materials.

Material Type	F_{TP}	$F_{Allowable}$	F.S.
EIA-RCF	4473 N/M	96,300 N/M (550lb/in)	21.5
PPE/CSPE	5570 N/M	35,000 N/M (200 lb/in)	6.3
HDPE	5422 N/M	16,800 N/M (100 lb/in)	3.1

Table 2. Summary of Forces and Safety Factors for Dry Deployment Scenario

All geomembranes considered in this "dry"scenario analysis have safety factors greater than unity. However, the reinforced EIA Coated Fabric was 3 times as reliable as the laminated materials and 6 times as reliable as the HDPE film in this analysis. These conditions, of course, represent worst case conditions, but are representative of the possible forces to be encountered in this field operation. Folded panels ready for installation along the bund are shown in Figure 6.

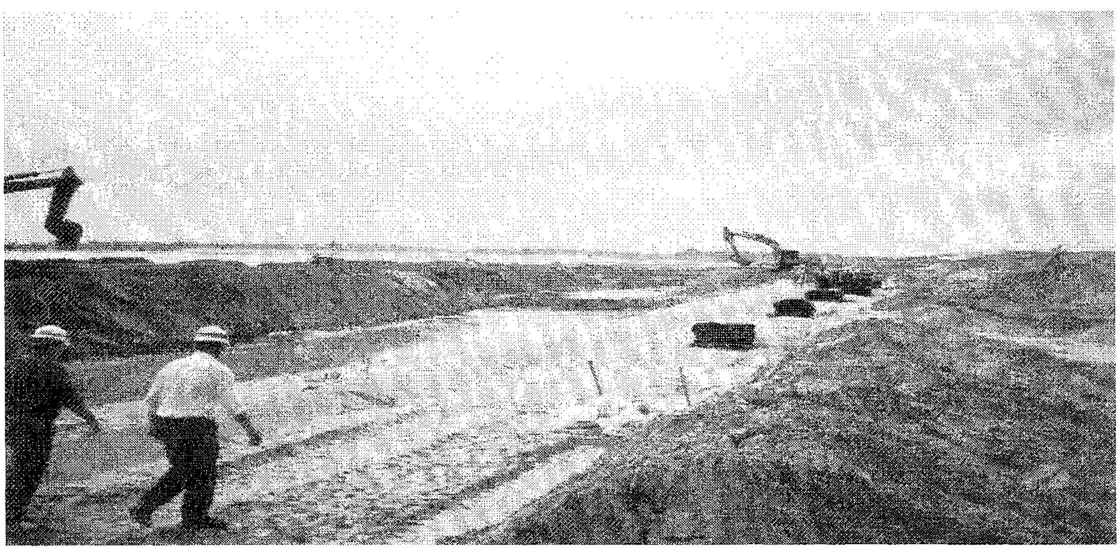

Figure 6. Folded Panels for Dry Installation

CASE 2: OFF SHORE DEPLOYMENT

Figure 7 illustrates the forces anticipated in deploying and placing the geomembrane in the "wet" installation scheme:

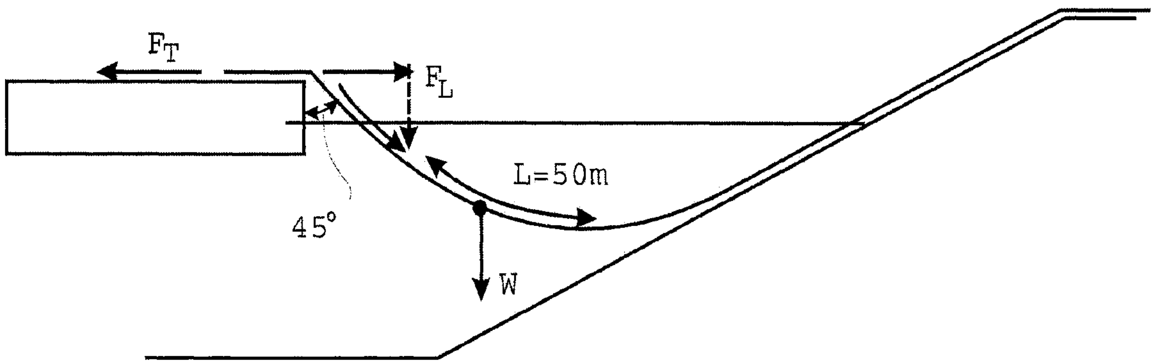

Figure 7. Forces Anticipated in Deploying and Placing Geomembrane in Wet Installation Scheme.

Calculate Buoyant Weight of Geomembrane, w

W = Geomembrane Area (50m x 20m) x Bwu (5)

Where Bwu = Buoyant Geomembrane Unit Weight

F_L = Force of Geomembrane in Water
F_T = Force of Geomembrane on Barge

Note: Assume Ballast is assumed to be added to provide $HDPE_{S.G.}$ = 1.2

Calculate force on Geomembrane as it is deployed from the barge:

FTP = (w x Impact Load Factor)/(Tan 45° x No. Tug Points) (6)

Calculate Factor of Safety (F.S.) in offshore dragging operations:

F.S. = $F_{allowable}$/FTP (7)

Note the materials with specific gravities (SG) less than 1 were assumed to require added ballast in order to provide a SG equal to the EIA-RCF, 1.25.

Table 3 summarizes the forces and theoretical safety factors for each material. While all exceed 1.0, the EIA-RCF geomembrane greatly exceeds the other materials.

Material	B_{uw}	F_{TP}	F.S.
EIA-RCF	21.5	1,050 N	91.7
PPE/CSPE	6.29	1.633 N	21.4
HDPE	3.1	544 N	30.9

Table 3. Summary of Forces and Safety Factors for Wet Deployment Scenario

Based on the constructability analysis, the following construction features were essential in the selection of the geomembrane:

- A portion of the geomembrane would be installed underwater and therefore a Specific Gravity >1 was needed.

- Ultimately, clay and rock would overlay the geomembrane which could result in some damage. A material was needed which would be most resistant to puncture.

- Large panels were needed which could be custom prepared based on both width and length. Field preparation of the material for fitting was to be minimized or eliminated.

- Overlapping rather than field seaming was to be used and then covered with the clay layer. Width was to be maximized in order to minimize amount of overlapping.

- Panel seams were to have maximum strength to withstand dragging and placement in the tropical environment, often under sustained loading. Abrasion strength was to be sufficient for installation.

The project designers created a specification that demanded the properties, listed in Table 4.

Ultimately, the supplied material was a reinforced Ethylene Interpolymer Alloy (EIA), manufactured as a Reinforced Coated Fabric.

Material Type:	Reinforced EIA Geomembrane
Yield Tensile Strength:	250 Kg (550 lbs) minimum
Dead Load Seam Strength (Mil-T-52983E Modified,Para 4.5.3.19, 25 mm strip, ASTM D751)	
20 deg C	Pass @ 900N (210 lbs), 4 hour sustained load
70 deg C	Pass @ 240N (105 lbs), 4 hour sustained load
Prefabrication Capability:	
Width	30.5 m (100') minimum
Size	1860 sm (20,000 sf) minimum
Specific Gravity	>1.2
Thickness	1 mm (0.040") minimum

Table 4. Project Geomembrane Specifications

INSTALLATION

The selected material allowed the contractor to install the geomembrane and clay layer in sections as bund construction proceeded. The geomembrane was prefabricated into large panels of widths up to 18.2 m (60') and lengths as determined by ocean depth and subsequent bund design. Fabricated panels were accordion-folded for shipment to Singapore. This folding technique made installation of the Geomembrane very efficient with an unfolding sequence that minimized material handling. All sheet manufacturing and fabrication activities were subject to QA/QC procedures and field activities were conducted according to a CQA plan, all approved and monitored by the Singapore Ministry of the Environment.

Figures 8 through 10 illustrate the Geomembrane unfolding and installation. Underwater divers were used to key the leading edge of the geomembrane to the ocean floor, shown in Figure 9. Figure 10 illustrates a completed bund area with the geomembrane in place. Sand and riprap were dumped over the geomembrane once it was installed. Installation of a typical panel required 1 day.

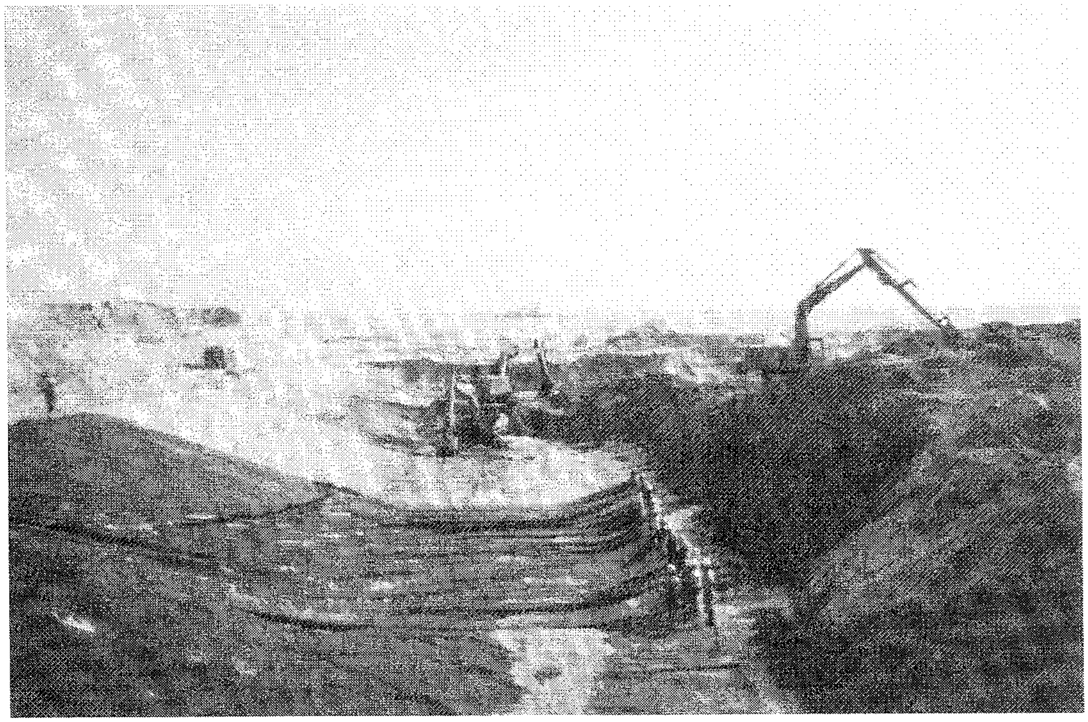

Figure 8. Panel Spreading

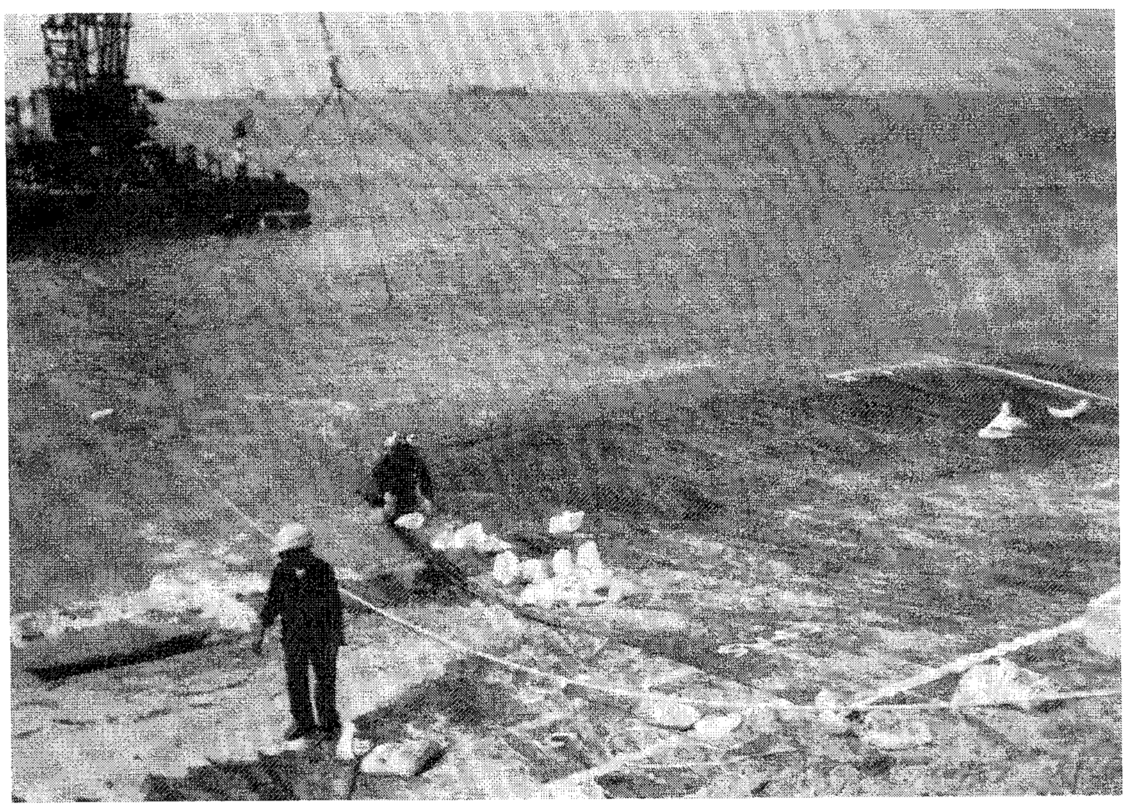

Figure 9. Underwater Panel Deployment

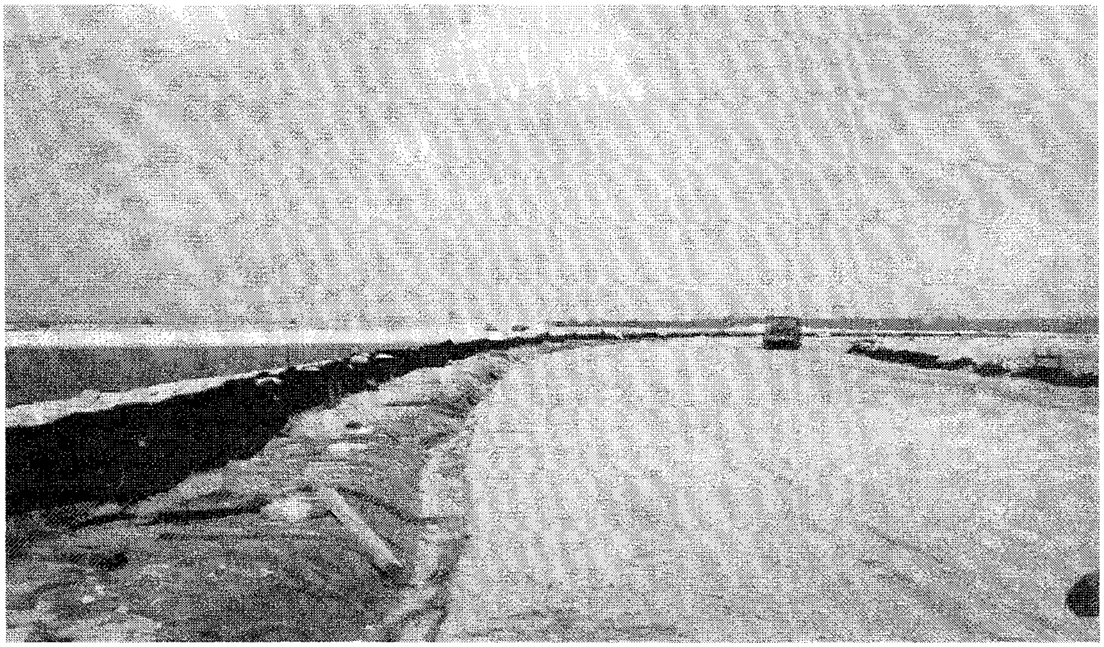

Figure 10. Completed Lined Bund

CONCLUSIONS

This project illustrates the versatile constructability of geomembranes as opposed to traditional clay-type materials. Without the use of a geomembrane, it is estimated that construction of the entire disposal facility would have been impractical, requiring different design techniques and different environmental constraints.

The Pulau Semakau accepted its first shipment of waste in March 1999.

ACKNOWLEDGEMENTS

The geomembrane used in the bund construction was XR-5, manufactured by Seaman Corporation, Wooster, Ohio, USA. The Panel fabricator was Lange Containment Systems, Denver, Colorado, USA. Project designers were Camp, Dresser and McKee Intl and Specs Consultants Pte. Ltd., both of Singapore.

REFERENCES

Tan, S.A., et al, "Leakage Study Across an Offshore Waste Containment Bund", Proceedings, 1998 Sixth International Conference on Geosynthetics, Atlanta, Georgia, 1998.

HYDRAULIC CONDUCTIVITY OF PARTIALLY PREHYDRATED GEOSYNTHETIC CLAY LINERS PERMEATED WITH AQUEOUS CALCIUM CHLORIDE SOLUTIONS

SCOTT M. VASKO
GEOSYNTEC CONSULTANTS, ACTON, MASSACHUSETTS, USA

HO YOUNG JO, CRAIG H. BENSON, AND TUNCER B. EDIL
GEO ENGINEERING PROGRAM, UNIVERSITY OF WISCONSIN-MADISON, USA

TAKESHI KATSUMI
DEPT. OF CIVIL ENGINEERING, RITSUMEIKAN UNIVERSITY, JAPAN

ABSTRACT: Tests were conducted to determine how prehydration water content affects the hydraulic conductivity of geosynthetic clay liners (GCLs) permeated with calcium chloride ($CaCl_2$) solutions of various concentrations. Results of the tests show that prehydration may not prevent the hydraulic conductivity of GCLs from increasing when permeated with divalent solutions. Hydraulic conductivities generally increased with $CaCl_2$ concentration, regardless of the prehydration water content, with hydraulic conductivities as much as 85,000 times higher than that obtained with deionized water. Application of a light confining stress during prehydration did not consistently result in lower hydraulic conductivities. Hydraulic conductivities much higher than anticipated were obtained when prehydration did not occur uniformly, indicating that prehydration must be carefully implemented in the field if it is to be reliable. Hydraulic conductivity was inversely correlated with void ratio, which is consistent with differences in the swelling of the bentonite granules for fully and partially prehydrated GCLs.

INTRODUCTION

Geosynthetic clay liners (GCLs) are used for lining waste containment systems because they have very low hydraulic conductivity (~10^{-9} cm/s) when permeated with dilute waters (i.e., deionized, distilled, or tap water). Their low hydraulic conductivity is due to constrictions in the pore space that occur when the bentonite swells as the surfaces and interlayer regions of the montmorillonite particles hydrate (Low 1979, Shackelford et al. 2000). An issue of prime concern when using GCLs for waste containment is the potential for adverse chemical interactions with the liquid being contained; i.e., the liquid will prevent swelling and cause the hydraulic conductivity to increase (Petrov and Rowe 1997, Shackelford et al. 2000). One method that has been suggested to prevent alterations in hydraulic conductivity of GCLs and other clay barrier materials is prehydration (Daniel et al.1993, Shackelford 1994, Gleason et al. 1997, Ruhl and Daniel 1997, Stern and Shackelford 1998); i.e., the barrier material is hydrated with deionized (DI) water, distilled (DS) water, or tap water before permeation with the chemical solution (Shan and Daniel 1991, Ruhl and Daniel 1997, Shackelford et al. 2000). Henceforth, the prehydrating fluid is referred to simply as "water."

Prehydration may be imposed (e.g., by spraying) or may occur naturally as the GCL adsorbs water from adjacent soils (Daniel et al. 1993, Bonaparte et al. 1996, Petrov and Rowe 1997). Prehydration may be full or partial. Full prehydration corresponds to saturation of the GCL with water prior to chemical permeation. Partial prehydration corresponds to hydration to a particular water content without saturating the GCL. The water content existing prior to introduction of chemical solution is referred to as the "prehydration water content."

The objectives of this study were to determine if prehydration can preclude increases in hydraulic conductivity caused by permeants where the cations primarily are divalent and to assess how increases in hydraulic conductivity are related to the prehydration water content. Leachates where the inorganic fraction is predominantly divalent are present in some municipal solid waste landfills, mine waste disposal facilities, fly ash landfills, and process water lagoons. Hydraulic conductivity tests were conducted using GCL specimens prehydrated to water contents ranging from approximately 9% (air dry) to 250% (saturated) and aqueous solutions of calcium chloride having various concentrations.

BACKGROUND

Daniel et al. (1993) studied how prehydration affected the hydraulic conductivity of GCLs permeated with five organic liquids (benzene, gasoline, methanol, tertbutylethylether, and trichloroethylene). Specimens were air dry (non prehydrated) or were partially prehydrated to water contents of 50%, 100%, 125%, and 145%. The non-prehydrated and the partially prehydrated specimens were permeated for two months with one of the organic liquids. Non-prehydrated specimens and those prehydrated to a water content of 50% had similar hydraulic conductivities (~2×10^{-5} cm/s). When the prehydration water content was increased to 100%, the hydraulic conductivity decreased by 3-4 orders of magnitude. Tests on specimens prehydrated to initial water contents of 125% and 145% were not completed. No permeant liquid flowed through these specimens during the two-month test period. Petrov et al. (1997) suggest that chemical equilibrium may not have been established in the specimens that retained low hydraulic conductivity.

Shackelford (1994) describes hydraulic conductivity tests conducted on compacted sand-bentonite mixtures that were permeated with a mine waste solution saturated with calcium. The mixtures contained 16% sodium bentonite by weight and were tested with and without initial permeation with water. The composition of the mine waste solution was not reported. Hydraulic conductivity of the sand-bentonite mixture initially permeated with water and then with mine-waste solution was approximately two orders of magnitude lower than the hydraulic conductivity of the sand-bentonite mixture permeated directly with the mine-waste solution.

Ruhl and Daniel (1997) conducted hydraulic conductivity tests on prehydrated and non-prehydrated GCLs using a simulated municipal solid waste (MSW) leachate designed to represent a worst-case scenario. When the GCLs were permeated directly with the simulated MSW leachate, the GCLs had hydraulic conductivities between 2×10^{-6} and 8×10^{-6} cm/s. When the GCLs were prehydrated with tap water prior to permeation with simulated MSW leachate, the hydraulic conductivities ranged between 3×10^{-10} and 2×10^{-9} cm/s. Ruhl and Daniel (1997) indicate that the prehydrated GCLs may not have been in equilibrium, and that the hydraulic conductivity of the GCLs may have increased had the tests been run longer. An analysis by Shackelford et al. (2000) confirms this supposition. They show that the specimens permeated with simulated MSW leachate that retained low hydraulic conductivity were not in pH equilibrium when the tests were terminated, whereas equilibrium had been reached for the specimens that exhibited large increases in hydraulic conductivity.

Gleason et al. (1997) investigated how prehydration affected the hydraulic conductivity of calcium (Ca) bentonite permeated with 0.25 M calcium chloride ($CaCl_2$) solution. The hydraulic conductivity of Ca-bentonite permeated directly with 0.25 M $CaCl_2$ solution was almost an order of magnitude higher than Ca-bentonite permeated initially with tap water and then with 0.25 M $CaCl_2$ solution. Shan and Daniel (1991) report similar findings from testing a sodium bentonite that was permeated first with water and then with 0.25 M $CaCl_2$ solution.

Petrov and Rowe (1997) indicate that, under the same confining stress, GCLs fully prehydrated under greater confining stress have lower void ratio and lower hydraulic conductivity than GCLs fully prehydrated at low confining stress. Specimens fully prehydrated at confining stresses of 3-4 kPa were typically two to four times more permeable than specimens fully prehydrated at confining stresses between 101-108 kPa, regardless of the confining stress applied during permeation. Petrov and Rowe (1997) also suggest that the hydraulic conductivity of a GCL is directly related to its final void ratio.

MATERIALS AND METHODS

Geosynthetic Clay Liner (GCL)

The GCL used in this study consisted of granular sodium bentonite encased between two geotextiles that were needle-punched together. One geotextile was a slit-film monofilament woven geotextile (170 g/m^2). The other was a non-woven staple-fiber geotextile (206 g/m^2). The surface of the geotextiles was heat burnished to retain the needle-punching fibers. The air-dry gravimetric water content of the bentonite was 9% and its specific gravity was 2.66. The mass/area of bentonite was 5 kg/m^2, the initial air dry thickness ranged from 7.5 to 8.5 mm, and the median granule size was 0.25 mm. X-ray diffraction showed that the bentonite in the GCL consisted of 67% sodium montmorillonite, 11% plagioclase feldspar, 10% quartz, and 12% other non-clay minerals (Jo 1999, Vasko 1999).

Permeant Liquids

Various aqueous solutions of $CaCl_2$ (0.005, 0.01, 0.025, 0.1, and 1 M $CaCl_2$) were used as permeant liquids. Solutions were prepared by dissolving anhydrous powdered $CaCl_2$ in deionized (DI) water. Only $CaCl_2$ was used because Jo (1999) found that the hydraulic conductivity of GCLs permeated with solutions having different species of divalent and trivalent cations differed by less than one-half order of magnitude provided the concentration of the permeant liquid was the same. Therefore, the hydraulic conductivities obtained with $CaCl_2$ solutions are believed to be representative of the behavior for other divalent and trivalent salt solutions.

Sample Preparation and Prehydration

Square specimens 150 mm x 150 mm were cut from a roll of GCL using a razor knife. Samples were cut from areas away from the edges of the roll or any other areas that appeared to have lower mass of bentonite in comparison to the rest of the roll. After cutting, the sample was weighed to obtain an initial dry weight.

Most specimens were prehydrated without confinement. The GCL specimen was placed on top of a piece of filter paper laying on a pedestal consisting of PVC tubing and a rigid plastic screen (Figure 1). The pedestal and GCL were then placed in a sealed tank filled with deionized water. The water level in the tank was maintained just below the bottom of the plastic screen.

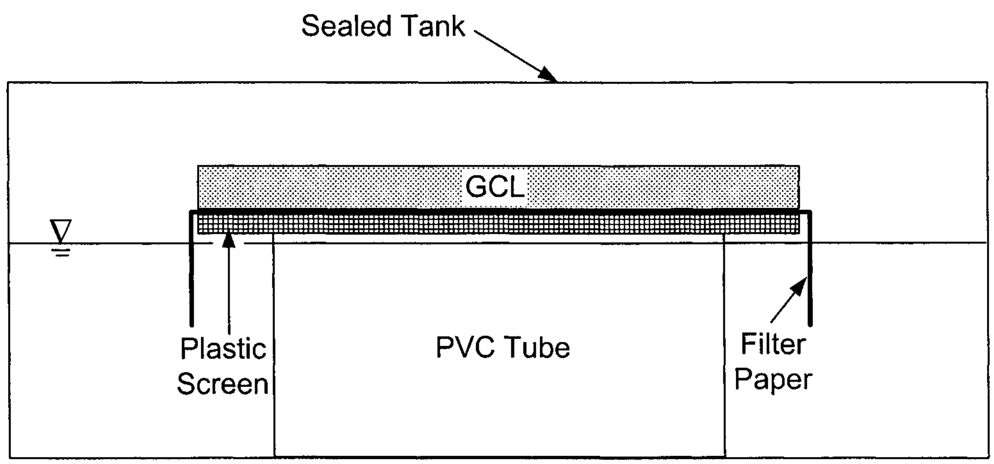

Figure 1. Set-up Used to Prehydrate GCLs.

Prehydration by vapor phase diffusion was attempted initially. However, prehydration water contents obtained by diffusion were limited to about 50%. This finding is consistent with surface hydration studies conducted by Fu et al. (1990), which show that sodium montmorillonites cannot be hydrated beyond 50% by vapor phase diffusion alone. Increases in water content beyond 50% must be achieved through capillary effects or direct application of water. To achieve higher prehydration water contents, the filter paper was made larger so that it would drape over the edge of the plastic screen and into the underlying water (Figure 1). The filter paper wicked water upward and into contact with the bottom (non-woven side) of the GCL. The non-woven side of the GCL was selected for contact based on preliminary comparisons that showed that the water content distribution in the bentonite was more uniform when the non-woven geotextile was in contact with the filter paper. Typical distributions of water content for contact with the non-woven and woven geotextiles are shown in Figure 2.

To monitor water content during hydration, the GCL specimens were regularly removed from the water tank, quickly weighed, and placed back into the tank. When a specimen achieved the target water content, it was removed and trimmed into a circular shape with a diameter of 100 mm. The thickness was measured in 7-10 locations using a caliper, and the specimen was placed in a flexible-wall permeameter for testing.

Specimens prehydrated with light confinement were prepared using the same procedures, with the following exceptions. The specimens were trimmed to a diameter of 100 mm prior to prehydration. Extreme care was used to minimize loss of bentonite during trimming because the specimens would not be trimmed any further after prehydration. Trimmed specimens were placed on the pedestal mentioned previously, and then retained within a stainless steel confining ring 15 mm high. The confining ring prevented lateral squeezing during hydration when the confining stress was applied. Confinement was applied using a cylindrical lead weight that applied an average stress of 8 kPa. This stress was selected to simulate the confining stress provided by a leachate collection layer in an unfilled landfill cell.

<u>Permeation</u>

Falling-head hydraulic conductivity tests with constant tailwater level were conducted on the GCLs using flexible-wall permeameters in general accordance with ASTM D 5084. No backpressure was applied, and the cell and influent pressures were applied using a gravity system. The average effective confining stress was 20 kPa and the average hydraulic gradient was 100. This hydraulic gradient is higher than specified in D 5084, but is typical of hydraulic gradients used for testing GCLs (Shackelford et al. 2000). In addition, Shackelford et al. (2000) show that the higher gradients used for testing GCLs induce the same level of effective stress as the gradients specified in D 5084 since GCLs are much thinner than the soil specimens for which D 5084 was originally developed.

Hydraulic conductivity tests were continued until the hydraulic conductivity data exhibited no trend and varied < 25% for four consecutive values, the ratio of outflow to inflow was between 0.75 and 1.25, the ratio of the pH of the outflow to the pH of the inflow was between 0.9 and 1.1, the ratio of the electrical conductivity (EC) of the outflow to the EC of the inflow was between 0.9 and 1.1, and at least 2 pore volumes of the permeant liquid flowed through the specimen. Shackelford et al. (1999) show that these EC and pH termination criteria ensure that chemical equilibrium is established. At termination, the permeameter was immediately disassembled, the specimen was weighed, the final thickness was measured at 7-10 locations using a caliper, and samples were collected for water content measurements.

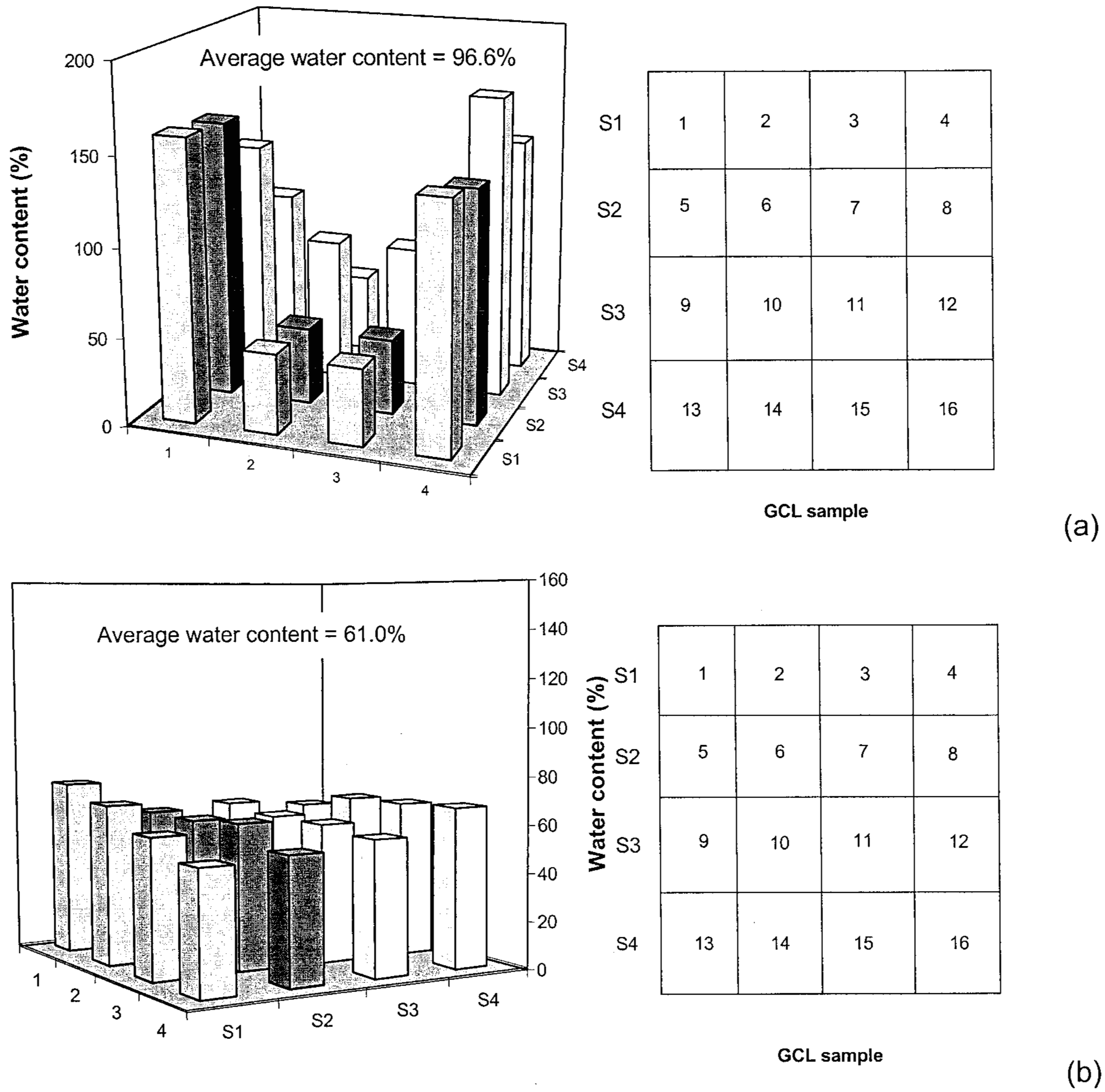

Figure 2. Distribution of Water Content in Prehydrated Specimens with Different Geotextile Contacting the Filter Paper: (a) Woven Geotextile in Contact with Filter Paper, (b) Non-Woven Geotextile in Contact with Filter Paper.

Occasionally the final hydraulic conductivity of a GCL specimen appeared unreasonably high. In such cases, rhodamine WT dye was added to the influent solution after the hydraulic conductivity test was completed to mark the flow paths. Stains left by the dye indicated that most of the flow in such specimens passed through only a portion of the GCL that apparently had much higher hydraulic conductivity than the remainder. No staining was observed along the sidewalls, indicating that sidewall leakage was not responsible for the elevated hydraulic conductivity. Non-uniform hydration was believed to be the cause of these permeable zones and the unexpectedly high hydraulic conductivity of these specimens. Thus, in such cases, the GCL was partitioned into 16 relatively equal sections to measure the spatial distribution of water content. An example of a water content distribution is shown in Figure 3 for a non-uniformly hydrated specimen that had an average prehydration water content of 100% and hydraulic conductivity of 1.0×10^{-4} cm/s to 0.1 M $CaCl_2$. The region with the lowest final water content (location 2 x S2 in Figure 3) was clearly stained by dye and apparently controlled the hydraulic conductivity. The hydraulic conductivity of this specimen is approximately 10 times higher than that of a uniformly hydrated specimen prehydrated to the same average water content and permeated with the same solution (9.6×10^{-6} cm/s). However, the hydraulic conductivity is less than two times higher than that of non-prehydrated GCLs permeated with the same solution (5.7×10^{-5} to 6.4×10^{-5} cm/s).

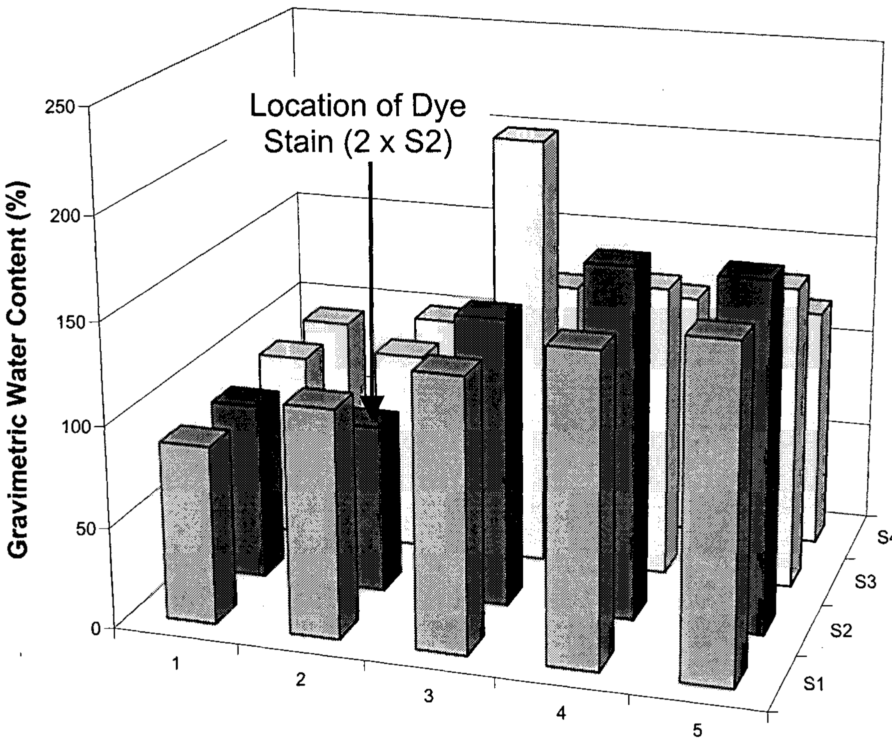

Figure 3. Distribution of Water Content in Non-Uniformly Hydrated Specimen.

RESULTS

Results of all tests on reasonably uniformly hydrated specimens are summarized in Table 1. A summary of all the data is in Vasko (1999).

Table 1. Summary of Hydraulic Conductivity Tests.

$CaCl_2$ Conc. (M)	Prehydration Water Content (%)	Void Ratio After Prehydration	Void Ratio After Permeation	Confined Hydration ?	Hydraulic Conductivity (cm/s)
0.005	9	2.24	5.05	No	1.3×10^{-9}
0.01	9	2.33	4.78	No	1.2×10^{-9}
0.01	250	6.70	7.20	No	1.5×10^{-9}
0.025	9	2.36	2.41	No	2.7×10^{-7}
0.025	9	2.27	2.64	No	5.0×10^{-8}
0.025	50	2.43	2.57	No	2.4×10^{-8}
0.025	50	3.18	3.64	No	9.0×10^{-9}
0.025	100	3.61	3.57	No	4.5×10^{-8}
0.025	150	5.37	3.89	No	2.7×10^{-7}
0.025	277	8.53	6.82	No	5.9×10^{-8}
0.1	9	2.41	2.49	No	6.4×10^{-5}
0.1	9	2.13	2.28	No	5.7×10^{-5}
0.1	50	3.74	4.32	No	9.7×10^{-5}
0.1	50	4.38	4.58	No	1.1×10^{-4}
0.1	100	3.99	4.07	No	9.6×10^{-6}
0.1	133	5.46	4.15	No	2.5×10^{-6}
0.1	150	5.16	4.56	No	7.8×10^{-8}
0.1	200	6.51	4.75	No	1.9×10^{-7}
0.1	258	7.71	6.41	No	2.0×10^{-7}
1.0	7	2.16	2.20	No	4.7×10^{-5}
1.0	9	2.36	2.41	No	8.7×10^{-5}
1.0	9	1.95	2.03	No	7.4×10^{-5}
1.0	50	2.61	3.01	No	7.2×10^{-6}
1.0	100	4.75	3.13	No	8.3×10^{-6}
1.0	150	5.47	5.12	No	5.2×10^{-6}
1.0	200	6.50	4.99	No	4.0×10^{-7}
1.0	258	8.10	6.96	No	1.0×10^{-6}
1.0	277	8.39	6.59	No	2.9×10^{-7}
0.1	50	3.31	3.41	Yes	1.0×10^{-4}
0.1	100	3.49	3.19	Yes	5.2×10^{-7}
0.1	133	4.61	-	Yes	2.6×10^{-7}
1.0	50	3.56	3.20	Yes	8.6×10^{-5}

Effect of Prehydration Water Content

Hydraulic conductivity vs. prehydration water content is shown in Figure 4 for specimens that were uniformly prehydrated without confinement. The data are segregated into three groups of similar behavior as exhibited by the trend lines: weaker solutions (DI water and 0.01 M $CaCl_2$), intermediate solutions (0.025 M $CaCl_2$), and stronger solutions (0.1 and 1 M $CaCl_2$).

Hydraulic conductivity increases as the concentration of $CaCl_2$ increases, which is most likely due to exchange of Ca^{2+} for Na^+ and the reduced swelling that is associated with the Ca^{2+} ion (Zhang et al. 1995, Jo 1999, Shackelford et al. 2000). Prehydration water content has no apparent effect on hydraulic conductivity for the intermediate and weaker solutions ($\leq$ 0.025 M). For 0.025 M $CaCl_2$, the hydraulic conductivity varies between $1x10^{-8}$ cm/s and $3x10^{-7}$ cm/s, and is approximately $1x10^{-7}$ cm/s on average. For concentrations $\leq$ 0.01 M $CaCl_2$, the hydraulic conductivity is about that obtained with DI water ($1.2x10^{-9}$ cm/s) and is independent of the prehydration water content. For the stronger solutions (0.1 or 1 M $CaCl_2$), lower hydraulic conductivity is obtained with higher prehydration water content. The hydraulic conductivity decreases from approximately $1x10^{-4}$ cm/s to $3x10^{-7}$ cm/s as the prehydration water content increases from 9% to 150% and then remains approximately constant at $3x10^{-7}$ cm/s as the prehydration water content is increased further.

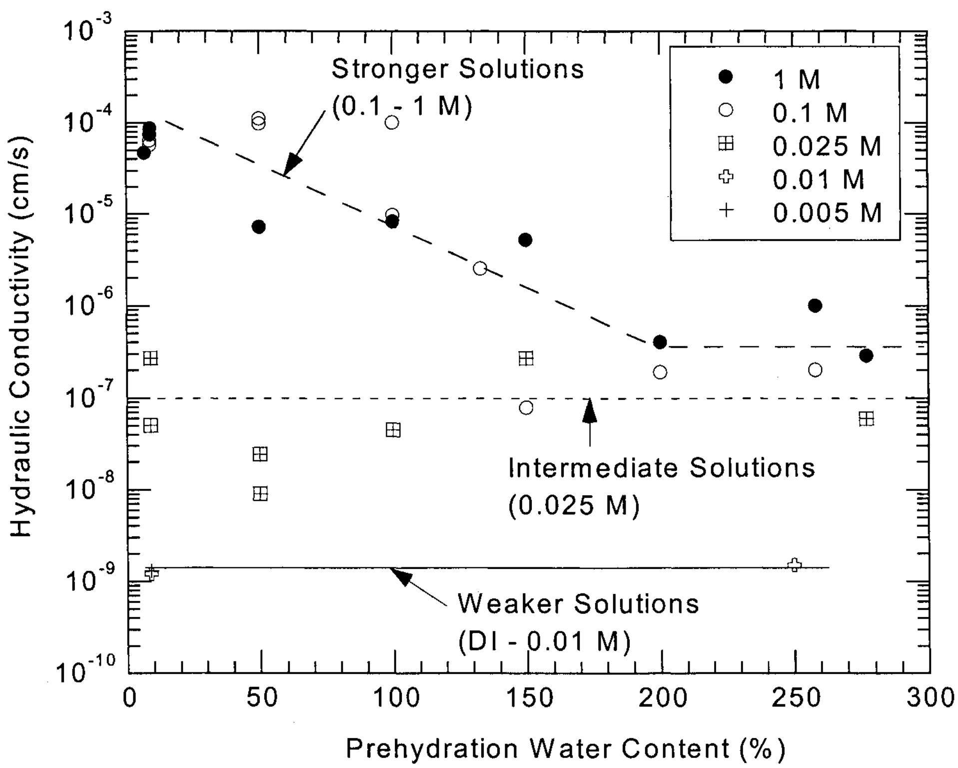

Figure 4. Hydraulic Conductivity vs. Prehydration Water Content for Unconfined Specimens.

The hydraulic conductivities reported here for concentrations ≥ 0.025 M are much higher than those reported by Daniel et al. (1993) for specimens prehydrated to water contents ≥ 100% and permeated with organic chemicals, and are typically above the value considered acceptable for liners (10^{-7} cm/s). Apparently the benefits accrued by hydration with water followed by permeation with a non-wetting organic liquid are not obtained when the permeant liquid is a wetting aqueous solution. One possible explanation for this difference in behavior is that the film of hydration water surrounding particles in a prehydrated GCL prevents the non-wetting and immiscible organic permeant liquid from interacting with the particle surface, and thus prevents a reduction in the volume of adsorbed water. In contrast, when the permeant liquid is an aqueous solution, mixing and exchange can readily occur between the hydration water and the permeant liquid, resulting in a reduced volume of adsorbed water and an increase in hydraulic conductivity. Another viable explanation is that provided by Petrov et al. (1997); i.e., the tests conducted by Daniel et al. (1993) were terminated before equilibrium was established.

Influence of Confinement During Prehydration

A limited number of tests were conducted with confinement during prehydration. Hydraulic conductivities of unconfined and confined specimens prepared and permeated under similar conditions are shown in Table 2. The ratio K_c/K_u in Table 2 corresponds to the hydraulic conductivity of a confined specimen (K_c) relative to that of a similar unconfined specimen (K_u). Hydraulic conductivities of the confined specimens are not consistently lower than those of the unconfined specimens, as was observed by Petrov and Rowe (1997). However, Petrov and Rowe (1997) fully prehydrated their specimens and used NaCl solutions as permeating liquids, whereas the specimens in this study were partially prehydrated and permeated with $CaCl_2$ solutions. By fully prehydrating their specimens, Petrov and Rowe (1997) allowed the bentonite to swell during prehydration with no restriction on the availability of hydration water. When access to hydration water is unlimited, the bentonite granules become soft, resulting in bentonite that appears as a gel. This condition probably results in more uniform pore structure and more well behaved conditions than existed in the partially prehydrated specimens tested in this study. When partially prehydrated, stiffer bentonite granules with larger inter-granule pores are readily visible when a GCL is opened (Vasko 1999).

There is a tendency for lower hydraulic conductivities under confinement when the prehydration water contents are higher (100 and 133%), which may be due to compression of softer bentonite granules that exist at higher prehydration water contents. Lower initial void ratio should correspond to lower hydraulic conductivity. Nevertheless, all of the hydraulic conductivities reported here are above the common maximum value of 10^{-7} cm/s, regardless of the stress applied during prehydration.

Table 2. Hydraulic Conductivity of Unconfined and Confined Specimens.

Prehydration Water Content (%)	Permeant Concentration (M)	Hydraulic Conductivity (cm/s)		K_c/K_u
		Confined Hydration	Unconfined Hydration	
50	0.1	$1.0x10^{-4}$	$9.7x10^{-5}$	1.0
50	1.0	$8.6x10^{-5}$	$7.2x10^{-6}$	6.3
100	0.1	$5.2x10^{-7}$	$9.6x10^{-6}$	0.05
133	0.1	$2.6x10^{-7}$	$2.5x10^{-6}$	0.1

Hydraulic Conductivity and Void Ratio

Petrov and Rowe (1997) and Shackelford et al. (2000) show that the hydraulic conductivity of GCLs and bentonites permeated with NaCl solutions is directly related to void ratio, and that a unique relationship between hydraulic conductivity and void ratio exists for each NaCl concentration. The data from this study were graphed in a similar manner to see if partially prehydrated GCLs permeated with $CaCl_2$ solutions follow similar trends. Hydraulic conductivity of the GCLs is shown in Figure 5 as a function of void ratio after prehydration (e_p) (Figure 5a) and void ratio after permeation (e_f) (Figure 5b). For both pre- and post-test conditions, the hydraulic conductivity either is unrelated to void ratio (intermediate or weaker solutions) or decreases with increasing void ratio (stronger solutions). These trends contrast those reported by Petrov and Rowe (1997), and the data exhibit more scatter than they observed. The trends differ because Petrov and Rowe (1997) obtained different void ratios by changing the effective stress on fully prehydrated GCLs, whereas in this study the stress was held constant and the prehydration water content was varied.

The decreasing trends in Figure 5 can be explained in terms of the texture and pore spaces of granular bentonites that are partially prehydrated and then permeated with stronger primarily divalent solutions. When fully prehydrated, bentonite granules disperse into individual particles and form a gel. This gel, while having high void ratio (e.g., e_p = 5-7), typically has low hydraulic conductivity because most of the voids are filled with essentially immobile bound water associated with the montmorillonite particles. When partially prehydrated, inadequate water exists for the bentonite granules to disperse and form a gel. A gel does not form during permeation either, because the Ca^{2+} ions prevent expansion of the interlayer region (Prost et al. 1998). Thus, the void ratio of a partially prehydrated specimen is lower (e_p = 3-5) than that obtained with a fully prehydrated specimen when permeated with the same solution. However, even though the void ratio of partially prehydrated GCLs is lower, the voids between the bentonite granules probably act as larger and more conductive pathways for flow relative to the voids that exist in bentonite in a gel state. Consequently, partially prehydrated GCLs can have higher hydraulic conductivity even though they have lower void ratio than fully prehydrated GCLs.

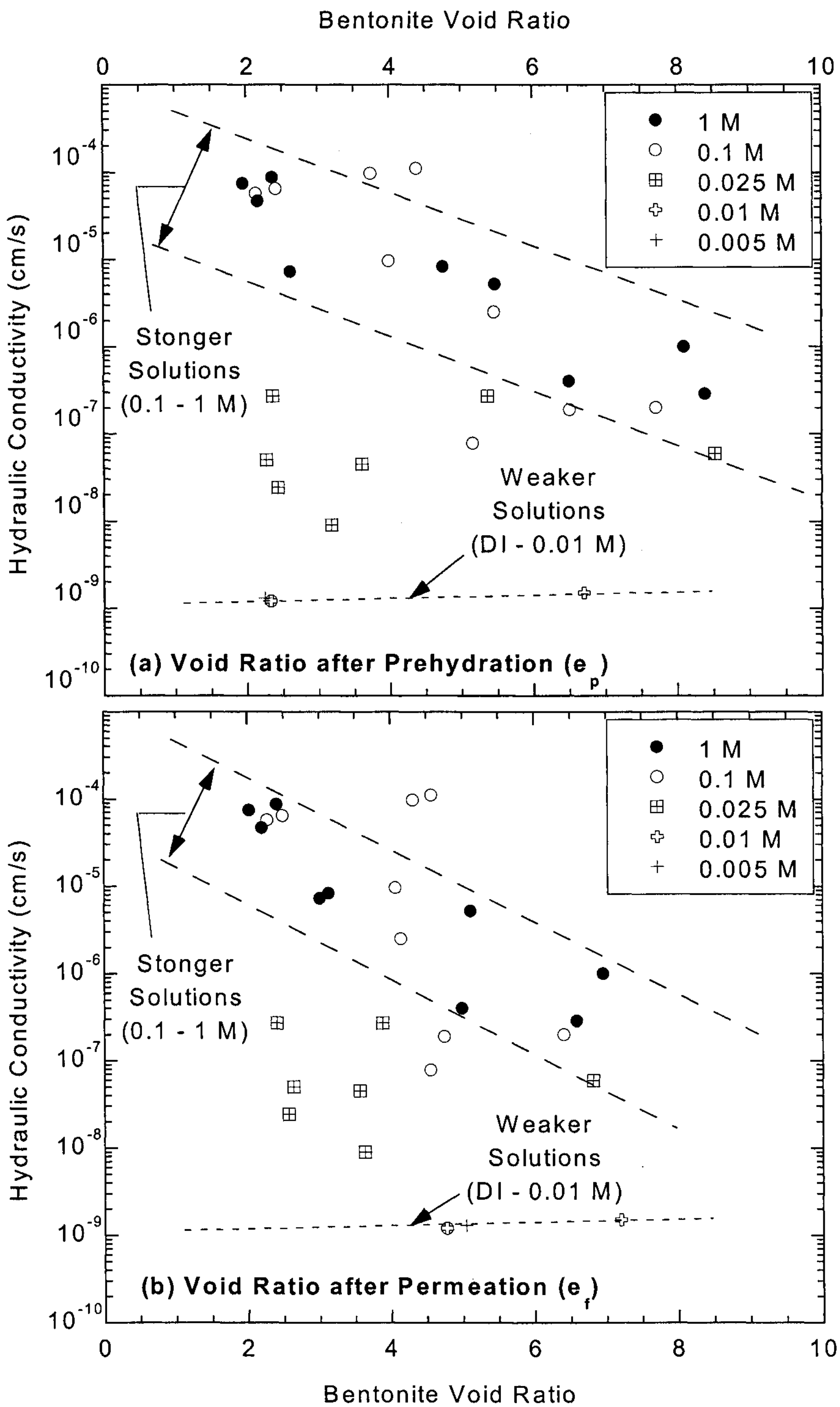

Figure 5. Hydraulic Conductivity vs. Void Ratio: (a) After Prehydration and (b) After Permeation.

The difference in void ratio caused by prehydration is shown in its most exaggerated state in Figure 6, which depicts void ratio after permeation (e_f) as a function of $CaCl_2$ concentration for non-prehydrated and fully prehydrated GCL specimens. The non-prehydrated specimens consistently have lower void ratio than the fully prehydrated specimens for all concentrations, but generally have similar or higher hydraulic conductivity (Figure 4).

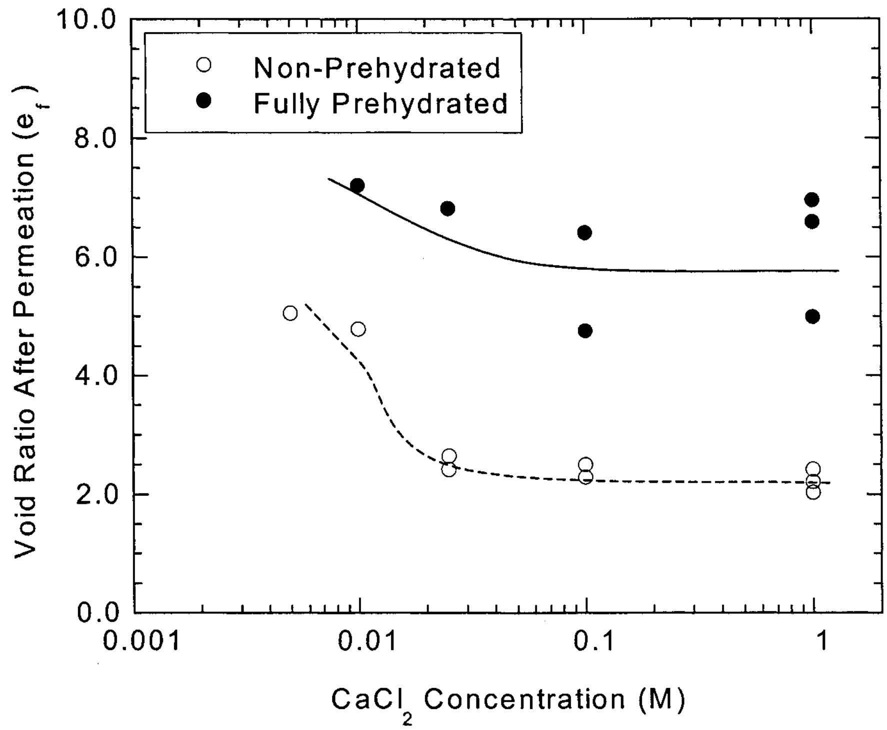

Figure 6. Void Ratio after Permeation (e_f) as a Function of $CaCl_2$ Concentration for Non-Prehydrated and Fully-Prehydrated GCL Specimens.

CONCLUSIONS

The objective of this study was to determine how prehydration water content affects the hydraulic conductivity of GCLs permeated with divalent inorganic chemical solutions of various concentrations. Specimens were prehydrated to differing water contents in a water tank and then permeated with $CaCl_2$ solutions using flexible-wall permeameters. Based on the results shown, the following conclusions are drawn:

- Prehydration with distilled, deionized (DI), or tap water may not prevent the hydraulic conductivity of GCLs permeated with inorganic salt solutions from increasing substantially above the base-line hydraulic conductivities obtained with DI water (~10^{-9} cm/s). Hydraulic conductivities comparable to those with DI water were only obtained for dilute solutions ($\leq$ 0.01 M $CaCl_2$). For the other solutions, the hydraulic conductivity was 10 to 85,000 times higher than that obtained with DI water, with higher hydraulic conductivities being obtained with stronger solutions, and in some cases at lower prehydration water contents.

- Application of a light confining stress during prehydration comparable to that provided by a leachate collection system did not consistently result in lower hydraulic conductivities. In some cases, higher hydraulic conductivities were obtained with confinement. Confinement does appear to result in somewhat lower hydraulic conductivities when the prehydration water content is at least 100%, which is probably due to softening of the bentonite aggregates at higher prehydration water contents. More testing is needed to clearly define the importance of confinement during prehydration.

- Hydraulic conductivities higher than anticipated were obtained when prehydration did not occur uniformly. Thus, if prehydration is to be relied on to provide lower hydraulic conductivity (e.g., for containment of organic liquids), steps must be taken to ensure uniform prehydration exists throughout the GCL. More study is needed to determine conditions that result in uniform prehydration.

- Hydraulic conductivity was uncorrelated or inversely correlated with void ratio for the specimens tested in this study, which were partially prehydrated and then permeated with $CaCl_2$ solutions. This inverse relationship can be explained by the differences in the swelling of bentonite granules and the pore structures obtained at high and low prehydration water contents.

ACKNOWLEDGEMENT

The United States National Science Foundation provided a portion of the support for this study through grant no. CMS-9900336. Dr. Katsumi conducted some of his effort on this study while on leave at the University of Wisconsin-Madison. The Kajima Foundation of Japan provided support for Dr. Katsumi's stay at the University of Wisconsin-Madison.

REFERENCES

Bonaparte, R., Othman, M., Rad, N., Swan, R., and Vander Linde, D. (1996), "Evaluation of Various Aspects of GCL Performance," Report of 1995 Workshop on Geosynthetic Clay Liners, Report No. EPA/600/R-96/149, USEPA, Washington, DC, F1-F34.

Daniel, D., Shan, H., and Anderson, J. (1993), "Effects of Partial Wetting on the Performance of the Bentonite Component of a Geosynthetic Clay Liner," *Geosynthetics '93*, IFAI, St. Paul, MN, 3, 1482-1496.

Fu, M., Zhang, Z., and Low, P. (1990), "Changes in the Properties of a Montmorillonite-Water System During the Adsorption and Desorption of Water: Hysteresis," *Clays and Clay Minerals*, 38(5), 485-492.

Gleason, M., Daniel, D., and Eykholt, G. (1997), "Calcium and Sodium Bentonite for Hydraulic Containment Applications," *J. Geotechnical and Geoenvironmental Engineering*, 118(5), 438-445.

Jo, H. (1999), Hydraulic Conductivity and Swelling of Non-Prehydrated GCLs Permeated with Inorganic Chemicals, MS Thesis, University of Wisconsin-Madison.

Low, P. (1979), "Nature and Properties of Water in Montmorillonite-Water Systems," *Soil Science Society of America J.*, 43, 651-658.

Petrov, R., and Rowe, R. (1997), "Geosynthetic Clay Liner (GCL) – Chemical Compatibility by Hydraulic Conductivity Testing and Factors Impacting its Performance," *Canadian Geotechnical J.*, 34, 863-885.

Petrov, R., Rowe, R., and Quigley, R. (1997), "Selected Factors Influencing GCL Hydraulic Conductivity," *J. Geotechnical and Geoenvironmental Engineering*, 123(8), 683-695.

Prost, R., Koutit, T., Benchara, A., and Huard, E. (1998), "State and Location of Water Adsorbed on Clay Minerals: Consequences of the Hydration and Swelling-Shrinkage Phenomena," *Clays and Clay Minerals*, 46(2), 117-131.

Ruhl, J., and Daniel, D. (1997), Geosynthetic Clay Liners Permeated with Chemical Solutions and Leachates," *J. Geotechnical and Geoenvironmental Engineering*, 123(4), 369-381.

Shackelford, C. (1994), "Waste-Soil Interactions That Alter Hydraulic Conductivity," *Hydraulic Conductivity and Waste Contaminant Transport in Soil*, STP 1142, ASTM, Daniel, D. and Trautwein, S., eds., 111-168.

Shackelford, C., Malusis, M., Majeski, M., and Stern, R. (1999), "Electrical Conductivity Breakthrough Curves," *J. of Geotechnical and Geoenvironmental Engineering,* 125(4), 260-270.

Shackelford, C., Benson, C., Katsumi, T., Edil, T., and Lin, L. (2000), "Evaluating the Hydraulic Conductivity of GCLs Permeated with Non-Standard Liquids," *J. Geotextiles and Geomembranes*, 18, 133-161.

Shan, H. and Daniel, D. (1991), Results of Laboratory Tests on a Geotextile/Bentonite Liner Material," *Geosynthetics '91*, IFAI, St. Paul, MN, 2, 517-535.

Stern, R. and Shackelford, C. (1998) "Permeation of Sand-Processed Clay Mixtures with Calcium Chloride Solutions," *J. Geotechnical and Geoenvironmental Engineering*, ASCE, 124(3), 231-241.

Vasko, S. (1999), Hydraulic Conductivity of Prehydrated GCLs Permeated with Calcium Chloride Solutions, MS Thesis, University of Wisconsin-Madison.

Zhang, F., Low, P., and Roth, C. (1995), "Effects of Monovalent, Exchangeable Cations and Electrolytes on the Relation between Swelling Pressure and Interlayer Distance in Montmorillonite," *J. Colloid and Interface Science*, 173, 34-41.

MATERIALS TESTING III—GEOMEMBRANES

GEOSYNTHETICS CONFERENCE 2001
Portland, Oregon USA
Economics, Performance & Constructibility • February 12-14, 2001

FROM BURST TEST TO BI-AXIAL TENSILE TEST

STÉPHANE LAMBERT, CEMAGREF,
FRANCE
CHRISTIAN DUQUENNOI, CEMAGREF,
FRANCE

ABSTRACT

The aim of this paper is to present results obtained performing strain controlled biaxial tensile tests and using an original real thickness estimation. Apparatus is described and calculations are presented. Test results on different kinds of geomembranes (HDPE, PVC, flexible PP and bituminous), and on five HDPE geomembranes made of the same compound and of different thicknesses are presented and discussed. Interesting conclusions concerning the method and its interest are drawn from these results showing that it brings real additional information to other methods but also that it should be enhanced.

INTRODUCTION

Geomembranes are used to act as barrier against fluids in geotechnical applications. They are submitted to different kinds of mechanical stresses due to field conditions. The main mechanical stress is tensile stress. Even if tensile stress should be avoided by a proper design this stress occurs more or less in every project and may lead to rupture of the geomembrane or dysfunction of the system. Geomembranes are submitted to tensile stress when placed on a slope, when the underlying support is subject to localized subsidence or even when the geomembrane shrinks as a consequence of temperature variations or aging.

Designers generally refer to the well-know uniaxial tensile test to assess the resistance of the geomembrane to on-site stress. Nevertheless, this test does not seem to be the most adapted. The first reason is that most on sites stresses, e.g. over subsiding material, are biaxial. Another reason is the narrowing of the geomembrane sample during uniaxial tensile test. This obviously cannot happen on site, even in cases where stress is usually considered uniaxial, e.g. on a slope. From a mechanical point of view, on site stress is not a uniaxial tensile stress (Soderman and Giroud 1995). Thus, the biaxial tensile test, or multi-axial tensile test, is sometimes preferred to the uniaxial tensile test. The term 'biaxial' is preferred here because it is thought to better reflect the involved phenomena.

The test consists in submitting a circular specimen of geomembrane clamped on its periphery to a hydraulic pressure. This out-of-plane stress deforms the geomembrane and the pressure is increased up to the rupture of the geomembrane. Pressure and deformation are generally recorded to calculate both stress and strain during the whole test.

Many studies have been carried out on the biaxial tensile test in the past 10 years. The initial burst test has been enhanced to better measure real biaxial characteristics. Some studies concern the method itself, and others the results and their interpretation. For instance, the effects of the diameter of the cell have been investigated, and a comparison between pressure control and strain control tests has been made (Merry and Bray 1995). The influence of strain rate and the influence of temperature on geomembranes properties have also been investigated (Nobert 1993, Merry and Bray 1997).

For the study presented herein, biaxial tensile tests were performed on different kinds of available geomembranes (HDPE, PVC, PP and bituminous), and on geomembranes made of the same HDPE compound of different thicknesses. Tests were performed controlling the strain. Stress was calculated using a new estimation of the thickness. Results are presented and discussed. Other possible uses of this test are also presented. For instance, a proposed use is the determination of the degree of damage of geomembranes. The results confirm the interest of this test, and point out aspects to be addressed.

MATERIALS AND METHOD

General Method

As previously mentioned, the test consists in increasing pressure under a circular specimen of geomembrane up to its rupture while measuring deflection of the specimen.

Tests presented in this study were performed increasing pressure in such a way that the strain rate was constant and equal to 5 % per minute. This method has been demonstrated to be the only one applicable to test different kinds of geomembranes in a comparable way (Merry Bray 1997).

Strain controlled tests required closed-loop-feedback; after measurement of the center point deflection the real strain was calculated, and according to this value, the pressure was readjusted.

Apparatus and calculations necessary for this strain controlled test are presented hereafter together with hypotheses on which calculations are based.

Apparatus

The apparatus (Figure 1) was composed of a cell, a deflection measuring device, a pressure delivery system and a computer. The apparatus allowed free deformation of the geomembrane for any deformation shape and height.

The cell was 200 mm in effective diameter (d), which is thought to be enough to avoid any size effects for geomembranes (Merry Bray 1995). The base of the cell was oriented upwards. The clamping ring was fixed on the base by sixteen bolts.

Deflection of the center point was measured with a laser and a light stick. The origin for deflection measurements was designated as the lower face of the clamping ring. A pressure gauge placed near the center of the cell provided pressure measurements. Measurement devices were connected to the computer.

Pressure was applied using water at a 22°C +/- 1°C temperature. The pressure delivery system was composed of a piston controlled by the computer. The volume of water available to inflate the geomembrane was insufficient to reach rupture for highly deformable geomembranes.

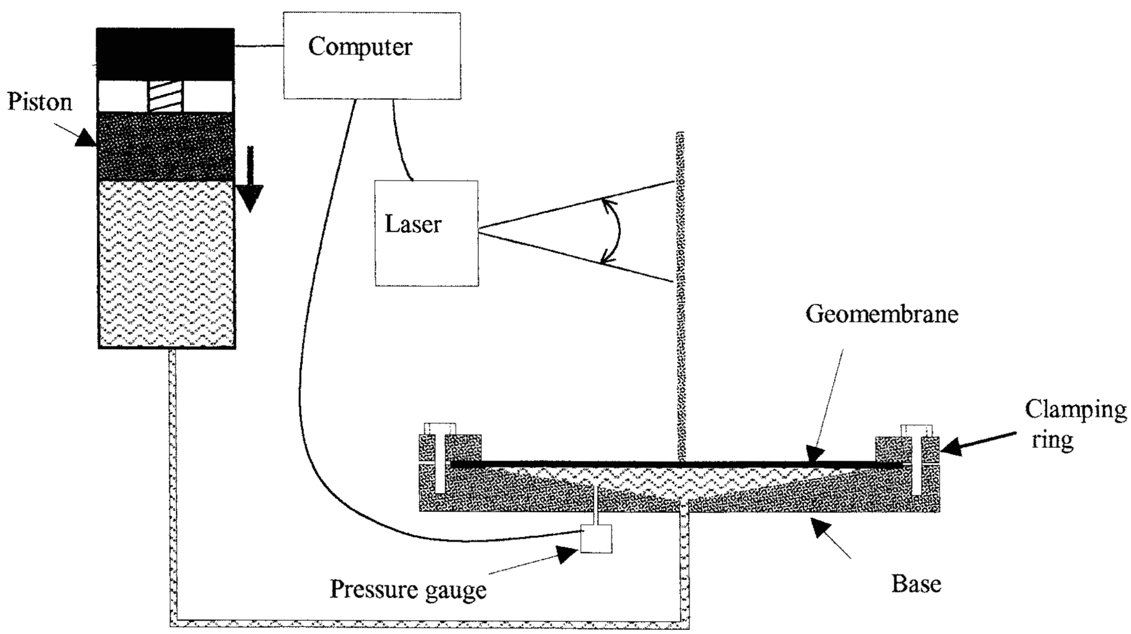

Figure 1. Schematic of the Equipment

Because clamping strength induced a deformation of the geomembrane in the installation process prior to the test, it was necessary to inflate the geomembrane before beginning the test. Thus, there are no measurements for low deflections.

Results are presented with the help of two kinds of graphs: pressure versus deflection and stress versus strain. The first one gives values of raw data, and thereby allows a direct comparison with other studies results providing the diameter of the cell is the same. The second are calculated results, obtained with the help of equations 2 and 3 presented hereafter.

Calculations

Main measurements are water pressure and deflection of the center point. Theoretical calculations based on geometrical considerations and some assumptions allow estimation of strain and stress.

Strain only depends on the deflection. Assuming that during the test the geomembrane deforms as a portion of a sphere, the strain is given by equation 1.

$$\varepsilon = \frac{R \times \alpha}{\left(\frac{d}{2}\right)} - 1 \qquad (1)$$

where

$$R = \frac{\delta^2 + \frac{d^2}{4}}{2 \times \delta} \quad \text{and}$$

$$\alpha = Arc\tan\left[\frac{d}{2 \times (R - \delta)}\right] \text{ when } \delta \le d/2 \text{ and } \alpha = \Pi + Arc\tan\left[\frac{d}{2 \times (R - \delta)}\right] \text{ when } \delta \ge d/2$$

with d the inner diameter of the cell (m), δ the deflection of the geomembrane specimen at the center point (m), R the radius of the sphere (m) and α the half-angle (radius) of the portion of circle between the center point and the edge of the cell (Figure 2). Notations used in this study are adapted from Koerner et al. (1990) taking into account IGS recommendations.

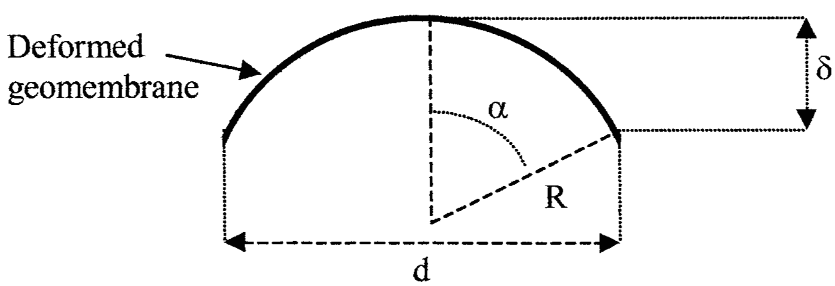

Figure 2. Geometrical Notations

Equation 1 is used during the test to control the way the deflection increases. These calculations are the same as specified by ATSM D 5617-99 and by Merry et al. (1993) when the deformed shape is spherical. In this study, these equations have also been used for other deformed shapes.

The stress was calculated taking into account the variation of thickness of the geomembrane and using the following equation:

$$\sigma = \frac{P \times R}{2 \times t'} \tag{2}$$

with t' the actual thickness (m) of the geomembrane and P the applied pressure (kPa). For this equation, it is assumed that the deformation is spherical and that stress across the geomembrane is uniform.

The estimation of the real thickness of the geomembrane is based on two assumptions: uniform thickness and geomembrane volume conservation (i.e. the material is considered incompressible).

Considering an elementary volume of the geomembrane, for which initial thickness, length and width are respectively t, L_i and W_i, and thickness, length and width during the test are respectively t', L' and W', it comes:

$$dV_i = t \times L_i \times W_i \quad \text{and} \quad dV' = t' \times L' \times W'$$

For this elementary volume, volume conservation gives:

$$t' = t \times \frac{L_i \times W_i}{L' \times W'}$$

But, geometrical considerations show that:

$$\frac{L_i \times W_i}{L' \times W'} = \frac{\alpha_i \times R_i}{\alpha' \times R'}$$

Thus, for the center point of the sphere:

$$t' = t \times \left(\frac{d}{2 \times \alpha \times R} \right)^2 \tag{3}$$

Equation 3 considers the center of the sphere, which is the area of main concern of the tested specimen. It is different from the one proposed by Merry et al. (1993) who considers the whole geomembrane for the real thickness calculation. As deflection increases, Equation 3 gives lower values of t', and thus higher values of σ.

Nevertheless, comparison between results obtained using equation 3 or Merry's equation is possible when the deformed shape is spherical, providing the relation giving the stress from R and P is known (see 'Discussion on the method'). Indeed, specimens are submitted to the same stress during the test and thickness estimation is only used after the test.

Testing Procedure Details

The bottom of the cell was filled with water before placing the specimen. The torque applied on the 16 bolts was 60 daN/m, except for bituminous geomembranes. Then, the geomembrane was inflated by gently introducing water so that its surface was regular in shape. The pressure and deflection necessary to reach this state depended on the type of geomembrane. The test started and stopped after specimen failure, or when the maximum available volume was reached.

Graphs and results presented in this study were obtained on one specimen. Graphs were smoothed for clarity purpose. Indeed, curves exhibited small oscillations for high deflections. Nevertheless, deflections versus time curves do not present such characteristics. The origin of these oscillations is supposed to be the pressure controlling system.

TESTS ON DIFFERENT TYPES OF GEOMEMBRANES

Five common geomembranes made of HDPE, LDPE, PVC, PP and bitumen were tested according to the previously described method. These smooth geomembranes had respective thickness of 1, 1.5, 1, 1.5 and 4 mm.

Results

During the tests, deformed shapes differed from one type of geomembrane to another. At the beginning of the test, all geomembranes deformed in a spherical way but, for HDPE, PP and LDPE, the shape of the geomembrane changed to resemble a cone or a quasi-cylinder with a spherical extremity.

Test results are presented in Figure 3 and Figure 4. Different geomembranes exhibit very different behaviors. These differ from those obtained with uniaxial tensile tests, especially when performed on a narrow specimen.

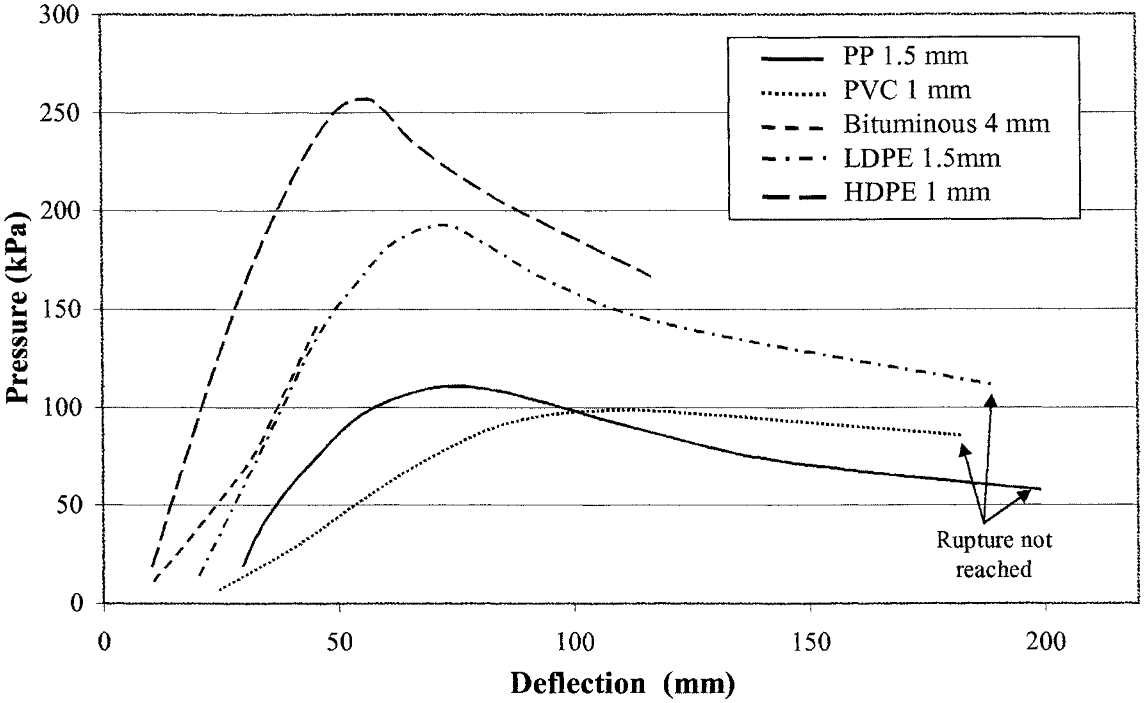

Figure 3. Pressure-deflection Biaxial Test Results on the 5 Geomembranes

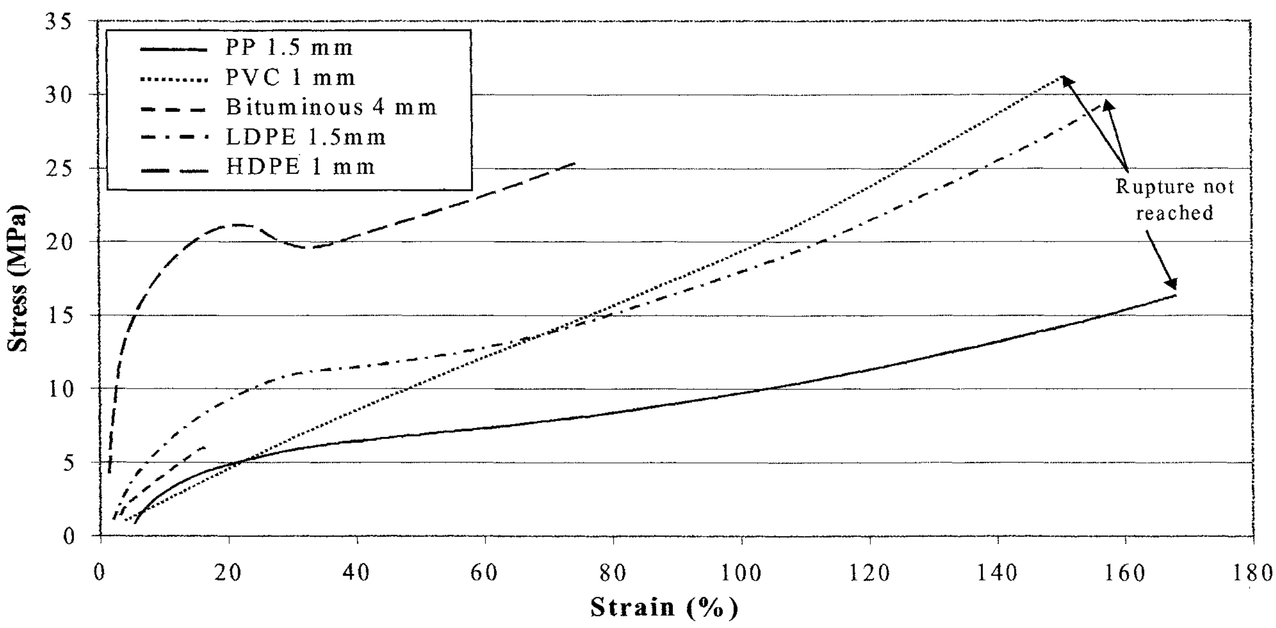

Figure 4. Stress-strain Biaxial Test Results on the 5 Geomembranes

For instance, using the biaxial tensile test, the HDPE geomembrane has smaller values of strain and stress at break than the PVC geomembrane with the same thickness. This is clearly the opposite of what is observed in uniaxial tensile test with a narrow specimen. This leads to a different ranking of products, proving that biaxial tensile testing is not redundant.

Rupture was not reached for PVC, PP and LDPE geomembranes. Nevertheless, after the test, every unbroken specimen exhibited residual deformations, showing that it has been deformed over its elastic limit.

The bituminous geomembranes failed rapidly. In fact, this is due to the incorporated geotextile, which has a low deformation at break. In this case, geotextile failure immediately leads to geomembrane failure.

Table 1gives characteristics at failure, excepting geomembranes labeled with a star. For these, the given value is the last one recorded during the test.

Type of Geomembrane	Stress at Break (kPa)	Strain at break (%)
HDPE	25.8	74.2
LDPE	29.7*	157*
PVC	30.3*	150*
PP	11.6*	167*
Bituminous	6	16.6

Table 1. Geomembranes Characteristics at Break

The moment when the shape becomes different from a sphere depends on the properties of the material. It has been observed that the shape seems to become non-spherical just after the 'peak' observed on pressure-deflection curves. For the HDPE geomembrane this happened for a deflection smaller than d/2, which is in contradiction with ASTM D 5617-99 requirements that suggest that the spherical assumption is valid until the deflection reaches d/2. This is only a visual observation and it is not possible to say if this occurs at the 'peak' or at the yield point, as defined by Soderman and Giroud (95). In the following we will mainly refer to the peak as the moment when the specimen changes of behavior.

For HDPE, and PP geomembranes, the specimen deforms quite spherically until the peak is reached. Then, the plastic zone, that is to say the zone in which the specimen actually changes its mechanical state, propagates from the center of the specimen to a generally circular area around the center of the specimen. From this moment all the deformation will be localized in the plastic zone. For HDPE, and PP geomembranes the rupture is ductile but for PVC geomembranes it is fragile. The rest of the specimen endures almost no deformation.

Contrary to homogeneous geomembranes, the thickness of the bituminous geomembrane should not be taken into account, as the bitumen itself does not really contribute to the resistance of the geomembrane. This method is therefore not adapted to bituminous geomembranes, and the results presented in terms of stress should not be considered. Raw data, that is pressure versus deflection curves, are the only ones to be considered.

Peaks observed on pressure-deflection curves do not correspond to peaks in strain-stress curves. This is due to the fact that the decrease of pressure is over-compensated by the decrease in thickness, leading to an overall increase of stress. This is visible on samples of PP, PVC and LDPE. This also influences HDPE results. In fact, the deflection at 'peak' observed in Figure 3 does not exactly correspond to the peak observed in Figure 4. The latest is about 2 % greater in deflection. This shows that both curves should be examined: the first (pressure vs. deflection) to determine the state of the geomembrane, and the second (stress vs. strain) for characteristics. Differences shown previously may be due to inconsistent calculations. Estimation of thickness and stress is based on many assumptions that may not be valid. Further research on the measurement of the geomembrane thickness at the center of the specimen should be conducted.

This test also allows evaluation of the heterogeneity of the material. This has been observed with tests on HDPE (Badu-Tweneboah et al. 1998) and PP geomembranes performed by the author and not presented herein. This observation can be made both from the deformed shape during the test and from the aspect of the specimen after the test. In fact, heterogeneity can cause a nonsymmetrical shape or an irregular plastic zone. In the latter case, the plastic zone can propagate in the machine direction, following a line of weakness.

TESTS ON FIVE HDPE GEOMEMBRANES OF DIFFERING THICKNESSES

Five geomembranes of 1, 1.5, 2, 2.5 and 3 mm thickness coming from the same producer and made of the same HDPE compound were submitted to the test according to the previously described method. The 1mm thick geomembrane is the same as mentioned in the previous paragraph.

Results

Tests always led to rupture. No heterogeneity of the material was observed from failed specimens. Results are presented in Figure 5 and Figure 6. Figure 5 illustrates the differing of behavior of each geomembrane as a function of its thickness.

For all the geomembranes, the peak is reached at a deflection value of about 55 mm and pressure at peak is proportional to the geomembrane thickness. The thickness does not seem to have any influence on deflection at break, but only on pressure at break.

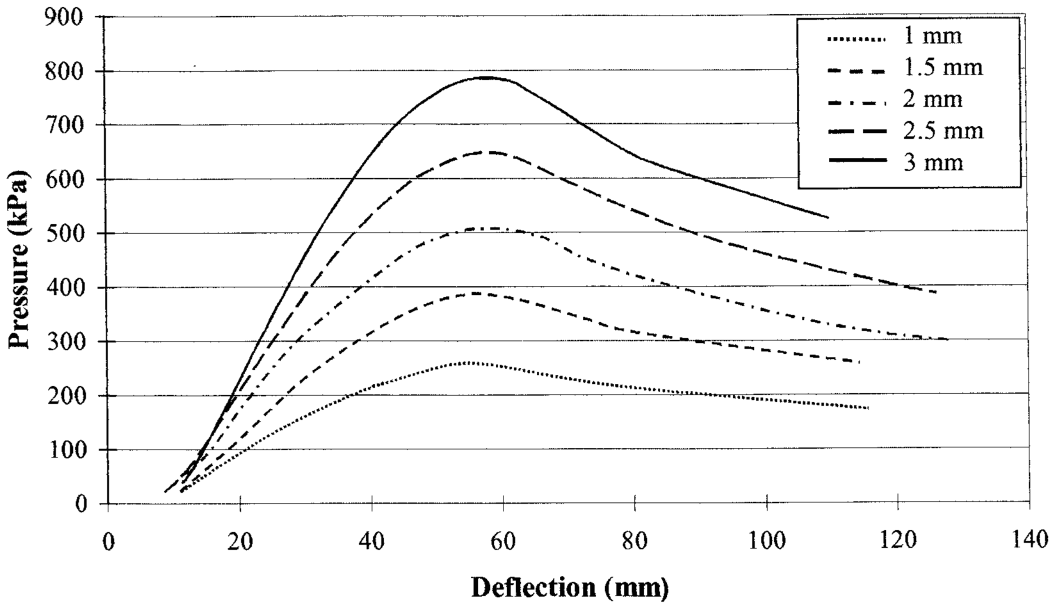

Figure 5. Pressure-deflection Biaxial Test Results on the 5 HDPE Geomembranes

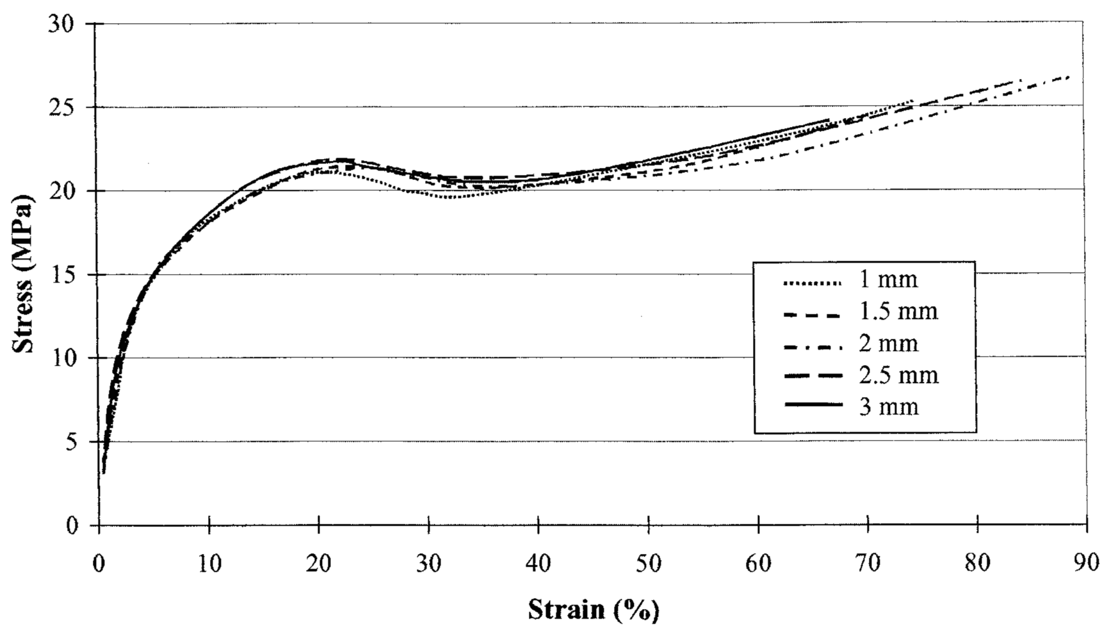

Figure 6. Stress-strain Biaxial Test Results on the 5 HDPE Geomembranes

The pressure that an HDPE geomembrane can endure is relatively high. Nevertheless these values should not be considered "as is" for design purpose because test conditions are not representative of field conditions. The main difference is the relatively high strain rate compared to that in a real application; the test does not take creep into account.

Strain-stress curves (Figure 6) are very similar. Modulus, strain and stress values at peak are shown in Table 2. The secant modulus as defined by Giroud (1992) has been calculated at 4 % strain. This value is the limit of linearity of the curves. Figure 6 shows that this limit is hard to establish and 4 % is a low value. In the limits of validity of the test, and mainly due to the fact that only one specimen has been tested for each geomembrane, it seems that the thickness has no influence on the modulus and on the characteristics at peak.

Geomembrane Thickness (mm)	Secant Modulus at 4 % (MPa)	Peak Stress (kPa)	Peak Strain (%)
1	294	21.6	22
1.5	292	21.7	24.3
2	338	21.9	23.3
2.5	316	22.4	24.3
3	299	22.1	22.8

Table 2. HDPE Geomembrane Biaxial Characteristics

All the remarks made in the previous chapter concerning the 1mm HDPE geomembrane are valid for all the different thickness. The shape was relatively spherical under a deflection smaller than d/2. Peak observed in Figure 6 is 2 % greater in strain than that observed in Figure 5.

OTHER USES OF THE TEST

The biaxial tensile test may also be used for the determination of the degree of damage of geomembranes, due to stones or other elements. This has been previously mentioned in many studies (Badu-Tweneboah et al. 1998). Indeed, one way to characterize the effect of damage is to measure the loss of mechanical properties of the geomembrane. The advantage of the biaxial tensile test is that it allows testing of large-scale specimens, as opposed to uniaxial tensile test. Thus the effective damaged specimen submitted to the biaxial test may present a statistically significant number of puncture points. Figure 7 shows biaxial tensile test losses due to damage on a HDPE geomembrane and on a PVC geomembrane. The HDPE specimen was exposed to severe gravel puncturing. Break was initiated by a dent visible before biaxial test.

This approach is not appropriate to estimate local effects of damage on mechanical properties. Indeed, this method may only determine the influence of localized damage of undetermined initial position on the behavior of a large specimen. Thus, the loss of biaxial mechanical properties due to damage should be considered with great care when trying to estimate a degree of damage.

Finally, the same apparatus may be used for creep tests. This test consists in applying a constant pressure under the geomembrane. Such tests have been performed on different geomembranes at low pressure (about 20 kPa). After a few days a small bubble was observed in the thickness of a transparent PP geomembrane, which finally led to a leak trough the geomembrane. The same thing occurred with a bituminous geomembrane. These simple tests allowed observation of otherwise invisible defects of the material when submitted to low deformation rates.

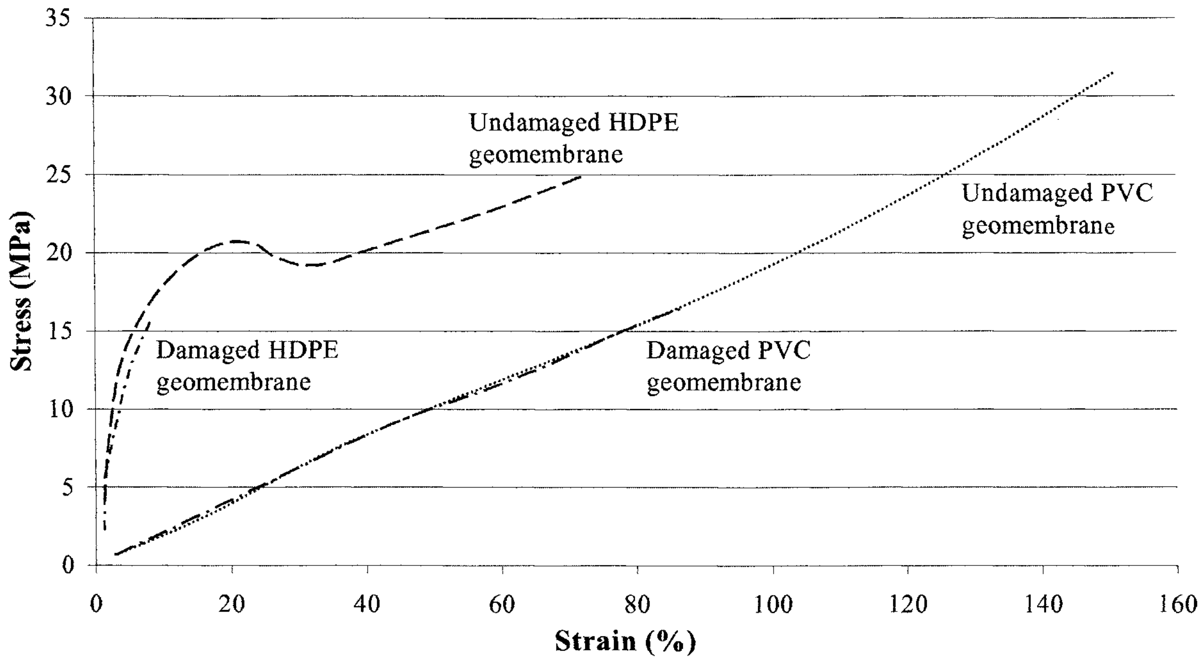

Figure 7. Example of Effects of Damage on Biaxial Characteristics of Geomembranes

DISCUSSION ON THE METHOD

The choice of only considering the spherical assumption for deformation calculations was due to the fact that even if the geomembrane deforms in a non-spherical way, there is no easy and simple method to define its exact shape, and the sole manner is to estimate it visually. Thus, even if the spherical assumption is incorrect, there is no available method to enhance results in a significant and more precise way.

Moreover, a non-spherical deformed shape mainly occurs after the strain is such that the peak is reached and then other assumptions are no longer valid (e.g. uniform thickness). For the same reason results before peak are comparable when performed on different products.

R, α and t' calculations are based on geometrical considerations, and thus depend only on the deflection H, and not on pressure under the geomembrane. The strain rate is constant during the test and D is also a constant. Thus, H, R, α and t'/t only depend on time regardless of the type of tested geomembrane (Figure 8). This graph allows conversion of any stress result of this study into stress values without taking thickness variations into account. This may be necessary to compare the results of this study with other studies or to compare biaxial test results with uniaxial test results where thickness variations are generally not taken into account.

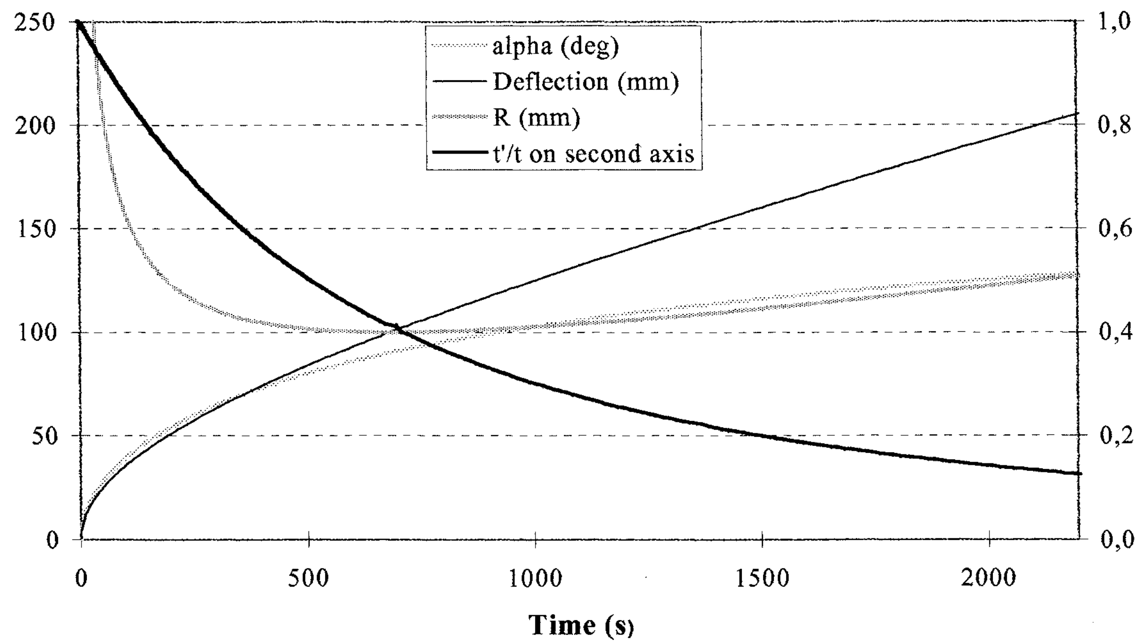

Figure 8. δ, α, R and t'/t as Functions of Time for a 200 mm Diameter Cell

Stress-strain results are greatly influenced by the real thickness estimation. This estimation can be based on a global approach considering the whole specimen, or on a local approach considering the center of the specimen as proposed herein with equation 3. These two estimates lead to different stresses, especially for high deflection. As we are mainly interested in the center of the specimen, the second approach seems to be more appropriate. Moreover, the global approach considers a uniform thickness, which is obviously not the case when performing the test. Nevertheless, the estimation of the strain, as proposed by equation 1 is a global approach. Then, our results are based on two different approaches and this may introduce inconsistency.

CONCLUSION

The results of this study show that the biaxial tensile test, performed at a constant strain rate, is a useful tool providing additional information to uniaxial tensile test. This test can be used to characterize the material itself. Indeed it appeared that results obtained for geomembranes made of the same HDPE compound but of different thickness are very similar in terms of strain-stress relationship.

The method relies on theoretical calculations that are based on assumptions such as spherical deformation and constant thickness. Limits of these have been underlined in this study. Calculations are thus to be enhanced and the so-called biaxial tensile test still needs to be improved to be fully satisfactory. Thus, the evolution from burst test to biaxial tensile test is not yet absolutely achieved. For instance, the test method should be significantly improved by measuring the real thickness of the center of the specimen.

REFERENCES

Badu-Tweneboah, K., Giroud, J.P., Carlson J.P., Scmertmann, G.R., 1998, "Evaluation of the Effectiveness of HDPE Geomembranes Liner Protection", *Sixth International Conference on Geosynthetics Conference Proceedings*, Atlanta, vol 1, pp. 279-284

Giroud, J. P., 1992, "Biaxial Tensile State of Stress in Geosynthetics", *Geotextiles and Geomembranes*, vol. 11, pp 319-325.

Koerner, R. M., Koerner, G. R., Hwu, B, 1990, "Three Dimensional Axi-symmentric Geomembrane Tension Test", Koerner, R. M., Editor, *Geosynthetic Testing for Waste Containement Applications*, Philadelphia, American Society for Testing and Materials, pp. 170-184.

Merry, S. M., Bray, D. B., Bourdeau, P. 1993, "Axisymmetric Tension Testing of Geomembranes", *Geotechnical Testing Journal*, Vol 16, n°3, pp 384-392.

Merry, S.M., Bray, D. 1995, "Size Effects for Multi-Axial Tension Testing of HDPE and PVC Geomembranes", *Geotechnical Testing Journal*, vol. 18, n°4, pp 441-449

Merry, S.M., Bray, D. 1997, "Time-Dependant Mechanical Response of HDPE Geomembranes", *Journal of Geotechnical and Geoenvironmental Engineering*, vol. 123, n°1, pp 57-65

Nobert, J., 1993, "The Use of Multi-axial Tensile Test to Assess the Performance of Geomambranes", *Geosynthetics '93 Conference Proceedings*, Vancouver, Canada, vol. 2, pp 685-702.

Soderman, K. L., Giroud, J. P. 1995, "Relationship Between Uniaxial and Biaxial Stresses and Strains in Geosynthetics", *Geosynthetics International*, vol. 2 n°2, pp 495-504.

GEOMETRIC AND SPATIAL PARAMETERS OF GEOMEMBRANE WRINKLES ON LARGE SCALE MODEL TESTS

NATHALIE TOUZE-FOLTZ, CEMAGREF, FRANCE
JEAN SCHMITTBUHL, ENS PARIS, FRANCE
MICHEL MEMIER, SINTEGRA, FRANCE

ABSTRACT

Photogrammetry was used to evaluate the distribution of wrinkles on three geomembranes: two made of high density polyethylene and one made of polypropylene. Results are presented in terms of the geometry of wrinkles and relative position of the various wrinkles obtained in the HDPE geomembranes. In all cases wrinkles developed in two preferential directions, nearly normal to each other. The maximum height of wrinkles is about 0.1m with a maximum distance between wrinkles equal to 1.6 m. Lengths of wrinkles vary between 0.5 and 4 m, widths between 0.1 and 0.8 m. Results obtained were used to feed a mathematical model for estimating the liquid flow rates through composite liners in the case of two interacting wrinkles. Results obtained with the polypropylene geomembrane could not be interpreted.

INTRODUCTION

Geomembranes used for the sealing of landfills often have holes caused by inadequate seaming, puncture, tears, etc. A recent synthesis of studies involving electrical leak detection systems (Rollin and Jacquelin 2000) reports a hole density varying from 2 to 26 defects per hectare after installation of the geomembrane. These defects form preferential advective leachate flow paths through the geomembrane. A number of analytical solutions (Brown et al. 1987; Rowe 1998; Touze-Foltz et al. 1999) and empirical solutions (Giroud 1997) have been developed to quantify rates of liquid flow for holes in flat or wrinkled geomembranes.

Nine large scale tests, about 50 m^2 each, have been conducted during the summer 1999, on the landfill site of Claye-Souilly, France. The purpose of these tests was to quantify the hydraulic performance of composite liners when the geomembrane is damaged, and thus check the validity of the existing analytical and empirical equations.

One of the key parameters to understanding the flow patterns obtained at the soil-geomembrane interface in these experiments is the spatial distribution of voids between both components, namely clay and geomembrane, of the composite liners. In practice, it is likely that soil and geomembrane surfaces are not flat and parallel. Vallejo and Zhou (1995) and Dove and Frost (1996) have shown that geomembrane surfaces are not perfectly smooth and exhibit a certain roughness. Moreover, in the field geomembranes expand when they are heated by the sun, and wrinkles appear. This is one of the three sources of imperfections affecting contact conditions between the soil and the geomembrane as identified by Rowe (1998). The other two concern the soil surface: protrusions related to particle size distribution and undulations/ruts appearing when the soil is compacted close to its plastic limit.

In order to evaluate this distribution of voids in composite liners between the compacted clays and the geomembranes, photogrammetry was conducted on three of these large scale tests. Specifically, photogrammetry was used to quantify the topography of two pieces of high density polyethylene (HDPE) geomembranes, and one piece of flexible polypropylene (PP) geomembrane which had been placed over the compacted clays.

The objectives of this paper are first of all to detail the materials and methodology used to quantify the features of the observed wrinkles. Then the main results obtained are presented, and compared to existing results. Finally, an analytical solution previously developed to predict the reduction of rates of liquid flow through a composite liner due to two interacting wrinkles will be used with the data collected from these large scale tests.

MATERIALS AND METHODS

Geomembranes

Photogrammetry was used to determine the features of wrinkles observed on three of the large scale tests conducted at a landfill site in Claye-Souilly, France. These three large scale tests were made of a compacted clay liner (CCL), 0.3 m thick and a geomembrane. Two different geomembranes were tested:

- an HDPE geomembrane, 2 mm thick. The dimensions of the two pieces of HDPE geomembranes used were 7.5×7.5 m^2; they will be called HDPE 1 and HDPE 2 in the following; the coefficient of linear thermal expansion of HDPE geomembranes varies between 14 and 30×10^{-5} °C (Pelte 1993);
- a PP geomembrane, 1.5 mm thick. The dimensions of the piece of PP geomembrane used was 5.8×5.8 m^2. The coefficient of linear thermal expansion of PP is 10×10^{-5} °C (Montell 1998).

These three pieces of geomembrane were installed on a CCL, 10×50 m^2, as shown on Figure 1. In order to prevent the geomembranes from flying away, they were anchored by sand berms at their periphery, 0.5 m wide and 0.3 m high. There was no seam at all in the geomembranes.

Photogrammetry

The first step of the photogrammetry process consists in preparing the geomembrane and in locating the coordinates of spherical targets installed on the geomembrane.
The geomembranes used were black. In order to increase the visual contrast, necessary to allow a good perception of the stereoscopic model, some white paint was randomly spread on the three pieces of geomembrane.

Figure 1. View of the Anchored Geomembranes. From left to right: HDPE 1, HDPE 2, PP.

Ground control point measurements consisted of determining the coordinates of particular points visible on the photographs to deduce the position and orientation of the photographs. Thus, thanks to the observation of image coordinates (x,y) on at least two photographs taken from different points and under different orientations, one can calculate the spatial coordinates (X,Y,Z) of the observed point calculating the intersection of the two homologous perspective rays (see Figure 2). The particular points of interest were the centers of twelve spherical targets placed on each geomembrane as shown on Figure 1. In order to know the exact position of each of these targets, a topographic survey was carried out using a theodolite.

In a second step, photographs were taken. The photographs must be taken in good lighting to clearly show the image coordinates, with a camera which internal geometry is well known. The camera used had a 100 mm focal length. The serviceable format of negatives used was 160 x 110 mm^2.

Two stereoscopic couples of photographs were taken for each geomembrane at a scale of 1/70. This corresponds to a vertical distance equal to 7 meters between the camera and the geomembrane. The camera was installed on an engine which lifted it up, as shown on Figure 3. Position and approximate orientation of the points from which the photographs were taken were controlled thanks to observations realized with the theodolite.

Photographs were taken between 10:00 AM and 1:00 PM. The weather was cloudy and the outside temperature was about 24 °C. The temperature at the surface of the geomembranes was not measured.

The third step, called survey, consisted in calculating the necessary parameters and identifying homologous perspective rays by correlation and spatial transforms. This step was carried out using a stereocomparator, by stereoscopic binocular vision. As geomembrane deformations are continuous, they could be objectively modeled by a sowing of points 0.1 m apart. The precision of data obtained was 1.2 mm.

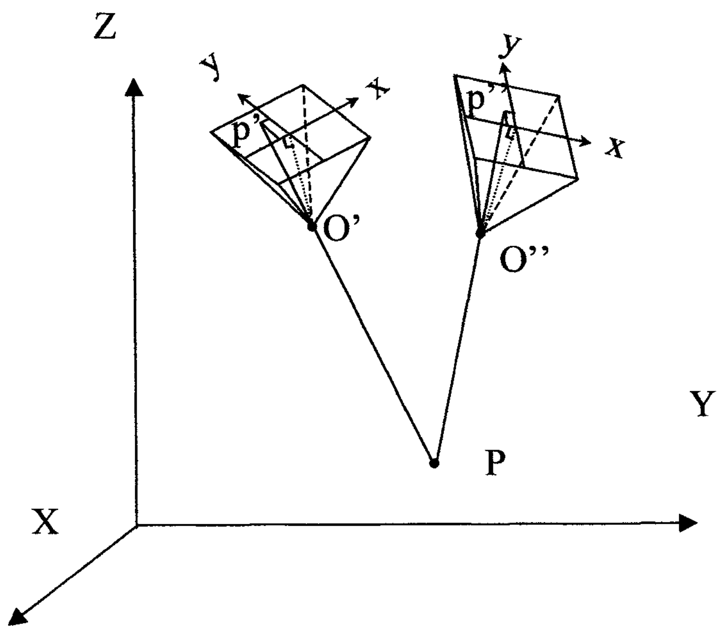

Figure 2. Location of Object P Using Two Images in Perspective

Figure 3. View of the Camera and of the Engine Used to Lift Up the Camera Before Taking Photographs

RESULTS OBTAINED

HDPE Geomembranes

Figures 4 and 5 show the position of the wrinkles in geomembranes HDPE 1 and HDPE 2, respectively. One can observe that the maximum height of wrinkles was about 0.12 m for HDPE 1 and 0.09 m for HDPE 2. Detailed results are presented in the following regarding the length, width, height, orientation of wrinkles and distance between centers of gravity of adjacent wrinkles. Since data were obtained only for 34 small to large wrinkles, no attempt was made to fit a statistical law to the obtained data.

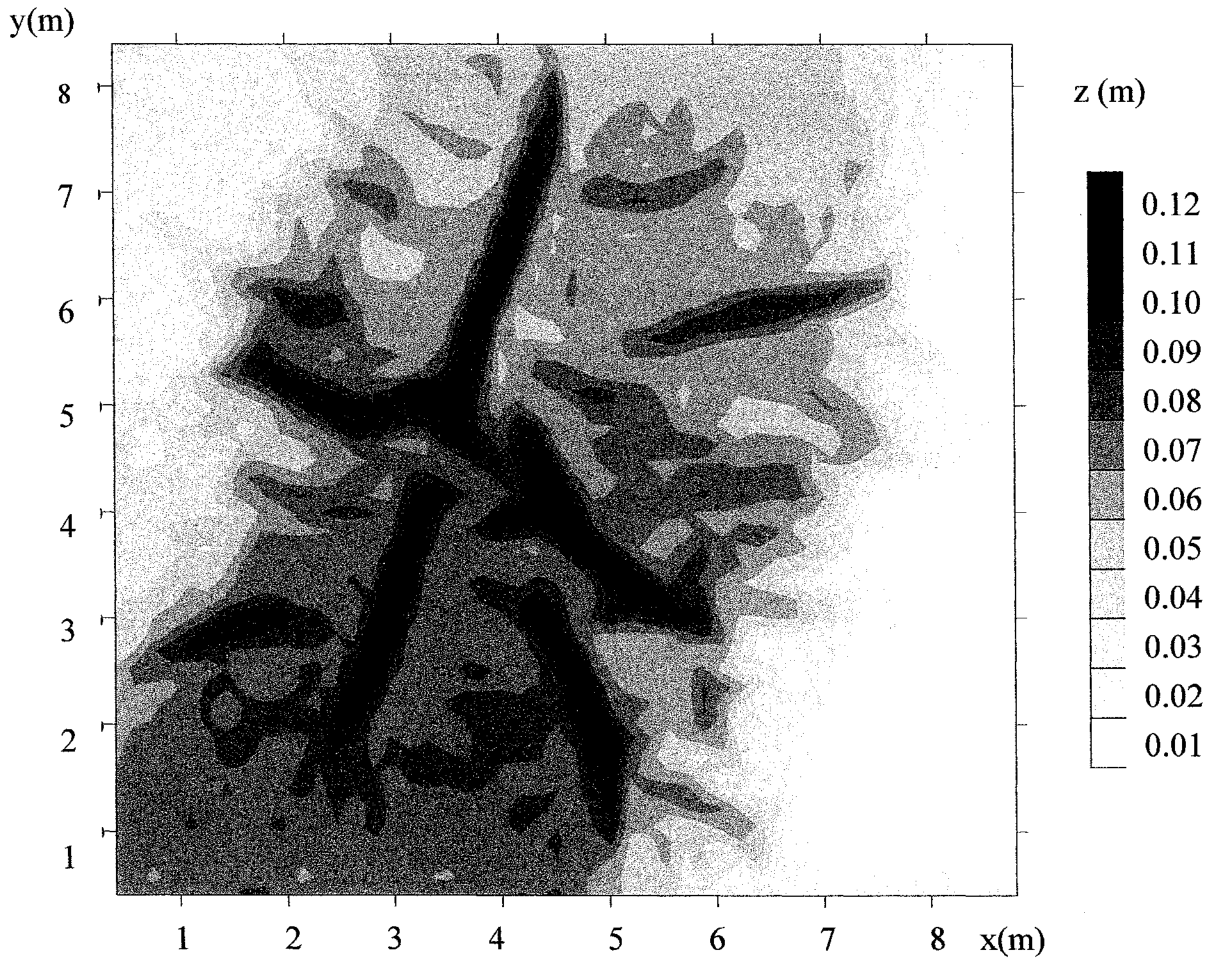

Figure 4. Geometry and Respective Positions of Wrinkles in Geomembrane HDPE 1

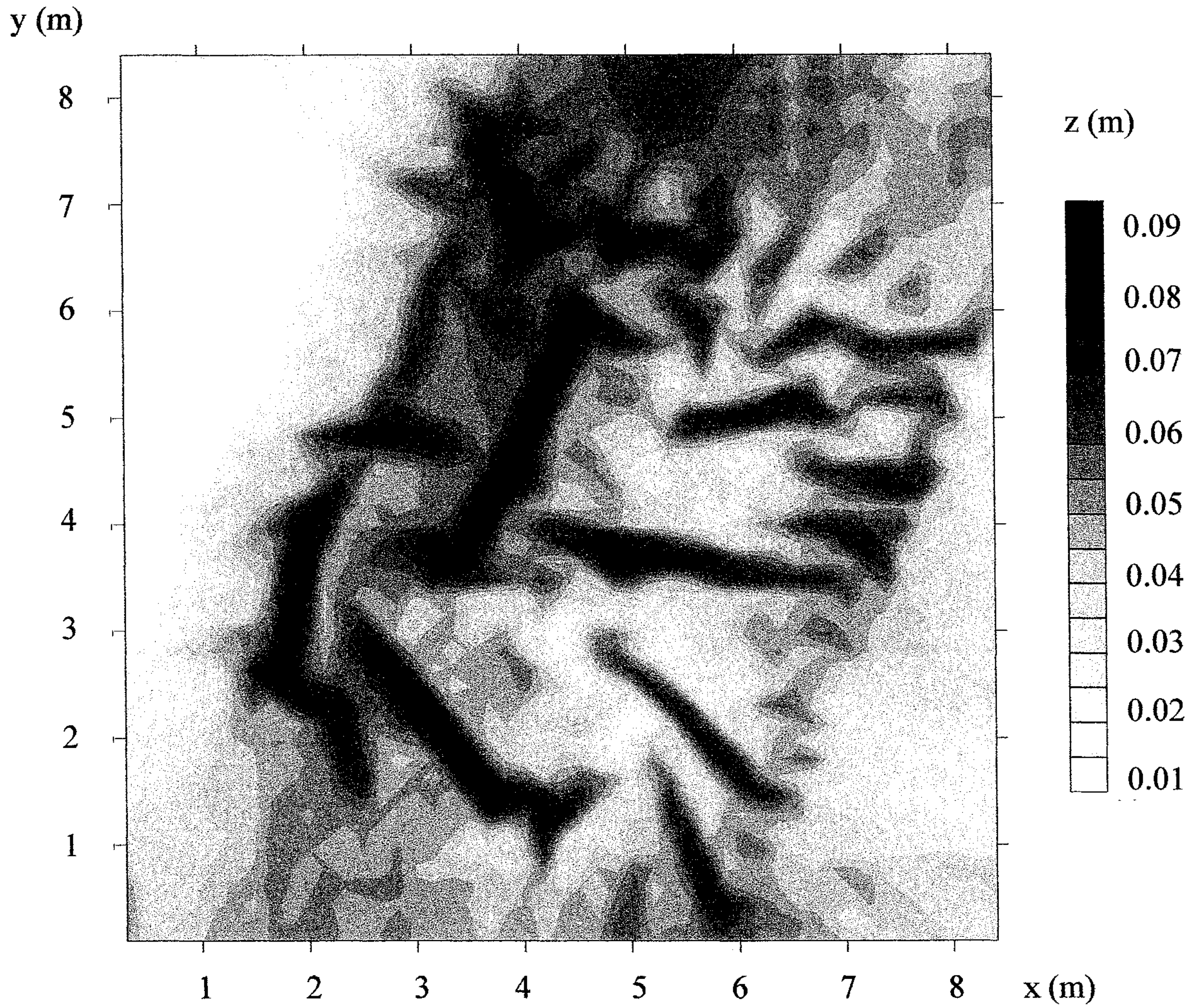

Figure 5. Geometry and Respective Positions of Wrinkles in Geomembrane HDPE 2

Lengths of wrinkles measured were less than 4 m on both large scale tests. Most wrinkles were 1 to 2 meters long as shown on Figure 6. These small lengths can be explained by the dimensions of the geomembranes used, that are not representative of real size geomembranes.

As shown by Figure 7, the mean width of wrinkles varies between 0.1 and 0.8 m. Most wrinkles are 0.3 to 0.6 m wide.

As far as the maximum height of wrinkles is concerned, it varies, as shown by Figure 8, between 0.05 and 0.13 m. A peak is obtained for maximum heights greater than 0.07 m and less than 0.09 m.

Distances between centers of gravity of adjacent wrinkles vary between 0.3 m and 1.6 m (See Figure 9). Maximum values were obtained for HDPE 1 at distances of about 1 m and at distances varying between 0.6 and 0.7 m for HDPE 2.

Figure 10 shows that most wrinkles developed in two directions, normal to each other. These directions are nearly the same for both HDPE geomembranes. They correspond to the machine and cross directions.

Comparison to Existing HDPE Results

The size and spacing of wrinkles have been shown to depend on temperature and on geomembrane characteristics such as color, coefficient of thermal expansion, roughness and flexibility. Giroud and Morel (1992) theoretically calculated the distance l_{bw} between two adjacent parallel wrinkles of infinite length to be of the order of 10 m with a height of the wrinkle of the order of 0.1 m for high density polyethylene (HDPE). Pelte et al. (1994) compared site measurements and mathematical calculations and found that for a 1.5 mm thick HDPE geomembrane l_{bw} was about 5 meters with a wrinkle height of around 0.1 m and a wrinkle half-width, b, of about 0.15 m.

The results presented in this paper tend to show that predictions given by Giroud and Morel and Pelte underestimate the wrinkling of geomembranes. Indeed, if the height of wrinkles observed are in good agreement with existing data, distances measured between adjacent wrinkles are lower than predictions. Nonetheless, one has to observe that we did not make a distinction between wrinkles and that we did not only consider parallel wrinkles but all wrinkles observed. This can be an explanation. A second possible source of difference may be linked with the size of the geomembranes tested here.

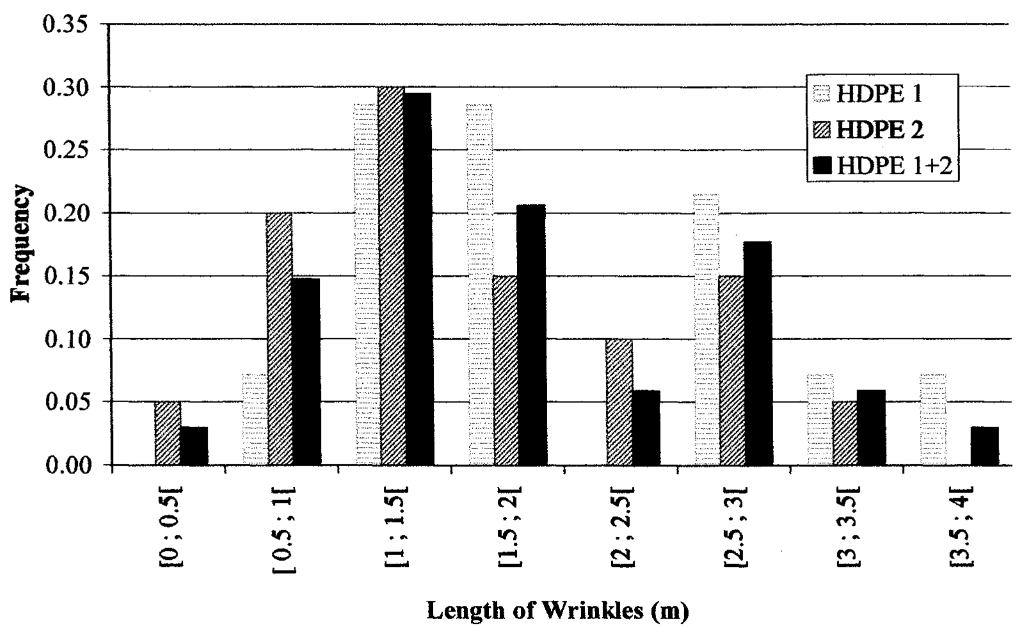

Figure 6. Length of Wrinkles Measured on Geomembranes HDPE 1 and HDPE 2

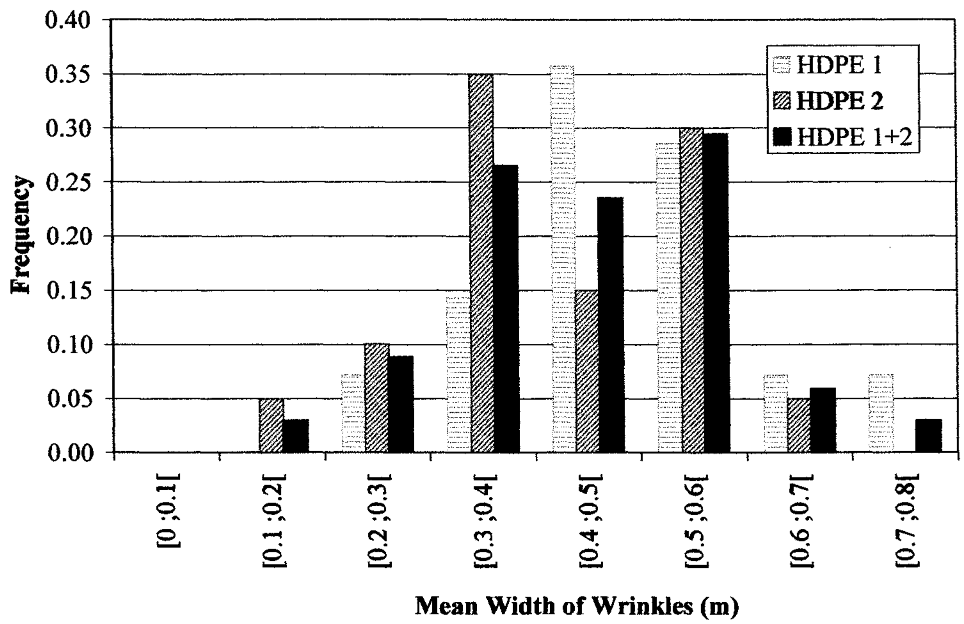

Figure 7. Mean Width of Wrinkles Measured on Geomembranes HDPE 1 and HDPE 2

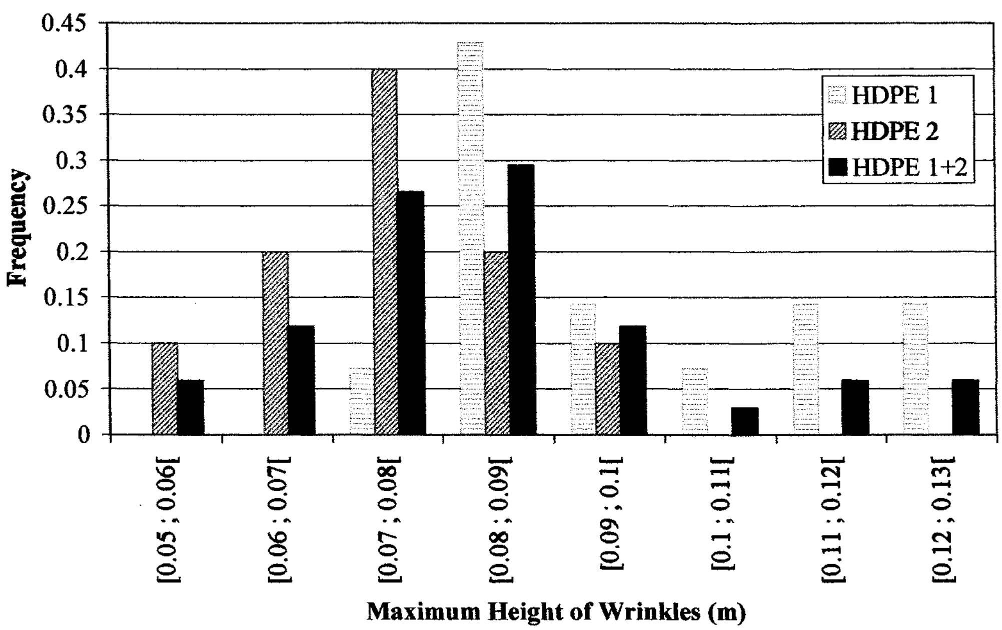

Figure 8. Maximum Height of Wrinkles Measured on Geomembranes HDPE 1 and HDPE 2

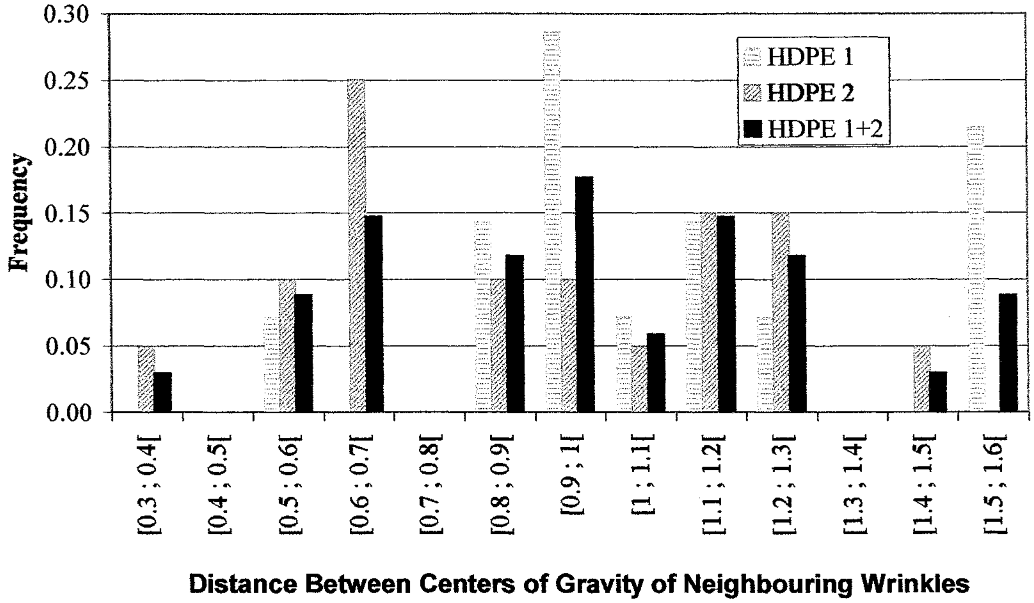

Figure 9. Distance Between Centers of Gravity of Neighboring Wrinkles Measured on Geomembranes HDPE 1 and HDPE 2

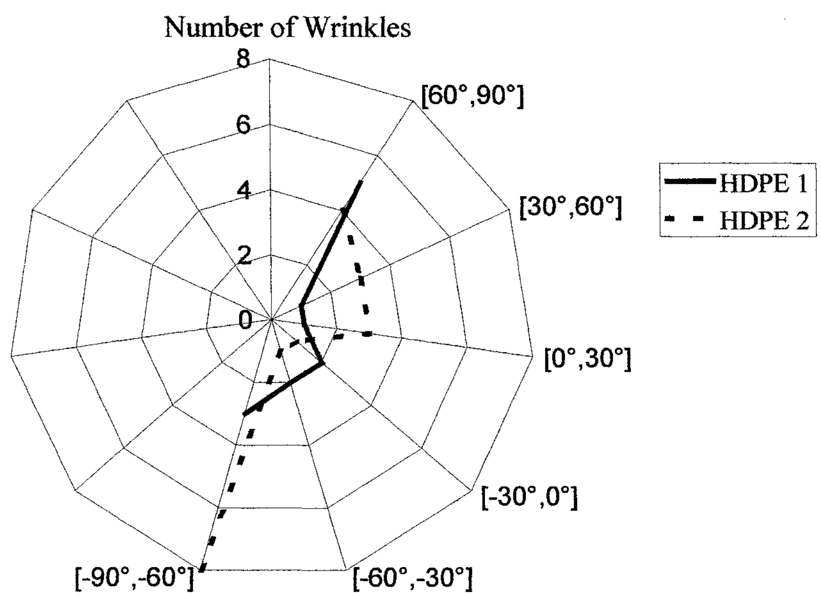

Figure 10. Orientation of Wrinkles on Geomembranes HDPE 1 and HDPE 2

PP Geomembrane

As far as the PP geomembrane is concerned, Figure 11 shows the spatial repartition of elevations in it. One can first notice that they are lower than 0.04 m and that no wrinkles clearly appear. Results could not be interpreted in the same way as those obtained with HDPE.

As a result, it seems that PP is less subject to wrinkling than HDPE, but this tendency needs to be confirmed all the more as the coefficients of linear thermal expansion for both geomembranes are in the same order of magnitude. Indeed, results obtained with HDPE and PP geomembranes cannot be compared since the dimensions of the geomembranes were different.

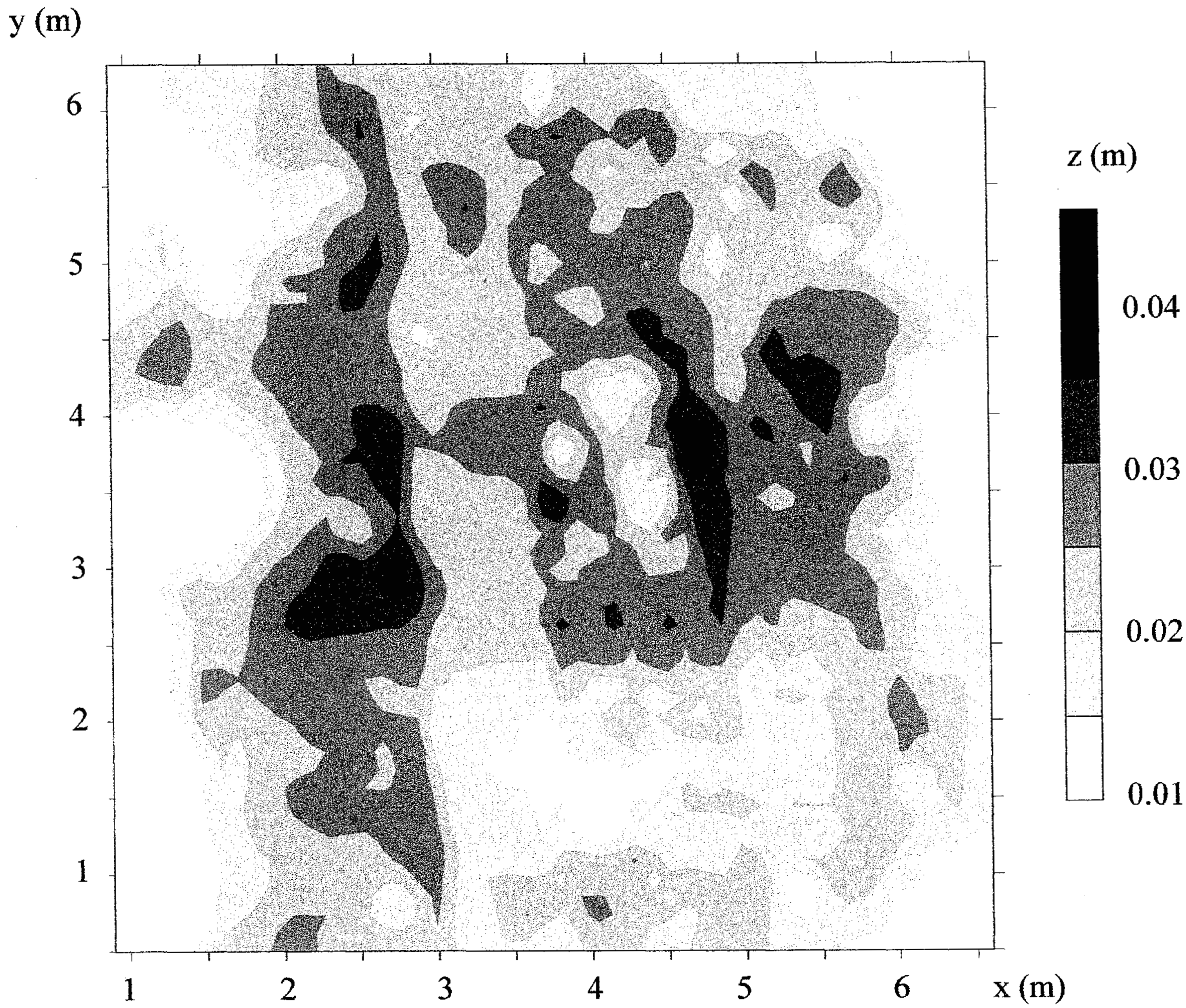

Figure 11. Geometry and Respective Positions of Wrinkles in the PP Geomembrane

EVALUATION OF THE REDUCTION OF RATES OF FLOW DUE TO TWO INTERACTING WRINKLES

Assumptions

The general liner system considered (Figure 12) follows from Rowe (1998) and Touze-Foltz et al. (1999) and includes a geomembrane resting on a low-permeability clay liner of thickness H_L and hydraulic conductivity k_L. The z-axis origin corresponds to the top of the soil liner with upward being positive. The soil liner rests on a more permeable foundation or attenuation layer of thickness H_f and hydraulic conductivity k_f which itself rests on a highly permeable layer that can be either an aquifer or a leakage collection layer. Following from Brown et al. (1987) it is assumed that the geomembrane is not in perfect contact with the soil liner and that there is a uniform transmissive zone or wetted area between the geomembrane and the soil liner surface that is referred to as the "transmissive layer." In the following, it is assumed that: (i) liquid flow is under steady state conditions; (ii) the soil liner and the foundation layer are saturated; and (iii) liquid flow through the liner and foundation layer is vertical.

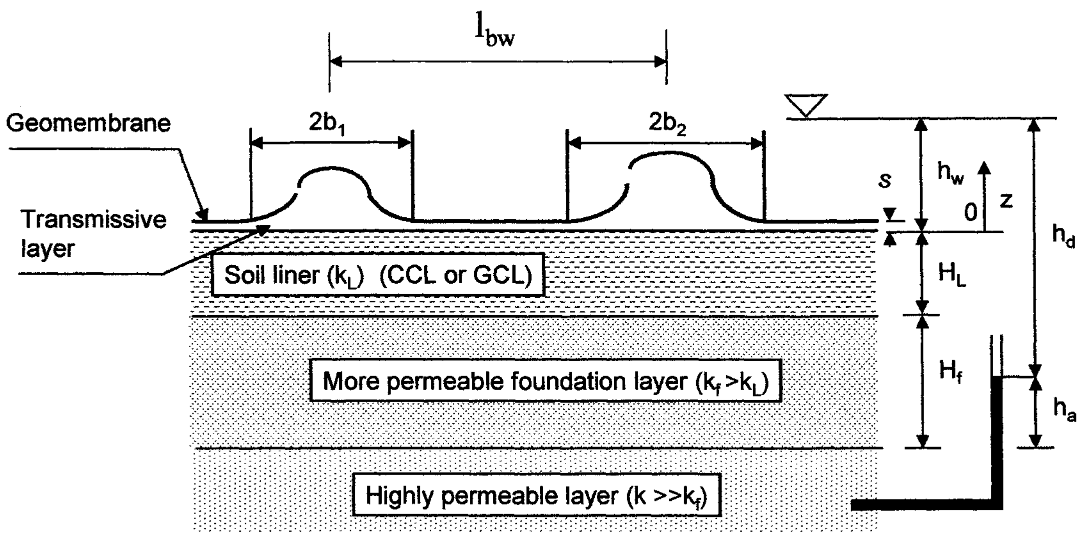

Figure 12. Schematic Showing two Parallel Damaged Wrinkles and the Underlying Strata (Modified from Rowe (1998) and Touze-Foltz et al. (1999))

No particular assumptions are made regarding the dimension, position, or the number of holes in the wrinkles, but rather it is assumed that the rate of liquid flow through the composite liner is not limited by the holes (the hole limiting case is discussed by Rowe (1998) and Touze-Foltz et al. (1999)). Liquid flow in the transmissive layer is assumed to be in the x-direction (see Figure 12), normal to the longitudinal axis of the wrinkle. The problem shown schematically in Figure 12 involves two parallel wrinkles that are long enough to neglect the end effects. It is assumed that both the hydraulic head on top of the geomembrane and the hydraulic transmissivity between the geomembrane and the soil liner are uniform.

A subscript 1 refers to the wrinkle at the left hand side of Figure 12 and subscript 2 to the one at the right hand side. The origin of abscissa is positioned at the centre of Wrinkle 1. The length between wrinkles, l_{bw}, is the total distance between the centres of Wrinkle 1 and Wrinkle 2.

Rate of Liquid Flow

Touze-Foltz et al. (1999) obtained the total rate of liquid flow between the wrinkles, Q, taking into account the liquid flow into the soil liner under the wrinkles:

$$Q = Lk_s i_s\left[b_1 + b_2 + \frac{2}{\alpha}\tanh\left[\alpha\left(\frac{l_{bw} - b_1 - b_2}{2}\right)\right]\right] \tag{1}$$

where b_1 and b_2 are respectively the half-width of Wrinkles 1 and 2, L is the length of wrinkle considered and i_s is the maximum mean hydraulic gradient through the liner and foundation (Rowe 1998):

$$i_s = 1 + \frac{h_w - h_a}{H_L + H_f} \tag{2}$$

When a hydraulic head, h_w, is applied on top of the composite liner, and where h_a is the hydraulic head in the highly permeable layer. The equivalent hydraulic conductivity, k_s, corresponding to the liner and the foundation layer is (Rowe, 1998):

$$\frac{H_L + H_f}{k_s} = \frac{H_L}{k_L} + \frac{H_f}{k_f} \tag{3}$$

α is defined by (Rowe 1998):

$$\alpha = \sqrt{k_s / \theta (H_L + H_f)} \tag{4}$$

where θ is the hydraulic transmissivity of the transmissive layer. The rate of liquid flow contribution Q' from the zone between the edges of the wrinkles is:

$$Q' = \frac{2Lk_s i_s}{\alpha}\tanh\left[\alpha\left(\frac{l_{bw} - b_1 - b_2}{2}\right)\right] \tag{5}$$

The maximum value of Q', Q'_{max}, is obtained when the wrinkles no longer interact under saturated flow conditions and can be derived from Touze-Foltz et al. (1999) under the form:

$$Q'_{max} = \frac{2Lk_s i_s}{\alpha} \tanh\left[\cosh^{-1}\left(\frac{h_w + H_L + H_f - h_a}{H_L + H_f - h_a}\right)\right] \quad (6)$$

Reduction of the Rate of Liquid Flow Through a Composite Liner Due to Two Interacting Wrinkles

Touze-Foltz et al. (1999) have shown that the potential interaction between wrinkles is an issue of interest for CCL–geomembrane composite liners when the distance between two adjacent wrinkles varies between 2.5 and 8.7 m for a hydraulic head, h_w, equal to 0.3m on top of the composite liner. Therefore, considering the distance between wrinkles measured in HDPE geomembranes as described in this paper, the interaction between wrinkles can be an issue of interest. The following illustrates the potential reduction of the rate of liquid flow through a composite liner due to two interacting wrinkles in the case of a geomembrane in good contact with a CCL. Good contact conditions have been defined by Giroud (1997).

For a 0.6 m thick CCL, with k_L equal to 1×10^{-9} ms^{-1}, the hydraulic transmissivity, θ, between the geomembrane and the CCL is equal to 1.6×10^{-8} m^2/s, according to Rowe (1998). If we assume that l_{bw} is 1.6 m, the maximum value observed in the study presented here, and b_1 and b_2 are respectively 0.15 m and 0.3 m, then Q' is equal to 0.15 l/d for one meter of wrinkle if we assume a hydraulic head equal to 0.3 m on top of the composite liner. Q'_{max}, calculated from Equation (6) is equal to 0.6 l/day for one meter of wrinkle. As a consequence, the reduction of flow rate due to the interaction between both wrinkles is 75 %.

CONCLUSION

Photogrammetry has proved to be a very useful tool to quantify wrinkles parameters in HDPE geomembranes, such as length, width, height, orientation and distance between adjacent wrinkles. Data obtained are consistent with previous results as far as the maximum height of wrinkles is concerned, but not for the mean distance between adjacent wrinkles. Results obtained on this particular experiment will have to be checked on larger pieces of geomembranes. The data presented in this paper will be used for future predictions of rates of liquid flow through composite liners thanks to existing analytical solutions of mathematical models.

ACKNOWLEDGEMENTS

The Claye-Souilly experiment has been conducted in collaboration with the INSA de Lyon. The authors gratefully acknowledge the Routière de l'Est Parisien who welcomed the experiments, and Siplast, for providing the geomembranes.

REFERENCES

Brown, K.W., Thomas, J.C., Lytton, R.L., Jayawickrama, P. and Bhart, S. (1987) "Quantification of Leakage Rates through Holes in Landfill Liners", U.S. EPA Report CR810940, Cincinnati, 147 p.

Dove, J. E. and J. D. Frost (1996). "A Method for Measuring Geomembrane Surface Roughness." *Geosynthetics International,* Vol. 3, No. 3, pp. 369-392

Giroud, J.P. (1997) "Equations for Calculating the Rate of Liquid Migration Through Composite Liners Due to Geomembrane Defects", *Geosynthetics International*, Vol. 4, No. 3-4, pp. 335-348.

Giroud, J.P. and Morel, F. (1992) "Analysis of Geomembrane Wrinkles", *Geotextiles and Geomembranes*, Vol. 11, No. 3, pp. 255-276 (Erratum : 1993, Vol. 12, No. 4, p. 378).

Montell Polyolefins (1998) "Polypropylene. Astryn Flexible PP. High Performance Materials for Geomembranes". Documentation.

Pelte, T. (1993) "Etude théorique et expérimentale de la fonction étanchéité et du comportement thermique des géomembranes" Thèse de doctorat, Université Josph Fourier, Grenoble, France, 253 pages.

Pelte T., Pierson P. and Gourc J.P. (1994) "Thermal Analysis of Geomembrane Exposed to Solar Radiation", *Geosynthetics International*, Vol. 1, No. 1, pp. 21-44.

Rollin, A.L. and Jacquelin, T. (2000) "Geomembrane Failures: Lessons Learned from Geo-Electrical Leaks Surveys" to be published in *Lessons Learned from Failures Associated with Geosynthetics*, J.P. Giroud. (To appear).

Rowe, R.K. (1998) "Geosynthetics and the minimization of contaminant migration through barrier systems beneath solid waste", Keynote paper, *Proceedings of the Sixth International Conference on Geosynthetics*, Atlanta, March 25-29, Vol. 1, pp. 27-103.

Touze-Foltz, N., Rowe, R.K. and Duquennoi, C. (1999) "Liquid Flow Through Composite Liners due to geomembrane Defects: Analytical Solutions for Axi-symmetric and Two-dimensional Problems", *Geosynthetics International*, Vol. 6., No. 6, pp. 455-479.

Vallejo, L. E. and Y. Zhou (1995). "Fractal Approach to Measuring Roughness of Geomembranes." *Journal of Geotechnical Engineering*, Vol. 121, No. 5, pp. 442-446.

COMPARISON OF RESULTS USING THE STEPPED ISOTHERMAL AND CONVENTIONAL CREEP TESTS ON A WOVEN POLYPROPYLENE GEOTEXTILE

THOMAS.L. BAKER, BP
UNITED STATES OF AMERICA
J. SCOTT THORNTON, TEXAS RESEARCH INTERNATIONAL, INC.
UNITED STATES OF AMERICA

ABSTRACT

The objective of this effort was to determine the validity of the stepped isothermal method (SIM) as a tool for investigating the long-term creep performance of woven polypropylene geotextile products. Creep data for a woven polypropylene geotextile were obtained using both SIM and conventional methods of time-temperature superposition (TTS). Applied load levels varied from 20% to 70% of the ultimate tensile strength (UTS). The tests were continued until rupture or the maximum strain, as determined by equipment travel limitations. Shifted rupture or run-out times in excess of ten years were readily obtained with either method, but the test times were orders of magnitude shorter for SIM. The results for creep strain and rupture time were the same for both SIM and conventional methods within anticipated variation attributed to lot-to-lot and sample-to-sample differences that are normally encountered with this material.

INTRODUCTION

Conventional ambient temperature creep tests coupled with elevated temperature creep tests to allow time-temperature superposition and projection of long-term creep performance have a long history. The validity of these procedures is accepted but it is generally time consuming to perform all the necessary testing, with a complete sequence of tests taking 18 months or more. The stepped isothermal method (SIM) of time-temperature superposition (TTS) offers a much quicker method of acquiring the same information. Using SIM, 10,000-hour creep test information can be obtained in less than 24 hours. The stepped isothermal method of characterizing long term creep performance has been shown to work with polyester geosynthetics (Thornton et al. 1998), but has not previously been used on polypropylene. This paper presents the results of a series of tests comparing SIM and the conventional creep and TTS testing method for characterizing the long-term creep performance of a woven polypropylene geotextile.

The details of the mechanics of performing and analyzing SIM have been given in detail previously (Thornton et al. 1997 and 1998). In brief, SIM is a method of performing a creep test in which one specimen is placed under load and subjected to a sequence of incremented temperatures. Strain, temperature and load are measured continuously throughout the test. For each step in temperature a time equivalent to the starting point time, which would be obtained if the temperature step were performed by itself and not in sequence, is determined. The initial time, referred to as t' in previous work, is obtained by iteratively varying the time until a close match between the slope of the creep modulus/log time plot of the beginning portion of the temperature step under consideration matches the ending slope of the previous temperature step. After the equivalent starting times have been determined (ending and beginning creep modulus/log time slopes matched), the shift factor (log A_T) is determined by iteratively varying it until the log time at the beginning of the step under consideration matches that at the end of the previous step. After completing these steps, a composite creep modulus/log time has been constructed which can be converted into a more conventional creep strain/log time plot. By use of SIM, material responses that can take over a year to determine by conventional TTS methods can be measured in 24 to 36 hours.

PROCEDURES

For this work a sequence of SIM tests were performed on both the warp (machine) and fill (cross machine) directions of a woven polypropylene fabric. These were compared to conventional creep tests at ambient and elevated temperatures, which had been performed previously. The BP, Fabrics and Fibers Business Unit Research and Technology Center (Lab 1) performed the testing except for four tests performed by TRI/Environmental (Lab 2), which are shown to demonstrate the interlaboratory reproducibility of results.

The SIM tests performed at Lab 1 were done using an Instron 5500R load frame with Instron Merlin software for load and strain control and measurement. Strain measurements were made using either an Instron 25mm travel LVDT (linear voltage differential transducer) or an Epsilon 3543, 50mm gage length and 50mm travel, extensometer interfaced into the load frame. The tests were performed inside an Instron model 3119-007 environmental chamber, which had been modified by replacing the stock controller with a Watlow F4 programmable controller. The environmental chamber was later further modified by installing a faster responding thermocouple than the factory original, as it was found that the relatively slow response time of the stock thermocouple on the environmental chamber inhibited control at a steady temperature. A homemade cooling coil operated off a surplus lab chiller was installed inside the chamber to provide a background level of cooling and facilitate initiating the tests at 20°C. Without the cooling coil the chamber operated at about 25°C. Temperatures were measured and recorded using an Omega data logger with an Omega model SRTD-2 RTD (resistance temperature detector) temperature probe. This model RTD is about the size and thickness of a postage stamp and responds to temperature changes quickly. The RTD was clipped onto the geotextile during the test. Initially a larger RTD was used during testing of the fill direction samples. Later it was determined that the slower response time of this larger RTD was "averaging" the temperature readings and giving a misleading impression of the stability of the temperature. Load and strain data were recorded every thirty seconds and temperature every minute.

Because of the enormous effect of temperature on creep rate, temperature control is very important. A 1°C change in temperature will result in a 20% or greater change in creep rate for most polymers. Thus, loss of temperature control will affect the shape of the creep curve, which can lead to under or over-estimation of service life. To achieve the desired quality of results, temperatures during tests were maintained in a range of ±1°C. This necessitates a great deal of care in setting-up the environmental chamber controller and monitoring the temperature during performance of tests.

The first SIM tests, in the fill direction, were performed using Instron "seat belt" type roller grips. For the cross-head travel available only about 35% geotextile strain was possible with this configuration, which was less than desired for some tests. Thus, when testing in the warp direction was performed, a set of Instron pneumatic/hydraulic grips with 50mm by 75mm (2 inch by 3 inch) grips were used inside the environmental chamber. Using these grips it was necessary to loop the geotextile over a rod and back down into the grips to prevent individual yarns from sliding out of the grips. This configuration worked well with the material tested and did not appear to result in premature rupture of the geotextile. With this configuration strains in the geotextile up to 100% were possible.

The SIM tests utilized somewhat over 50mm (two inch) wide specimens. After attaching the extensometer and RTD the outside yarns were cut to obtain a 50mm (two inch) wide test specimen. The temperature was then allowed to equilibrate at about 20°C. The test was initiated by applying the load at an extension rate equivalent to about 10% strain per minute. Load levels of 25% to 45% of the ultimate tensile strength (UTS) were used in the initial fill (cross machine) direction tests. In the later warp (machine) direction tests load levels of 20% to 70% of the UTS were used. The load was maintained throughout the test. The temperature was increased in about 7°C steps starting at about 20°C. The time to accomplish the step up to each new temperature was two to four minutes. Each temperature was held for a dwell time of 10,000 seconds. During the hold period the temperature was kept within a range of 2°C (±1°C).

The conventional ambient temperature creep tests were performed in accordance with ASTM D 5262. Samples 200mm (eight inches) wide were used. The same load levels as for the SIM tests were used. The loads were held and strains measured for periods up to about 10,000 hours, or until the maximum travel of the available equipment was reached. In some cases the tests were extended out beyond 10,000 hours. During the tests, the strain measurements were made manually, by reading of dial gages or LVDTs. Elevated temperature tests were performed using a creep test load frame in a temperature controlled room. Procedures followed were the same as for the conventional ambient temperature creep tests. Tests were performed at temperatures of 38°C and 49°C in the fill direction and 50°C in the warp direction.

In addition to the SIM and conventional creep tests a series of short term ramp and hold tests were performed. The purpose of these was to characterize the material creep variability and give a common initial strain for all of the tests (Thornton et al. 1999). The ramp and hold tests used a 50mm (2 inch) wide specimen. The load in these was held for 1000 seconds.

FINDINGS

Test Results

Composite plots of the strain as a function of the logarithm of time in seconds are shown in Figures 1 and 2 for the warp and fill directions, respectively. These plots include the results of all the SIM, and ambient and elevated temperature conventional creep tests performed by Lab 1. In these plots the superposition of the elevated and ambient temperature tests has already been performed. In some cases multiple tests were performed and are shown. The SIM and creep tests have all been normalized to the average 1000-second strain from the ramp and hold tests.

Data are shown for strains up to 50%. This is the approximate limit of the equipment used for the ambient and elevated temperature conventional creep tests. The set up used for the SIM tests in the fill direction using roller grips was only capable of testing up to about 35% strain, where the maximum available travel was reached. Rupture did not occur in any of the fill direction tests. The revised set up used for the tests in the warp direction, which used pneumatic/hydraulic grips inside the environmental chamber, was capable of obtaining up to 100% strain. Using this configuration, in the warp direction rupture at a load level of 50% of UTS occurred at about 68% strain. At load levels below 50% of UTS rupture did not occur even up to strains approaching 100%. For strains above about 50% it became difficult to assure that the extensometer attachment was actually moving with the geotextiles. This was to some degree mitigated by applying latex adhesive to two areas of the fabric and pinning the extensometer mounting in these areas.

The SIM tests were performed using 7°C temperature steps starting at about 20°C. At each step the temperature was held for 10,000 seconds. Using these procedures it was possible to obtain the equivalent of a 10,000-hour conventional creep test in roughly 18 hours. This involved seven temperature steps ending at 62°C. In the tests reported in this paper, the equivalent of 100 years of data was obtained in 26 to 28 hours after 11 temperature steps ending at 90°C. Smaller time savings were realized for shorter duration conventional creep tests. An eight-hour conventional creep test was replicated using SIM in about 5 hours after two temperature steps.

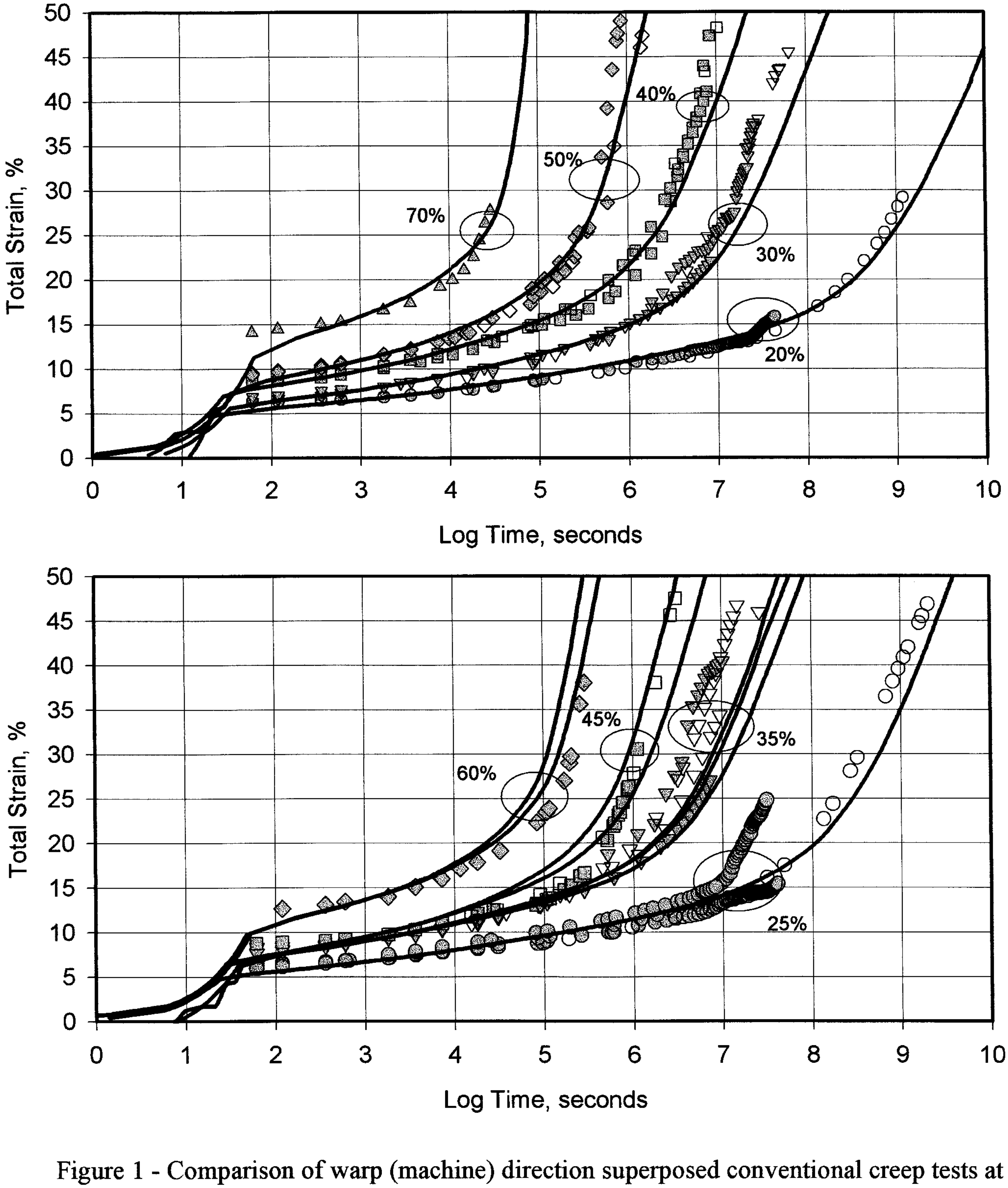

Figure 1 - Comparison of warp (machine) direction superposed conventional creep tests at ambient and elevated temperatures to SIM results at load levels indicated as a percent of UTS after adjustment to initial strain from 1000 second ramp and hold tests. Solid symbols are ambient temperature tests, open symbols are 50°C. Solid lines are SIM results.

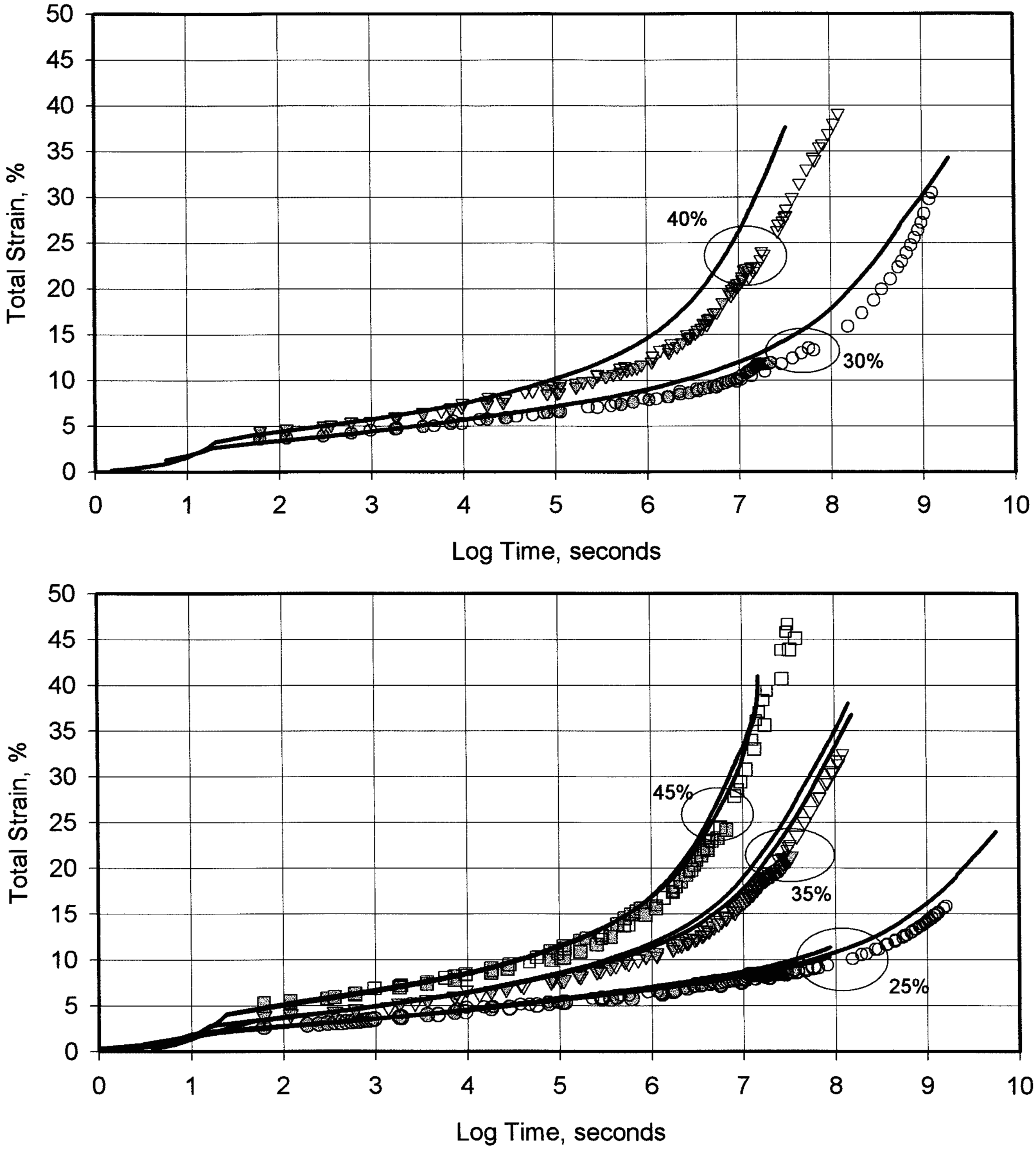

Figure 2 - Comparison of fill (cross machine) direction superposed conventional creep tests at ambient and elevated temperatures to SIM results at load levels indicated as a percent of UTS after adjustment to initial strain from 1000 second ramp and hold tests. Solid symbols are ambient temperature tests, open symbols are 38° and 49°C. Solid lines are SIM results.

Analysis Of Comparison

From the data shown in Figures 1 and 2 the overall correlation between methods appears relatively good. Unfortunately, it was not possible to perform the SIM tests on the same fabric roll samples used in the conventional creep tests. Therefore, some of the variation in the data shown may be a function of material variability and not differences in methods. To compare the SIM results to results obtained from conventional creep tests at ambient and elevated temperatures, isochronous plots were constructed. The plots are of strain taken from the test results at each of 10^4, 10^5, 10^6, 10^7, 10^8 and 10^9 seconds. The isochronous plots are shown in the plots in Figure 3. The relationship between SIM and conventionally obtained data is not as good as might be desired in the warp direction at load levels of 35%, 45% and 60% of UTS. In the cases of the tests at 35% and 45% of UTS, the isochronous plots shown in Figure 3 indicate that for the conventional creep higher strains occurred than the overall trend would indicate. The isochronous plots also indicate that at the 60% load level the SIM test overestimated the strain and the conventional test underestimated the strain at that load level. The significant thing to note is that in all these cases the isochronous plots indicate that the conventional tests may be at greater fault than the SIM generated results.

Based on the combined data from SIM and conventional creep testing shown in the isochronous plots, a best-fit regression was calculated for each time interval. A logarithmic relationship was calculated using the strain as the independent variable and load level as the dependent variable. Based on the relationship calculated, residuals were determined as a percent of the predicted load level. The residual is the variation of the actual data from the load level calculated from the regression relationship. The analysis of the residuals as a percent of the load level predicted from the regression calculation is summarized in Table 1. In the table the average is based on the residuals of all of the tests performed from their respective time interval regressions. The minimum and maximum numbers are the values furthest below and above, respectively, any of the calculated regression lines.

Table 1 - Residuals of Data from Calculated Regressions as Percentage of Predicted Load Level

Fabric	Average		Minimum		Maximum	
Direction	SIM	Creep	SIM	Creep	SIM	Creep
Warp	-0.8%	+0.7%	-14.7%	-11.8%	+8.6%	+21.9%
Fill	-2.9%	+1.6%	-7.1%	-6.5%	+2.1%	+7.8%

As shown in the table, the average variations from the calculated regression lines are approximately equal for SIM and the conventional methods. SIM on average yields a slightly lower load level to obtain a given strain at a given time than the conventional method, thus producing slightly conservative results. SIM also produced less overall scatter than the conventional method. The conventional method results in an overall spread of the data from the regression lines of 33.7% in the warp direction and 14.3% in the fill, compared to 23.3% in the

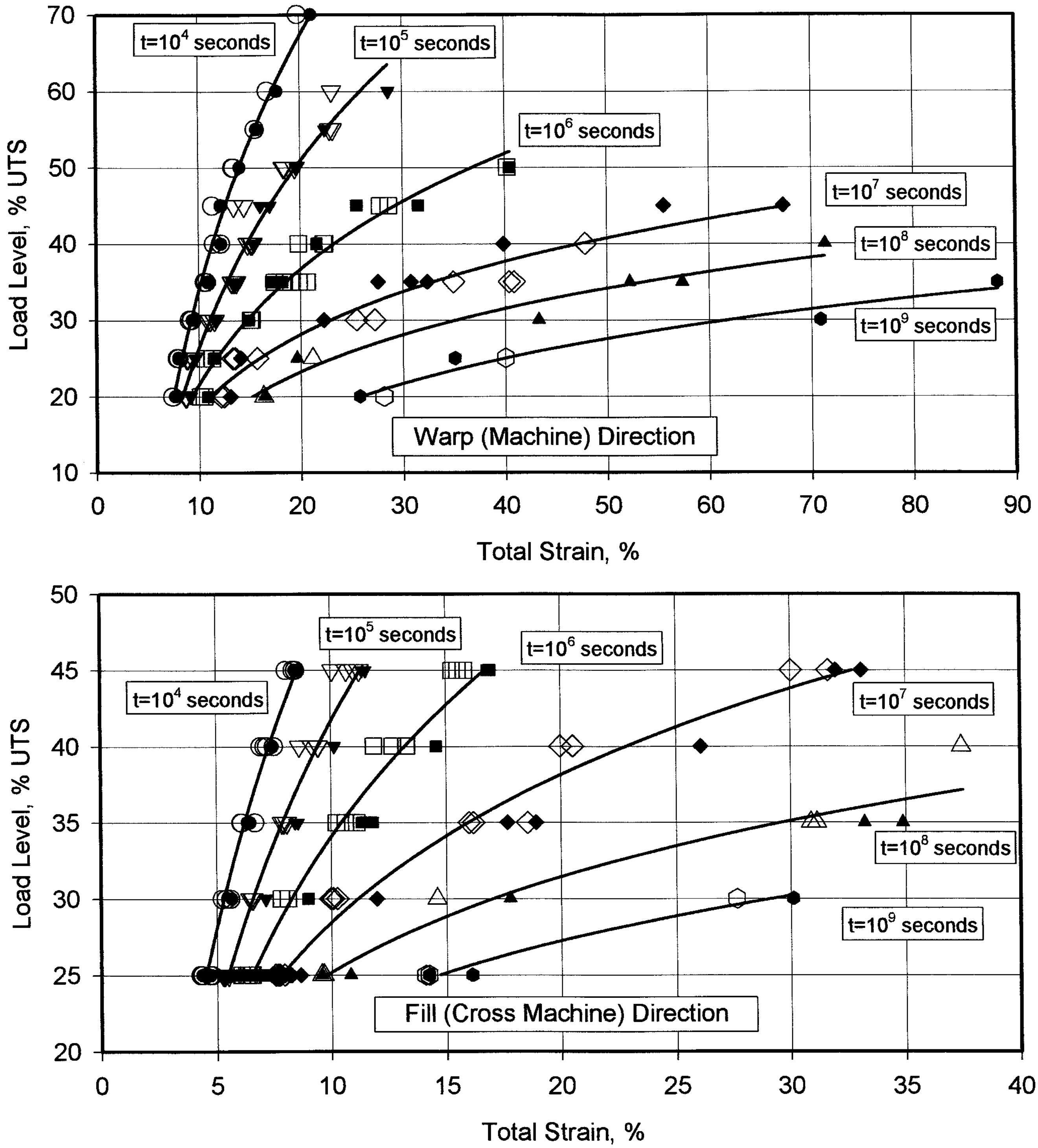

Figure 3 - Isochronous plots of warp (machine) and fill (cross machine) direction ambient and elevated temperature conventional creep test and SIM data. Open symbols represent data from ambient and elevated temperature conventional creep tests after superpositioning. Filled symbols represent SIM data. Regression lines are based on the combined data.

warp and 9.2% in the fill for SIM. Based on this analysis of the residuals, the SIM data that was developed produced results consistent with trends of conventional and elevated temperature creep tests. Additionally, SIM data was more consistent and less scattered than that from the conventional procedures.

The second comparison to be made of the applicability of SIM to conventional creep tests is an examination of the cumulative shift factors (log A_T) relative to 20°C due to time acceleration obtained by elevated temperature from both methods. The plots in Figure 4 show the cumulative shift factors obtained from the SIM tests and elevated temperature tests in the warp and fill directions as a function of temperature. The SIM data are further subdivided by load levels. As can be seen the relationship of the cumulative shift factors determined by both methods is good. Also observable is a slight load dependence in the shift factors as has been previously noted for polyester (Thornton et al. 1998).

Reproducibility

As mentioned previously in addition to the work performed by Lab 1, Lab 2 also performed four SIM tests on the same material used in this study. These included two tests each in the warp and fill directions. Comparisons of these results are shown in Figure 5. Figure 5 displays four SIM test results at 25% of UTS and three at 35% of UTS in the fill (cross machine) direction. One curve in each set was generated by Lab 2, and the others were by Lab 1. The agreement between multiple tests by Lab 1 as well as that between the two laboratories is excellent. On the other hand the top portion of the figure shows significant differences in the warp (machine) direction results between the two labs. Again the applied stress levels are 25% and 35% of UTS. A detailed examination of the rescaling and shifting parameters developed independently by the two labs indicated no significant differences. For this reason we concluded that the differences in the reported results are due to differences in the material tested. That such differences could occur is demonstrated by the conventional ambient temperature creep data shown in the figure, and is further supported by observed variations in the 1000 second ramp and hold tests.

CONCLUSION

The most difficult part of performing SIM was found to be temperature measurement and environmental chamber control to ±1°C. The response time of the thermocouple operating the environmental chamber was found to be an important element in obtaining better control. The response time of the temperature probe used to record temperatures during the test was also found to have an impact on interpreting the temperature profile.

The stepped isothermal method (SIM) offers a way of developing long-term creep data in a much shorter time than is possible using conventional and elevated temperature creep test

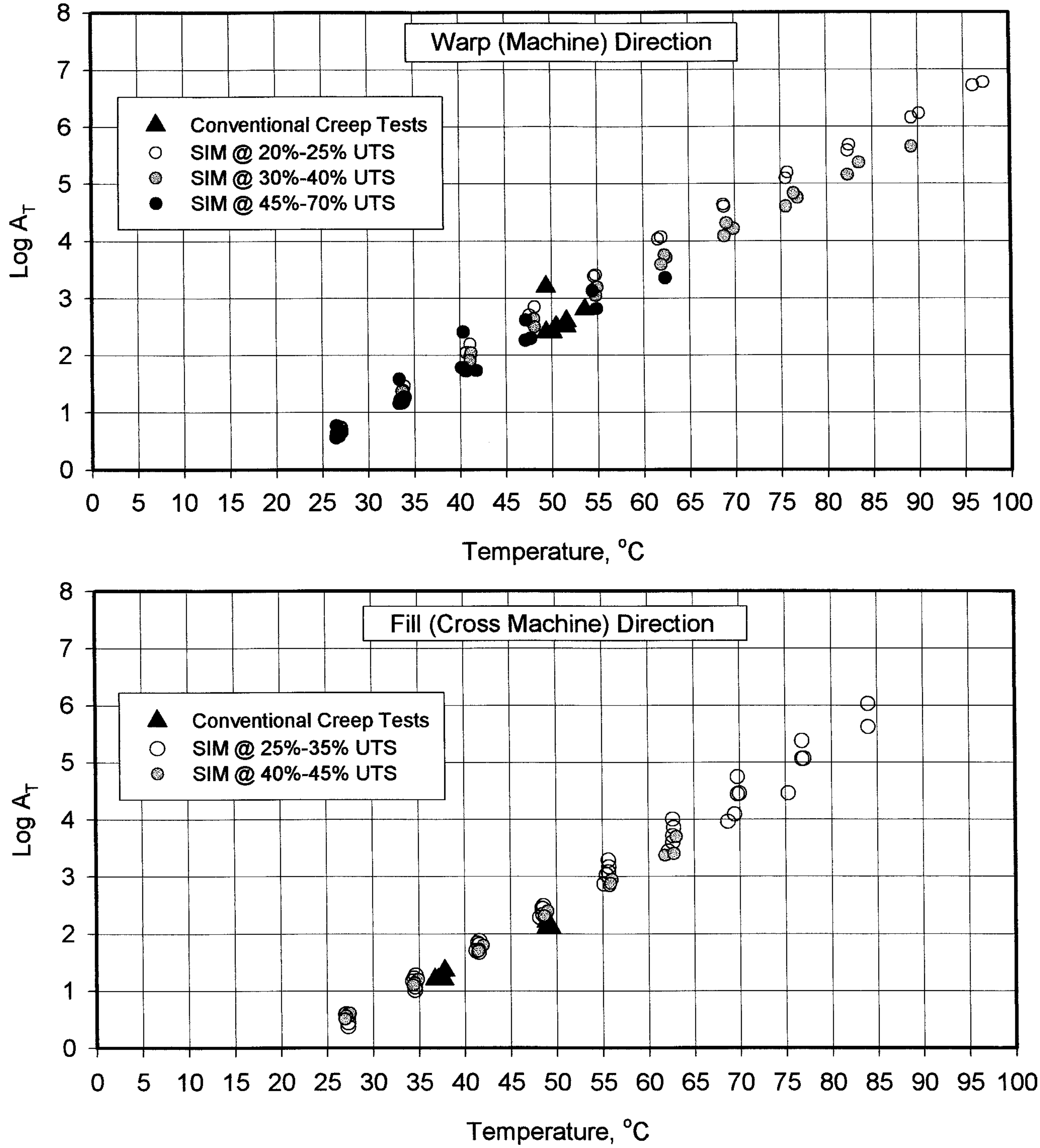

Figure 4 - Cumulative shift factors relative to 20°C from SIM and elevated temperature conventional creep tests.

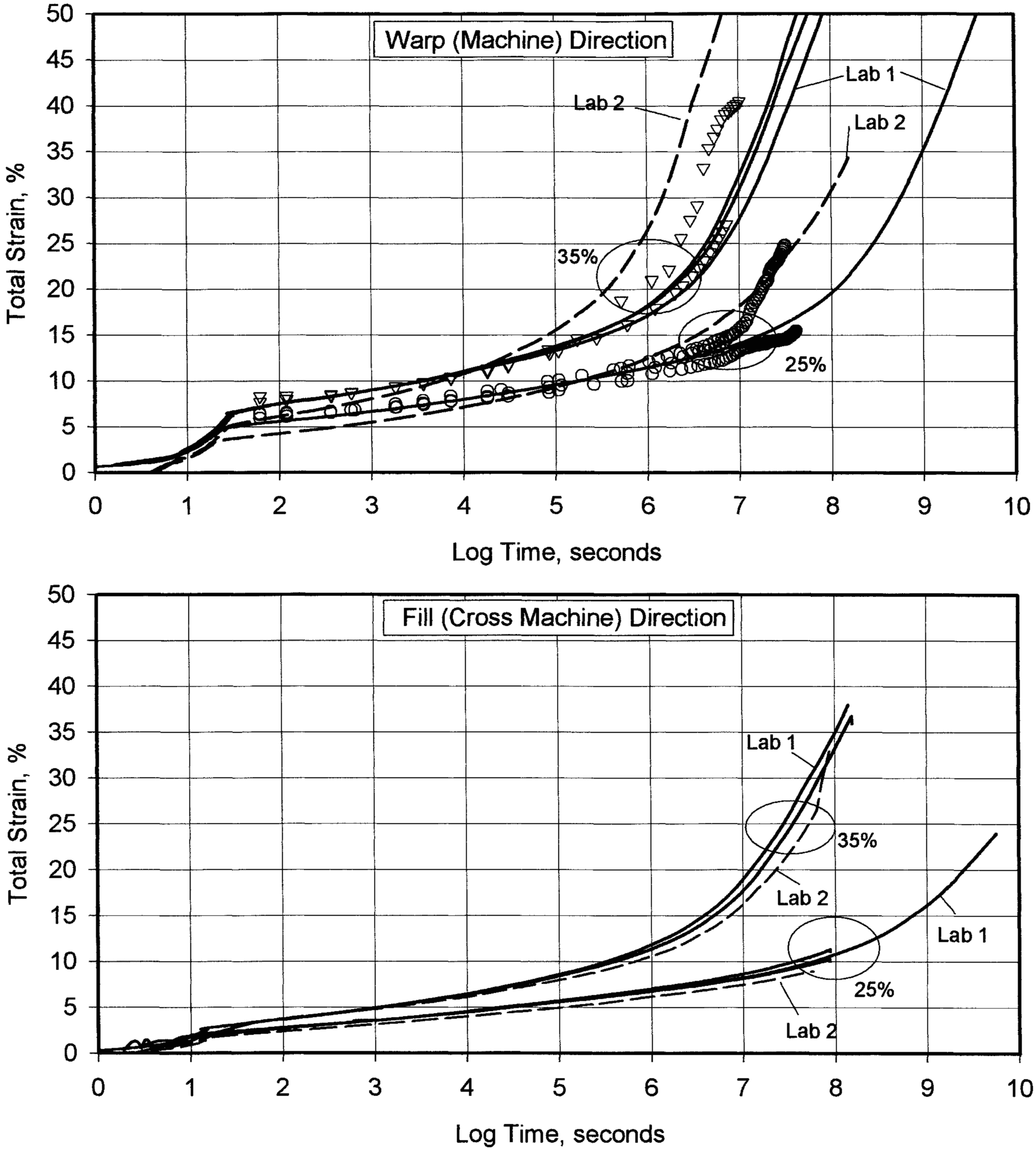

Figure 5 - Comparison of warp (machine) and fill (cross machine) direction SIM test results by Labs 1 and 2 at indicated load level as percent of UTS. Solid lines are results from Lab 1 and dashed lines are results from Lab 2. The conventional ambient temperature creep data for the warp direction is shown for reference.

methods. SIM has been shown to work with polyester products in previous papers. No previous work using SIM with polypropylene is known. In this paper the results of conventional creep tests at ambient and elevated temperatures of from eight hours to projected times over 100 years on a woven polypropylene geotextile have been presented. Strains shown for these tests were up to 50%. Results of SIM tests at the same load ranges have also been shown. The SIM tests for the similar load levels took 5 to 28 hours to develop the same data. The log time/strain relationships developed have been demonstrated to be at least as good using SIM as the conventional methods and with generally somewhat less scatter than was observed with the conventional creep testing. The time-temperature shift factors (log A_T) obtained using SIM have also been shown to be comparable with those obtained using conventional time temperature superpositioning. Data demonstrating the repeatability and reproducibility of SIM have also been shown. We believe that SIM is a viable way of measuring long-term creep performance of polypropylene geotextiles.

REFERENCES

Thornton, J.S., Paulson, J.N., and Sandri, D., 1998, "Conventional and Stepped Isothermal Methods for Characterizing Long Term Creep Strength of Polyester Geogrids", *Sixth International Conference on Geosynthetics*, IFAI, Atlanta, Georgia, USA, March 1998, pp 691-698.

Thornton, J.S., Allen, S.R., Thomas, R.W., and Sandri, D., 1998, "The Stepped Isothermal Method for Time-Temperature Superposition and Its Application to Creep Data on Polyester Yarn", *Sixth International Conference on Geosynthetics*, IFAI, Atlanta, Georgia, USA, March 1998, pp 699-706.

Thornton, J.S., Allen, S.R., Thomas, R.W., 1997, "Approaches for the Prediction of Long Term Viscoelastic properties of Geosynthetics from Short Term Tests", *Geosynthetics '97*, IFAI, Long Beach, California, USA, March 1997, pp 277-290.

Thornton, J.S., Sprague, C.J., Klompmaker, J., and Wedding, D.B., 1999, "The Relationship of Creep Curves to Rapid Loading Stress-Strain Curves for Polyester Geogrids", *Geosynthetics '99*, IFAI, Boston, Massachusetts, USA, April 1999, pp 735-744.

WALLS, SLOPES & EMBANKMENTS II

GEOSYNTHETICS CONFERENCE 2001
Portland, Oregon USA
Economics, Performance & Constructibility • February 12-14, 2001

DESIGN CONSIDERATIONS OF GEOSYNTHETIC FOR REINFORCED EMBANKMENTS SUBJECTED TO LOCALIZED SUBSIDENCE

BLIVET J.C., KHAY M., LABORATOIRES DES PONTS ET CHAUSSÉES, CETE N-C, ROUEN, FRANCE
GOURC J.P., LIRIGM, UNIVERSITÉ, GRENOBLE 1, FRANCE
GIRAUD H., SNCF, DIRECTION DE L'INGÉNIERIE, PARIS, FRANCE

ABSTRACT

Road and rail infrastructure is increasingly routed through areas likely to contain cavities that are too small to be detected. A geosynthetic used under the fill gets a deformation as a membrane that does not prevent surface settlement but helps to limit its extent and thus reduce risks for traffic. A design method is proposed, based on a wide-ranging experimental program that was partly presented at "Geosynthetics 99" conference. The influence of various hypotheses concerning failure mechanisms is assessed and typical charts are proposed for selecting stiffness modulus and tensile strength values for the geosynthetic.

INTRODUCTION

Problem : the lack of space available for new road and rail infrastructure often means that new routes have to run through areas where the subsoil may contain or allow the formation of cavities, leading to localized subsidence. The development of such sinkholes poses enormous problems of public safety when vehicles travel through these areas.

An experimental program conducted by a group of research workers from universities, public technical centers and industry has been described in previous publications. The full-scale experiments on real sites (SCET, Société d'Autoroutes Scetauroute and SNCF, Société Nationale des Chemins de Fer Français) were discussed by Gourc and his co-authors (1999) and the experiments at the Rouen Road Studies Center (SCER) by (Blivet et al., 2000). A CD-ROM has also been released (Gourc et al., 2000). These experiments concentrated on maximum-sized cavities of 4 m, as it was considered that small cavities were the most difficult to detect by geotechnical investigations.

These experiments were aimed at assessing the benefits of placing geosynthetics under fill in order to reduce the risk posed by surface subsidence for traffic. It was a matter of determining whether :

- a geosynthetic can absorb a load corresponding to the weight of fill suspended over the cavity without failure,
- a geosynthetic can confine the area of collapsing fill, prevent the formation of “steps” at the ground surface that can be seen without any geosynthetic, corresponding to the complete collapse of fill into the cavity, and contain differential surface settlement within acceptable limits for at least temporary use by traffic.

Detailed analysis of these experiments showed that the answer was yes in both cases (Villard et al., 2000).

The next stage is to propose a design method for the geosynthetic. As far as the authors are aware, only one method exists at present (Kempton et al., 1996). This has been included in a standard (BS 8006, 1995) but it is based essentially on observations of sinkholes in the absence of any geosynthetic. The aim of the present article is to define design principles and to demonstrate the effect of various assumptions numerically on the basis of real experiments conducted on site, but without taking any stance with regard to existing or future standards, which must include safety coefficients that are not considered here.

MAIN RESULTS OF THE FULL-SCALE EXPERIMENTAL PROGRAMME

The full-scale experimental program comprised two parts, RAFAEL 1 (Gourc et al., 1999) and RAFAEL 2 (Blivet et al., 2000). RAFAEL 1 was conducted on an actual site. The circular cavities (figure 1) had a diameter L = 2 m and L = 4 m. The fill, a sandy gravel (grain size : 0 to 300 mm), was compacted above the artificial cavity that had been filled previously with clay beads. The fill was 1.5 m thick. The cavity was created by sucking out the clay beads. The geosynthetic was a dual-function geotextile, i.e. a non-woven geotextile reinforced in a single direction (the same as that of traffic movement). For this reason, the geosynthetic will be referred to as "monodirectional". The stiffness modulus in the direction of traffic is equal to J. When the cavity is emptied of clay beads, the geosynthetic sags like a membrane to absorb the weight of the fill. If the structure permits, trucks or trains are sent across it.

Table 1 shows the main characteristics of the tests conducted in the RAFAEL 1 program. (f) is the deflection in the center of the strained geosynthetic acting as a membrane and (s) the corresponding settlement at the surface of the fill.

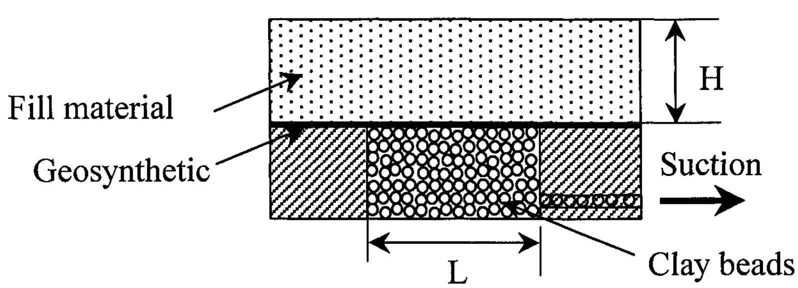

Figure 1. Geometry of the field experimentation (RAFAEL 1)

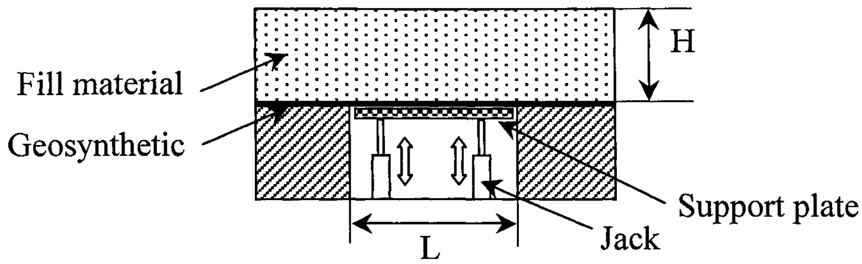

Figure 2. Geometry of the large scale tests (RAFAEL 2)

The second part of the experimental program, entitled RAFAEL 2, is distinguished from the first mainly in terms of the method of cavity formation, as in this case a hydraulic jack lowers a plate placed under the geosynthetic (figure 2), and in the type of fill material. In light of the RAFAEL 1 tests, it was felt that the mechanical characteristics of the fill could usefully be changed to demonstrate the effect of the type of soil on fill deformation mechanisms (table 2).

Table 1. Main features and results of the field experience (RAFAEL 1)
Characteristics and results of tests after traffic

Type of test	L (m)	H (m)	H/L	Fill material	γ kN/m³	w (%)	J (kN/m)	s (m)	f (m)	Fill Behaviour *
SCET1	2	1.5	0.75	sandy gravel 0/300 mm	21.1	6	1818	0	0.22	Stable arch (a)
SCET2	4	1.5	0.375		21.1	6	1818	0.2	>0.6	Arch Collapse (b)
SCET3	4	1.5	0.375		21.1	6	3600	0.2	0.48	Partial Collapse (b)
SNCF	2	1.5	0.75		21.1	6	455	0	0.28	Stable arch (a)
SNCF	4	1.5	0.375		21.1	6	1818	> 0	0.51	Arch Collapse (b)
SNCF	4	1.5	0.375		21.1	6	x 1818	0.1	>0.51	Partial Collapse (b)
SNCF	2	1.5	0.750		21.1	6	1818	0	0.20	Stable arch (a)

* the different fill behaviours (a to d) are illustrated in figure 4

Table 2. Main features and results of the large scale tests (RAFAEL 2)

Type of test	L (m)	H (m)	H/L	Fill materia	Grain size (mm)	γ (kN/m³)	w %	J kN/m	s (m)	f (m)	Fill Behaviour*
CER	.07	.03	.497	Sand	0.08/5	18.15	.9	938	0.150	.203	Arch collapse (b)
CER	.07	.86	.415	Sand	0.08/5	18.2	.2	3600	0.123	.143	Arch collapse (b)
CER	.07	.05	.507	Ballast	25/50	14		3600	0.092	.152	Progressive collapse (c)
CER	.07	1.1	.531	Silt	0/0.1	20.8	8	938	0.075	.195	Bent beam (d)

* the different fill behaviours (a to d) are illustrated in figure 4

FILL DEFORMATION MECHANISMS IN THE CASE OF SINKHOLES

Membrane Deformation of Geosynthetic

When a cavity appears, the geosynthetic behaves as a membrane and is deformed to confine the collapsing area of fill and absorb the weight of the subsidence through tensile force. This mechanism has been studied in detail elsewhere (Gourc et al., 2000). If the weight of fill on the geosynthetic is assumed to be uniformly distributed (vertical stress q), the deformation profile in the direction of "monodirectional" reinforcement (i.e. the direction of traffic) is a parabola. According to (Giroud, 1990), an approximate value may be obtained for maximum tensile force in the geosynthetic by the following equation :

$$T_{max} = J.\,\varepsilon_{max} \approx J.(8/3).(f/L)^2 \qquad [1]$$

in which ε_{max} is the maximum strain.
It will be recalled (figure 3) that the vertical equilibrium condition :

$$2.T_{max}.\sin\alpha = q.L \qquad [2]$$

shows that the activated tensile force T_{max} (fixed q.L) is greater if the geosynthetic is only slightly deflected, i.e. if the stiffness value J is high.

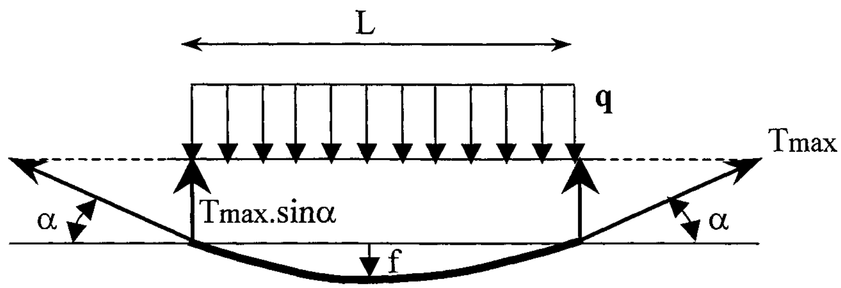

Figure 3. Membrane behavior

Fill Deformation Profile

Four types of deformation mode could be identified in the fill (figure 4). The transition from one to another depends on the geometry (especially H/L), the nature of the fill material and the tensile stiffness of the geosynthetic. Tables 2 and 3 indicate the types of deformation.

The arching effect was clearly observed in the RAFAEL 1 series of experiments. By generalizing the calculation proposed by Terzaghi (1943), it was possible to find a theoretical relation between the relative height of the arch (h/L) and the relative height of the fill (H/L) (figure 5) (Villard et al., 2000). Observations on the actual site are in good agreement with this theoretical relation, as shown on the figure.

When (H/L) has a low value, the thickness of the overlying soil (d) at the keystone level is too small to withstand the live load created by traffic, and surface subsidence occurs instantaneously (mode b – figure 4) or progressively (mode c). (s) is the settlement occurring at the center.

In the case of fill material with a certain tensile and hence bending strength, such as silts, another type of global deformation (mode d) could be identified, equivalent to that of a bending beam. The experiment concerning slopes or retaining structures showed that the tensile strength of soils tends to disappear with time.

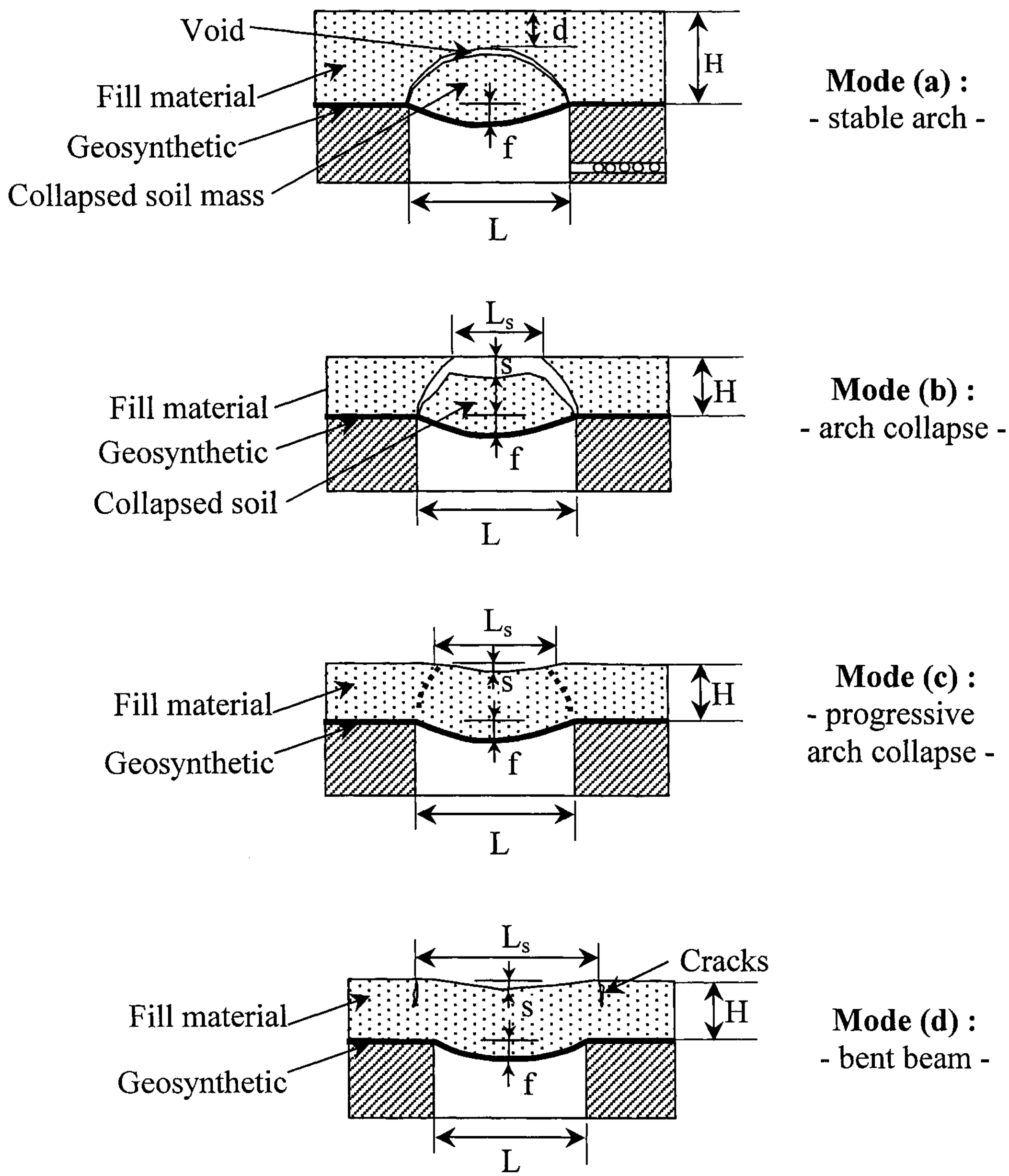

Figure 4. Different fill behaviours above cavity with existing geosynthetic

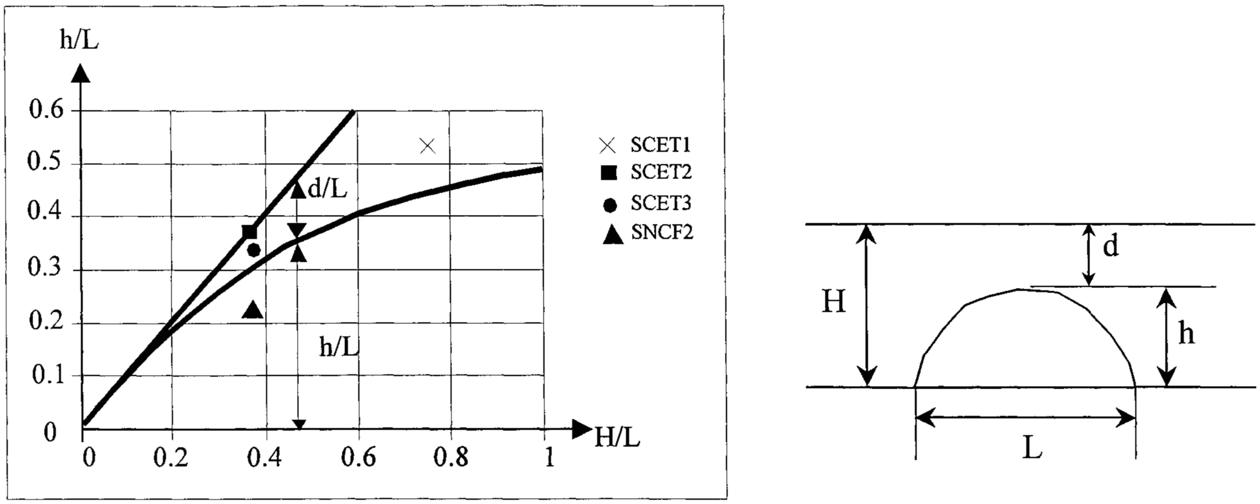

Figure 5. Height of the stable arch for a circular cavity
(Fill $\phi = 38°$, $\gamma = 21.1$ kN/m^3, p = 0)

Mechanisms Proposed for a Design Method

In view of the observations made in the RAFAEL 1 and RAFAEL 2 experimental programs, it is proposed that :

- with a high H/L value, the thickness of soil (d) above the arch is sufficiently large to be stable, and no surface settlement (s) is observed,
- with a low H/L value, the soil arch is not stable and arch failure occurs. It seemed reasonable to consider that the collapsing soil mass would adopt a cylindrical shape (figure 6) as a result of the arch crumbling (mode b – figure 4).

By taking into account a safety factor applied to the mechanism in figure 5, it is possible to fix the limit value of H/L above which no failure occurs, but it may also be suggested as a precaution that a cylinder of fill material will collapse irrespective of H/L.

The trunconical failure mode proposed by British Standard BS 8006 (1995) was also considered at the same time. This failure mode corresponds to drawdown of the fill material into the cavity at the same angle as the natural ground slope (β=ϕ). This drawdown mechanism, which is likely to occur in the absence of any geosynthetic, appears to be prevented by the membrane, provided that the latter does not undergo excessive deflection (f).

Another observation made in the RAFAEL experimental program was that the space freed by the geosynthetic membrane deformation profile (ΔV_g) (figure 6) was always larger than the corresponding volume of settlement at the surface (ΔV_{sub}). It was deduced from this that the fill material expanded as it collapsed. Hence V_s is the initial volume before failure and V_{se} the volume after expansion. This dilatance capacity (under low stress) was characterized by an expansion coefficient C_e:

$$V_{se} - V_s = \Delta V_s = (C_e - 1).\ V_s = \Delta V_g - \Delta V_{sub} \qquad [3]$$

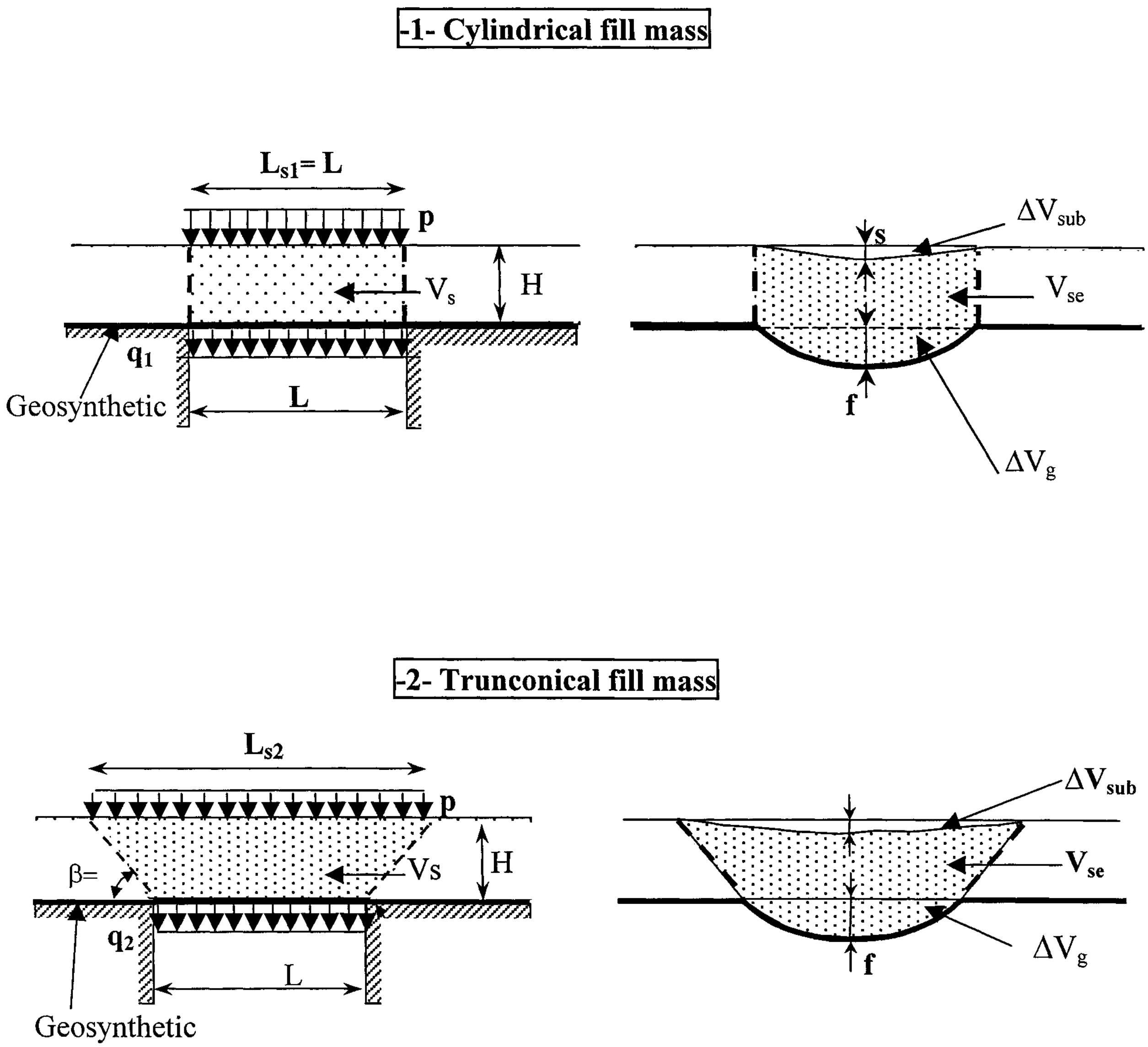

Figure 6. Proposed mechanisms and compatibility of volume

DESIGN OF GEOSYNTHETIC – INFLUENCE OF HYPOTHESES

The numerical cases considered above correspond to the RAFAEL 1 experiments (ϕ fill = 38°, thickness H = 1.5 m, unit weight = 21.1 kN/m^3, no live load at the surface, p = 0) using circular cavities of diameter L = 2 m and L = 4 m. The geosynthetic is monodirectional, with a modulus J in the direction of traffic movement. It should be recalled that monodirectional reinforcement has been shown to be the most effective with the same mass of reinforcement fibers (Villard et al., 1998).

Loading of Geosynthetic Membrane

The two cases shown in figure 6 are considered, namely :

- Case 1: cylindrical collapsing fill mass

Let q_1 be the equivalent normal vertical stress exerted on the membrane (Villard et al., 2000). The mass is assumed to be subject to lateral shear at the edges of the cylinder :

$$q_1 = \left[\frac{L.\gamma - 4.c}{4.K.\tan\phi}\right] . \left[1 - e^{\left(-4K\tan\phi.\frac{H}{L}\right)}\right] + p.e^{\left(-4K\tan\phi.\frac{H}{L}\right)} \qquad [4]$$

with (c, ϕ) being the mechanical characteristics of the fill material and K the active earth pressure coefficient.

- Case 2: trunconical collapsing fill mass

Let q_2 be the equivalent normal vertical stress. The lateral soil mass is assumed to be retained at the edges of the truncated cone by friction ; in conformity with British Standard BS 8006, it is assumed that :

$$q_2 = \gamma H + p \qquad [5]$$

Membrane-Type Behavior of the Geotextile

In both cases 1 and 2, the same membrane-type behavior is considered :

$$T_{max} = \frac{q.L}{2} . \sqrt{\left(\frac{L}{4f}\right)^2 + 1} \qquad [6]$$

The relations T_{max} (f/L) shown in figure 7 may be obtained for cases 1 and 2 with a descending load corresponding to the cylindrical or trunconical collapsing mass and for cavities with diameters L = 2 m or L = 4 m. On the basis of equations [1] and [6], the variation in (q L) with a fixed value of J produces the diagrams shown in figure 8. By combining figures 7 and 8, it is possible to determine the deflection F and maximum tensile force T_{max} in the membrane for a geosynthetic with a fixed tensile stiffness J and cavity of fixed diameter L, for both cases 1 and 2, i.e. f_1 and f_2 (figure 9).

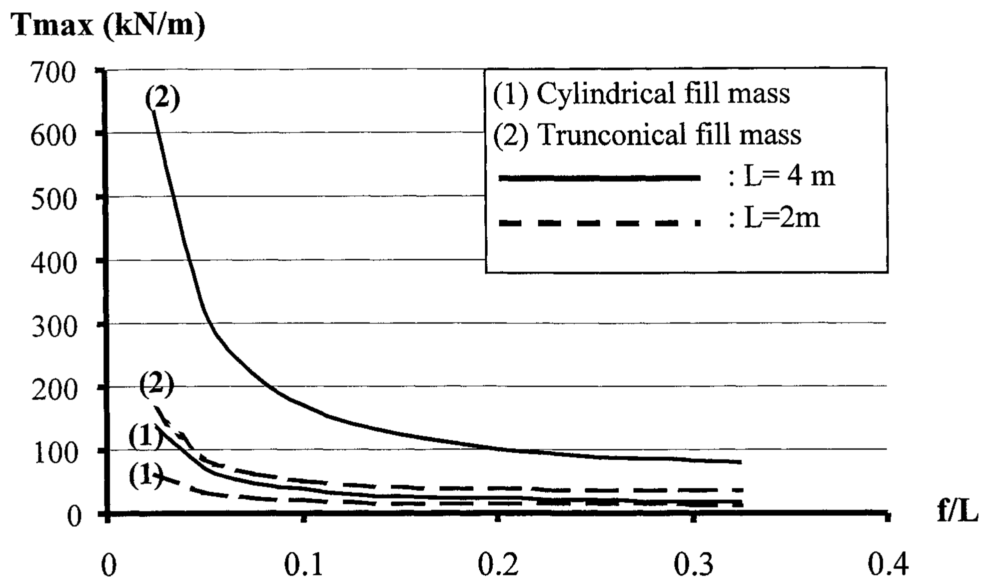

Figure 7. Tensile mobilisation of the geosynthetic (circular cavity, diameter L – monodirectionnal geosynthetic – fill height H = 1.5 m, $\gamma = 21.1$ kN/m^3, p = 0, $\phi = 38°$)

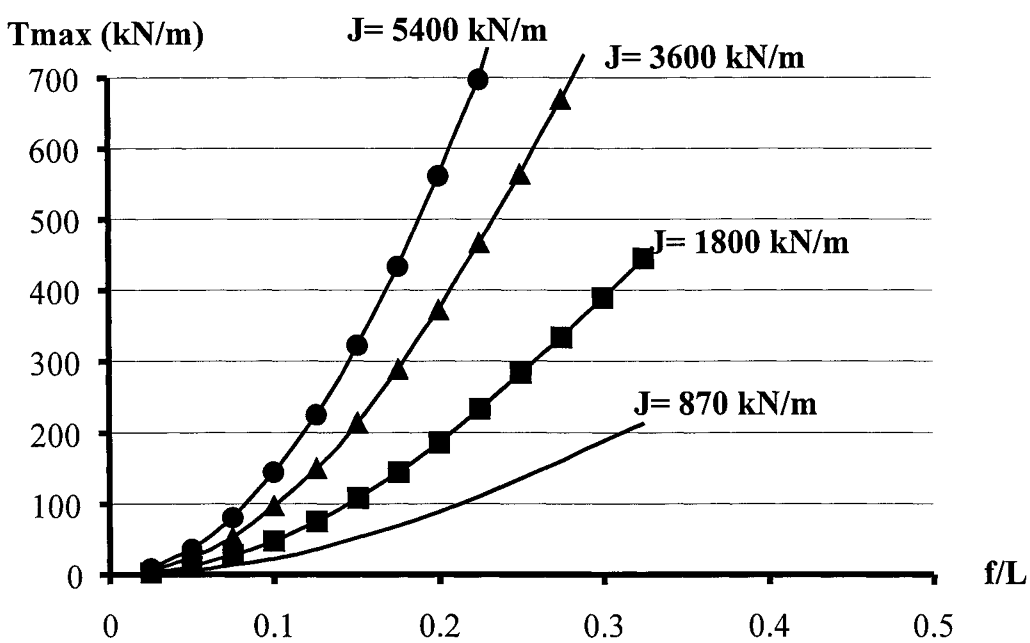

Figure 8. Membrane behaviour under increasing loading (qL) relationship between tensile mobilisation (Tmax) and relative deflection (f/L) for different tensile stiffness of the geosynthetic.

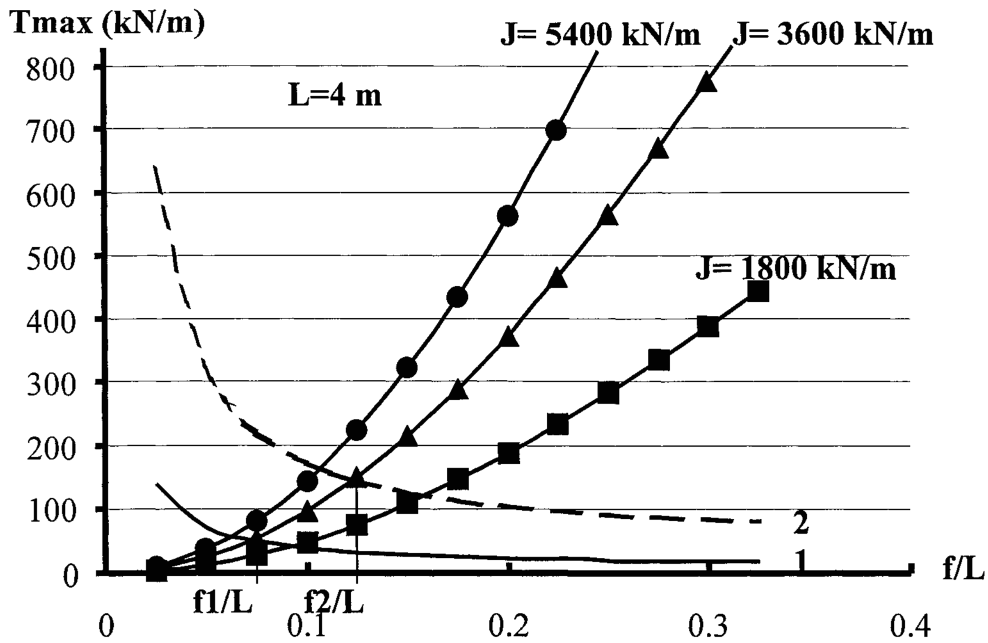

Figure 9. Diagrams for determination of elastic deflection and tensile force in the geosynthetic for different geosynthetic stiffness (circular cavity, diameter L – monodirectional geosynthetic – fill height H = 1.5 m, p = 0)

Settlement at Fill Surface

The deformation profiles of the geosynthetic membrane and of the free surface of the fill are assumed to be parabolic (figure 6). It is thus possible to evaluate the volumes involved :

$$\Delta V_g = \frac{\pi . f . L^2}{8} \quad [7]$$

$$\Delta V_{sub} = \frac{\pi . s . Ls^2}{8} \quad [8]$$

If the expansion coefficient C_e of the fill material is fixed using relation [3], the relation between geosynthetic deflection (f) and surface settlement (s) can be determined. It is thus possible to obtain the results shown in table 3 for two extreme values of the expansion coefficient C_e (C_e = 1.00 zero expansion and C_e = 1.10 extreme expansion). Test SCET3 shown in table 1 is the only one that corresponds to the same conditions for a cavity (L = 4 m). The result is very close to that obtained by BS 8006, even if the mechanism observed is very different (f and s are the experimental values but L_{S1} and L_{S2} are the theoretical values).

Table 3. Surface settlements for different design assumptions
(Geosynthetic : J = 3600 kN/m – Fill : H = 1.5m, $\gamma = 21.1$ kN/m^3, p = 0, $\phi = 38°$)

Cavity L(m)	Subsidence mechanism	Soil expansion Ce	f/L	s/Ls
2	Cylindrical	1.00	0.0689	0.0689
	Trunconical *	1.00	0.0959	0.0113
	Cylindrical	1.10	0.0689	-0.0811
	Trunconical	1.10	0.0959	-0.0617
4	Cylindrical	1.00	0.0721	0.0721
	Trunconical *	1.00	0.123	0.0320
	Cylindrical	1.10	0.0721	-0.0029
	Trunconical	1.10	0.123	-0.0124
SCET 3 (L=4m)	Ls_1 (cylindrical) Ls_2 (trunconical)	Experimental	0.120 0.120	0.0625 0.0319

* BSI 86006 conditions

Design of Geosynthetic

The following method will be used to design a reinforced fill structure in an area where localized subsidence is likely to occur :

- choice of diameter (L) for the largest cavity likely to occur,
- choice of limit value for allowable differential surface settlement (s/L_s),
- choice of failure mechanism for the fill material (cylindrical or trunconical) and expansion coefficient C_e.

Each curve of figure 10 can be used to obtain the tensile stiffness of the geosynthetic as a function of the differential surface settlement for a given geometry and collapse mechanism. In addition T_{max}, the maximum tensile force mobilized, could be determined with the relationship between s/Ls and s/L. After that, the tensile strength T_f is obtained, taking into account an appropriated safety factor.

The experimental values obtained in the RAFAEL program are shown in figure 10. The straight line corresponding to the permissible differential surface settlement (s/L_s) = 0.025, considered to be realistic for a roadway, is shown on the same figure. The tensile stiffness values J required for the assumed mechanisms and corresponding to the RAFAEL program are indicated in table 4.

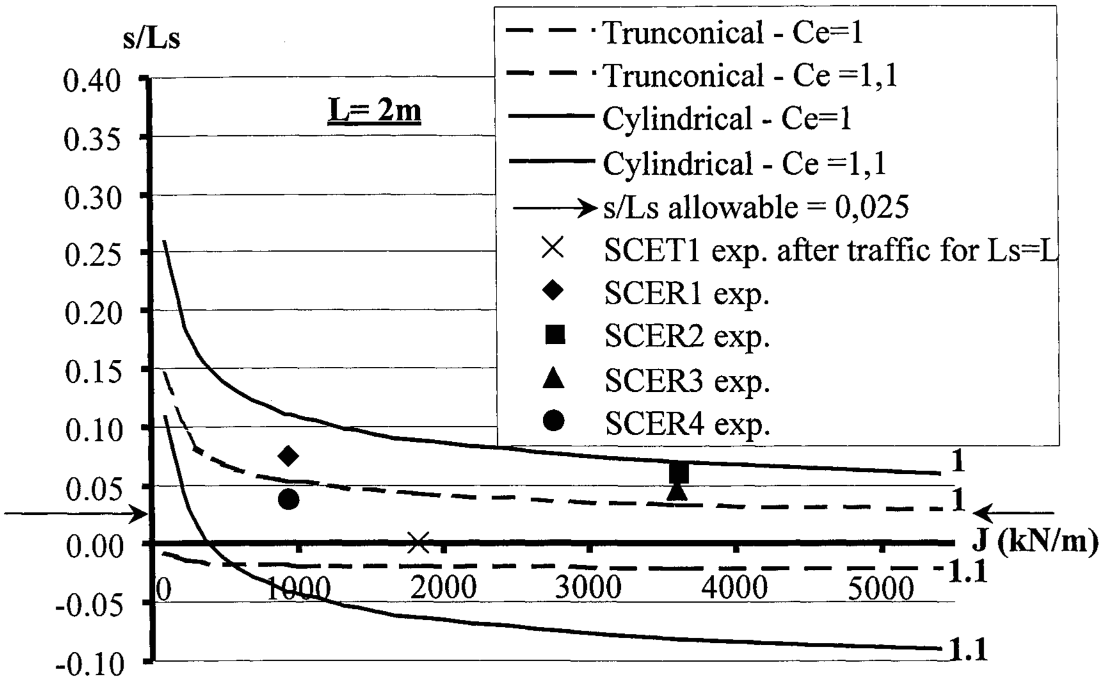

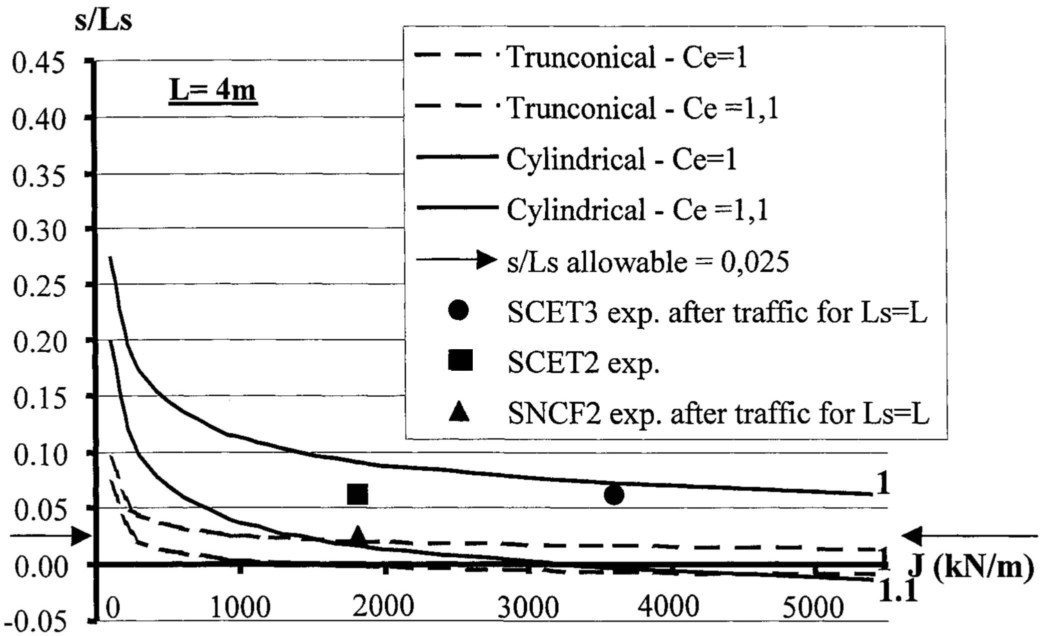

Figure 10. Minimum value of geosynthetic stiffness for a maximum allowable relative surface settlement (s/Ls = 0.025), following different design assumptions. (Fill H = 1.5 m, $\gamma = 21.1$ kN/m^3, p = 0, $\phi = 38°$)

The major influence of the expansion coefficient C_e in comparison with that of the fill collapse mechanism is quite clear, but the value $C_e = 1.10$ must be considered as an extreme.

Moreover, there is a negative settlement in certain cases, which is unrealistic. A value of C_e = 1.05 appears to be more realistic.

Table 4. Minimum value of geosynthetic stiffness J for a maximum allowable relative surface settlement (s/Ls = 0.025) – (Fill H = 1.5m, γ = 21.1 kN/m^3, p = 0, ϕ = 38°)

Cavity L(m)	Subsidence mechanism	Soil expansion Ce	J (kN/m)
2	Cylindrical	1.00	7310
	Trunconical *	1.00	5500
	Cylindrical	1.10	270
	Trunconical	1.10	60
4	Cylindrical	1.00	83000
	Trunconical	1.00	1050
	Cylindrical	1.10	1400
	Trunconical	1.10	250

* BSI 86006 conditions

CONCLUSIONS

The aim of this article is to help in defining a design method in which the tensile stiffness J of a geosynthetic can be chosen in accordance with the geometry of the problem and the characteristics of the fill material used. The same method can be used to determine the minimum tensile strength from the value of T_{max} determined on the figures.

Figure 10 shows the influence of the hypotheses made with regard to the failure mechanism occurring above the cavity.

ACKNOWLEDGEMENTS

The authors wish to thank the Centre d'Études Routières de Rouen, Société d'Autoroutes Scetauroute, Société Nationale des Chemins de Fer Français (SNCF) and geosynthetic manufacturer BIDIM for their technical and financial contribution to the RAFAEL experimental program.

REFERENCES

Blivet, J.C., Khay, M., Villard, P., Gourc, J.P., 2000 "*Experiment and design of geosynthetic reinforced to prevent localised sinkholes*", GeoEng 2000, Melbourne, Australia

British Standard (BS 8006), 1995, "*Code of Practice for strengthened / reinforced soils and other fills*", British Standard Institution, London, UK.

Giroud, J.P., Bonaparte, R., Beech, J.F. and Gross B.A., 1990, "*Design of soil layer-geosynthetic systems overlying voids*", Geotextiles and Geomembranes, Vol. 9, N° 1, pp. 11-50.

Gourc, J.P., Villard, P., Giraud H., Blivet, J.C., Khay, M., Imbert, B., Morbois, A. and Delmas, Ph., 1999 "*Sinkholes beneath a reinforced earthfill - a large scale motorway and railway experiment*", Geosynthetics'99 Conference, April 28-30, 1999, Boston, Massachusetts, USA (Award of Excellence of the North American Geosynthetics Society - Boston April 1999)

Gourc, J.P., Villard, P., 2000, "*Special Lecture : Reinforcement by membrane effect : Application to embankments on soil liable to subsidence*", 2nd Asian Geosynthetics Conference, GeoAsia 2000, Kuala Lumpur, Malaysia, 18 p.

Gourc, J.P., Villard, P., 2000, "*Reinforcement by membrane effect : Application to embankments soil liable to sinkhole*", CE-Rom, distributed by IGS, Educational Committee.

Kempton, G.T., Lawson, C.R., Jones, C.J.F.P. and Demardash, 1996, "*The use of geosynthetics to prevent the structural collapse of fills over areas prone to subsidence*" Proceedings of the first European. Conference on Geosynthetics : Applications, Design and Construction, Maastricht 1996, De Groot, Den Hoedt and Termaat Editors, Balkema, pp. 316-324.

Terzaghi, K., 1943, "*Theoretical Soil Mechanics*", John Wiley and Sons, New York.

Villard, P., Giraud H., 1998, "*Three-Dimensional Modeling of the Behavior of Geotextile Sheets as Membranes*", Textile Research Journal 68 (11), November 1998, pp. 797-806.

Villard, P., Gourc, J.P., Giraud, H., 2000, "*A geosynthetic reinforcement solution to prevent the formation of localised sinkholes*", Canadian Geotechnical Journal, August 2000.

ELASTICIZED GEOFOAM FOR REDUCTION OF COMPACTION-INDUCED LATERAL EARTH PRESSURES

J. Nathan Reeves and George M. Filz
Virginia Polytechnic Institute and State University, USA
David D. Van Wagoner
GeoTech Systems Corporation, USA

ABSTRACT

Compaction of backfill adjacent to retaining walls that are restrained from movement can induce large lateral earth pressures, requiring substantial wall sections. Several pilot-scale tests were performed in which elasticized geofoam was placed on the backfill side of a 2-m-high instrumented retaining wall. Sand backfill was placed in lifts and compacted with either a vibrating plate compactor or a rammer compactor. The test results show that the lateral earth pressures on the wall are smaller with geofoam than without it and that the lateral earth pressures are smaller for thick layers of geofoam than for thin layers of geofoam. A 150-mm-thick layer of elasticized geofoam resulted in lateral earth pressures approximately 50 percent smaller than the pressures on the wall without geofoam. Cost comparisons demonstrate that substantial savings can be achieved when elasticized geofoam is used to reduce compaction-induced lateral earth pressures.

INTRODUCTION

Retaining walls and basement walls retain soil to create useable spaces below adjacent ground surfaces, and the retained soil exerts lateral pressures on these walls, which must be designed to withstand the pressures. The retained soil is typically compacted to improve its properties, but compaction can increase the lateral earth pressures (Broms 1971, Duncan and Seed 1986, and Filz and Duncan 1996). Compaction-induced lateral pressures are larger for walls that are restrained against movement, like basement walls and mass-concrete walls on rock foundations, than they are for walls that are able to move.

One proposed method to reduce compaction-induced lateral earth pressures is by the use of a synthetic compressible inclusion between the wall and the retained soil (Horvath 1995, 1997). If a compressible inclusion is placed against a retaining wall prior to placing and compacting the backfill, the magnitude of lateral earth pressures may be reduced. As the inclusion compresses under the lateral pressures, the backfill expands laterally, and the strength of the backfill becomes more fully mobilized. Lateral earth pressures are smaller when the soil strength is mobilized by lateral expansion than when it is not.

A series of instrumented retaining wall experiments were performed to study the effect that an elasticized geofoam product has on reducing compaction-induced lateral earth pressures. Elasticized geofoam is an expanded polystyrene geofoam that has been subject to a large compressive strain during the manufacturing process. Applying this compressive strain permanently alters the geofoam structure, producing a material with reduced stiffness at low stress magnitudes (Horvath 1995).

The elasticized geofoam product used in this research has an average density of 14.4 kg/m^3 (0.9 pcf), as delivered. A limited laboratory testing program was conducted to assess the compressibility of the elasticized geofoam.

This paper provides a description of the laboratory and instrumented retaining wall experiments that were performed. A discussion of the impact of elasticized geofoam on the cost of non-moving, mass-concrete walls is also provided.

LABORATORY TESTS

Laboratory creep tests were performed to measure the compressibility of elasticized geofoam under sustained loads. Cubes of geofoam, 50 mm on a side, were subjected to unconfined compression. The value of Poisson's ratio for geofoam is close to zero (Horvath 1995), so the values of stiffness in unconfined and confined compression should be similar. The samples were loaded perpendicular to the sheets from which they were trimmed, which is the same direction as the field loading. The room temperature during testing was approximately 25° C.

A consolidometer device was used to apply the loads. Two steel plates, 76 mm square by 6 mm thick, served as load platens. The elasticized geofoam specimens were placed between the two steel plates, and loads from the consolidometer were then applied. Compression measurements were made with a dial gage.

Creep testing was performed to develop a set of isochronous stress-strain curves for the elasticized geofoam. In these tests, a constant load was applied to a specimen and strain measurements were taken over time. Each measurement provides a data point on a stress-strain isochrone. Four creep tests were performed at compressive stresses of 9.6 kPa (200 psf), 14.4 kPa (300 psf), 19.2 (400 psf), and 24.0 kPa (500 psf). Deflection readings were taken at 0.1 hours, 1 hour, 10 hours, and 100 hours for each test, with these times representing the total duration from the beginning of load application. Deflection readings were then converted to values of strain. These readings produced stress-strain curves for load durations of 0.1 hours, 1 hour, 10 hours, and 100 hours.

The isochronous stress-strain curves from the creep tests are shown in Figure 1. It can be seen that there is a progressive decrease in the slope of each curve between 0 kPa and 19.2 kPa compressive stress. The slopes of the curves begin to increase between 19.2 kPa and 24.0 kPa.

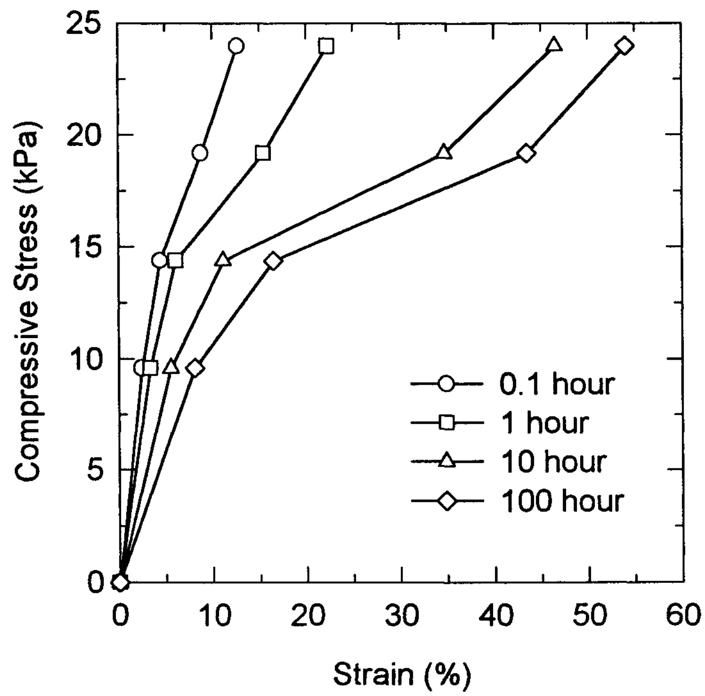

Figure 1. Stress-Strain Isochrones for Elasticized Geofoam

INSTRUMENTED RETAINING WALL TESTS

Instrumented retaining wall tests were performed using two different hand operated compactors and geofoam thicknesses ranging from 50 to 250 mm. Tests were also performed without geofoam to provide a basis for comparison. The following sections provide descriptions of the instrumented retaining wall test facility, the backfill soil, the test procedures, and the test results.

Test Facility

The instrumented retaining wall consists of four, 200-mm-thick concrete panels located within a very stiff reinforced concrete structure, as shown in the oblique view in Figure 2. Each of the panels is 0.76 m wide by 2.13 m tall, so the overall wall size is 3.05 m long by 2.13 m high. The backfill area is 1.83 m wide, 2.13 m high, and 3.05 m long. An access ramp leads to the bottom of the backfill area and is 1.83 m wide by 3.66 m long. During backfill operations, the backfill area and access ramp are both filled with compacted soil.

Lateral support for the instrumented wall is provided by the 380-mm-thick concrete reaction wall shown in Figure 2. A cross-section through the reaction wall and lateral support system for the instrumented wall is shown in Figure 3. The lateral support system includes load cells, a steel frame, and screw jacks. Each panel is directly supported by three load cells (not shown in Figure 3) that react against a steel frame. The steel frame is, in turn, supported by four screw jacks, two located toward the bottom of the wall and two located near the top. The screw jacks bear on the 380-mm-thick concrete wall. The reaction wall is part of a massive U-frame structure that contains the backfill area and instrumented wall, as shown in Figure 3. The base of the U-frame structure is 530 mm thick. The U-frame structure is essentially non-deflecting under lateral loads from the backfill. Although the screw jacks permit the instrumented wall to be moved toward or away from the backfill, this capability was not used for the test results reported in this paper.

The three load cells that support each panel were used to obtain the lateral force applied by the backfill to the instrumented wall. The instrumented wall is equipped with other instrumentation (Sehn and Duncan 1990), but only the lateral load cells were used in this research.

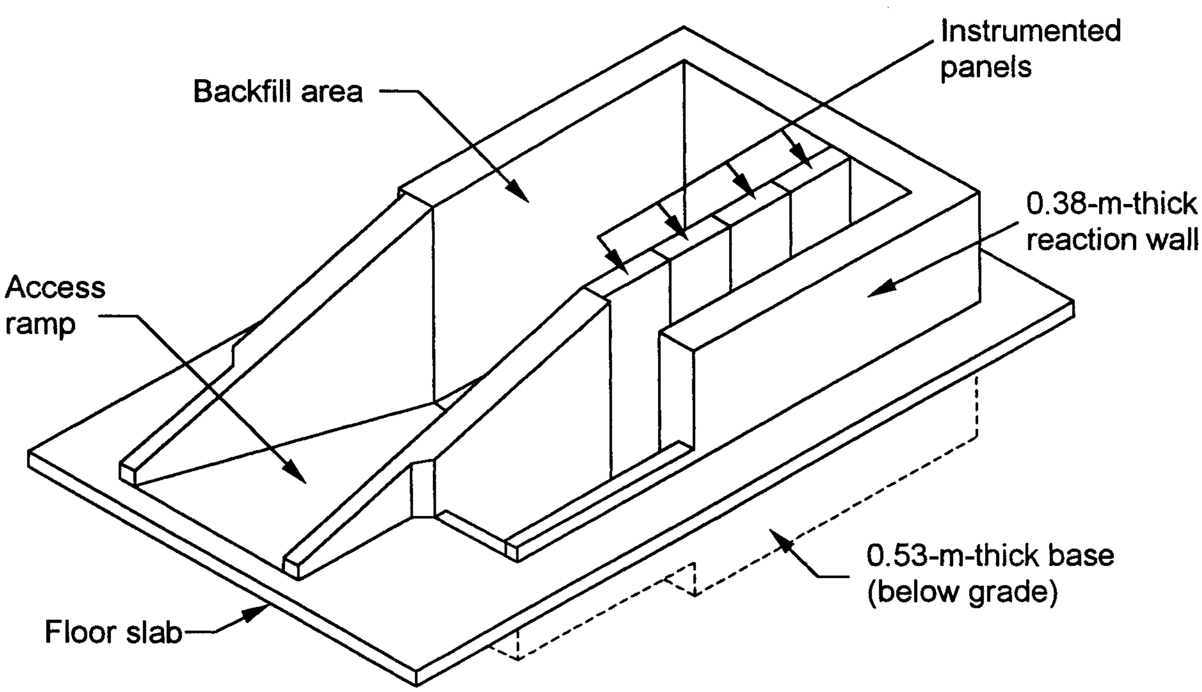

Figure 2. Instrumented Retaining Wall Test Facility (after Sehn and Duncan 1990)

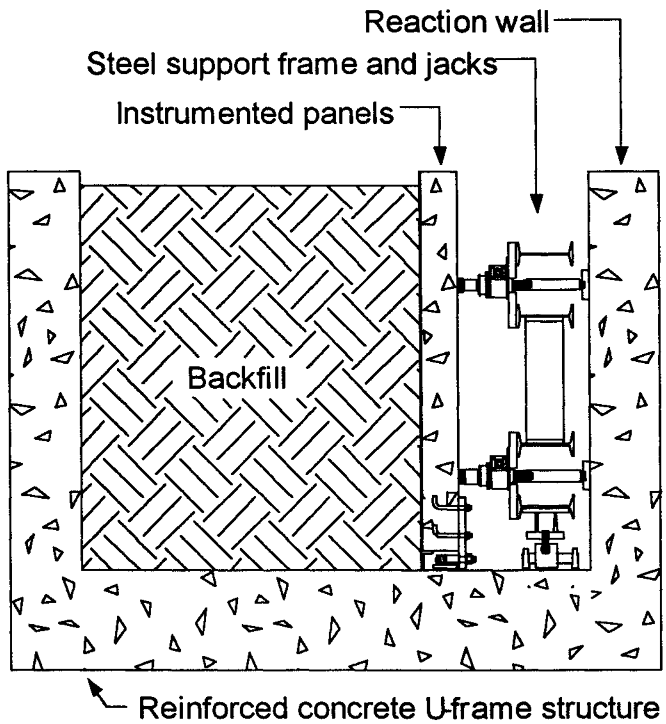

Figure 3. Cross-section through the Instrumented Retaining Wall Facility (after Sehn and Duncan 1990)

Backfill Soil

Light Castle sand obtained from a quarry in Craig County, Virginia, was used as the backfill soil for the instrumented retaining wall tests. Light Castle sand is a clean, fine sand consisting predominantly of subangular quartz grains. About 68 percent of Light Castle sand passes the No. 40 sieve, and less than 1 percent passes the No. 200 sieve. The coefficient of uniformity and coefficient of curvature are 1.8 and 0.9, respectively, and the sand classifies as a poorly graded sand (SP) according to the Unified Soil Classification System. The specific gravity of solids is 2.65. The maximum and minimum densities determined according to ASTM D4253-83 and ASTM D4254-83 are 16.6 and 13.9 kN/m^3, respectively. According to Filz and Duncan (1992), the friction angle of the Light Castle sand is about 42 degrees when it is at its maximum density.

Test Procedures

Preparation of the test facility included 1) lubricating the end wall and the far wall and 2) placing elasticized geofoam against the instrumented wall. Lubrication of the end wall and the far wall was performed to reduce shear stresses on these walls and thereby create a condition approximating a backfill area of broad lateral extent. Lubrication was accomplished by taping a 6-mil sheet of polyethylene against the walls, spreading a thin layer of wheel bearing grease on the polyethylene sheet, and then covering the grease with another sheet of 6-mil polyethylene. The elasticized geofoam was secured to the instrumented wall with an adhesive supplied. The geofoam was applied over the full height and length of the instrumented wall, and extended 0.75 m onto the wall in the access ramp area so that there would not be an abrupt transition at the beginning of the instrumented wall.

The Light Castle sand was dried to a water content of less than 0.1 percent and placed in a dry stockpile area. The sand was moved from the stockpile area to the backfill area by a hopper lifted by an overhead crane. After depositing the sand in the backfill area, it was spread by hand in loose lifts of sufficient thickness to produce compacted lift thicknesses of 0.15 m. Thirteen lifts were used in each test to produce a compacted backfill height of 2.0 m.

For this study, two hand-operated compactors were used: a rammer compactor (Wacker model BS60Y) and a vibrating plate compactor (Wacker model BPU 2240A). For tests using the rammer compactor, each backfill lift was compacted with 2 passes. For tests using the vibrating plate compactor, 5 passes were used to compact each lift. Both compaction procedures produced dry unit weights of about 16.5 kN/m^3, which corresponds to a relative density of nearly 100 percent.

The rammer and vibrating plate compactors used in this study are commonly employed for compaction in confined areas and adjacent to various types of structures, including retaining walls. In a separate study (Filz and Brandon 1993), it was found that the rammer compactor delivers a much higher peak contact force to the soil backfill than the vibrating plate compactor. When operated during the final pass on Light Castle sand, the average measured peak contact forces for the rammer and vibrating plate compactors were 21.3 kN (4,780 lb) and 5.8 kN (1,310 lb), respectively. Because of the higher peak contact forces, higher compaction-induced earth pressures are expected in backfill compacted with the rammer compactor than in backfill compacted with the vibrating plate compactor.

Horizontal load cell readings were taken immediately after backfill placement and for a period of several days thereafter.

Test Results

The results of the instrumented retaining wall tests are expressed in terms of the lateral earth force coefficient, K_h, which is defined as follows:

$$K_h = \frac{F_h}{\frac{1}{2}\gamma H^2} \tag{1}$$

where F_h is the lateral earth force on the wall (kN/m), γ is the unit weight of the backfill soil (kN/m^3), and H is the height of the backfill against the wall (m). The values of F_h used in equation (1) were obtained from the horizontal load cell measurements.

The test results are presented in Table 1 and Figures 4 and 5 for the five instrumented retaining wall tests performed for this research and one test performed as part of a previous study (Filz and Duncan 1992). It can be seen in Table 1 that the values of K_h are higher for the rammer compactor than for the vibrating plate compactor, they decrease with increasing geofoam thickness, and they decrease with time after backfill placement.

Table 1. Instrumented Retaining Wall Test Results

Test	Geofoam thickness (mm)	Compactor	K_h at end of backfill placement[a]	End-of-test values: Elapsed time after backfill placement (hours)	End-of-test values: K_h	End-of-test values: Reduction in K_h due to geofoam (percent)
1	50	Rammer	0.62	131	0.54	38
2	100	Rammer	0.64	135	0.46	47
3	250	Rammer	0.47	140	0.38	56
4	0	Rammer	0.89	62	0.87	--
5	150	Vib. Plate	0.31	140	0.20	56
EP 16[b]	0	Vib. Plate	0.45	96	0.46	--

[a] Backfill placement took about 25 hours for test 1, 8 hours for tests 2 through 5, and 18 hours for test EP 16.

[b] Test EP 16 was performed as part of a previous study (Filz and Duncan 1992) and is included here to provide a basis for evaluating test 5.

Figure 4 shows the influence of time after backfill placement on values of K_h for Tests 2 through 5. There is relatively little change in the value of K_h for Test 4, which did not have any geofoam placed against the instrumented retaining wall. Significant decreases in the value of K_h were measured for the tests that did have geofoam placed against the instrumented wall. Most of the decrease occurred during the first 24 hours after backfill placement. Decreases in values of K_h with time after backfill placement are consistent with the creep behavior of elasticized geofoam shown in Figure 1.

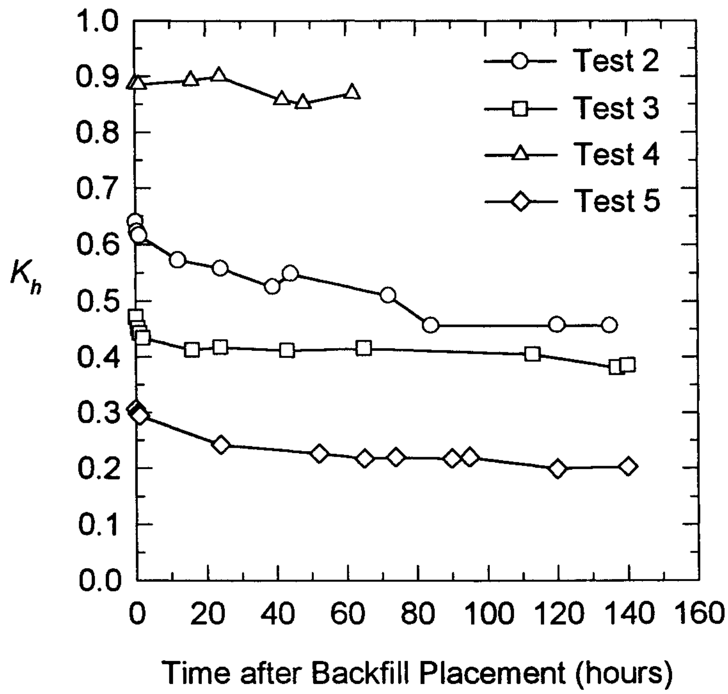

Figure 4. Influence of Time on K_h Values

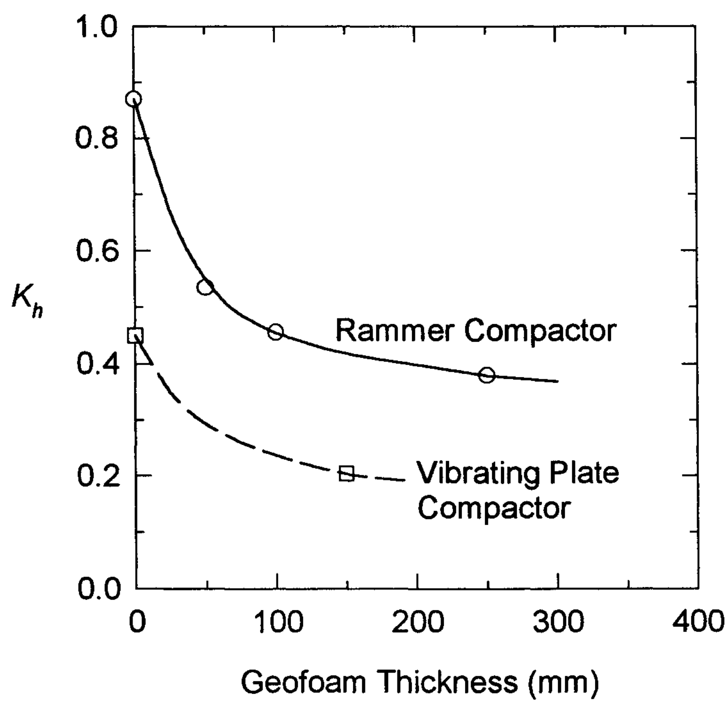

Figure 5. Influence of Elasticized Geofoam Thickness on K_h Values

Figure 5 shows the influence of the thickness of elasticized geofoam on the end-of-test values of K_h for all the tests listed in Table 1. The trend of decreasing values of K_h with increasing geofoam thickness is clear. This trend holds for both the rammer compactor and the vibrating plate compactor, even though the compaction-induced lateral earth pressures for the rammer compactor are much higher than for the vibrating plate compactor. Based on the data presented in Table 1 and Figure 5, a geofoam thickness of 150 mm provides about a 50% reduction in compaction-induced lateral earth pressures for both compactors.

Economic Impact on Mass-Concrete Retaining Walls

One way to evaluate the significance of reductions in compaction-induced lateral earth pressures is to estimate the impact on the cost of mass-concrete retaining walls. For the purposes of this evaluation, a simple trapezoidal shape is assumed for a non-moving, mass-concrete wall on a rock foundation, as shown in Figure 6. Assuming that bearing capacity of the rock is not a limitation, the controlling design criteria for a wall like that shown in Figure 6 are sliding and overturning.

In the absence of vertical shear forces on the back side of the wall, the minimum width to prevent sliding, $B_{MIN\text{-}SL}$, is given by

$$B_{MIN-SL} = \frac{2(FS)(K_h)\gamma}{3\mu\gamma_{conc}}H \tag{2}$$

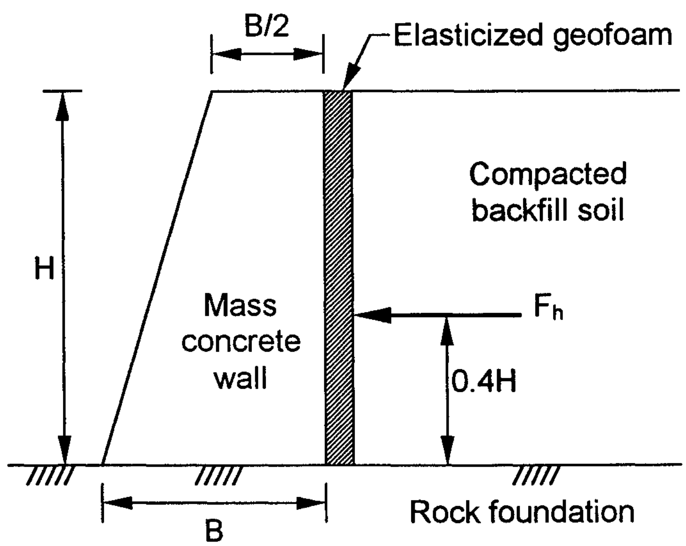

Figure 6. Mass-Concrete Wall for Cost Assessment

where FS is the factor of safety against sliding, μ is the coefficient of friction at the concrete-wall interface, and γ_{conc} is the unit weight of the concrete (kN/m^3).

According to Duncan et al. (1990), an adequate margin of safety against overturning is provided for a wall on a rock foundation by requiring that the resultant normal force on the base of the wall be within the middle half of the base, provided that the elevation of the lateral force is taken at 0.4H above the base. These considerations imply that the minimum width to prevent overturning, $B_{MIN\text{-}OV}$, is given by

$$B_{MIN-OV} = 0.86\sqrt{K_h \frac{\gamma}{\gamma_{conc}}}\, H \tag{3}$$

Considering both sliding and overturning, the minimum width necessary for stability is the larger of the values given by equations (2) and (3). These equations apply only for the geometry and conditions shown in Figure 6.

To evaluate the impact of a 150-mm-thick layer of elasticized geofoam on the cost of a 4-m-high wall, the following assumptions were made: $FS = 1.5$, $\gamma = 20$ kN/m^3, $\mu = 0.8$, and $\gamma_{conc} = 23.5$ kN/m^3. It was also assumed that the values of K_h are 0.6 for a wall without a compressible inclusion and 0.3 for a wall with a 150-mm layer of elasticized geofoam. For the wall without a compressible inclusion, equation (2) controls, and the required base width is 2.55 m. For the wall with 150 mm of elasticized geofoam, equation (3) controls, and the required base width is 1.74 m. If the cost of mass-concrete is \$200/m^3 and the installed cost of a 150-mm layer of elasticized geofoam is \$12/m^2, then the cost of the wall without a compressible inclusion is \$1,530/m, and the cost of the wall with 150 mm of elasticized geofoam is \$1,090/m. The cost reduction due to use of a compressible inclusion for this hypothetical example is 29 percent.

Summary and Conclusions

A series of instrumented retaining wall tests were performed to investigate the influence that elasticized geofoam has on the magnitude of compaction-induced lateral earth pressures applied to non-moving walls. Laboratory creep tests were also performed to determine the stress-strain-time relationships for elasticized geofoam.

The laboratory tests showed that elasticized geofoam experiences significant creep, with strains increasing from 22 percent to 54 percent under a constant stress of 24 kPa (500 psf) during the time period from 1 hour to 100 hours. The stress-strain curves are nonlinear, and the nonlinearity increases as the duration of loading increases.

The instrumented retaining wall tests showed that elasticized geofoam effectively reduced compaction-induced lateral earth pressures produced by a vibrating plate compactor and a rammer compactor. After backfill compaction, the lateral earth pressures acting through the geofoam onto the instrumented wall continued to decrease, with most of the reduction occurring within 24 hours. A geofoam thickness of 150 mm reduced the long-term lateral earth pressures by about 50 percent compared to the pressures on walls without geofoam.

The economic benefit of elasticized geofoam was shown with a hypothetical mass-concrete retaining wall, 4 m high, on a rock foundation. A 150-mm layer of elasticized geofoam produced a cost savings of 29 percent.

Acknowledgements

The substantial contributions of Mr. Jesus Gomez, Mr. Brian Metcalfe, Dr. John Horvath, and Dr. Richard Barker to this research are gratefully acknowledged. Financial support was provided by Virginia's Center for Innovative Technology and GeoTech Systems Corporation.

References

Broms, B., 1971, "Lateral Earth Pressures Due to Compaction of Cohesionless Soils," *Proceedings of the Fourth Budapest Conference on Soil Mechanics and Foundation Engineering*, Budapest, 373-384.

Duncan, J.M., Clough, G.W., and Ebeling, R.M., 1990, "Behavior and Design of Gravity Earth Retaining Structures," *Proceedings of the Conference on Design and Performance of Earth Retaining Structures*, ASCE Geotechnical Special Publication No. 25, New York, 251-277.

Duncan, J.M., and Seed, R.B., 1986, "Compaction-Induced Earth Pressures Under K_0-Conditions," *Journal of the Geotechnical Engineering Division*, ASCE, 112(1), 1-22.

Filz, G.M., and Brandon, T.L., 1993, "Compactor Force and Energy Measurements," *Geotechnical Testing Journal*, ASTM, Philadelphia, 442-449.

Filz, G.M., and Duncan, J.M., 1992, "An Experimental and Analytical Study of Earth Loads on Rigid Retaining Walls," Geotechnical Engineering Division, Dept. of Civil Engineering, Virginia Polytechnic Institute and State University, Blacksburg, Virginia, 334 p.

Filz, G.M., and Duncan, J.M., 1996, "Earth Pressures Due to Compaction: Comparison of Theory with Laboratory and Field Behavior," *Transportation Research Record* No. 1526, National Academy Press, Washington, D.C., 28-37.

Horvath, J.S., 1995, *Geofoam Geosynthetic.* Horvath Engineering, P. C., Scarsdale, New York, 217 p.

Horvath, J.S., 1997, "The Compressible Inclusion Function of EPS Geofoam," *Geotextiles and Geomembranes*, 15, 77-120.

Sehn, A.L., and Duncan, J.M., 1990, "Experimental Study of Earth Pressures on Retaining Structures," Geotechnical Engineering Division, Department of Civil Engineering, Virginia Polytechnic Institute and State University, Blacksburg, Virginia.

MISSION VALLEY SHOPPING CENTRE: PREFABRICATED VERTICAL DRAINS KEEP EMBANKMENT CONSTRUCTION ON SCHEDULE

BRIAN L.J. MYLLEVILLE, Ph.D., P.Eng., GOLDER ASSOCIATES LTD.
BRITISH COLUMBIA, CANADA
TREVOR FITZELL, P.Eng., GOLDER ASSOCIATES LTD.
BRITISH COLUMBIA, CANADA

ABSTRACT

The recently completed Mission Valley Shopping Centre in the Fraser Valley of British Columbia, Canada included development of a highway interchange with a 14 m high approach fill embankment constructed on soft and relatively weak floodplain deposits. The use of prefabricated vertical drains within the underlying soft foundation soils was a key design element which allowed the embankment to be constructed to full height in less than 4 months. This paper describes the interchange development, the soil conditions at the site, considerations included in the design and construction of the approach embankment, geotechnical instrumentation and the performance of the embankment.

INTRODUCTION

The Fraser Valley of British Columbia, Canada, has undergone rapid growth in urban development in the last decade or so, resulting in the need for upgrading of the transportation infrastructure. The floodplain deposits of the Fraser River Valley present unique geotechnical challenges for development, and for the upgrading of transportation infrastructure. Many of the development sites located on the floodplain deposits of the Fraser River Valley require significant ground improvement treatment to address geotechnical engineering considerations such as bearing capacity, stability, settlement and seismic liquefaction resistance. One such development was the Mission Valley Shopping Centre and Interchange which was constructed in the summer of 1998. This paper describes the design and construction aspects of the interchange development and the key role that treatment of the site with prefabricated vertical drains played in keeping the development on schedule.

SITE LOCATION AND INTERCHANGE DEVELOPMENT

The Mission Valley Shopping Centre site is located approximately 68 km east of Vancouver, B.C. near the north bank of the Fraser River (see Figure 1). The new grade separation Interchange provides access to the Shopping Centre from Provincial Highway No. 11, just south of the community of Mission, B.C.

The Interchange project was jointly funded by the Government of the Province of British Columbia, the District of Mission and Mission Valley Shopping Centre Ltd., a subsidiary of Schroeder Properties Ltd. (the Developer). Upon completion, and following the post-construction maintenance period, the Ministry of Transportation and Highways of British Columbia assumes ownership and maintenance of this interchange facility.

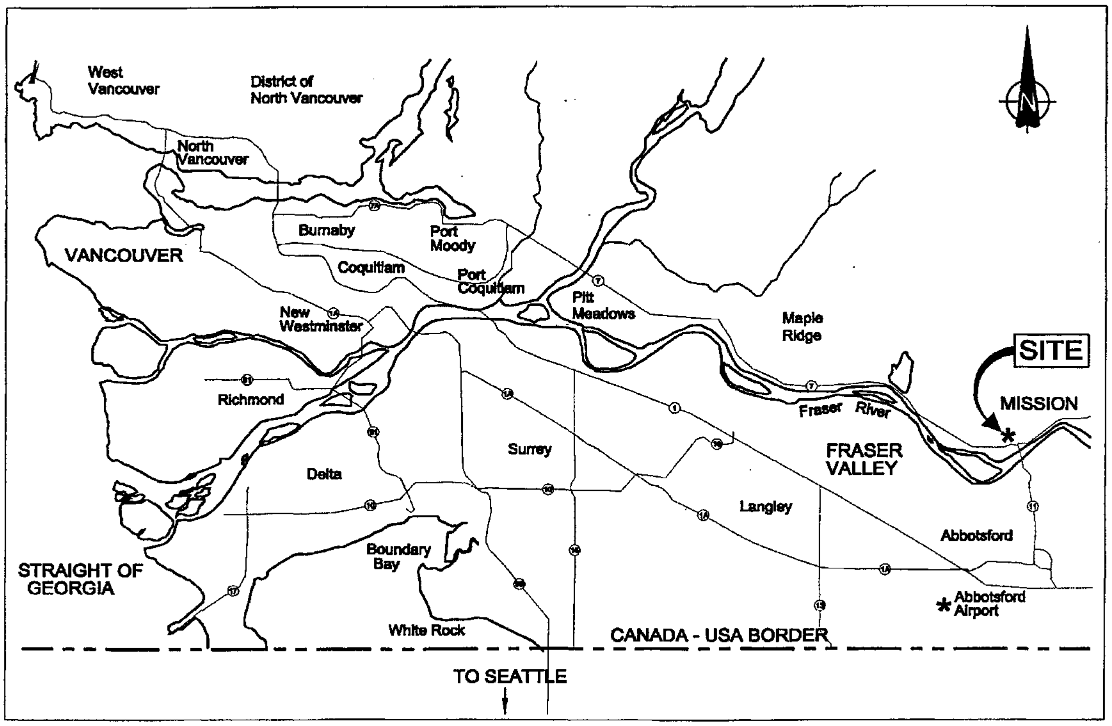

Figure 1. Site Location Plan

The Interchange development includes two single-span bridge structures supported on Mechanically Stabilized Earth structures (an underpass crossing of Highway No. 11 and an overpass along London Avenue to provide improved future access to the shopping mall) together with engineered fill approach embankments. Figure 2 shows the general plan arrangement of the interchange development. A "bird's eye" view of the completed interchange looking toward the southwest is shown on Figure 3. The embankment of interest in this paper is that embankment on the south side of Highway No. 11.

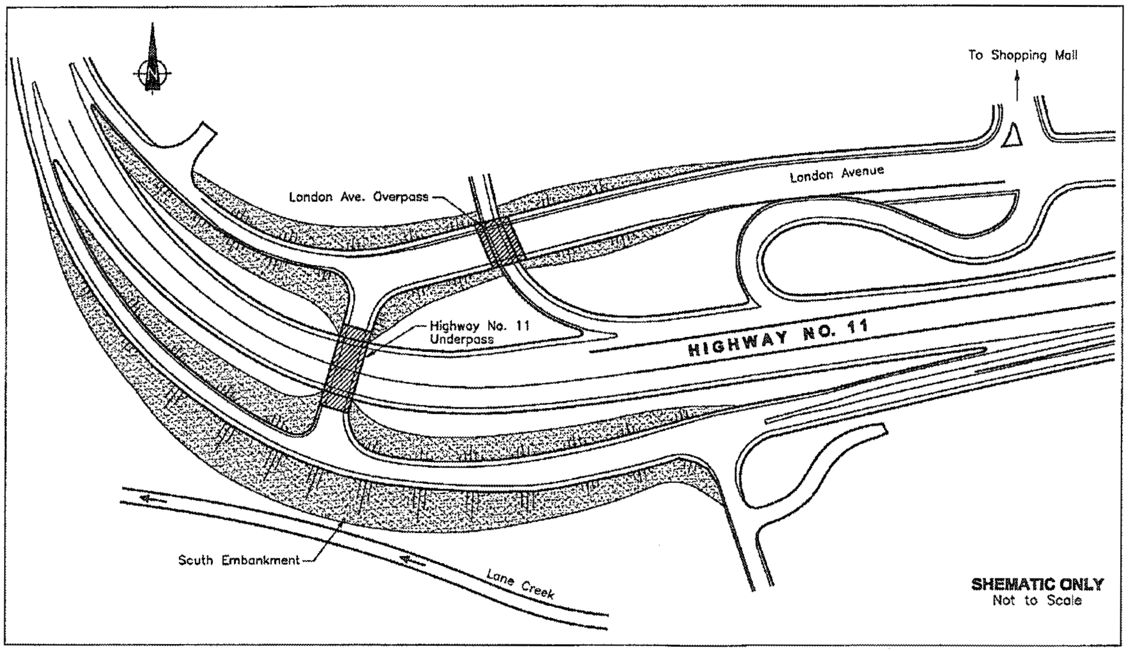

Figure 2. Mission Valley Shopping Centre Interchange General Arrangement

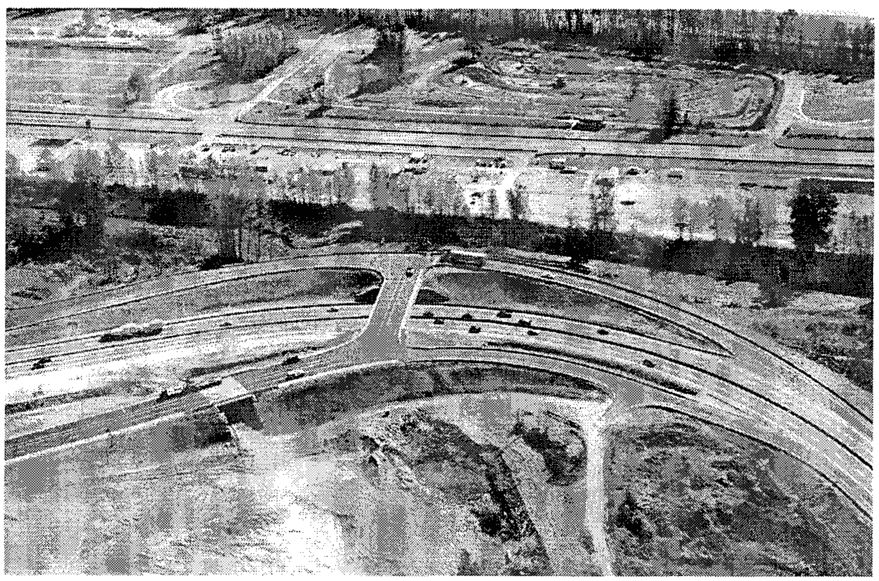

Figure 3. Bird's Eye View of the Completed Interchange

The embankment on the south side of the Highway No. 11, was constructed up to a height of some 14 m above the original ground surface using dredged Fraser River Sand for the bulk embankment fill. The final embankment geometry was developed with 1.75 Horizontal to 1 Vertical side slopes and a slightly back-sloping bench located about mid-height on the embankment. The cross-section geometry of the embankment, looking east at the point of maximum embankment height, is shown on Figure No. 4. The new embankment fill was constructed immediately adjacent to an existing lower height fill embankment supporting Highway No. 11 at that location. The toe of the south embankment is located within some 5 m of the original alignment of a tributary stream to the Fraser River, locally known as Lane Creek. This stream was later realigned to the south during construction to re-establish a minimum 15 m fisheries setback from the toe of the highway embankment. However, because most of the floodplain lowland near the toe of the embankment was inundated as a result of the annual spring flood on the Fraser River, this stream re-alignment work could not be completed until the water levels had receded, and in the meanwhile construction of the embankment was well underway.

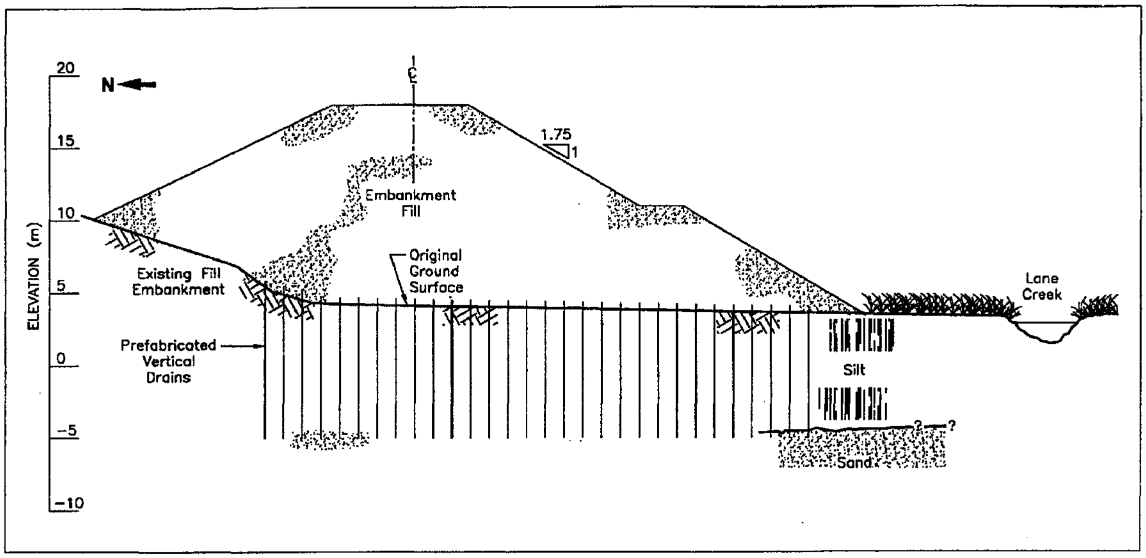

Figure 4. Embankment Geometry

GEOTECHNICAL INVESTIGATION

The Fraser River floodplain deposits are highly variable in nature, with many areas underlain by weak and poorly consolidated sediments, as well as, highly compressible organic deposits. The use of specialized geotechnical ground improvement techniques is commonly required to permit development on these floodplain soils.

Published Surficial Geology Map 1485A, Mission, B.C., indicates the interchange site is underlain by channel and over-bank sediments deposited by the Fraser River. The more recent surficial over-bank sediments typically comprise a highly interlayered sequence of fine sand, silt, and in some areas clay. These deposits are in turn underlain by the older channel deposits of the Fraser River and/or deltaic sediments, which are comprised predominantly of sand and gravel to depths of 100 m or more.

In January 1998, a detailed geotechnical investigation was carried out at the site by putting down a number of small diameter boreholes and electronic Cone Penetration Tests (CPT). In-situ field vane shear testing was carried out within the near-surface silt deposit to investigate the in-situ undrained shear strength properties of the silt stratum. Figure 5 shows the approximate locations of the various boreholes and CPTs put down at the interchange site.

The results of CPT 98-4, put down near the base of the highest part of the embankment are shown on Figure 6. The measured very low tip resistance together with development of excess porewater pressure during cone advance and high friction ratio down to about 8 m depth indicate the presence of relatively soft fine-grained soils. CPT 98-4 was terminated at a depth of 20 m below the original ground surface. Results of a borehole put in the proximity of CPT 98-4 confirmed the presence of a deposit of relatively soft silt to a depth of some 8 m which was in turn underlain by an interlayered sequence of loose to compact silty sand to sand. In-situ vane shear testing was carried out within the silt strata in a borehole put down adjacent to CPT 98-4. With the exception of the upper desiccated crust, which was about 1 m in thickness, the measured undrained shear strength of the soft silt deposit ranges between about 25 and 30 kPa.

Shelby tube samples were collected from the silt deposit. Atterberg limit tests carried out on a sample of the silt indicate Liquid and Plastic Limits of 45 and 30 per cent, respectively, indicating a silt of moderate compressibility. Grain size distribution analyses carried out on samples of silt indicates that the silt contains approximately 20 per cent clay. Results of one-dimensional oedometer testing carried out on the silt gave a coefficient of consolidation, C_v of 3×10^{-3} cm/sec over the stress range equal to the applied stresses from the new embankment fill.

The presence of this relatively soft silt deposit raised concerns relating to the constructability and stability of the south approach embankment, in particular given the short time line available for construction (3 ½ months from mid July 1998 to the end of October 1998). The Developer was contractually committed to complete the interchange development and provide access to the shopping mall to coincide with the scheduled opening of the new shopping mall in late November 1998. As outlined in the next section, a number of important considerations needed to be addressed during both design and construction of the south embankment to meet this objective.

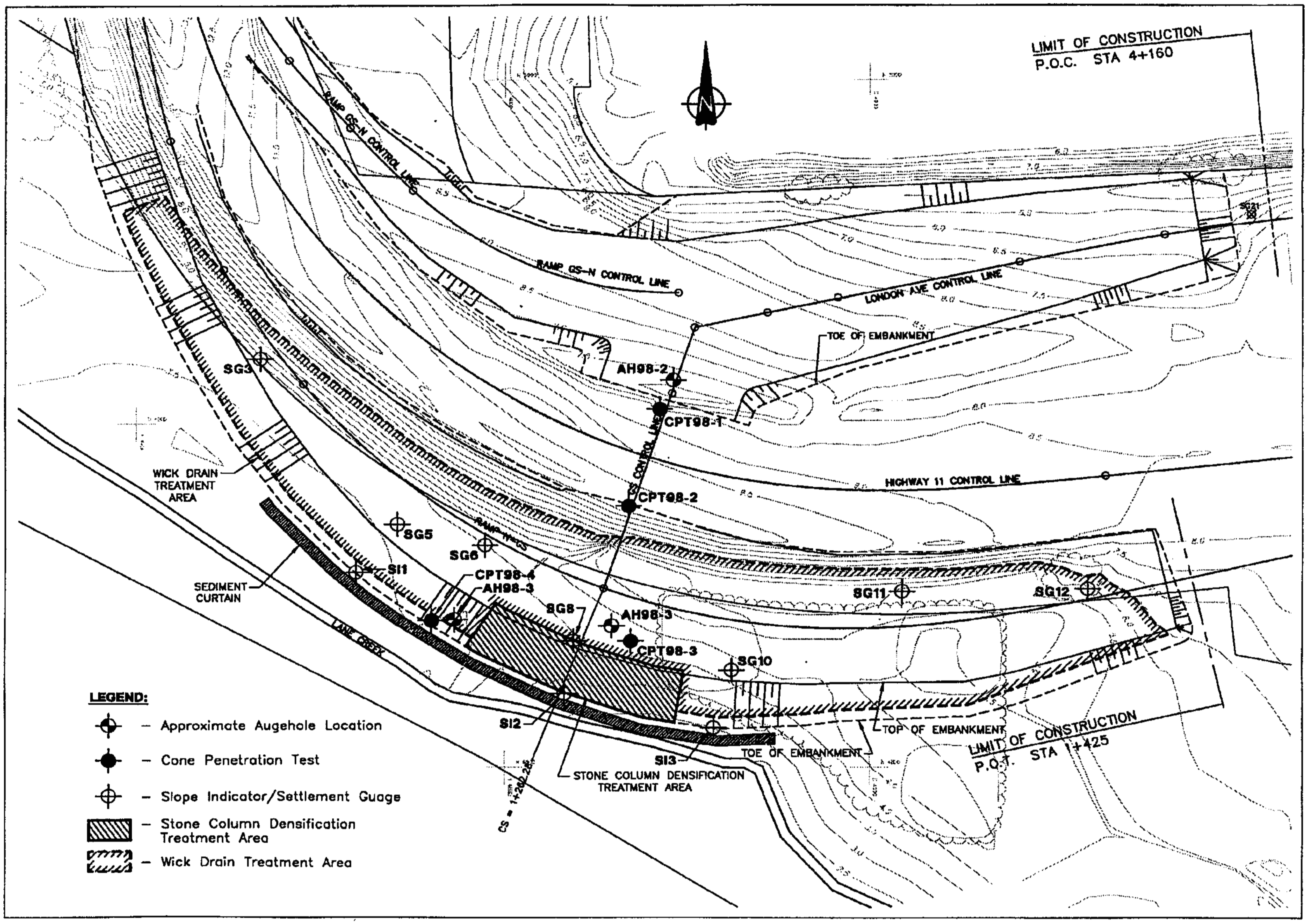

Figure 5. Location Plan of Ground Improvement and Instrumentation

Results of in-situ vane shear testing carried out in several other boreholes put down to the north and adjacent to the existing Highway No. 11, indicated higher undrained shear strengths within the silt strata. The silt deposit in these areas is overlain by varying thickness of previously placed fill materials, most of which was likely deposited as part of the original highway construction. The results of the in-situ vane shear testing carried out in the boreholes put down in the filled areas to the north confirmed that a significant strength gain was achievable as a result of consolidation under relatively modest fill loading. For example, in one borehole put down at the north end of the Highway No. 11 underpass, where the silt deposit was overlain by some 4 m of granular fill, the measured undrained shear strength of the silt ranged between about 80 and 100 kPa. This indicated that, providing excess porewater pressure dissipation could occur quickly enough to facilitate drained loading conditions, foundation soil strengths required to safely support the high embankment could likely be achieved.

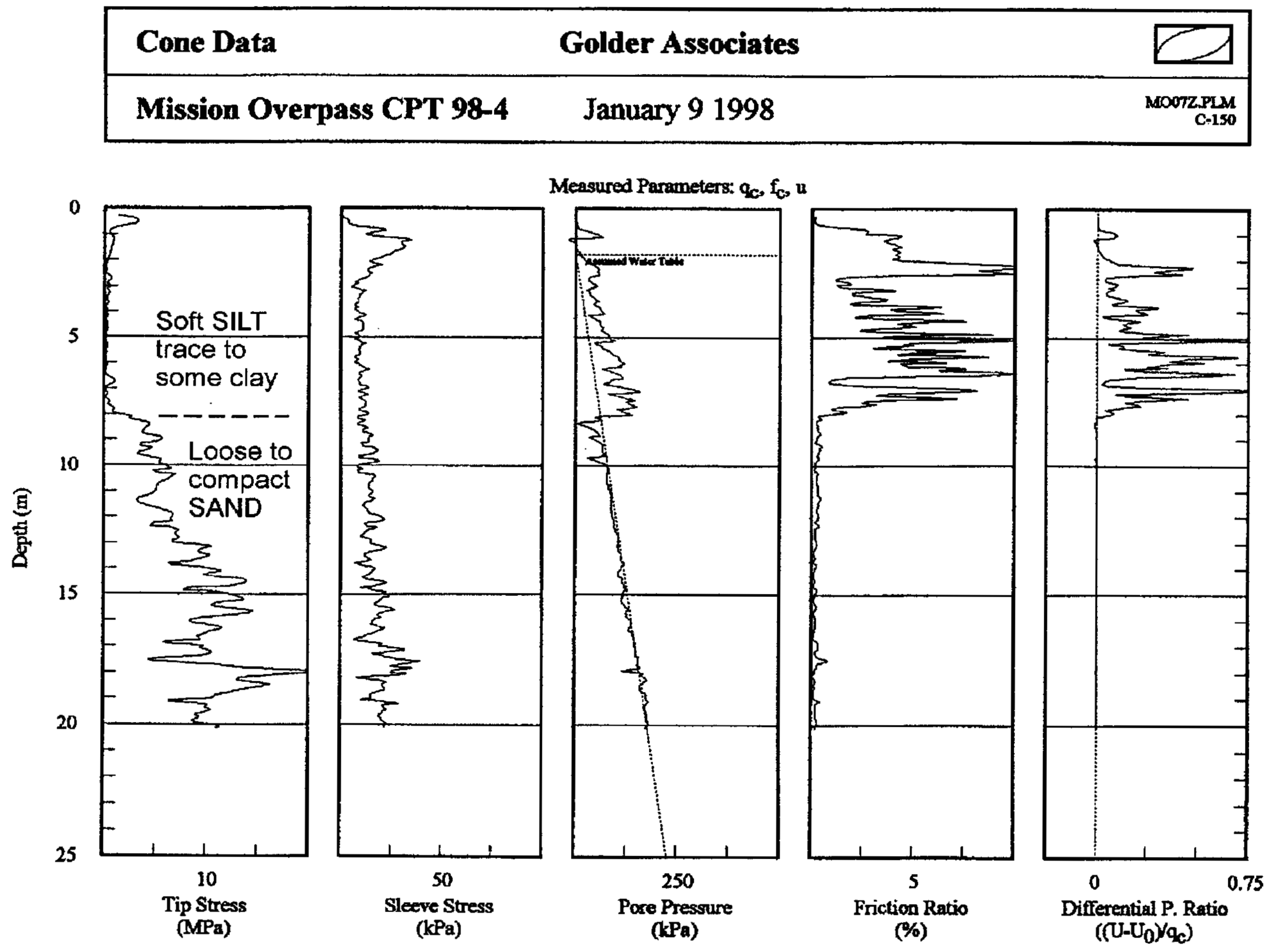

Figure 6. Results of Cone Penetration Testing at Toe of South Embankment

DESIGN CONSIDERATIONS

The design of the south embankment required careful consideration of a number of details to ensure successful completion of the interchange within the project schedule.

First and foremost, the primary geotechnical design consideration was the constructability and stability of this high embankment which was to be located on top of a deposit of soft silt. Results of stability analyses indicated that the embankment could not be built to full height under undrained conditions. In order to achieve an acceptable factor of safety of at least 1.5 under static conditions a significant increase in the strength of the existing soft foundation soils would be required. Data from the existing fill embankment to the north indicated that sufficient strength gain could be achieved through consolidation. However, in order to realize this increase in strength the foundation soils would have to be loaded in carefully controlled stages with sufficient time between fill stages to permit consolidation to occur.

Using the results of one-dimensional consolidation testing, it was estimated that the time for primary consolidation to occur would exceed one year. Given the tight construction schedule, it was considered necessary to try to implement practical and economical means of accelerating drainage of the silt deposit, thus increasing the rate of strength gain within the silt and hence allowing for faster embankment construction

Initially sand drains were considered; however, based on economics and speed of installation, prefabricated vertical drains were ultimately selected to meet the construction schedule. With the objective of achieving primary consolidation in less than four months, the required spacing of the drains was established using a modified procedure as outlined in John (1987) which includes relationships originally developed by Barron (1948) and Kjellman (1948). Estimates of coefficient of consolidation were obtained from the results of one-dimensional oedometer testing on samples of silt. The prefabricated vertical drains were installed to improve drainage and dissipation of excess pore water pressure within the foundation soils, thus accelerating the rate of increase in soil shear strength as the embankment was constructed. Furthermore, the enhanced drainage of the silt deposit also allowed consolidation settlements to occur faster, thus reducing the magnitude of post-construction embankment settlement.

In addition to foundation drainage improvement, a contingency allowance was also made to incorporate lightweight fill (such as Geofoam, or expanded polystyrene, EPS) in the upper part of the embankment in the event that drainage alone did not result in sufficient shear strength improvement within the available time. Fortunately, this was not required in the actual construction.

Although geosynthetic reinforcement was also considered as an option to improve stability of the embankment; the use of reinforcement alone could not have accelerated consolidation settlements and offered improved seismic performance by reducing liquefaction risk. The use of reinforcement together with prefabricated vertical drains was not considered cost effective in this case.

The stability of the south embankment was a concern from an environmental as well as a geotechnical perspective. The toe of the embankment was initially constructed within some 5 m of the original alignment of an existing stream, known locally as Lane Creek. This stream, being a direct tributary stream to the Fraser River, is classified as prime fish-bearing habitat for both anadromous and non-anadromous fish species. The consequences of a slope failure impacting this sensitive riparian habitat would have had negative implications for the project, likely resulting in the inability to complete the interchange within the project schedule.

GROUND TREATMENT FOR IMPROVED EMBANKMENT PERFORMANCE

Ground improvement methods, including vibro-compaction/vibro-replacement ground densification and installation of prefabricated vertical drains, were required both to assist in construction of the south embankment and to ensure satisfactory post-construction performance.

Vibro-compaction/Vibro-replacement ground densification treatment of the loose sandy portions of the foundation soils was required to reduce the risk of seismic liquefaction beneath the toe and side slopes of the higher section of the embankment in proximity to the new Highway No. 11 underpass structure. The extent of ground densification was limited to an area measuring some 60 m in length by 15 m in width in plan area, adjacent to the south end of the underpass abutment structure (see also Figure 5), and extended to a depth of about 14 m. The stone columns formed at about 3 m (centre to centre) spacing during the vibro-replacement process provided the necessary foundation drainage within the silt strata, and also resulted in stiffening of the soils in the treated zone; consequently, additional drainage measures were not required in this area.

Prefabricated vertical drains were installed along the remainder of the footprint of the south embankment (outside of the densified zone) where the proposed fill thickness was greater than 5 m. The prefabricated vertical drains consisted of a polypropylene core with a spun-bonded polypropylene geotextile filter jacket measuring some 100 mm wide by 3 mm in thickness. Using a track-mounted excavator and specially designed mandrel, the drains were installed to a depth of about 9 m, penetrating the entire soft silt deposit and just into the underlying sand strata. The prefabricated vertical drains were installed in a triangular pattern at a spacing of 1.5 m. The Approximate Limits of prefabricated drains is shown on Figure 5.

GEOTECHNICAL INSTRUMENTATION

Geotechnical instrumentation, including settlement gauges, inclinometers (slope indicators) and pneumatic piezometers, was installed to permit monitoring of embankment performance during construction. These instruments were installed just prior to fill placement at the approximate locations shown on Figure 5.

- The settlement gauges consisted of rigid wooden plates with 38 mm diameter steel pipe (and couplings) attached by means of pipe flanges. The settlement gauges were installed immediately following completion of ground improvement.

- The casings for the inclinometers (slope indicators) were installed to depths of between 14 m and 15 m below the original ground surface using auger drilling equipment prior to embankment fill construction. The inclinometer casings were installed along the toe of the embankment at about maximum fill height, with one inclinometer casing located along the outside edge of the densified zone and the other two on either side of the densified zone. The inclinometer casings consisted of 70 mm diameter ABS plastic casing with two sets of orthogonal grooves to guide the slope indicator probe. The inclinometer casings were installed with one set of grooves (axes) oriented as close as possible to perpendicular to the road alignment (or in the expected direction of maximum horizontal movement of the foundation soils).

- Two pneumatic piezometers were also installed within the south embankment; however, one was destroyed shortly following installation and the other malfunctioned giving erroneous results.

Initial baseline readings were taken on all instruments prior to fill placement.

EMBANKMENT CONSTRUCTION AND PERFORMANCE

The south embankment was constructed using Fraser River Sand in a series of about 8 stages, each of which comprised between about 1.5 to 2 m thickness of fill. Construction of the entire embankment was completed in only 3½ months, with fill placement for each stage occurring almost immediately following review of monitoring data and authorization to proceed.

Results of monitoring data collected on a number of settlement gauges installed within the south embankment are plotted together with the filling sequence on Figure 7. The locations of the settlement gauges are shown on Figure 5. The results of settlement monitoring data collected to the end of embankment construction indicate that the range of settlements for the higher part of the embankment was generally between about 250 and 500 mm. This compares well with estimates of construction settlement calculated during design which range between 300 mm and 500 mm. Based on the settlement data collected during construction, long-term post-construction settlements for the highest part of the south embankment were projected to range between 150 and 200 mm, which is within the project design criteria.

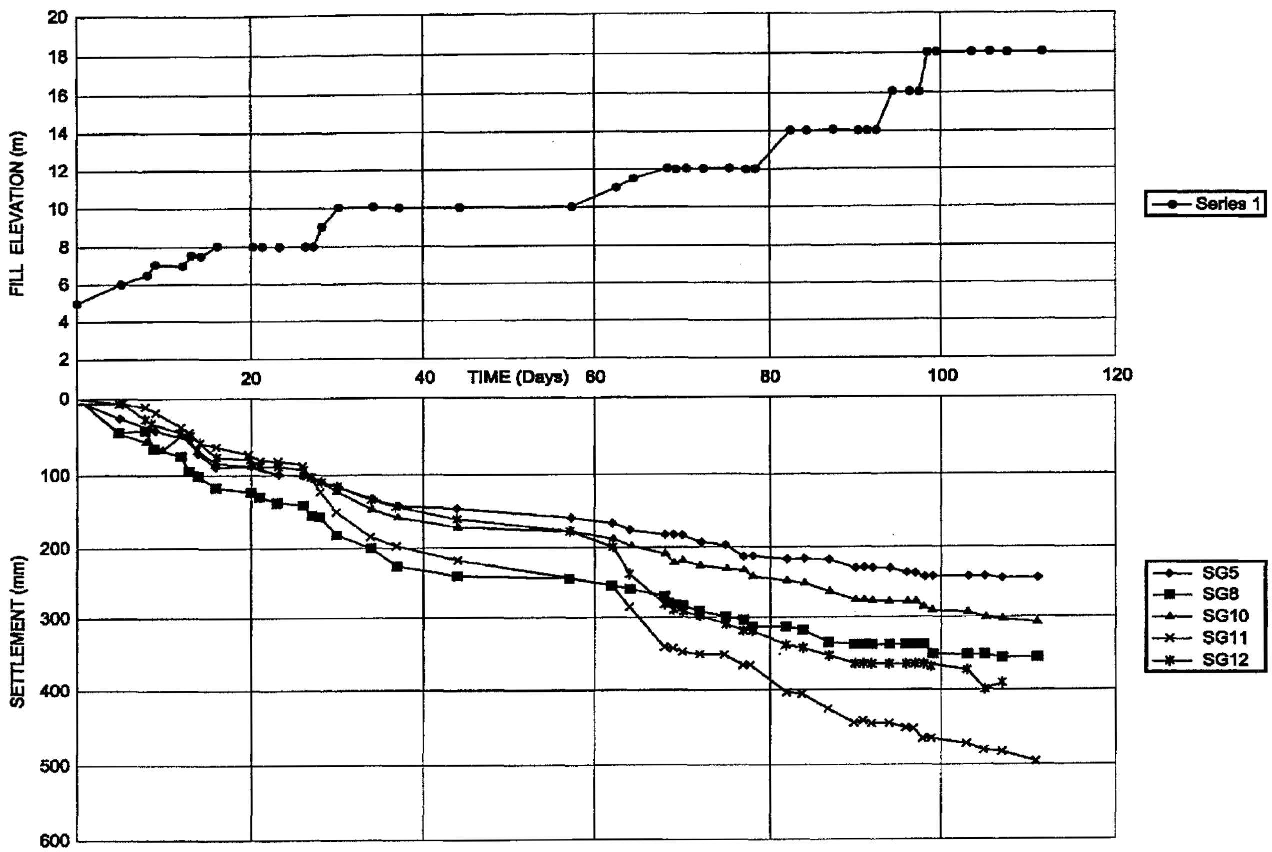

Figure 7. Results of Settlement Monitoring, South Embankment

Results of Inclinometer readings are shown on Figure 8. Inclinometer SI 98-2 was located along the toe of the embankment adjacent to the zone that was densified by Vibro-Compaction/Vibro-Replacement treatment. Cumulative lateral (horizontal) displacements of up to some 90 mm were measured in SI 98-2, with measurable displacements having occurred down to some 8.5 m below the ground surface. In the inclinometer located further east and beyond the densified zone, the cumulative lateral displacements were greater and measured to be as much as about 150 mm. This is not entirely surprising, and illustrates the stiffening benefit of the stone columns. It is interesting to note that the depth of measurable lateral displacement is some 2 m deeper in SI 98-3 than in SI 98-2. This can attributed to the greater depth of the silt strata east of the densified zone. The depth of measurable lateral displacement coincides well with depth of the silt deposit encountered in both the boreholes and the CPTs.

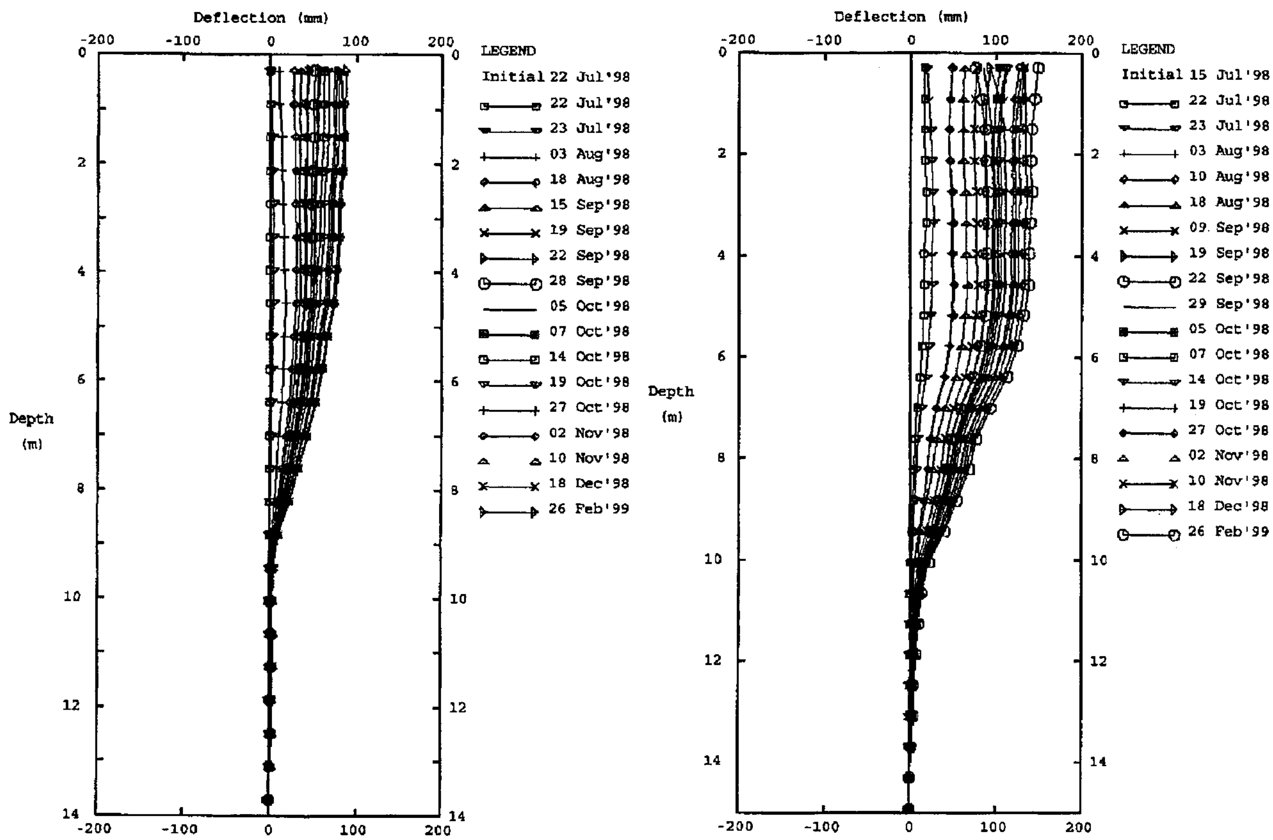

Inclinometer SI 98-2 Inclinometer SI 98-3

Figure 8. Results of Inclinometer Readings at Toe of South Embankment

During construction, rates of settlement and/or lateral displacement were also plotted for the various instrumentation to monitor the performance of the embankment at the various fill stages as input to decision analysis pertaining to the rate of fill placement. The instrumentation proved to be invaluable for analysis of the embankment performance so as to minimize the waiting period between the fill stages and maintain the project schedule.

Figure 9 shows a view (looking east) of the south slope of the completed approach embankment at about maximum fill height. The concrete abutments and superstructure for the Highway No. 11 underpass were completed and opened to traffic in only four weeks following completion of the south approach embankment.

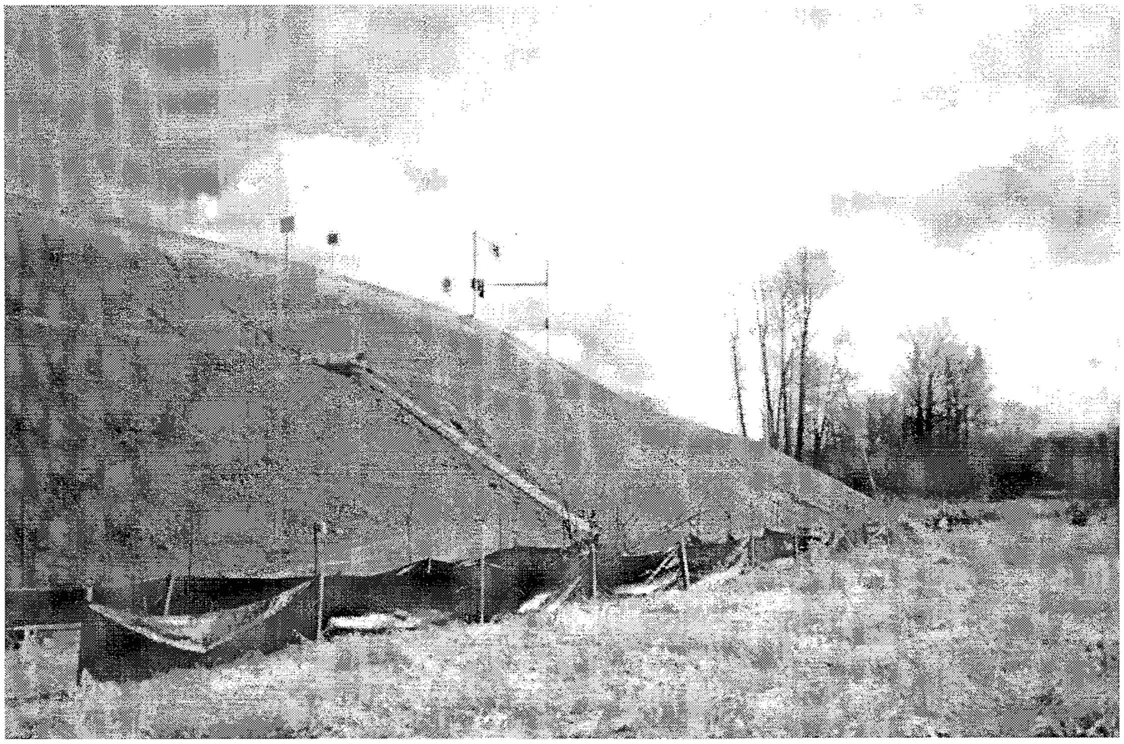

Figure 9. Completed South Embankment (Looking East)

SUMMARY AND CONCLUSIONS

Installation of prefabricated vertical drains was selected as a practical and economical means of accelerating the rate of strength gain and consolidation settlements within the underlying soft silt strata at the site. Given the tight project schedule, this was the most effective approach to ensuring stability of the 14 m high embankment during construction, as well as satisfactory settlement performance following construction. It is expected that, without the benefit of the prefabricated vertical drains, the embankment construction rate would have been much slower, and there would have been serious geotechnical and environmental concerns about embankment stability. The embankment and interchange construction could not have been completed without the improved foundation soil drainage provided by the prefabricated vertical drains.

The geotechnical instrumentation installed at the site proved to be invaluable for monitoring and analysis of embankment performance during construction. This was the basic input data to decision analysis on the rate of fill placement which would ensure an acceptable risk of slope instability during construction while maximizing the rate of embankment construction.

Based on the results of the field monitoring program, the predicted post-construction performance of the south embankment is expected to be well within acceptable geotechnical criteria for the project.

ACKNOWLEDGEMENTS

The authors gratefully acknowledge the cooperation of Dillon Consulting Ltd., Schroeder Properties Ltd. and the Ministry of Transportation and Highways of British Columbia. The authors also wish to acknowledge the assistance of Mr. Pierce Bakker for assembling and plotting the monitoring data, Mr. Shaun Schmidt for preparing the figures and Ms. Teresa Klassen for assistance in preparing the final manuscript.

REFERENCES

Barron, R. A., (1948) "*Consolidation of Fine Grained Soils by Drain Wells*", Trans. ASCE, Vol. 113, pp. 718-754.

John, N.W.M. (1987) *Geotextiles*, Blackie and Son Ltd., London, England.

Kjellman, W., (1948) "Accelerating Consolidation of Fine-Grained Soils by Means of Card-Board Wicks", *Proceedings of 2nd International Conference on Soil Mechanics and Foundation Engineering*, Vol. II, pp. 302-305.

PAVEMENT & RAILWAY SYSTEMS

LENGTH OF SINGLE REINFORCEMENT IN FOUNDATIONS TO MAXIMIZE BEARING CAPACITY

CHRISTOPHER ELVIDGE
DBA ENGINEERING LTD.
CANADA

GERALD RAYMOND
QUEEN'S UNIVERSITY
CANADA

ABSTRACT

Part 1 reports a monotonic load testing program on a surface footing that investigates the effect of geogrid length (Lr) on the ratio of the Ultimate Bearing Capacity (UBC) using a reinforced foundation to the UBC using an unreinforced foundation. From these investigations the optimum (minimum length to give maximum UBC) geogrid length was established to be between 1.2 to 1.5 times the footing width when placed at the optimum depth to result in the maximum UBC.

Part 2 reports a cyclic loading program that investigates the effect of geogrid length (Lr) on the performance of a surface footing on a granular soil reinforced by geogrids of different lengths placed at the optimum depth of placement to give the maximum UBC. The optimum (minimum length to give minimum Settlement) geogrid found to be between 1.0 and 1.5 times the footing width. Finally, the UBC of the post-repeated loading of the footings was observed to be 30 to 50% higher than the similar directly loading of the footings.

INTRODUCTION

The growth of geosythetics has provided engineers with new tools for the construction and transportation industries. Among geosynthetic functions is the reinforcement of granular bases in roads and railroads. This research is part of a program aimed at finding the optimum location for reinforcement in railroad granular bases.

Increasing traffic on former railroad spurlines has lead to the retrofit of these lines using geosynthetics. In order to make such line upgrades as economical as possible it is desirable to maximize the Ultimate Bearing Capacity (UBC) of the granular material by placing the reinforcement at the proper depth. As important as the increase in UBC, the reinforcement reduces the amount of settlement for a given load.

Using a plain strain model of a foundation on a shallow granular layer the following factors were investigated.

1) The effect of geogrid length for two different thicknesses of granular soil on the UBC and pressure distribution of the system.

2) The effect of scale on the results, via a number of different footings tested at the same depth of soil to width of footing ratio (H/B).

3) The effect of geogrid length on the UBC the system when subject to cyclic loading.

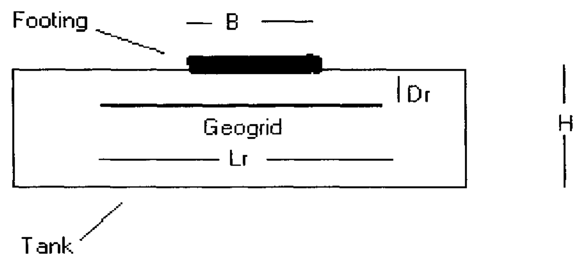

Figure 1 Test Variables

EQUIPMENT

The experiments were performed in a large tank. The tests were conducted in plane strain. The tank had glass sides to reduce friction effects and measured 900 mm long by 200 mm wide by 330 mm deep by 13 mm thick. The rest of the tank was made of 13 mm thick aluminum. Up to 650 kPa of air pressure could be provided by the lab air pressure line. The load was applied by a 193.5 cm^2 Bellofram piston. Figure 2 shows the setup of the testing apparatus.

The primary footing used in the tests was a 200 mm long by 200 mm wide by 19 mm thick aluminum plate. Four thrust bearings allowed slight horizontal movement of the loading piston. The other footings were 75 mm wide, 150 mm wide, and 300 mm wide.

The settlement was recorded by four LVDTs placed at the corners of the footing. The four readings were recorded individually to ensure little differential settlement was occurring and then averaged. The load was measured with a 450 kN load cell attached to the loading piston.

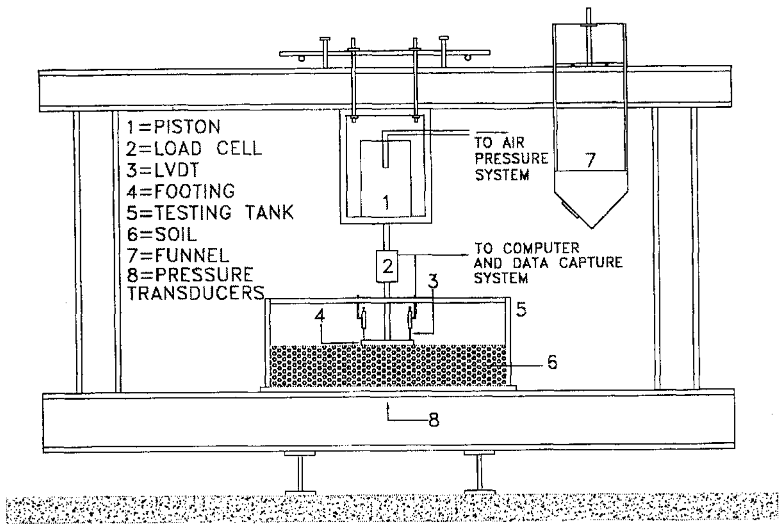

Figure 2 Test Apparatus

MATERIALS

The soil was modelled with a 3 mm diameter ceramic bead. The specific gravity was found to be 2.4 and the angle of internal friction was 33^0 (Ismail, 1994). The placement density using a drop height of 350 mm was 1.5 g/cm^3. A round synthetic soil was used to ensure a constant effective internal friction angle.

The geogrid was a full scale woven polyester grid with PVC coating. The wide-width strength of the grid was 30.5 kN/m in the machine direction and 23.3 kN/m in the cross-machine direction (GFR, 1998). At 5% strain these strengths are 10 kN/m and 4.4 kN/m respectively. A variety of grid lengths were used. The full scale grid was used because 1/10 scale grids sometimes ruptured during testing. Walters (1998) found in preliminary testing that the full scale geogrid and 1/10th scale geogrid produced the same test results.

TESTING PROCEDURE

The soil was measured out and placed into the hopper. The hopper was opened and run back and forth across the I-beam at a rate of 100 mm/s. As each lift was placed the hopper was raised to ensure a drop height of 350 mm for each lift. The thickness of soil varied from 56.25 mm to 225 mm. The thickness of the soil was limited by the height of the tank, but was meant to provide a range of typical ballast thickness, from 50 to 225 cm at 1\10th scale. For the last layer, only half of the lift was placed. After which the soil was levelled and the geogrid was laid down. Then the final half-lift was placed and soil was graded out and slightly compacted. The footing was placed at the centerline of the tank and attached to the loading piston. Then the LVDT assemblies were positioned and clamped in place.

For Monotonic Loading the air pressure in the bellofram was increased at a rate of 0.5 kPa/s until failure. For Cyclic Loading a constant load of 35 kPa for the 200 mm wide footing and 60 kPa for the 300 mm wide footing was applied. The cyclic loading was started and continued until 10 000 cycles. After the cyclic loading the footing was loaded statically from 0 kPa to failure.

Test Program for Part One - Monotonic Loading

The monotonic loading portion of the research program consists of two Phases. In Phase One the effect of soil thickness (H), geogrid length (Lr), and geogrid depth (Dr) at two depths are investigated for a 200 mm wide surface footing (B) and a 150 mm wide surface footing. The two reinforcement depths used were Dr/B = 0.06, and Dr/B = 0.12. These two depths were determined in previous research by Walters (1998) to maximize the bearing capacity of the footing. In Phase Two the effect of scale (different H and B, but same H/B ratio) for various geogrid lengths is investigated.

Test Program for Cyclic Loading

Once the static tests were complete two sets of cyclic tests were performed using a soil thickness (H) of 150 mm, and reinforcement depth (Dr) of 25 mm giving a Dr/B ratio of 0.12. Two different surface footing widths (B) of 200 mm and 300 mm were used. The load was repeatedly applied between 0 and 35 kPa, for B = 200 mm, or 0 and 60 kPa, for B = 300 mm, for 10 000 cycles. The 35 kPa represents approximately 55% of the failure load of the unreinforced test for B = 200 mm, and the 60 kPa represents approximately 35% of the failure load of the unreinforced test for B = 300 mm. Once the cyclic loading was complete the footing was subjected to an increasing monotonic load from zero load until failure.

RESULTS OF PART ONE

Part One investigated the effect of Footing Width (B), Soil Thickness to Footing Width Ratio (H/B), and Depth of Reinforcement to Footing Width Ratio (Dr/B) on the UBC and Settlement of the footing.

Test Results for Phase One

Figure 3 shows the Load-Settlement curves for the B = 200 mm, H/B = 0.75 and Dr/B = 0.06, series. This curve is typical of the curves generated from monotonic loading. The curve typically has an initially linear shape to about 50% failure load after the first 5 kPa of loading. The loading up to 5 kPa is regarded as the load required to seat the footing on the prepared foundation surface. As the test approaches failure, settlement increases and the curve steepens. Eventually the stress becomes too great and the soil-geogrid system fails.

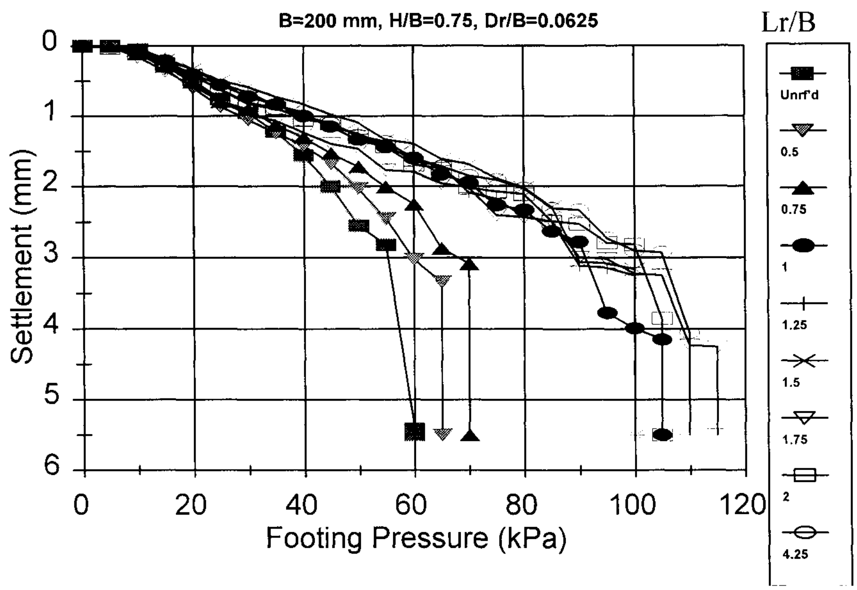

Figure 3 Load Settlement Curves for B = 200 mm, H/B = 0.75, Dr/B = 0.0625, Lr/B = variable

Figure 4 shows the relationship between the Bearing Capacity Ratio (BCR) and the length of geogrid to footing width ratio (Lr/B). The Bearing Capacity Ratio is the ratio of a bearing capacity at a given reinforced condition to the unreinforced bearing capacity.

Figure 4 compares the failure BCR values for the 200 mm footing width at two different H/B ratios. It is apparent when the data is presented in this manner that for H = 150 mm the optimum ratio of geogrid is around Lr/B = 1.0, and that for H = 75 mm the optimum ratio of the geogrid is around Lr/B = 1.50. This suggests that when H/B is small a greater optimum length is required.

Additional Testing

Other sets of tests investigated different depths of geogrid placement and footing widths. The results are similar to those illustrated above. All results for Phase One are summarized in Table 1.

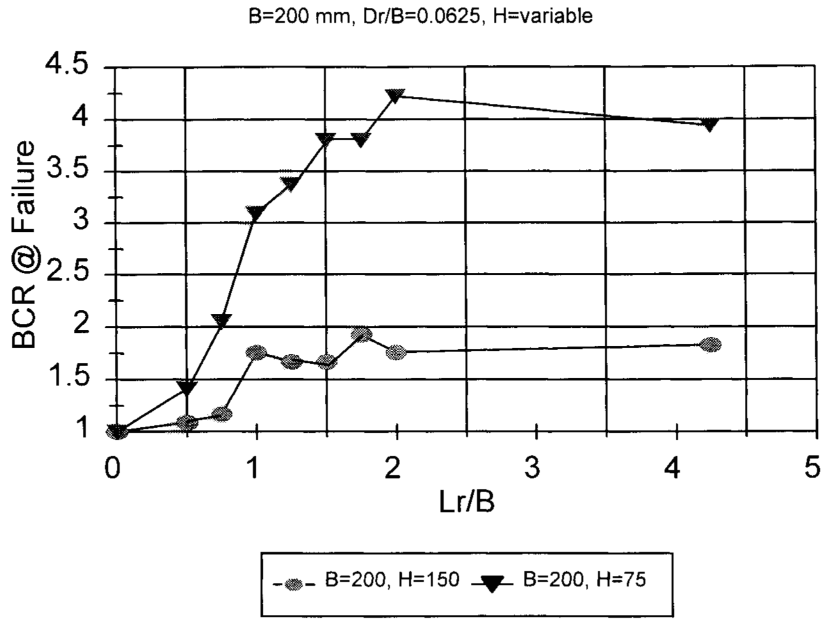

Figure 4 BCR values for B = 200 mm

Table 1: Summary of Phase One Results

B (mm)	H (mm)	Dr (mm)	H/B	Dr/B	Optimum Lr/B
200	150	12.5	0.75	0.06	1.0
200	75	12.5	0.375	0.06	1.5
200	150	25	0.75	0.12	1.25
150	112.5	9.4	0.75	0.06	2.0
150	112.5	18.7	0.75	0.12	1.33

Test Results for Phase Two

The Phase Two tests compare results with footing widths to soil thicknesses ratios (H/B)of 0.75. Two sets of tests from Phase One (series 2 and series 5) and two additional sets. Figure Five shows the Load-Settlement curves for the one of the new series (B = 300). These are similar in shape to the results of Phase One that showed very little settlement for the first 5 kPa of load and then a semi-linear curve to failure.

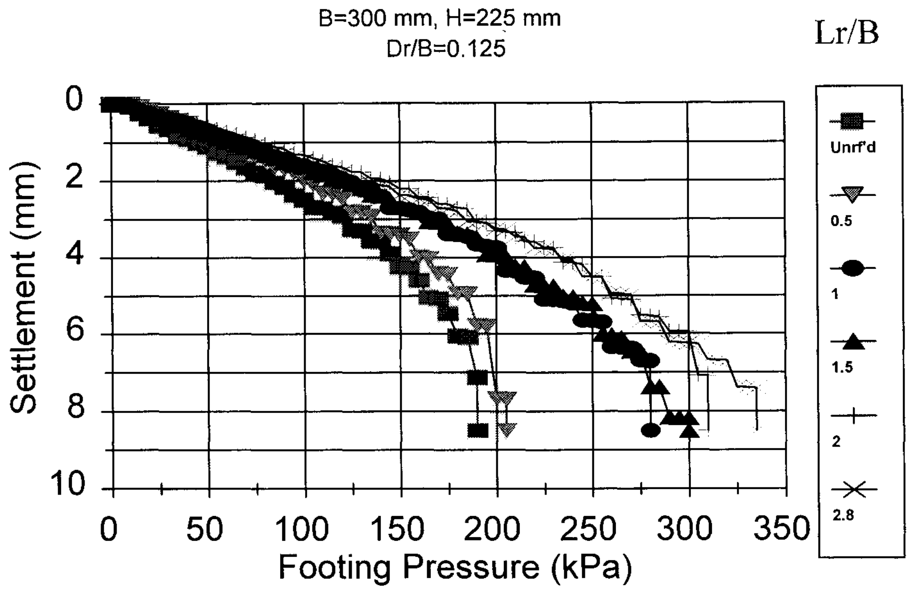

Figure 5 Load Settlement Curves for B = 300 mm, H/B = 0.75, Dr/B = 0.125, Lr/B = variable

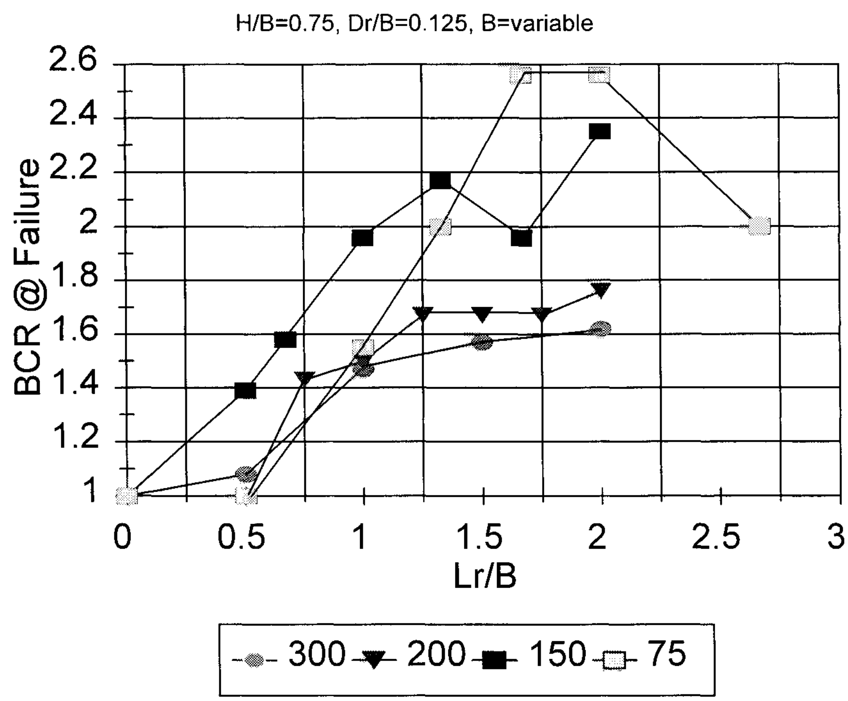

Figure 6 BCR for Various Footing Widths

The Load-Settlement curve for B = 300 mm (Figure 5) shows an increase in load at failure, with no apparent optimum length, although there is a grouping at the highest footing pressures, ranging from 275 to 325 kPa with a minimum Lr/B = 1.0 at 275 kPa and maximum Lr/B = 2.8 at 325 kPa. The Load-Settlement curves for B = 200 mm have been discussed in Phase One, with the optimum length being around Lr/B = 1.25. The Load-Settlement curves for B = 150 mm were discussed in Phase One and showed an optimum length of Lr/B = 2.0 for Dr/B = 0.06 and Lr/B = 1.33 for Dr/B = 0.12. For B = 75 mm the Load-Settlement curve shows the full length (850 mm) failure load being the same as the failure load for Lr/B = 1.33, and 2.66, at 20 kPa, and less than the failure load for Lr/B = 1.67, and 2.00 (25 kPa) suggesting an optimum around Lr/B = 1.33.

Figure 6 shows the bearing capacity ratio (BCR) curves for the four different footing widths. This figure can confirm the optimum length ratios for the different B values. For a B of 300 mm the optimum length is about 1.50. For B = 200, 150, and 75 mm the optimum length is between 1.25 and 1.50.

RESULTS FOR PART TWO

Test Results for Repetitive Loading Using B = 200 mm

Figures 7 and 8 show the curves for all repetitive loading tests using the B = 200 mm

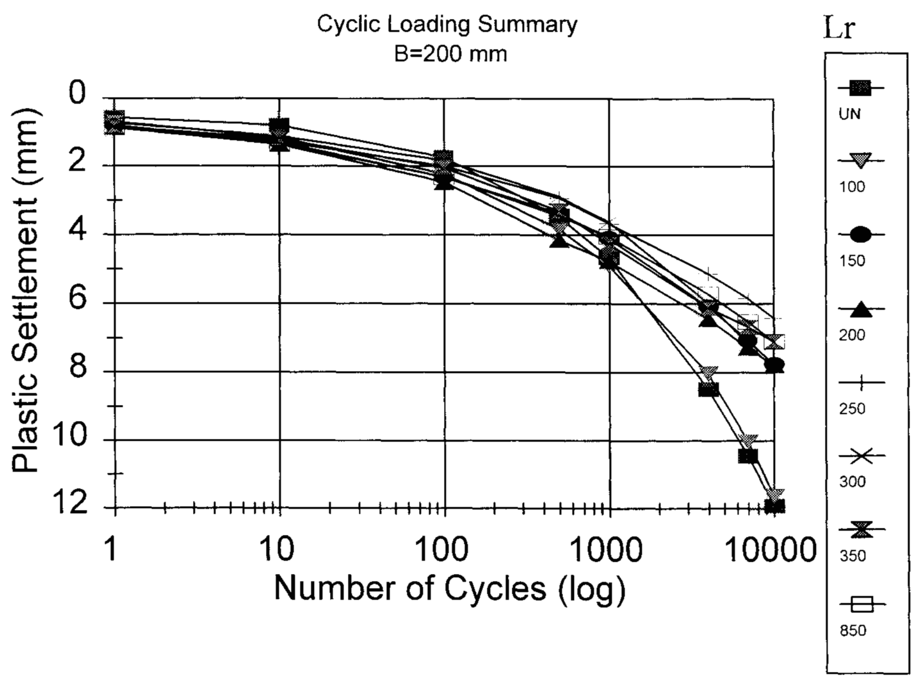

Figure 7 Summary of Plastic Settlement for Cyclic Loading Tests (B = 200 mm, Lr = variable, Load = 0 - 35 kPa)

footing. The Settlement curve illustrates the common shape of each test. It can be seen that, in addition to increased Settlement with increasing number of loading cycles, the addition of the geogrid generally also affects the amount of Settlement. Figure 7 illustrates the value of the reinforcement after the number of repeated loadings N = 1000 cycles. At N = 100 the Settlements for Lr > 100 are slightly less than the Settlements for Lr < 100. At N = 1000 the Settlements for the reinforced tests are up to 1.0 mm less than the Settlements for the unreinforced and Lr = 100 mm tests.

The elastic unloading rebound curves using the B = 200 mm footing (Fig 7) also show a relationship between geogrid length and elastic rebound. The curves all have the same shape, but are linearly displaced vertically on the plot. For most portions of the figure the lowest rebound value is associated with the unreinforced case and the highest rebound is for the 350 or 400 mm geogrid length. At higher number of cycles the spread of the curves narrows from about 0.045 at cycles 1 to 10^3 to about 0.03 at cycles 7000 and 10^4.

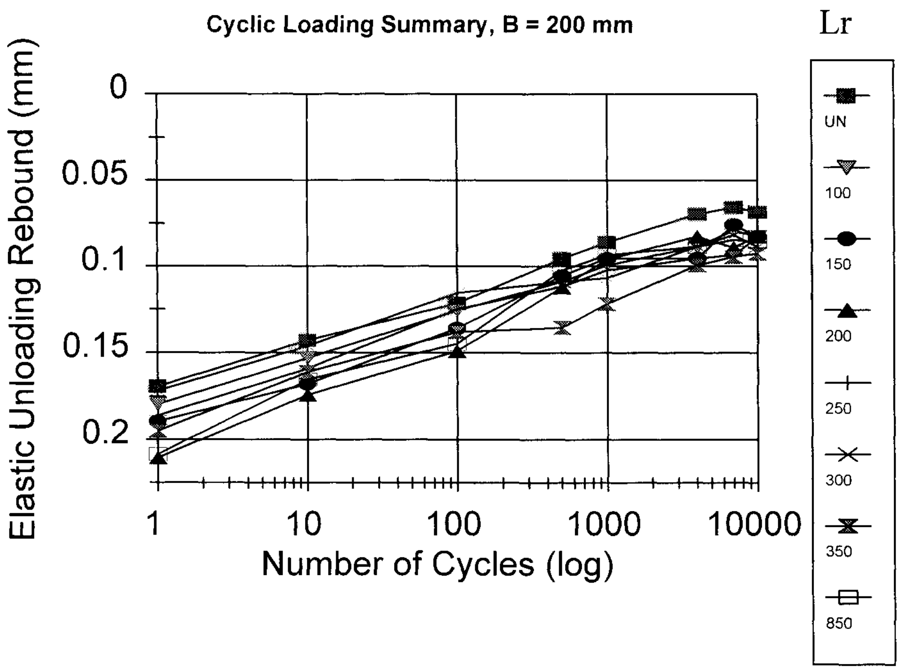

Figure 8 Summary of Elastic Unloading Rebound for Cyclic Loading Tests
(B = 200 mm, Lr = variable, Load = 0 - 35 kPa)

Test Results for (Monotonic Loading)

Figure 9 presents the Load-Settlement curves for the monotonic loading of the 200 mm wide footing over 150 mm of granular material using various lengths of geogrid after 10^4 cycles from 0 to 35 kPa of cyclic stress. The figure has the same features as the same situation without the cyclic loading. There are two groups of curves; one group around the unreinforced failure pressure, and another group around the failure pressure of the optimum geogrid length.

From Figure 9 the UBC load for the various Lr/B values may be obtained. As the geogrid

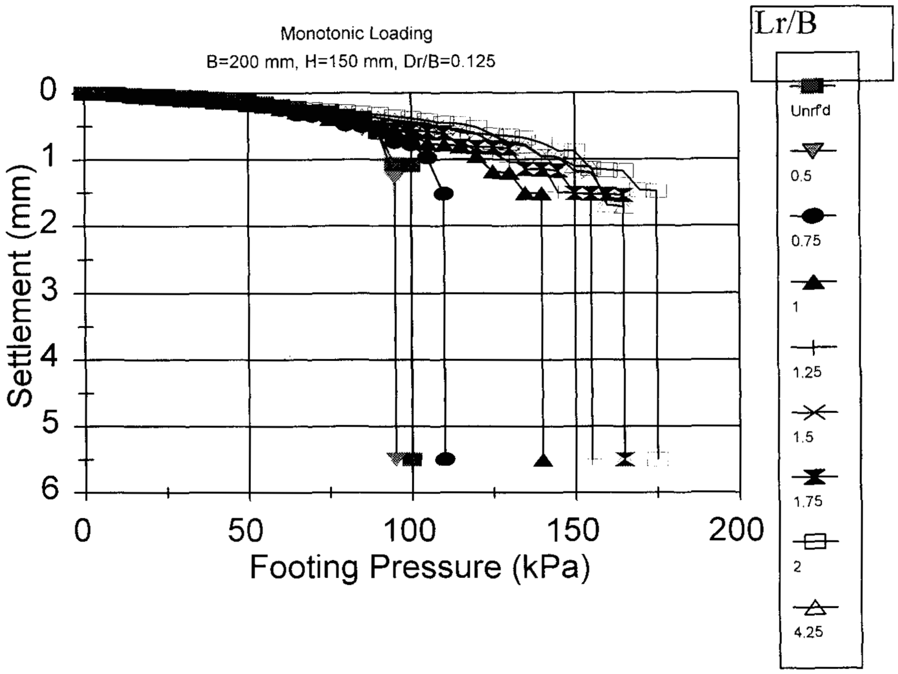

Figure 9 Load Settlement Curves for Cyclic Tests (B = 200 mm, Lr/B = variable)

length increases the footing pressure at failure increases. The results tend to separate into two groups of results. The first group consists of the unreinforced condition, as well as Lr/B = 0.50 and 0.75. The Lr/B = 1.00 test is between the two distinct groups. The optimum geogrid length grouping contains the remaining tests, with the 1.25 Lr/B ratio being at the lower end of the group. There is some scatter in each of the two groups. The optimum geogrid length is between 1.25 and 1.50.

Figure 10 shows the BCR at failure for the post-cyclic static tests and the static tests performed for Part One. There is fairly good correlation between the two curves. The major difference is that the curve for the static condition is slightly higher than the curve for the cyclic tests. The BCR curve confirms that the optimum length is about 1.50 times the footing width.

Additional Test Results

A second series of tests were performed using the B = 300 mm footings and a cyclic load of 35% of the unreinforced failure load. The results are similar to the tests using B = 200 mm. The optimum length was found to be 1.0 B for cyclic loading and 1.0 to 1.5 B for monotonic loading.

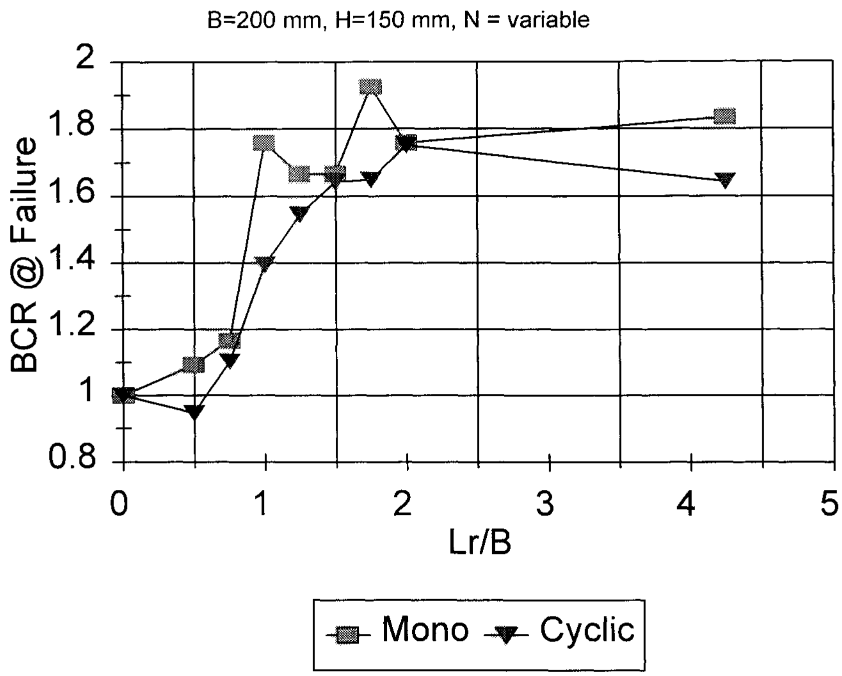

Figure 10 BCR comparing Cyclic and Non-Cyclic loading

DISCUSSION

Part One - Monotonic Loading

An increase in geogrid length leads to an increase in the failure load. This relationship is not linear. The increase in failure load ceases to be significant past Lr/B = 2.0. The relationship between Lr and failure load is best illustrated by the BCR plots. The BCR plots show an average optimum geogrid length of 1.5 times B.

Geogrid depth increases the failure load, but has little affect on the BCR.

Two granular thickness were used, 75 mm and 150 mm. The thinner (75 mm) soil thickness showed higher failure loads and lower settlements. The reduced settlement is most likely due to the fact that there is half the amount of material that is able to deform. The BCR at failure decreases as the footing width increases. This indicates that, in this testing, the effect of the geogrid is more pronounced at smaller scales.

Part Two - Repetitive Loading

The second part of the research program examined the effect of geogrid length on the plastic settlement and elastic rebound of a footing on granular material. Additionally a comparison can be made between the UBC of statically and cyclically loaded footing to determine the effect of cyclic loading.

The presence of the geogrid reduces the amount of plastic settlement. This becomes most evident after 10^3 cycles. Geogrid lengths less than 0.5 B have little effect on the plastic settlement.

Usually the unreinforced test shows the least amount of elastic rebound and the reinforced tests show no distinct pattern. This indicates that the presence of the geogrid effects the elastic rebound, but the length of geogrid makes little difference.

Comparing the static and post-cyclic load settlement curves for B = 200 mm it can be noted that cyclic loading increases the failure load and decreases the settlement at failure. The increase in failure load can be as high as 66% and the reduction in settlement can be as high as 50%.

CONCLUSIONS

For Part One - Monotonic Loading

1) The optimum geogrid length in most cases is 1.5 times the footing width.
2) The depth of geogrid length, within the optimum range as determined by Walters (1998), does not effect the BCR.
3) Thinner soil depths lead to increased failure loads, increased BCR at failure, and reduced settlements.
4) Wider Footings at the same H/B ratio increase the failure load (at a proportion of B^2) and decrease the BCR at failure.

For Part Two - Cyclic Loading

1) The inclusion of a geogrid greater than Lr/B = 0.5 reduces the plastic settlement by 27 to 41 percent. The optimum Lr is most effective at reducing the plastic settlement.
2) The inclusion of a geogrid increases the amount of elastic unloading rebound.
3) Preloading the soil with 10^4 cycles at 50% of the unreinforced failure load increases the failure load by 66% and reduces the settlement at failure.

REFERENCES

Ismail, I., 1994, *"Geosynthetic Reinforcement of Granular Layered Soils"*, Ph.D Thesis, Queen's University, Kingston, Canada.

Walters, D.L., 1998, "*Geogrid Reinforcement of Finite-Depth Granular Material Subjected to Monotonic and Repetitive Loading*", M.Sc Thesis, Queen's University, Kingston, Canada.

Design of Geogrid Reinforcement for Heavily Loaded Pavement Systems

ROSS T. MCGILLIVRAY, PE, ARDAMAN & ASSOCIATES, INC.
EDWARD J. GARBIN, JR., UNIVERSITY OF SOUTH FLORIDA
ALAA K. ASHMAWY, PHD, PE, UNIVERSITY OF SOUTH FLORIDA
UNITED STATES OF AMERICA

ABSTRACT

This paper describes the design of a heavily loaded pavement system using geogrid reinforcement of a granular base material. The project required that the pavement system support cargo handling equipment with axle loads exceeding 890 kN at the port facility in Tampa, Florida. Finite difference modeling of the pavement system was carried out as part of the design process in order to determine the optimum location of the geogrid layer within the pavement system cross section. Contrary to the current practice, the numerical model indicated that optimum performance was obtained by placement of the geogrid at very shallow depths within the base course. The numerical model conclusions were verified by means of in-situ, full-scale plate load tests.

INTRODUCTION

The Port of Tampa, like most ports, is located in an area where the subsoils are soft sediments or deep fill materials. The subgrade soils immediately below pavements may be firm, but the soil profile can include debris fills and dredge spoil material that are undergoing consolidation. Therefore, consideration in the design of cargo yard pavement systems must be given to the potential for large, post construction settlements. Figure 1 shows a typical soil profile in the cargo yard area of one berth at the Port of Tampa. The subsoil profile is highly variable in thickness and type of soft soil, so total and differential settlements can be expected to be large, and in the case of dredge spoil material, independent of the surface loads applied by site grading and operations.

Cargo handling in the Port of Tampa is typically done with large top-loader type equipment, the largest of which, the TEC 950L, has an axle loaded at 890 kN. In addition, materials such as coils of wire, steel pipe and other general cargo are stacked on pavement surfaces. Therefore, the pavement systems must be designed for high loads and the pavement surface must be tough.

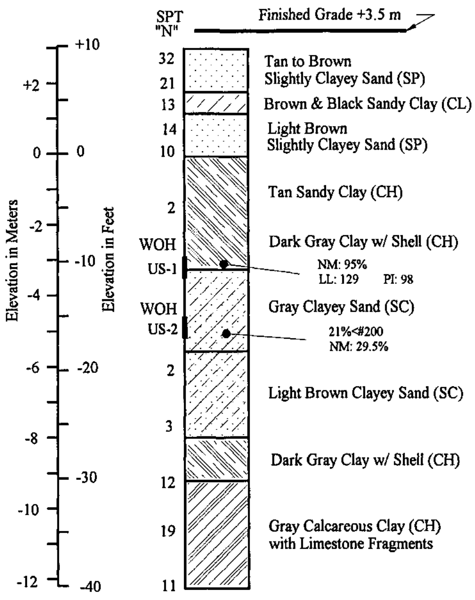

P-1 A (Typical soil conditions)
FIGURE 1

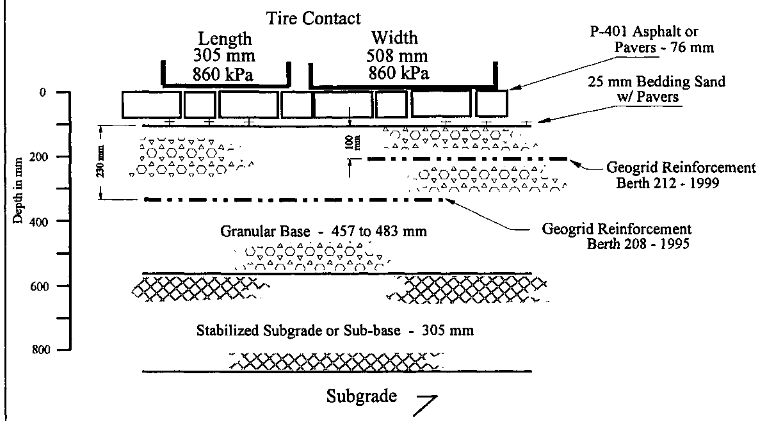

Typical Pavement Section
Figure 2

TYPICAL PAVEMENT DESIGN

Prior to 1994, pavement systems in cargo yards at the Port of Tampa were designed in accordance with design procedures established by the Florida Department of Transportation (FDOT) using soft limestone, roadbase limerock, with an LBR of 100 (FDOT 1991). The LBR is a test developed by the FDOT based on modifications to the CBR test (SRDF, 1960). An LBR of 100 is equivalent to a CBR of about 80 (ASTM D1883). Also, the pavement subgrade was stabilized or compacted to an equivalent CBR of about 30. The surface course was standard S-1 asphalt, used in Florida for highway construction. This pavement system was compliant in that it could withstand some differential settlement without excessive cracking, but it was not tough. Most roadways and cargo yard pavements in the Port exhibited severe distress within a short period of time after construction, and maintenance demands were high.

REVISED PAVEMENT DESIGN

Design Procedures

Because of the problems with the typical pavement systems, the Port Engineer decided to evaluate alternative pavement systems for a new cargo yard at Berth 208. A decision was made by the Port Engineer to use brick pavers. The design was also based on operational loads higher than typical highway pavement loads used previously, in this case, containers with a top-loader type equipment. The design of the pavement system was initially done based on the methods described in the British Ports Federation design manual (Knaption, 1990). The design was also evaluated using the program Lockpave (Edgeware, 1991). The results of the analyses in both methods resulted in the apparent need to use a bound base course such as strong soil cement or lean concrete. In fact, Knapton recommends that the CBR of any granular base should not be less than 80, and that the elastic modulus used in design should not be taken as exceeding 1000 MPa. The point in British practice is to discourage the use of granular bases (Knapton, 1990). No provision is made to allow for reinforcement of granular base using geogrids in the British Ports Federation document.

Soil Stratigraphy

The soil profile in the area varied from deep very loose clayey sands to thick layers of soft clay; for example, the more than 5 meters of CH-clay found in the boring shown in Figure 1. Therefore, large total and differential settlements were expected at the site. The designer believed that large differential settlements could be destructive of bound base systems such as strong soil cement or lean concrete. Also, the use of a concrete base system would make adding, repairing or moving buried utilities very difficult. Therefore, the recommendation was made in the design of the Berth 208 Cargo Yard to use the granular base course with brick pavers (McGillivray, 1995).

Engineering Properties of Materials

Analyses were conducted using the Lockpave and Knapton methods with a hard, durable granular base. However, an elastic modulus higher than the maximum of 1,000 MPa recommended by Knapton was used in the design. The base material was specified with a minimum CBR of 150. In order to assure a durable material, and to eliminate the possibility of the contractor substituting soft limestone for the granular base material, an LA Abrasion resistance of 40%, and soundness losses of 10% by the Sodium Sulfate method (ASTM) and 15% by the Magnesium Sulfate Method (ASTM) were specified.

A decision was also made to use geogrid reinforcement to improve the performance of the pavement system base. The specifications were written for a generic FDOT Type 2 Geogrid (FDOT, Section 985, SSRBC, 1991). The Type 2 grid is a biaxial grid with relatively high strength and moduli. Engineering properties such as tensile strength and moduli, aperture size and minimum grid and joint thickness are specified. However, the table is silent as to the number of sheets or layers of geogrid required to meet the structural requirements. The FDOT specification does not specify a method of manufacture or the materials used in manufacture of the geogrid. Table 1 lists the geogrid properties specified in FDOT Section 985.

Table 1: FDOT Type 2 Biaxial Geogrid Specifications

	Units	Standard
Modulus @ 2% Elongation:	kN/m	269
Strength @ 2% Strain:	kN/m	5.2
Peak Strength:	kN/m	16
Elongation at Peak Strength:		12.5%
Junction Strength:	kN/m	14
Junction Efficiency:		90%
Aperture Size - Minimum:	mm	25
Maximum:	mm	50
Thickness - Rib:	mm	1.5
Junction:	mm	3.0

Design Pavement Section

No specific analyses were done to evaluate the optimum location of the geogrid for the Berth 208 project. The geogrid was placed at the midpoint of the base because the designer believed that it was more important to confine the base course than to reinforce the subgrade. Figure 2 shows the design cross section that was developed during the initial design process with the geogrid located about 230 mm below the surface of the finished base (Berth 208, 1995). The geogrid was a punched/drawn sheet polypropleyene type material that met the FDOT Type 2 specifications.

Field Tests

Plate load tests were run to evaluate the effect of the geogrid, and to confirm that a granular base system could be used for the proposed pavement system. A large bucket loader was used as a reaction with test plates 178 mm (7 inches) and 457 mm (18 inches) in diameter. Because the reaction load was limited, the 1oad was limited to 827 kPa, the nominal tire pressure of the large top-loader cargo handler, for the 457 mm diameter plate.

Figure 3 presents the result of the set of tests for the 178-mm diameter plate. It can be clearly seen that the reinforcement improved the stiffness of the base, but that the thickness of the base was the primary contributor to the strength of the system. Unfortunately, the strength of the base was greater than could be tested using the equipment available for the field tests at that time. The same can be shown for the 457 mm plate tests summarized in Figure 4. Again, the major improvement in system stiffness came from increasing the thickness of the base course. However, the geogrid reinforced section had about twice the stiffness of the unreinforced section. The residual settlement below the 457 mm plate in the reinforced section was about 0.5 mm, while the net settlement after rebound on the unreinforced section was about 2.7 mm. Clearly, the lower rebound under the initial loading indicates more elastic behavior and a lower tendency for rutting of the pavement surface.

178-mm Diameter Plate Load Tests on Aggregate Pavement Base
FDOT Type 2, Punched/Drawn Type Geogrid

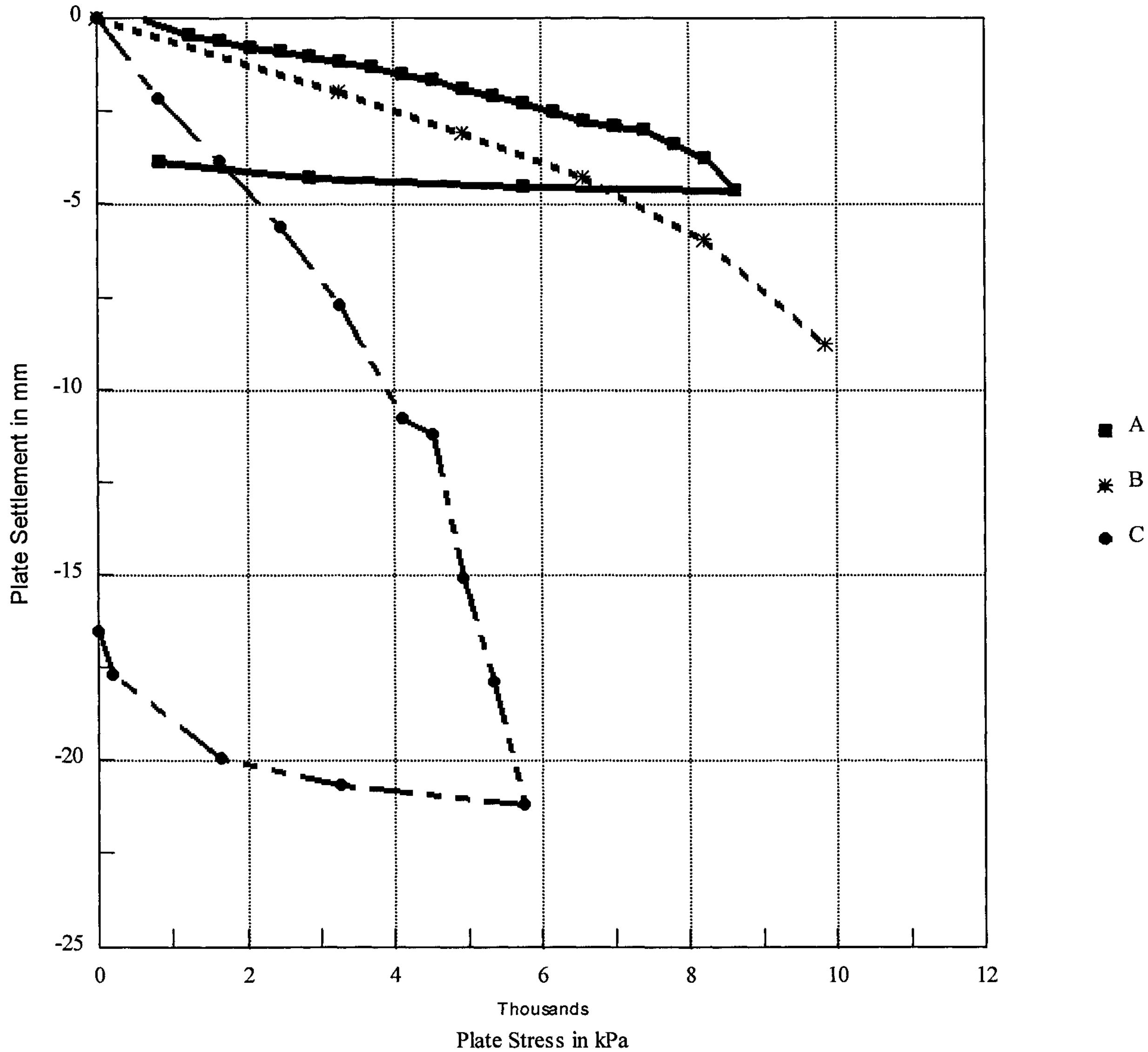

A: 457 mm Base with Geogrid at 229-mm - B: 457-mm Base without Geogrid
C: 229-mm Base without Geogrid - FIGURE 3

457 mm Diameter Plate Load Tests on Aggregate Pavement Base
FDOT Type 2, Punched/Drawn Type Geogrid

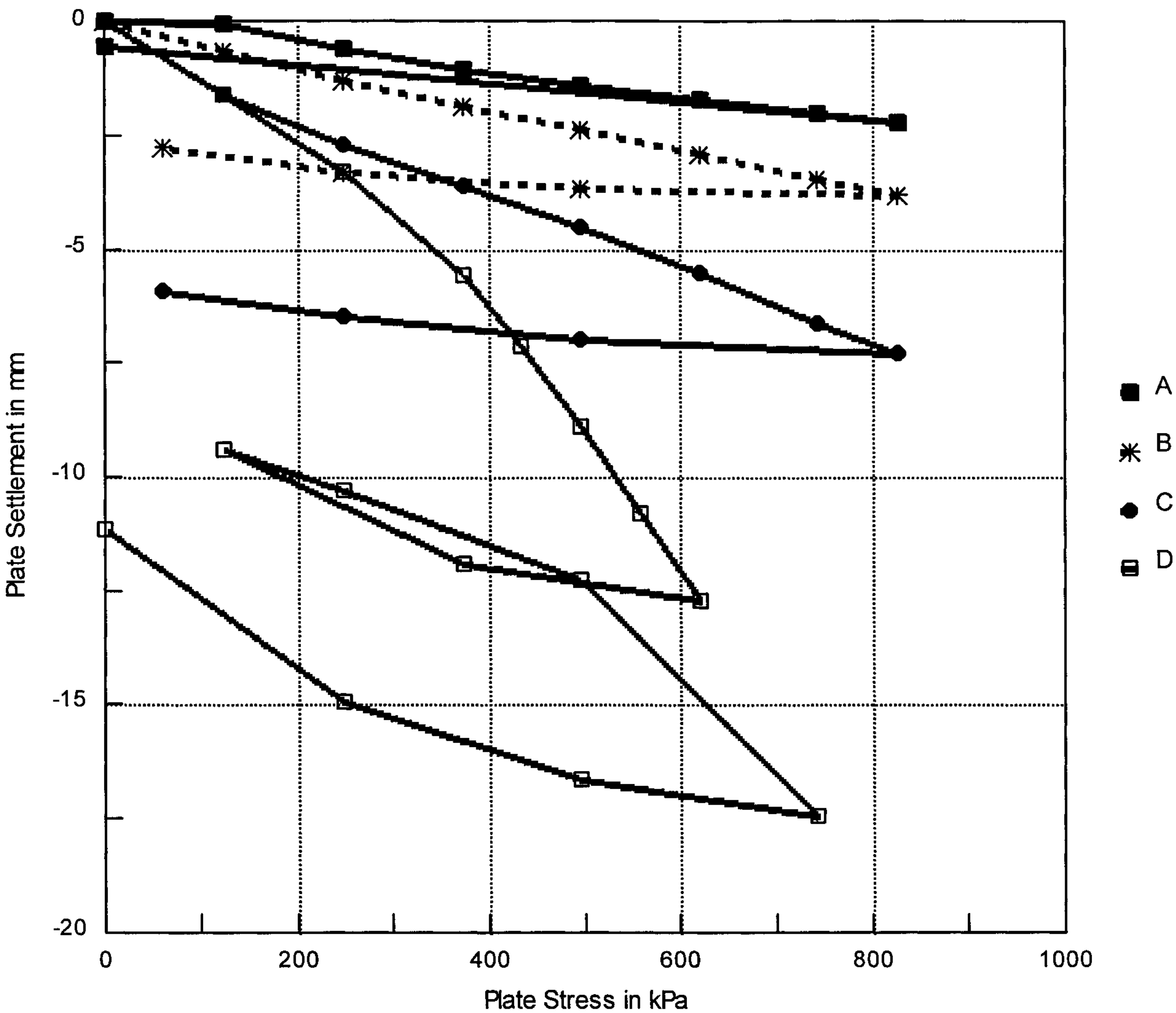

A: 457 mm Base with Geogrid at 229 mm - B: 457 mm Base without Geogrid
C: 229 mm Base without Geogrid - D: Subgrade - FIGURE 4

Evaluation of Optimum Geogrid Location

The typical use of geogrid when it is included in the design of granular base courses appears to be to reinforce the pavement system over a soft subgrade. That is, treating the base course as a beam with the geogrid as a tension member (Ashmawy, 1995). For soft subgrades, the effect is to achieve better performance with the geogrid at the interface between the base and the subgrade, even with thick bases. Most field testing and research for evaluation of geogrid effectiveness have been done with the geogrid at the interface between the subgrade and the base course, and with subgrade strength varying between CBR values of 1 to 24 (Knapton, 1990; Webster, 1992; Perkins, 1999). The "improvement" achieved by adding geogrid to the pavement section decreased as the thickness of the base increased (Webster, 1992). Also, the Webster study indicated that some coated polyester geogrids with a woven structure and a multi-layered thin-section polypropylene filament geogrid had little to no effect on the measured rutting over the control section without geogrid although all of the geogrids met the tensile strength and moudli criteria established for their class of geogrid. However, the tests were run with a CH clay subgrade that had a CBR ranging from 3 to 8. It is possible that the results may have been different if a subgrade with a CBR significantly greater than 8 had been used in the study.

The mechanism causing rutting in pavement systems that have strong subgrades and thick base courses might primarily be lateral movement of the particles in the granular base, rather than compression/compaction of the base or subgrade soils. This thesis appears to be confirmed by work done by Dr. Thomas C. Kinney who has proposed a test for geogrid effectiveness: "Grid Aperture Stability by In-Plane Rotation" (Appendix A, Webster, 1992). His work indicates that a stiff grid limits the migration of particles laterally from below the wheel path. Tests using the "Grid Aperture Stability" method showed good correlation with field tests with respect to reduction in rutting. Our interpretation was that this problem should be greatest near the upper part of the base, close to the pavement surface. Therefore, we believed that the geogrid might be more effective if it was higher in the pavement section. It was resolved to complete modeling using numerical methods to evaluate the issue of grid location within the base for thick bases on strong subgrades.

The Tampa Port Authority had adopted the design of the Berth 208 pavement system discussed above as the standard pavement for cargo yards, and Berth 206 Cargo Yard was built without any additional analyses using the Berth 208 section shown in Figure 2. We believed that there was a possibility of improving the system. Therefore, a recommendation was made to the Port Engineer that analyses should be conducted to evaluate the optimum location of the geogrid in the pavement cross section for the design of the Berth 212 Cargo Yard pavement system.

Finite Difference Analyses

The Finite Difference models used for the Berth 212 Cargo Yard pavement system analyses were developed using FLAC, an explicit finite difference program (Itasca, 1998). The pavement section shown in Figure 2 was used to develop the model geometry, with an upper, stabilized subgrade underlain by a softer soil. The soil moduli were estimated based on correlations with soil and base CBR (Knapton, 1990). The engineering properties of the soil and the geogrid used for the analyses are summarized in Table 2.

Table 2 - Material Properties for Finite Difference Analyses

Material	cohesion, c, Pa	Friction Angle	Density, T/M^3	Modulus of Elasticity, E, MPa
Joint Sand	0	38°	1.60	300
Base Material	0	50°	2.05	1,000
Stabilized Subgrade	0	35°	1.95	200
Subgrade	0	32°	1.92	150

Type 2 Geogrid

Modulus @ 2% Elongation:	270 kN/m	
Peak Strength:	16 kN/m	@ 12% Strain
Cross Sectional Area per meter:	667 sq. mm	

The Pavers were 79x79x152 mm with 3-mm spacers on the sides. The unit weight of the pavers was 2.40 T/M^3. The unconfined compressive strength was 55 MPa and the Modulus of Elasticity was 35.4 Gpa.

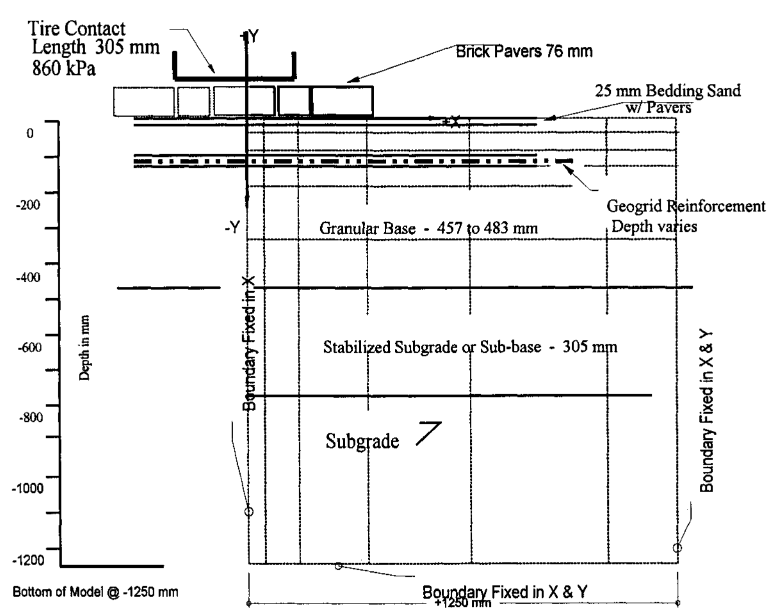

Finite Difference Grid Representation
Not all Grid Lines Shown for Clarity

Figure 5

Figure 5 is a representation of the grid used for the analyses, with a finer grid close to the load. The grid origins are the top of the bedding sand and the center of a large (side-on) brick paver. The model is a 2-D plane with the 0-X boundary fixed in the X-direction. The brick paver joints interact with friction of 38 degrees to model the joint sand, and the load was applied over the center full brick and half of the brick end-on. The model represents conditions observed in the field with respect to tire contact on the pavers. The load was ramped-up to the full contact pressure and the model was allowed to step until a solution was reached with respect to X and Y displacements.

The location of the geogrid was varied at 229, 152 and 102 mm below the surface of the base. The geogrid was modeled using a beam-structural element. The interface between the base material and beam element (geogrid) was modeled as a Coulomb Material with a friction angle of 32 degrees. The results were then evaluated for the variation in stress in the geogrid and the stresses and strains in the soil.

Figure 6 shows the graphs of the beam element (geogrid) stresses for each depth location of the geogrid. The analyses showed that there were no detectable differences in model stresses and strains in the stiff base/subgrade sections with variations in geogrid location. There were minor differences in peak geogrid stresses depending on the depth of the geogrid. However, there was a greater distribution of stress in the geogrid as it was moved upward in the base section. The analyses also indicated that the geogrid was not acting as a tension reinforcement in the sense that the stresses in the beam element did not extend significantly beyond the loaded zone. Especially at the maximum test depth of 229 mm, the tension stresses were concentrated over a

Figure 6 - Axial Forces In Geogrid from the Finite Difference Analyses

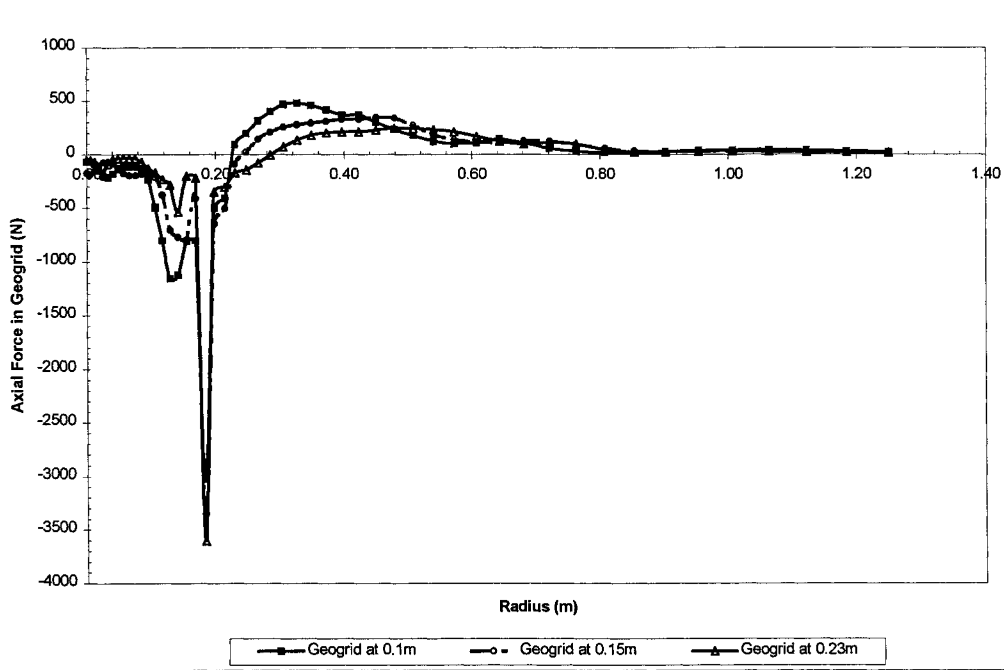

beam element length of 50 mm with a second, zone about 100 mm long at about half the peak stress. At a depth of 102 mm, the beam element tension stresses were distributed over a length of about 300 mm, varying more or less uniformly over that length. The results were interpreted by the designer to show that the geogrid might work best at a depth as shallow as 102 mm below the finished surface of the base course (McGillivray, 1997).

A command in FLAC, "Plastic", shows the nodes that are at yield in the model. At a geogrid depth of 229 mm, the plastic zone is well developed. Figure 7a shows the plot of nodes at yield in the model with the geogrid depth at 102 mm. At a geogrid depth of 152 mm, the zone of yielded nodes is significantly modified, with more concentration along the vertical line below the joints.

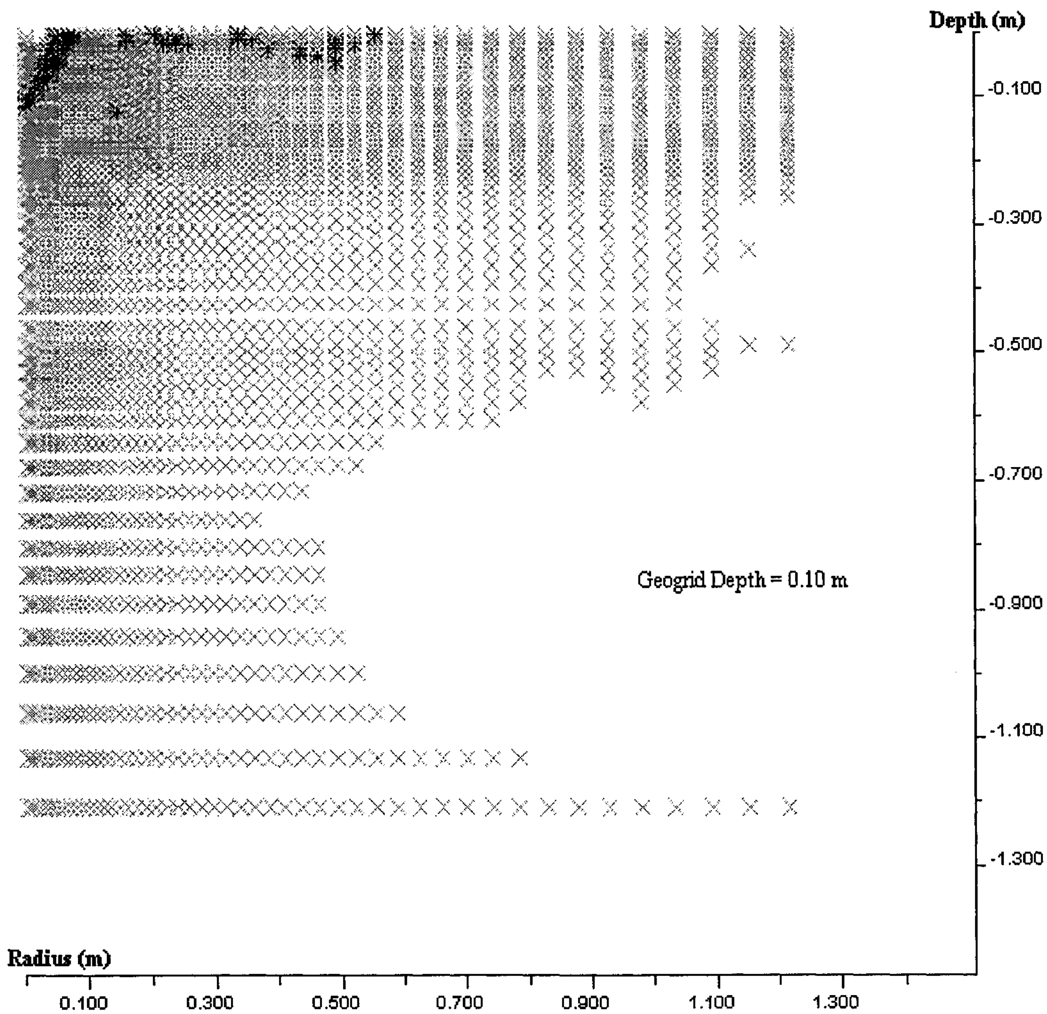

Figure 7a. Plastified zone with geogrid at 0.10 meters.

Figure 7b shows the pattern of nodes at yield for the geogrid located at a depth of 229 mm. The yielded zone is much smaller at the shallow geogrid depth, indicating that a greater volume of the base is behaving elastically.

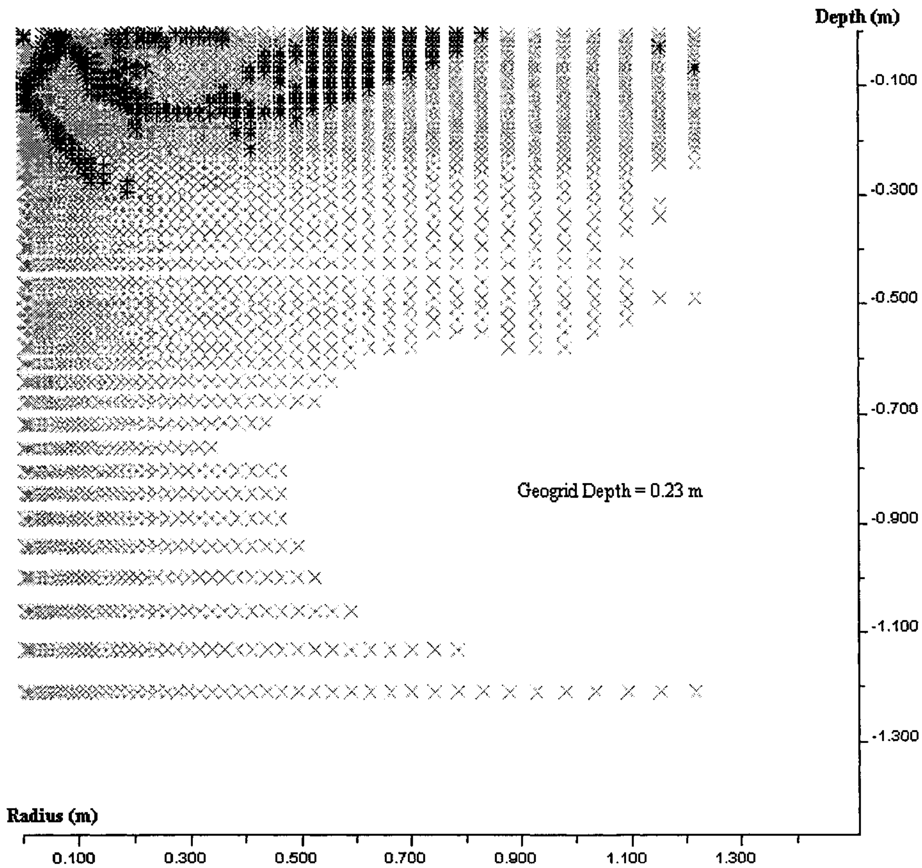

Figure 7b. Plastified zone with geogrid at 0.23 meters.

BERTH 212 PROJECT RECOMMENDATIONS

Based on the results of the Finite Difference Analyses, a recommendation was made to utilize the pavement section shown in Figure 2 with the geogrid placed at a depth of 102 mm below the top of the base course. The base material was to be a dense-graded dolomitic limestone or granite gravel with a minimum LBR, a minimum CBR of 150 and with low LA Abrasion, Magnesium Sulfate and Calcium Sulfate Soundness Test losses.

The original concept for the pavement system was to use pavers as a surface course. The paver systems installed at cargo yards at Berths 208 and 206 had performed well, and the Port was satisfied with the basic pavement system. However, the Finite Difference Analyses indicated that the pavers could concentrate stresses in the base course, and adversely affect its performance. Therefore, an alternative pavement section using P-401 (FAA Airport) asphalt was allowed in the specifications for the Berth 212 Cargo Yard.

CONCLUSIONS

Finite Difference numerical analyses proved to be a valuable tool in the evaluation of geogrid reinforced pavement systems. The analyses were capable of revealing mechanisms of pavement failure that were not considered in typical analyses.

The geogrid reinforcement system was found to be more effective at a shallow depth below the top of the base in a pavement system with a relatively stiff subgrade. The analyses indicated that the reinforcement mechanism caused a decrease in the size of the zones that might undergo plastic displacements under the expected traffic loads in Cargo Yards.

The Finite Difference model indicated that the geogrid did not act as tension reinforcement in the classical sense. The zone of geogrid in tension was very small, even when it was located at a shallow depth. Consideration should be given to the stability of the geogrid apertures. The aperture stiffness of the geogrid may control its effectiveness in limiting rut formation in pavement systems. Additional modeling and full scale field testing would be required to evaluate the effects of higher modulus and aperture stability on the behavior of reinforced pavement systems.

The Finite Difference analyses indicated that a pavement system with a surface course comprised of brick pavers might not distribute wheel loads as effectively as a continuous pavement surface such as strong asphalt. In fact, it is possible that the pavers could amplify the stress at the top of the base due to placement that allows some pavers to be above adjacent pavers.

ACKNOWLEDGMENTS

We want to thank Mr. Bruce Laurion, PE, the Tampa Port Authority Port Engineer for his permission to use the data presented in this paper. Also, we want to thank Mr. Lauren Lorig, Manager, Civil Engineering of Itasca Consulting Group, Inc. for his assistance in developing the FLAC models used for these analyses.

REFERENCES

Asmawy, A. K. and Bourdeau, P. L., 1995, "Geosynthetic Reinforced Soils Under Repeated Loading: A Review and Comparative Design Study", Geosynthetics International, Vol. 2, No. 4, pp. 643-678

ASTM D1883, (1995). "Standard Test Method for California Bearing Ratio Test" Annual Book of American Society for Testing and Materials, Volume 4.08

Edgeware Corp, (1991). "Lockpave Program No. 466, Program Manual, Version 6

Florida Department of Transportation (FDOT) (1991). "Standard Specifications for Road and Bridge Construction", pp. 645-646, Section 985

Florida Department of Transportation, (1990). "Flexible Pavement Design Manual for New Construction and Pavement Rehabilitation", April 1, 1993, Table 3, Figure 5.1.11 & 12

Itasca Consulting Group, Inc., (1998). "FLAC Version 3.4 User's Guide.", Minneapolis, Minnesota."

Knapton, J. and Smith, D. R., (1990). "Port and Industrial Pavement Design with Concrete Pavers", Second Edition,

McGillivray, R.T. & Fielland, C. E., (1995). "Selection of a Pavement System for Heavily Loaded Marine Terminal" Ports 95, March 1995, pp.1057-1067

McGillivray, R. T., "Pavement System Recommendations, Proposed Berth 212, Port of Tampa" Ardaman & Associates, Inc. report to Gee & Jenson, September 5, 1997.

Perkins, S. W., (1999). "Geosynthetic Reinforcement of Flexible Pavements: laboratory Based Pavement Test Sections", Technical Report FHWA/MT-99-001/8138

State Road Department of Florida (SRDF), (199\60) "Research Bulletin 22-B, Flexible Pavement Design Manuel"

Webster, S. L., (1992). "Geogrid Reinforced Base Courses for Flexible Pavements for Light Aircraft, DOT/FAA/RD-92/25, Waterways Experiment Station, Cops of Engineers

APPLICATIONS OF GEOTEXTILES, GEOGRIDS, AND GEOCELLS IN NORTHERN MINNESOTA

WALTER LEU, P.E.
DISTRICT STATE AID ENGINEER
MINNESOTA DEPARTMENT OF TRANSPORTATION

LUANE TASA, P.E.
DISTRICT STATE AID ENGINEER
MINNESOTA DEPARTMENT OF TRANSPORTATION

ABSTRACT

This presentation describes four different applications of geosynthetics in the reconstruction of roads in northern Minnesota. Installations are on paved and unpaved low volume county roads, medium volume paved county roads, and a state trunk highway. County road projects use geotextiles for separation and strengthening of weak, lake deposited, subgrade soils; including a unique project at the Northwest Angle (the chimney of Minnesota) where geotextiles were used to provide a passable road during spring breakup. The state trunk highway project consists of geocell, geogrid, and geotextile sections constructed in sequence to determine which is the most cost effective. Most installations will have been inplace in excess of 5 years by 2001. Maintenance benefits to date include reduced longitudinal and transverse cracking of pavements, reduced or eliminated frost heave, and reduced blading and regraveling of aggregate surfaced roads. Design benefits include reduced base course thickness requirements and improved constructability of roadbed over soft subgrades. Construction techniques used allowed for ease of placement and efficient contractor operations. Rules of thumb have been developed through practical experience to determine when and where to use geotextiles.

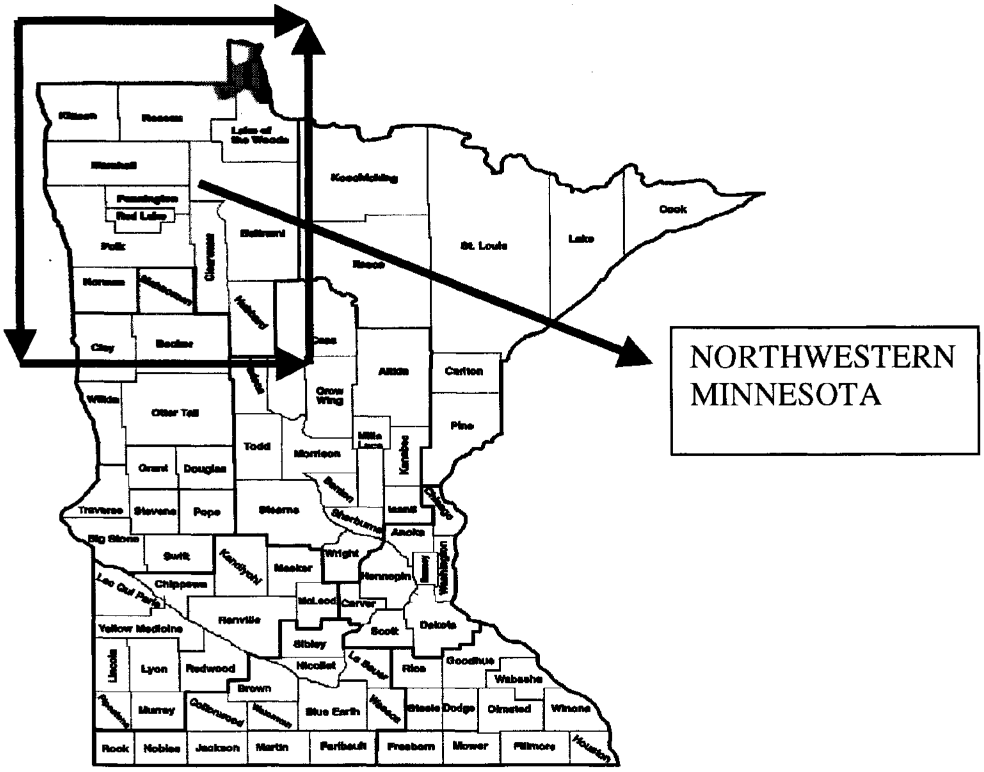

APPLICATIONS OF GEOSYNTHETICS IN NORTHERN MINNESOTA

Geosynthetics have been used in northern Minnesota for roadway construction ranging from gravel surface to paved road applications. They have been used as a means to stabilize poor subsoils and subgrades in order to provide a passable gravel surfaced roadway during spring breakup and also in one situation, to accomplish paving operations. Geosynthetics have also been used as part of the typical roadway design (without reducing the gravel equivalence) in several new construction projects, anticipating improved strength and reduced future maintenance activities. One research application on a state highway is using four different types of geosythetics in a 1.6 km section to determine which will be more effective in eliminating severe longitudinal cracking. In all of the applications mentioned, the geosynthetic was not anchored, but covered with gravel of varying thickness.

The above applications occur in five northern Minnesota counties, Lake of the Woods, Polk, Roseau, Hubbard, and Beltrami. In addition to improving the constructability of the roadbed, there may be long term maintenance benefits resulting from these applications through reduction of transverse and longitudinal cracks. What we are planning to do is to monitor the longitudinal cracks on these and any future segments of geosynthetic installations through low level uncontrolled aerial photos or through the use of the Minnesota Department of Transportation's Pavetech van. The Minnesota Department of Transportation flew low level uncontrolled aerial photos of all the segments in April, 2000. At the writing of this paper it is unknown whether this method to monitor roadway cracking will be feasible.

Lake of the Woods County, the Northwest Angle Story

The Northwest Angle portion of Lake of the Woods County is a very unique area in terms of both geography and geology. Being the northern most point in the continental United States, it was actually created by a surveying and mapping error. Geologically, the area was created when an ancient glacial lake receded, resulting lake deposited organic silts. Tremendous growth in the recreational development of the area severely damaged the existing limited road system.

Local aggregate resources are almost non-existent, and any gravel materials needed are imported from Canada. In addition, because of the environmental sensitivity of the area, any

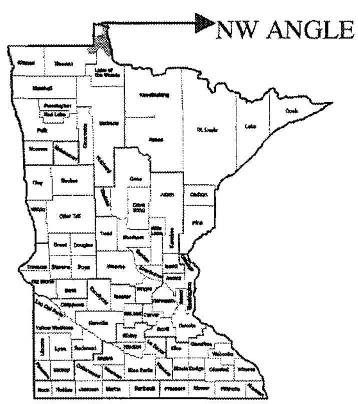

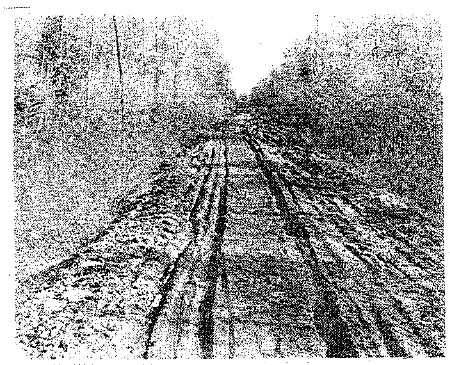

The Angle road after the sun had shone for a day. This was the beginning of one of the easier stretches.

proposed improvement must have minimal impact.

Lake of the Woods County Highway Department, with assistance from the Minnesota Department of Transportation (MnDOT), office of State Aid, developed a project proposal to stabilize and improve the road system that was efficiently constructed, minimized environmental impact, and was reasonable in cost.

The Northwest Angle system of roads is 24 km in length with no detour available. There is only one road to access the entire area. The initial project proposed to improve 8 km of the poorest sections. Construction included reshaping of the existing grade to a 9 m top width and 4% crown, placement of 9 m width pre-sewn woven geotextile with a grab tensile strength of 0.9 kN bi-directional (MnDOT type V), 200 mm thickness of stabilizing aggregate (pit run), and 75 mm of Class 5 aggregate surfacing resulting in a finished top width of 7.2 m as shown in Figure 2.

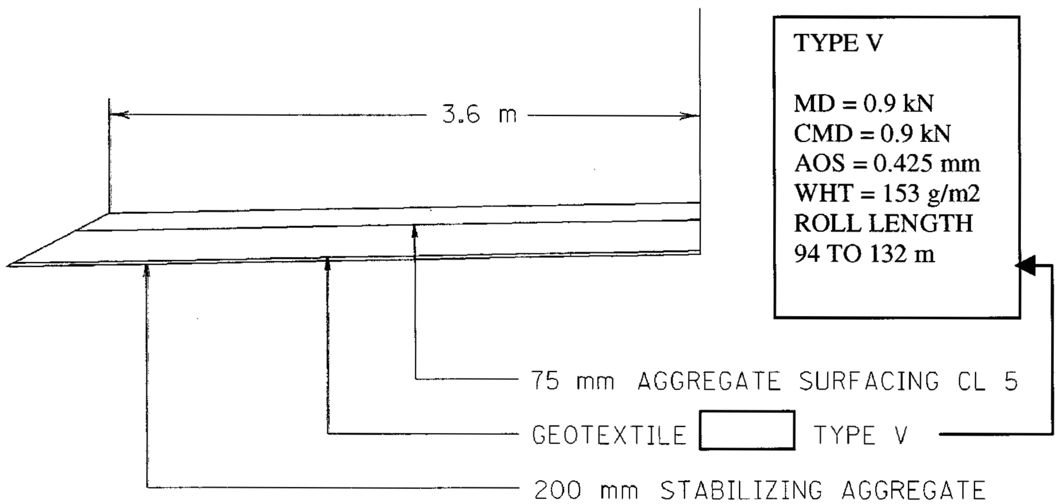

Figure 2, NWA Typical Section

To speed construction and minimize traffic delay, geotextile was pre-sewn at the factory, re-rolled and delivered to the site. Each roll was then unrolled longitudinally, unfolded, and edges temporarily held down with wood fiber u-nails or shovels of gravel. Trucks, along with traffic, were allowed to drive on the fabric (centered on the road). Slow vehicle speed and no turning on geotextile resulted in no physical damage. Bottom dump trailers placed gravel along the centerline, while a motor grader bladed material out towards the sides. This method of placement resulted in a pre-stretching of the fabric and elimination of wrinkles. The next piece of fabric was unrolled and lapped approximately 2 m under the previous roll so that it lapped in the direction of the work. A rubber tired roller and water was used to compact the aggregate material. Using this method, approximately 1.6 km of fabric and initial aggregate surfacing could be placed each day. Cost for this construction method was approximately $50,000 per km. Geotextile cost was $7,000 per km, aggregate subbase $29,000 per km, and aggregate base $13,000 per km.

Eventually all 24 km of roadway were improved with some modifications to the original construction method. A stronger 1.35 kN grab tensile strength fabric (MnDOT type VI) was substituted for the type V, as it was stiffer, stronger, easier to place, less susceptible to wind and had minimal increase in material costs. In addition, it was more economical to substitute the higher quality class 5 aggregate surfacing in place of the stabilizing aggregate (pit run) subbase and the overall thickness reduced to approximately 175 mm based on gravel equivalency method, where 2 mm of subbase is needed for 1 mm of base. Once completed, each section received a topping of calcium chloride to keep the aggregate from raveling. Figure 3 shows how the road is today.

Figure 3, NWA Today

The first reconstructed segments of the NWA road have been in place for over 10 years without a springtime subgrade failure. Geotextile is successfully preventing the siltly subgrade from penetrating the aggregate bases during spring thaw. Today there is over 200 000 square meters of geotextile placed at the "Angle". Calcium Chloride and minor blading are the only maintenance activities.

The Story of Pete

As can happen sometimes in the most remote areas of Minnesota, Lake of the Woods County Highway Department became involved with the reconstruction of a County Road, the Corps of Engineers, and someone or something called Pete (also known as Peat). Typical construction practice called for removal of all underlying peat when widening a road for future bituminous surfacing. Disposal was normally just a matter of placing the material out to the sides. This was not acceptable to the Corps of Engineers as this was depositing fill in a wetland. The County Commissioners were notified that the project was shut down because of problems with peat.

The Commissioners then called in the engineer to find out who this "Pete" was and by what authority could this gentleman shut down our road construction. After much explaining by the engineer, the Commissioners decided to "cover up" the matter by using geotextile.

The project was redesigned to cut vertically next to each side of the existing roadbed to a depth of one meter, excavated peat temporarily stored to the side, a MnDOT type V woven geotextile placed on top of subgrade and over the existing roadbed. All seams were sewn in the field. The geotextile was approximately 18m wide to cover the subgrade, vertical cut, and existing roadbed. Excavated and graphic section shown on Figure 4.

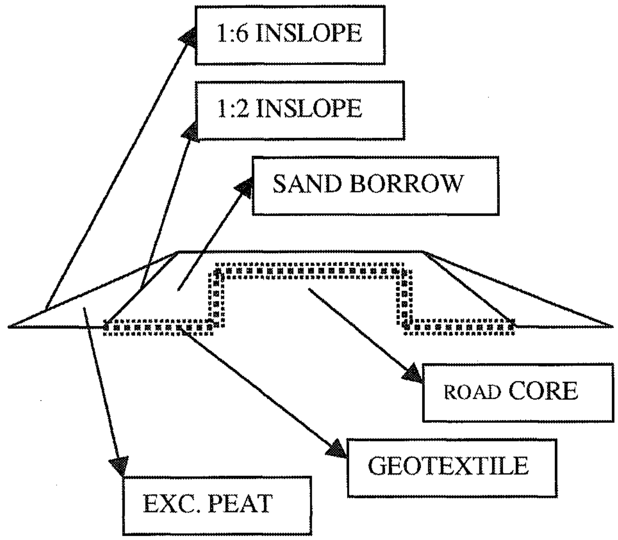

Figure 4, Vertical Cut next to Grade

Sand borrow was then placed on top of the geotextile to the planned grade elevation with a 1:2 inslope. The entire 13m roadtop then had a 200 mm layer of aggregate base applied. The inslopes were flattened to 1:6 by using the excavated peat that was temporarily placed to the side. Bituminous surfacing was placed the following year after grade reconstruction. In place now for over 10 years, this roadway is performing very well with no longitudinal cracks or settlement at the interface between the old roadbed and the widened sections.

To Fabric or not to Fabric, that was the Question

Because good gravel resources are scarce in Lake of the Woods County, it was decided to eliminate the placement of pit run aggregate subbase and instead use geotextile for Lake of the Woods County Road #3, a road reconstruction project in an area of poor drainage and very weak silty-clay soil. Figure 5 shows a typical section for the placement of geotextile. The project was 8 km in length with 4.8 km having the geotextile section and 3.2 km having only aggregate subbase.

The non-geotextile section had 150 mm of pit run aggregate subbase placed in addition to the 240 mm of class V aggregate base. The geotextile selected was a MnDOT type V, woven with a grab tensile strength, bi-directional of 0.9 kN. The contractor elected to sew the fabric on the prepared subgrade, as the width was approximately 12.8 m. During construction, the roadbed was constantly subjected to rain and although the center of the road was hard, the newly

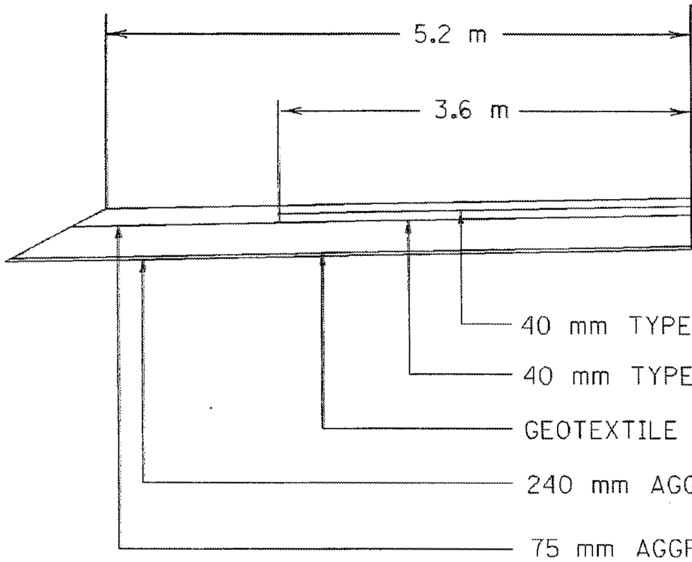

Figure 5, Typical Geotextile Section LOW County Road #3

constructed shoulders were very soft. During construction heavy equipment was kept off of the soft shoulders. Gravel base was placed with belly dumps driving on the fabric along the road centerline. The motor grader spread the aggregate material forward and to the sides to stretch out the fabric. See figure 6.

Figure 6, Spreading aggregate base over geotextile

Gravel base was placed in 120 mm lifts to carry construction equipment. Although it was communicated many times to keep equipment off of the soft shoulders, one errant motor grader

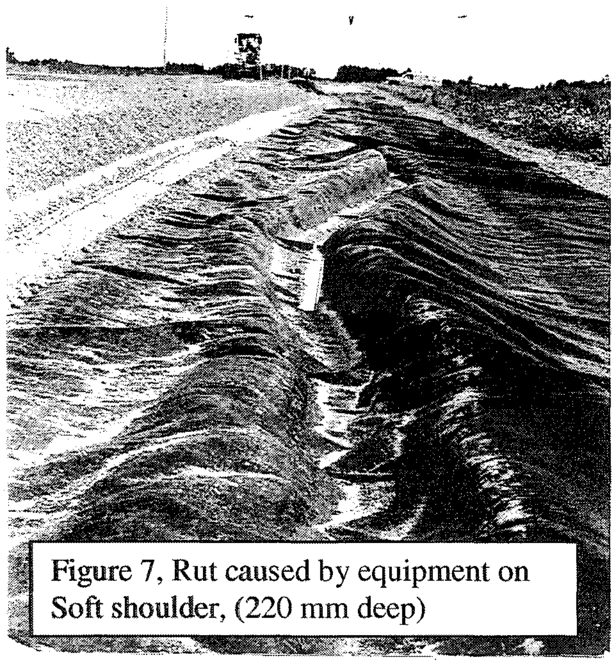

Figure 7, Rut caused by equipment on Soft shoulder, (220 mm deep)

created the 220 mm rut shown in Figure 7.

The non-fabric section was even more difficult to construct because of the wet subgrade. Additional pit run was used in some locations just to carry the gravel trucks.

The road was surfaced with 80 mm of plant mixed bituminous the following year. To try and quantify the strengthening effect of the geotextile, a falling weight deflectometer was used. Tests were taken every 30 m on both the fabric and non-fabric sections. Test results indicated similar deflections along the entire road length, leading one to believe that the section, with geotextile and less aggregate material, was as strong as the non-geotextile section. In addition, the geotextile section had a cost saving of $9,000 per km. One side benefit noticed was improved ride. The silty nature of the soils along with the wet construction season resulted in somewhat of a "rolling" ride caused by construction equipment operating on the saturated subsoils. This "roll" was much more pronounced on the non-geotextile section. This project is now over 9 years old. A recent drive-by survey indicated approximately 50 percent less transverse cracking of the bituminous pavement on the geotextile sections when compared with the non-geotextile section.

Over the years, Lake of the Woods County has placed over 1 000 000 square meters of geotextile in many applications. The cost of geotextile is less than $10,000 per km, a bargain of an insurance policy when reconstructing any road over fine-grained soils. Cost savings in reduced aggregate subbase, increased strength, protection from contamination of gravel base from frost boils, and apparent reduction in cracking of bituminous pavements are all excellent reasons to use geotextile as part of your typical section.

Other Projects and Test Sections

In Roseau County approximately 240 000 m^2 of type V woven fabric has been used. The earliest installation was in 1992 was on County State Aid Highway 13 as shown in figure 8.

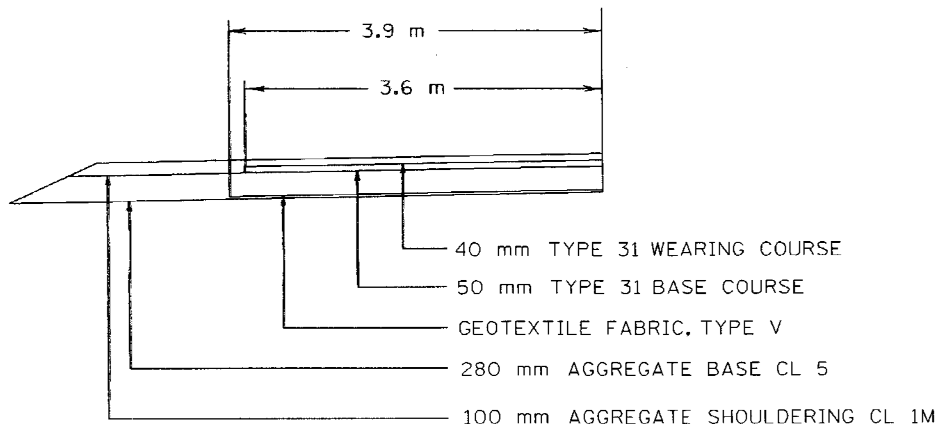

Figure 8, Typical Section for CSAH 13

Geotextile was installed in several segments for a total length of 1.3 km of this 6.5 km project.

On County State Aid Highway 20 (10km in length) the geotextile was installed under 175 mm of class five aggregate in 1995, fig. 9. Paving of this roadway occurred the following year. The successful paving contractor informed the county that they bid the project based on

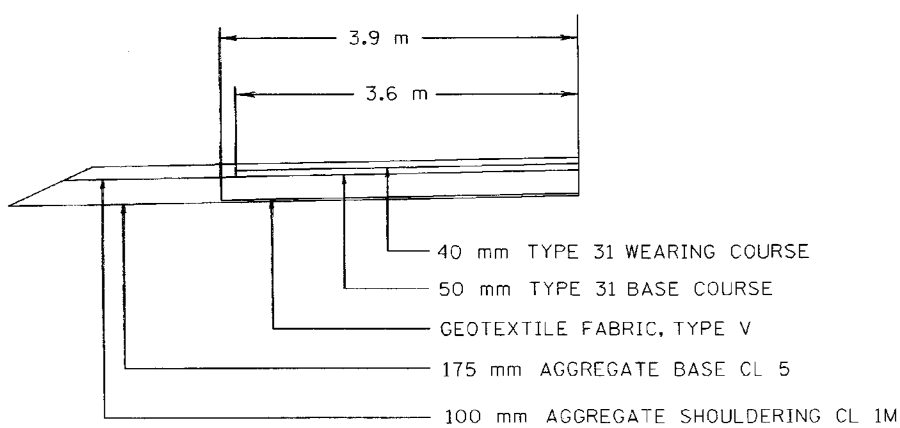

Figure 9, CSAH 20 typical section

overlay prices as they had confidence in being able to pave with minimal roadway preparation due to the geotextile presence below the class 5. Transverse cracks in this segment have varying distances between them. They range from about 75 m to 1200 m with 75 m – 100 m average spacing.

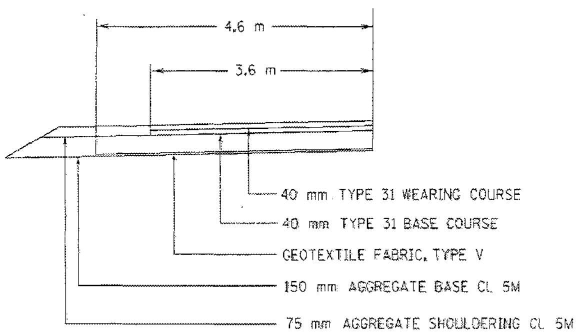

FIGURE 10 POLK CSAH 58

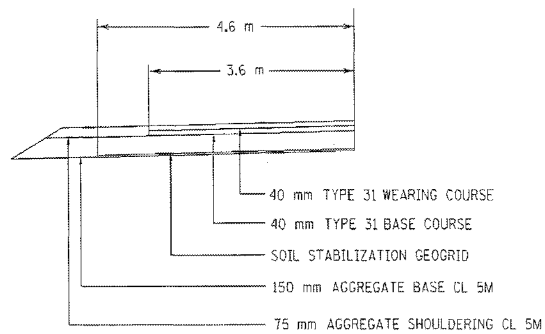

FIGURE 11 POLK CSAH 59

Polk County has installed both the geotextile type V and a biaxial geogrid on County State Aid Highways 58 and 59 (fig.'s 10 and 11). There is also an inplace control section. This project was constructed in 1997 and serves as a good segment for comparing non-geotextile, geotextile and geogrid segments as all have the same depth of class five aggregate and bituminous pavement. To date there is one minor transverse crack about

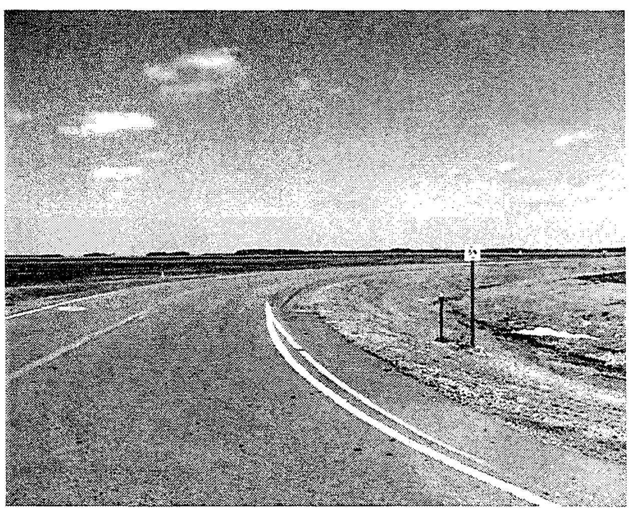

Figure 12, Polk Co. CSAH 59 (after 3 winter seasons)

Figure 13, Polk Co. CSAH 15 at Jct. CSAH 59, Paved in 1953, overlaid in 1974 and 1987 typical transverse and longitudinal cracking.

2 m long in one geogrid segment. There are no other visible longitudinal or transverse cracks in the geotextile, geogrid, or control section after 3 winter seasons. Generally these cracks start showing 3 – 4 years after the paving is completed. These installations total 134 000 m^2 of geogrid and 4000 m^2 of type V geotextile. Polk County is also constructing another 12.9 km aggregate base and bituminous project with geogrid on their County State Aid Highway 18, in 2000 (fig. 14).

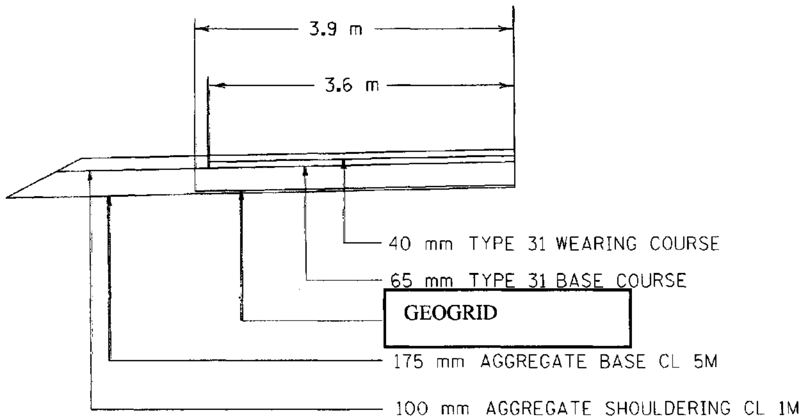

Fig. 14, Polk Co. CSAH 18 typical section (yr. 2000 const.)

In Hubbard County geogrid was used in a segment of County State Aid Highway 3 across a swamp section (fig. 15). The existing paved road was experiencing some settlements and the county was planning an overlay of the road. Through the swamp section, the existing pavement was removed and the underlying 75 mm of gravel reshaped.

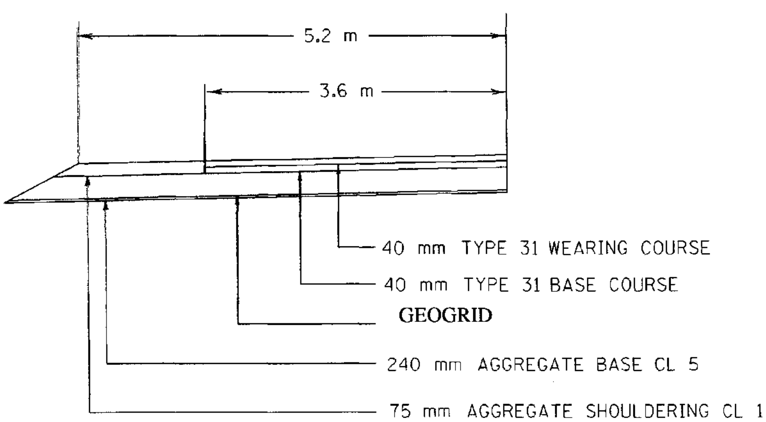

Fig. 15, Hubbard CSAH 3 typical section

About 20 000 m^2 of geogrid was laid on the reshaped gravel and 240 mm of class five gravel and 80 mm of bituminous pavement was placed over it. This was constructed in 1996 and to date, for the total length of 1.9 km, there are only 4 visible transverse and no longitudinal cracks in the surface after 4 winter seasons.

The Minnesota Department of Transportation has a research section of a variety of geosynthetic applications on Trunk Highway 72 in Beltrami County. This consists of four consecutive 400 m test sections (fig.'s 16, 17, 18, 19). The geosynthetics used are type V woven, Type VI woven, biaxial geogrid, and 200 mm geocell. The objective is to determine the most effective geosynthetic of these 4 to eliminate the severe longitudinal cracking being experienced on the majority of this highway section. Each 400 m segment was constructed in 1997 with the same typical section except for the type V geotextile. To date the geogrid visually appears to be performing the best according to a field review in the fall of 1999.

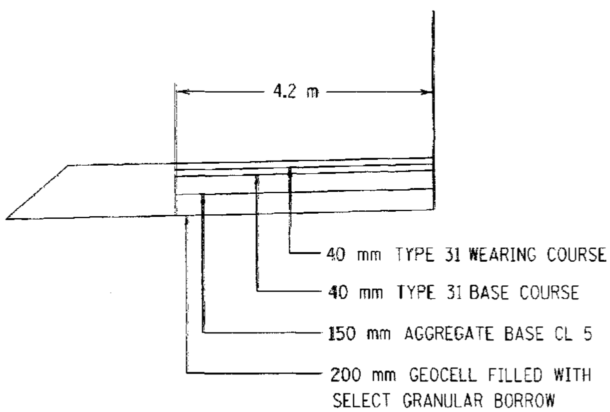

Figure 16, TH #72, Geocell typical section

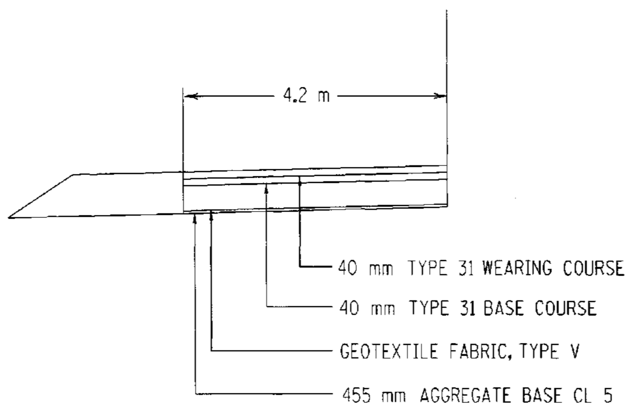

Figure 17, TH #72, Geotextile, Type V, typical

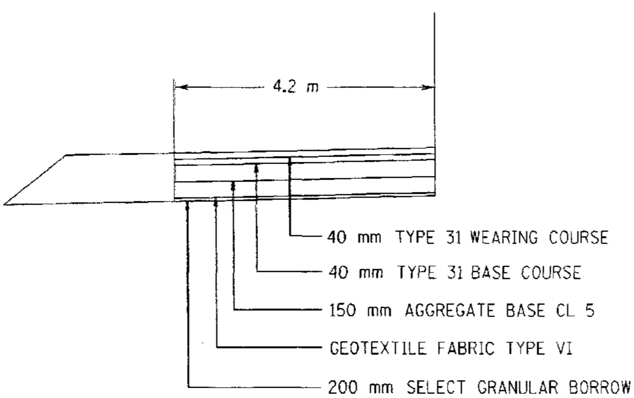

Figure 18, TH #72, Geotextile, Type VI, typical

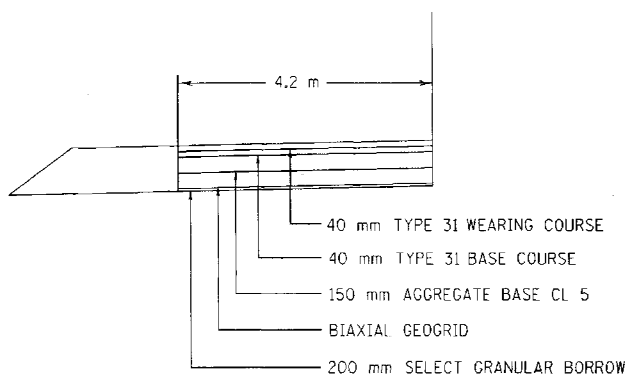

Figure 19, TH #72, Biaxial Geogrid typical

All geosynthetics used in these applications in northern Minnesota have been specified according to the 1988 or 1995 Edition of the Minnesota Department of Transportation Standard Specifications for Construction.

Typical Physical Properties of Geosynthetics:

Property	MnDOT Type V Geotextile	MnDOT Type VI Geotextile
Grab Tensile	0.9 kN	1.4 kN
Elongation (min)	15%	15%
AOS (max)	0.300 mm	0.425 mm

Geogrids

Tensile MD	12.47 kN/m
Tensile CMD	20.43 kN/m
Weight	215 g/m2
Aperture	2.5 cm by 3.3 cm

Hubbard County will be installing two – 300 m segments on their County State Aid Highway 6 this summer, one with a biaxial geogrid and the other with type V nonwoven geotextile. Installations will be similar to the typicals discussed in this paper. These two segments are constructed in granular type soils which is typical of the soils for the entire project. This will provide a comparison between the heavy clay type soils and the granular sandy type soils for any effects on the transverse and longitudinal cracking in addition to the remainder of the constructed roadway.

CONCLUSIONS:

The applications of geosynthetics generally have been used in situations where there is some concern for soil stabilization or poor soil conditions. The authors have found that it is very cost effective to use a somewhat stiffer geotextile (grab tensile strength bi-directional of 1.4 kN) because of the added benefits with minimal additional material costs. The type VI geotextile with 1.4kN tensile strength only costs an additional $0.10 per m2 versus the type V geotextile (0.9 kN tensile strength). Also, by allowing the contractor to carefully drive over placed fabric and sewing rolls longitudinally, we greatly reduce the placement cost. To expedite placement of geotextile and to maintain seam quality, we recommend factory sewing if overall fabric widths are 9 meters or less.

There are also field test results that indicate geosynthetics have strengthening effects that could reduce the thickness of the gravel base course while maintaining the original designed load carrying capacity. Our conclusion from actual field experiences with geosynthetics is that they have potential long term benefits when applied as an integral part of the design without reducing the gravel or bituminous thickness.

Long term benefits observed are reduced maintenance of transverse and longitudinal cracking and stronger road to resist rutting which could offer more economical future preservation type fixes such as thin (40mm) overlays or seal coats rather than the traditional 80mm overlays. There is also the benefit of having a gravel road somewhat immune to frost boil action during spring breakup which results in an all weather year around road.

Typical contract costs for furnishing and installing a Type VI woven geotextile is $10,000 per kilometer. This initial cost is small compared to the opportunity to reduce subbase, improve constructablity of aggregate base courses, reduced pavement rutting and cracking, and protection of gravel bases from frost boil migration and contamination.

The authors plan to continue to monitor all these and future applications of geosynthetics for benefits and unforeseen problems. Also the documentation of any progression of transverse and longitudinal cracking would be included. The more data gathered from constructed projects the more it will help us in future designs of roadways for longer service life in northern Minnesota.

MATERIAL SCIENCE & DURABILITY III

GEOSYNTHETICS CONFERENCE 2001

Portland, Oregon USA

Economics, Performance & Constructibility • February 12-14, 2001

MANUFACTURING VARIABILITY OF COEXTRUDED GEOMEMBRANE SURFACE TEXTURE

J.E. DOVE, Ph.D., P.E., VIRGINIA TECH
UNITED STATES OF AMERICA
MATTHEW W. ADAMS, GSE LINING TECHNOLOGY, INC.
UNITED STATES OF AMERICA
MAX L. JOHNSON, URS CORPORATION
UNITED STATES OF AMERICA

ABSTRACT

The results of an investigation to quantify the variability of high density polyethylene geomembrane surface texture due to manufacturing are presented. Specimens of two coextruded textured high density polyethylene geomembrane products were sampled from two manufacturing lines over an eight-month period. Surfaces were characterized using parameters obtained from stylus profilometer traces. For the materials and manufacturing processes used, the results show that surface texture remained within discernable ranges that have not previously been defined for coextruded geomembranes. Coefficients of variation of the roughness parameters range from 14.2 to 29.4 percent and are comparable to coefficients of variation for other geotechnical design parameters.

INTRODUCTION

Use of geosynthetics in civil engineering has created a specialized design science and numerous innovative methods for constructing interfaces between soils and geosynthetic, and interfaces between two geosynthetics. An outgrowth of this rapidly emerging area is the idea of designing an interface to meet specific project requirements. The ability to design interfaces within the engineered structure is a distinct advantage that geosynthetics have over traditional civil construction materials.

For construction involving geomembranes, it is known that the surface texture greatly influences the shear strength of critical interfaces. For this reason, various types of textured polyethylene geomembranes have been developed. In the United States, the two primary manufacturing methods are coextrusion and spray-on. This study focuses on coextruded high density polyethylene (HDPE) because of the recognized variability in surface texture due to the influence of many factors of the manufacturing process. Texture variability influences the finished product appearance, and can reduce tensile elongation at break for coextruded geomembrane with an extremely high degree of texturing.

Two applications where quantitative surface data is critical for the engineer, quality control organization, contractor, and the geomembrane manufacturer include: 1) material selection, and 2) verification that a given interface material combination meets project design criteria. For example, when engineers design using geomembranes, it is done on the basis of performance properties and experience with the product or group of products. Index tests, such as thickness and the tensile strength, are reviewed and candidate materials chosen. A program of direct interface shear tests may be conducted to evaluate interface friction. If the group of materials meets design and regulatory requirements, these materials are found to be adequate for use on the project. Once a contractor has secured a project, such as a landfill, the specified geomembrane is purchased. After the geomembrane has arrived at the job site, a third-party quality control engineer typically inspects the geomembrane. Inspection may include any or all of the following: visual inspection, evaluation of geomembrane thickness, evaluation of tensile strength, evaluation of asperity height and evaluation of the friction angle.

Visual inspection of texturing is subject to different interpretations brought about by the spatial characteristics of the surface. For instance, a surface with large asperity height but large peak spacing will appear "smoother" than a surface with the same asperity height but smaller peak spacing. This can lead to disputes about the degree of texture and delays in a project. If necessary, a series of supplemental shear tests may be carried out. However, the report relating to these tests may take several weeks to obtain causing further project delay. Quantifying the surface texture of geomembranes has the potential to prevent these delays. A quality assurance program would compare surface parameters of the geomembrane in question with statistical data from the manufacturer which gives ranges of the expected degree of texture variation. If the texture is found to be within the established range of variation for that product, the material would be accepted.

There is presently no published information known to the authors regarding surface texture variability for HDPE geomembrane products. Developing a database of statistics such as the expected value, $E[X]$, standard deviation, σ, and coefficient of variation, $V(x)$, for values of roughness parameters can provide a framework to determine if a textured geomembrane product delivered to a project site is within established manufacturing ranges. Previous limitations to collecting this information have been removed with development of innovative surface characterization techniques.

Knowledge of product variability could provide geomembrane manufacturers with a quantitative basis for quality control and product characterization. Engineers would gain confidence in knowing the product specified is actually used in construction, and variations in engineering performance could be quantified (reliability-based engineering). Finally, field quality assurance and dispute avoidance would be facilitated as surface parameters of a questioned geomembrane are obtained and compared with established manufacturing data.

Therefore, this paper presents the results of a study to investigate the manufacturing variability in surface texture over time, and over two different production lines. This study focuses on two coextruded HDPE textured geomembrane products over a period of approximately eight months.

BACKGROUND

Currently, there is no universally adopted test to quantify the texture of the geomembrane after it is produced. Manufacturing quality assurance typically is limited to a visual inspection of the sample, which is compared to a benchmark sample. If the newly produced sample has texture visibly different than a desirable benchmark sample, then the whole roll of the geomembrane may be rejected. The manufacturing parameters are then modified in order to produce a texture that is congruent with the benchmark sample.

There have been efforts in the past to create an index test that would permit quantification of surface texture. The Geosynthetics Research Institute (GRI) created such a test that incorporated a tilt-table. The test consisted of wrapping a wood block with a standard carpet and then setting this composite block onto the geomembrane sample, which was secured in place upon the tilt table. The angle of the table was increased until, at some critical angle, the composite block would slide off the geomembrane. The GRI tilt-table test was eventually retired because the variance in results for repeated tests was unacceptable. The lack in precision is realized in considering that the carpet/geomembrane interface in not a well reproduced or controlled test. Furthermore, the lack of a normal load greatly contributed to the high variability of data.

A second method of quantifying texture is through use of the Asperity Measurement (GRI Method GM12). This method calls for measuring asperity height using a depth gage that extends from a flat base plate resting on the tops of the asperities down to a point on the geomembrane sheet. It is a rapid test that may be conducted on the production floor. The asperity height is the average of ten measurements made over the roll width. The asperity height as determined by GM12 provides information only at discrete points, and has a high degree of operator dependence. While point estimates can be useful in many applications, a major limitation is that they are unable to provide spatial information about the surface such as the different scales of texture and their distribution within the sheet. This information facilitates interface engineering and design through use of surface parameters determined at the scale of the soil grain or geotextile fiber.

Methods to quantify geomembrane texture using a stylus profilometer were presented by Dove and Harpring (1999) and Johnson (2000). A stylus profilometer is a standard measurement device that has been used in mechanical engineering applications since for about 50 years. It records two-dimensional surface topography in a vertical plane perpendicular to a surface. In contrast to point measurements, spatial relationships between asperities can be measured and expressed by various parameters. While product quality control applications are discussed herein, the profilometry method provides an ability to extract surface geometry information for use in engineering design.

For example, Irsyam and Hryciw (1991), Hryciw and Irsyam (1993), and Dove and Jarrett (1999) have shown that for a given asperity height, asperity spacing and slope (discussed below) control the mechanics of interface shear with granular materials. This is illustrated in Figure 1 where the influence of asperity spacing and average slope on efficiency of an ideal machined surface and Ottawa 20/30 sand is shown. Note that asperity spacing is normalized with respect to the median grain diameter (D_{50}) of Ottawa sand which yields a relative measure of interface roughness. Thus the information gained from the profilometry technique is ideally suited for both quality control and for engineering design purposes.

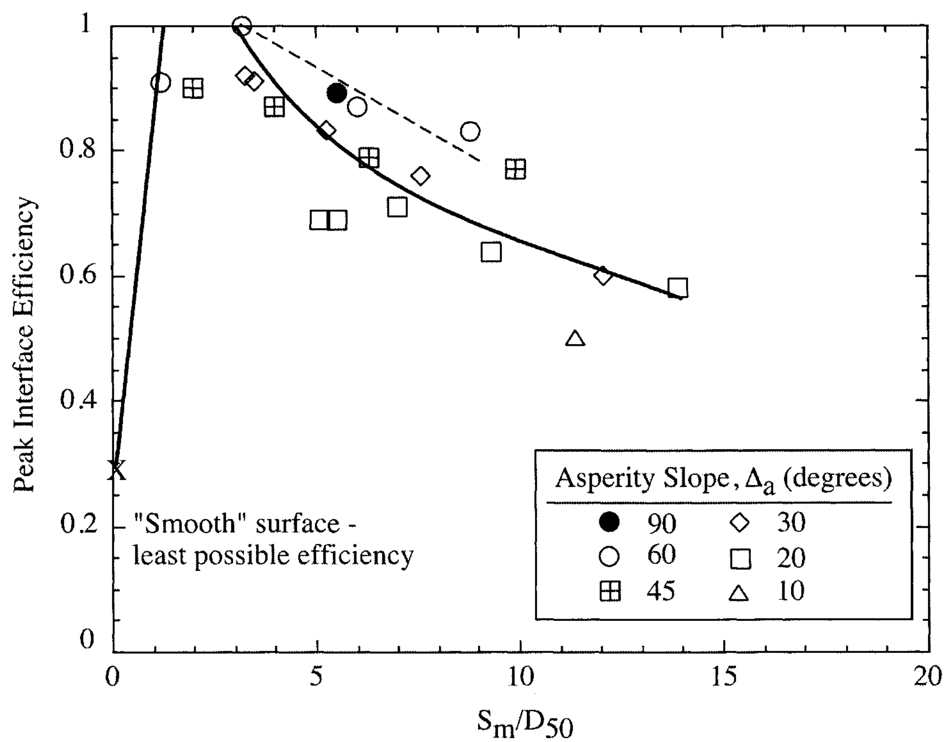

Figure 1. Normalized Spacing Relationships for Ottawa 20/30 Sand at Peak State

EXPERIMENTAL

Geomembrane Specimens. Specimens approximately 30 cm x 30 cm in plan dimension were made from material collected from Production Lines 1 and 2 during routine manufacturing quality assurance sampling of standard production geomembranes. Surface characterization specimens were made on approximately one-week intervals over the eight-month period from May 1999 to February 2000. The geomembrane materials used in this project are manufactured by a coextrusion process using a circular die 2.2 m in diameter. During manufacturing, a core layer of polyethylene is extruded through a die. Nitrogen gas is introduced into extruders feeding polyethylene to layers on both sides of the core layer. As the three layers are coextruded from the die, the exterior layers are joined to the core layer while the polymer is molten. The nitrogen gas in the exterior layers expands on contact with atmospheric pressure, creating the texture. The tube of geomembrane is then split, and opened into a flat sheet.

Materials 1.0 mm, 1.5 mm, and 2.0 mm (40 mil, 60 mil, and 80 mil) in thickness were randomly sampled. Specimens included HDPE coextruded geomembranes with black surfaces on both sides and with black on one side and white on the other side.

Surface Characterization. Each specimen was characterized in the machine direction with four random 40 mm long profiles on both sides. A Taylor-Hobson S3F inductive profilometer with an extended range stylus (see Dove and Harpring, 1999) was used to record the surface profiles. Characterization in directions other than the machine direction was not performed as most textured materials are deployed with machine direction in the direction of shear. As the profiles were located randomly, variations in texture within a specimen are implicitly included. The four 40 mm profiles for one side were averaged to give representative parameters for that side. Texture was characterized using the following parameters:

- Average Roughness, R_a,
- Maximum Peak to Valley Height, R_t,
- Average Centerline Spacing, S_m, and,
- Average Asperity Slope, Δ_a.

R_a and R_t are height parameters, S_m is a spacing or wavelength parameter, and Δ_a incorporates both height and spacing. The physical meaning of the parameters are indicated for an ideal surface in Figure 2. R_a is the average of the absolute values of profile height measured from a centerline through the data. Thus portions of a profile below the centerline are negative height values. Taking the absolute value of these heights gives the dashed lines shown on Figure 1. The resulting positive heights are averaged.

R_t is the maximum vertical relief (distance from highest peak to lowest valley) in the profile length. Conceptually, R_t is analogous to the Asperity Measurement in that it is a peak to valley height. Dove and Harpring (1999) found that R_t was about 20 percent less than the Asperity Measurement obtained by GM12 for similar coextruded geomembranes.

Asperity spacing is critical to mechanical behavior of the interface, as shown in Figure 1, and as demonstrated by Dove and Jarrett (1999) and Dove and Harpring (1999). S_m is the average value of the distance between adjacent points located at the intersection between the mean line and the profile. Δ_a is the average of the absolute values of instantaneous slope between data points. Asperity slope is a hybrid parameter that accounts for both height and spacing.

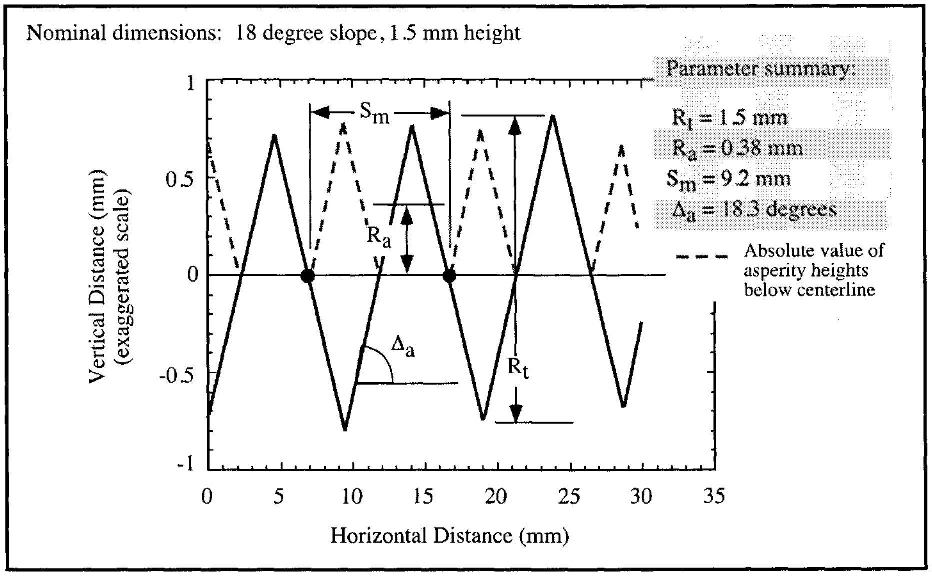

Figure 2. Definitions of Surface Roughness Parameters

RESULTS

Black/Black Geomembrane. Figures 3 and 4 present results for R_a, R_t, S_m, Δ_a, respectively, for the geomembrane with black on both sides (black/black) manufactured on production line Number 1. In these plots, the two data points connected by vertical lines given for each point in time represent the two sides of the geomembrane. Statistics were computed for each parameter and each geomembrane side. The centerline is the expected value, E[X] (the average of data which has variability). Limits representing one standard deviation (σ) above and below the expected value are designated E[X]+σ and E[X]-σ.

In Figure 3a, the average roughness values, R_a, are shown with respect to time. The expected value for R_a is 88 μm (0.088 mm) and the standard deviation is 26 μm (0.026 mm). The data indicates that variations in roughness on opposing sides of the material are typical. For instance, a set of measurements in late-September show that one side has up to three times the roughness value as the other side. In general, however, the difference in roughness between the two sides is much less, as indicated by the number of closely spaced data points. No global trend of increasing or decreasing roughness over time was observed for this texture. However, the data suggests that the samples produced in January and February of 2000 have very similar roughness values on both sides of the geomembrane.

Figure 3b shows the trend of peak to valley height, R_t, values for this geomembrane over time. The expected value for R_t over the study is 685 μm (0.685 mm) and the standard deviation is 136 μm (0.136 mm). The coefficient of variation, V(x), for R_t is around 20 percent as compared to around 30 percent for average roughness, R_a. Therefore the height between the maximum peaks and the lowest valleys has less variation than the deviation of the surface from the profile mean line.

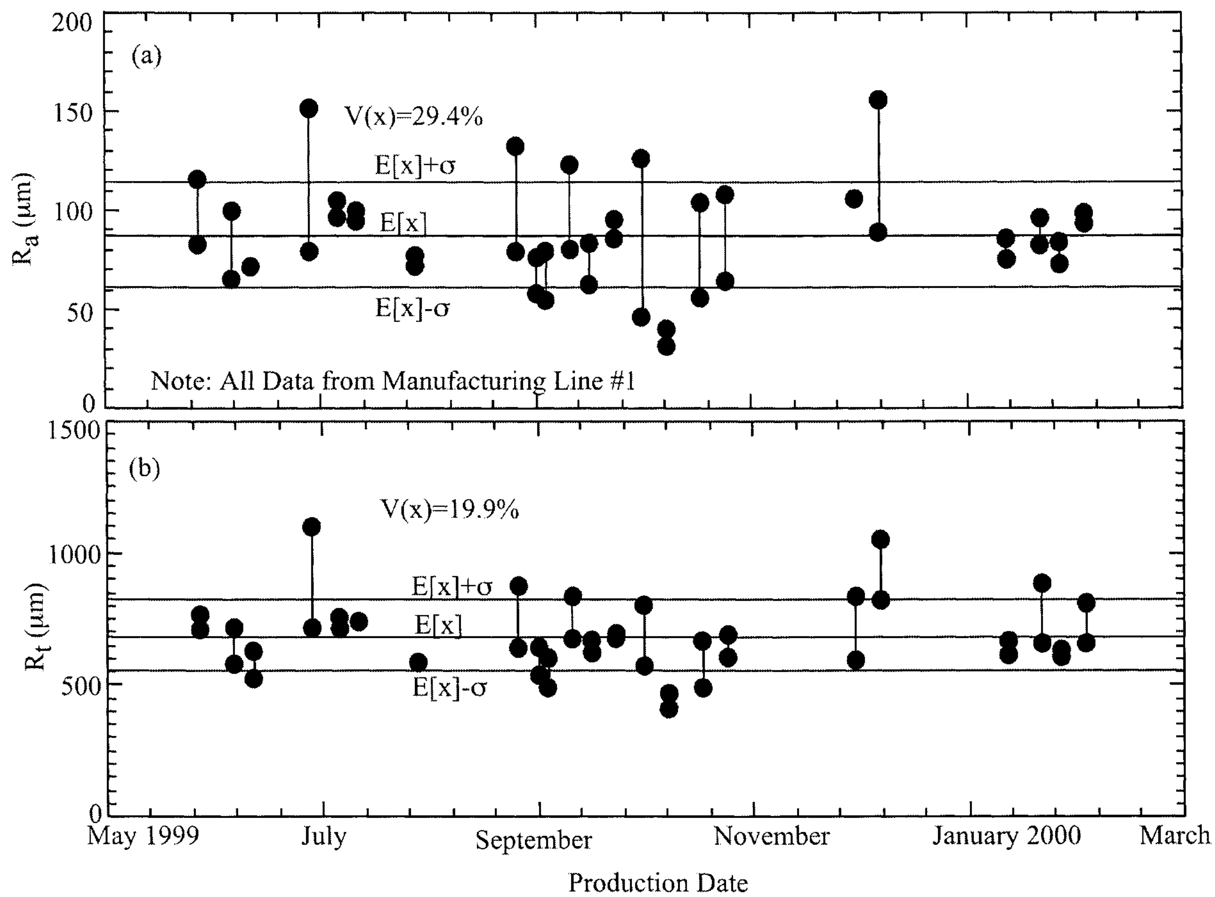

Figure 3. Variation of (a) R_a, and (b) R_t of Black/Black Coextruded Geomembrane

Figure 4a shows the trend of mean line spacing, S_m, values over time for the black/black geomembrane. The expected value for S_m throughout the entire study is 3.4 mm and the standard deviation is 0.8 mm. The coefficient of variation, V(x), for S_m is around 25 percent. As shown, a sample produced in early December had a S_m value twice that of the other side of the membrane. This is highly unusual as compared to the entire data set. It is known that the surface properties of coextruded textured geomembranes are impacted by a number of manufacturing variables. These include speed of manufacturing, equipment, thickness of the geomembrane, resin type and percentage of nitrogen gas in the molten polyethylene. In addition, changes in equipment or polymer mixture also can affect the end product. It is not known at this time which if any of these possible influences were responsible for the large deviation in the mean line parameter spacing that occurred with this sample. Analysis of roll test data showed there was no correlation between roughness parameters and properties such as melt flow index and tensile elongation to break.

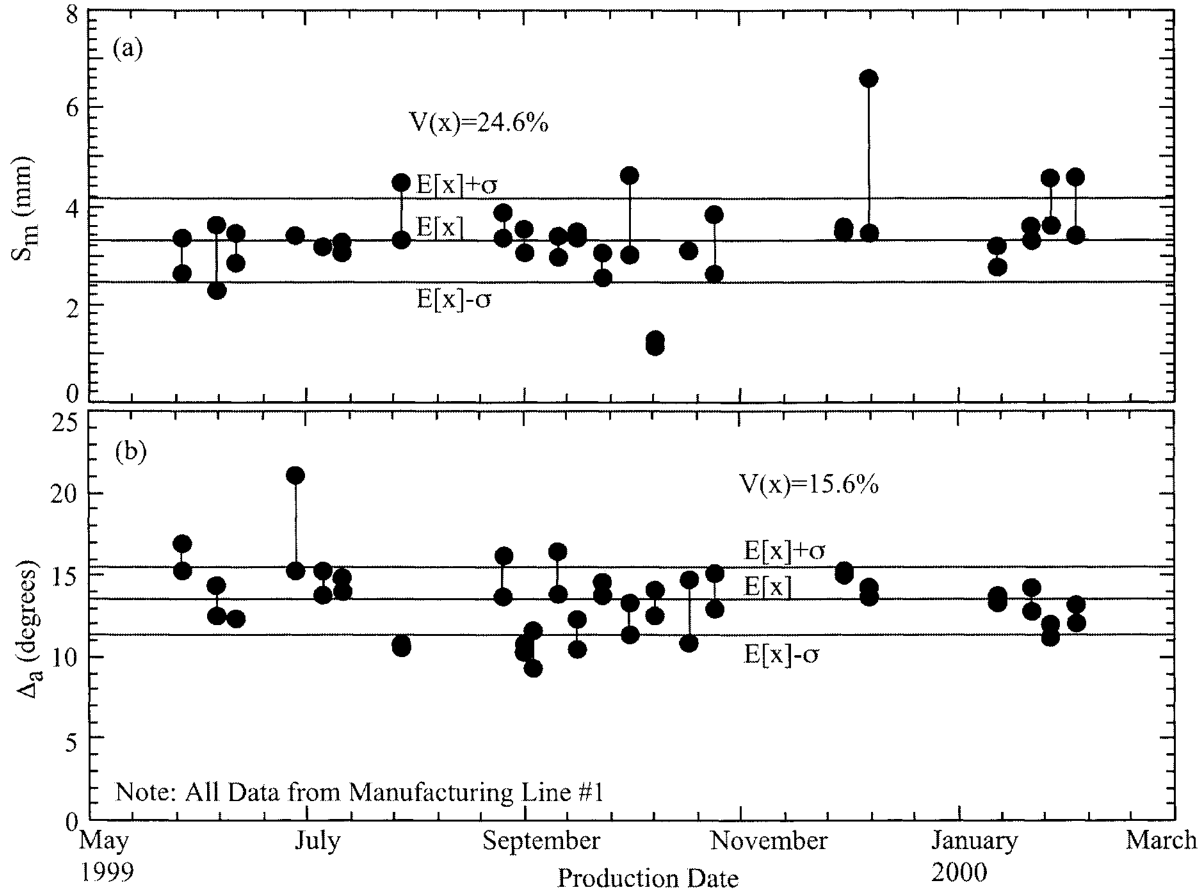

Figure 4. Variation of (a) S_m, and (b) Δ_a of Black/Black Coextruded Geomembrane

The results for average asperity slope, Δ_a, during the 8-month period are given in Figure 4b. The expected value for Δ_a throughout the entire study is 13.5 degrees and the standard deviation is 2.1 degrees. The coefficient of variation, V(x), for Δ_a is about 16 percent, which is the lowest of the four parameters in these plots. As with the other parameters, there is little to no shift in the parameter over the course of the study.

Black/White Geomembrane. Figures 5 and 6 provide results in terms of parameters R_a, R_t, S_m, Δ_a, respectively, for white/black geomembrane manufactured on production line Number 2. In these plots, the closed data points represent the black side and the open data points represent the white side of the product. Each data point represents the average value of the parameter from 4 random 40 mm long profiles. To avoid confusion, the statistics for each side have been placed in a table on the figure instead of being graphically illustrated with horizontal lines as shown on Figures 3 and 4.

In Figure 5a, the roughness value, R_a, is shown over time. The expected values for the black and white sides are given above the plot. In general, both sides have similar expected R_a

values and coefficients of variation. The difference in expected value between sides is 16.9 μm (0.017 mm), which is considered small. In observing the data, there is no global trend in increasing or decreasing surface roughness.

Similar observations can be made in terms of R_t. Both sides have similar expected values with differences less than 0.1 mm. Coefficients of variation for the parameter are also similar. The parameter S_m, as shown in Figure 6a, has a slightly higher expected value (0.4 mm) for the black side of the membrane. However, the coefficient of variation is only slightly greater for the black side.

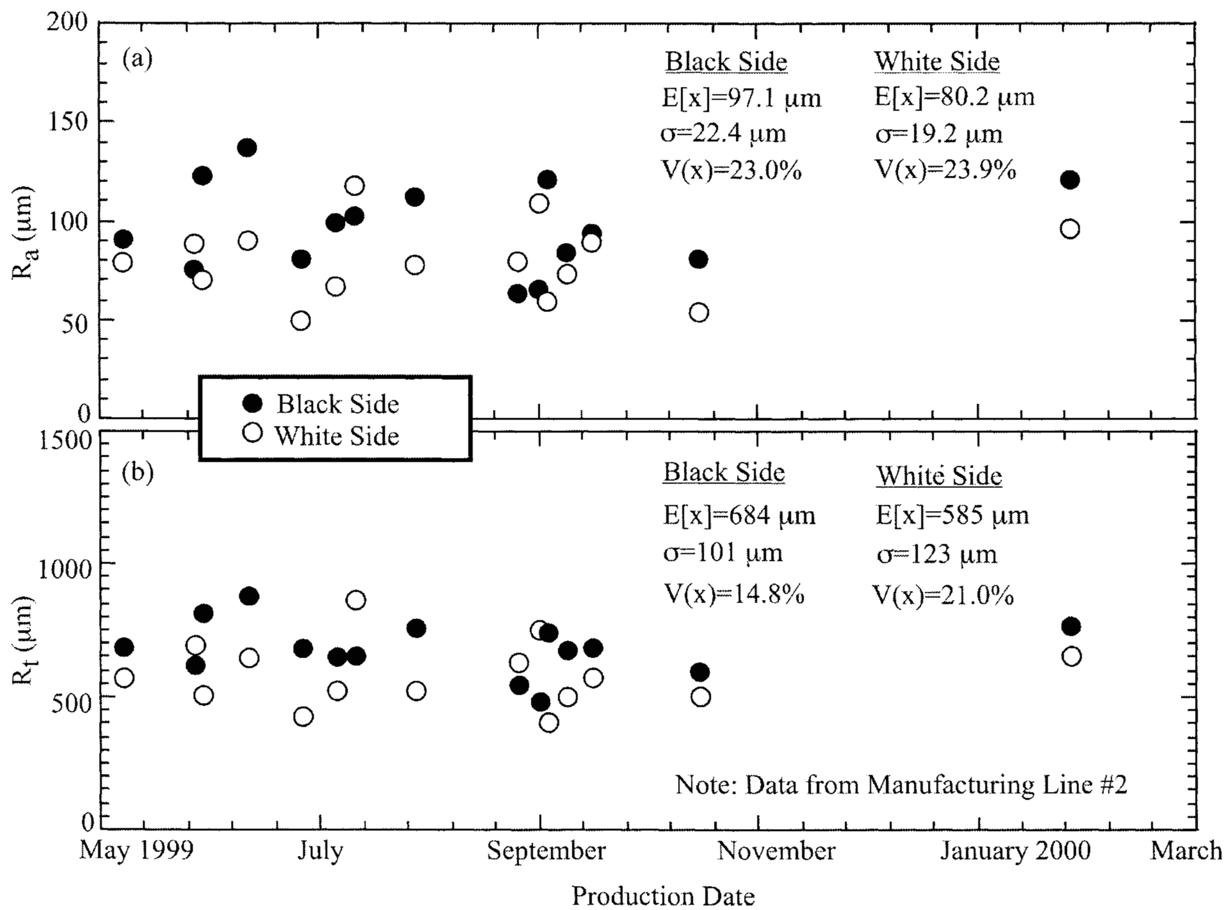

Figure 5. Variation of (a) R_a, and (b) R_t for White/Black Coextruded Geomembrane

Figure 6b shows the variation in average asperity slope, Δ_a. This figure indicates that the expected value and standard deviation are nearly equal for the black and white sides of the product.

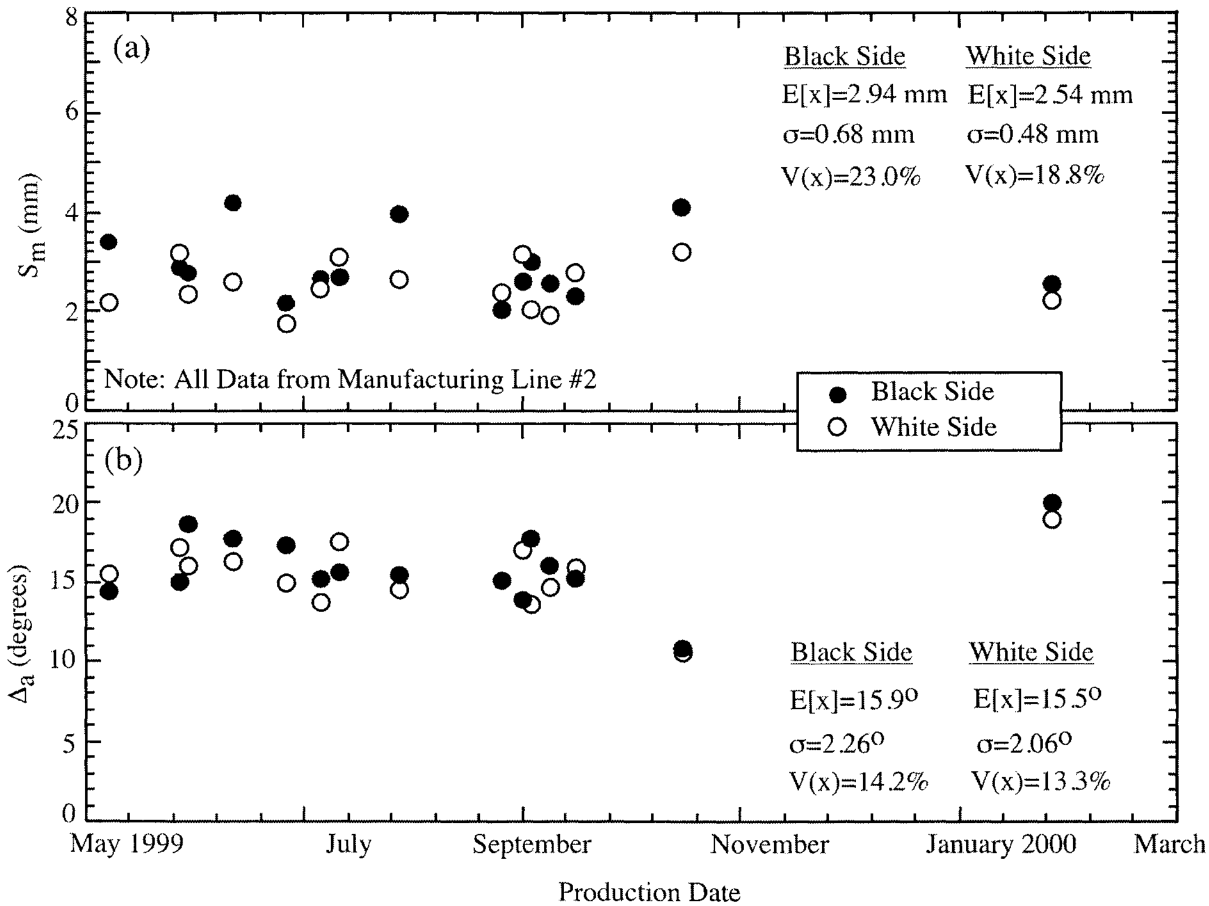

Figure 6. Variation of (a) S_m, and (b) Δ_a, for White/Black Coextruded Geomembrane

Results Summary. The results of this study show that there is no overall increase or decrease in surface texture over the eight-month period for both the black/black and the black/white geomembranes. A major research finding is that the coefficients of variation for the roughness parameters used range from 14.2 percent to 29.4 percent with R_t and Δ_a having the least variability. Therefore, it would be expected that any given sample taken from the materials used in the study would have variation in the roughness parameters of between 14 and 29.4 percent from the mean value. These coefficients of variation are comparable to those of other geotechnical parameters, as shown in Table 1.

CONCLUSIONS

This study has presented data to quantify the variability of in the degree of texture in the machine direction for two coextruded geomembranes. For the materials and manufacturing equipment used, there is no overall increase or decrease in surface texture over the eight-month period. It was found that the black/white product has similar degrees of texturing and coefficients of variation for each side. It has also been shown that the coefficients of variation in roughness parameters for the materials used herein are similar to those of other geotechnical parameters.

Table 1. Typical Coefficients of Variation for Geotechnical Parameters (after Harr, 1987)

Geotechnical Parameter	Coefficient of Variation (%)
Porosity	10
Specific Gravity	2
Water Content	13 to 20
Degree of Saturation	10
Hydraulic Conductivity	90 to 240
Preconsolidation Pressure	19
Compression Index	26 to 30
Standard Penetration Test	26
Cone Penetrometer Test	37
Friction Angle	7 to 12
Cohesion Intercept	40

The practical significance of this study is in showing that the manufacturing process for the materials used produced coextruded geomembranes with definable bounds of texture over the duration of the project. The profilometry method is shown to have the capability to quantify this variability for quality control purposes. In the future, a database of manufacturing data could be used to determine if the texture of a geomembrane sample is within normal ranges of variation for the manufacturing process and manufacturing equipment. This use requires that an acceptable variation from the mean be established (quality limit).

Additional data is needed to conclude if variations in the degree of surface texture observed in this study are typical for the coextrusion process. This requires that additional data be collected over a longer time period. It should be noted that variability in these materials has been visually observed in the past with no negative impact on performance. Further research is also needed to determine the sensitivity of interface strength and deformation behavior to texture variations, and how each of the processing variables influences the final product.

ACKNOWLEDGEMENTS

This material is based on work supported by the National Science Foundation under Grant No. CMS-9800291. This support is gratefully acknowledged. The authors thank GSE Lining Technology, Inc. of Houston, Texas for providing the geomembrane material used in the study. Ms. Angela Booth, Undergraduate Research Assistant at Georgia Tech, collected many of the surface profiles used in this study.

REFERENCES

Dove, J.E. and Jarrett, B.J., 1999. "Friction Behavior of Granular Materials on Ideal Counterfaces". Proceedings of Workshop: *"Tribology on the 300th Anniversary of Amontons' Law"*, Materials Research Society, San Jose, CA, USA, June 1999, pp. 29-31.

Dove, J.E. and Harpring, J.C., 1999, "Geometric and Spatial Parameters for Analysis of Geomembrane/Soil Interface Behavior", *Proceedings of Geosynthetics '99*, Vol. 1, IFAI, Boston, MA, USA, April 1999, pp. 575-588.

Geosynthetic Research Institute, GRI Test Method GM12. *"Asperity Measurement of Textured Geomembranes using a Depth Gage"*, Drexel University, Philadelphia, PA, USA.

Harr, M.E., 1987, *"Reliability-Based Design in Civil Engineering"*, Dover Publications, Mineola, New York, USA, 291 p.

Johnson, M.L., 2000, *"Characterization of Geotechnical Surfaces via Stylus Profilometry"*, Master of Science Thesis, School of Civil and Environmental Engineering, Georgia Institute of Technology, Atlanta, GA, USA, 503 p.

Hryciw, R.D. and Irsyam, M., 1993, "Behavior of Sand Particles Around rigid Ribbed Inclusions During Shear", *Soils and Foundations,* Vol. 33, No. 3, pp. 1-13.

Irsyam, M and Hryciw, R.D., 1991, "Friction and Passive Resistance in Soil Reinforced by Plane Ribbed Inclusions", *Geotechnique*, Vol. 41, No. 4, pp. 485-498.

CHARACTERIZATION OF SHORT AND LONG TERM CREEP AND RELAXATION PROPERTIES OF A POLYPROPYLENE GEOGRID

J. S. THORNTON, TEXAS RESEARCH INTERNATIONAL, INC., U.S.A.

ABSTRACT

An objective of this effort has been to support improved understanding of the long term performance of reinforcement members of mechanically stabilized earth walls. Tests were performed to define the trajectory of creep and relaxation modulus curves for a commercial polypropylene geogrid. Short term data were obtained to generate isochronous stress-strain curves which showed that nonlinear viscoelastic behavior was displayed at strain levels above 0.5%. Long term tests were conducted using the stepped isothermal method. Those tests showed that for equivalent starting stresses and strains, the creep modulus fell more rapidly than the relaxation modulus for times greater than 1000s. This divergence in creep and relaxation modulus responses is attributed to non-linear viscoelastic behavior. It would appear non-conservative to design using long term creep and relaxation data interchangeably, but overly conservative to use creep data alone. Further work is needed to evaluate intermediate paths combining of creep and relaxation processes.

INTRODUCTION

A prime motivator for this effort has been the need to better understand the long term performance of mechanically stabilized earth (MSE) walls (Bathurst, et al., 2000). Studies have shown that the long term "aging" paths of geosynthetic materials in a soil reinforcement context include both creep and stress relaxation components (Boyle, 1995). Creep refers to the strain response of a material subjected to a constant stress and stress relaxation to the stress response of a material subjected to a constant strain. With time, we should expect both an increase in strain and a reduction of stress as the reinforcement seeks to achieve thermodynamic equilibrium within the soil structure. Individually, creep strain or stress relaxation vs. log time curves are not adequate to describe this behavior. Perhaps some combination of creep and relaxation moduli will be found useful for modeling long term geosynthetic reinforcement performance. The creep and stress relaxation moduli are defined similarly and both are secant moduli. Both are the quotient of total stress by total strain. For creep the stress is constant and the strain time dependent, while for relaxation the stress is time dependent and the strain is held constant.

BACKGROUND

Linear Vs Non-linear Viscoelastic Behavior In general, stress vs. strain curves developed from rapid loading tensile tests on polymeric materials show negative curvature during the load-up ramp. Some of this behavior can come from the viscoelasticity of the material and some from plastic deformation or other material non-linearity. If the negative curvature is due to viscoelasticity only, then the material is said to be a linear viscoelastic material. If this is not the case, then the material is said to be nonlinear viscoelastic. Another kind of stress vs. strain curve, called an isochronous stress vs. strain curve, is constructed from creep data (time dependent strain data collected at constant stress) or stress relaxation data (time dependent stress data collected at constant strain). With a series of such curves, a number of stress, strain pairs for a given test time (e.g. 1000s or 1000h) may be assembled to construct an isochronous plot. Time is effectively removed as a variable since all the points for the plot will have had the same test time. A good test for linear viscoelastic behavior is a linear isochronous stress-strain plot. Most polymeric materials exhibit linear viscoelastic behavior at small strains (one-half percent or less). Most engineering applications engage polymers in large strain situations; so it would seem that engineers need not take an interest in linear viscoelasticity. Notwithstanding that most don't, they should because linear models are much easier to understand. Non-linear viscoelastic theory has been developed for some materials in some stress-strain regimes and some temperature ranges, but the theories are not at all general and tend to be exceedingly complex. The best guidance may come from the simplest models, but the limitations imposed by simple models must be realized.

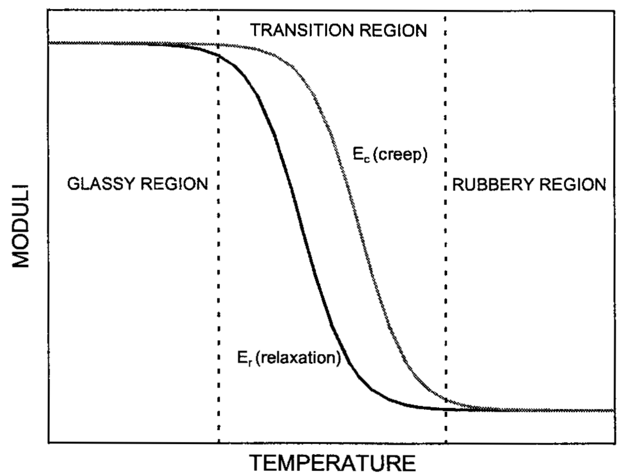

Figure 1. Creep (E_c) and relaxation (E_r) moduli for an ideal linear viscoelastic material as a function of temperature

Transition Behavior Figure 1 diagrams the temperature dependence of an ideal linear viscoelastic material. This plot of the creep and relaxation moduli as a function of temperature shows the range of mechanical behavior possible with a polymer. At a suitably low temperature in the "glassy" region, the material has high creep and relaxation moduli. Also in the glassy region the creep and relaxation behaviors are nearly indistinguishable. At a suitably high temperature in the "rubbery" region the material has low moduli, and again the creep and relaxation responses are nearly indistinguishable. Then in a relatively narrow range of intermediate temperatures called the "transition" region, the material displays a range of behaviors that change from glassy (stiff, brittle) through leathery (tough) to rubbery (compliant, resilient) as the temperature is increased from low to high. The transition region is defined approximately by the glass transition temperature (T_g) at the low temperature end and 50°C above the T_g on the high end. In the transition region the creep and the relaxation moduli are no longer indistinguishable. This means that in this temperature region one could not use creep data to estimate relaxation behavior directly and visa versa. The creep modulus is always larger than the relaxation modulus for linear viscoelastic materials in this region [Smith, (1963)]. Because of the equivalence of time and temperature in understanding polymer behavior, the abscissa of Figure 1 could be renamed log time and the discussion above amended to read log time instead of temperature with no change of meaning.

Response Paths Figure 2 is a stress vs. strain diagram which depicts load-up OA, creep path AD, stress relaxation path AB and a combined creep and relaxation path AC. The path lengths are chosen arbitrarily so that the moduli (given by the slope of the dashed line OBCD) are the same. The path AC can be thought of as a combination of creep and relaxation segments (stair case fashion), but in general it will be a smooth path, the trajectory of which is governed by the boundary conditions (machine stiffness if in a test fixture, or soil stiffness if an in-soil application).

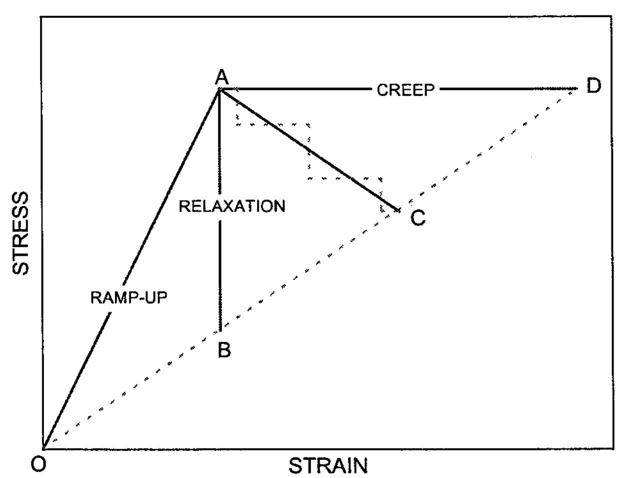

Figure 2. Stress vs. strain diagram showing ramp up (OA), relaxation (AB), creep (AD) and general viscoelastic response (AC)

CHARACTERIZATION OF A POLYPROPYLENE GEOGRID

Material The material studied was a polypropylene (PP) geogrid designated BX 1100 SB. This material has been used in recent investigations of MSE walls (Bathurst, et al., 2000). The viscoelastic behavior of this material at relatively low values of stress and strain is of interest to confirm the findings of these investigations especially where independent measurements of stress and strain could not be accomplished. The glass transition temperature of PP is around –20°C; so that at +20°C the material behavior should be as in the upper part of the transition region or the lower part of the rubbery region as defined in Figure 1.

Rapid Loading Tensile (RLT) Tests The first step was to perform rapid loading tensile (RLT) tests on single ribs of the material to determine the properties in both the machine and cross machine directions. Most of the creep and relaxation tests were to be done in the machine direction since it was the one most studied in the MSE test walls. The tests were conducted at 20°C in an Instron Model 4500 testing machine equipped with a temperature controlled chamber. The strain rate used for the ramp was 10%/min. The results are shown in Tables 1 and 2. The machine direction turned out to be the more compliant of the two. Of concern was the rather high coefficient of variation (%CoV in the tables), which foretold the need for numerous replicates in accomplishing the short term creep and relaxation tests.

Table 1. RLT Summary Results
Machine Direction

Specimen number	Strain at max. stress %	Maximum stress N/rib	Secant modulus N/rib
1	10.61	552.0	5203
2	11.51	564.5	4905
3	9.43	557.7	5915
4	9.58	559.6	5842
5	9.26	548.7	5929
6	9.88	551.1	5580
Avg.	10.04	555.6	5562
Std Dev	0.86	6.00	423.7
% CoV	8.57	1.08	7.62

Table 2. RLT Summary Results
Transverse Direction

Specimen number	Strain at max. stress %	Maximum stress N/rib	Secant modulus N/rib
1	8.13	661.2	8129
2	7.80	685.2	8779
3	7.92	669.2	8455
4	8.00	663.6	8291
5	7.69	684.5	8900
6	7.07	678.6	9597
Avg.	7.77	673.7	8692
Std Dev	0.38	10.49	529.8
% CoV	4.83	1.56	6.10

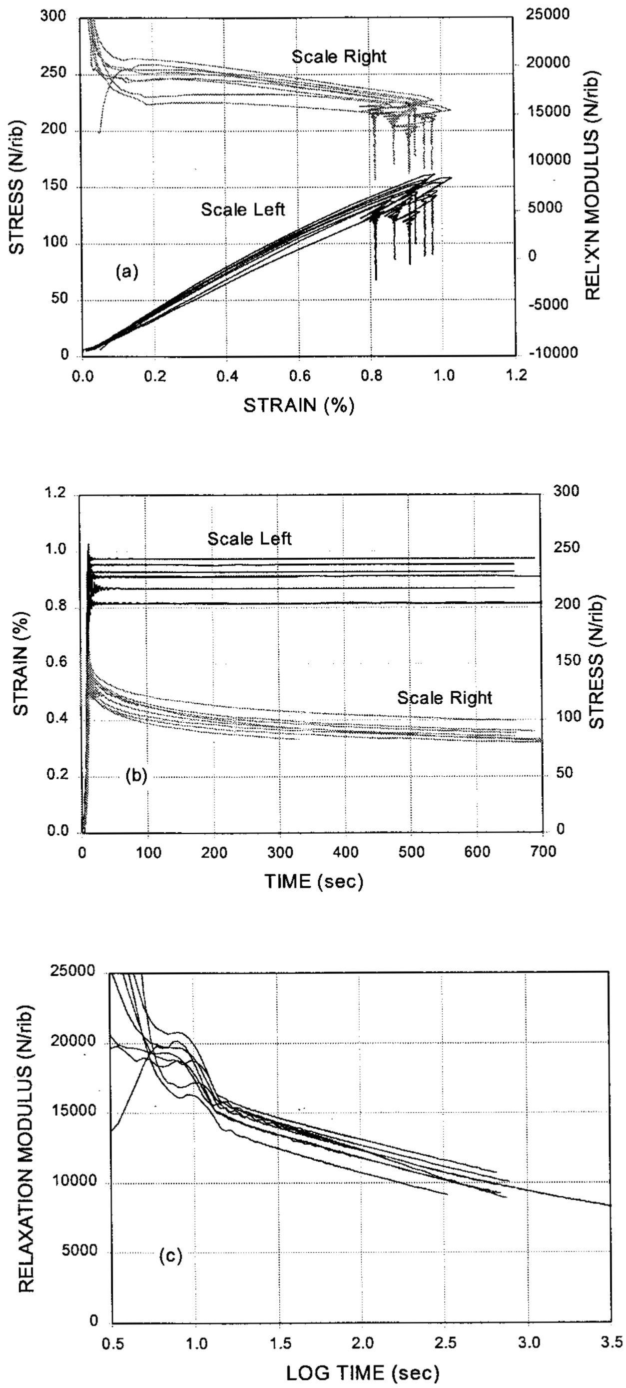

Figure 3. Typical short term stress relaxation test results for a PP geogrid (a) stress and relaxation modulus vs. strain, (b) stress and strain vs. time, and (c) relaxation modulus vs. log time

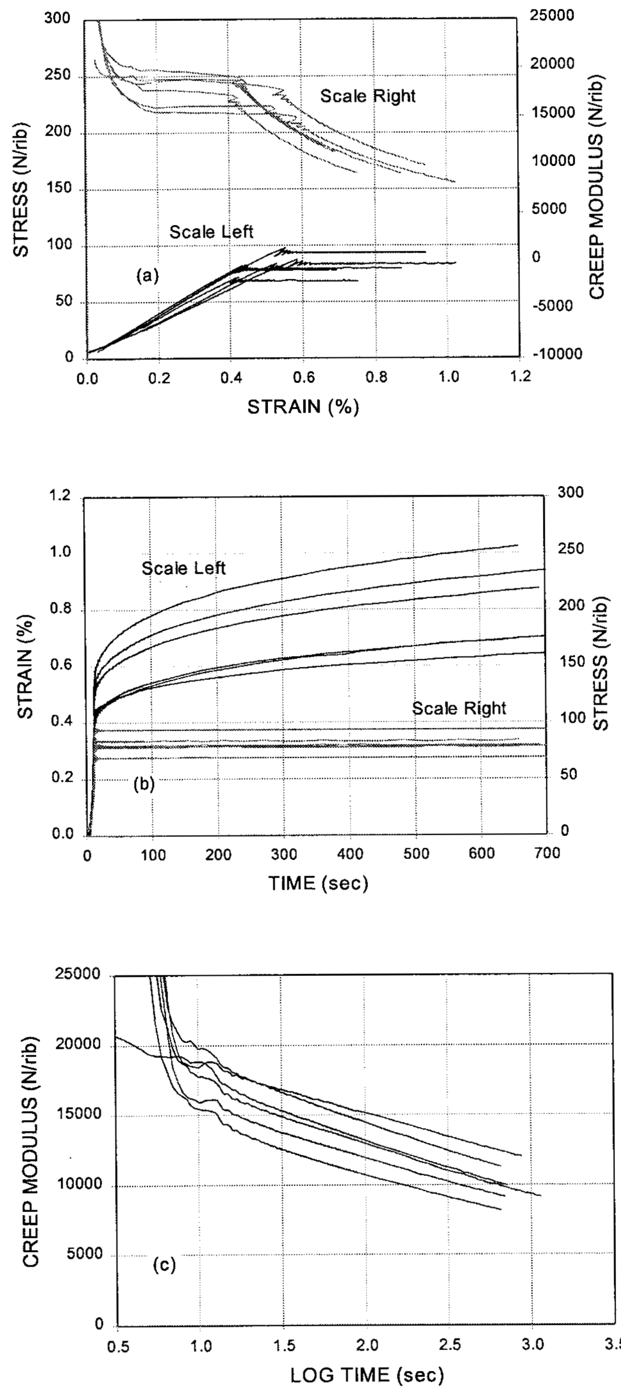

Figure 4. Typical short term creep test results for a PP geogrid (a) stress and creep modulus vs. time, (b) stress and strain vs. time, and (c) creep modulus vs. log time

Ramp and Hold (R+H) Tests The next step was to perform short term creep and relaxation tests in the machine direction. We accomplished forty of these short term tests, which we call ramp and hold (R+H) tests, in the ranges 0.25% to 1.1% initial strain and 8% to 30% initial stress. These tests were performed at 20°C in the same testing machine and chamber used for the RLT tests. Load control was utilized for the creep tests and strain control for the relaxation tests. Figures 3 and 4 show typical results. The scatter in the data was minimized by "pointing" the curves (Thornton, et al., 1999), but scatter remains. The figures show stress relaxation results at 0.8 to 1.0% applied strain, and creep strain results for 70-90N/rib applied stress. From data such as these we obtained 120s and 600s isochronous stress-strain pairs as shown in Table 3. Note that included in the table are 120s and 600s isochrones from accelerated creep and relaxation tests that were performed later. The 120s and 600s isochronous stress-strain curves displayed in Figures 5 and 6 were constructed from the Table 3 data.

Polynomial curves were fit to the creep and relaxation data sets separately. R^2 for these curves are quite high as shown in the figures indicating that there is sufficient data density to offset uncertainty between individual test replicates (high CoVs). Note that in both Figures 5 and 6 the creep and relaxation isochronous curves are nearly indistinguishable, although the relaxation curves are very slightly below the creep curves. This indistiguishability confirms that at 20°C the polymer is sufficiently above its glass transition temperature to be considered at least in the upper transition region of Figure 1. The data in Figure 5 support linear viscoelectic behavior up to 0.35% strain and 60-50N/rib stress (about 10% of the UTS). The Figure 6 data support linear viscoelestic behavior to 0.45% strain and 40-50N/rib (about 8% of the UTS). For realistic engineering applications we can expect this polymer to exhibit non-linear viscoelastic behavior, but it is encouraging that the creep and relaxation properties are nearly the same, at least out to 600s.

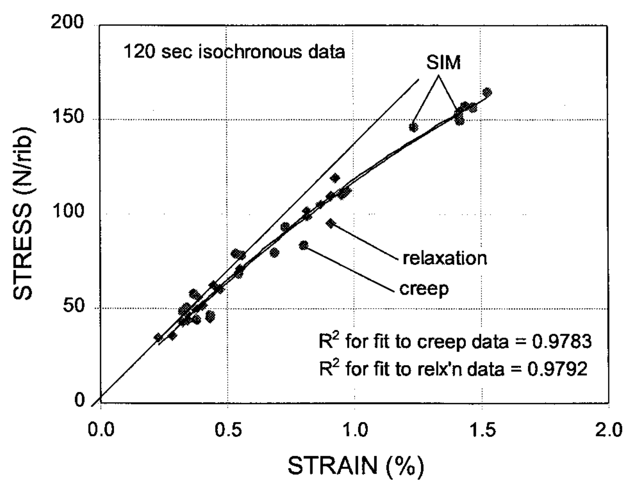

Figure 5. Isochronous (120 s) stress vs. strain curves for PP geogrid constructed from both creep and relaxation data

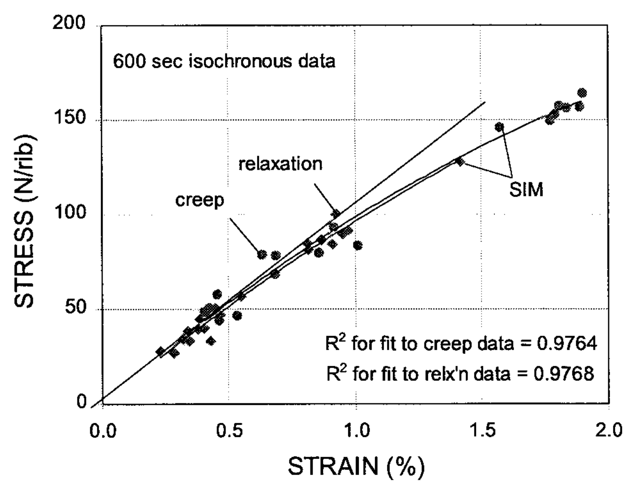

Figure 6. Isochronous (600 s) stress vs. strain curves for a PP geogrid constructed from both creep and relaxation data

Table 3. 120 and 600s Isochronous Stress vs. Strain Pairs

	Creep				Relaxation			
Nominal	120s		600s		120s		600s	
Strain	stress	strain	stress	strain	stress	strain	stress	strain
	N/rib	%	N/rib	%	N/rib	%	N/rib	%
	164.5	1.526	164.3	1.897	119.2	0.927	100.2	0.927
	157.4	1.439	157.4	1.807	101.3	0.815	84.3	0.814
	156.3	1.468	156.3	1.835	105.0	0.868	86.4	0.869
	149.4	1.418	149.4	1.773	112.0	0.975	91.3	0.974
	156.8	1.469	156.8	1.888	109.5	0.952	89.1	0.952
	152.4	1.414	152.8	1.791	95.1	0.909		
					98.5	0.817	81.2	0.815
					109.3	0.911	84.1	0.911
SIM tests	146.2	1.234	146.2	1.571	154.3	1.416	127.6	1.417
0.6%	68.6	0.543	68.6	0.684	49.4	0.378	39.5	0.378
	83.4	0.801	83.3	1.008	44.9	0.431	33.1	0.429
	79.7	0.685	79.7	0.856	55.8	0.383	44.8	0.385
	93.4	0.728	93.2	0.916	60.1	0.47	46.6	0.47
	79.2	0.532	78.9	0.63	70.8	0.552	56.2	0.552
	78.1	0.554	78.2	0.686	62.1	0.446	50.4	0.445
0.3%	57.8	0.365	57.6	0.452	51.7	0.402	39.6	0.402
	48.4	0.324	48.5	0.403	43.6	0.344	32.9	0.344
	50.4	0.336	50.4	0.421	42.5	0.321	34.0	0.32
	44.0	0.376	43.9	0.46	47.1	0.339	38.3	0.339
	46.6	0.432	46.7	0.535	34.6	0.229	27.8	0.229
					35.5	0.284	26.6	0.284

Effect of Switching Between Load and Strain Control Two short term tests of about 1200s duration were conducted to illustrate the effect of repeated switching between load control (creep) and strain control (relaxation) at the testing machine control console. On one of these we started with creep and on the other started with relaxation. Individual results of strain and secant modulus are shown in Figures 7 and 8 plotted against a linear time scale, and again in Figure 9 against a log time scale. Note that at all the switch points (circled in the figures) the relaxation modulus falls more rapidly than the creep modulus.

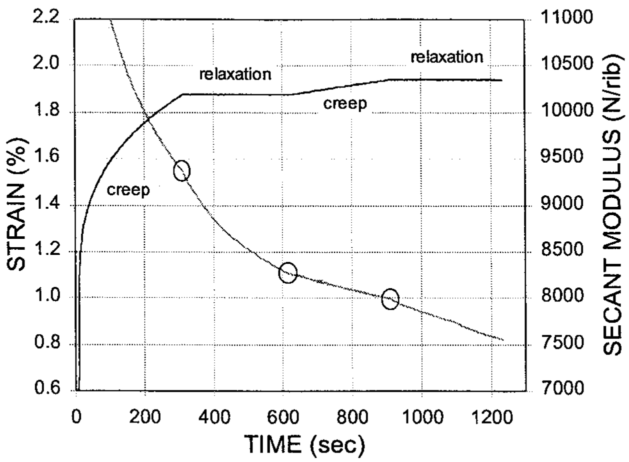

Figure 7. Strain and secant modulus plots vs. time for alternating creep and relaxation responses beginning with creep

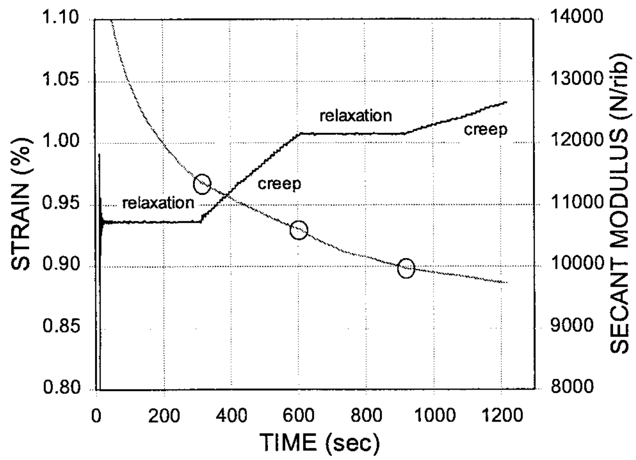

Figure 8. Same as Figure 7 except beginning with relaxation

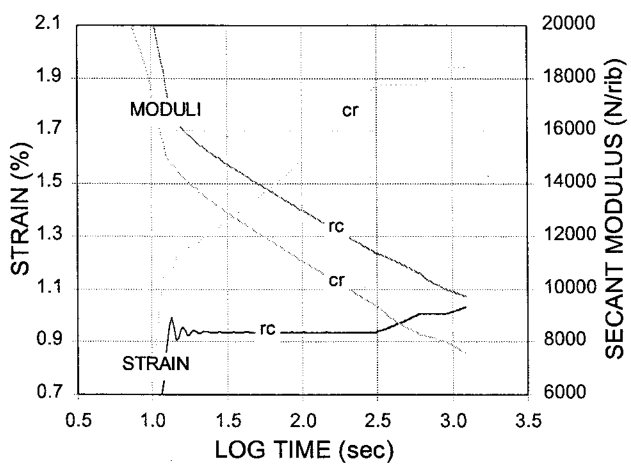

Figure 9. The data of Figures 7 and 8 plotted vs. log time. The CR curves begin with creep and the RC curves begin with relaxation response

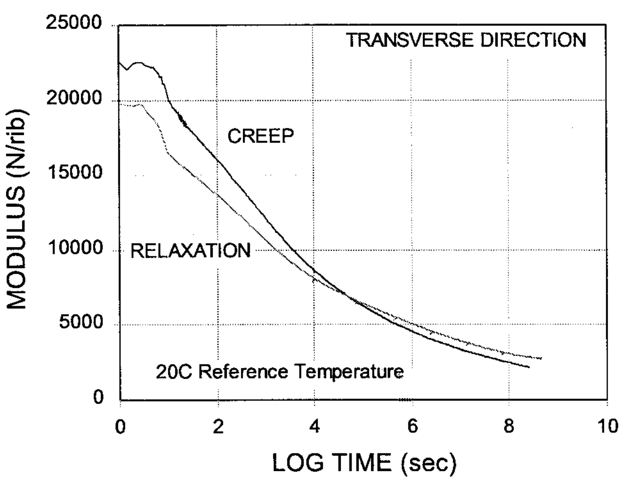

Figure 10. Long term creep and relaxation moduli vs. log time at % UTS for transverse direction PP geogrid specimens

Long Term Tests Long term creep and relaxation results were obtained for both machine and transverse direction specimens using the stepped isothermal method (SIM) of time-temperature superposition (TTS). The experimental setup for SIM has been described previously [Thornton et al, (1998)]. The creep stresses and relaxation strains for the transverse direction SIM tests were 21% UTS and 1% respectively and those for the machine direction SIM tests were 26% UTS and 1.4% respectively. Thus, the tests were begun in the nonlinear viscoelastic regime, but not beyond the range investigated in the short term tests (recall that 120s and 600s machine direction SIM data were used in earlier figures). Figures 10 and 11 present the SIM test results for the machine and cross machine directions. The creep and relaxation modulus curves do not start from a common point because of "specimen-to-specimen variation" also known as variations in test technique. Further illustration of the initialization difficulty is shown in Figure 12 which is a re-plot of fourteen machine direction R+H tests on the same scale as Figures 10 and 11. Figures 13 and 14 display the same information as Figures 10 and 11 except the relaxation curves have been "initialized " to the creep curves, and the data are presented on a log-log scale. The log-log presentation also suggests that the relaxation curves are seeking equilibrium, while the creep curves continue to decrease with time with a linear (power law) trajectory. These curves show the effect of initializing the creep and relaxation moduli at log time = 2 (100s) by implementing a vertical shift of the relaxation data. It is felt that the distortion of the relaxation data by this shift is not as problematic as a shift in the creep data because the relaxation path does not result in increasing viscoelastic non-linearity, while the creep path does. With the log-log format we can clearly see a divergence of the creep and relaxation curves at longer times.

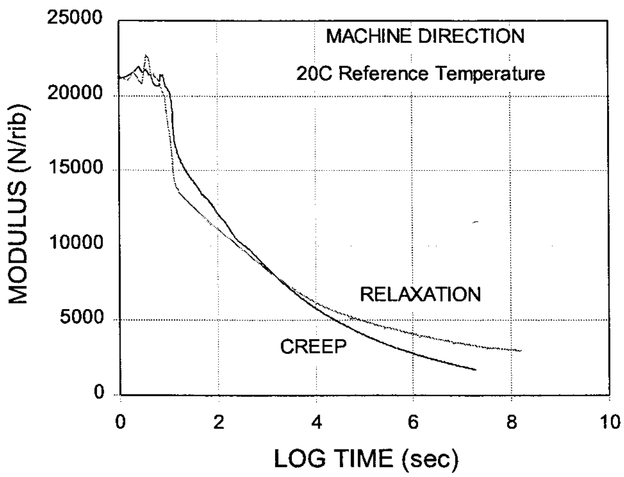

Figure 11. Long term creep and relaxation moduli vs. log time at % UTS for machine direction PP geogrid specimens

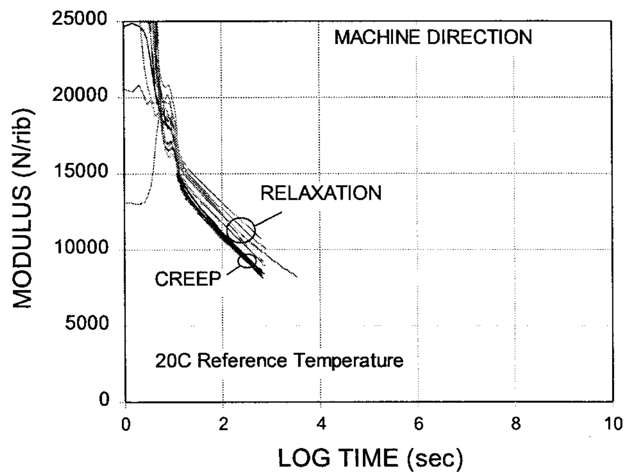

Figure 12. Short term creep and relaxation moduli vs. log time for machine direction PP geogrid specimens

INTERPRETATION OF RESULTS

Linear viscoelasticity theory teaches that for an ideal material the relaxation modulus lies below the creep modulus in the transition region. The results of the present experimental work on PP, which nominally took place in the upper transition region or lower rubbery region, show that the relaxation modulus can be less than, nearly the same as or greater than the creep modulus depending on the test time. At very short times the creep and relaxation moduli are nearly indistinguishable, but there is a tendency for the relaxation modulus to be slightly less than the creep modulus. This tendency is illustrated in Figures 7 and 8, which show that the relaxation modulus falls more rapidly than the creep modulus at the points in time where control is switched from constant load to constant strain or visa versa at least for sample loading histories up to 1000s. For times of 120s and 600s, the isochronous plots of Figures 5 and 6 show that the stress vs. strain plots using creep data or relaxation data are nearly the same demonstrating that the two moduli are nearly the same for this intermediate range of test times. For long times it has already been noted that the creep modulus becomes substantially less than the relaxation modulus over long periods of time. Figures 13 and 14 depict the relaxation modulus curves above the creep modulus curves for times from 1000 seconds (log time = 3) to beyond five years (log time = 8.2). For the machine direction results of Figure 14, the creep modulus is less than half the relaxation modulus at log time = 7.26. Were these trends to continue the creep modulus would fall to less than one quarter of the relaxation modulus, at 100 years (log time = 9.5).

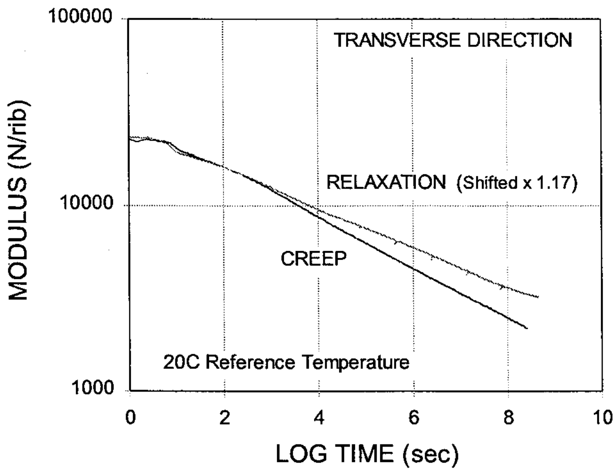

Figure 13. Long term creep and relaxation moduli data from Figure 10, "initialized" at log time 2 (1000 s) and presented as a log-log plot

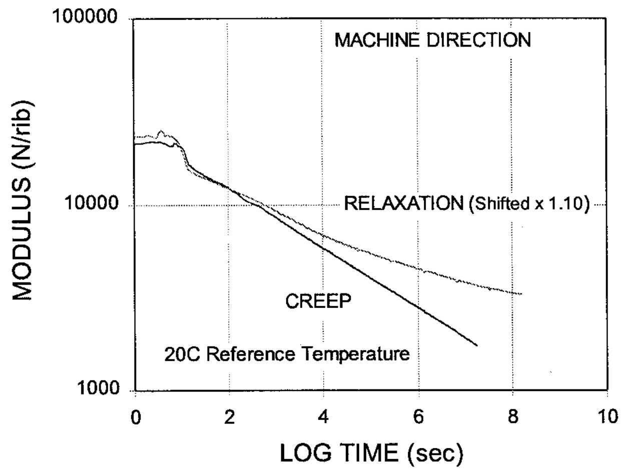

Figure 14. Long term creep and relaxation moduli data from Figure 11, "initialized" at log time 2 (1000 s) and presented as a log-log plot

It seems that at short times the material tested behaves as if it were a linear viscoelastic solid in the transition region. Referring to Figure 1, the short time just referred to would be equivalent to reducing the temperature to one from the upper transition region or lower rubbery region to well within the transition region. Thus, in the brief times following a switch of control mode the creep modulus is larger than the relaxation modulus. At the intermediate times between 120s and 600s the material behaves as a rubbery solid, linear at low strains but while non-linear at high strains, the creep and relaxation moduli are nearly the same as if linear out to nearly 2% strain. Beyond 1000s the non-linear behavior of the PP becomes more pronounced. Apparently, the creep path AD of Figure 2 takes the material further into non-linear territory while relaxation path AB does not. The linear theory is helpful in interpreting the results obtained even though due to non-linearity of the PP studied, the results are exactly the opposite of a casual prediction using the linear theory.

Using the creep modulus to predict the stress using strain data from MSE walls may lead to underestimates of stress, while using relaxation modulus may lead to overestimates. Intermediate paths of time-dependent load decay and strain along the approach illustrated by Figure 9 should be investigated.

IMPLICATIONS FOR DESIGN

The line AC in Figure 2 is illustrative of one of an infinite number of possible time dependent combined stress relaxation and creep paths which are governed by the constraints of the complete system being observed. If the system is a testing machine, then the negative of the ratio of the testing machine elastic stiffness to the specimen elastic stiffness governs the slope of AC. If the machine is very stiff compared to the specimen, then the slope of AC approaches that of AB and relaxation dominates the response of the specimen to the ramp-up. If the machine is very compliant compared to the specimen, then the response will be dominated by creep along a path closer to AD. In MSE wall applications the ratio of the elastic stiffness of the soil to that of the reinforcement governs the slope of AC. Returning to Figures 13 and 14, the relaxation and creep modulus curves represent the upper and lower limits of the possible modulus/time dimension trajectories of the path AC. In principle, intermediate trajectories, based on soil properties, reinforcement properties and reinforcement spacing are predictable. While a conservative approach would be to simply use the creep modulus of the reinforcement to estimate the useful lifetime of MSE walls, it is likely to be overly conservative to do so. Additional work is needed to identify the most probable time-dependent modulus trajectories to use in realistic MSE wall designs.

REFERENCES

Bathurst, R.J., Walters, D., Vlachopoulos, N., Burgess, P., and Allen, T.M., 2000, "Full Scale Testing of Geosynthetic Reinforced Walls", *Proceedings of Geo-Denver 2000*, Special Publications 103, ASCE, Reston, VA, pp 201-217

Boyle, S.R., 1995, *Deformation Prediction of Geosynthetic Reinforced Soil Retaining Walls*, Ph.D. Dissertation, University of Washington

Smith, T.L., 1963, "Ultimate Tensile Properties of Elastomers. I. Characterization by a Time and Temperature Independent Failure Envelope," *J. Polymer Science: Part A*, Vol. 1, Wiley & Sons, New York, NY, pp. 3597-3615.

Thornton, J.S., Allen, S.R., Thomas, R.W., and Sandri, D., 1998, "The Stepped Isothermal Method for Time-Temperature Superposition and Its Application to Creep data on Polyester Yarn," *Sixth International Conference on Geosynthetics*, Vol. 2, Atlanta, IFAI, Roseville, MN, pp. 699-706

Thornton, J.S., Sprague, C.J., Klompmaker, J., and Wedding, D., 1999, "The Relationship of Creep Curves to Rapid Loading Stress-Strain Curves for Polyester Geogrids," *Geosynthetics '99*, Vol. 2, Boston, Industrial Fabrics Association International, Roseville, MN, pp 735-744

TEXTURED HDPE GEOMEMBRANE VARIABILITY EFFECTS ON CONSTANT LOAD STRESS CRACK TESTING

MARK W. CADWALLADER
CADWALLADER TECHNICAL SERVICES (CTS), USA,

ABSTRACT

This paper examines the variability of stress crack resistance in commercially common types of textured HDPE geomembranes. It reports the conclusions reached in correlating stress crack test results with resin quality, asperity height and variability, thickness variation, and break elongation for three different sources of textured HDPE (Samples A, B, and C). To focus on the "effective notching" which may be present for texture type, degree, and variation within the type of texturing, stress crack tests are run as single point un-notched constant tensile load (SP-UCTL) stress crack tests. The current focus on base resin qualification "only" for stress crack resistance via single point notched constant tensile load (SP-NCTL) testing is questioned. The paper attempts to isolate resin effects in the data reported here, and it reviews other published data regarding surface blemishing effects on stress crack resistance. Suggestions for better specification of long term durability of textured HDPE geomembranes are made following the results and discussion.

INTRODUCTION

Plastics may be notch-sensitive. Deep-set asperities and surface blemishes in textured HDPE may act effectively as "notch" locations to initiate and accelerate stress cracking. The deeper the notch, the more accelerated the crack development. Long term durability of HDPE geomembranes is largely a function of stress crack resistance, and whether stress crack resistance is compromised by the degree, type, and variability of texturing is important for the industry to assess.

Since their development ten to fifteen years ago, rough textured geomembranes have grown to account for nearly half of the HDPE geomembrane deployed in North America. The asperities of texture grip interfacial materials and improve slope safety and stability as measured routinely by interface friction. Considering the importance of providing these functions in geomembrane design and construction, and the wide acceptance they have enjoyed from owners and engineers, textured geomembranes have been arguably the most important innovation to lining with geomembranes.

But the variability of textured surfaces is known to be high. Wide ranges of measurement of interface friction, texture asperity heights, tensile break properties, and destructive weld tests are routinely expected in conformance and field testing. The different ways in which the asperities of different types of texture join to the geomembrane, their size, shape, and uniformity, affect not only interface friction, but provide lingering questions of long term durability due to reductions in stress crack resistance. The different textured materials in many cases also experience highly reduced tensile break properties, erratic peaks and valleys in the texture, and variable and compromised thickness.

Is there a correlation of un-notched constant tensile load (UCTL) stress crack test results to the more easily measured and observed texture physical properties which may indicate the "effective notching" of textured surfaces? Can we specify these easily tested items as indirect QC tests for good long term durability against stress cracking? Reduction in stress crack performance would seem to relate to reduction in break elongation since rougher (more indented/notched) samples tend also to elongate less than smoother samples of the same textured sheet. Have resin improvements driven by NCTL testing made up for the potential crack initiation effect or "effective notching" potentially inherent in many textured geomembrane surfaces?

The UCTL testing reviewed and performed for this paper utilizes a procedure developed by the German Federal Institute called the Bundesanstalt für Materialforschung und-prüfung (BAM), the BAM procedure. It is contrasted with the ASTM D5397 NCTL test in Table 1.

Table 1. Comparison of BAM UCTL test with ASTM NCTL test
(after Thomas and Woods-DeSchepper, 1993)

Parameter	ASTM D5397 SP-NCTL	BAM ESCR SP-UCTL
Temperature	50°C	80°C
Load	30% of Yield	4 N/mm^2
Solution	10% Igepal CO 630	5% Igepal CA 720
Notch	Yes	No
Specimen Dimensions:		
Overall Length	60 mm	165 mm
Central Region Length	15 mm	80 mm
Central Region Width	3 mm	12.5 mm

BACKGROUND

Modern fracture mechanics technology in polyethylene gas transmission pipe has produced an empirical method for estimating lifetimes in polyethylene for tension stresses sustained across a notch defect at various temperatures. The method has also been extended to HDPE geomembranes.

According to the empirical model presented for HDPE geomembranes by Kanninen et al (1993), the difference between a 0.08 mm (3 mil) notch depth and a 0.3 mm (12 mil) notch depth is 20% in lifetime for a "no slack" initial condition and a temperature drop of 2 °C. The difference in lifetime between the same two notch depths becomes 50% for a "no slack" initial condition and a temperature drop of 15 °C. A difference in surface blemishing, notching, can yield a very large difference in geomembrane lifetime. Given the facts of liner tension, buried wrinkle stresses, and temperature contraction stresses, "effective notching" from textured sheet surface blemishes and discontinuities could well be a significant factor in long term durability.

Hsuan (1999) points out that the stress crack failures from 16 project sites evaluated in a 1990 EPA funded study occurred mostly at the "discontinuity" formed by overlapping seams. The study's findings led to the replacement of bent strip (constant strain) stress crack testing with the current constant tensile load (CTL) stress crack testing in most North American specifications. In these and other field problems evaluated, stress cracking has occurred at abrupt discontinuities such as seams functioning as "effective notching" much the way that laboratory notching in NCTL testing initiates stress cracking in lab tests such as ASTM D5397.

Thomas and Woods-DeSchepper (1993) have reported results of textured HDPE in UCTL tests done according to the BAM procedure and have found dramatic differences due to type of texture and degree of surface roughening. Large embossed cones reduced failure times. Applying a "thick" versus "thin" texturing in a secondary coating process for making textured HDPE geomembrane increased failure times by an order of magnitude. They concluded that the textured sheet they considered in their study provided high stress locations in the sheet, and that dramatic improvements could be made by modifying the manufacturing process to reduce residual stress and stress risers.

Thomas et al (1995) studied the effects of different degrees of blemish inducing wedge and wheel combinations in hot wedge welding. Though high quality resins as measured by NCTL tests using ASTM D5397 dramatically increased stress crack failure times for both a high and low surface-blemishing wedge/wheel combination, very dramatic effects were seen simply by changing the degree of blemishing. Reducing the "effective notching" of the surface significantly increased stress crack failure times. It is instructive to consolidate the Thomas et al (1995) data (see Table 2) and to explore some of their findings more closely since much of the significance of the information has been dropped with the idea that resin quality is a stress crack cure-all.

Note from their data, that in the case of resin D, a >5,000 hr resin, the high blemish inducing wedge/wheel #1 combination failed in 159 hours in the un-notched test while resin C, a mere 300 hr resin, failed in 206 hours in the low effective notching configuration, wedge/wheel #2. The high effective notching arguably ruined the contribution to long term durability of a high stress crack resistant resin. For resin B, a 500 hr resin, the high effective notching geometry (wedge/wheel #1) yielded a faster stress crack failure time by a whole order of magnitude (28 hours vs 206 hours) than did resin C, the 300 hr resin, in the low effective notching geometry (wedge/wheel #2).

Table 2. Times to Failure for NCTL and UCTL Stress Crack Testing after Two Degrees of Blemishing by Seaming with Different Hot Wedge/Wheel Combinations – consolidated from Thomas et al (1995)

Resin Type	SP-NCTL ASTM D5397 (hr)	Wedge/Wheel #1 (High Effective Notching) SP-UCTL (hr)	Wedge/Wheel #2 (Low Effective Notching) SP-UCTL (hr)	% Improvement
A	25	3 ± 1	11 ± 2	267
B	500	28 ± 3	139 ± 59	396
C	300	28 ± 1	206 ± 148	636
D	>5000	159 ± 27	>2400	>1409
E	>5000	283 ± 133	>3300	>1066

Improving the resin from a 300 hr resin to a >5000 hr resin increased the wedge/wheel #1 failure times from 28 hours to 283 hours, a 911% improvement. Yet changing the surface blemishing of the geomembrane of those resins from wedge/wheel #1 to wedge/wheel #2 (from high to low effective notching) increased failure times >1400% for the same resin.

Such data suggests that the effects of surface blemishing can supercede the contribution to durability in stress crack tests which resin selection can provide. The German BAM criterion for its UCTL test is >700 hr. By that criterion the high quality resins D and E would not have been enough to overcome the blemishing imposed upon the sheet in the first blemishing instance, wedge/wheel #1.

If good resin selection can be negated through overly blemishing, roughening, and thus effectively notching HDPE geomembranes, shouldn't specifications include considerations for stress crack resistance, beyond base resin quality? This is particularly important for textured geomembrane, where surfaces are intentionally blemished in a wide variety of ways to a wide variability of "effective notching".

EXPERIMENTAL INVESTIGATION

Materials and Procedures

Textured HDPE geomembrane samples for this study were obtained from three different sources of common commercially available material. These styles of texture represent over 95% of the current North American market for textured geomembrane. Multiple samples from each manufacturer were tested with each style of texture given a letter designation A, B, and C. Samples A were embossed styles of texture, using calender rolls to allow extruded polyethylene sheet to fill patterns for texture asperities in the calendering rolls while in the molten phase. Samples B and C were samples from two different manufacturers of co-extruded texture, prepared by depositing separate foamed/turbulent-flow layers of polyethylene on a geomembrane through a three layer co-extrusion die.

Samples were tested in one or more of the following tests: SP-NCTL (ASTM D5397), SP-UCTL (BAM), asperity height and variability (GRI GM 12), tensile break elongation (ASTM D638), and core thickness and variability (ASTM D5994). Not all samples were tested in all tests due to lack of retained specimens and limited funds. Asperity heights were averaged from measurements on both sides of the textured sheet samples.

Where samples were tested in more than one test, the locations for individual specimens in that test were as close to being the same as was possible. For example, specimens cut for samples tested in both tensile break elongation and UCTL stress crack testing were cut closely adjacent to each other and alternating one with the other. Those samples tested in NCTL stress crack testing were melted and pressed out of their original textured samples into smooth plaques per ASTM D1928, which were then notched to focus the stress on the notch and test the resin as intended for NCTL testing.

Results

From the results of the tests conducted, presented in Table 3, we can note a number of interesting observations. First, low stress crack resistance times can occur in textured geomembrane sheet tested without an accelerating notch cut into the lab specimens. Sample C1 went only 21 hours in the UCTL test. This result began the entire inquiry and regretfully could not be compared to a corresponding NCTL test to evaluate the resin, or tested for other parameters for lack of retained sample. C1's base resin likely gave at least 100 hrs in NCTL testing, since it was a modern resin. Somehow the surface blemishing of this textured sample unexpectedly accelerated failure times to a very low value in the UCTL test.

Samples C2 and C3 clarify the emerging picture. C2 was made with a relatively lower quality 164 hr base resin per smooth plaques pressed from the textured sample for NCTL, yet went over 700 hours in the UCTL stress crack resistance test. From its asperity height measurements, thickness variation, and break elongation, C2 can be seen to be not as blemished, or not as "effectively notched", as C3, a >1000 hr base resin by NCTL stress crack testing of plaques pressed from the textured sample. C3 went only 324 hours in UCTL testing, failing the BAM criterion of >700 hours.

Complicating the emerging picture is that several of the co-extruded texture samples clearly contained different resin for their textured surfaces. As noted in Table 3 these were found to be samples C2, C3, and C4. Tan and white particles and agglomerations were observed in the textured surfaces (see Figures 1,2,and 3). Pressing the bad textured surface resin into a blend with the geomembrane core did not uncover the flaw of a stress crack initiating resin on the textured surface of C3. C2, though a relatively poor result for NCTL (one which would have failed the GRI GM 13 specification of 200 hr for HDPE) passed the BAM requirement for UCTL testing of 700 hr. As noted C2's surface was not as blemished as C3's. In the case of Sample C4, the effect of foreign resin in the textured surface was enough to fail the BAM criterion for UCTL testing.

Table 3. Compilation of Average Stress Crack Times, Asperity Heights, Break Elongations, and Core Thickness for Textured HDPE Geomembranes

Samples	SP-NCTL (hr)	BAM SP-UCTL (hr)	Asperity Ht. (mm) ± S.D.	Tensile Break Elong (%) ± S.D.	Core Thickness (mm) ± S.D.
A1		>2000	0.46 ± .07		
A2	>1000		0.48 ± .09	417 ± 29	2.11± .08
A3	165	184	1.26 ± .04	31 ± 3	1.50 ± .03
B1	799	>700	0.58 ± .12	293 ± 115	1.72 ± .08
B2		>700	0.48 ± .09	430 ± 53	1.57 ± .05
B3		1279	0.45 ± .09		
B4	901	>700	0.58 ± .11	76 ± 65	1.77 ± .10
C1		21			
C2*	164	>700	0.62 ± .06	231 ± 69	1.72 ± .08
C3*	>1000	324	0.90 ± .23	74 ± 48	1.86 ± .21
C4*		407	0.51 ± .09	296 ± 144	1.59 ±.08

* These samples of co-extruded texture were observed by microscope to have different material in textured layers, containing particles of uncompounded resin and foreign particulates.

Sample A3 displays a correlation with inordinately high roughness as measured by asperity height and poor tensile break elongation results with a low UCTL stress crack failure time. Under magnified view, an "effective notch" at the base of a large asperity in the sample to initiate stress crack failure is clearly visible (see Figure 4). Further detail for the effect of asperity structure on stress crack resistance would concern the angle at which the asperity contacts the geomembrane.

Sample B4 passed stress crack testing even though its tensile break elongation was quite poor. In this case the other factors of good resin in the textured surface and geomembrane core, and asperity structure were evidently enough to pass the UCTL.

The results here show correlation between UCTL stress crack failure times and the following physical measurements and tests: 1) poor resin in the textured layer, 2) low tensile break elongation results, and 3) inordinately high asperity height. These easily-measured and/or specified requirements taken together would act as a safe-guard against low results in UCTL tests.

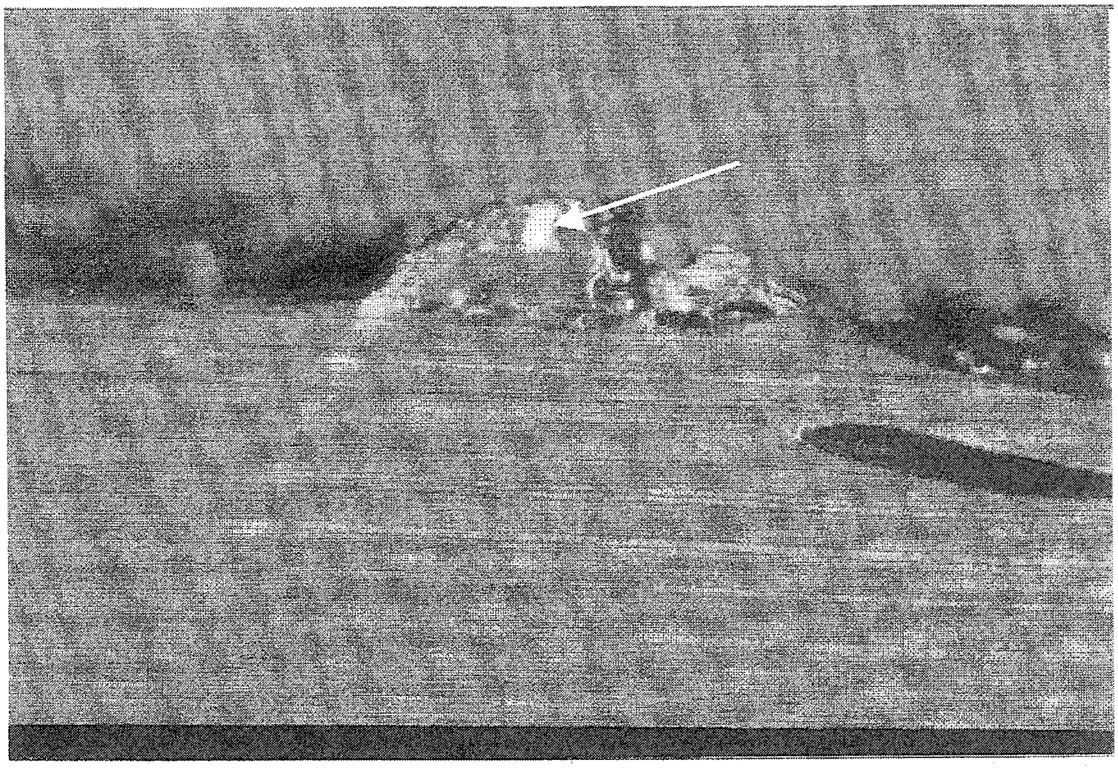

Figure 1. Although containing different resins for core and texture (note unblended resin in texture), relatively less blemished C2 (cross section 40X mag) did not stress crack in >700 hours of UCTL testing.

The results demonstrate that good base resin may be "ruined" by bad texturing. Furthermore they point to a correlation between easily measured and/or specified physical performance features, and times-to-failure in more difficult, time consuming, and costly UCTL stress crack testing.

IMPLICATIONS FOR SPECIFICATIONS

Good specification of textured geomembranes should address the potential for surface roughening to promote failure in UCTL stress crack testing, and thus to promote earlier failure

Figure 2. Numerous stress cracks initiating through surface resin containing particulates and unblended resin, in highly textured surface of sample C3 (cross section 25X mag). Stamped plaque gave NCTL result >1000 hours which by itself would have made this textured sheet acceptable while failing in UCTL.

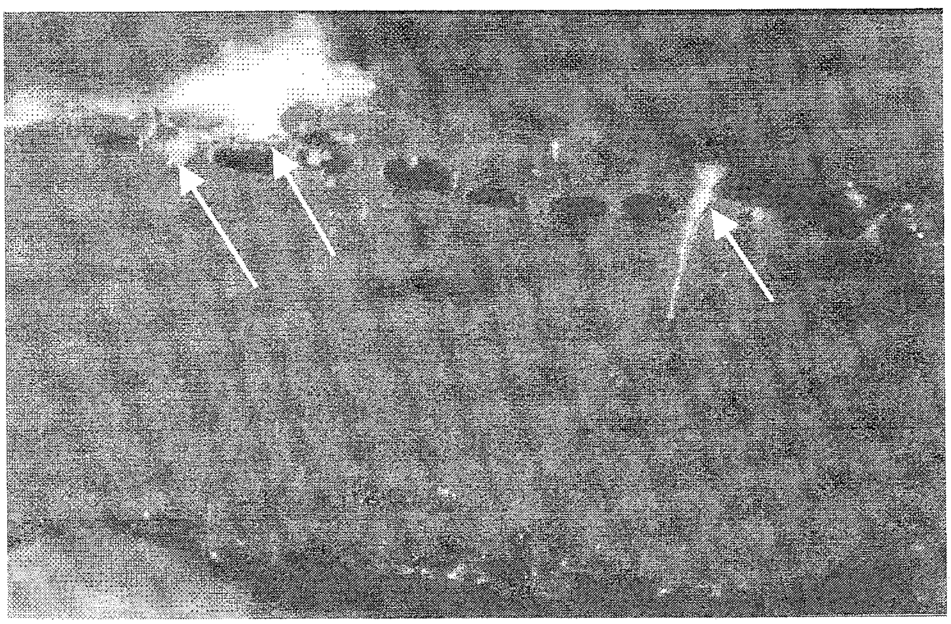

Figure 3. Stress crack failure in UCTL testing caused by different material in textured surface of sample C4 (cross section 40X mag).

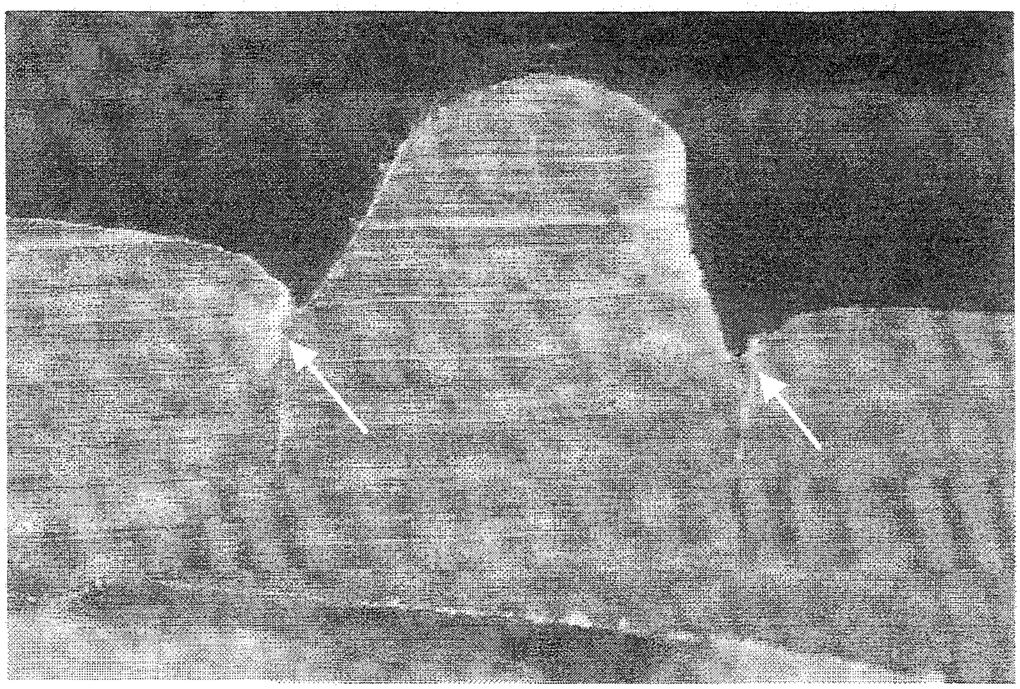

Figure 4. Sharp edge of a very large texture asperity is location of these stress cracks in Sample A3 (cross section 30X mag).

in application. The data presented here confirm earlier published work noting that good base resin selection can be thwarted by surface blemishing. Specifiers should address this concern when specifying textured sheet, not simply depend on NCTL testing for base resin quality.

The importance of these considerations for specifications is clarified by the recent demonstration that stresses are not entirely relieved in wrinkles trapped beneath landfills. Soong and Koerner (1998) studied the behavior of waves buried in landfills and report that wave distortion under loads produce stresses not entirely overcome by stress relaxation, with residual tensile stress varying from 1% to 22% of yield at 10,000 hours under load. Koerner et al (1998) exhumed HDPE geomembrane after eight years of landfill liner service and found waves remaining trapped in place with reduced stress crack resistance in the "waved" versus non-waved geomembrane samples. Stresses remain in buried geomembranes. Therefore it is important for those geomembranes to resist stress cracking to their achievable and best ability.

It would be burdensome to run UCTL tests for conformance quality testing. But measuring key physical properties, and specifying the quality and consistency of the textured blemishing should go a long way in avoiding the undesirable procurement of stress crack prone material.

Blemish reductions for tensile break elongation are arguably similar to blemish reductions for stress crack performance. Both performance properties are compromised by locations of "effective notching" in the material, for either premature tear (break) or possible stress crack initiation. Tensile break elongations for textured sheet have been allowed to drop way below break elongations allowed for smooth sheet. For example the GRI GM 13 specification calls for 700% break elongation for smooth while only 100% is necessary for textured sheet. This would seem to be too much of an allowance of reduced performance considering the implications of stress cracking. Certain specifying engineers have been concerned about allowing such reduced performance and have been requiring 200% and 400% break elongations.

Asperity heights of textured sheet are tested at great frequency and are direct measurements of surface blemish quality which arguably impact stress crack resistance. These properties can also be specified to higher levels of consistency in conformance testing in order to indirectly control quality for long term stress crack resistance.

For specifying engineers, field performance in stress cracking due to the effects of textured blemishing (i.e. UCTL testing) can be indirectly safe-guarded against by specifying the following recommended target conditions.

1) The textured surface must be made with similarly high quality resin as is in the base resin of the sheet itself.
2) Minimum tensile break elongations should be increased to 300% in order to prevent the roughening process from creating locations of premature tear (break) i.e., effective notch locations in the geomembrane surface.
3) Asperity height measurements should not only require minimum asperity height (eg 0.25 mm), but also a maximum asperity height of 0.8 mm.

In all likelihood the specification of asperity height really depends on the angle at which asperities contact the geomembrane sheet, but barring further test developments and measurement techniques the generalized correlation is that taller asperities mean more opportunity for "effective notching".

SUMMARY AND CONCLUSION

Base resin stress crack tests do not tell us enough about the potentially harmful effects that surface blemishing via rough texturing may provide. An un-notched constant tensile load (UCTL) stress crack test such as the BAM procedure has been able to uncover reduced stress crack resistance performance from the textured blemishing undetected by the notched constant tensile load (NCTL) test designed for resin quality control.

Melting textured sheet to stamp plaques for NCTL tests, cutting notches below textured surfaces, or cutting notches in smooth edges of textured sheet does not tell us about the damaging effects of the textured surface itself. The textured surface may damage stress crack performance due to asperity structure, the creation of geomembrane locations for premature tear (low break elongation), or due to lower quality resin deposited as texture to initiate stress cracking.

It is interesting to note that the German testing authority (BAM) sets its requirement for a UCTL stress crack test at >700 hr. Their philosophy seems to imply that sheet blemishing is at least as important if not more important than resin quality. Yet our approach in North America is at present entirely base resin focused.

Due to textured sheet variability, and in the interest of not having to run such long duration tests as UCTL stress crack on textured sheet, we could adopt a short suite of physical tests and requirements beyond NCTL. For example, engineers could easily specify a maximum asperity height (in addition to the currently specified minimum per GRI GM 13). Engineers could easily specify a higher tensile break elongation to take advantage of the well known phenomenon of effective notching from textured blemishing reducing break elongation (a quick test) as well as initiating stress crack failure (a long test). Engineers could specify that similarly high quality resin as the sheet itself be used to manufacture the textured surface for those textured geomembranes which apply a separate resin flow to the textured surface.

The data here presented, in addition to a review of previously published findings, as well as stress crack failure theory itself, demonstrate a correlation between time in an un-notched stress crack test and the degree and quality of surface blemishing. Such blemishing in textured sheet can be controlled through the specification of currently standardized physical property measurements. The specification of expensive and time consuming UCTL stress crack tests may arguably be replaced by modifying current specifications as noted above. This approach to specifying conformance testing of textured sheet is here advanced for better long term durability in geomembrane applications.

REFERENCES

Hsuan, Y. G., 1999, "Data Base of Field Incidents Used to Establish HDPE Geomembrane Stress Crack Resistance Specification", *Proceedings of the 12th GRI Conference on Lessons Learned from Geosynthetic Case Histories*, GII Publications, Philadelphia, PA, USA, pp 153-176.

Kanninen, M.F., Peggs, I.D., and Popelar, C.H., 1993, "A Methodology for Forecasting the Lifetimes of Geomembranes that Fail by Slow Crack Growth", *Proceedings of Geosynthetics '93*, Vol 2, Industrial Fabrics Association International, Vancouver, BC, Canada, March/April, pp 831-844.

Koerner, G.R., Eith, A.W., and Tenese, M., 1998, "Properties of Exhumed HDPE Field Waves and Selected Aspects of wave Management", *Proceedings of the GRI-11 Conference on Field Installation of Geosynthetics*, GII Publications, Philadelphia, PA, USA, pp 155-169.

Soong, T. and Koerner, R. M, 1998, "Behavior of Waves in High Density Polyethlene Geomembranes: A Laboratory Study", *Proceedings of the GRI-11 Conference on Field Installation of Geosynthetics*, GII Publications, Philadelphia, PA, USA, pp 131-154.

Thomas, R.W. and Woods-DeSchepper, B., 1993, "Stress Crack Testing of Unnotched HDPE Geomembranes and Seams", *Proceedings of the 7th GRI Seminar*, Philadelphia, PA, USA pp116-125.

Thomas, R.W., Kolbasuk, G.M., and Mlynarek, J., 1995, "Assessing the Quality of HDPE Double Track Fusion Seams", *Sardinia '95 Landfill Conference*, Sardinia, Italy, pp 415-428.

Thomas, R.W., 1998, "Evaluating the Stress Crack Resistance of HDPE Seams", *Proceedings of the 6th International Conference on Geosynthetics*, Industrial Fabrics Association International, Atlanta, GA, USA pp 349-352.

ACKNOWLEDGEMENTS

The author wishes to thank TRI/Environmental, Austin, TX and Chevron Chemical, Orange, TX for the testing conducted in this paper. The author also thanks Rick Thomas of TRI/Environmental and Ian Peggs of I-Corp International for helpful suggestions and comments.

WASTE & LIQUID CONTAINMENT II—FINAL COVER

GEOSYNTHETICS CONFERENCE 2001
Portland, Oregon USA
Economics, Performance & Constructibility • February 12-14, 2001

GEOMEMBRANE/GCL COMPOSITE FINAL COVER FOR A HAZARDOUS WASTE LANDFILL

MARK SWYKA, P.E., IT CORPORATION
UNITED STATES OF AMERICA
JIM OLSTA, CETCO
UNITED STATES OF AMERICA
RON COTTON, G.E. CORPORATION
UNITED STATES OF AMERICA

ABSTRACT

The incorporation of a geosynthetic clay liner (GCL) in the closure of a permitted hazardous waste landfill resulted in both an increase in waste disposal capacity and a reduction in final cover construction costs. The state regulatory authority required a composite final cover. The cross section originally designed for the site consisted of a 60 cm (24-inch) compacted clay layer overlain by a 40-mil textured geomembrane overlain by 1.1 m (42 inches) of protection soil, and 15 cm (6 inches) of topsoil.

The final cover cross-section was revised to a total of 0.8 m (30 inches) consisting of a needlepunched nonwoven GCL, overlain by a 40-mil textured geomembrane overlain by a 30 cm (12 inch) drainage layer, 30 cm (12 inches) of protection soil, and 15 cm (6 inches) of topsoil. The equivalency issues evaluated included hydraulic issues, physical/mechanical issues, construction issues, and economic issues. An evaluation determined the GCL provided superior performance to a compacted clay liner while accelerating construction and reducing overall costs.

INTRODUCTION

As a component of its materials management system, a major New York industrial manufacturer maintains an active Hazardous Waste Disposal Unit at its facility. This Disposal Unit is necessary to accept hazardous by-products of its manufacturing and on-site waste water treatment processes. As the permitted air-space of this facility was depleted, IT reviewed opportunities to modify the landfill design to extend site life and defer the expense associated with the construction of a new landfill facility.

- In 1995, a permit modification application was prepared for the vertical expansion of the facility. The permit modification application had three fundamental components and included the following changes to the permitted design: An increase in the facility sideslopes from the currently permitted slopes of 4H:1V and 5H:1V to 3H:1V (the maximum allowed by regulation) and a 3 meter (10-foot) increase in the top elevation of the landfill. These changes increased facility capacity by 30,000 m^3 (39,000 cubic yards).
- Replacement of the 60 cm (24-inch) low permeability soil layer with an equivalent geosynthetic clay liner (GCL). This change increased facility capacity by 14,000 m^3 (19,000 cubic yards).
- Reduction in the total thickness of cover soils above the liner from 1.2 m (4 feet) to 0.8 m (2.5 feet). This change increased facility capacity by 11,000 m^3 (14,000 cubic yards).

These modifications, shown in Figure 1, resulted in a total landfill capacity increase of 55,000 m^3 (72,000 cubic yards). While not a huge increase for typical landfills, the hazardous waste capacity is at a premium and the above modifications effectively extended hazardous waste disposal capacity within this landfill for an additional five years. The key to the modification was the use of a GCL in place of compacted clay in the cover design. This paper will focus on the considerations addressed in evaluating the use of a GCL in place of compacted clay.

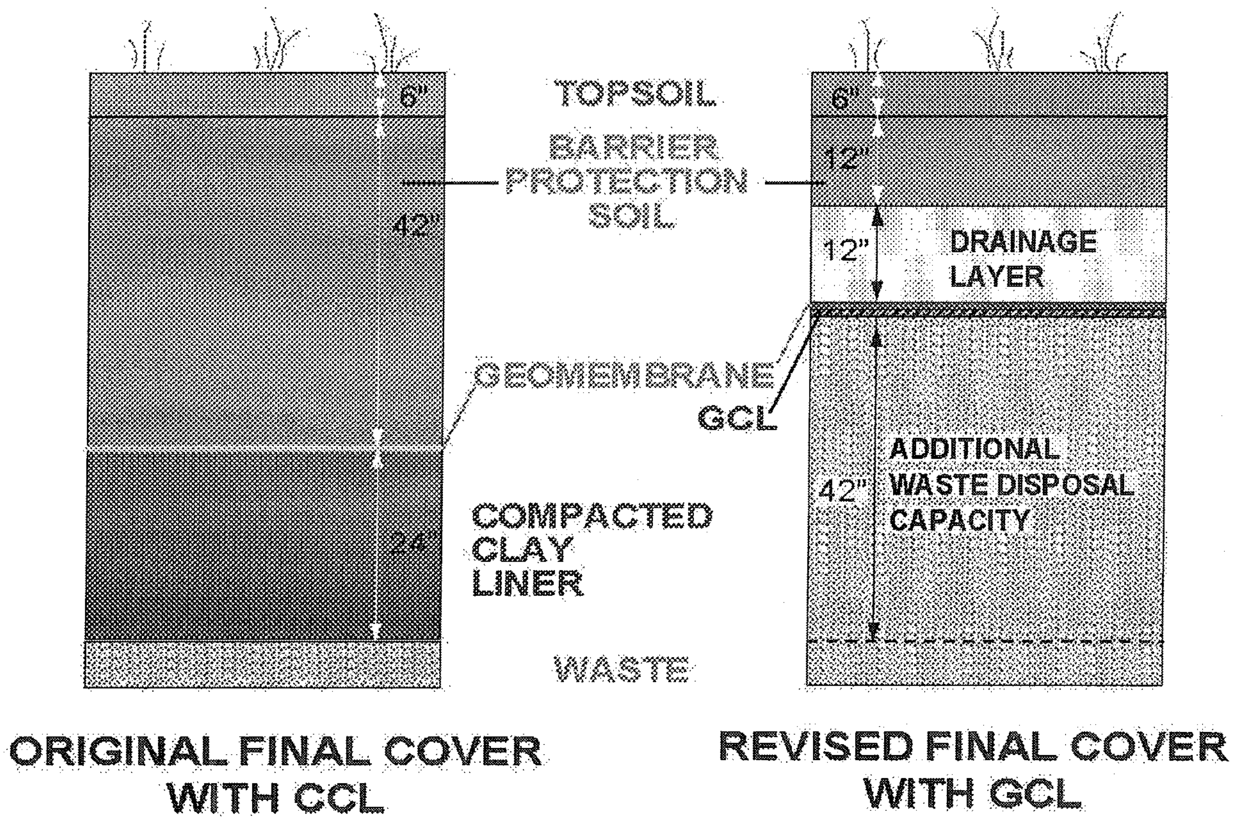

Figure 1. Original and Revised Final Cover Designs

GEOSYNTHETIC CLAY LINERS

A GCL is a factory manufactured hydraulic barrier that consists of a layer of sodium bentonite bonded to one or more geosynthetics. There are several different types of GCLs currently produced in the United States, 1) bentonite adhesive-bonded to two geotextiles, 2) bentonite needlepunch-bonded between two geotextiles, 3) a membrane laminated to one of the above, and 4) bentonite adhesive-bonded to a geomembrane.

Bentonite is primarily composed of montmorillonite, a high swelling clay. Under a confining pressure of 35 kPa (5 psi) GCLs have a hydraulic conductivity of $< 5 \times 10^{-9}$ cm/s. Since their introduction in the 1980s, GCLs have become a common material in the design of landfill liners as an alternative to compacted clay liners. Due to final cover stability concerns, a double-nonwoven needlepunched GCL was chosen for evaluation as the alternative in this project.

DESIGN CONSIDERATIONS

The design considerations for the modifications described above, included global landfill stability, final cover stability, protection of final cover barrier layers from freeze/thaw damage and equivalency of cover barriers.

A cross-section was developed using the information from the site topographic mapping, as-built baseline topography for the landfill, the hydrogeologic investigation, the existing grade of waste, and the proposed final grade of the landfill. The slope stability analyses were primarily based on this cross-section.

Because of the relatively low strength of the silty clay layer and the low interface strengths of the baseliner system, the global stability analysis focused on the following:

- The stability of the base soil underlying the baseliner of the landfill
- The stability of the side slopes
- The stability of the baseliner system

The global stability analyses of the landfill were performed using the computer program, PCSTABL5M, developed by Purdue University. This program is capable of conducting two-dimensional slope stability analysis under various circumstances. Seismic stability analyses were also conducted on the long-term global stability of the landfill.

The final cover stability calculations were performed using the infinite slope stability approach. Based upon the proposed final cover profile, stability of the proposed cap is controlled by three primary factors:

- The shear strength of the various interfaces and the internal shear strength of the GCL,
- The shear strength of the soils used above the geomembrane,
- The development of seepage forces or pore pressures above the geomembrane associated with infiltration from rainfall.

The behavior of the geomembrane soil interface is well understood and has been documented many times since the use of geomembrane caps first began. Of greater interest in the design was the interface between the GCL and the geomembrane and the shear forces that may pass directly through the GCL.

GCL DIRECT SHEAR TESTING

Based upon previous discussions and submissions to the NYDEC, the minimum factor of safety against sliding that would be acceptable was 1.25. This factor of safety was based upon the engineered nature of all the products used, the repairable nature of any damage that may occur in the cap and the limited consequences of any failure in the cap with respect to potential loss of life or irreversible damage to the environment.

The stability of the proposed composite cap containing the GCL was evaluated. Two interface direct shear tests were performed at normal loads of 7.5, 15 and 25 kPa (150, 300 and 500 psf) between the 40-mil textured geomembrane and a double-nonwoven needlepunched GCL with no fiber melting process. The design analyses incorporated data from recent laboratory test results of the materials proposed for construction. The results of these analyses supported factors of safety in excess of 1.25 based upon the residual interface shear strengths. Conformance testing of materials supplied for construction exceeded minimum strength requirements. Conformance testing yielded peak friction angles of 37.5 and 32 degrees with respective cohesion values of 118 psf and 111psf. Residual friction angles of 27.1 and 18.5 degrees were measured with cohesion intercepts of 51 psf and 80 psf, respectively.

Internal shear was not considered to be the critical factor for needlepunched GCLs placed against geomembranes at low normal stresses. An EPA sponsored large-scale field study that was in progress at the time of design did not show any internal shear failures for needlepunched GCLs on 2H:1V slopes (Koerner et al., 1996). When loaded in the shear testing apparatus, the GCL/other interface can be constructed to have a multi interface sandwich consisting of the two layers of geotextile, the bentonite, and the other material being tested. In all cases, the GCL/other interface failed before failing the GCL internally. As a result, the internal strength of the GCL is considered greater than the interface strength at relatively low (15 kPa) loads. Also, historical internal direct shear data from an independent laboratory for the double-nonwoven needlepunched GCL under low normal loads had yielded a 44 degree friction angle.

FREEZE/THAW

Based upon the molecular composition of bentonite as well as the results of laboratory and field testing, no impact to the GCL's hydraulic properties due to freeze/thaw is expected. This is due to the weak interbonding in montmorillonite clays that results in interlayer expansion whenever polar molecules, such as water, are available. This is quite in contrast to most naturally occurring clays in the Northeast U.S., which do not expand or swell in the presence of free water. This results in the development in compacted clay of increased permeability upon successive freeze/thaw cycles due to flow channels created by the formation of micro lenses during the freezing process. The moisture that forms the micro lens is drawn from the surrounding clay peds, desiccating the clay. For non-montmorillonite clays, these desiccated zones do not significantly swell upon release of the moisture during thawing. This results in an increase in permeability. Comparatively, bentonite, a montmorillonitic clay, does swell upon thawing and therefore would not be expected to exhibit an increase in permeability associated with freeze-thaw cycles.

Several laboratory and field tests have been performed on geosynthetic clay liners and compacted clay liners, to specifically analyze the affects of freeze/thaw cycles on them. Reports and papers have been written based upon these results. Specifically, Nelson (1993) demonstrated by laboratory testing that the permeability characteristics of a GCL product do not appear to be affected by exposure to multiple freeze/thaw cycles. Kraus et al. (1997) demonstrated by laboratory and field testing that the hydraulic conductivity of needlepunched GCLs did not change significantly after freezing and thawing through one winter. However, Benson et al. (1995) and Chamberlain et al. (1995) have shown through field and laboratory studies that compacted clay does form micro cracks that do not heal upon thawing resulting in increased permeability.

It is evident from this literature that GCLs outperform compacted clay liners with respect to freeze-thaw. Therefore, the thickness of the cover soil of the final cover could be reduced.

EQUIVALENCY

The NYDEC prescriptive cover is a composite cover consisting of 60 cm (24 inches) of compacted clay, with a permeability of no greater than 1×10^{-7} cm/s, overlain by a geomembrane. The idea of using a geomembrane over a clay liner to form a composite liner takes advantage of the beneficial properties of each of the materials in a synergistic manner. The geomembrane provides the primary impermeability of the lining system. Small defects in the geomembrane can be backed up and blinded off by the clay, greatly reducing the leakage potential. In effect, the geomembrane limits flow through the clay liner to relatively small areas.

The specific issues for a technical comparison of GCLs to compacted clay liners have been well documented and presented in literature by Koerner and Daniel (1993). The issues can be divided into two categories: hydraulic and physical/mechanical.

Empirical modeling and field monitoring (Giroud, et al., 1997) have demonstrated that leakage through a circular hole in a geomembrane is a function of the underlying clay permeability, liquid head above the hole, hole size, and degree of intimate contact between the geomembrane and the soil. Leakage rates can be theoretically predicted according to the following equation:

$$Q = C\,[1 + 0.1(h_w/t_s)^{0.95}]\; a^{0.1}\; h_w^{0.9}\; k_s^{0.74} \qquad (1)$$

Where Q = rate of leakage through a hole; C = a constant related to the quality of the intimate contact between the geomembrane and the underlying clay liner; a = area of hole in geomembrane; h_w = head of liquid on top of the geomembrane; t_s = clay liner thickness and k_s = permeability of the underlying clay liner.

By inspection of the parameters involved in equation (1), it can be deduced that the possibilities of reducing potential liner leakage in terms of the soil component of a composite liner are related to the quality of its surface for creating an intimate interface with the overlying geomembrane and its permeability.

A paper by Harpur, et al. (1993) describes experiments that were performed on five different GCLs to evaluate the quality of their intimate contact with geomembranes in terms of hydraulic transmissivity along the contact. They present a very revealing graph that demonstrates the effectiveness of a GCL in limiting the horizontal flow of liquid coming through a defect in a geomembrane. The graph indicates that GCLs would be 2 to 3 orders of magnitude more effective in reducing horizontal transmissivity than theoretically excellent field conditions with a compacted clay liner. This would have a direct impact on the amount of leakage that would occur through a geomembrane defect.

The permeability of needlepunched GCL, even at low normal loads, has been shown to be on the order of 5×10^{-9} cm/s (Estornell and Daniel, 1992). This compares favorably to the prescriptive compacted clay liner permeability of 1×10^{-7} cm/s.

Thus, regarding liner leakage through geomembrane defects, the above analysis indicates that GCLs are at least technically equivalent, and most likely superior, to compacted clay liners. This is supported by an EPA funded study of actual leakage through double-lined composite liner systems in municipal solid waste landfills. Data (Bonaparte et al., 1999) indicates that geomembrane/GCL composite liner systems yielded the lowest flow in leachate detection systems in both active and post-closure cells.

From a physical/mechanical perspective, the most important factor for the final cover is differential settlement. Differential settlement could result in separation, cracking or tearing of various elements of the final cover system. In a related sense, deformation from a seismic event, could cause defects or failures in liner elements in a similar manner to differential settlement.

Koerner and Daniel (1993) describe reports and tests that document needlepunched GCL's ability to withstand relatively high levels of tensile strain (on the order of 10 to 15 percent) without undergoing significant increases in permeability. Standard compacted clay liners, on the other hand, generally cannot tolerate strains approaching one percent without cracking. GCLs are generally considered superior to compacted clay liners in terms of their ability to resist damage from deformation. Slope stability and freeze/thaw behavior are other key elements in the equivalency demonstration. These elements, discussed previously, also indicated that the GCL is equivalent, or superior, to compacted clay.

CONSTRUCTION ISSUES

The final cover was constructed in several phases. Phase I was completed in July 1997, Phase II was constructed in July of 1998, and Phase III was constructed in May of 1999. Construction issues, when comparing GCLs to compacted clay liners, include subgrade preparation, material availability, speed and ease of installation, and construction quality assurance.

A GCL's relative thinness requires that more attention be given to subgrade preparation than for a compacted clay liner. The subgrade for the GCL was the in-place soil-like hazardous waste material. This material is a fine-grained soil-like material that when delivered for disposal contained no sharp stones or other objects that could damage the liner. This material was graded to a 3H:1V (33%) slope and covered with a temporary tarp to shed rainwater until the final cover construction was initiated. Prior to GCL placement, the deployment area was inspected and hand picked for large or sharp objects which may have been included with the waste during the process of landfilling and that might damage the liner. After grading and inspection of the subgrade, the GCL could be safely pulled over the waste surface without damage.

Although the additional attention to subgrade preparation may appear at first to be a disadvantage for a GCL compared to a compacted clay liner; it is actually an advantage. The reason for this is that the most critical subgrade preparation is for the geomembrane. In the case of a compacted clay liner, this means the top surface of the clay liner requires very careful finishing. This is often difficult, requires special equipment, and is often at odds with the aim of covering up the clay as soon as possible to reduce desiccation.

In the case of GCLs, the subgrade can be smoothed out to fit the convenience of the construction schedule without worrying about moisture loss. Even though the same subgrade preparation specifications would be used for the GCL as would be used for a geomembrane, it is actually slightly less critical because of the cushioning effect of the GCL. The surface of the GCL will be much more ideal for a composite liner than the finished compacted clay surface.

Regarding material availability, needlepunched GCLs are readily available from two suppliers.

A GCL can be installed much quicker and easier than a compacted clay liner. Once the GCL material is approved through manufacturers' certifications, conformance testing and on site inspection, its installation is very quick and straightforward. As shown in Figure 2, a backhoe with spreader bar attachment and a four-wheel all-terrain vehicle were used to initially deploy the GCL. A work crew then moved the GCL into final position and placed bentonite between the overlapping seams. In good weather, a crew can typically install one and one-half acres a day with production often limited by the geomembrane installation.

Figure 2. Geosynthetic Clay Liner Deployment

The most critical item during installation is to prevent excessive hydration of the GCL prior to loading. Hydration sources come from precipitation before the GCL is covered with the geomembrane and moisture absorbed from the subgrade waste. Hydration from precipitation was controlled by covering all in-place GCL with geomembrane on the same day that it was deployed (Figure 3).

Hydration from moisture in the subgrade materials is somewhat less defined. If the GCL hydrates before the soil cover is placed, adequate strength can not be guaranteed to support the soils and the placement equipment. Therefore it is necessary to place the soil cover in a timely fashion. In general, a window of 10 to 20 days is available between the time of GCL placement

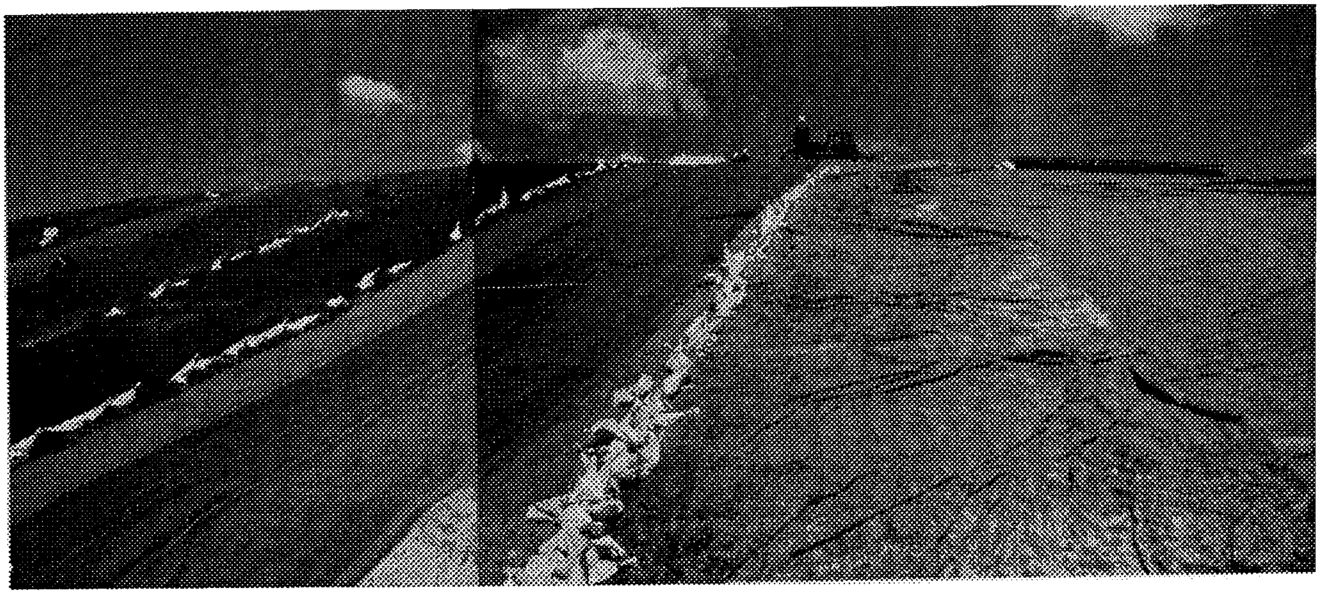

Figure 3. Layers of Geomembrane, Geosynthetic Clay Liner, Subgrade and Tarp

and the need to have cover soils in place. All placement of soils in the final cover was performed within this window with no stability issues.

Comparatively, a compacted clay liner must be moisture conditioned, compacted in lifts at controlled moistures and densities, inspected for good lift bonding and breakdown of clods, and finished smooth enough for overlaying of a geomembrane.

In general, both a GCL and compacted clay liner can be satisfactorily constructed during moderate weather. However, during wet, rainy weather neither a GCL nor a compacted clay liner can be installed. During hot, dry weather a GCL would be superior to a compacted clay liner. While this type of weather is actually advantageous to a GCL, it would tend to desiccate a compacted clay liner.

COST ANALYSIS

The GCL barrier layer was overall less costly to construct than the compacted clay barrier. The actual construction cost paid to the contractor to construct the GCL final cover was $112,000 per acre. This cost includes all of the soil and geosynthetic components of the final cover but is exclusive of other ancillary activities associated with the construction. By comparison, using the same unit rates, the cost to construct the final cover with the recompacted clay barrier would have been $154,000 per acre. The direct savings in construction cost were determined to be $42,000 per acre. This cost difference is specific to construction and does not include the value of the additional waste disposal capacity created through the implementation of this modification.

There are five aspects of cost to consider when comparing the overall costs of the original compacted clay liner/geomembrane composite final cover to the revised GCL/geomembrane composite final cover:

- Material Quantities
- Material Cost (Material, Transportation, Installation)
- Construction Time
- Construction Quality Control (CQC) and Construction Quality Assurance (CQA) Cost
- Airspace

The revised final cover design reduced the overall quantity of material that was incorporated into the closure. In total, the cover soil thickness was reduced from 1.2 m (48 inches) to 0.8 m (30 inches). Therefore a total of 1,850 cubic meters (2,420 cubic yards) of material per acre were saved.

The comparison of the cost of the materials suggests that due to the reasonable availability of naturally occurring clay in the area of the project site, the unit cost per square foot of barrier layer were essentially equivalent. If clay soils had to be purchased from off-site, the GCL would have been less expensive. All other material prices were equivalent between the two final cover cross-sections.

The time required to construct the GCL barrier layer is significantly less than the time required to construct a recompacted clay barrier layer. This reduction in contract time is reflected in the contractor's unit prices for various activities. Savings in "G&A", General and Administrative costs throughout the period of construction were not accounted for in this assessment.

The differential in construction quality control costs were minimal compared to the other parameters. However it is necessary to note that as a reduction in construction time, CQA costs would also be lower for the revised final cover cross-section.

The airspace savings were a key element. Air space for the disposal of Hazardous Waste is at a premium. At the time of this evaluation, the cost for trucking and off-site disposal at a commercial facility is on the order of $105 to $130 per cubic meter ($80 to $100 per cubic yard). Therefore the commercial value of the air space generated by this design change is in the range of $5.7 million to $7.2 million. Without the airspace savings, waste would need to be sent to an off-site disposal facility or another cell would have to be constructed. Both options represent a significant increase in cost over the option selected.

PERFORMANCE

Performance of the composite landfill final cover has been excellent. The measured quantities of leachate collected at the facility have decreased dramatically with the introduction of the final cover. Leachate generation is monitored very closely at this facility. Daily leachate generation data is monitored and reported to NYSDEC on a monthly basis. The first phase of construction was performed in the Spring of 1997. Prior to final cover construction, an average of 867,000 liters (229,000 gallons) of leachate were collected each month (approximately 13,000 lphd or 1,400 gpad). Upon the completion of the Phase I final cover construction, leachate generation dropped to an average of approximately 352,000 liters (93,000 gallons) per month (5,200 lphd or 560 gpad). With the completion of the Phase III final cover construction in May of 1999, leachate generation was reduced to approximately 250,000 liters (66,000 gallons) per month (3,700 lphd or 400 gpad).

It is interesting to note that the reduction in leachate generation observed with this waste material appeared to correspond directly with the placement of the final cover. At the point of completion of the Phase III final cover, approximately 78% of the landfill had received final cover and leachate generation had been reduced by approximately 71% indicating a very close correlation.

CONCLUSION

The use of a GCL in place of a compacted clay liner in a hazardous waste landfill cover design resulted in significant cost savings, accelerated construction time, and improved performance over compacted clay liners.

ACKNOWLEDGEMENTS

The authors would like to acknowledge the firms and individuals without whose efforts the project could have never been completed. Rasheed Ahmed of the EMCON/IT Geosynthetics Laboratory for his dogged persistence and excruciating detail with the interface strength testing; R.J. Kennedy & Sons, Inc.; William J. Keller & Sons Construction Corp.; GSE Lining Technology, Inc.; Solmax Geosynthetics; New England Liner Systems; geotechnical wizards Peter Carey and Nagesh Koragappa; Don Hullings for his critical review and being a buddy; and most of all Casey Cowan, Matt Hamilton, and Ken Kerr for their copious field notes and proactive approach to construction problem avoidance.

REFERENCES

Benson, C., Abichou, T., Olson, M., and Bosscher, P., 1995, "Hydraulic Conductivity of Compacted Clay Frozen and Thawed In-situ", *Journal of Geotechnical Engineering,* ASCE, Vol. 121, pp. 69-79.

Bonaparte, R., Daniel, D.E. and Koerner, R.M., 1999, Assessment and Recommendations for Optimal Performance of Waste Containment Systems, Grant No. CR-821448, Final Report to U.S. EPA Office of Research and Development, Cincinnati, OH.

Chamberlain, E., Erickson, A., and Benson, C., 1995, "Effects of Frost Action on Compacted Clay Barriers", *GeoEnvironment 2000,* ASCE, New York, NY, USA, pp. 702-717.

Estornell, P. and Daniel, D.E., 1992, "Hydraulic Conductivity of Three Geosynthetic Clay Liners", *Journal of Geotechnical Engineering,* ASCE, Vol. 118, pp. 1592-1606.

Giroud, J.P., 1997, "Equations for Calculating the Rate of Liquid Migration Through Composite Liners Due to Geomembrane Defects", *Geosynthetics International,* IFAI, Vol. 4, pp.335-348.

Harpur, W.A., Wilson-Fahmy, R.F. and Koerner, R.M., 1993, "Evaluation of the Contact Between Geosynthetic Clay Liners and Geomembranes in Terms of Transmissivity", *7th GRI Conference: Geosynthetic Liner Systems; Innovations, Concerns and Designs,* Geosynthetic Research Institute, Philadelphia, PA, USA, December 1993, pp. 138-149.

Koerner, R.M. and Daniel, D.E., 1993, "Evaluation of the Contact Between Geosynthetic Clay Liners and Geomembranes in Terms of Transmissivity", *7th GRI Conference: Geosynthetic Liner Systems; Innovations, Concerns and Designs,* Geosynthetic Research Institute, Philadelphia, PA, USA, December 1993, pp. 255-275.

Koerner, R.M., Carson, D.A., Daniel, D.E. and Bonaparte, R., 1996, "Current Status of the Cincinnati GCL Test Plots", *10th GRI Conference: Field Performance of Geosynthetics and Geosynthetic Related Systems,* Geosynthetic Research Institute, Philadelphia, PA, USA, December 1996, pp. 147-175.

Kraus, J.F., Benson, C.H., Erickson, A.E., and Chamberlain, E.J., 1997, "Freeze-Thaw Cycling and Hydraulic Conductivity of Bentonitic Barriers", *Journal of Geotechnical Engineering,* ASCE, Vol. 123, pp. 229-237.

Nelson, R.L. & Associates, 1994, "Report of Bentomat Freeze/Thaw Test Results", *Report to CETCO,* Schaumburg, IL.

AN ALTERNATIVE LINER DESIGN FOR A PIGGYBACK LANDFILL

ROBERT J. GRILLO, P.E., SR. ENGINEER
CMA ENGINEERS, INC., USA
JEFFERY S. MURRAY, P.E., PROJECT ENGINEER
CMA ENGINEERS, INC., USA
BEN LEBER
INTERNATIONAL PAPER COMPANY, USA

ABSTRACT

A Maine paper mill is applying for a permit to expand its residue landfill. Siting constraints require that the expansion overlap the existing landfill side slopes. Maine regulations require a clay/geomembrane primary liner and a single geomembrane secondary liner for this expansion. This paper presents a proposed alternative liner design that incorporates thinner geosynthetic barrier and drainage layers. Use of the alternative liner increases landfill capacity by about eight percent and adds more than one year to the expected life of the landfill expansion, with an associated small construction cost premium.

The paper includes an evaluation of the relative performance, costs, and constructability of the alternative liner design. The alternative design provides a superior barrier to leakage, more efficient leak detection, and increased tolerance of differential settlement. The alternative design is also easier to build, and is less sensitive to weather and less susceptible to erosion during construction.

INTRODUCTION

A Maine paper mill is applying for a permit to expand a 24-hectare landfill that is nearing its design capacity. This paper presents the design of an alternative liner for the overlap portion of a landfill expansion. The liner design incorporates geosynthetic barrier and drainage layers, in lieu of natural soils, to provide thinner and more effective lining and leachate collection systems. The landfill is used for disposal of sludge from a paper mill wastewater treatment plant, along with other mill wastes and residuals. The landfill design has been completed, and a permit application is pending with the Maine Department of Environmental Protection.

The overlap portion of the landfill expansion covers about 8.5 hectares. The existing landfill slopes in the expansion area range from about 3 horizontal to 1 vertical (3H:1V) to 4H:1V. An approximately 1 hectare area on the top portion of the overlap is sloped at a seven percent grade. The existing slope has a total height of about 55 meters. The proposed landfill expansion is divided into five phases. Figure 1 presents the existing and proposed limits of waste, and delineates the limits of the five phases.

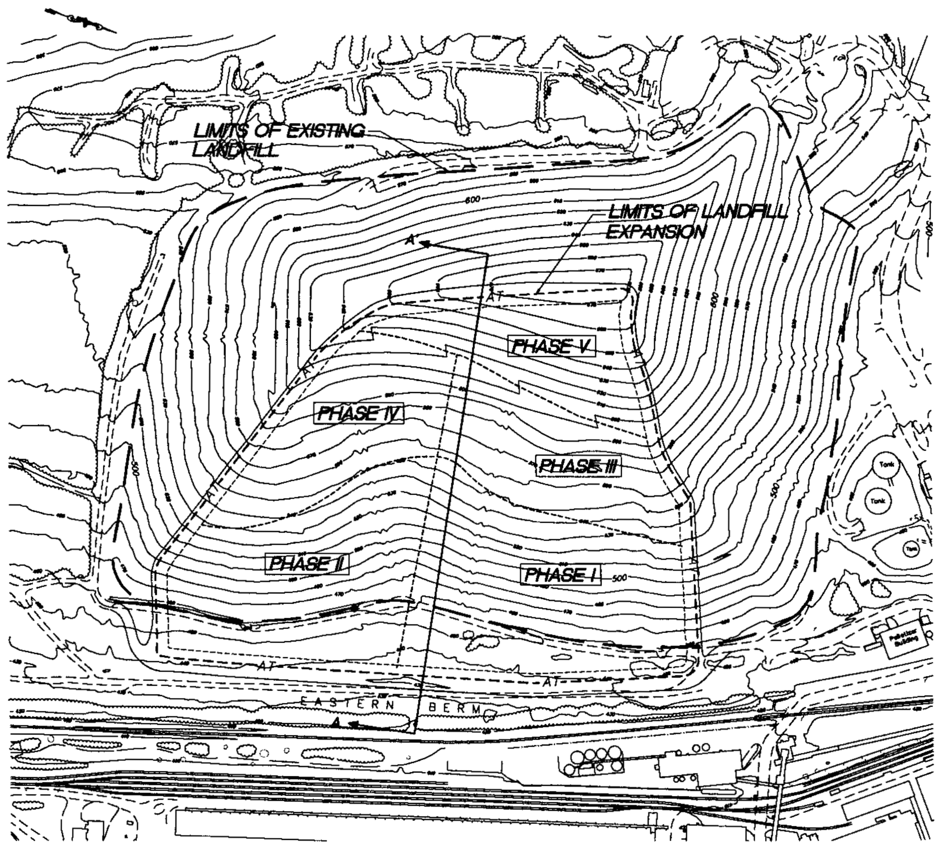

Figure 1. Site Plan

BACKGROUND

The paper mill site presently contains an active landfill located to the south of the main mill complex. The landfill has been operating since 1976. The proposed landfill expansion abuts and overlaps the eastern-facing portion of the existing landfill. Due to siting constraints, the only viable expansion area is limited to a narrow 1.6 hectare strip over virgin ground abutting the east side of the landfill. An additional 8.5 hectare overlap is required to gain the required disposal capacity. The thickness of waste in the proposed expansion is limited by geometric constraints to an average of less than 12 meters. These constraints include the narrow area of the expansion on virgin ground, regulatory and practical limitations on the steepness of the expansion final grades, and the relatively steep slopes of the existing landfill which form the expansion base grades. The thickness of existing waste beneath the overlap area ranges from zero at the toe of the slope to a maximum thickness in the range of 35 to 40 meters beneath Phase V of the proposed expansion. A typical cross-section through the proposed expansion area is presented on Figure 2.

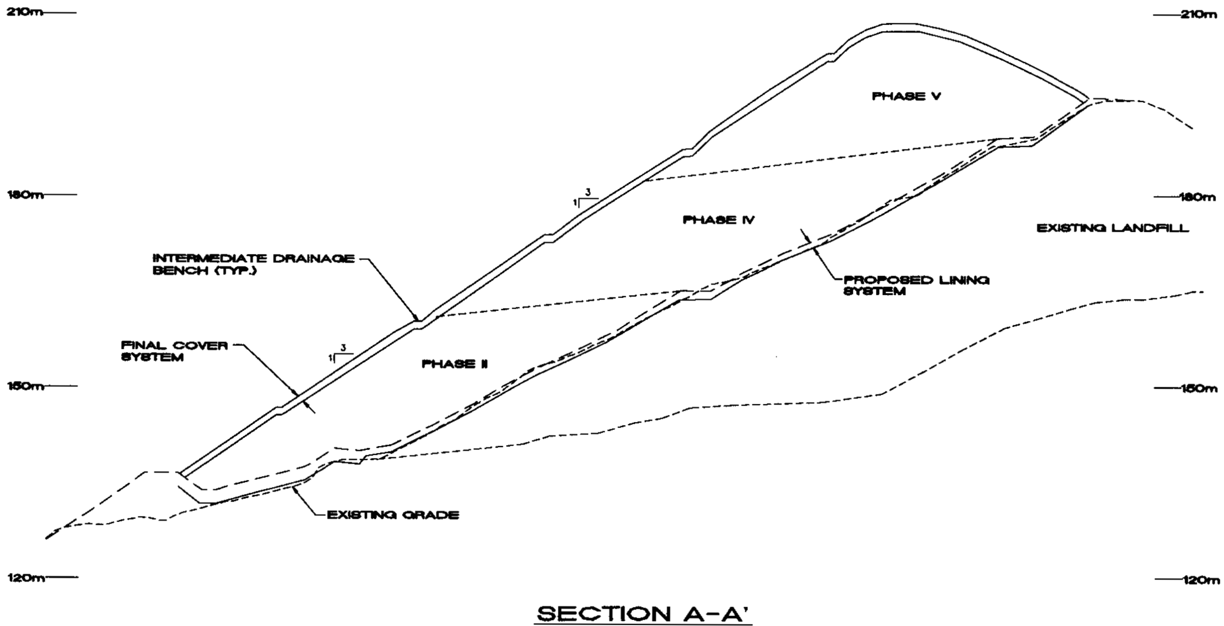

Figure 2. Landfill Cross-Section

The State of Maine through its Department of Environmental Protection (MEDEP) has established minimum design standards for landfill liners. Landfills are required to have a single composite liner, consisting of a 0.15 cm high density polyethylene (HDPE) membrane underlain by 0.6 meters of compacted clay exhibiting a maximum hydraulic conductivity of 1 X 10^{-7} centimeters per second (cm/sec). A 0.75-meter clay layer is typically required considering the difficulty of compacting the lowest 0.15 meters to hydraulic conductivity specifications without damaging underlying liner materials or mixing the clay with subgrade soils. Further, the regulations require more stringent design standards to account for certain site conditions. In this instance, travel times to sensitive receptors in the event of a leak were estimated to be as low as four years. The closest sensitive receptor at this site was deemed by the MEDEP to be fractured bedrock beneath the landfill. The regulations require a second liner consisting of 0.1 cm HDPE, and a leak detection system, if travel times to sensitive receptors are between four years and six years. The liner section required by the regulations for this project is hereinafter referred to as the "regulatory design."

The regulations allow permit applicants to propose alternatives to the minimum design standards, provided the applicant submits the following documentation to "clearly and convincingly" demonstrate technical equivalency of the proposed alternative:

- a discussion of the benefits of the proposed alternative technology;
- a discussion of the risks and drawbacks of the proposed alternative technology;
- an assessment of similar applications of the proposed alternative technology;
- a demonstration that the alternative technology will provide equal or superior performance to the component it is proposed to replace, or that its inclusion within a system will result in equal or superior performance of that system;
- an assessment of the feasibility of constructing the proposed alternative, including the ability to provide an adequate level of quality assurance and quality control (a demonstration of the feasibility of construction may be required), and;
- an assessment of the likelihood that the proposed alternative will perform as designed through landfill operations, closure, and post-closure periods.

An alternative liner system was proposed for the landfill expansion within the context of this regulatory provision. The liner system incorporates geosynthetic clay liners (GCLs), in lieu of compacted clay, to form composite primary and secondary liners, and a drainage geocomposite (HDPE drainage net bonded to non-woven geotextile fabric) for leak detection. Schematic details of the regulatory and alternative liners are provided on Figure 3.

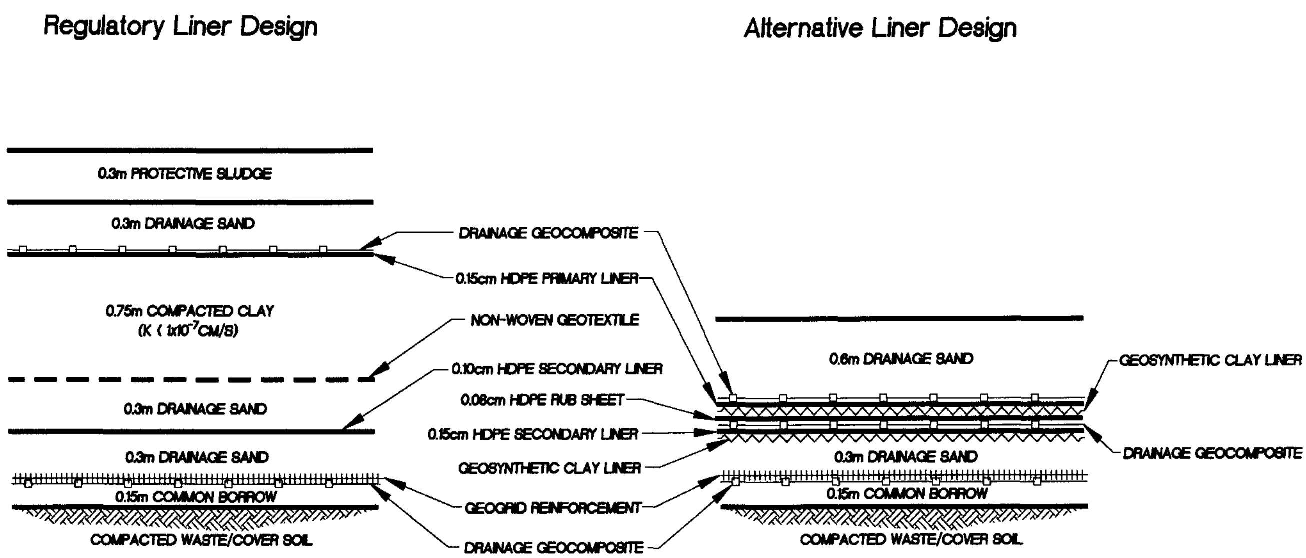

Figure 3. Liner System Schematics

The thickness of the liner and cover systems has a larger than usual impact on capacity at this site because of the limited available waste thickness. For this reason, a major objective of the alternative design process was to develop a thinner liner system than one that would meet the design prescribed by the regulations. Additional objectives included developing a liner section that is easily built on side slopes and meets the project design criteria presented in the following section.

The permit application for this project was prepared using a "milestone" review process with the MEDEP. The milestone process involves the MEDEP regulatory review team (engineer, hydrogeologist, and licensing specialist) with all of the major design and siting decisions as the permit application is being prepared. For design aspects of the project, such as the alternative liner design, the milestone process typically includes a sequence of meetings and MEDEP review of progress prints and supporting calculations for each major component of the work. The milestone process is intended to streamline the application review by essentially eliminating unacceptable design concepts and major review comments on the application that could result in a total redesign or denial of the permit. Although MEDEP did not provide formal approvals of the alternative liner and other design aspects of the project at the conclusion of the milestone process, it is implicit in the process that the design concepts presented were acceptable and judged to be in general conformance with the regulations.

LINER DESIGN CRITERIA AND CONSTRUCTION CONSIDERATIONS

The following design criteria and construction considerations were assessed in evaluating the alternative design relative to the regulatory design:

- **Barrier Properties** - The alternative design must provide an equal or superior barrier to leakage than the regulatory design.

- **Settlement Tolerance** - Calculations indicate primary settlements of up to about 2.75 meters are expected shortly after the landfill is filled to capacity, with an additional 2.75 meters of secondary settlement occurring during the post-closure period. The settlement properties of the sludge were estimated from laboratory consolidation tests and long-term settlement monitoring of the landfill surface. Localized differential settlements are also expected due to the nature and variability of the waste.

- **Interface Stability** - The landfill lining system is required to have sufficient internal and interface shear strength to provide an adequate factor of safety against slope instability.

- **Liner Thickness** - The thickness of the liner substantially impacts landfill capacity.

- **Wet/Dry Behavior** - The liner is expected to be subjected to cycles of wetting and drying during and after the construction period.

- **Puncture Resistance** - The liner is susceptible to damage from construction and operating equipment.

- **Leak Detection** - The leak detection system must be capable of transmitting a rapid and large leak (9,400 liters per hectare per day) in accordance with the landfill Action Leakage Rate/Response Action Plan.

- **Quality Assurance** - The quality of the liner installation depends in part on quality assurance measures taken before and during construction.

- **Weather Constraints** - The liner will likely be subjected to wet/dry and hot/freezing conditions during construction.

- **Vulnerability to Erosion** - Rain falling on the landfill side slopes during construction has the potential to cause erosion and sediment transport.

- **Ease and Speed of Construction** - The time and effort required to construct the liner on the side slopes will impact overall construction costs.

TECHNICAL EQUIVALENCY EVALUATION

This section presents an evaluation of the technical equivalency and relative merits of the alternative liner design as compared to the regulatory design. The two designs are evaluated for the project design criteria and construction considerations listed above.

Barrier Properties

The flux (leakage) rate for each liner design was analyzed using procedures outlined by Giroud and Bonaparte[1], and the following equation:

$$Q = 1.15\, a^{0.1}\, h^{0.9}\, k_s^{\,0.74}$$

where:
- Q = flow through hole in m^3/sec
- a = area of hole in m^2
- h = head on liner in meters
- k_s = permeability of soil under geomembrane hold, in m/sec

For comparative purposes, the leakage through one 1 cm^2 hole in the liner was estimated assuming the overlying drainage layer was saturated. These assumptions were used to evaluate both the primary and secondary liners. The leakage through the alternative primary liner was estimated to be 3.1 x 10^{-3} liters/day, versus 3.0 x 10^{-2} liters per day for the regulatory liner. The Giroud and Bonaparte equation is empirical, however, and does not account for gradient. Considering the significantly higher gradient for the alternative design due to the relative thicknesses of the GCL and compacted clay layers, it was judged that the flow through the primary liner hole for each design would be approximately equivalent. For the secondary liner, however, calculations indicate the alternative design is expected to provide a more positive barrier to leakage by a factor of many orders of magnitude (leakage of 3.1 x 10^{-3} liters/day versus 576 liters/day). This superior performance is due to the composite nature of the secondary liner (HDPE membrane/GCL) in the alternative design, versus the single secondary HDPE geomembrane in the regulatory design.

Settlement Tolerance

Large total and differential settlements are expected due to consolidation of the underlying waste, and the nature of the waste. Although the underlying waste consists mostly of wastewater treatment plant sludge, bulky wastes had been landfilled in the past. Shallow sinkholes indicative of such settlement have been observed on existing landfill sideslopes filled to final grades. In addition, gas vents and leachate collection pipes have been constructed in vertical stone-filled wire baskets within the waste mass. The pipes and surrounding stone have the potential to settle much less than the surrounding waste. Although these pipes will be cut off about 15 feet below the proposed lining system, there is a long-term potential for these "hard spots" to create differential settlement of the liner. The GCLs in the alternative design are much more tolerant of differential settlement than the compacted clay in the regulatory design. GCLs can accommodate tensile strains in the 15 percent range and maintain their barrier properties, whereas compacted clay cracks when strained in tension to the 1 or 2 percent range.

Interface Stability

Stability calculations indicate both liner designs would be stable, with a factor of safety of at least 1.5 for static conditions. In the alternative design, a 0.08-cm textured rub sheet was required between the GCL and drainage geocomposite due to a low interface shear strength between those two materials. The calculations were based on limited project-specific interface tests, along with published data and test results on file. Project construction specifications require direct shear tests for each liner interface, as well as the internal strength of the GCL, on the actual materials to be used in the expansion.

Favorable properties of the landfilled sludge material are a major factor in the overall stability of the lining systems. The sludge is relatively light, having a total unit weight of about 1.1

grams per cubic centimeter. The sludge also has a high shear strength, with an effective friction angle of about 40°, due to the reinforcing effects of residual fibers from the paper making process. The friction angle of the sludge was determined by in-situ vane shear testing and laboratory direct shear tests.

The base grade configuration on the sideslopes also aids lining system stability. Three 9-meter wide lateral benches are located on the overlap portion of the landfill expansion. The benches are intended to provide for temporary liner anchorage and cell access as the expansion is developed sequentially, and to aid in managing surface water runoff and leachate collection. The benches, in effect, also provide a "shear key" effect relative to liner interface stability. The benches force potential failure surfaces to pass through the stronger waste materials either above or below the lining system, thereby raising the overall factor of safety.

Liner Thickness

The alternative liner is 1.1 meter thinner than the regulatory liner. The additional corresponding 1.1-meter thick layer of waste results in a volume of 93,000 cubic meters, or an eight percent increase in capacity over the regulatory design. With the alternative liner, the landfill expansion has a capacity of about 1.2 million cubic meters.

Puncture Resistance

Regarding the primary liner, the GCL's thinner section is more susceptible to damage from construction equipment than compacted clay. GCLs have self-healing properties, however, for punctures up to about five centimeters in diameter. The potential for large-scale damage to GCLs during construction should be greatly reduced by Construction Quality Assurance (CQA) activities. If damage occurs, it should be obvious. Damaged GCLs are more easily repaired than compacted clay. For the primary liner, the alternative design includes an extra 0.3 meters of drainage sand (0.6 meters total) and a drainage geocomposite (included in both designs but not required by the regulations) as added mechanical protection for the geomembrane and GCL liners. Large-scale puncture damage to compacted clay is not likely. Regarding the secondary liner, the thicker liner (0.15 cm vs. 0.1 cm) and the presence of the GCL and drainage geocomposite make the alternative design more resistant to puncture than the required design (0.1 cm liner only).

Leak Detection

Both liner designs are capable of transmitting the rapid and large leak of 9,400 liters per hectare per day. For the regulatory design, 0.3 meters of drainage sand (or similar material) are required above the secondary liner for mechanical protection during overlying clay placement operations. The drainage sand can also serve as a drainage layer, negating the need to use a drainage geocomposite for this function. A drainage geocomposite is used in the alternative design. The drainage geocomposite is thinner and more transmissive than the drainage sand layer.

Other Factors

Evaluations of the relative merits of GCLs versus compacted clay have been widely published. In general, GCLs are viewed as being equivalent or superior to compacted clay liner with respect to wet/dry behavior, quality assurance, weather constraints, vulnerability to erosion, and ease and speed of construction.

COST COMPARISON

The estimated costs to construct the alternative and regulatory liner designs is presented below. The cost estimates are based on the following material unit rates obtained from landfill construction experience in the region. The unit costs reflect the cost to purchase and place/install the materials in accordance with project specifications.

Table 1. Estimated Liner Construction Costs

Regulatory liner			Alternative liner		
Material	Cost per m^2	(ft^2)	Material	Cost per m^2	(ft^2)
0.3 m Sludge	$1.20	($0.11)	0.6 m Sand	$9.60	($0.89)
0.3 m Drainage Sand	$4.80	($0.45)	Drainage Geocomposite	$7.00	($0.65)
Drainage Geocomposite	$7.00	($0.65)	0.15 cm Liner	$5.40	($0.50)
0.15 m Liner	$5.40	($0.50)	GCL	$6.00	($0.56)
0.75 m Compacted Clay	$12.00	($1.11)	0.08 cm Rub Sheet	$2.40	($0.22)
Non-woven Geotextile	$1.30	($0.12)	Drainage Geocomposite	$7.00	($0.65)
0.3 m Drainage Sand	$4.80	($0.45)	0.15 cm Liner	$5.40	($0.50)
0.10 cm Liner	$4.30	($0.40)	GCL	$6.00	($0.56)
Drainage Geocomposite	$7.00	($0.65)	Drainage Geocomposite	$7.00	($0.65)
0.3 m Drainage Sand	$4.80	($0.45)	0.3 m Drainage Sand	$4.80	($0.45)
Geogrid	$10.80	($1.00)	Geogrid	$10.80	($1.00)
0.15 m Common Borrow	$1.60	($0.15)	0.15 m Common Borrow	$1.60	($0.15)
TOTAL:	**$65.00/ m^2**	**($6.04/$ft^2$)**	**TOTAL:**	**$73.00/ m^2**	**($6.78/$ft^2$)**

Extending the unit costs over the entire 8.5 hectares overlap area, the regulatory design would cost about $5.5 million and the alternative design would cost about $6.2 million. Assuming a total life cycle cost of $55 per megagram to build and operate the landfill, and a weight of landfilled waste of about one megagram per cubic meter, the value of the 93,000 cubic meters capacity gained by using the alternative design is about $5 million.

CONCLUSIONS

1. The results of the technical equivalency evaluation of the alternative and regulatory designs indicates the alternative design is better suited to this project and expected site conditions. In particular, the alternative design provides superior leachate barrier layer performance, is easier to install, is less vulnerable to erosion and the effects of weather, and is much more tolerant of settlement. Any risks or drawbacks of the alternative design are accounted for in the design (i.e., extra mechanical protection against puncture of the GCL, and superior puncture resistance of the secondary liner). The technical benefits of the alternative design are due in large part to the substitution of GCLs for compacted clay liners.

2. Overall, the alternative design is more economical than the regulatory design. For a premium construction cost of about $700,000, the alternative design provides an additional $5 million of disposal capacity. The economic benefits of the alternative design are due to the substitution of thin geosynthetic materials (GCLs and drainage geocomposites) for compacted clay barrier and sand drainage layers.

ACKNOWLEDGMENTS

The authors would like to thank Mr. Alan Jones of Integrated Waste Solutions, Inc. for coordinating the efforts of the permit application team and providing valuable insight into historical practices at the site. Mr. Steven Cole of S.W. Cole Engineering, Inc. completed the project geotechnical engineering including stability analyses and settlement estimates.

REFERENCES

Giroud, J.P. and Bonaparte, R., 1989, *"Leakage through Liners Constructed with Geomembranes, Part I: Geomembrane Liners, and Part II: Composite Liners"*, Geotextiles and Geomembranes, Vol. 8.

COST EFFECTIVE ALTERNATIVE TO AN UNREINFORCED GCL FOR LANDFILL FINAL COVER SYSTEMS

DAMON BROWN
CHRISTOPHER J. BRUMMER
MICHAEL A. DELMANOWSKI
EBA ENGINEERING, SANTA ROSA, CALIFORNIA, USA

ABSTRACT

A geosynthetic clay liner (GCL) may be installed at a fraction of the cost of a California prescriptive standard compacted clay liner (CCL) when low-permeability material is not available on-site and soils must be either amended or imported. The engineered alternative selected for the final cover system at the 32 ha (79 acre) Hanford Landfill located in Kings County, California incorporates a new GCL product that offers a cost-effective alternative to both unreinforced GCLs and the State's prescriptive standard CCL, while exceeding applicable performance standards. Economic analyses comparing three design alternatives demonstrated a 41 to 63 percent cost savings over a prescriptive CCL cover system. This paper discusses the first use of a new, lightweight, woven/nonwoven, needle-punched GCL product in a landfill final cover application and presents results from conformance testing and construction quality assurance monitoring. Bentonite migration has been reported in unreinforced GCLs; however, at the Hanford Landfill, field observations of GCL panels exhumed approximately five weeks after initial placement indicated significant hydration, but no discernable bentonite migration.

INTRODUCTION

This paper utilizes a case study to present results of the first use of a new, lightweight, woven/nonwoven needle-punched geosynthetic clay liner (GCL) product in a landfill final cover application. The scope of work for the case study consists of the final closure of the Hanford Landfill, an unlined municipal solid waste (MSW) disposal facility located in the Central Valley of California (Figure 1). Average annual precipitation at the site is approximately 211 mm (8.29 in) and occurs as rain, 90 percent of which falls during the months of November through April. Subgrade excavation and refuse filling throughout the operating life has resulted in a nearly square, 32 ha (79 acre) footprint rising a maximum of 6.4 m (21 ft) above the surrounding flat terrain with refuse ranging from 7.6 to 12 m (25 to 40 feet) in thickness. The top of the landfill has been graded at 3 percent to form a series of alternating ridges and swales designed to drain the interior. The extreme northern and southern ridges steepen to approximately 10 percent away from the center and constitute a minor portion (4 percent) of the total landfill surface requiring closure. A 1.8 to 3.0 m (6 to 10 ft) high operational soil berm forms 3H:1V perimeter side-slopes.

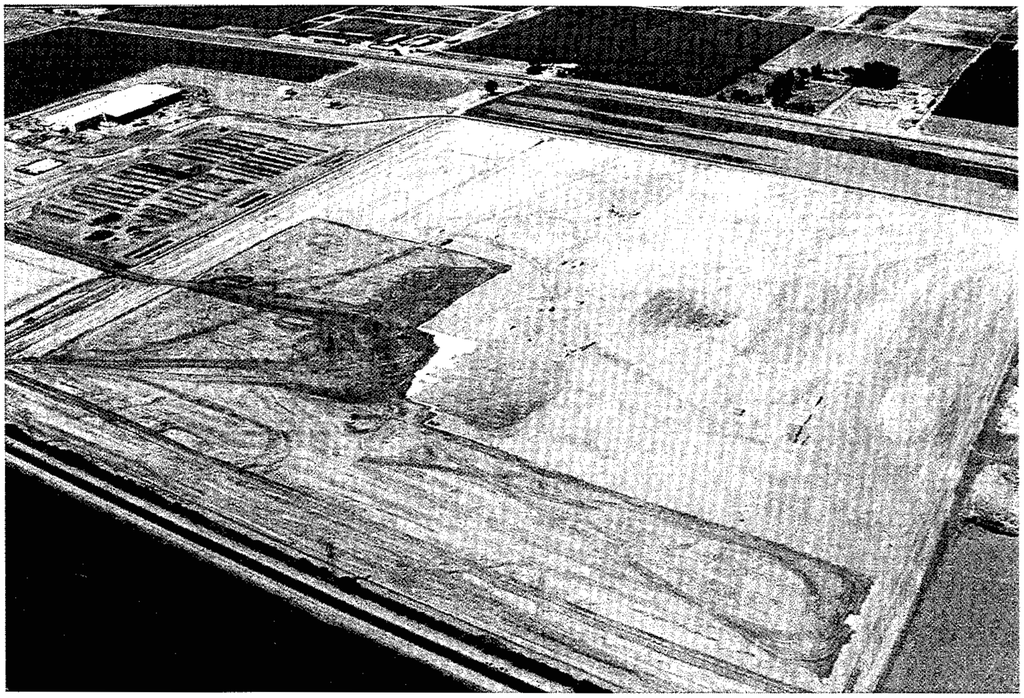

Figure 1. Oblique aerial view of the Hanford Landfill taken during GCL and cover soil placement.

The combined absence of a local source for low-permeability material, low seismic activity, and the gently sloping surface of the landfill requiring placement of the final cover system provided an opportunity to explore possible benefits offered by the use of an unreinforced GCL. In this paper we present results of an economic analysis comparing various final cover system designs which led to the selection of a preferred GCL alternative, and discuss conformance testing and construction quality assurance monitoring during construction.

FINAL CLOSURE DESIGN

Final closure of MSW landfills in California is subject to requirements promulgated under California Code of Regulations (CCR) Title 27. The prescriptive standard for unlined waste management unit final cover systems in California consists of the following in ascending order:

- foundation layer consisting of 61 cm (24 in) of engineered fill, typically compacted to at least 90 percent relative density (modified proctor),
- compacted clay liner (CCL) consisting of 30 cm (12 in) of fine-grained material compacted to attain a saturated hydraulic conductivity no greater than 1×10^{-6} cm/sec, and
- an erosion resistant layer, typically in the form of a vegetative layer consisting of 30 cm (12 in) of soil capable of sustaining native, shallow-rooting plant growth and resisting foreseeable erosion.

Several geotechnical investigations were conducted at the Hanford Landfill to determine the suitability of on-site borrow soils for use in construction of the low-permeability clay layer and other components of the final cover system. Early investigations identified a silty-clay horizon located approximately 3 to 5 m (10 to 15 ft) below the ground surface. In addition to the onerous task of excavating this material, results of laboratory testing of undisturbed samples indicated a hydraulic conductivity that only marginally met requirements for the low-permeability layer. Hence, the on-site silty-clay material was eliminated as a potential source for low-permeability clay material. Subsequent testing of silty-clayey material exposed at the ground surface was performed to determine possible bentonite admix ratios which would allow more accessible on-site material to meet hydraulic conductivity requirements. Based on results of laboratory testing, a 3 percent bentonite admix ratio was required and was subsequently increased to 6 percent to account for variability in material and degree of mixing achieved during construction.

California allows the consideration and approval of engineered alternatives to the prescriptive standard when the prescriptive standard is not feasible and if there is a specific engineered alternative that is consistent with the performance goals addressed by the prescriptive standard, and which affords equivalent protection against water quality impairment. To establish that compliance with the prescriptive standard is not feasible, it must be demonstrated that the prescriptive standard is either unreasonably and unnecessarily burdensome and will cost substantially more than alternatives which meet the State's criteria, or is impractical and will not promote attainment of applicable performance standards.

Because the majority of slopes on the landfill surface do not exceed 3 percent, we also investigated the use of an unreinforced GCL product. We performed an economic analysis comparing three final cover system designs to assist in selection of the preferred alternative. The alternatives evaluated in the analysis included the following:

1) a prescriptive standard cover system utilizing 100 percent clay imported from the nearest commercial source,

2) a prescriptive standard cap utilizing on-site material with a 6 percent bentonite admix, and

3) an engineered alternative incorporating an unreinforced GCL.

As anticipated, the estimated cost for Alternative 1 was significantly higher than the other alternatives, with clay acquisition and transportation expenditures accounting for the cost differential. Costs, normalized to Alternative 1, are shown in Figure 2. Amending on-site soils with imported bentonite (Alternative 2) provided an estimated cost savings of 37 percent over that of Alternative 1. Alternative 3 provided a cost savings of 63 percent with respect to Alternative 1 and 41 percent with respect to Alternative 2, and was selected as the preferred engineered alternative.

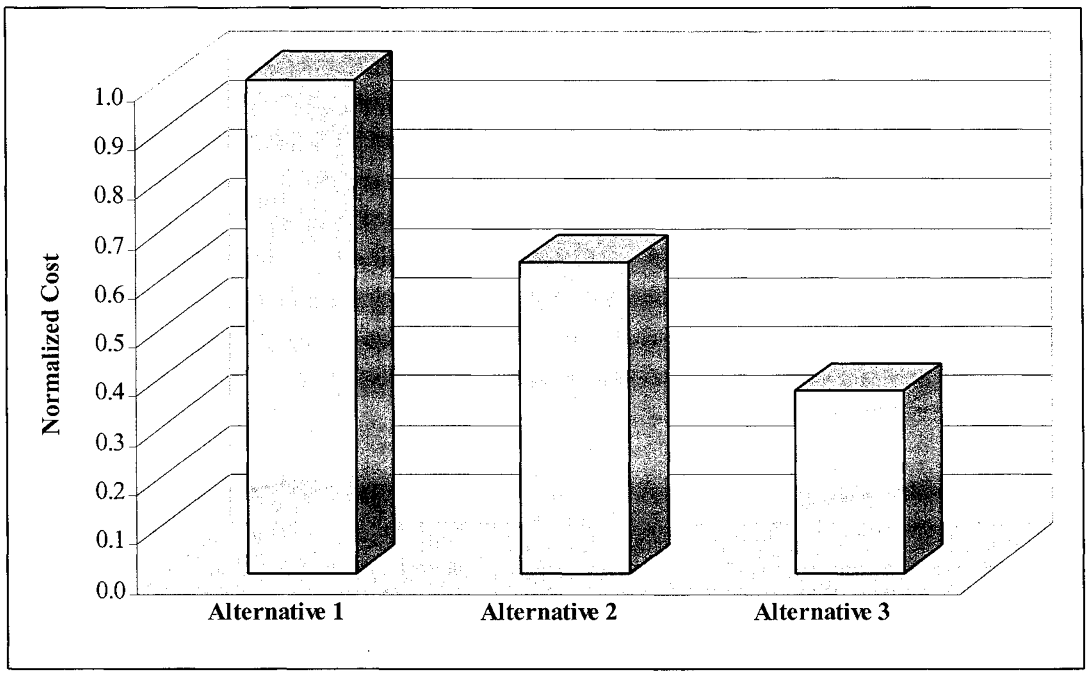

Figure 2. Relative costs for final closure alternatives described in this paper, normalized to Alternative 1.

Specifications for the engineered alternative cover on slopes less than 10 percent at the Hanford Landfill consisted of the following components in ascending order:

- a 30 cm (12 in) foundation layer placed over the existing intermediate cover and compacted to at least 90 percent relative compaction (modified proctor),
- An unreinforced GCL consisting of an approximately 3.7 kg/m^2 (0.75 lbs/ ft^2) dry weight sodium bentonite layer sandwiched between and continuously adhered to two lightweight (95 g/m^2, nominal [2.8 oz/yd^2]) woven geotextiles, and
- A 46 cm (18 in) vegetative soil layer track-walked to approximately 85 percent relative compaction (modified proctor).

Various manufacturers of GCLs have reported swelling of their products when installed in final cover systems applications in conjunction with the minimum 30 cm (12 in) vegetative layer required by the prescriptive standard. Therefore, the thickness of the vegetative layer was increased to 46 cm (18 in) to provide additional normal stress and prevent swelling of the GCL during hydration. The additional thickness also provides greater protection of the GCL against equipment damage following installation. The prescriptive standard requires a foundation layer of 61 cm (24 in) for the purpose of providing a firm and unyielding subgrade for compaction of the low permeability clay layer. However, for the GCL alternative, the main purpose of the foundation layer is to provide a smooth subgrade free of protrusions and deleterious objects which could damage the GCL. Therefore, the foundation layer thickness was reduced to 30 cm (12 in).

We petitioned the regulatory agencies and were successful in gaining approval of the preferred GCL engineered alternative. Project specifications were written to require the unreinforced GCL described above. However, the selected geosynthetics supplier proposed the use of a new, lightly needle-punched, woven/nonwoven GCL product designed specifically for the project which not only exceeded the project specifications, but also was bid at a cost savings of 4 percent to that of other bids submitted for an unreinforced GCL. The new product consists of sodium bentonite at the approximate dry weight of 3.7 kg/m^2 (0.75 lbs/ft^2) carried between a woven geotextile with a nominal weight of 95 g/m^2 (2.8 oz/ yd^2) and a nonwoven geotextile with a nominal weight of 100g/m^2 (3.0 oz/yd^2) that are lightly needle-punched together. For slopes exceeding ten percent, a standard double nonwoven needled punched (NWNP) reinforced GCL overlain by a geonet composite drainage layer was specified. Depending on the application, the authors commonly specify a minimum peel strength of 110 to 130 N (25 to 30 lbs) performed on a 10 cm (4 in) wide sample using the modified ASTM D 4632 test method. However, due to the shallow 10 percent slopes at the Hanford Landfill, the minimum acceptable peel strength was reduced to 67 N (15 lbs) using ASTM D 4632 (modified).

CQA AND INSTALLATION

Manufacturers present geosynthetic physical properties in terms of a minimum average roll value (MARV) in a particular manufacturing lot. The MARV is the value which is exceeded by 97.5 percent of the test data and is derived statistically as the average value minus two standard deviations (Koerner, 1997). Unfortunately, it can be difficult to define a manufacturing lot which can be the compilation of many tests over months or years. The average of all testing on any roll was required to be greater than the value listed in the project specifications shown in Table 1.

Table 1. GCL Specifications

Test	Method	Value	MQC[1] Testing Frequency
Base Bentonite			
Moisture Content	ASTM D 2216	25 percent (max.)	1 per 50 tons
Swell	ASTM D 5890	24 ml/2 g (min.)	1 per 50 tons
Fluid Loss	ASTM D 5891	18 ml (max.)	1 per 50 tons
Geotextiles[2]			
Mass per Unit Area	ASTM D 5261	95 g/m^2	1 per 50,000 ft^2
GCL[2]			
Grab Strength[3]	ASTM D 4632	330 N	1 per 200,000 ft^2
Bentonite Mass Per Unit Area	ASTM D 5993	3.66 kg./m^2 (oven-dried)	1 per 50,000 ft^2
Index Flux	ASTM D 5887	5 x 10^{-9} cm/sec	1 per production-week

[1] Manufacturing Quality Control.
[2] Values for geotextiles and GCL are Minimum Average Roll Values (MARV) and the average of all measurements on any roll shall not be less than the MARV specified.
[3] Tested in machine direction.

The manufacturer of the lightly-needled GCL reports a nominal internal shear strength of 2.4 kPa (50 lbs/ft^2) and a minimum peel strength of 22 N (5.0 lbs) for the lightly-needled GCL. Peel strengths of the lightly-needled GCL for the Hanford project ranged from 24 N to 93.0 N (5.5 lbs to 20.9 lbs) with a typical value of 44 N (10 lbs). These values exceed the internal shear strength reported for unreinforced GCL.

Lightly-needled GCL rolls were delivered to the site in standard widths of 4.72 m (15.5 ft) and lengths of either 45.7 m (150 ft) or 67.1 m (220 ft). Sample coupons of GCL delivered to the site were collected for Construction Quality Assurance (CQA) testing to verify that the product met the project specifications. A compilation of CQA test results and Manufacturing Quality Control (MQC) test results for the lightly-needled GCL are presented in Table 2.

Table 2. Combined Results of CQA Testing and MQC Testing

Material	**Base Bentonite**			**Geotextile (MARV)**[1]		**GCL (MARV)**[1]		
Test[2]	Moisture Content	Swell	Fluid Loss	Upper Mass	Lower Mass	Grab Strength	Bentonite Mass (dry)	Index Flux
Project Specification	25% (max)	24 ml/2 g (min)	18 ml (max)	95 g/m^2 (min)	95 g/m^2 (min)	330 N (min)	3,662g/m^2 (min)	5.0×10^{-9} cm/sec (max)
Min.	7.3	24.0	10.4	122.0	103.0	333.6	3662	1.1×10^{-9}
Max.	11.0	30.0	16.4	259.0	347.0	631.6	5714	5.0×10^{-9}
Avg.	9.2	25.5	12.5	151.3	118.9	375.0	4088	4.9×10^{-9}
s.d.	0.9	1.4	1.3	33.6	30.4	70.3	309	6.2×10^{-10}

1 The average of all measurements on any roll shall not be less than the MARV specified.
2 A total of 164 MQC tests and 31 CQA tests were conducted for this project.

GCL rolls were deployed using a forklift boom and steel bar inserted through the core tube (Figure 3). Panels were oriented parallel to the slope and placed with adjacent GCL panels overlapped a minimum of 30 cm (12 in) along the length and 2 feet along the width (butt-seams). For slopes greater than 10 percent, a standard reinforced GCL overlain by a geocomposite drainage layer was installed prior to vegetative layer placement (Figure 4). Because non-woven geotextiles inhibit the extrusion of internal bentonite, seams were required to be augmented with powdered bentonite at a minimum rate of 0.37 kg/m (0.25 lb/ft) in a continuous bead within 15 cm (6 in) of the edge of the lower GCL panel (Figure 5). GCL rolls held up well to the handling associated with field installation activities.

Project specifications also required that all GCL panels be covered with soil by the end of each day. Scrapers delivered borrow material to the leading edge of the vegetative layer where the soil was pushed by small bulldozers over installed GCL panels in a single 46 cm (18 in) lift. Kamatsu Model D65 bulldozers equipped with 106-cm (42-in) wide, low ground pressure tracks were used to place the soil (Figure 6). Scrapers were limited to those areas where the full 46 cm (18 in) lift had been placed. The rate of GCL installation was limited to approximately 0.93 ha/day (2.3 acres/day), the maximum amount of vegetative layer material that equipment was capable of placing in one day.

A manufacturing deficiency was identified in the lightly-needled GCL by quality assurance monitors during field installation. The deficiency was characterized by a 2.5 to 7.6 cm (1.0 to

3.0 in) wide bentonite void running longitudinally along affected GCL rolls and was determined to be related to over-tensioning of the lower woven geotextile during manufacturing, requiring a minor modification of manufacturing operational procedures. Effected rolls were rejected and replaced with approved material.

FIELD PERFORMANCE

Bentonite creep has been reported in unreinforced GCLs under low normal confining loads (LaGatta et al., 1997). LaGatta et al. (1997) concluded that unreinforced GCL suffered bentonite migration, which was influenced in part by the lack of confinement from needle-punched fibers. Field observations of lightly-needled GCL panels exhumed approximately five weeks after initial placement at the Hanford Landfill indicated significant hydration, but no discernable bentonite migration. The presence of needle-punched fibers may be helping to inhibit bentonite migration, providing potentially better performance than unreinforced GCL.

Due to a construction-sequencing problem caused by a staking error, a number of lightly-needled GCL panels were required to be exhumed and replaced. Approximately five weeks after placement, the panels were exhumed with a backhoe and examined. Consistent with the observations of Daniel et al. (1998) and Bonaparte et al. (1997), the GCL had undergone significant hydration by absorbing moisture from the surrounding soils. The GCL was carefully examined for installation damage, and bentonite migration. Other than damage caused by the backhoe teeth during exhumation, the GCL panels were intact and in good condition. Although the panels appeared fully hydrated, no signs of tensile strain, swelling, or lateral shearing were observed. It should be noted that only a visual inspection was conducted and no mass per unit area or moisture content measurements were performed on the exhumed GCL. These observations suggest that the 18-inch thick soil cover provided sufficient normal stress to prevent swelling of bentonite during hydration and prevent differential normal loads which can result from heavy vehicle wheel loads over the final cover (Richardson and Marr, 1999; and Richardson, 1996).

CONCLUSION

Based on the authors' experience with cover system designs prepared for other landfill closures, a prescriptive final cover system incorporating a CCL is typically more economical than a GCL engineered alternative when suitable low-permeability clay material is available on-site. For this case study, construction of the prescriptive standard would have required import of clay or amendment of on-site soils. The cost savings incurred through substitution of a GCL for a CCL was the primary basis for selection of a geosynthetic alternative for the Hanford Landfill. A new, lightly-needled GCL product was developed for this project that provided a higher internal shear strength; a lower potential for bentonite migration; and high installation survivability at a slightly lower-cost than an unreinforced GCL product.

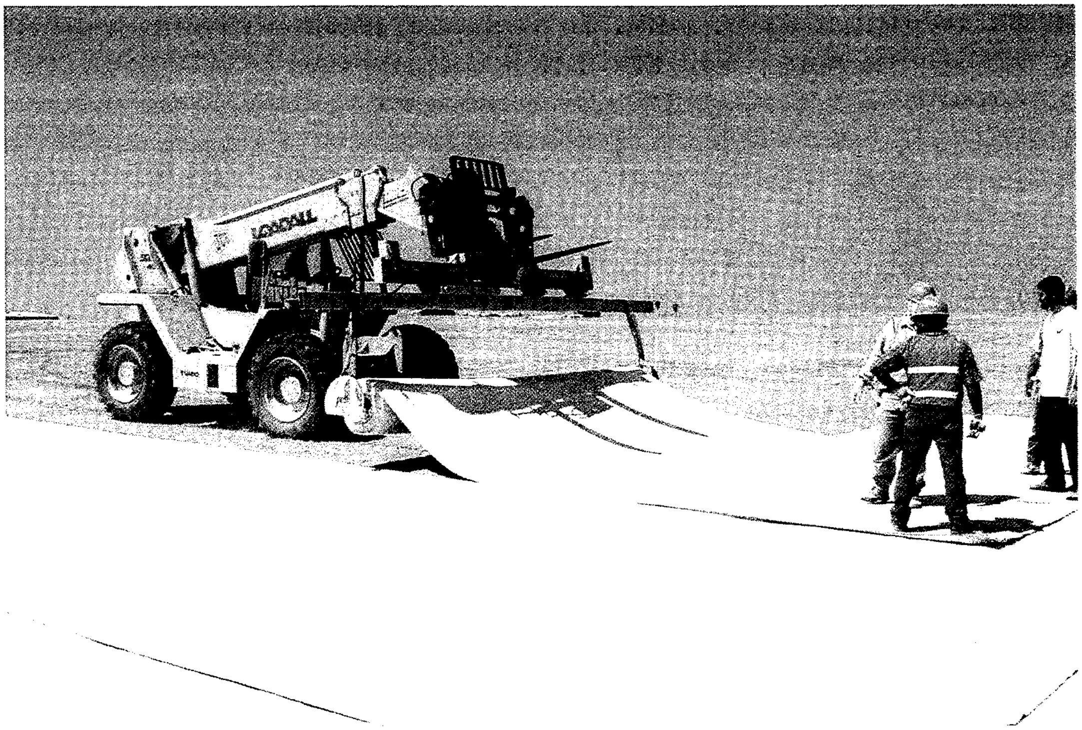

Figure 3. GCL installation over prepared subgrade.

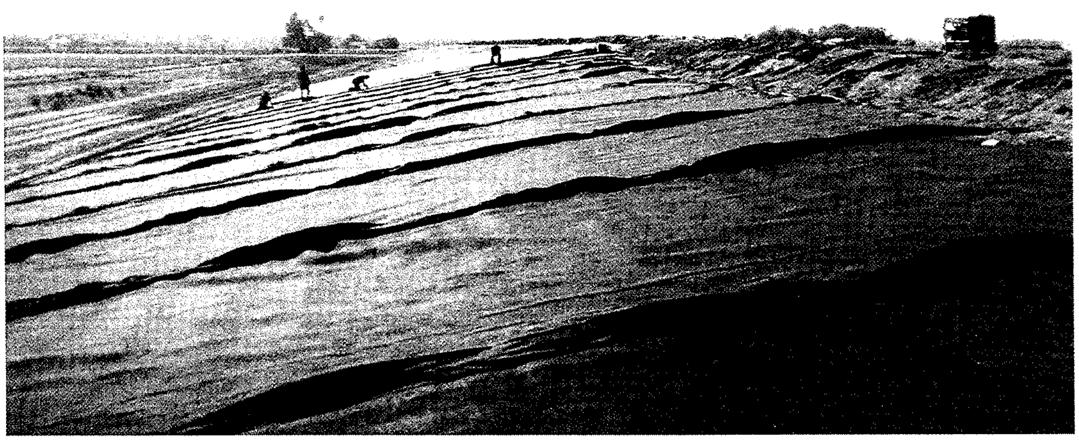

Figure 4. Placement of standard double NWNP reinforced GCL and overlying geonet composite drainage layer on 10 percent refuse slope.

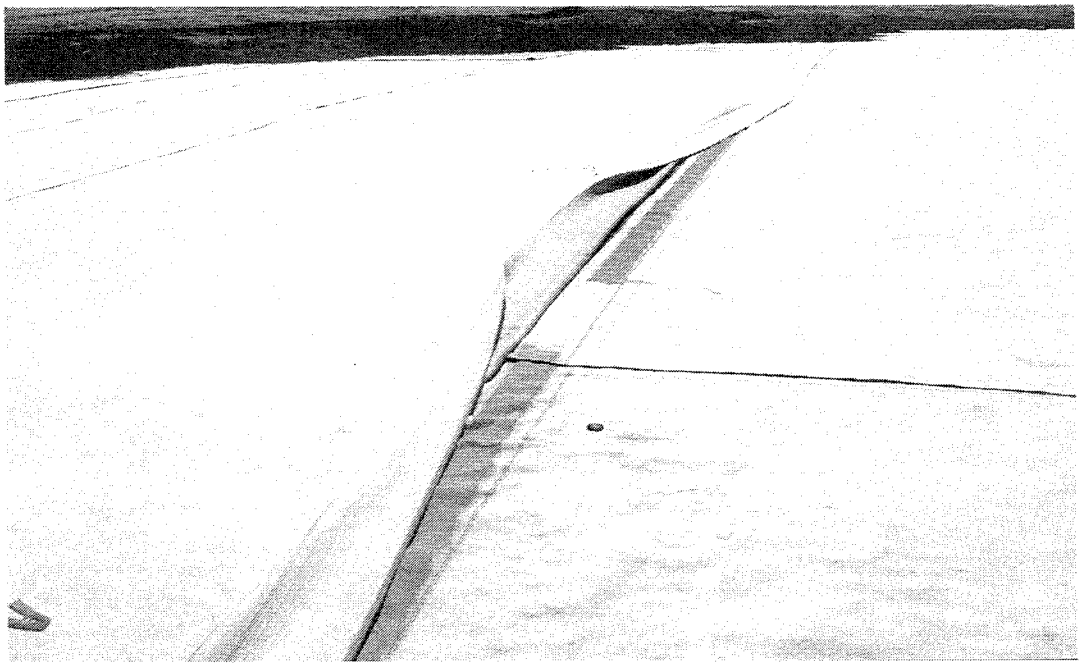

Figure 5. Bentonite powder augmenting GCL seams. Photo taken prior to hand application of bentonite at butt-seam. Note lens cap for scale.

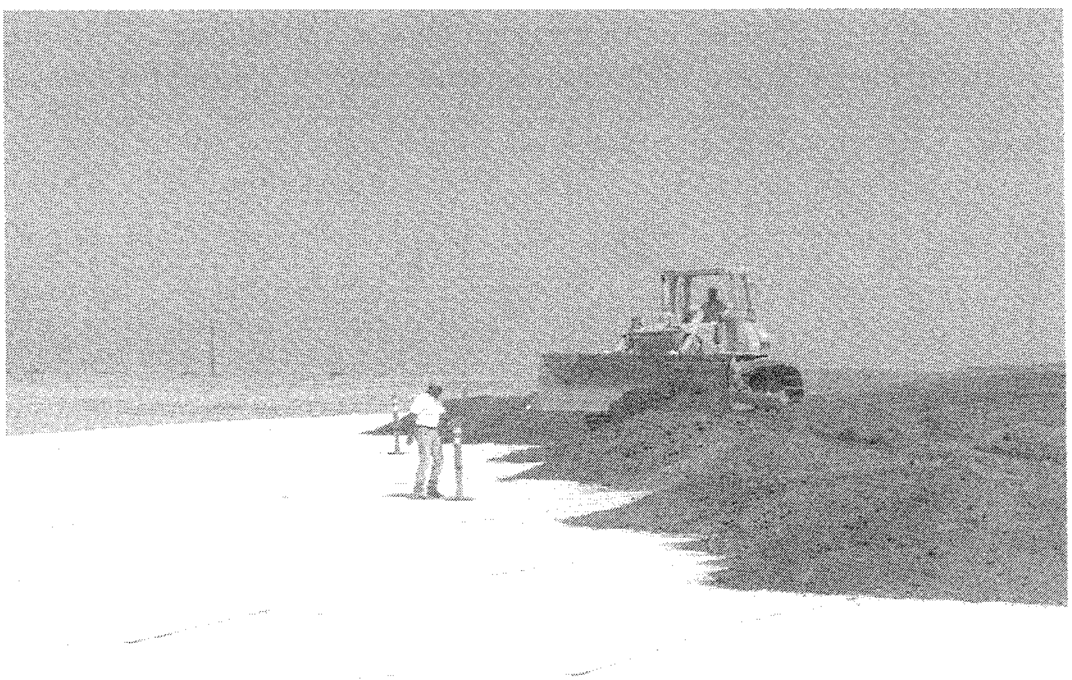

Figure 6. Vegetative Soil layer placement over GCL on 3 percent refuse slope.

A manufacturing deficiency identified during placement of GCL panels further emphasizes the importance of a rigorous quality assurance program during the installation of new geosynthetic products.

ACKNOWLEDGMENTS

The authors wish to thank and acknowledge the cooperation of Mike Adams and the Kings Waste and Recycling Authority for allowing the use of their case history in this paper.

REFERENCES

Bonaparte, R., Othman, M.A., Rad, N.S., Swan, R.H., and Vander Linde, D.L., 1997, Evaluation of Various Aspects of GCL Performance, *1995 Workshop on Geosynthetic Clay Liners*, U.S. EPA, Rept. No. EPA/600/R-96/149.

Daniel, D.E., Koerner, R.M., Bonaparte, R., Landreth, R.E., Carson, D.A., and Scranton, H.B., 1998, Slope Stability of Geosynthetic Clay Liner Test Plots, ASCE, *Journal of Geotechnical and Geoenvironmental Engineering*, Vol. 124, No. 7, pp. 228-637.

LaGatta, M.D., B.T. Boardman, B.H. Cooley, and D.E. Daniel, 1997, Geosynthetic Clay Liners Subject to Differential Settlement, *Journal of Geotechnical and Geoenvironmental Engineering*, ASCE, Vol. 123, No. 5, pp. 402-410.

Koerner, R.M., 1997, *Designing with Geosynthetics*, 4th ed., Simon & Schuster, New Jersey, USA.

Richardson, G.N., 1996, GCL Internal-Shear Strength Requirements, *Geotecnical Fabrics Report*, IFAI, Vol. 15, No. 2, pp. 20-25.

Richardson, G.N., and Marr, A., 1999, Developing a Standard of Practice for GCLs, *Geotecnical Fabrics Report*, IFAI, Vol. 17, No. 6, pp. 20-25.

USING HELP MODEL FOR DESIGNING GEOCOMPOSITE DRAINAGE SYSTEMS IN LANDFILLS

GHADA ELLITHY, PH.D., TENAX CORPORATION
UNITED STATES OF AMERICA
AIGEN ZHAO, PH.D., P.E., TENAX CORPORATION
UNITED STATES OF AMERICA

ABSTRACT

The US EPA's HELP (Hydraulic Evaluation of Landfill Performance) model is by far the most used tool for analyzing water balance in landfill lining and capping systems. However, a proper simulation of geocomposite lateral drainage layers in the HELP Model is not well established. A misinterpretation of the model's output results can lead to an unsafe design of the drainage systems in landfills. A parametric study was conducted to show the importance of using measured geocomposite properties -versus default ones- as input values and their effect on the estimated amount of lateral drainage and the head on the liner as presented in the model's output. It was demonstrated that the maximum head on the liner, as calculated by McEnroe's equation, is valid only when it lies within the thickness of the geocomposite. A design example is presented to demonstrate the proper use and interpretation of HELP model input and output data. Also, the effect of incorporating updated weather data was investigated.

INTRODUCTION

The use of geonets, and geocomposites (geonets with laminated geotextile on one or both sides) as drainage layers in landfills to replace soil drainage layers, was introduced to save space and simplify construction on slopes. Also, when soil drainage layer materials are not readily available, geosynthetics provide a viable alternative. However, design methodologies of geosynthetics drainage systems, based on the HELP model output, are not well established.

Figure 1 shows a typical cross section in a landfill. There are two main functions of a lateral drainage layer in a cover system: 1) to reduce the seepage forces in the overlying soil layer to increase the factor of safety with regard to slope stability, and 2) to reduce the head on top of the GCL, geomembrane or compacted clay liner.

The flow capacity in a drainage geonet or geocomposite is highly dependent on the applied load, hydraulic gradient and the seating period. The hydraulic conductivity of a soil drainage layer is relatively constant under the practical ranges of normal loads encountered in such applications. Also, the flow rate in drainage geonets or geocomposites is not linearly proportional to the hydraulic gradient. This indicates a non-Darcian flow at higher hydraulic gradients. Geosynthetics are made of polymeric materials that tend to creep with time. Additionally, the structure of the geonet plays a role in the level of that creep. Other factors such as geotextile/ soil intrusion, chemical and biological degradation reduce the flow capacity of geosynthetic drainage materials. All these factors indicate the importance of considering the difference between geosynthetics and typical soil drainage materials in design.

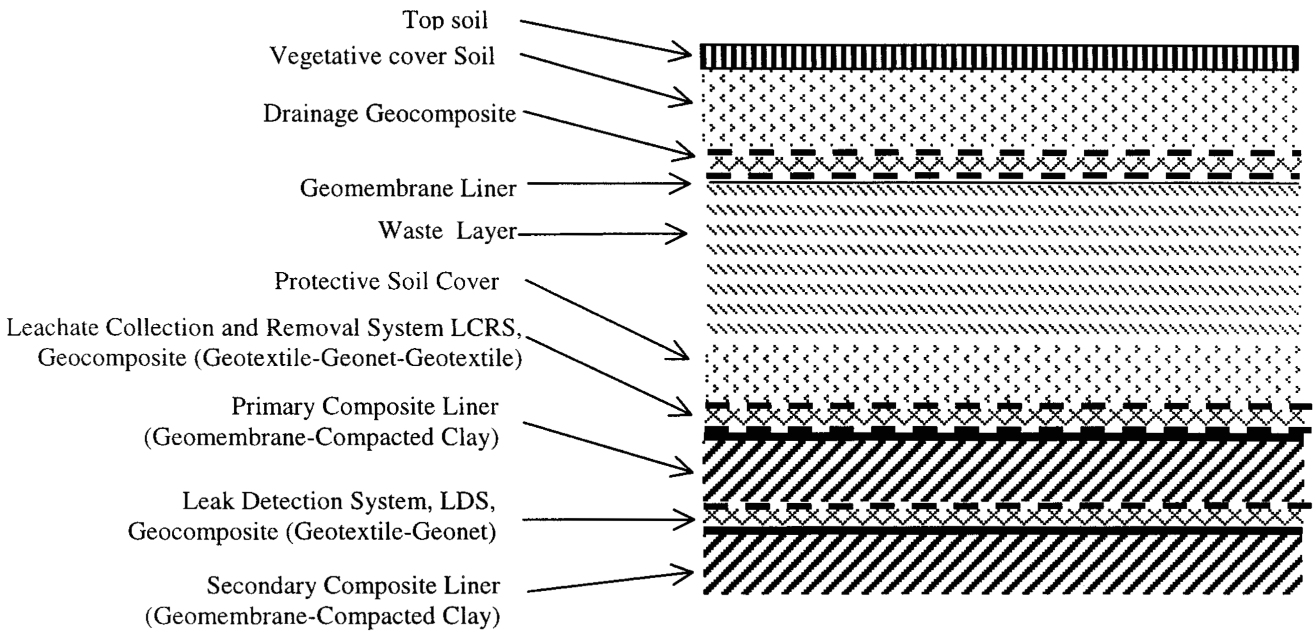

Figure 1: Typical Cross Section in a Landfill

In this paper, the input data for the HELP model for a geosynthetics drainage layer are reviewed, including geometric and hydraulic properties. A parametric study is conducted on a typical landfill cover cross-section to show the effect of using geocomposite properties measured under simulated field conditions as an input compared to the default values. The results are presented in terms of the estimated amount of lateral drainage and the head on the liner as shown in the HELP Model output. The validity of using the maximum head on the liner, as calculated by McEnroe's equation, McEnroe, 1993, is also discussed.

A design example is presented to demonstrate the proper use and interpretation of HELP model input and output data. The effect of incorporating updated weather data in the simulations compared to the historic weather data used by the HELP Model will also be investigated.

THE HELP MODEL

The HELP model is a quasi –two-dimensional hydrologic model of water movement across, into, through and out of landfills. The model accepts weather, soil and design data and uses solution techniques that account for more than ten above-surface and subsurface hydraulic processes including precipitation, snowfall, runoff, and evapotranspiration. The three main weather data required for the HELP model are: precipitation, temperature, and solar radiation.

The HELP model supports three types of soil layers;1) a vertical percolation layer, e.g. the waste layer, in which the downward flow is modeled by unsaturated vertical gravity drainage, and the upward flow due to evapotranspiration by an extraction. 2) A lateral drainage layer, e.g. LDS layer, to conduct drainage laterally to a collection and removal system. The lateral flow in this layer is modeled as saturated flow. 3) A barrier soil liner to restrict vertical leakage or percolation in which a saturated vertical flow is allowed. The liner soil layer is assumed to be saturated all the time, which means that all the percolation through it will be considered leakage.

The following are input data required by the HELP model to simulate a lateral drainage layer:

- Layer Thickness (cm)
- Moisture Retention Parameters:
  - Porosity (vol/vol), the ratio of active pore volume to the total volume
  - Field Capacity (vol/vol), the maximum volumetric water content that does not result in gravity drainage.
  - Wilting Point (vol/vol), the lowest volumetric water content that can be achieved by plant transpiration
- Saturated hydraulic conductivity (cm/sec)
- Max Drainage Length (m), the horizontal projection of the slope
- Drain Slope (%), from 0 to 50%

It's very important to note that all dimensional and hydraulic input data for a geosynthetic drainage layer should be specified under the anticipated field conditions. Therefore, for a particular geosynthetic drainage layer, measured values of thickness, porosity, and saturated hydraulic conductivity are used in the parametric study. Field Capacity, and Wilting Point apply more to soils. For geosynthetic materials, the two properties are not well defined values. Default values, as suggested in the HELP model, of 0.01 and 0.005 respectively, will be used in the parametric study.

PARAMETRIC STUDY

Slopes in landfill final closure systems are among the largest man-made slopes. Careful design considerations need to be taken to ensure both hydraulic and mechanical stability. Several cases have been reported of landfill capping systems that failed due to an inadequate flow capacity of the drainage systems, Soong and Koerner, 1994. Figure 2 shows a cross section of the flat slope in a typical landfill cap profile which consists of a cover soil, geocomposite lateral drainage layer and a geomembrane liner. The slope is assumed to be 3% and 33% (1.7°, 18.4°) with a horizontal length of 40 m (131 ft). The hydraulic conductivity of the cover soil was assumed within a typical range of a vegetative support layer. Bare (no vegetation) and no surface runoff were modeled. Table 1 shows the relevant properties of the three layers.

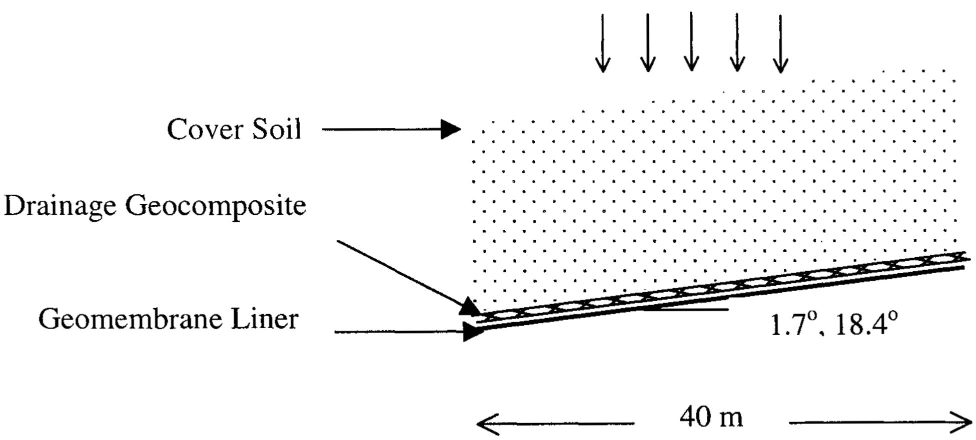

Figure 2: Landfill Cover System Example

Table 1: Layer Properties

Layer	Thickness (cm)	Saturated Hydraulic Conductivity (cm/sec)	Moisture Retention Parameters (vol/vol)		
			Porosity	Field Capacity	Wilting Point
Cover Soil	45.00	$1.0 \times 10^{-5} - 1.0 \times 10^{-3}$	0.40	0.15	0.01
Drainage Geocomposite	0.50 – 0.75	1.0×10^{1} - 5.0×10^{1}	0.85	0.01	0.005
Geomembrane Liner	0.15	2×10^{-13}	-	-	-

The parametric study was conducted to evaluate the effect of the variation in the saturated hydraulic conductivity of the cover soil on the collected lateral drainage and maximum head on the liner calculated by McEnroe's equation and as presented in the HELP model output. The precipitation minus runoff, evapotranspiration, and moisture storage change will infiltrate into the lateral drainage system. The drainage collected from the lateral drainage layer, as calculated by the HELP model, is the difference between the vertical percolation from the layer directly above and the leakage from the liner. For the purpose of this parametric study, the geomembrane liner is modeled with no pinholes or installation defects to minimize the leakage through it. This maximizes the lateral drainage collected and hence the head on top of the liner for a given infiltration rate.

Each case was run for a simulated period of time of one year, based on the default precipitation, temperatures, and solar radiation weather data of Baltimore, Maryland. Two drainage geocomposites GC1 and GC2 were considered with thickness and hydraulic conductivity of 0.5 cm, 10 cm/sec and 0.75 cm, 50 cm/sec respectively. GC1 is a default geocomposite in the HELP model. The results presented are from the "Peak Daily" summary table of the HELP model output. The data in this table don't necessarily correspond to a single day from the analysis period of time. For example, the peak daily drainage collected might not be on the same day as the peak daily precipitation, because on the day of the peak precipitation, a high level of runoff might take place that reduces the amount of infiltration into the sub-layers, hence reducing the amount of collected lateral drainage. For that reason, a water- balance analysis shouldn't be conducted by subtracting the "Runoff" value from the "Precipitation" value as presented in the "Peak Daily" summary table.

Flat Slopes

Figure 3 shows the effect of changing the hydraulic conductivity of the cover soil on both the amount of lateral drainage collected from the geocomposites (thin lines), and the maximum. head on the liner (thick lines). Both drainage geocomposites GC1 and GC2 seem to have an adequate flow capacity until a point close to an infiltration rate of 30 mm/day. Here, the flow capacity of GC1 starts to be exceeded and the head on the liner is higher than GC1 thickness. Up to this point, the lateral drainage collected from both geocomposites is approximately equal. Beyond this point, GC1 becomes saturated, and the head on the liner and the amount of lateral drainage of GC1 increase significantly. However, these values lack accuracy as will be explained below. The infiltration rate that will saturate GC1 at the toe section of the 40 m slope, can be estimated as follows:

Infiltration rate = thickness x hydraulic conductivity x gradient / slope length
= 0.5 cm x 10 cm/sec x 0.03 / 4000 cm = 3.75×10^{-5} cm/sec (32.4 mm/day)

For GC2, the saturation infiltration rate is estimated at 1.48×10^{-4} cm/sec or 128.3 mm/day. At approximately 32.4 mm/day of infiltration into the drainage layer, the head on the liner in GC1 dramatically increases and exceeds the thickness of the geocomposite. In the case of GC2, the

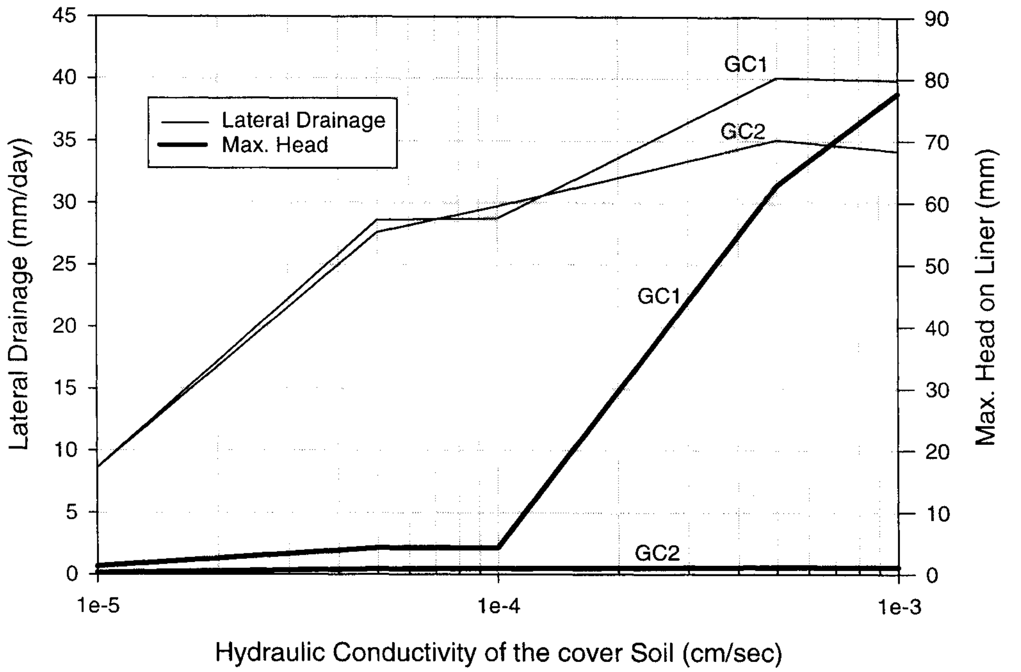

Figure 3: Effect of Cover Soil Hydraulic Conductivity on Lateral Drainage and Max. Head, Default Precipitation Data, Slope; 3%

maximum head on the liner stays within the thickness over the selected range of cover soil hydraulic conductivities, since it requires a higher value of infiltration rate to saturate.

The default maximum daily precipitation rate for this particular location is 76.4 mm/day (8.8×10^{-5} cm/sec). A lateral drainage of approximately 40 mm/day is the maximum daily precipitation minus evapotranspiration. When the lateral drainage system is saturated and the head above the liner extends into more than one layer as in case of GC1, the HELP model assigns a weight- averaged saturated hydraulic conductivity of the saturated zone. This is based on the ratio of the head in the layers and has a value that lies between the high value of the drainage layer, and the lower value of the cover soil. This weighted value is used in calculating the maximum head with McEnroe's equation. Back calculating this value in the case of GC1 and a maximum head of 77 mm, a value of approximately 0.15 cm/sec is estimated. This value lies between 10 cm/sec for GC1 and 1×10^{-3}cm/sec for the cover soil.

It's the authors opinion that such a weighted hydraulic conductivity for the saturated zone is only valid when using a soil drainage layer and only when its hydraulic conductivity is within one or two orders of magnitude of the cover soil's. In such cases, the weighted hydraulic conductivity could be a representative value of the continuous vertical movement of the water between the cover soil and the lateral drainage layer. However in the case of using a geocomposite as a drainage layer, where its hydraulic conductivity could be as high as 5 orders of magnitude higher than that of the cover soil, it's unlikely that the water movement is going to be continuous between the two layers, and it's going to be drained immediately through the geocomposite. Assigning a weight-averaged hydraulic conductivity for such a system will tend to significantly underestimate the head over the liner.

Side Slopes

For the configuration in Figure 2, the same parametric study has been conducted on a slope of 3H: 1V slope (18.4°) and a hypothetical weather pattern with high daily precipitation rates manually input into the HELP model to ensure a fully saturated condition of the cover soil. The maximum impingement rate is the lowest saturated hydraulic conductivity of the sub-profile layers above the liner, or the infiltration rate whichever is lower. So in this case the hydraulic conductivity of the cover soil is the controlling factor on the amount of the collected lateral drainage.

Figure 4 shows the lateral drainage amount collected from geocomposites GC1 and GC2 (thin lines), and the max. head on the liner (thick lines). A direct relationship between the amount of lateral drainage and the cover soil hydraulic conductivity exists when that layer is fully saturated and the flow capacity of the drainage layer is adequate to drain away the infiltrated water. At a hydraulic conductivity of $1\text{x}10^{-4}$ cm/sec, a drainage amount of 86.4 mm/day was collected from both GC1 and GC2 since their flow capacity of $4.1\text{x}10^{-4}$ cm/sec and $3.1\text{x}10^{-3}$ cm/sec respectively, wasn't exceeded. When the hydraulic conductivity of the cover soil is increased to $1\text{x}10^{-3}$ cm/sec, the flow capacity of GC2 is still not exceeded, and the head over the liner is kept within the thickness of the geocomposites. Here again, the amount of the lateral drainage corresponds to the maximum impingement rate. However, with GC1, the resulting head of approximately 800 mm exceeds the thickness of the cover soil, therefore the lateral drainage is not correct.

For the design of a geocomposite lateral drainage system, the head over the liner, as shown in the peak daily summary table, should not exceed the thickness of the geocomposite. If the resulting maximum head, as calculated by McEnroe's equation, exceeds the thickness of the geocomposite, neither its value nor the lateral drainage amount are correct values. Another geocomposite material with higher performance values should be considered and the simulation repeated until the resulting maximum head is within the thickness of the geocomposite.

UPDATED WEATHER DATA

The default weather data stored in the HELP model are for the five years from 1974 to 1978. All synthetically generated weather data for the analysis period years are based on the statistical seasonal patterns of those five years. The HELP model accepts different formats of user input

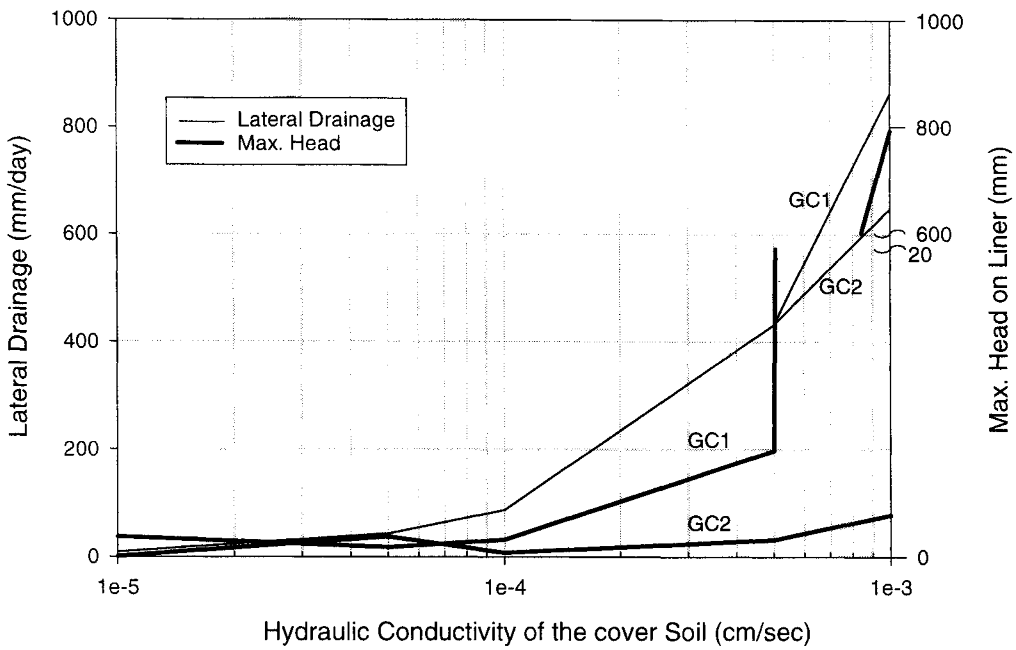

Figure 4: Effect of Cover Soil Hydraulic Conductivity on Lateral Drainage and Max. Head, Hypothetical Precipitation Data, Slope; 33%

from weather data files such as NOAA, ASCII, and Canadian Climatological. In recent years climatical changes have occurred due to some phenomena such as El Ninio, resulting in an increase in the precipitation rates above the reported averages nation wide.

On the National Oceanic Agency (NOAA) web site on the Internet; http://www.nndc.noaa.gov/ temperature, and precipitation data are available for most of the weather stations in the nation for a nominal price. However, more effort is required to make these weather data files compatible with the HELP model. For the purpose of this study, precipitation data from January 1999 to December 1999 for Baltimore, Maryland were manually input into the HELP model and the previous simulations were run for the 3% slope and GC1.

Figure 5 shows the effect of using updated precipitation data on both the maximum head on the liner and the amount of lateral drainage. The data of 1999 show a maximum daily precipitation of 127.5 mm/ day corresponding to only 76.4 mm/day from the historic data used by the HELP model. At a hydraulic conductivity of $1x10^{-4}$ cm/sec for the cover soil, the GC1 geocomposite is no longer capable of providing enough flow capacity, and the maximum head on the liner far exceeds the thickness of the geocomposite. Thus, another geocomposite with higher flow capacity should be considered.

The HELP model precipitation data is based on an average daily rate. This may not be as critical as considering a 6 hour average, as noted by Soong and Koerner, i.e., within a few hours during a storm event, the cover soil could be saturated. This may not be simulated if the storm event is reported on a daily average.

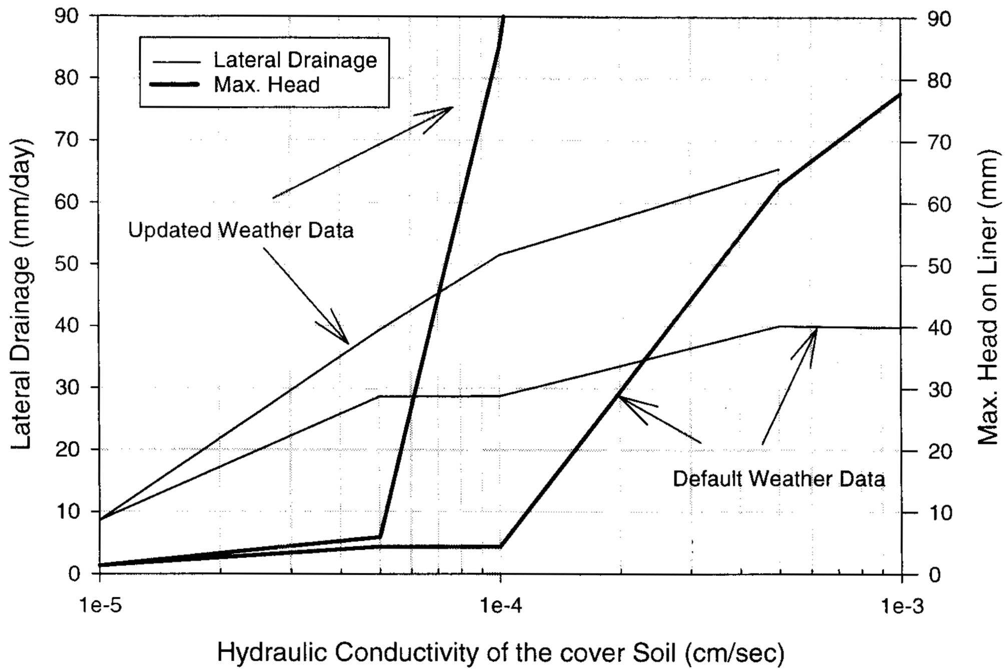

Figure 5: Effect of Cover Soil Hydraulic Conductivity on Lateral Drainage and Maximum Head, Default and Updated Precipitation Data, GC1, Slope: 3%

DESIGN EXAMPLE

A simple example for designing a drainage geocomposite system is presented utilizing the above discussed parametric study;

Given:

- Slope 3% with horizontal length of 40 m
- Cover soil is 45 cm thick, hydraulic conductivity: $1x10^{-4}$ cm/sec

Required:

- Ultimate Transmissivity of the drainage geocomposite

Solution:

- From Figure 5, at a hydraulic conductivity of $1x10^{-4}$ cm/sec, and considering the updated weather data, the head on the liner is approximately 85 mm. This exceeds the geocomposite thickness and indicates that the default geocomposite GC1 (thickness 5 mm, hydraulic conductivity of 10 cm/sec) is not adequate to provide the required flow capacity.

- Another simulation has to be run, this time using GC2 (thickness 7.5 mm, hydraulic conductivity of 50 cm/sec). The resulting maximum head is 1.58 mm and the lateral drainage is 51.73 mm/day. The results indicate that the design properties of the selected drainage geocomposite are adequate. However, since the resulting maximum head is less than the thickness of the geocomposite, another trial may be considered this time with less thickness and/or lower hydraulic conductivity. These trials should be run until a reasonable convergence occurs between the thickness of the geocomposite and the maximum head.

- A quick hand calculation could be done to verify the above results by calculating the required design Transmissivity (thickness x hydraulic conductivity) of the current slope configuration using the unit gradient design, Richardson and Zhao 1999:

  $$\text{Transmissivity}_{\text{required}} = \text{Slope Length x Hydraulic Conductivity}_{\text{cover soil}} \,/\, \text{Gradient}$$
  $$= (4000\text{ cm}) \times (1\text{x}10^{-4}\text{ cm/sec}) / (0.03) = 13.33\text{ cm}^2\text{/sec}$$

  For example, if a geocomposite has a hydraulic conductivity of 50 cm/sec, the required thickness is 13.33/ 50 = 0.27 cm or 2.7 mm. The difference between this thickness and the maximum head calculated by the HELP model (1.58 mm), is due to the fact that only 51.73 mm/day ($6\text{x}10^{-5}$ cm/sec) was considered as an impingement rate. This indicates an unsaturated condition of the cover soil. The hand calculations account for the worst case scenario where the cover soil is fully saturated.

- Applying the design by function approach, a safety factor of 8 (including the overall safety factor and the reduction factors) as suggested by Richardson and Zhao, 1999, is applied on the required design transmissivity to determine the ultimate required transmissivity from the manufacturer (8 x 13.33 = 106.64 cm^2/sec or $1.07\text{x}10^{-2}$ m^2/sec). This transmissivity value has to be verified in the laboratory at the anticipated field conditions as explained before, i.e., at soil boundary conditions, gradient of 0.03 (or preferably 0.1 for less testing variability), a normal stress of 50 kPa (typical for landfill closure systems), and a seating period of 100 hours or until the material stabilizes under the load whichever is less.

SUMMARY AND CONCLUSIONS

The HELP model is a useful tool for the hydraulic evaluation of the required flow capacity of the drainage layers in landfill systems. However, the output results should be properly interpreted, and carefully considered. The main limitation of the program is the precipitation data being handled on a daily average basis which results in an underestimation of the maximum head over the liner. Quick hand calculations, using the unit gradient method, could be done to verify the results, as explained above in the design example. The parametric study conducted in this paper showed the following main results:

1) The "Daily Peak" summary table in the HELP model should be considered to obtain the results of both the maximum head and amount of lateral drainage. No water- balance calculation should be conducted by subtracting the "Runoff" value from the "Precipitation" value as presented in this table because the data don't necessarily correspond to a particular day.

2) McEnroe's equation gives an accurate estimate of the maximum head on the liner beneath the geocomposite drainage layer as long as the head is kept within the thickness of the geocomposite.

3) The weight-averaged hydraulic conductivity, as estimated in the HELP model, may significantly underestimate the maximum head on the liner beneath a geocomposite lateral drainage system.

4) For all practical purposes, it could be assumed that the cover soil will be saturated if the lateral drainage flow capacity is exceeded and the maximum head on the liner exceeds the thickness of the geocomposite.

5) Updated weather data could be utilized in the HELP model to give a more accurate representation of the current precipitation patterns which are more critical than the default ones.

REFERENCES

1) McEnroe, B.M. (1993), "Maximum Saturated Depth over Landfill Liner", Journal of Environmental Engineering, Vol. 119, No.2, pp:262-270

2) Richardson, G., and Zhao, A. (1998), "Design of Lateral Drainage Systems for landfills", GRI 12th conference proceedings pp:177-196

3) Schroeder, P.R., Dozier, T.S., Zappi, P.A., McEnroe, B.M., Sjostrom, J.W., and Peyton, R.L. (1994). "The Hydrologic Evaluation of Landfill performance (HELP) Model: Engineering Documentation for version 3," EPA/600/9-94/xxx, U.S. Environmental Protection Agency Risk Reduction Engineering Laboratory, Cincinnati, OH.

4) Soong, T. Koerner, R.M. (1997), "The Design of Drainage System Over Geosynthetically Lined Slopes", GRI Report # 19, June.

EXPOSED GEOMEMBRANE COVER SYSTEMS: TECHNOLOGY SUMMARY

MARK H. GLEASON, P.E., GEOSYNTEC CONSUNTANTS, INC., USA

MICHAEL F. HOULIHAN, P.E., GEOSYNTEC CONSULTANTS, INC., USA

JEFFREY R. PALUTIS, WASTE MANAGEMENT, INC., USA

ABSTRACT

Exposed geomembrane cover systems (EGCS) were designed and constructed at four landfill sites in the United States. The EGCS represents a new direction in landfill cover system design and construction because it does not include the overlying soil and drainage layer components of a typical final cover system. Accordingly, it can be installed at significantly less cost than a typical final cover system.

For each landfill site, the purpose of the EGCS is to prevent exposure of the waste to the environment, to manage the collection of landfill gas, and to minimize infiltration of stormwater into the landfill. However, at each of the four landfill sites, the design and operations criteria for the EGCS, as well as the rationale for constructing the EGCS, were significantly different. In this paper, the range of economic and technical applications of EGCS technology are reviewed and examples of EGCS applications are presented.

INTRODUCTION

Solid and hazardous waste landfills are typically required to be closed with a final cover system consisting of layers of soil and geosynthetics (Figure 1). The purposes of the final cover system are to prevent exposure of waste to the environment, to enhance collection of landfill gas, and to minimize infiltration of stormwater (which causes leachate) into the landfill. Landfill closure can represent a significant cost to owners and operators when the combined costs of cover system construction, maintenance, and the stormwater management system are considered. Owners and operators may realize a significant cost savings by constructing an exposed geomembrane cover system (EGCS) that consists of an exposed geomembrane without the drainage, vegetative support, and topsoil layers of the typical final cover system, thereby eliminating the construction and maintenance costs associated with these materials (Figure 2). An EGCS is particularly applicable to sites where the design life of the cover system is relatively short (i.e., 10 to 20 years), when future removal of the cover system may be required (e.g., for landfill reclamation), when the landfill sideslopes are steep, when cover soil materials are prohibitively expensive, or when the landfill may be expanded vertically (i.e., overfilled) in the future.

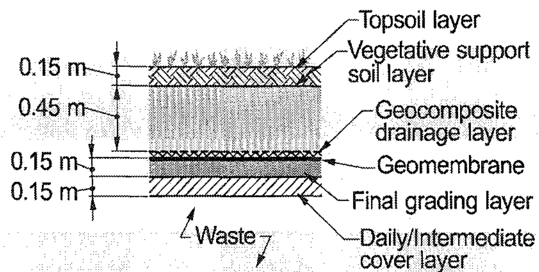

Figure 1. Typical Final Cover System

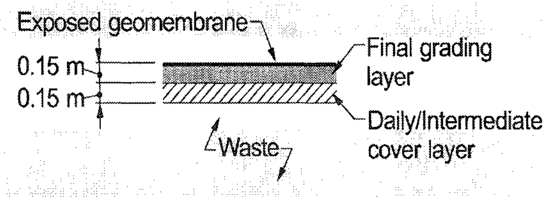

Figure 2. Exposed Geomembrane Cover System

An EGCS was designed and constructed at four landfill sites in the United States. At each landfill, the EGCS was constructed to prevent exposure of the waste to the environment, to manage the collection of landfill gas, and to minimize infiltration of stormwater into the landfill. However, at each of the four landfill sites, the design and operations criteria for the EGCS, as well as the rational for constructing the EGCS were significantly different, as outlined below.

- At a site in Delaware, an EGCS was designed and installed over a 17-hectare (ha) landfill to provide a long-term cover system (i.e., 10 to 20 years) over waste that may be reclaimed at a later date.
- At a site in Maine, an EGCS was designed and installed over a 2-ha landfill that had reached its allowable interim grades based on site subsurface stability. With time, the subsurface strata of clay beneath the landfill will consolidate and gain shear strength, thus allowing for additional waste placement.
- At a site in Florida, an EGCS was designed to provide a temporary cover over a 9-ha landfill for two purposes: (i) the EGCS was constructed a year prior to the planned construction of a typical final cover system in order to control odors associated with landfill gas and; and (ii) on two of these slopes, the EGCS was installed over areas that will be overfilled in the near future.
- At a site in Louisiana, an EGCS was designed and installed over a 6-ha landfill that had severe erosion and long, steep sideslopes that could not be reasonably closed using conventional closure system technology.

The EGCS represents an innovative and economic approach to landfill cover system design and construction. In this paper, the following topics for this cover system are addressed: (i) the advantages and disadvantages of an EGCS; (ii) a discussion of wind uplift design criteria for the

EGCS; (iii) a discussion on geomembrane selection for the EGCS; (iv) a review of the economics of an interim and long-term EGCS as compared to a typical final cover system; and (v) case histories of the four landfills where the EGCS has been designed and constructed. These discussions demonstrate that exposed geomembrane cover systems are an innovative, viable, low-cost approach to a variety of landfill closure applications.

ADVANTAGES AND DISADVANTAGES

As indicated by comparing Figures 1 and 2, the EGCS represents a design that is simpler than the typical final cover system, which results in several advantages. However, the functions performed by the materials overlying the geomembrane in the typical final cover system (i.e., protection of the geomembrane, evapotranspiration and retention of stormwater, etc.) are not performed in the case of the EGCS, which results in disadvantages. These advantages and disadvantages are briefly summarized in the following sections.

Advantages

Compared to a typical final cover system, the advantages of an EGCS include:

- *Reduced construction cost.* Elimination of topsoil, cover soil, drainage, and vegetation components of a typical final cover system may reduce construction costs by as much as $60,000 to $140,000 per hectare, depending on site-specific conditions and the availability of construction materials at the site. A detailed discussion of the economic advantages of an intermediate and/or long-term EGCS as compared to a typical final cover system is presented in a later section of this paper. An estimate of these costs is provided in Table 1.
- *Reduced Annual Operation and Maintenance requirements.* Because there are no exposed soils on an EGCS, repairs to eroded areas and mowing of vegetation are eliminated. An estimate of costs associated with these repairs is provided in Table 1.
- *Increased landfill volume.* By eliminating the cover soils components of a typical final cover system an EGCS can result in added capacity for a landfill if the EGCS is placed at permitted final grades, is used to temporarily cover a landfill slope prior to a lateral expansion, or is used to justify steeper landfill slopes. For landfill overfill situations, eliminating the cover soils would result in added landfill volume when the overfill disposal area is developed.
- *Easier access to landfilled materials for reclamation.* In the event of future landfill reclamation, the EGCS allows the owner access to the waste without having to remove the existing cover soils of a typical final cover system.
- *Reduced post-construction waste settlement.* Because an EGCS is very light, post-construction settlement of the waste is reduced, thereby minimizing damage to geomembrane boots around landfill structures such as landfill gas wells and differential settlement of drainage structures.

- *Reduced hydraulic head on the geomembrane.* Surface water is rapidly drained off of an EGCS and is not restricted by the hydraulic conductivity of the cover drainage materials (i.e., soils and/or geocomposite drainage layer). As a result, the hydraulic head on the geomembrane and subsequent infiltration into the waste is minimized.
- *Slope stability.* Unlike a typical final cover system, there are no soils on the sideslopes of the EGCS, therefore, interface stability associated with slope inclination, water seepage forces, and material property interface friction values are not design concerns.
- *Enhanced visual inspection.* Because the geomembrane is exposed, it may be easily inspected for damage, which, if identified, may be easily and inexpensively repaired.

Disadvantages

Compared to a typical final cover system, the potential disadvantages of an EGCS must be considered prior to and during the design, including:

- *Increased vulnerability to environmental damage.* Because the geomembrane is not protected by overlying cover soils, an EGCS is susceptible to damage from vandalism, animals, exposure to sunlight, low temperatures, and extreme weather (i.e., wind uplift, hail, lightning strikes, etc.). A general discussion of wind uplift design is presented later in this paper.
- *Increased volume and velocity of stormwater runoff.* Because there are no soils and no vegetation on the EGCS, stormwater runoff is conveyed quickly off of the cover system, resulting in increased peak flow quantities and increased runoff velocities. The increased peak flow quantity requires an increased capacity for stormwater drainage features (i.e., ditches and culverts) and a significantly increased peak storage capacity for the on-site stormwater management ponds.
- *Increased susceptibility to uplift by landfill gas.* Because there are no cover soils on the geomembrane of the EGCS, uplift resulting from landfill gas generated beneath the geomembrane must be controlled. A landfill gas collection system must be designed to effectively collect or vent the landfill gas and to control uplift of the geomembrane.
- *Limited access.* Access to a landfill cover system is usually required to allow maintenance of stormwater management and landfill gas management features and to make repairs to damaged features on the cover system. On a typical final cover system, vehicles are allowed access to all soil portions of the landfill cover system. However, in order to protect against puncture or other damage to the geomembrane component of an EGCS, vehicular access is either restricted to a landfill cover access road or not provided at all. In addition, personnel access on the EGCS may be limited for safety reasons when the geomembrane is wet.
- *Limited Design Life.* Because the geomembrane component of the EGCS is not protected from environmental damage (i.e., due to exposure), its design life may be shorter than a geomembrane in a typical final cover system.

- *Limited regulatory approval.* Because the EGCS represents a departure from typical final cover systems, permit approval for an alternative final cover system from the governing regulatory agency is required, and there may be misperceptions among regulators regarding the technical feasibility of an EGCS.
- *Aesthetic concerns.* A large landfill that is covered by an EGCS could be perceived as less visually appealing than a landfill with a fully-vegetated typical final cover system.
- *Limited Post-Closure Use.* Because access on an EGCS must be limited to protect the exposed geomembrane, the post-closure use for an EGCS is very limited. In addition, the EGCS can not provide the potential wildlife habitat (i.e., animal burrows, nests, and grazing) that a typical final cover system can.

WIND UPLIFT DESIGN CONSIDERATIONS FOR AN EGCS

The resistance to wind uplift of the exposed geomembrane component of the EGCS is a governing factor in the design of the EGCS. Wind uplift of the geomembrane is a function of the tensile characteristics of the geomembrane, the landfill geometry, and the design wind velocity. Procedures for the analyses of geomembrane wind uplift are presented by Giroud et al. (1995), extended by Zornberg and Giroud (1997). The analyses are for two criteria: (i) resistance of the exposed geomembrane to tensile failure (i.e., rupture) caused by wind uplift; and (ii) resistance of the geomembrane anchor (i.e., ballast or anchor trenches) to the tensile forces caused by wind uplift on the geomembrane. The forces acting on the geomembrane that cause geomembrane uplift, geomembrane tension, and tensile forces at the geomembrane anchors are a function of the wind velocity and the exposed length of the geomembrane, which is based on site-specific characteristics (i.e., landfill height, side slope inclination, and distance between geomembrane anchors).

To evaluate the potential for tensile failure of the geomembrane caused by wind uplift, the suction force acting over the exposed length of geomembrane is compared to the ability of the geomembrane to resist this force. The properties of the geomembrane required for this analysis can be obtained from the stress-strain curve of the geomembrane, which may be established by performing a wide strip tensile test (for example, according to the American Society for Testing and Materials (ASTM) test method D 4885, "Standard Test Method for Determining Performance Strength of Geomembranes by the Wide Strip Tensile Method"). The properties to be obtained from the stress-strain relationship are: (i) the allowable tensile strain (a fraction of the tensile strain at break for the reinforcing component of a reinforced geomembrane, or a fraction of the tensile strain at yield for unreinforced geomembranes); and (ii) the tensile stiffness of the geomembrane. A discussion of the application of these design methods is presented in Gleason et al. (1998).

To evaluate the resistance of the geomembrane anchor to wind uplift, the uplift force that is exerted on the geomembrane ballast or anchor trench is calculated. The uplift force on the geomembrane anchor is a function of the tensile force in the uplifted geomembrane, the angle between the uplifted geomembrane and the landfill slope at each geomembrane anchor, and the landfill slope angle. A detailed discussion of anchoring methods for the exposed geomembrane is presented in Giroud et al. (1999). As discussed in Giroud et al. (1995), ballast (i.e., tires, sand bags, sand tubes, etc.) is relatively ineffective in limiting uplift when the geomembrane is exposed to wind speeds that are associated with storm events, unless the ballast is placed at very frequent intervals (i.e., 1 to 2 m^2 per ballast).

GEOMEMBRANE SELECTION

The selection of the geomembrane component of the EGCS is a critical element of the EGCS design. The geomembrane component of the EGCS should be designed to meet the following design criteria: (i) the geomembrane polymer should resist exposure to sunlight, which generates heat and contains ultra-violet radiation; (ii) the geomembrane polymer should not become brittle when subjected to low temperatures; (iii) the geomembrane should resist damage caused by tensile stress due to gradual downslope movement (the combined action of gravity and thermal expansion/contraction of the geomembrane over long periods of time could lead to downslope movement of the geomembrane, thus creating additional stresses at the anchors); (iv) the geomembrane should resist mechanical damage caused by extreme weather (i.e., puncture from hail stones (see Gleason, et al. 1998)) and by maintenance activities (i.e., personnel walking on the geomembrane for inspection of the EGCS and to maintain the landfill gas collection system, if present); and (v) the geomembrane should have sufficient tensile strength to resist the tensile stresses caused by uplift from the design wind speed.

ECONOMIC ADVANTAGES OF EGCS

As described in the case histories presented in this paper, an EGCS was selected at each landfill site because it had unique economic advantages over a typical final cover system. The EGCS was selected and installed at these sites as either an intermediate cover system or as a long-term cover system. A detailed cost comparison of materials, construction, and maintenance for a typical final cover system, an intermediate EGCS, and a long-term EGCS is presented in Table 1. Based on the parameters presented in Table 1, the intermediate EGCS and long-term EGCS can provide a cost savings of up to \$140,000 and \$60,000 per hectare, respectively, over the cost of constructing and maintaining a typical final cover system. Examples of when an intermediate and a long-term EGCS could be considered are presented below.

An intermediate EGCS (i.e., a cover system intended for a 1 to 5 year period) may be constructed for one or more of the following reasons:

- on landfill areas that will be overfilled or mined in the future;
- to limit leachate generation before final closure occurs;

- to allow subsurface stratigraphy time to gain strength and allow for additional waste placement and/or construction of a typical final cover system;
- as a means of landfill gas or odor control by enhancing gas collection capability; and
- as a partial final cover system to delay future capital costs associated with construction of a typical final cover system in the future.

A long-term EGCS (i.e., a cover system intended for a 5 to 30 year period) may be constructed for one or more of the following reasons:

- along with an active landfill gas collection system as a long-term means of enhancing landfill gas collection and odor control;
- where operations at the landfill site intends to maintain the EGCS as a final cover system as long as feasible; and
- closure where typical final cover is not feasible (i.e., because existing landfill side slopes are too steep to support a typical final cover system, where adequate final cover soils are not available, where environmental conditions do not permit the growth and sustenance of a vegetative erosion control layer, etc.)

CASE HISTORIES

Cell 1 and 2 Landfill Cover System
Delaware Solid Waste Authority
Southern Solid Waste Management Center
Sussex County, Delaware, USA

The Cell 1 and 2 Landfill consists of two double-lined cells that have been filled to form one monolithic landfill with an area of approximately 17-ha. Solid waste was placed in Cell 1 from 1984 to 1988; solid waste was placed in Cell 2 from 1988 to 1997. In 1997 and 1998, a long-term EGCS was constructed over the Cell 1 and 2 Landfill (Figure 3). As part of the permit condition for the Cell 1 and 2 EGCS, the cover system is considered to be a long-term rather than a final cover system. As a result, its permit will be reviewed by the governing regulatory agency on a 10-year recurring basis. This criteria for this review will be focused on the long-term integrity and durability of the geomembrane and the effectiveness of the EGCS as a barrier to stormwater infiltration and exposure of waste.

The geomembrane component of the EGCS is a 0.9-mm thick green polypropylene geomembrane with a polyester scrim reinforcement. Based on the local building code for structures in the area, the design wind velocity was selected to be 130 km/hr. The landfill has 4H:1V slopes, is approximately 40-m high, and has cover benches with corresponding drainage swales and geomembrane anchors spaced at 12-m vertical intervals (for an exposed geomembrane length of approximately 50 m). The constructed geomembrane anchor trench is located at each cover bench and has a cross sectional area of 2.3 m^2. A detailed summary of the design calculations for the Cell 1 and 2 EGCS is presented by Gleason et al. (1998); a summary of construction of the Cell 1 and 2 EGCS is presented by Gleason et al. (1999).

The limited availability cover soil material in the region and the possibility of future waste mining and/or capacity recovery at the site made the EGCS an economically attractive option for this landfill. By constructing an EGCS for the Cell 1 and 2 landfill, a cost savings of approximately $60,000 per hectare was realized, compared to constructing a typical final cover system.

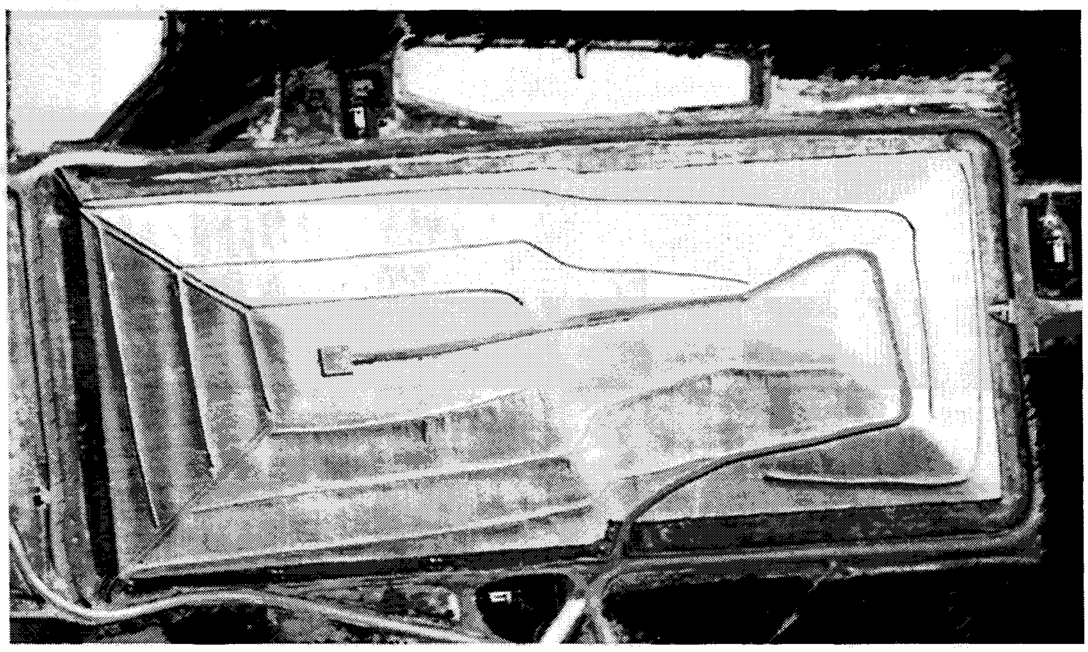

Figure 3. Cell 1 and 2 Exposed Geomembrane Cover System

Phase 7 Landfill
Crossroads Landfill
Waste Management Disposal Services of Maine
Norridgewock, Maine, USA

The Phase 7 Landfill occupies an area of approximately 2 ha and is a "special waste" (i.e., non-municipal solid waste) landfill. In 1996 an intermediate EGCS was constructed over the Phase 7 landfill (Figure 4). Although only 8 m in height, the landfill had reached its allowable interim grades based on stability of the subsurface glacio-marine clay materials. With time, the pore pressures in the clay resulting from waste placement will dissipate (i.e., the clay will consolidate) and the clay will gain strength, thereby allowing additional waste placement. As part of the permit condition for the Phase 7 Landfill, the cover system is considered to be a temporary cover system.

The geomembrane component of this intermediate EGCS is a 1.0-mm thick high-density polyethylene (HDPE) geomembrane. Because of the low profile of the landfill and the relatively short-term life of this EGCS, the geomembrane is ballasted with sandbags (ultra-violet light resistant) at a spacing of one per 9 m^2. Stormwater is collected in a drainage swale that was constructed around the perimeter of the Phase 7 Landfill and is drained to one of the site stormwater management ponds. Because the special waste landfill produces little gas, a passive gas vent system was designed and installed for the EGCS.

The time-dependent nature of consolidation and associated strength gain in the subsurface clay materials made the intermediate EGCS an economically attractive option for this landfill. By constructing an EGCS for the Phase 7 Landfill, a cost savings of approximately $120,000 per hectare was realized, compared to constructing a typical final cover system.

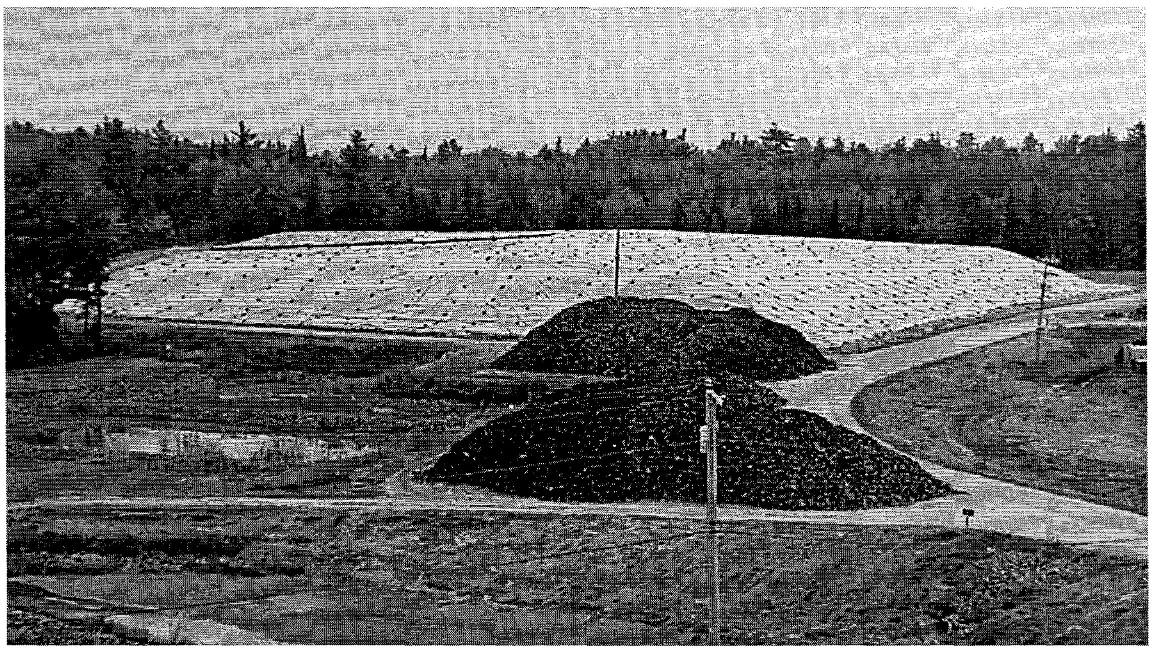

Figure 4 – Phase 7 Landfill Exposed Geomembrane Cover System

Cell 6 - Naples Landfill
Waste Management of Florida, Inc.
Naples, Florida, USA

The Cell 6 Landfill in occupies an area of approximately 9 ha. In 1999 an intermediate EGCS was constructed over the Cell 6 landfill (Figure 5). The EGCS was constructed in association with an active landfill gas collection system to control landfill gas and odors at the site. The design of the EGCS was selected for two purposes: (i) on two slopes, the EGCS was constructed to provide an interim cover to collect landfill gas in an area that would eventually be covered with a typical final cover system and; and (ii) on the other two slopes, the EGCS was installed over areas that will be overfilled in the near future.

On the western and northern slopes of Cell 6, a 1.0-mm thick HDPE geomembrane was installed. These slopes were covered with a geocomposite drainage layer and soil components of a typical final cover system in the 2000 construction season. A 1.5-mm thick HDPE geomembrane was constructed on the top, southern, and eastern slopes of Cell 6. These slopes of the landfill are currently exposed and will likely be overfilled with waste at a future date. Due to the short-term exposure of the western and northern slopes, minimal geomembrane ballast was used on these slopes; geomembrane anchor trenches were constructed on the top, southern, and eastern slopes because of longer-term exposure. The design wind velocity used at the site was 100 km/hr.

The need for odor control at the site, the ability to install the EGCS quickly and convert it to a typical final cover system on two slopes, and the future potential for overfilling of portions of the Cell 6 Landfill made the EGCS an economically attractive option for this site. By constructing an EGCS on the western and northern slopes of the site, landfill gas odors were controlled and approximately $1 million in construction costs were delayed for one year. On the top, southern, and eastern slopes, a savings of approximately $100,000 per hectare was realized, compared to the costs associated with constructing a typical final cover system.

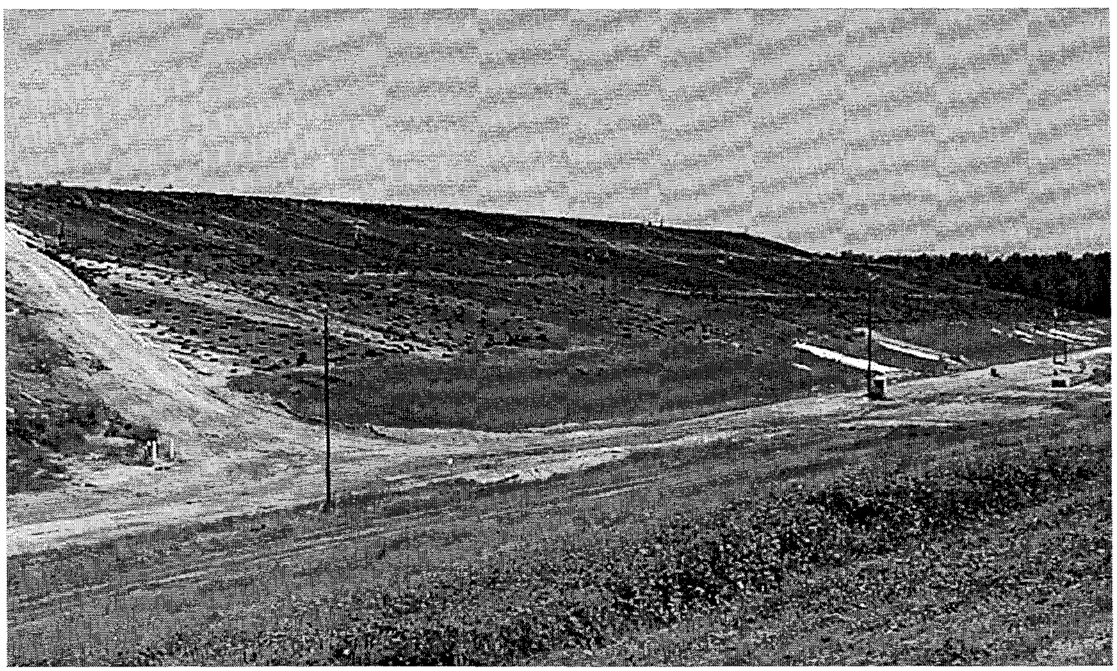

Figure 5. Naples Landfill Cell 6 Exposed Geomembrane Cover System

Phases I and III - Sabine Parish Landfill
Waste Management, Inc.
Many, Louisiana USA

Prior to constructing an EGCS, Phases I and III of the Sabine Parish Landfill had long, steep sideslopes and was experiencing severe erosion of the existing poorly vegetated soil cover (Figure 6). A long-term EGCS was designed and constructed on the 6 ha landfill in 1999 (Figure 7). Because the geomembrane component of the EGCS satisfied the minimum permeability requirements for the cover system for this site of 1 x 10^{-5} cm/s, the EGCS was approved and permitted as a final cover system.

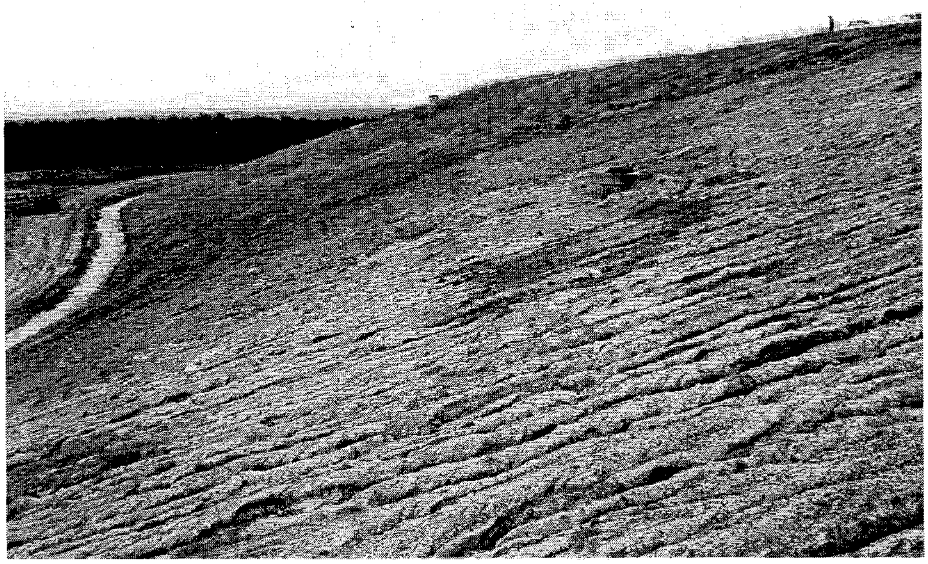

Figure 6. Pre-Construction Slope Conditions at Sabine Parish Landfill

As a result of side slopes with an average inclination of 2.8:1 (horizontal to vertical), a maximum inclination of up to 2.5:1, and a height of approximately 25 m without benches, the site could not be reasonably closed using conventional closure system technology (i.e., typical final cover system). The geomembrane component of the EGCS was a 1.5-mm thick green HDPE textured geomembrane that was designed to be restant to long-term exposure to ultraviolet light. The design wind velocity for the project was selected to be 100 km/hr. Landfill cover anchor trenches were constructed at approximately 10 to 12-m vertical intervals for an exposed geomembrane length of between 35 and 40 meters. The constructed geomembrane anchor trenches correspond to drainage swales and have cross-sectional areas of between 1.0 and 1.2 m^2. Because the site does not have an active landfill gas collection system, passive gas vent flaps were installed in the EGCS.

The difficulty in maintaining a sustainable vegetative cover, the long and steep sideslopes, the severe erosion experienced at the site, and the regulatory acceptance of this type of alternative cover system made the EGCS an economically attractive option for this landfill. By constructing an EGCS for the Phase I and III landfill, a cost savings of at least $130,000 per hectare was realized, compared to constructing a typical final cover system. The site is currently in its 30-year post-closure period. As such, inspection, maintenance, and repair (if necessary) of the EGCS is part of post-closure care for the site.

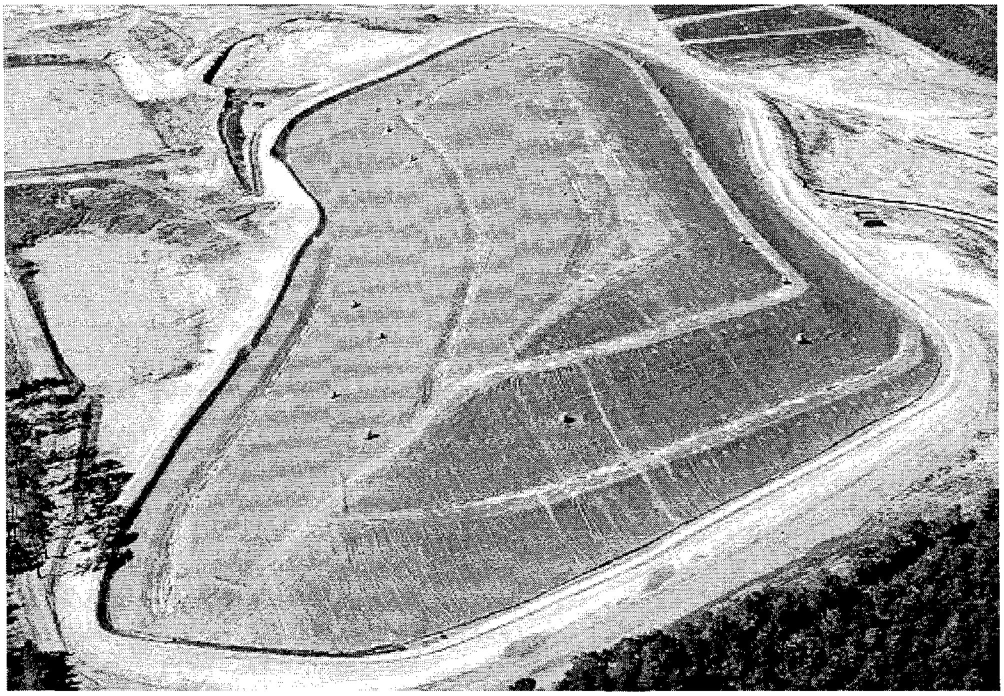

Figure 7. Phase I and III Exposed Geomembrane Cover System

CONCLUSIONS

Based on the discussions in this paper, landfill owners, operators, and design engineers should consider the advantages, disadvantages, and design parameters associated with designing and constructing an EGCS at a landfill site. In particular, the expected cover system design life and the operational requirements for the site should be reviewed to assess whether an EGCS is appropriate for a particular landfill. References are provided to address detailed EGCS design issues.

As described in this paper, an exposed geomembrane cover system has been successfully designed and constructed at four landfill sites in the USA. The design criteria and economics associated with both an intermediate EGCS (1 to 5 year) and long-term EGCS (5 to 30 year) EGCS are discussed. As described in this paper, the rationale for selecting an EGCS for each site is very different; however, at each site, constructing an EGCS presented a clear economic advantage over constructing a typical final cover system.

Table 1

Economic Analysis
Typical Final Cover System
vs.
Intermediate and Long-term Exposed Geomembrane Cover System

Component	Typical Final Cover System			Intermediate EGCS (1 to 5 years)			Long-Term EGCS (5 to 30 years)		
	Quantity	Unit Rate	Cost	Quantity	Unit Rate	Cost	Quantity	Unit Rate	Cost
Construction									
Grading/Initial Cover (0.15 m)	1,500 m^3	$8.00	$12,000	1,500 m^3	$8.00	$12,000	1,500 m^3	$8.00	$12,000
Geomembrane	10,000 m^2	$4.40	$44,000	10,000 m^2	$2.00	20000	10,000 m^2	$6.50	65000
Anchor/Ballast	-	-	-	LS	$3,000	3000	LS	$15,000	15000
Cover System Drainage Layer	10,000 m^2	$6.00	$60,000	-	-	0	-	-	0
Vegetative Support Soil (0.45 m)	4,500 m^3	$10.00	$45,000	-	-	0	-	-	0
Topsoil (0.15 m)	1,500 m^3	$12.00	$18,000	-	-	0	-	-	0
Stormwater Management	LS	$25,000	$25,000	LS	$20,000	$20,000	LS	$40,000	$40,000
Seeding	LS	$4,000	$4,000	-	-	-	-	-	-
Total/Hectare:			**$208,000**			**$55,000**			**$132,000**
Total/Acre:			**$84,000**			**$22,000**			**$53,000**
Annual Operation and Maintenance									
Mowing/Revegetation	LS	$1,500	$1,500	-	-	$0	-	-	$0
Regrading	LS	$1,500	$1,500	-	-	$0	-	-	$0
Stormwater Management Repairs	LS	$1,500	$1,500	LS	$500	$500	LS	$750	$750
Anchor/Ballast Repair	-	-	$0	LS	$1,000	$1,000	LS	$500	$500
Geomembrane Repair	-	-	$0	LS	$1,000	$1,000	LS	$750	$750
Total/Hectare/Year:			**$4,500**			**$2,500**			**$2,000**
Total/Acre/Year:			**$1,800**			**$1,000**			**$800**

REFERENCES

Giroud, J.P., Pelte, T., and Bathurst, R.J., (1995) "Uplift of Geomembranes by Wind", *Geosynthetics International*, Special Issue on Design of Geomembrane Applications, Industrial Fabrics Association International, Vol. 2, No. 6, pp. 897-952.

Giroud, J.P., Gleason, M.H., and Zornberg, J.G., (1999) "Design of Geomembrane Anchorage Against Wind Action", *Geosynthetics International*, Vol. 6, No. 6, pp.481-507.

Gleason, M.H., Houlihan, M.F., and Giroud, J.P., (1998) "An Exposed Geomembrane Cover System for a Landfill", *Proceedings, Sixth International Conference on Geosynthetics*, Atlanta, Georgia, pp. 211-218.

Gleason, M.H., Germain, A.M., Vasuki, N.C., and Giroud, J.P., (1999) "Design and Construction of an Exposed Geomembrane Cover System for a Solid Waste Landfill", *Proceedings Sardinia '99, Seventh International Waste Management and Landfill Symposium*, Caligliari, Italy, pp. 335-342.

Zornberg, J.G., and Giroud, J.P., (1997) "Uplift of Geomembranes by Wind - Extension of Equations", *Geosynthetics International*, Industrial Fabrics Association International, Vol. 4, No. 2, pp. 187-207.